

Green Energy and Technology

Sudipta De
Santanu Bandyopadhyay
Mohsen Assadi
Deb A Mukherjee *Editors*



Sustainable Energy Technology and Policies

A Transformational Journey, Volume 1

 Springer

Green Energy and Technology

More information about this series at <http://www.springer.com/series/8059>

Sudipta De · Santanu Bandyopadhyay
Mohsen Assadi · Deb A Mukherjee
Editors

Sustainable Energy Technology and Policies

A Transformational Journey, Volume 1

 Springer

Editors

Sudipta De
Department of Mechanical Engineering
Jadavpur University
Kolkata, West Bengal
India

Mohsen Assadi
Natural Gas Technology
University of Stavanger
Stavanger
Norway

Santanu Bandyopadhyay
Department of Energy Science
and Engineering
Indian Institute of Technology Bombay
Mumbai, Maharashtra
India

Deb A Mukherjee
Energy and Environment Committee
The Bengal Chamber of Commerce
and Industry
Kolkata, West Bengal
India

ISSN 1865-3529

Green Energy and Technology

ISBN 978-981-10-7187-4

<https://doi.org/10.1007/978-981-10-7188-1>

ISSN 1865-3537 (electronic)

ISBN 978-981-10-7188-1 (eBook)

Library of Congress Control Number: 2017958612

© Springer Nature Singapore Pte Ltd. 2018, corrected publication 2018

This work is subject to copyright. All rights are reserved by the Publisher, whether the whole or part of the material is concerned, specifically the rights of translation, reprinting, reuse of illustrations, recitation, broadcasting, reproduction on microfilms or in any other physical way, and transmission or information storage and retrieval, electronic adaptation, computer software, or by similar or dissimilar methodology now known or hereafter developed.

The use of general descriptive names, registered names, trademarks, service marks, etc. in this publication does not imply, even in the absence of a specific statement, that such names are exempt from the relevant protective laws and regulations and therefore free for general use.

The publisher, the authors and the editors are safe to assume that the advice and information in this book are believed to be true and accurate at the date of publication. Neither the publisher nor the authors or the editors give a warranty, express or implied, with respect to the material contained herein or for any errors or omissions that may have been made. The publisher remains neutral with regard to jurisdictional claims in published maps and institutional affiliations.

Printed on acid-free paper

This Springer imprint is published by Springer Nature

The registered company is Springer Nature Singapore Pte Ltd.

The registered company address is: 152 Beach Road, #21-01/04 Gateway East, Singapore 189721, Singapore

Foreword

The 2017 Energy Conclave of the Bengal Chamber of Commerce & Industry focused on the “Transforming Face of Energy,” and the discussions at the Conclave, including the papers in the two volumes, address various aspects (technological, financial, policy, and institutional) of the paradoxes associated with high greenhouse gas emissions cohabiting with development goals. This leads to many debates, including that of the comparative economics of renewable energy from new installations and of coal-based power generation from existing plants. It also tells us that this is a longer-term transition, with many challenges along the way, and with public policy priorities that also change over time. During the past couple of years, climate change has risen to the top of public policy concerns, which have traditionally included energy security, energy access, business competitiveness, and air quality.

Low Carbon Energy Growth is Steadily Increasing in India

In 2015, on Gandhi Jayanti, India submitted its Intended Nationally Determined Contributions (INDCs) to the United Nations Framework Convention on Climate Change (UNFCCC). We pledged that in the energy sector, at least 40% of our electricity generating capacity would not be based on fossil fuels (and on renewables, hydro, and nuclear) and that the carbon intensity of our economy (i.e., total greenhouse gas emissions divided by the GDP) would be 33–35% less in 2030 as compared to 2005¹. For the sake of comparison, in 2015 ~30% of electricity generation capacity did not depend on fossil fuels and our carbon intensity was 13% less than the level prevailing in 2005.

¹ INDIA'S Intended Nationally Determined Contribution <http://www4.unfccc.int/submissions/INDC/Published%20Documents/India/1/INDIA%20INDC%20TO%20UNFCCC.pdf>.

If we draw a straight line from 2005 to 2014 and onto 2030, it seems that we are on target to meet these goals. The recent success in the growth of renewables and of energy efficiency, largely driven by business models which have also led to sharp decline in the price of energy efficient and renewable energy products (such as LED bulbs and the solar photovoltaic modules), also suggests a similar trend. Yet, at the same time coal-based power generating stations in India are operating at historically low plant load factors and are able to sell, on an average, no more than two-thirds of the electricity that they are designed to produce. And, it is also true that while the cost of electricity from solar photovoltaic is now less than that from coal power stations, it is available only when the sun is shining—whereas nowadays the demand for electricity in summer months in cities like Delhi, occurs at midnight, when all households who have air conditioners switch them on as they go to sleep.

These trends present competing visions. On the one hand, solar energy is becoming cheaper and the demand for energy is rising more slowly than in the past. But on the other hand, our existing fleet of coal power stations is thirsting to sell more electricity in order to be able to payback the loans that they have taken from our banking systems, and a large amount of our energy use occurs at times of the day when solar energy cannot meet that demand.

The Transformation is Turbulent ... and is not Inevitable

This suggests that the Indian electricity sector is presently going through a major transformation. The accelerated pace of generation capacity addition over the past few years has led to a situation where the electricity supply potential is greater than the economic demand, a scenario which has never before existed in the history of the Indian electricity sector. At the same time, we have also been witnessing changes in the energy mix due to enhanced policy focus on climate change, energy security concerns, etc., due to which the penetration of renewable electricity, especially from wind and solar energy, has been increasing steadily and is projected to grow much faster in the coming years. The demand for electricity is increasing, primarily due to increased space conditioning loads, but the growth in demand is slower than expected, in part due to the adoption of energy efficiency (EE) initiatives. As India's energy mix and demand patterns change, due to significant addition of RE in the grid and new EE measures, it is important that the policy and regulatory environment in the power sector rapidly adapts itself to the changing landscape so that new technologies, and more significantly, new business models (in addition to the current business model of a distribution company supplying electricity to all consumers within its geographical jurisdiction, while sourcing electricity from power generation companies on the wires of electricity transmission companies) come into place which provide space for newer low carbon technologies, as well as newer ways for local electricity generation and the distribution and sales of this electricity to nearby neighbours and other consumers.

The Government of India's (GoI) resolve to combat climate change and decarbonize India's energy systems is clearly spelt out in India's Intended Nationally Determined Contributions (INDCs). To enable the goals, a range of policies and programs to promote RE is in place at the central and state level in India, which suggests the possibility of an early initiation of de-carbonization of India's electricity sector. There is a high probability that if the costs of storage technologies continue to decline at the same rate as in the past ten years, then it is quite possible that, by 2025, all new electricity generation capacity that is added—and a lot of generating capacity still needs to be added to ensure that there is an adequate provision of energy services in the country so that all citizens have a high quality of life—comes from renewable energy, with storage providing the means to ensure that the electricity from the sun harnessed during the day by solar cells is available for use even when the sun is not shining.

In the interim (till storage costs become economically viable), a recent study carried out by the Power System Operation Corporation India (POSOSO), NREL, and LBNL has demonstrated that India's electricity grid can manage the variability and uncertainty of adding large amounts of renewable energy into the grid. The studies demonstrate that balancing the Indian power system in 2022 with 100 GW solar and 60 GW wind is achievable with minimal curtailment of renewable energy output². However, economically viable electricity from solar+storage means that we will need to continue to expand the competitive procurement of solar electricity, and in addition, start the procurement of storage capacity as well. Only this will ensure that prices of electricity from renewables+storage keep declining—so that when new generation capacity needs to be added (in about 2025), this will be competitive with the price of electricity from new coal-based generation capacity.

The tension in enhancing renewables at present, when the coal-based power sector is facing low utilization, was captured in the 16th Darbari Seth Memorial Lecture³ that Dr. Arvind Subramanian, the Chief Economic Adviser, delivered at TERI on the August 17, 2017. His analyses suggested that the social cost of electricity from renewables is more than the social cost of electricity from coal, and that the country could not both provide relief to the coal power plants operating at low plant load factors (and to the banks whose NPAs are increasing as a result), as well as subsidize renewable electricity. This suggests that the straight-line movement to 40% nonfossil fuel generating capacity in 2030 is not preordained. It also means that several ancillary goals will have to be achieved in order that we meet our INDC pledges.

All these changes are occurring while we, as a country, will have to make adequate and affordable energy, including electricity, available to all citizens. Current estimate suggests more than 40 million households still do not have an electricity connection, and that of those that are connected, more than half gets

² GREENING THE GRID: Pathways to Integrate 175 Gigawatts of Renewable Energy into India's Electric Grid, Vol. I—National Study <https://www.nrel.gov/docs/fy17osti/68530.pdf>.

³ <http://www.teriin.org/themes/teriday/darbariseth2017.php>.

electricity for less than some 16 hours per day. The recently announced Saubhagya program⁴ promises to ensure connectivity to all households by the end of 2018, but the challenge to provide 24x7 electricity supply to all of them will need new initiatives. We also note that the average electricity consumption in India is still only about 1075 kWh⁵ per person per year—which is way below that needed for ensuring a good quality of life. And, there is no country in the world with a standard of living—with a Human Development Index (HDI) of 0.9 or more—with electricity consumption of at least 5000 kWh per person per year. Consequently, electricity demand growth is both inevitable and essential. At the same time, the ability of most of the newly connected electricity households to purchase electricity is limited; affordable and adequate electricity supply is a necessary prerequisite for development.

The Next Steps

In view of the uncertainties associated with the transition, and the changing comparative economics of coal- and renewables-based electricity for the next decade or so, it is difficult to suggest next steps. What is clearer is that we will pass through at least three phases during this period during each of which a different set of strategies will need to be followed.

In the first phase, till about 2023, the current backlash from the coal sector would continue—primarily because the installed coal capacity is being used at very low load factors (of the order of 50%). We expect the load factors, electricity generation, and revenues of the coal-based power stations would increase during this period (as electricity demand increases), and that the plants may become viable by 2023 which will reduce the push back to renewables. In this short term, the primary goal is to ensure that renewable electricity continues to have breathing space, while the coal plants are also able to survive. In the short and medium term, the bulk of electricity would continue to be provided from the coal-based power stations. This is both because the vast of our current electricity capacity is based on coal power and also goes on a full cost basis (which includes the need to provide electricity when the sun is not shining and wind is not blowing). Consequently, in the short term coal plants are able to survive the financial stress that they are currently undergoing. The TERI analyses , ‘Transitions in Indian Electricity Sector 2017–2030⁶’, showed

⁴ Government of India notification for Pradhan Mantri Sahaj Bijli Har Ghar Yojana http://powermin.nic.in/sites/default/files/webform/notices/OM_SAUBHAGYA_SIGNED_COPY_0.pdf .

⁵ CEA executive summary, Page 11 http://www.cea.nic.in/reports/monthly/executivesummary/2017/exe_summary-09.pdf.

⁶ Transitions in Indian Electricity Sector- A Report by TERI http://www.teriin.org/files/transition-report/files/downloads/Transitions-in-Indian-Electricity-Sector_Report.pdf.

that the coal-based capacity (the current capacity that is already installed and that which is currently under installation) would reach an average plant load factor of at least 60% by 2023, or so. This PLF level of utilization is significant since most plants would be able to operate profitably at this level of utilization. Beyond 2023, the PLFs would increase further, and the coexistence of electricity from renewables and from coal would be easier.

In the second phase, beyond 2023 and probably the 2026–27, the already-installed coal capacity and renewables will coexist and will together be able to meet the still increasing demand. The challenge during this period will be to demonstrate that the cost of renewable electricity is less than the *variable* cost of coal-based electricity—about Rs. 1.50 per kWh. This is because distribution companies are already committed to paying the fixed costs of coal-based electricity (about Rs 2 per kWh), and the merit order scheduling is based only on the variable cost of coal electricity (which is largely the coal cost the O&M cost). With a decline in the cost of renewable energy to be less than the variable cost of coal-based electricity, there would be an increasing preference for the procurement of the lower cost renewable energy, and for the use of existing coal capacity as surrogate storage capacity, to provide electricity when renewable electricity is not available.

In the third phase, beyond 2027, there will be a need to add new generation capacity. At this time, if the full costs of renewable electricity (including the cost of storage) are less than that of new coal capacity. This is important because as we move into the third phase, beyond 2027, there will be a demand for new capacity as the already installed coal capacity would be operating at peak levels of utilization. If the cost goal is achieved and demonstrated, then all new capacity that is added would come from renewables + storage. The challenge beyond 2027 (and possibly till 2032 or so) would be to ensure that the Indian grid is able to move toward an operational regime that is increasingly comfortable in absorbing ever-increasing amounts of renewable energy. As this challenge is met, India will move toward the long-term goal of the replacement of retiring coal capacity by renewables + storage.

The successful achievement of this long-term goal requires us to address different questions of political economy at different times in the years ahead. It would mean that the public discourse which influences the technical investments, institutional design, and policy decisions would also need to be tweaked over time.

New Delhi, India

Ajay Mathur, Ph.D.
Director General
The Energy and Resources Institute (TERI)

Preface

With the growing concern for environmental degradation and specifically climate change problem, energy sector all over the world is facing the difficult challenge to meet the ever-increasing energy demand with minimum/no degrading effects on the environment in an economic way. Energy is a vital component for modern civilization, and often per capita consumption of energy is considered as the index of life standard of people of a country. Supplying energy for a decent living at an affordable price and in an environment-friendly way is the critical challenge.

Sustainability is the concept of meeting the present demand without compromising the needs of the future generation. Optimum planning of use of natural resources to meet the need of the present as well as future generations is very critical for sustainability. Solutions must be socially and environmentally acceptable as well as economically feasible. For a long period, fossil fuels were the main source of useful energy for rapid development of human civilization. Technologies for using these fuels have matured over a long period and are available at an affordable cost all over the world. However, limited remaining reserves of these fuels have forced energy technologists to explore alternative options. On top of that, climate change problem may force us to 'leave fossil fuels before they leave us.' Renewable resources are considered to be only future options of energy in a longer time frame as these are virtually inexhaustible. However, technologies for using different renewable resources are widely varying and most of them are still developing. Economic feasibility as well as social acceptance of these new options has to be checked thoroughly before they can emerge as reliable options for future. Intermittency of most of these resources is another problem. These are to be used when 'these are available rather than when we need these for our use.' Different ways of addressing this challenge are under active investigation, including suitable technology development for energy storage and 'hybridization' of different resources available locally. Thus, solutions may be site specific and no unique solution may be available for the whole world. Removing fossil fuels immediately may not be a feasible solution too as other options are neither capable to meet the huge demand nor their reliability is assured under all possible adverse situations. Also, a large capital is already 'locked' in fossil fuel-based technologies. A planned

smooth phasing out of these technologies is required with the development of alternative ones within a specified time frame. This needs proper energy policy with multilevel governance. Moreover, suitable change of existing fossil fuel-based technologies during this transition is critical, most specifically due to climate change problem. Energy sustainability is a global challenge, though many issues of it are site specific. Addressing energy sustainability is thus a global issue as well as local one—starting from a country even up to a small village of that country.

Sustainability of Indian energy sector needs thorough introspection. Presently, coal dominates with 54% of installed generation capacity and ~69% in terms of actual power generation. Also, most of these coal-based power plants are of conventional PF fired with low efficiency. Large transmission and distribution losses with minimum environmental regulation are other limitations of these plants. Hydropower has the next largest share (21% of total installed). Other renewable and nuclear power have steady growth but with some constraints—technological, social, economical, and even political. Transport sector is mostly dependent on imported oil with large uncertainty, economical as well as political. Traditional sources of energy also have a good share, though decreasing. To have a sustainable plan for the Indian energy sector, assessment of the present scenario and future planning based on this assessment is very urgent.

In two volumes of this book, experts from all over the world have addressed energy sustainability from different viewpoints in several articles. Specifically, Indian energy sustainability is also explored with a background of this global perspective.

In the introductory chapter, Sikdar has reported his perception about the different terminologies, say, clean, green, and sustainable energy. Solar photovoltaic technology is considered to be one of the most widely used renewable technologies worldwide as an alternative to fossil fuel-based electricity. Roy discussed this technology starting from the very basic fundamentals up to the most advanced research findings in this field. Integration of intermittent renewable electricity to the conventional grid is a real challenge. Microgrids are considered to be emerging solutions for utilizing different distributed intermittent renewable energies. N. K. Kishore et al. have presented an overview of the present status of microgrids. Transmission and distribution losses affect the overall energy efficiency. Lakshmi and Ganguly presented a state-of-the-art review of transition of power distribution systems. Distributed generation is emerging as a sustainable solution in place of large-scale fossil fuel-based energy systems. Iaria et al. have reported such a system using solar energy. Design of this system has been developed up to the full-scale implementation. Unexplored potential of distributed generation in India has been reported by Jana and De. Full utilization of this potential may make a paradigm shift of energy sustainability of India. Delivery of multiple utility with single or multiple inputs is called polygeneration. It increases the overall energy efficiency with optimal design. A mathematical optimization process using linear programming for such systems has been discussed by Tan and Aviso. Though increasing renewable share is always desired, fossil fuel-based electricity will continue to remain as the major source of electricity. Detoxification technology during

processing of crude oil has been reported by Jarullah et al. CO₂ capture is required to use fossil fuels in power plants in a longer time frame. Different technologies are being developed for this purpose. An overview of state of the art of this technology has been discussed by Maria et al. Prospects of use of algae specifically for this purpose have been discussed by Chowdhury et al. In spite of all challenges, coal plays a critical role in energy sustainability of India. This complex issue is addressed by Bhattacharyya, former chairman of the largest coal producing company of India. Finding new fuels and to use those in innovative ways also add to future energy sustainability. A chapter on use of gas hydrates has been contributed by Nair et al. Biofuel is undoubtedly one important option to substitute fossil fuels in future, specifically in transport sector. Several chapters discuss this important issue both from global perspectives as well as in Indian context. Two chapters by Verma and Kishore and other two by Chowdhury et al.; Yadav and Sen discussed different aspects of biofuels. Energy sustainability cannot be achieved without improving energy efficiency. Building energy efficiency is considered to be a very important issue for future energy sustainability. Two chapters by Azad and Rakshit; Saikia et al. discussed this important issue including Indian context. In the concluding chapter, possible energy efficiency measures in a milk plant of India have been discussed by Srinivasan et al.

Editors thankfully acknowledge the support of experts in different disciplines as both authors and reviewers. The book is the outcome of one of the collaborations (INCP-2014-10086) under the Indo-Norwegian Cooperation Program between the Jadavpur University, India, and the University of Stavanger, Norway. Both coordinators from India and Norway of this collaboration are two editors of this book. Support from industry is specifically acknowledged. The Bengal Chamber of Commerce and Industry (BCC&I), the oldest industry chamber of India, was very much supportive to this effort of joint activity by academia and industry. Chamber is also represented by its Vice President as one of the editors of this book. Department of Energy Science and Engineering of the Indian Institute of Technology (IIT), Bombay, is one of the pioneering groups of India for higher studies and research of interdisciplinary sustainable energy. A Chair Professor of this department is also another editor of this book.

Kolkata, India
Mumbai, India
Stavanger, Norway
Kolkata, India

Sudipta De
Santanu Bandyopadhyay
Mohsen Assadi
Deb A Mukherjee

The original version of the book was revised: Incorrect Foreword version has been updated with correct version. The erratum to the book is available at https://doi.org/10.1007/978-981-10-7188-1_20

Contents

Sustainability of Energy Systems: Views from Technology Perspectives	1
Subhas K. Sikdar	
Solar Photovoltaic Technology	21
J. N. Roy	
Microgrids	57
N. K. Kishore, Saroja Kanti Sahoo and A. K. Sinha	
Transition of Power Distribution System Planning from Passive to Active Networks: A State-of-the-Art Review and a New Proposal	87
Shubh Lakshmi and Sanjib Ganguly	
Solar Dish Micro Gas Turbine Technology for Distributed Power Generation	119
Davide Iaria, Jafar Alzaili and Abdalnaser I. Sayma	
Distributed Energy Solution for India: Exploring the Possibilities	133
Kuntal Jana and Sudipta De	
Synthesis of Cogeneration, Trigeneration, and Polygeneration Systems Using Target-Oriented Robust Optimization	155
Charlle L. Sy, Kathleen B. Aviso, Aristotle T. Ubando and Raymond R. Tan	
Detoxification of Crude Oil	173
Aysar T. Jarullah, Iqbal M. Mujtaba and Alastair S. Wood	
The Sustainable Option of Power from Fossil Fuels with Carbon Capture and Storage: An Overview of State-of-the-Art Technology	195
Maria Elena Diego, Karen N. Finney and Mohamed Pourkashanian	

CO₂ Capture and Utilization (CCU) in Coal-Fired Power Plants: Prospect of In Situ Algal Cultivation	231
Ranjana Chowdhury, Sumona Das and Shiladitya Ghosh	
Sustainability of Coal as a Source of Energy in India	255
Partha S. Bhattacharyya	
Gas Hydrates as a Potential Energy Resource for Energy Sustainability	265
Vishnu Chandrasekharan Nair, Pawan Gupta and Jitendra S. Sangwai	
Current Advances in Bio-Oil Upgrading: A Brief Discussion	289
Anand Mohan Verma and Nanda Kishore	
A Succinct Review on Upgrading of Lignin-Derived Bio-oil Model Components	315
Anand Mohan Verma and Nanda Kishore	
Sustainability of Microalgal Biorefinery: Scope, Challenges, and Opportunities	335
Geetanjali Yadav and Ramkrishna Sen	
Indian Agro-wastes for 2G-Biorefineries: Strategic Decision on Conversion Processes	353
Ranjana Chowdhury, Shiladitya Ghosh, Biswajit Debnath and Dinabandhu Manna	
Energy Conservation and Sustainability Due to Passive Daylight System of Light Pipe in Indian Buildings	375
Abdus Salam Azad and Dibakar Rakshit	
Thermal Performance Evaluation of Building Roofs Embedded PCM for Multi-climatic Zones	401
Pranaynil Saikia, Abdus Salam Azad and Dibakar Rakshit	
Enhancement of Energy Efficiency at an Indian Milk Processing Plant Using Exergy Analysis	425
Babji Srinivasan, Jaideep Pal and Rajagopalan Srinivasan	
Erratum to: Sustainable Energy Technology and Policies	E1
Sudipta De, Santanu Bandyopadhyay, Mohsen Assadi and Deb A Mukherjee	

About the Editors

Sudipta De is currently a Professor at the Mechanical Engineering Department, Jadavpur University, Kolkata. He received his Ph.D. from IIT, Kharagpur, and was a guest researcher at the Department of Energy Sciences, Lund University, Sweden. He was an INSA (New Delhi) visiting scientist to Germany, selected faculty of Erasmus Mundus External Cooperation Window of the EU in sustainable energy. He delivered invited lectures in many programs/institutes including Indian National Clean Coal Technology Mission meeting, TU of Berlin and Munich, KTH, Stockholm, University of Stavanger, Norway, etc. He received his research funding from UGC, DST of India, EU, German Research Foundation, Swedish Research Council, Research Council, Norway, etc. Presently, he is the Coordinator/Coinvestigator of two EU projects. He is also closely associated with industry chambers.

Santanu Bandyopadhyay is currently an Institute Chair Professor, Department of Energy Science and Engineering, at the Indian Institute of Technology Bombay (IIT Bombay). He obtained his B.Tech. (Hons.) in Energy Engineering from IIT Kharagpur in 1992 and M.Tech. and Ph.D. in Energy Systems Engineering from IIT Bombay in 1995 and 1999, respectively. His research interest includes process integration, pinch analysis, industrial energy conservation, modeling and simulation of energy systems, design and optimization of renewable energy systems, etc. Since 1994, he has been associated with and contributed toward various developmental, industrial, and research activities involving different structured approaches to process design, energy integration, and conservation as well as renewable energy systems design. Prior to joining IIT Bombay, he worked for M/s Engineers India Limited, New Delhi. He is currently one of the Editor in Chiefs for Process Integration and Optimization for Sustainability (Springer Nature) as well as Associate Editor for Clean Technologies and Environmental Policy (Springer Nature), International Journal of Energy Technology and Policy (Inderscience), and INAE Letters (Springer Nature).

Mohsen Assadi is a Professor at Faculty of Science and Technology, University of Stavanger (UiS), Norway, Head of energy efficiency group for clean energy network at UiS, Head of monitoring and maintenance hub at CIAM, UiS, Visiting Professor at Sheffield University and London City university. Developing methods and tools for identification of optimized instrumentation for cost-effective monitoring and control of various types of power plants has been one of the focus areas for the conducted R&D activities during the past years. He has been a project leader for several national- and European-funded projects, dealing with performance monitoring and concept evaluation for conventional combined cycle plants using industrial gas turbines from various OEMs; a hybrid plant using a combination of biomass-fueled steam cycle and natural gas-fired gas turbine with HRSG delivering steam to a common steam turbine; an innovative cycle utilizing the humid air turbine concept, small-scale combined heat and power (CHP) units using mixtures of various gas fuels; an integrated gasification combined cycle plant, etc.

Deb A Mukherjee is an entrepreneur, professionally qualified as a lawyer, with over 33 years of work experience in diverse business domains, engineering systems, information technology solutions, and later in energy services for the last 15 years. He was the Executive Chairman of Eaga Energy India Pvt Ltd (subsidiary of Eaga plc UK FTSE 250 company) until 2012. Currently, he is an Investor and Country Director for Big Solar Ltd UK and also Managing Director of Cenergist Ltd UK, India Operations, an energy services business with operations in the UK, Spain, Germany, Italy, and now in India. He is also incubating an IT start-up Teknowlegion Ltd in Kolkata, India. He has served on various trade committees in India and the UK and spoken at several international seminars on sustainability issues, energy efficiency, renewables, water management, and business strategies. Currently, he serves as the Vice President and Chairperson of the Energy and Environment Committee and is also the Member of the Managing Committee/Board of the Bengal Chamber of Commerce & Industry, Kolkata, India.

Sustainability of Energy Systems: Views from Technology Perspectives

Subhas K. Sikdar

To take away today from England her steam engines would be to take away at the same time her coal and iron. It would be to dry up all her sources of wealth, to ruin all on which her prosperity depends, in short, to annihilate that colossal power.

—Sadi Carnot

Abstract Green, clean, sustainable—these three words are frequently used casually to connote some desirable attributes. When claimed for technical systems, however, the monikers of green, clean, and sustainable must be scientifically justified. Unfortunately, this objective of introducing scientific rigor into assessing the greenness or sustainability of technical systems has not been universally accepted or practiced. For energy systems, currently the debate is conspicuously driven by the phenomenon of global warming, which more recently is described as climate change. The nonfossil modes of energy production, delivery and use of solar, wind, hydro, nuclear, or biomass, are uncritically assumed to be green and sustainable in both scientific and popular literature. This should not be the case. This chapter will look at the issues that must be considered while designing energy systems that can be described as sustainable, clean, or green.

Keywords Energy sustainability · Energy systems · Sustainable energy Sustainability indicators · Sustainability assessment

1 Introduction

Recently a multinational corporation announced a global research collaboration on sustainable chemistries.¹ As in this example, we have in general cavalierly used “sustainable” as an adjective for all sorts of supposedly desirable objectives without making clear what sustainability means in the specific context. Sustainable energy is one such objective that national, regional authorities, as well as scientists and

¹Akzo Nobel, C&E News Jan 23, 2017, p. 10.

S. K. Sikdar (✉)

National Risk Management Research Laboratory, US EPA, Cincinnati, OH 45237, USA
e-mail: subhas.sikdar@gmail.com

engineers have been promoting at least for two decades. There are even some published textbooks on this topic [1–3]. The terms “energy sustainability” and “sustainable energy” appear in many texts to mean the same thing, but clearly they reveal different objectives. In energy sustainability, the focus is on a community of users of energy, such as a nation, a region, or a corporation. On the other hand, sustainable energy refers to a particular energy production technology or a combination of more than one technology.

The dictionary definition of the term “sustainable,” as used in colloquial or communication context, connotes the continuation of the current condition or a desired past or future condition. It is important to recognize that sustainability is not a scientific word, though it is extensively used in scientific and technical contexts. The sustainable development movement that produced the document, *Our Common Future* [4], came from sociopolitical arena. The word quickly became a universally common currency for all manners of discourse. This book will examine, in the various chapters, both the sustainable energy and energy sustainability objectives in various specific contexts.

A useful way to consider sustainability of energy is to think of it as a “system.” Attempts at achieving sustainability of an identified system amount to reducing the adverse environmental, societal, and economic impacts associated with the system—environmental, societal, and economic considerations being the three domains of sustainability. These three domains are, however, not independent of each other. They are interrelated: A change in one may affect another in positive or negative ways. Thus, it needs to be pointed out at the outset that it will not be in general possible to minimize each impact on a system. In other words, we would be looking for an optimized solution that offers the best conditions in the three domains for all possible solution alternatives. Energy sustainability refers to a system where the energy and power producing subsystems of a community together attain the most desirable combination of the three impacts mentioned above. Similarly, sustainable energy refers to an energy or power producing system, such as solar, wind, or bio-fuels, which has achieved a desirable optimum of its impacts on the three domains.

This chapter is mainly concerned with the broader issues of energy sustainability of the significant sources alternative to fossil energy. Detailed examinations and opportunities of specific energy systems, as they are relevant globally or regionally, would be dealt with in other chapters. Of the three impact domains, environmental impact is the most important, and arguably the main inspiration of the sustainable development movement. Raw energy is always derived from natural sources by mining operations in the cases of coal, oil, natural gas, and uranium. Similarly, wind power is derived by converting the kinetic energy of directional wind, solar thermal, or photovoltaic energy by exploiting solar photons, geothermal by capturing the heat of the earth’s interior, most notably from radioactive decays, and biofuels by converting carbohydrates of agricultural and forestry sources. Except for coal, petroleum, natural gas, and nuclear which are called “nonrenewable,” because they are obviously finite, all other forms of energy are referred to as “renewable” and generally recognized as infinite. Of the nonrenewables, coal, natural gas, and petroleum are also referred to as fossil, because they are derived

from geological carbon. The signal importance of energy sustainability is derived from the recognition that the fossil energy of coal, petroleum, and natural gas is dirty, coal being particularly so. These fossil energies are legacy products of biogenic sources transformed by geologic forces within the earth's crust over millions of years. The impurities of sulfur, nitrogen, mercury, arsenic, and other heavy metals in them upon combustion create noxious emissions that are harmful to humans as well as to ecological health. Added to these concerns are the emissions of carbon dioxide, the main combustion product of fossil fuel burning. Carbon dioxide is a recognized greenhouse gas and is considered by many as causing global warming and climate change. There are no known health concerns from carbon dioxide at 400 ppm in the atmosphere and is known as a trace gas in it. The renewable energies are thought to be the panacea for getting rid of fossil fuels and are considered by many as suitable for widespread development. Though these alternatives are supposedly carbon neutral, there has been little demonstration of a generalized case for sustainability of any of these alternative energy sources. Additionally, the concept of sustainability also applies to fossil fuels. All these energy carriers are much refined before use, and one is referred to any text on combustion and on petroleum refining for details on impurity removals from them.

Sustainability considerations of energy systems, regardless of whether they are based on fossil or renewable energies, require us to consider several important factors, both for energy sustainability and sustainable energy systems:

1. Sufficiency of the type of energy for a system's requirement in a particular context. In other words, is their enough for the objective of satisfying a need?
2. Intermittency of some of the sources (such as solar and wind).
3. Impacts of the source exploitation on the environment, society, and the economy over the "source to use" spectrum, otherwise known as life cycle impacts.
4. It needs to be remembered that alternative energy needs to be economic to be used on a long-term basis. It is always possible to use government force to mandate a form of energy that is not economic but deemed to be in the public interest, but such policies will distort the market forces that may produce unwanted, unintended consequences later on.

One other important aspect of the concept of sustainability that is not emphasized enough: Nothing can be absolutely sustainable in a dynamic world. Sustainability is always comparative. Thus, the goal of sustainability claims and determination must be to find solutions that are comparatively more sustainable. Human curiosity always finds improvement on existing solutions; an acceptable solution today will be invariably superseded tomorrow by superior solutions.

2 Basic Facts of Energy and Its Sustainability

Harnessing energy for improving human living and work conditions has been the mainstay of material progress through the centuries. Discovery of various energy sources has stimulated the steady progress from the days of wood to hydro, coal,

oil, natural gas, and nuclear. However, the form in which we use energy requires much processing so that the refined energy has a grade or quality that is directly useful. For instance, raw coal and petroleum are processed in huge processing plants at much cost to produce coke, gasoline, diesel, and various fractionation products of direct utility. Though solar photon is free, solar energy is not. Much of the environmental impacts of these energy sources reveal themselves in the processing steps even after elaborate safeguards are taken to contain and neutralize the various offending chemicals, the discharge of which would be of great concerns these days. The most convenient form in which we prefer energy is electricity, whose widespread use in the power sector is obvious, but it is also seen as a growing potential for transportation and heating. Already there is much interest in powering automobiles with electricity to eliminate local pollution from emissions of SO_x , NO_x , ozone, volatile organic compounds (VOCs), and particulates, especially $\text{PM}_{2.5}$, from internal combustion engines that use gasoline or diesel.

Electricity, however, must be used as it is produced, as current technologies do not allow large-scale storage. The fluctuating demands of electricity must be managed by producing and supplying organizations, requiring capacity modulation at the producing plants, and creating intricate pricing structures that create incentives and disincentives for consumption at certain times of day and seasons. A critical need is effective technologies for storing electricity for tackling the fluctuating demands. The storage batteries are usually named after the electrodes used. The familiar lead–acid batteries used in automobiles are the oldest. They are effective in small voltage applications but are bulky, unwieldy, and dangerous in large scales. Besides they use the toxic metal lead, which is not favored for environmental applications. Other batteries are based on nickel alone or in combinations with cadmium. Lithium in various forms have been developed, the most recent being the Li-ion batteries. In small scales, battery storage has been a continued success for a long time for specific uses, but despite much research on various battery technologies, there is still no clear winner for mass storage for large-scale supplies. The emerging interests in electric cars have created an interest in battery research, and this is the area that is likely to see success in the coming years, provided rate of recharge is speedy for convenience.

Processing to upgrade the form of energy also is necessarily associated with waste of energy [5]. The second law of thermodynamics provides a limit to each energy conversion we encounter. Fossil power through combustion of coal and natural gas is subject to Carnot efficiency, currently at 40%, which can be increased with temperature, but material of construction puts another limit on what can be used. Thus to have the tremendous utility benefit of electricity, we must accept 60% waste of the original energy content. Electricity can be directly used for lighting and heating, but it is also the basis of further upgrading to coherent power such as semiconductor lasers of extremely high power density for usage where common electricity (e.g., 110 V, 60 Hz) is of no use.² Thus, more energy must be wasted in

²For instance, power density of solid-state lasers is 20 MW/cm^2 , whereas utility's high-voltage line carries 100 MW/cm^2 .

upgrading the form of energy. This upgrading can be looked upon as creating more and more order, and the second law still limits us as this order creation is accompanied by entropy generation, which is a waste. The same principle applies to electricity from solar photons, nuclear reactions, wind, hydro, and any other conventional or alternative energy sources.

Some energy wastes inherent to particular use technologies, however, can be improved significantly. A prominent example is incandescent lighting, which gobbles up 22% of US electricity,³ yet is only 2% efficient, wasting the rest in the form of useless heat. In comparison, fluorescent lamps can produce more lumens per watt, and light-emitting diodes (LEDs) lamps would be a major improvement. Industry, especially chemical industry, has been using process heat integration techniques for sometime to improve energy efficiency of plants. These energies are usually thermal energy required at various points for heating streams using liquid fuels or natural gas. The motivation of these actions is cost reduction and profitability, which is why they are actively embraced in industry.

2.1 Nonrenewable Energy

Ever since the first commercial extraction of petroleum by Drake in 1859, there have been doubts expressed as to how long the limited supply of this new form of energy would last. Nevertheless, petroleum production kept on increasing and it replaced coal as the primary source of fossil energy. Hubbert⁴ was the first to formulate a peak oil theory which predicted that U.S. petroleum production will reach a peak in the 1980s and then decline eventually to be exhausted. This prediction, however, did not materialize as more and more sources began to be discovered, first on land and then offshore. This fashionable theory remained diehard and began to be revised, always failing in its prediction. Now with the advent of hydraulic fracturing and horizontal drilling, it appears that the potential for oil and gas exploration will last a very long time. Two important issues were missed by the protagonists of these failed predictions. First, although fossil oil and gas must be limited by dint of a finite planet, use rate of the potential reserves has been low. Second, petroleum availability is always related to price of oil. As the price of oil increased, more hitherto unprofitable wells became profitable, resulting in more availability. The story of shale oil is a result of that line of reasoning. Peak oil, however, has not lost its adherents, as argued recently by Hall [6].

Energy needs of the world are mainly satisfied by supplies of nonrenewable coal, natural gas, oil, and nuclear. About 20% of the primary energy needs is served by renewables, which includes hydroelectricity. Figure 1 shows that three of these fossil sources are very significant, of which natural gas portion has been gradually

³Forbes, October 2005, p. 71.

⁴Cornell University, http://www.geo.cornell.edu/eas/energy/the_challenges/peak_oil.html.

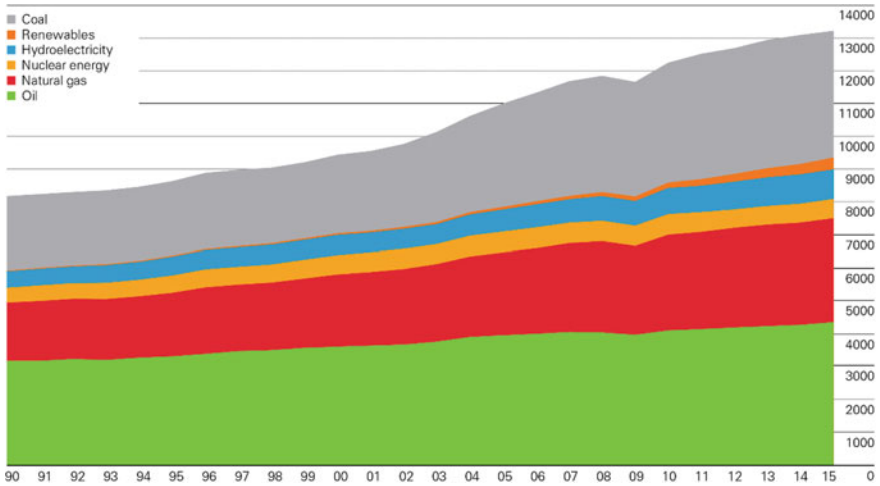


Fig. 1 Evolving use profile of various primary energy systems globally (in million tons of oil equivalent, BP Statistical Review: <https://www.bp.com/content/dam/bp/en/corporate/pdf/energy-economics/statistical-review-2017/bp-statistical-review-of-world-energy-2017-full-report.pdf>)

increasing due to the new phenomenon of hydraulic fracturing. The renewables that are being promoted by government policies worldwide, i.e., wind, solar, and biomass are but a tiny part still, though the growth rate of these is very high. Of these three, solar and wind are looked upon mainly as a means of supplying electricity, and biomass, mainly for transportation (for more details, please see later). Because of the intermittency of solar and wind, they cannot yet be looked upon as base power, until large scale, functional, and effective electricity storage systems are developed and deployed. There are many ideas on electricity storage, but none are in practice at present. Nuclear is an effective solution to the greenhouse gas emission problem. It is largely carbon neutral and is reliable as base power. However, because of Three Mile Island and Chernobyl accidents, public opinion in most countries has turned sour on nuclear. Recent Fukushima incident in Japan, where the nuclear plants were overwhelmed by earthquake and consequent flooding from tidal waves, did not help the cause of nuclear power. Apart from fear of accidental radiation discharge, which occurred in the poorly designed Soviet plant at Chernobyl, the nuclear waste is the other cause of concern. Currently, nuclear option faces more a political and societal barrier than a technical or economic one. In summary, it is certain that nonrenewables, which are mainly carbon-based, will stay with us for a very long time yet.

Figure 2 is a “source-to-outcome” diagram of approximately 100 quadrillion BTU (quad) of aggregate energy sourced in the USA for domestic use. The left side of the diagram shows the various sources, both nonrenewables and renewables. On the right-hand side are the four main use categories: residential, commercial, industrial, and transportation, showing what fraction of the total energy at the source reaches a particular use category. A significant part of these use categories is served by electricity. In the USA virtually no oil is used for power generation, and

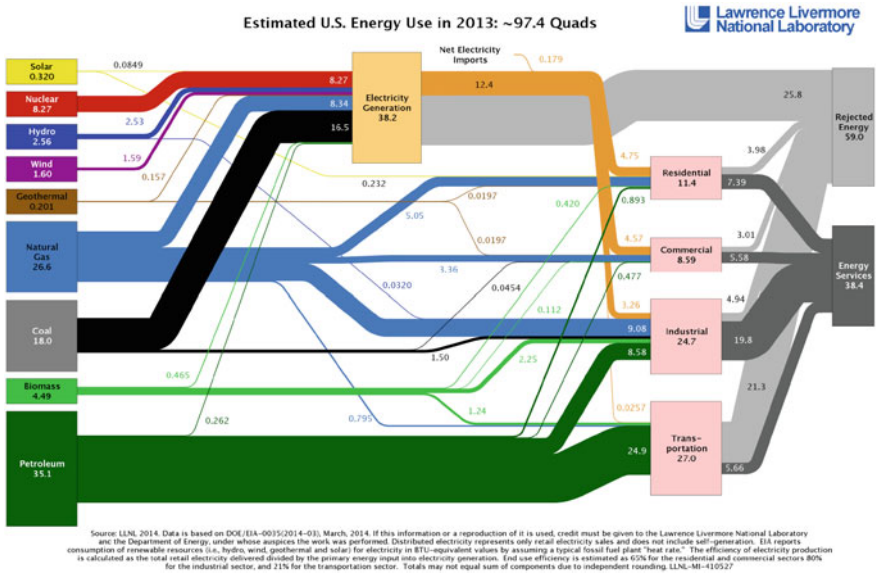


Fig. 2 Categories of use of various energy sources in the USA. *Source* Lawrence Livermore National Laboratory, http://flowcharts.llnl.gov/content/energy/energy_archive/energy_flow_3013/2013USEnergy.png

most all transportation needs are met by fossil fuels. At the far right end of the figure, we see that in order to get 38.4 quads of useful energy, i.e., ready to be used, we reject 60% of the total energy used at the source.

2.2 Renewable Energies

It would be clear from both Figs. 1 and 2 that the renewable portion of the total global or American energy budget is small, and it includes hydropower and biomass as well. It is important to focus on energy sustainability of communities in terms of the renewable sources available to those communities. First, hydropower is an established technology. It is also location-specific. Hydropower is seen as a growing source of renewable electricity in very specific locations, for instance, Bhutan. Adverse public reaction to large dams has of late created difficulty in implementing large projects. The three renewables that are really growing are solar, wind, and biomass. In the recent past, much government and private sector research funding has been made available, with consequent innovations in all three areas. As stated before, of these three candidates, solar and wind are mainly for power, i.e., electricity generation, and biomass is mainly for generating biofuels, such as alcohols through fermentation of sugar or starch derived from energy crops, or for

generating biodiesel from oil crops such as rape seed, soybeans, or from trees such as palm. Extracted oil from these latter sources is trans-esterified to yield monoesters of fatty acids, which are attractive as substitutes of fossil diesel. A third process that can produce a product that is similar to petroleum hydrocarbons depends on pyrolysis of cellulosic raw materials. Bio-oil, as the pyrolysis product is called, is still in the developmental stage. Bioethanol and biodiesel are already reality in large-scale production and are available in many countries of North and South America, Europe, and South-East Asia. Biomass development as a source of liquid fuel depends on land use limitation, and therefore there are other considerations emanating from land use that can and will limit the proliferation of biomass-based energy. These considerations are (1) food crops that are being used these days for bioethanol or biodiesel would not be a growth area for fuel, (2) energy crops exert land use impacts on the environment, such as impacts on biodiversity, species disappearance, ground water pollution, and an adverse economic impact on food prices, (3) biomass energy can only be looked upon as a component of a multi-source solution for displacing fossil fuels, but not as a unique solution. Globally and individually in most countries, the land area needed is woefully inadequate to supply all demands of transportation fuels.

There is a small contribution of biomass to combined heat and power (CHP). Where the biomass is essentially agricultural waste from farms that comprises vegetable wastes, agricultural refuse, and animal farm waste, this can be a desirable contribution to the economy of small rural communities. This approach offsets the fossil fuel that would have been used and in addition helps in eliminating or greatly reducing farm wastes.

Solar energy is the one renewable energy that has captured the imagination of people because it is plentiful and appears to be cost-free. Solar can be used for heat and power (CHP). The typical and the most visible application of solar power is the photovoltaic solar cells on rooftops in urban and suburban areas. Photovoltaic is the direct conversion of the visible part of the spectrum of solar radiation into electricity. There can of course be solar heating devices for capturing solar radiation and using a working fluid, such as water, to circulate the heat in living areas in a dwelling. Besides these household units for offsetting heating costs from fossil fuels, there are two large-scale community interests that are extremely important in the context of renewables as posing a challenge to fossil-based units. First is the solar thermal power plants, and the second, large photovoltaic power stations. Details about these can be found in standard texts such as Tester et al. [3]. Only the outlines of the sustainability issues will be discussed here in brief.

Solar thermal approach involves directing concentrated solar light onto a high temperature working fluid which is used to raise superheated steam to drive the Rankine cycle to produce electricity. The receiving fluid can also be water itself. Ground level mirrors direct light onto a receiver tower containing the working fluid. Over the last forty years or so, many relatively large-scale demonstration units have been built in the USA and elsewhere. In California, Solar One and Solar Two, funded by the US Government in the 1980s, demonstrated the utility of the solar

thermal approach.⁵ But the cost of electricity produced was not competitive with either fossil or nuclear. Projects were stopped when the government funding went away. Another approach of solar thermal used parabolic concentrators to directly heat the working fluid positioned on the focal plane of the mirrors. The fate of this technology is similar to the tower-heliostat system. Currently, there are no large-scale solar thermal power plants in operation anywhere in the world, despite their demonstrated feasibility at 100 MW level or higher. These technologies are desirable but not yet economic.

Photovoltaic solar cells have seen rapid and continuous improvements over the years. With innovations on solar cell designs, which accelerated with the impact of nanotechnology, both the capture efficiency and the cost of cell manufacture have decreased significantly. Small-scale power units capable of supplying electricity in the kW range are now available. Large-scale applications for serving a community for its need for electricity have really not been tried yet because a fossil-based base power would still be needed. Solar electricity at any power level, when compared to fossil-based electricity, is not cost-effective. We mentioned before that storage of electricity at a large scale is the greatest impediment to large-scale commercialization of solar or wind.

Wind is the only other renewable that needs to be mentioned here. In many developed countries wind mills are frequently seen in the country side, and offshore as well. Turbines for practical units are large and heavy and require sturdy structure to support the turbines from extreme weather events. One of these units can produce, when wind is blowing, at a rate of 2–4 MW. Typically, a large number of these turbines would have to be arranged in a large real estate. Considered in isolation, wind energy can be close to fossil power in cost. But a realistic life-cycle cost of wind energy has not been attempted. Storage of electricity is a dominant issue for wind power development just as it is for solar power.

3 Significance of Energy Use

Energy consumption is the life blood of material development of any society. Throughout history as we developed more implements to enable us to make useful things that improved comfort and living standards, we continued to use more energy per capita. Newer and newer energy sources have helped spur industrial and economic development as more energy was needed. There is a definite correlation between the size of an economy, measured in gross domestic product and its energy consumption. This correlation is valid for overall energy consumption, as it is for electricity use. The latter, as an illustration, is shown in Fig. 3. The relatively less advanced economies are currently attempting a rush to development with consequent increasing energy intensity of their economies. The brightest example of this development is China,

⁵https://en.wikipedia.org/wiki/The_Solar_Project.

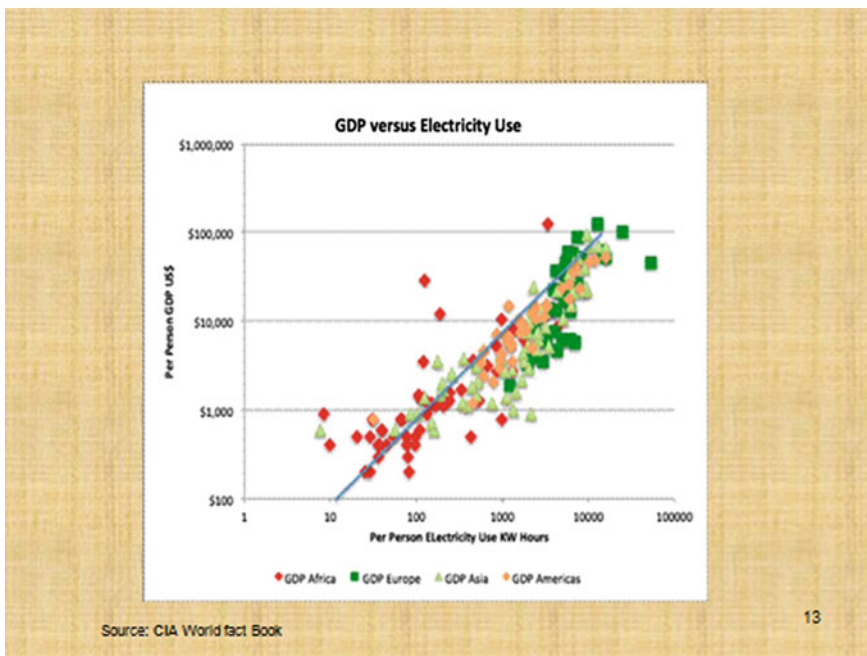


Fig. 3 Correlations between material progress of countries and per capita energy use, specifically electricity

which has made phenomenal advances in gross domestic product and has established an impressive built environment during the last three decades. Since the energy sources for these developments are mostly fossil-based, they end up in carbon dioxide emission. Carbon dioxide thus can also be looked upon as a rough surrogate indicator of material progress, as ironic as it may appear. The rapid development in China helped her to get ahead of the USA in carbon dioxide emission in the recent past owing to China’s decades-long 10% year over year GDP growth.

Energy sustainability of nations matters because energy, as the primary driver of material development, is also the main source of greenhouse gas emissions. All other kinds of pollutions having impacts on human health and the ecology also accrue from the use of fossil fuels. The question at this juncture is: are we, as humanity, at a cross-road where we must change the energy source from fossil-based to fossil-neutral form? The concerns arising from global warming or climate change have triggered roughly two choices ahead: first, if we have to use fossil energy, the capture and underground sequestration of post-combustion carbon dioxide for eternal burial, and second, abandon fossil fuel, albeit gradually in favor of solar, wind, and biomass. As we discussed before, this second option does not look practical, now and in the near future. Ultimately though, if solar energy at the point of use can be made cheap, reliable, and plentiful, that would be the future we

can look forward to. This is the overall global-scale picture. But smaller scale perspectives are equally important.

On a smaller scale of systems of engineering interest, however, there are plenty of opportunities to contribute to energy sustainability by way of better energy efficiency of fossil fuels, and also by way of alternatives to fossil energy in specific applications. We will move to that discussion now.

4 Energy Sustainability of Systems

The system in this discussion is a community, which uses various forms of energy carriers from fire wood to coal, oil, natural gas, hydro, geothermal, solar, wind, and nuclear. The query here is:

What combinations and proportions of these various energy carriers would be needed to achieve energy sustainability for a community?

This depends on the societal needs and wants. A primarily agrarian society would have its needs and wants different from a dominantly urban community. An important factor is having access to energy availability, either within the borders of the community or the ability to acquire such energy carriers from others through free trade. In either case, this is energy security, which is intimately tied to energy sustainability. For instance, hydropower is regional and may not be available to parties distant from the hydroelectric plant or they may not be able to establish a contract for sustained supply of electricity at the time the electricity needs are expressed. Petroleum, however, is a portable commodity and can be purchased at the world market from various national and private sector vendors, subject to disruptions because of embargo, war, or accidents. The other side of the ledger contains the environmental impacts of the use of these energy carriers. We can consider various environmental impacts of interest. As one example of these environmental impacts, we can take a look at water requirements of various energy production systems. Even having ready access to fresh water will have restrictive influence on the production choices for a community. Recently compiled water use data⁶ are quite revealing in assisting planners of sustainability communities. This is presented in Fig. 4.

A second example of environmental impact is life cycle-based fossil energy use, which can be expressed in two ways. The first is the net energy ratio, defined as the total produced useful energy from a source for a unit of fossil energy used to produce the energy carrier in question. The larger this ratio, more favorable is the renewable energy because smaller amount of fossil energy is used. For wind, for example, Fig. 5 shows a range of 30–60, which implies that 30–60 times wind energy is generated for a unit fossil energy used. Much of the fossil energy used in wind power is hidden from view because they are used to make the materials used

⁶Science, 23 October 2009, vol 326, 0516, NGCC represents gas plant.

Water Requirements for Energy Production
(Science, 23 October 2009, vol 326, 0516)

Energy operation	Water requirement (l/Mwh)
• Petroleum extraction	10-40
• Oil refining	80-150
• Oil shale surface retort	170-681
• NGCC closed loop cooling	230-30,300
• Coal gasification combined cycle	~ 900
• Nuclear, closed loop cooling	~ 950
• Geothermal, closed loop cooling	1900 – 4200
• Enhanced oil recovery	~7600
• NGCC, open loop cooling	28,400-75,700
• Nuclear, open loop	94,600 – 227,100
• Corn ethanol irrigation	2,270,000 - 8,670,000
• Soybean biodiesel irrigation	13,900,000 – 27,900,000

Fig. 4 Water requirements for energy production

to make the wind mill and its various parts. At the other end of the scale, the smallest number is coal-fired power, which from environmental perspective is the worst, and hence is used to show the superiority of the renewable energy forms. For coal-fired power plants, this number is 0.3, as we know we can generally achieve 30% efficiency, and the rest is wasted. The second expression is the carbon intensity, defined as the g CO₂ equivalent per kWh of produced energy. Again, for a coal-fired power plant, since carbon is the main input, the carbon intensity is very high, as shown in Fig. 5. The four renewable energies shown in Fig. 5 have net carbon ratio higher than 1 because little fossil-based energy is expected to be used when a renewable source is used as the feed. In general, higher this number, more fossil-neutral is the alternate form of energy. Biomass and photovoltaic are inferior to wind and hydro, per Fig. 5. Whatever little fossil-based energy is used in generating useful renewable energy, it will end up as carbon dioxide. Lower carbon intensity is obviously desirable, as compared to fossil-based intensity.

Figures 6 and 7 show other sustainability considerations for comparing an energy system with another energy system. Continuing to focus on production systems, we can consider land use of the various energy options. This is shown in Fig. 6. The data presented here are taken from Hodgson [7]. Though not a surprise, the very significant land use requirement of wind, solar, and hydro would limit the potential of these sources, especially the first two, for socioeconomic reasons.

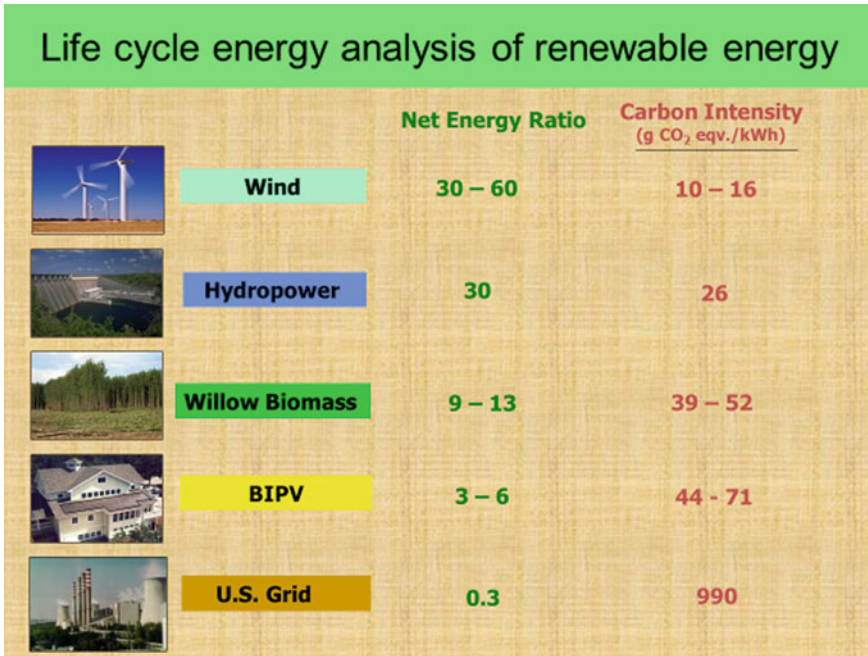


Fig. 5 Energy efficiencies of alternate energy sources (courtesy of Greg Keolian, University of Michigan)

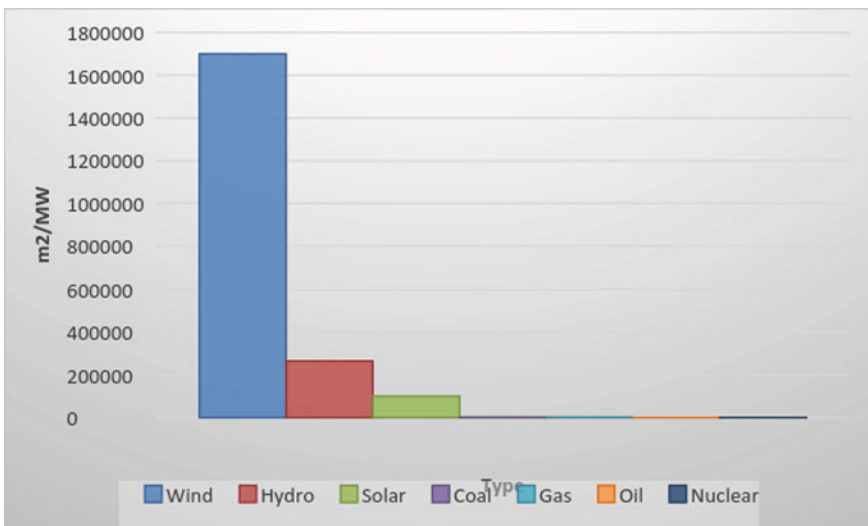


Fig. 6 Land use of power production systems

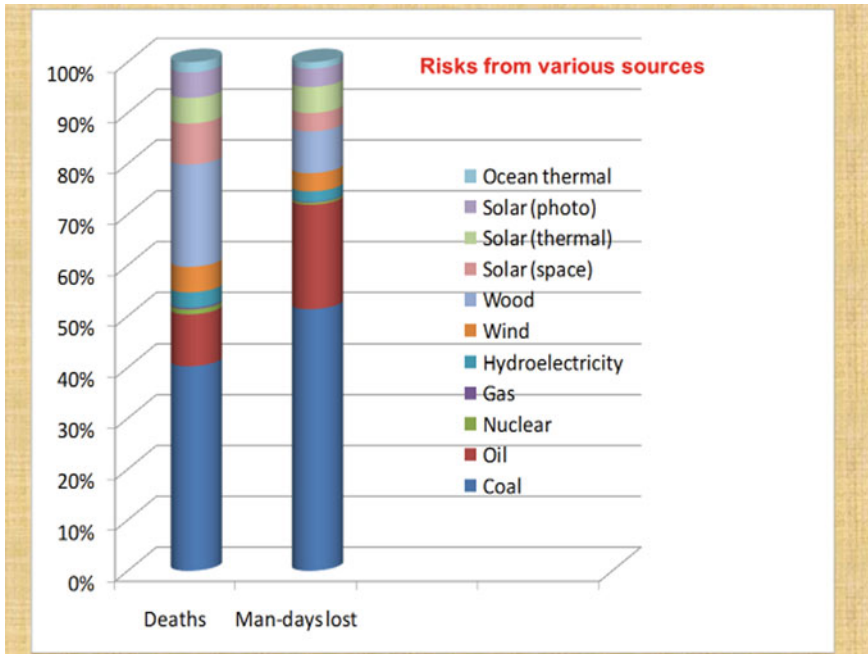


Fig. 7 Comparative safety records of various power systems

Figure 7 presents comparative data, also taken from Hodgson [7] for safety of these power producing installations. Fossil power in general has a bad track record of safety, including disease potential from work environment. But the ecological risks of solar and wind are also considerable, though not usually discussed. Comprehensive life cycle-based sustainability impacts have not been conducted for solar and wind. When the impacts of mining and other conversion steps ahead of the production installations are taken into account, these favored technology systems will look significantly worse, pointing to the need of rapid and steep improvements before these can be accepted as technically sustainable.

Since the race to replacing fossil fuels in the energy sector hinges on the efficacy and economic viability of solar and wind for power, and biomass for transportation, it would be interesting to look qualitatively at how these alternative forms of energy fare with respect to fossil-based energy for power or transportation. For each option, the positives are shown in green and the negatives in red. Figures 8, 9, and 10 present the relevant comparison for sustainability.



Fig. 8 Sustainability considerations for wind and solar power versus fossil power

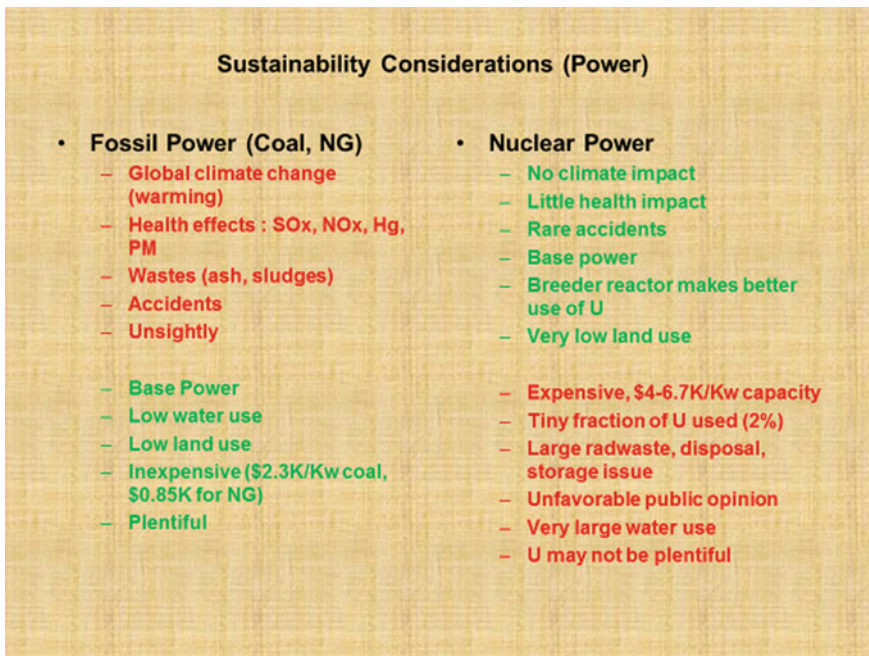


Fig. 9 Sustainability considerations for nuclear vis-a-vis fossil power

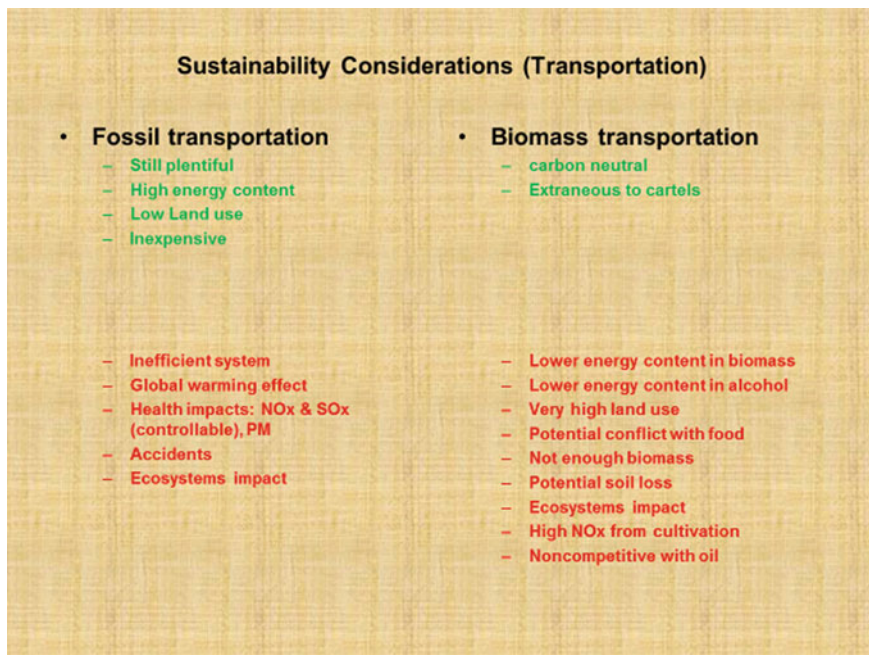


Fig. 10 Sustainability considerations of biomass for transportation vis-a-vis fossil fuels

5 Discussion and Conclusions

The main objective of this chapter has been to point out and discuss the sustainability issues of different energy types and their usages. Since fossil energy sources, such as coal, natural gas, and oil, have come under intense scrutiny both from global warming and sustainability viewpoints, the question of a comparative evaluation of fossil and nonfossil sources naturally arises. This scrutiny has led to the dominant view that fossil energy is not sustainable for human society, human health, and the ecology, and that we should learn to wean ourselves from fossil energy [8, 9]. Proponents of severe restrictions on the use of fossil energy derive their guidance from the Intergovernmental Panel on Climate Change or IPCC [10]. This guidance goes along the following line: We will probably suffer irreparable damage to human life if we incur greater than a 2 °C average global temperature increase, corresponding to about 550 ppm of atmospheric CO₂-eqv, compared to the preindustrial CO₂ concentration of 280 ppm (as of this writing it is 400 pm CO₂). Time is an essential element of sustainability discussion. IPCC has targeted year 2100 as the reference date for all future projections. Taken in this light, energy sustainability is a global-scale discussion and must be solved in global collaboration, as has been the case since the Rio Summit of 1992, the Kyoto Protocol following it, culminating in the recent climate conference in Paris known as COP

21. Energy sustainability is also considered central to all sustainability discussions. In fact, it is frequently used as the flagship metric, in terms of greenhouse gas emissions, for local and technological discussions as well.

Energy issues are also local, and the question of which combination of energy resources would be sustainable for a community is an important question to ask. To answer this question for satisfying its self-interest, the community in question may decide to seek solutions that are at odds with another community either nearby or far away.

But individual energy sources are either (i) nonrenewable such as nuclear or coal, or (ii) renewable such as solar, wind, and biomass. The individual energy source under consideration also emits pollution when the source is exploited for human use. Sustainability considerations of each energy source should include the specific method of exploitation as well. These considerations address sustainable energy at the technology scale, in contrast to community or global scale. In theory, we can make individual energy source as environment-friendly as we like, limited only by affordability considerations. For example, we can make natural gas power plant virtually free of CO₂ emission by capturing and sequestering it, regardless of the cost. In this chapter, an attempt was made to distinguish between energy sustainability of a community and the sustainability of a specific energy production technology. This distinction results in the different way we must approach the question of sustainability of a specific case.

Thus far in this chapter, we have identified the various necessary sustainability indicators one should use for a particular case. Globally, energy sustainability is driven by aggregate greenhouse emissions of energy systems. The almost total reliance of CO₂ for the assessment of energy sustainability maybe short-sighted if it turns out from life cycle studies that the most championed energy sources of solar and wind are not that promising from sustainability viewpoint for replacing fossil energy. Such a case has already been made by Giampietro and Mayumi for biofuels that are based on food crops [11]. These authors call the fascination of crop-based biofuels a delusion. If the nonfossil alternatives cannot be unequivocally certified as sustainable, the choice before an interested party will then narrow down to which particular alternative energy is superior from a sustainability viewpoint. More specifically, for a community, we need to know which combinations of energy sources and in what proportions provide optimum sustainability outcomes. Finding such optima for a community is still an art, and much scientific and engineering research opportunities exist for the future. These decisions, however, tend to be mainly political, even when scientific information is made available.

The list of necessary indicators for place-based community energy sustainability would consist of explicit community concerns, in addition to technical indicators to represent environmental and economic issues. Such community concerns are frequently aired by various interest groups for hydroelectric or coal-fired power plants. When the specific energy technology is for the narrow benefits of an industry, the community concerns are indirect, rather than up front. Depending on the nature of the energy technology, different sets of indicators will be necessary to reflect sustainability. So far in the energy sustainability debates, we have not encountered in

articulated details the relevant concerns that are associated with the sourced materials for wind and solar, for example. Huge quantities of heavy metals and rare earths as well as high purity silicon would be needed for these two renewable forms of energy, and sourcing these materials must be part of sustainability assessment of solar or wind. Not much work has been done in this area, partly because it has been conveniently assumed that these are sustainable sources, as if by definition. In the end, when the choice of a particular energy technology or a mix of technologies is needed, the least harmful choice would be deemed the most desirable.

The comparative assessment, however, must be quantitative. To date, not much work is in the literature on quantitative assessment of sustainability. Another deficiency is the relative lack of adequate focus on choosing the necessary and sufficient kinds of indicators for comparative assessment. Energy sustainability of a community would of course depend on very specific needs and wants of that community, and the sustainability indicators that would be needed for a quantitative assessment would have to be chosen to customize the set of indicators for that community.

For specific technology systems, the chosen set of indicators would again be different. Figures 4, 5, 6, 7, 8, 9, and 10 were constructed to highlight these indicators that differentiate one form of energy from another.

Quantitative expression of the sustainability of specific energy systems was proposed for communities by Tester et al. [3]:

$$S_e = [(P) \times (GDP/P) \times (E/GDP)] \sum_i w_i(t) [A_i(E)] \quad (1)$$

where

- S_e energy sustainability
- $A_i(E)$ i th impact related to energy
- $w_i(t)$ weighting factor for the i th impact
- n number of impacts
- P population
- E energy

As can be seen here, the specific impact indicators, A_i , still need to be identified and measured to provide an estimate of the aggregate S_e . Aggregating overall assessment in this fashion suffers from the difficulty of executing the summation when the indicators have different units of measurement.

Since comparison of energy technology scenarios is of interest to us, the various statistical distances proposed by Sikdar [12] and Sikdar et al. [13] are useful. The following expression uses the Euclidean distance to compare chosen scenarios. Here a reference case is synthesized from existing data to represent the most favorable values of the chosen indicators x_r . For each scenario i , the Euclidean distance is calculated using indicator data j . The least value of $D_{e,i}$ would then be for the scenario that is closest to the reference or ideal scenario. This expression is valid for any number of scenarios.

$$D_{e,i} = \sqrt{\sum_{j=1}^n \left[c_j \frac{(x_{ij} - x_{r,j})}{(x_{\max,j} - x_{r,j})} \right]^2} \quad (2)$$

Mukherjee et al. [14] have demonstrated the utility of this technique for a number of cases. A complete set of the various statistical distances is discussed quantitatively in Sikdar et al. [15].

Decisions on relative energy sustainability of a community or a specific energy technology can be made using Eq. 2 provided indicator data are available. Such decisions are retrospective and applied only to systems that have already been designed and built. Designing a more sustainable system a priori is very useful, but we do not yet have such prospective design techniques. Some multivariate simulation techniques do exist, but none is as yet capable of handling more than one, two, or three indicators (variables) at a time. Design of sustainable systems prospectively is a challenge for the future.

References

1. Dunlap R (2015) Sustainable energy. Cengage Learning, Stamford
2. Kreith F (2014) Principle of sustainable energy systems, 2nd edn. CRC Press, Boca Raton
3. Tester JW, Drake EM, Driscoll MJ, Golay MW, Peters WA (2005) Sustainable Energy: choosing among options. MIT Press, Cambridge
4. Bruntland G (1987) Our common future. Oxford University Press, Oxford
5. Huber P, Mills M (2005) The bottomless well. Basic Books, New York
6. Hall CA, Day JW (2009) Revisiting the limits to growth after peak oil. *Am Sci* 97:230–237
7. Hodgson PE (2010) Energy, the environmental, and climate change. Imperial College Press, London
8. Helm D (2012) The carbon crunch. Yale University Press, New Haven
9. Moriarty P, Honnery D (2011) Rise of fall of the carbon civilisation. Springer, London
10. Darwall R (2014) The age of global warming; a history. Interlink Publishing Group Inc., Northampton
11. Giampietro M, Mayumi K (2009) The biofuel delusion: the fallacy of large-scale agro-biofuel production. Earthscan, Washington, D.C.
12. Sikdar SK (2009) On aggregating multiple indicators into a single metric for sustainability. *Clean Technol Environ Policy* 11(2):157–161
13. Sikdar SK, Sengupta D, Harten P (2012) More on aggregating multiple indicators into a single index for sustainability analyses. *Clean Technol Environ Policy* 14(5):765–773
14. Mukherjee R, Sengupta D, Sikdar SK (2013) Parsimonious use of indicators for evaluating sustainability systems with multivariate statistical analysis. *Clean Technol Environ Policy* 15(4):699–706
15. Sikdar SK, Sengupta D, Mukherjee R (2016) Measuring progress towards sustainability: a treatise for engineers. Springer, Switzerland

Solar Photovoltaic Technology

J. N. Roy

Abstract There is all around focus on the development of renewable energy due to energy security, climate change and energy access. Solar photovoltaic deals with conversion of sunlight into electricity. Understanding the available energy resources at Earth's surface that can be used for this conversion is important. The single- and multi-crystalline silicon solar cells dominate the present PV market and occupy >85% of it. Advancements are continuously being made and efficiency of the most widely used cells using c-Si cells now touching up to 20%. Higher efficiency cells use III–V compound semiconductors. Commercial efficiency of more than 30% is now routinely achieved using high-efficiency multi-junction (MJ) III–V cells. Due to cost consideration, these cells are primarily being used in space. Concentrated Photovoltaic (CPV) using high-efficiency MJ cells are used in terrestrial application. Thin-film solar cell is relatively new technology and now occupies about 10% of PV market. The present conversion efficiencies of a-Si thin film solar cells are 8–10% (stabilized) and that of micromorph 9–11% (stabilized) at the production level. Amongst the compound semiconductor, thin-film solar cells CdTe are being produced on mass scale. The conversion efficiency is about 10%. For CIGS the production technology is not yet fully matured. There are several new types of solar cell technologies attracting attention. Dye-sensitized solar cell (DSSC) mimics photosynthesis process. The efficiency achieved is 15–16% in the laboratory scale. However, stability is a problem which is standing in the way of its commercial production. Organic and polymer-based solar cells have not been able to make much progress in terms of efficiency and stability. The other important R&D activities which are going to enhance the conversion efficiencies of solar cells are based on better light management so that current from the cell goes up. For this nanotechnology involving nanostructures are being used.

Keywords Solar cell · Solar resources · Concentrated photovoltaic (CPV) Band gap · Equivalent circuit · Maximum power point (MPP)

J. N. Roy (✉)

Advance Technology Development Centre and Energy Science and Engineering,
IIT-Kharagpur, Kharagpur 721302, India
e-mail: jatinroy2000@gmail.com

1 Introduction

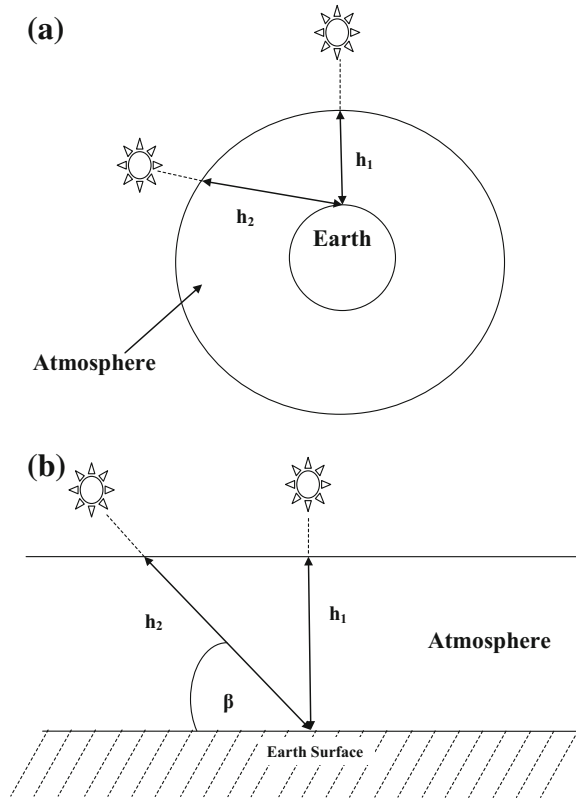
There is all around focus on the development of renewable energy due to energy security, climate change and energy access [1–5]. Solar photovoltaic deals with direct conversion of sunlight into electricity. Governments across the world realized the importance of solar power and many countries have introduced feed-in tariffs, capital subsidies and incentives for productions to promote wider adoption and advancement of solar PV. Renewable initiatives, particularly solar PV, have picked up pace in India. The Jawaharlal Nehru National Solar Mission (JNNSM) is a major initiative of the Government of India to give an impetus to the domestic solar power industry. Several State Governments have announced independent policies in solar PV.

The single- and multi-crystalline silicon solar cells [6] dominate the present PV market and occupy about 90% of it. Thin-film solar cell [7–9] is relatively new technology and now occupies about 10% of PV market. Amongst the compound semiconductor thin-film solar cells, CdTe [10–12] and CIGS [13, 14] have matured and are used in production. There are several new types of solar cell technologies attracting attention. Dye-sensitized solar cell (DSSC) [15] mimics photosynthesis process. Although it is a cost-effective solution, stability is a major issue and in the way of its commercial production. Organic- and polymer-based solar cells have not been able to make much progress in terms of efficiency and stability. Recently, a new type of solar cell, known as perovskite solar cell [16], has been discovered and is generating lot of attention. High-efficiency III–V solar cell exhibits very high efficiency. Due to much higher cost, use of such solar cells is limited to space and terrestrial concentrated photovoltaic (CPV) applications.

2 Solar Resources

Sun is a star and provides most of energy available at Earth. The energy generation in the Sun is due to nuclear fusion, and this energy is transmitted in all directions. The total power emitted can be estimated as about 3.9×10^{26} W by assuming Sun as a black body with a surface temperature of about 5800 K. A small part of this energy is intercepted by Earth as decided by the solid angle subtended from the Sun. This can be estimated as about 1370 W/m^2 outside the Earth's atmosphere. This is known as solar constant and has small variation throughout the year, as distance between the Sun and the Earth varies. Further attenuation happens due to absorption of portion of the energy as it travels through atmosphere. Therefore, the power received at the surface of the Earth, also known as “irradiance”, is lower than the solar constant and varies from place to place depending on the altitude. The irradiance value also changes throughout the day at a particular place as the travel path of the sunrays varies. This is shown in Fig. 1. Sunrays travel different

Fig. 1 **a** During two different times of a particular day, Sunrays travelling different distance through atmosphere to reach at a particular point on Earth surface. **b** Simplified version of (a) assuming flat Earth at the location of interest



distances through the atmosphere at two different times of the day to reach a particular point of the Earth as shown in Fig. 1a. A simplified version is shown in Fig. 1b assuming the Earth is flat at the location of interest. It can be seen that h_1 is the minimum possible distance. This happens when the Sun is directly overhead, which is also known as Zenith position. At any other location of the Sun, the distance travelled by the Sunrays through the atmosphere is always larger.

An important term, Air Mass (AM), is defined to quantify this. Sometime this is also called atmospheric mass (AM). AM0 corresponds to outside the atmosphere. The reference point at the Earth surface is AM1, when the Sun is at Zenith. At any other time of the day the air mass is defined as given in Eq. 1.

$$\text{Air Mass } m = (h_2/h_1) = (1/\sin \beta) \tag{1}$$

β is the altitude of the Sun. AM1.5 corresponds to $\beta \approx 42^\circ$, which is also approximated as the average irradiance received during the entire day at that particular location.

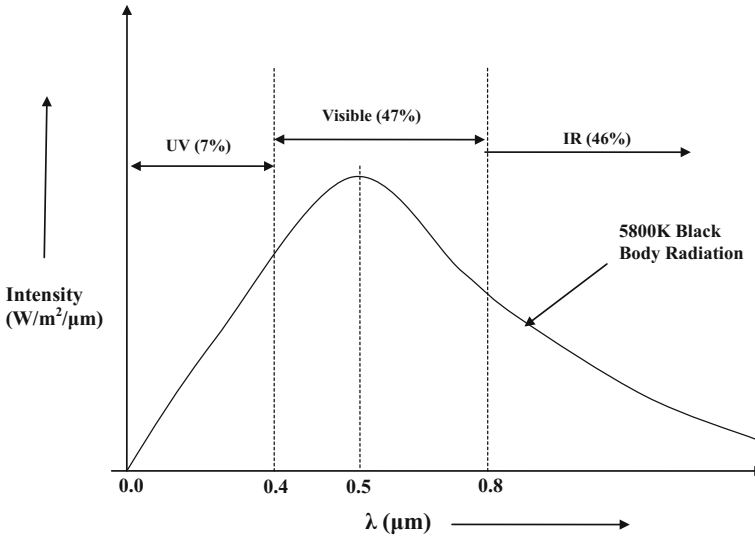


Fig. 2 Spectral distribution of 5800 K black body. The radiation received by the Earth at outside atmosphere (AM0) is also similar

The energy emitted by Sun has a spectral distribution corresponding to a black-body emitter having a temperature of 5800 K as shown in Fig. 2. The actual extraterrestrial radiation (AM0) closely resembles the spectrum shown in Fig. 2. The peak intensity is at $\lambda = 0.5 \mu\text{m}$, which corresponds to green part of visible spectrum. The total energy is roughly divided in ultraviolet (UV: $\lambda < 0.4 \mu\text{m}$): 7%, visible ($0.4 \mu\text{m} < \lambda < 0.8 \mu\text{m}$): 47% and infrared (IR: $\lambda > 0.8 \mu\text{m}$): 46%. The spectral distribution of intensity gets modified (not shown) as it travels through the atmosphere. The energy distribution also gets modified depending on altitude and air mass. The rough energy distribution at AM1.5 is 2.0% UV, 54% visible and 44% IR.

The total irradiance available at Earth's surface consists of mainly three parts. The major part is known as direct radiation denoted by direct normal incident (DNI). This is also known as global (G) part of the total irradiance. During cloudy weather, DNI is zero. Any collector receiving the direct radiation will receive full DNI, denoted here as I_{DG} , when the Sunrays are falling perpendicular on the collector surface as shown in Fig. 3. At any other Sun angle, the collector receive irradiance of $I_{DC} = I_{DG} \cos \theta$ as shown in Fig. 2. The collector can be a solar photovoltaic (SPV) module.

The other important portion of the irradiance received by Earth's surface is known as diffused radiation generated due to scattering of sunlight due to cloud, dust particles or even constituent gases in the atmosphere. During a cloudy day, although the DNI is zero, there are diffused radiations. Diffused radiation is modelled as if it is coming from all directions uniformly as shown in Fig. 4. The sky

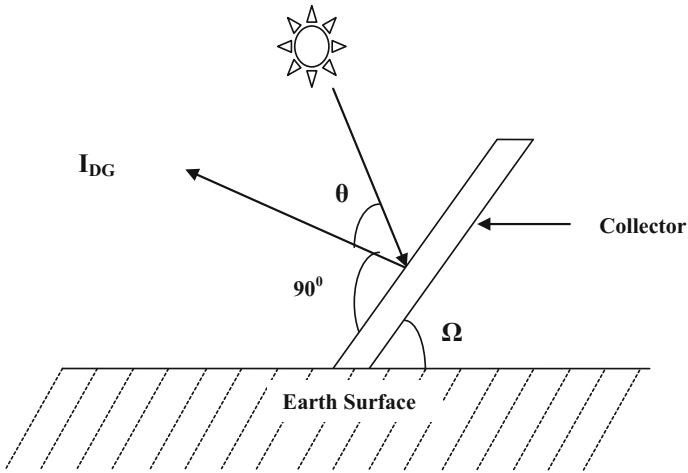


Fig. 3 Collector receiving direct radiation

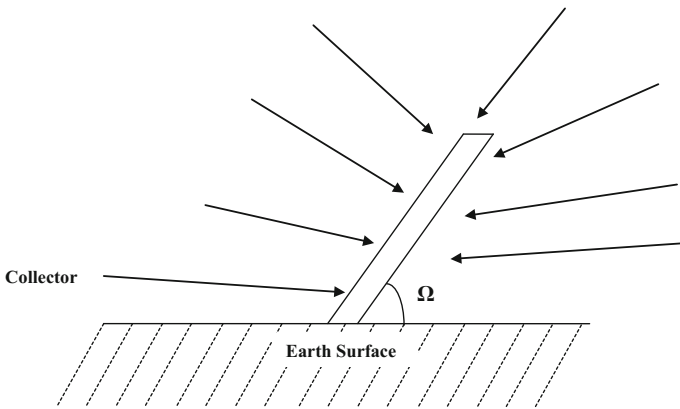


Fig. 4 Collector receiving diffused radiation

diffusivity factor (d) decides the amount of total diffused radiation (I_S), which eventually decided by the DNI. A simplistic model is shown in Eq. 2.

$$I_S = d I_{DG} \tag{2}$$

The total diffused radiation received by the collector (I_{SC}) depends on the tilt angle Ω (see Fig. 3) and it is given as shown in Eq. 4.

$$I_{SC} = d I_{DG} (1 + \cos \Omega) / 2 \tag{3}$$

In case the collector is kept horizontal to the ground, the entire diffused radiation will be available to the collector. On the other hand, in case the collector is perpendicular to the surface, the amount of diffused radiation received is 50% of the total.

Reflected radiation forms another small portion of the total radiation received by the collector. The reflection can be from the ground, adjacent mountain which may be covered by the snow and other structures such as buildings. This is very small and mainly depend on the ground material on which the collector are installed and surroundings.

The total radiation received by the collector is the sum total of direct and diffused radiation assuming the reflected radiation is negligible. On an average, the reflected radiation is about 0.5–1.5% depending on the location and surroundings. The direct radiation forms the major part of the total radiation, about 75%, if long-term average (e.g. a year) of a particular location is considered. Diffused radiation, about 25%, forms the other part. These figures will vary based on the climatic conditions of the location. For example, for a tropical country like India, the figures mentioned (75% direct and 25% diffused) would be close. Another place where there are more cloudy days, the diffused radiation contribution will be more. Estimation of direct and diffused radiation separately is important due to several reasons. Tracking-based SPV system only improves the direct radiation collection as the sunrays fall perpendicular to the collector most of the time. However, the amount of diffused radiation remains same as compared to a fixed SPV installation. In concentrated photovoltaic (CPV) [17], it is possible to only use direct part of the radiation to be concentrated to a point. Some SPV technologies, e.g. thin film amorphous silicon, diffused irradiance performance is better.

3 Photovoltaic Materials

Electrical conductivity of inorganic materials mainly gets decided by the nature of bonding prevailing amongst the constituent atoms or molecules. Semiconductor materials are formed due to strong covalent bond between constituent atoms or molecules. Elemental semiconductors are Si, Ge, etc. from group IV of periodic table and also compound semiconductors formed by two elements, one from group III and another from group V. Examples of compound semiconductors are GaAs, InP, etc. Compounds formed between one element of group II and another element of group VI, e.g. CdTe, are also semiconductor. In general, semiconductor materials have average valence electrons count as four. Other combinations such as Cu (group I), In (group III) can substitute Cd (group II) and if combined with group VI element such as Se forms semiconductor (Copper Indium Selenide-CIS). Band gap, which is introduced later, can be adjusted by using multiple elements from the same group retaining the basic requirement as discussed above. $Ga_xIn_{1-x}As$, $Ga_xIn_{1-x}P$, $Ga_xIn_{1-x}As_yP_{1-y}$ are examples of such semiconductors. Band gap can be tailored by varying x and y .

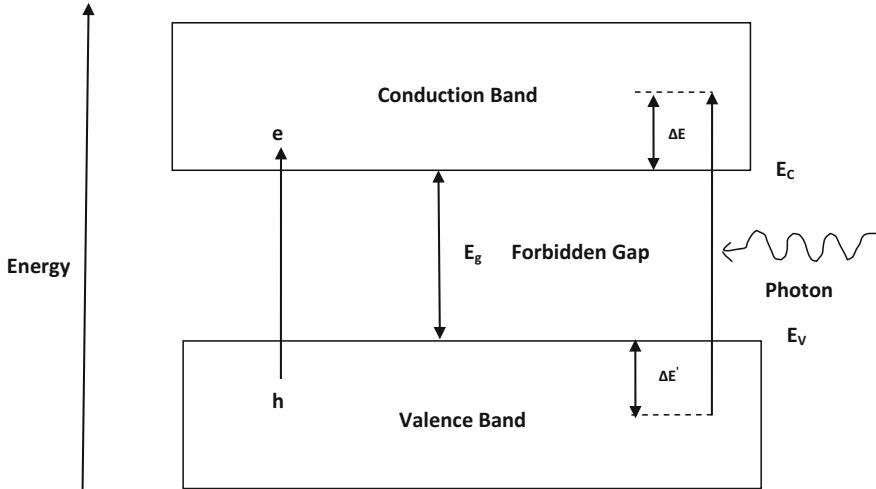


Fig. 5 Semiconductor band structure. E_V : Top of the valence band, E_C : bottom of the conduction band, E_g : band gap, h: hole, e: electron

The semiconductor [18] has a characteristic band structure as shown in Fig. 5. The valence band has allowed closely spaced energy levels (not shown) which are known as density of states. The number of such states is really large; in the order of $10^{23}/\text{cm}^3$. The highest allowed energy level in the valence band, also known as top of valence band, is denoted as E_V . Allowed energy levels do not necessarily mean that those are occupied by carriers, electron in this case. However, for intrinsic semiconductor at 0 K, all the available energy levels in the valence band are occupied by electrons. The free carrier concentration is zero and the material behaves like perfect insulator with zero conductivity.

The conduction band also has allowed closely spaced energy levels (not shown). The density of such states is also large: in the order of $10^{23}/\text{cm}^3$. The lowest allowed energy level in the conduction band, also known as bottom of the conduction band, is denoted as E_C . None of the energy levels in the conduction band are occupied by electrons for an intrinsic semiconductor at 0 K. There are no allowed energy levels in between top of the valence band and bottom of the conduction band. This is known as forbidden gap or band gap (E_g). Exciting electrons from the valence band to the conduction band require a minimum energy of E_g . At temperature other than 0 K, some of the carriers at the valence band acquire energy greater than E_g and get excited to the conduction band. Such carriers are called intrinsic carrier concentration, which strongly depends on temperature and band gap. If one electron gets excited from the valence band to conduction band, there is a corresponding hole which gets generated in the valence band as shown in Fig. 5. Both type of free carriers (electron and hole) can contribute to conductivity. Intrinsic carrier concentration for semiconductor materials is small. For example, for silicon with a band gap of about 1.1 eV, the intrinsic carrier concentration is about $1 \times 10^{10}/\text{cm}^3$.

It is possible to increase the free carrier concentration of electrons and holes by doping elements from group V and group III, respectively. These are known as n-type extrinsic semiconductor or p-type extrinsic semiconductor with extrinsic carrier concentrations decided by the level of doping, i.e. doping concentrations. The conductivity of the typical extrinsic semiconductors is therefore not as high as metal but much higher than insulator.

Photovoltaic devices use the energy of photons (see Fig. 2) to excite additional electrons from the valence band to the conduction band creating e–h pairs as shown in Fig. 5. The excitation and creation of additional e–h happens only if the energy ($E = hv = hc/\lambda$) of the photon is greater than the band gap. The photons having energy more than the band gap of the material are absorbed and create e–h pairs as shown in Fig. 5. The other photons with lower than this energy is simply passed through the material without contributing any e–h pairs generation. This is known as cut-off wavelength which is given as $\lambda_{\text{cut-off}} = hc/E_g$ or $\lambda_{\text{cut-off}}$ (in μm) $\approx 1.24 \text{ eV}/E_g$ (in eV). For example, this cut-off wavelength for silicon is about $1.13 \mu\text{m}$ with a band gap of about 1.1 eV. The additional e–h pairs generated effectively increase carrier which can be used for photoconductivity or electricity generation. Electricity generation requires a semiconductor device (p–n junction diode) which is discussed later.

The photoconductivity can be observed in a standard electrical circuit in which semiconductor material is used as a resistor. As the photons are absorbed by the semiconductor material and create additional carriers (e–h pairs), the resistance decreases resulting in higher current. However, this cannot be used to generate electricity. In case no external electric field in the form of voltage is applied, these photon-induced carriers are not separated from each other and recombine eventually without contributing to any current. The photo-generated carriers can be separated by creating an internal field. This is done by using a p–n junction made by n-type and p-type semiconductor material. The band diagram and the internal field are shown in Fig. 6. The photon-generated electron-hole pairs get separated due to internal electric field (ϕ_B).

The solar cell is essentially a p–n junction diode made of semiconductor material. Due to absorption of photons, e–h pairs are created and separated by the internal field of the p–n junction diode generating the electric power. These carriers can flow through the external load connected to the p–n diode. It is now important to understand the power, which is a product of voltage (V) and current (I). The current (I) will be decided by the amount of additional carriers generated due to irradiance and the voltage is decided by the potential energy of these carriers.

The total additional carriers generated due to irradiance depend on the spectral response and the band gap of the material. The spectral response curve is reproduced in Fig. 7. The total power of the irradiance as depicted in Figs. 2 and 7 can be estimated as the area under the entire curve. However, only a portion of this power is absorbed depending on the band gap of the material. For example, for a band gap of E_{g1} , the cut-off wavelength ($\lambda_{\text{cut-off } 1}$) is about $(1.24/E_{g1}) \mu\text{m}$ as shown in Fig. 7. The photons having wavelength of $\lambda_{\text{cut-off } 1}$ and below will be absorbed by the material. This can be estimated as the area of the curve between $\lambda = 0$ and

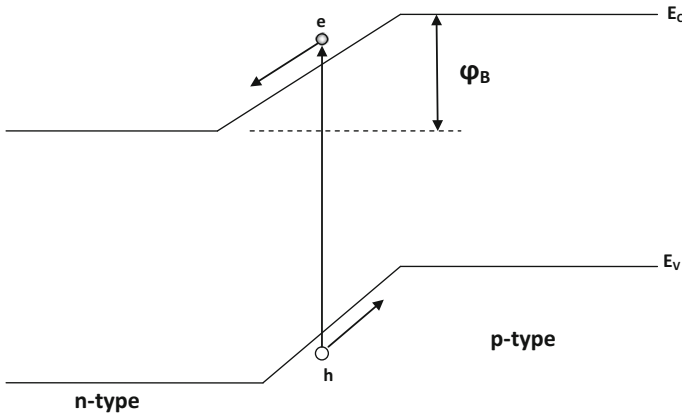


Fig. 6 Electron-hole pair separation due to potential barrier (ϕ_B) in p-n junction diode

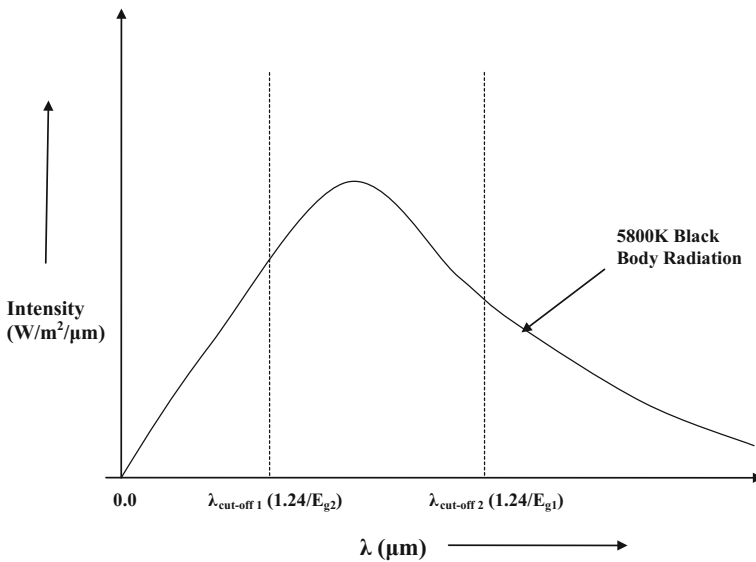


Fig. 7 Spectral response of radiation received by the Earth and the cut-off wavelengths

$\lambda = \lambda_{\text{cut-off } 1}$. Rest of the power, which falls on the right side of the $\lambda_{\text{cut-off } 1}$ curve is not absorbed and therefore does not contribute to carrier generation. As the band gap increases, the power which is absorbed by the material reduces. The material with band gap E_{g2} , which is higher than E_{g1} , absorbs less power as the area of the curve between λ and $\lambda_{\text{cut-off } 2}$ is lesser. It is clear therefore that the number of carriers generated due to absorbed irradiance depends on the band gap of material. The actual number of carriers generated can be estimated from the spectral response

knowing the total number of photons absorbed assuming one e-h pair is generated per one absorbed photon. This decides the current (I_L) produced by the photovoltaic device, which is also known as short-circuit current (I_{SC}). More about the short-circuit current are discussed later. It may be noted that the current produced by a photovoltaic device decreases as band gap increases.

The potential energy of the photo-generated carriers, which decides the voltage of the photovoltaic device, also depends on band gap. As shown in Fig. 5, the energy of the photon ($\lambda < \lambda_{\text{cut-off}}$) gets transferred to the electron in the valence band which then gets excited to the conduction band. Although the initial potential energy of the excited carrier is equal to the energy of the photon, ultimately it gets settled to the bottom of conduction band (top of the valence band for hole) by losing some energy as shown in Fig. 5. The total energy loss for e-h pair is $(\Delta E + \Delta E')$. This energy is lost and gets converted to heat. The voltage of the photovoltaic device therefore gets decided by the band gap. More the band gap more is the voltage.

The output power (P) of the photovoltaic device is the product of current (I) and voltage (V). The band gap of the material therefore decides the output power. As the band gap is increased from low to high, the current decreases but voltage increases. Limiting cases are $E_g \rightarrow 0$ ($I \rightarrow \infty$, $V \rightarrow 0$, and $P \rightarrow 0$) and $E_g \rightarrow \infty$ ($I \rightarrow 0$, $V \rightarrow \infty$, and $P \rightarrow 0$). There is then an ideal band gap which gives the maximum output power. The efficiency of the photovoltaic device is defined as (output power/input power). The input power is given by the entire curve of Figs. 2 and 7. The output power is less than the input power as some part of the spectrum gets unutilized due to $\lambda_{\text{cut-off}}$ issue and also due to the loss of $(\Delta E + \Delta E')$ as discussed earlier. The theoretical limit of the efficiency is calculated based on the above considerations. The practical efficiency obtained is less than the theoretical maximum due to several other factors, which are taken up later. The efficiency versus band gap plot is shown in Fig. 8. The maximum efficiency occurs at about $E_g = 1.45$ eV. Silicon has a theoretical efficiency of about 28%.

The higher theoretical efficiency can be achieved using multi-junction device. These are known as multi-junction (MJ) [19] or tandem [20] solar cells. Solar cells made using III-V compounds or amorphous silicon uses this technology. MJ or tandem solar cells use larger portion of the solar spectrum more efficiently by employing multiple semiconductor layers with different band gaps. Each layer absorbs different portions of the spectrum capturing more number of photons. This can be explained with the help of Fig. 9. The top layer (layer 3) absorbs the photons with energy more than the band gap energy (E_{g3}) and allows the lower energy photons to pass through. Layer 2 absorbs photons having energy between E_{g2} and E_{g3} . Similarly, in layer 3, photons having energy between E_{g2} and E_{g1} is absorbed.

It is possible to absorb all the photons having energy higher than E_{g1} by layer 1 alone. However, there is extra loss of energy in single-junction structure. The excess energy of a photon with reference to the band gap energy is lost mainly due to heat as explained earlier $(\Delta E + \Delta E')$. This loss is minimized by using MJ (tandem) structure. The voltages which are determined by the band gap is highest for cell 3 (V_3) and lowest for cell 1 (V_1). The open-circuit voltage of cell 2 (V_2) lies

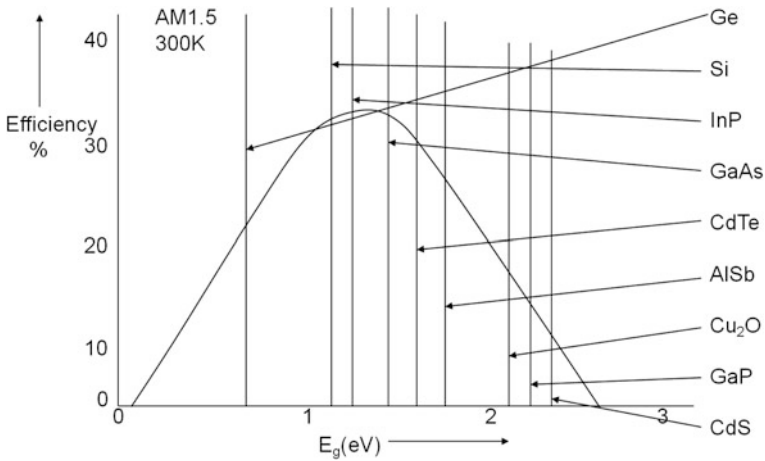
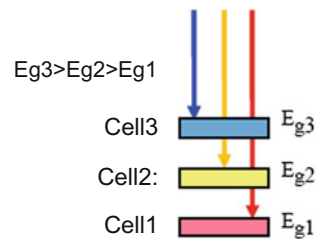


Fig. 8 Ideal (theoretical) efficiency of photovoltaic device as a function of band gap of the material. Maximum efficiency is at band gap of about 1.45 eV

Fig. 9 Three stacked materials absorbing larger part of the spectrum



in between. As the cells are connected in series, the effective open-circuit voltage of the MJ cell is the sum of these three voltages ($V_1 + V_2 + V_3$). The layers are to be carefully designed to have same short-circuit current (I_{SC}) for all the three cells as they are connected in series. Otherwise, the effective current is decided by the lowest current and there are losses of photo-generated carriers due to internal flow of current in the cell having lower current.

The band gap adjustment of the III–V compound semiconductor are done using ternary (e.g. $In_xGa_{1-x}P$) or quaternary (e.g. $In_xGa_{1-x}As_yP_{1-y}$) compounds by varying x or/and y . The band gap of amorphous silicon (a-Si) can be varied by incorporating germanium (a-Si:Ge) and carbon (a-Si:C).

The organic solar cells work on different principle as compared to inorganic solar cells described above. The photons absorbs by the organic materials generates excitons. These excitons are responsible for electrical conductions. The concept of valence band and conduction band are also not applicable in organic material. Instead, the highest molecular orbital (HOMO) and the lowest unoccupied molecular orbital (LUMO) are equivalent to valence and conduction bands. The detail description of the organic photovoltaic is out of the scope of this chapter.

4 Electrical Characteristics of Photovoltaic Devices (Solar Cells)

The cross section of a p-n junction diode acting as a solar cell is shown in Fig. 10. The photo-generated carriers denoted by + for hole and — for electron get separated due to internal electric field in the depletion region and flow through the load generating current. The current is decided by the amount of photons absorbed and the band gap of the material as discussed earlier. The spectral response of the solar cell is essentially decided by the spectral response of the material used to make the solar cells. The details have been discussed in Sect. 3.

The symbolic circuit representation of Fig. 10 is shown in Fig. 11 which is also known as equivalent circuit. Figure 11a represent the equivalent circuit under no irradiance. Under irradiance and due to the internal field of the diode, a photo-generated current (I_L) gets established and acts as current source. This current

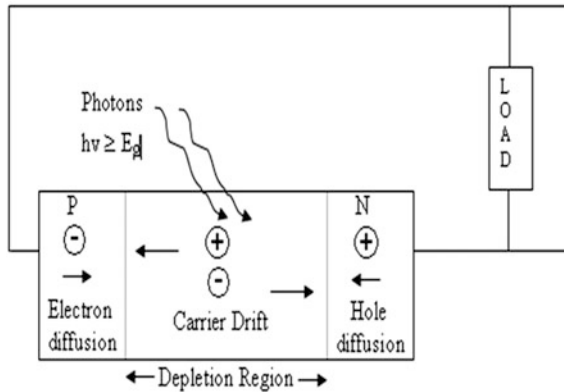


Fig. 10 Cross section of a p-n junction diode acting as a solar cell

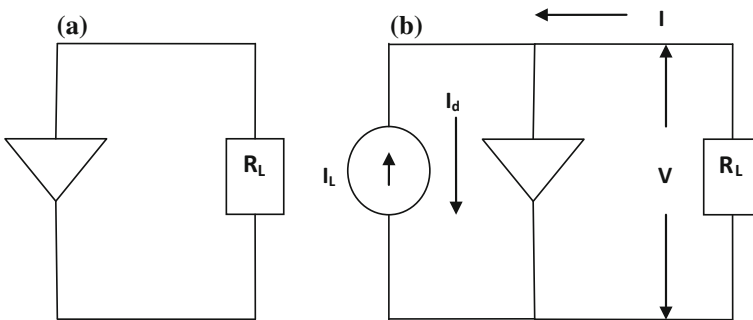


Fig. 11 a Ideal equivalent circuit in dark. b Ideal equivalent circuit under irradiance

flows through the load (R_L) and also through the diode. The diode current (I_d) which is given by Eq. 4 depends on the voltage (V) developed across it.

$$I_d = I_S \left(e^{qV/kT} - 1 \right) \quad (4)$$

where I_S is the reverse saturation current of the diode, k is the Boltzmann constant and T is the temperature. It is interesting to study the current (I) flowing through the load if the load resistance (R_L) varied from zero (short circuit) to infinity (open circuit). Under short-circuit condition ($R_L = 0$), there is no voltage drop and the voltage (V) across the load and the diode is zero. The diode current (I_d) is therefore zero (see Eq. 4). The entire current I_L flows through the load. The short-circuit current, denoted as I_{SC} is equal to I_L ($I_{SC} = -I_L$ for $R_L = 0$, $V = 0$). As the resistance becomes finite, there is a voltage drop across the resistor. This voltage (V) increases as the resistance increases. There is then a current (I_d) through the diode (see Eq. 4). The current through the load can be written as give in Eq. 5.

$$I = I_S \left(e^{qV/kT} - 1 \right) - I_L \quad (5)$$

Under open-circuit condition ($R_L = \infty$), there is no current across the load and the voltage developed only causes the current across the diode. This voltage is known as open-circuit voltage (V_{OC}) and can be determined from Eq. 5 by substituting $I = 0$ and $V = V_{OC}$. This expression is given in Eq. (6).

$$V_{OC} = (kT/q) \ln[(I_L/I_S - 1)] \quad (6)$$

This can be represented graphically as shown in Fig. 12. The current through the load (I) is a sum total of I_d and $-I_L$. The diode current is given by Eq. 4 can be drawn as per the voltage (V) across the load (and diode) and shown as I_d in Fig. 12. The photocurrent (I_L) is constant as shown. The current through the load ($I = I_d - I_L$) can be then drawn as shown in Fig. 12. The I_{SC} ($V = 0$) and V_{OC} ($I = 0$) is also shown in Fig. 12. It may be noted that the I–V characteristics appear at the fourth quadrant in which power ($P = V \times I$) is negative. This indicates the energy extracted from the device.

This I–V characteristic is an important representation of the solar cell. It is inconvenient to work always with a fourth quadrant characteristic. Therefore, for simplicity, the equivalent I–V characteristic drawn in first quadrant is used as shown in Fig. 13. Corresponding power versus voltage (P–V) characteristic is also shown. Maximum power (P_m) appears at a particular V_m known as maximum power point (MPP). The corresponding I_m is known as maximum current as shown in Fig. 13. The ideal power is the area of the rectangle defined by $V_{OC} \times I_{SC}$. However, the maximum power which can be extracted from a solar cell is the area of the rectangle defined by $V_m \times I_m$. It is to be noted that for extracting maximum power (P_m), the

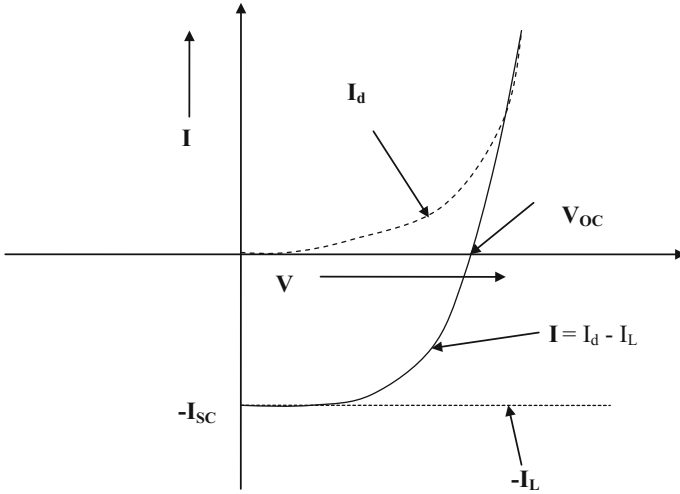


Fig. 12 I-V characteristics of a solar cell. I_d is the current through the diode, I_L is the photo-generated current, and I is the current through the load

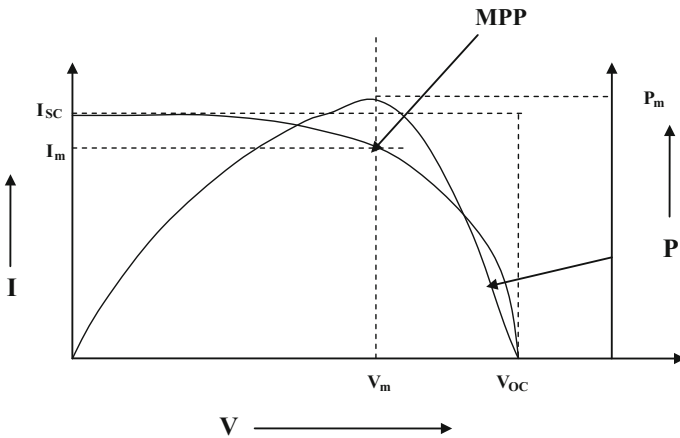


Fig. 13 Equivalent I-V drawn in first quadrant. P-V characteristic is also shown. Power is maximum at V_m (maximum voltage) and I_m (maximum current). The corresponding point is known as MPP (maximum power point)

solar cell has to be operated at MPP. The ratio between actual power and ideal power is an important parameter defined by fill factor (FF) as given in Eq. (7).

$$FF = (V_m \times I_m) / (V_{OC} \times I_{SC}) \tag{7}$$

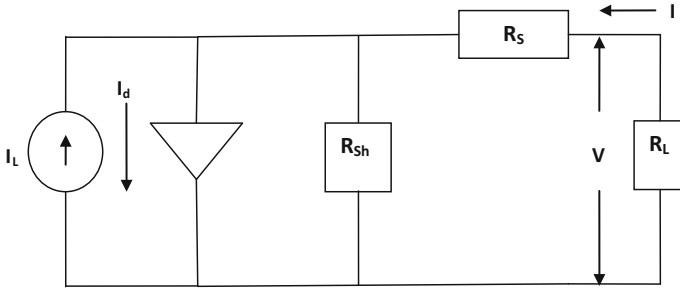


Fig. 14 Equivalent circuit of a practical solar cell with series (R_S) and shunt (R_{Sh}) resistance

The three important factors, V_{OC} , I_{SC} , and FF, together decide the power output and efficiency of a solar cell.

The equivalent circuit shown in Fig. 11 is assumed to be not affected by the internal as well as the external resistance. This is an ideal situation and not true for a practical device. There are series resistances (R_S) associated with the neutral (beyond depletion region) portion of the device material and also the external connection to be made to form the circuit. The diode has assumed to be an ideal device with infinite resistance. However, these have large but finite resistance. This resistance actually comes in parallel with the diode and the load. Therefore, this is known as shunt resistance (R_{Sh}). The equivalent circuit incorporating these resistances is shown in Fig. 14.

The current equation gets modified as given in Eq. 8.

$$I = I_S \left(e^{q(V-IR_S)/kT} - 1 \right) - I_L + (V + IR_S)/R_{Sh} \tag{8}$$

The I–V characteristics also get accordingly adjusted. The slopes at V_{OC} and I_{SC} move inwards reducing the fill factor. Details are not shown.

5 Solar Photovoltaic Technology

The common types of solar PV devices are shown in Fig. 15. Most of the terrestrial installations uses either c-Si or low-efficiency thin film technology such as a-Si, CIGS and CdTe. c-Si is most widely used PV technology capturing market share of about 90%. Multi-crystalline silicon (c-Si: multi) technology with efficiency range of 16–19% is more common. Higher efficiency in the range of 17–20% is achieved for monocrystalline silicon (c-Si: mono) technology. This is used mostly where there is a space constraint or space is available at premium. Both mono and multi c-Si are bulk technology which requires a silicon substrate of thickness of about 200 μm .

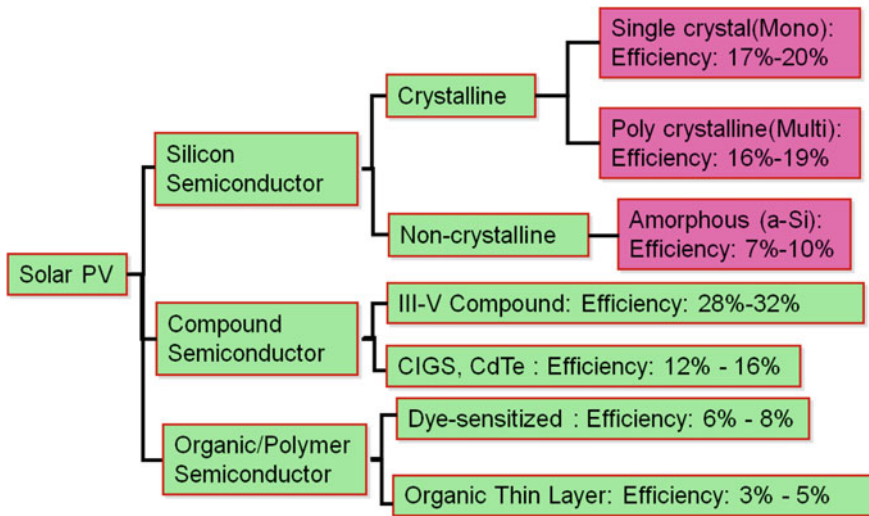


Fig. 15 Type of solar PV devices. The efficiency mentioned are stabilized efficiency and on large substrate

Thin film a-Si SPV devices are made by depositing thin layers of required materials on a glass substrate. The use of costly silicon substrate is therefore eliminated resulting in lower cost. However, the efficiency is lower (7–10%).

Other thin film technologies use materials such as CIGS and CdTe. Efficiency level of 14–16 and 12–14% are achieved for CIGS and CdTe technologies, respectively. Amongst the thin film technologies, CdTe is most commonly used and have a market share of about 10%. a-Si, which was introduced during the period when the cost of polysilicon was very high. c-Si substrates are made using polysilicon. As the prices of polysilicon came down subsequently, the a-Si technology lost its competitive advantage. CIGS technology is comparatively new amongst the thin film technologies and some recent installations are coming up. A hybrid technology, known as Heterojunction with Intrinsic Thin Layer (HIT), using combination of c-Si and a-Si thin film has been developed giving higher efficiency (~22%) [21].

Use of high-efficiency (28–32%) III–V thin film technology is not preferred in conventional terrestrial applications, except concentrated photovoltaic (CPV) systems [17, 22]. High-efficiency III–V SPV devices are used for space applications. Previously c-Si technology was used for space applications. This has now been completely replaced by the III–V technology.

Organic and polymer-based semiconductor materials are under current research. The concept has been proven and prototypes are made. Prominent amongst them are dye-sensitized solar cell (DSSC), organic thin layer solar cell [23, 24] and Perovskite solar cell [16, 25]. Solar cell technologies based on quantum mechanics [26] and nanotechnology [27] are under fundamental research.

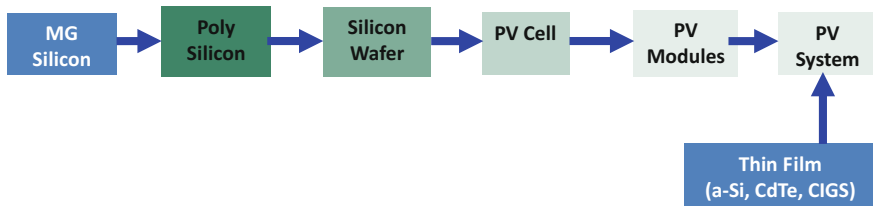


Fig. 16 Solar PV value chain

The complete solar PV value chain is shown in Fig. 16. The crystalline silicon-based solar cell has a long value chain. Each block of the value chain is a business model by itself. This starts by extracting metallurgical grade (MG) silicon from SiO_2 abundantly available in sand, quartz, etc. The MG-grade silicon is not so pure, and crystallinity level is low. This is further purified as polycrystalline silicon in the form of “chunks”. The next process is crystal growth in which more pure polycrystalline, known as multi c-Si or mono-crystalline, known as mono c-Si, ingots are formed. Parallelepiped-shaped ingots are formed for multi c-Si using a die casting method. Mono c-Si in the form of cylindrical ingots is made using a more sophisticated technology such as Bridgman and Czochralsky. The respective doping (n or p-type) is done during the crystal growth process. Thin slices, of the order of 200 μm , are cut out using advanced sawing techniques. These are known as wafers. These mono or multi c-Si wafers are then used to fabricate the solar cells. The solar PV modules are then made by electrically connecting several cells in series. SPV systems are configured by connecting modules in series and parallel combinations as required.

c-Si is categorized as first-generation technology. III–V high-efficiency cells, which is primarily used for space applications and also in concentrated photovoltaic (CPV), is also in first-generation technology category. In this, the cells are made by high-quality single-crystal thin films typically using a germanium substrate. These cells are then configured directly assembled as a system as per requirement. The intermediate requirement of module manufacturing is generally skipped.

Thin film a-Si, CdTe and CIGS cells are made directly on a large substrate such as a glass coated with transparent conductive oxide (TCO) such as indium tin oxide (ITO). These fall under second-generation technology. The value chain is much simpler, as shown in Fig. 16, as the cells in the size of module are directly made and several of them can be used to configure SPV system.

The third-generation technologies are dye-sensitized (DS) solar cells, organic solar cells, etc. These are yet to be matured and presently not used in commercial applications.

c-Si solar photovoltaics is the most proven and reliable technology at present. As mentioned before, the solar cells are made first, and several of them are connected together to make the modules. The cross-sectional diagram of a basic c-Si solar cell

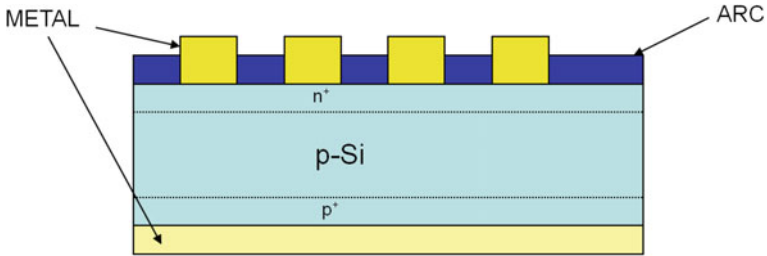


Fig. 17 Cross section of a basic solar cell

structure is shown in Fig. 17. The baseline c-Si cell manufacturing process flow is shown in Fig. 18. The c-Si solar cell is essentially a single p–n junction diode made on a single-crystal substrate. Present technology uses a 156 mm × 156 mm p-type (boron doped) silicon wafer as a substrate.

5.1 *c-Si Solar Photovoltaic Technology*

5.1.1 c-Si Solar Cell

Saw damage removal and texturization [28, 29] are the first step of the c-Si manufacturing process. During slicing of the ingot to take out wafers, there are damages on the surface which are to be repaired. A layer of about 10 μm is removed from the front surface where the p–n junction is formed. This is done by etching using a wet solution comprising of HF. The texturization step also uses wet solution, and this is done along with saw damage removal. Anisotropic etching in which the lateral etch rate is more than the vertical etch rate is employed to get pyramid-like structures on the surface as shown in Fig. 19. The light capture increases due to multiple reflections. Untextured and polished silicon surface have very high level of reflection. It can touch 40% which is essentially lost as it is not absorbed in the silicon bulk. Texturized surface reduces this reflection loss to as low as 4–5%. Further reduction of reflection loss is achieved through anti-reflection coating (ARC) [30, 31], which has been discussed later.

The texturization is straightforward and simpler in case of mono-crystalline silicon. Alkaline solutions such as NaOH and KOH with lower etch rate are used to form textured surface. The shape and height of the pyramids get decided by the horizontal and vertical etch rates decided by the concentration of etching solution. This gets complicated for multi-crystalline silicon as the etch rate of crystalline portion is different than that of grain boundaries. Slower etching using alkaline solutions result in irregular-shaped pyramids. Acidic solutions such as HNO₃ and HF with higher etch rates are used to circumvent this problem. However, the texturization of c-Si multi is not as good as c-Si mono. A common process for c-Si

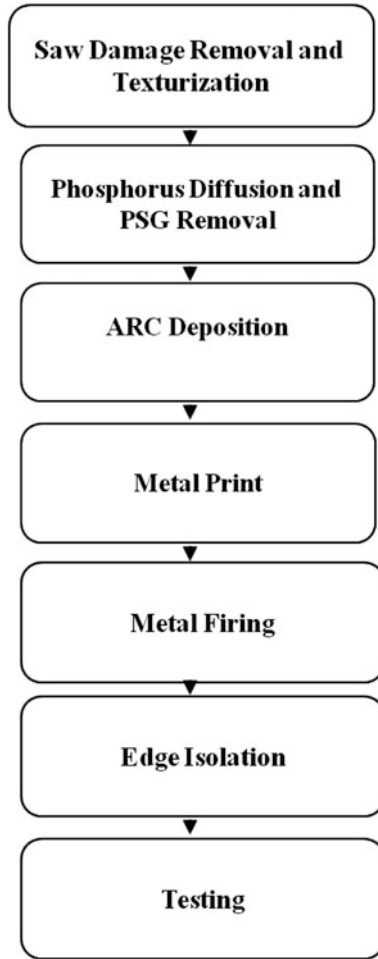


Fig. 18 Process flow of baseline c-Si cell manufacturing

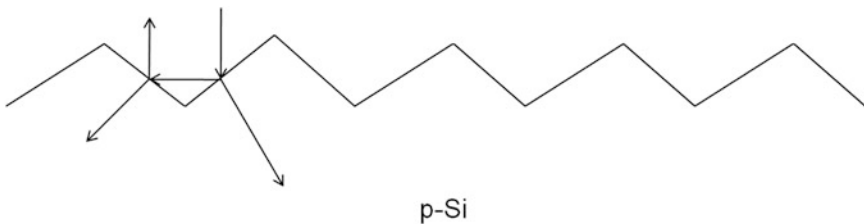


Fig. 19 Enhanced light capture due to texturized surface

mono and c-Si multi using a mixture of alkaline and acidic solution having an intermediate etch rate have been tried by researchers with limited success.

The p–n junction diode is formed by doping the top portion of the p-type substrate with phosphorus which is a n-type dopant in silicon (Fig. 17). Primarily, two processes are prevalent in solar PV industry. Dominant one uses furnace diffusion using POCl_3 as phosphorus-containing gas. This technique is in fact adopted from VLSI industry. POCl_3 along with an inert carrier gas is allowed to flow through the surface of the p-type silicon which is kept at high temperature ($\approx 800^\circ\text{C}$) in a furnace. The reactant gas, POCl_3 , gets decomposed to P, O_2 and Cl_2 . Phosphorus then diffuses to the silicon causing n-type doping. Alternative process, which was also been used in earlier VLSI fabrication known as pre-deposition, uses O_2 along with POCl_3 . An intermediate compound P_2O_5 is then formed at somewhat lower temperature. This when subjected to a high temperature ($800\text{--}850^\circ\text{C}$) reacts with Si and liberates phosphorus, which acts as a n-type dopant in silicon. A complex compound ($\text{Si}_x\text{P}_y\text{O}_z$), known as phospho silicate glass (PSG), is also formed. Direct decomposition of POCl_3 at high temperature, skipping the intermediate pre-deposition step, is more common in solar PV industry.

An entirely different process, although less common, using spray techniques is also used for solar cell manufacturing. In this, H_3PO_4 is sprayed on the silicon substrate kept at about 200°C . This gets decomposed in P_2O_5 and H_2O . The P_2O_5 -deposited substrate is then heated at high temperature ($800\text{--}850^\circ\text{C}$) to achieve phosphorus doping similar to the alternative POCl_3 process. This also results forming a PSG layer on top of the substrate after completion of doping process. The PSG layer is then removed by etching using HF and H_2O_2 .

As discussed earlier the reflection loss is reduced by texturization. Further, reduction of reflection loss is achieved through deposition of anti-reflection coating (ARC). Overall reflection loss of only 1–2% can be achieved with the help of ARC together with texturization. A thin film (600–800 Å) of silicon nitride (Si_3N_4), deposited by plasma-enhanced chemical vapour deposition (PECVD) technique, is generally used for ARC. The refractive index (n) of Si_3N_4 ($n \approx 2$) is in between air ($n = 1$) and Si ($n \approx 4.0$). As the thickness of ARC layer falls under thin film region, interference effect decided the overall reflection loss. The refractive index along with the thickness of this thin film layer determines the interference pattern, i.e. constructive or destructive, for a particular wavelength. Destructive interference for the wavelength range of interest can be achieved by choosing appropriate thickness of Si_3N_4 . The refractive index of the silicon nitride layer can also be varied by changing the stoichiometry of the film (Si_xN_y) by making either silicon rich ($n > 2$) or nitrogen rich ($n < 2$). The silicon nitride deposition is done by using SiH_4 and NH_3 . The composition of these gases can be altered to get varying x and y . SiH_4 rich gas composition gives higher refractive index and vice versa. Composite ARC layers with Si_3N_4 and SiO_2 ($n = 1.4$) for better control of interference effect have also been tried.

The metal connections from the front (n) and the back (p) are required for electrical connection to the p–n diode. The front connection is not straightforward mainly due to two reasons. First, metal used for the connection typically aluminium

(Al) is opaque to the light. No light can reach silicon in case the entire front surface is covered with metal. Second problem is due to the ARC layer, which is essentially an insulator. Special process is required so that the deposited metal on the front makes electrical contact with underlying silicon. Back side metal connection has no such problems. The front side metallization is done using a paste consisting mainly of silver (Ag) along with lead and an organic binder. The composition of this metal paste is a technology by itself and is closely guarded secret kept by the suppliers.

The front metallization is done by applying the paste through a mask, typically having mesh openings, defining the fingers and the bus bars (see Fig. 20a). This is known as printing and somewhat similar to what is used in printed circuit board (PCB) process. Two-stage printing process is used to define the front and back side metals including the back bus bars. There are no fingers type patterns on the back side (see Fig. 20b). The printing process is followed by a high-temperature firing. During this step, the Pb present in metal paste dissolves the ARC layer so that Ag can make contact to underlying silicon. Front and back side of a solar cell is shown in Fig. 20. Segmented three bus bar cells are shown. Cells with four bus bars are also in use.

The final process before testing is edge isolation. During doping to make n-p junction, the phosphorus also gets doped on the sides of the cells. This can result in short between front and back side rendering the n-p junction useless. A portion of the silicon is removed at the edges of the front side. The depth of etching is more than the junction depth of n^+ . This removal can be done either by LASER or by chemical etching, which is more popular for current technology.

The manufactured cells are then tested in a cell tester, which record the I-V and P-V characteristics and extracts electrical parameters such as V_{OC} , I_{SC} , V_m , I_m , fill factor and power. These cells are then segregated in BINs usually in terms of power. Dedicated test set up, known as sun simulator, is used for solar cell and module testing. Some stipulated standards have to be followed, such as tester accuracy, calibration procedure for the testing.

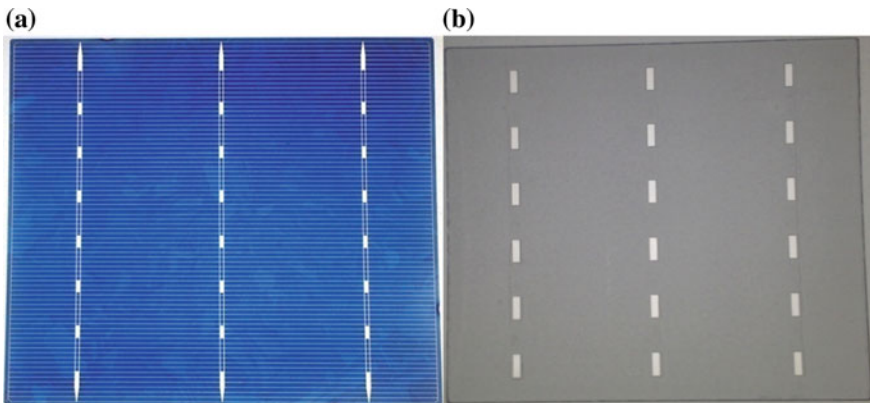


Fig. 20 a Front side and b back side of a solar cell

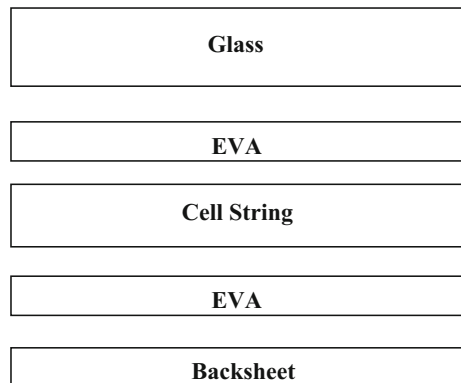
5.1.2 c-Si Solar Module

Several of c-Si solar cells are electrically connected, usually in series, to make a c-Si solar module. Modules with 60 cells or 70 cells connected in series are more popular. Modules with lower or higher than 60/70 cells are also available. V_{OC} of c-Si solar cell is about 0.6 V. I_{SC} depends on the efficiency of the cells and can be of the order of 9 A. As the cells are connected in series to make modules, V_{OC} of about 36 V and I_{SC} of about 9 A are achieved for a 60 cells module. Some smaller systems such as solar lantern, street light require higher voltage but less current. In such cases, “cut cells”, i.e. individual cells are cut into several pieces and they are then connected in series. For example, if one c-Si cell is cut into four pieces, each piece has $V_{OC} = 0.6$ V and $I_{SC} = 2.25$ A. If these four pieces are now connected in series, $V_{OC} = 2.4$ V and $I_{SC} = 2.25$ A is achieved instead of $V_{OC} = 0.6$ V and $I_{SC} = 9$ A for one uncut cell.

Apart from the electrical connection, further processing is required to protect the c-Si cells from the external harsh environment during the operation of the modules in the field. This is achieved by lamination. The lay-up of the different layers before lamination is shown in Fig. 21. The cells are sandwiched between a front glass and a back sheet. Polymer layers made of Ethyl Vinyl Acetate (EVA) are inserted between cell string array and front glass and also between cell string array and back sheet. The cell receives the irradiance through transparent front glass as the front side of the cells face the glass. Apart from electrical connection and lamination additional process steps, such as fixing the junction box for external connection and the frame insertion for fixing the module to the external structure, are required. The module manufacturing process flow is shown in Fig. 22. An overview of various process steps are discussed below.

The electrical connection of the cells is done through an automatic process known as tabbing and stringing (T&S). Typically, a certain number of cells, e.g. 10 for 60 cells module and 12 for 72 cells module, are connected in series to make the individual strings. Required number of such strings, e.g. 6 are placed in parallel and connected in series. This process is known as bussing. The lay-up as shown in

Fig. 21 Lay-up sequence of solar PV module



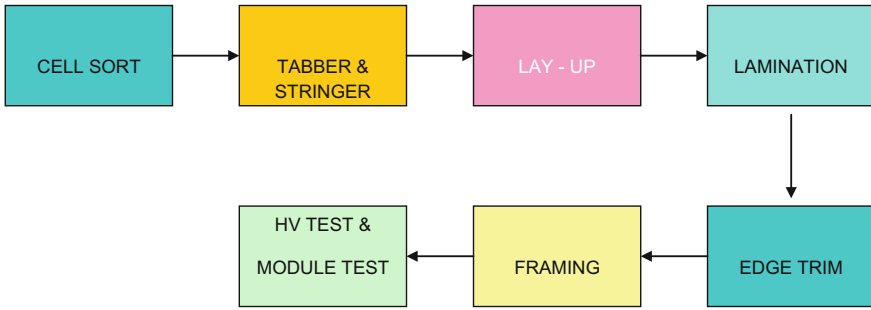


Fig. 22 Process flow of c-Si module manufacturing

Fig. 21 is then arranged. Modern manufacturing line uses automated lay-up through robotic machines. The lay-up is then laminated using an equipment called laminator. This process is in principle similar to the conventional lamination used for protecting, e.g. important documents. However, better accuracy of temperature, pressure, vacuum, etc. is needed for solar module lamination. The size of the laminator is large due to (a) large size of the module and (b) more than one module is generally laminated in one process cycle to increase the throughput. Lamination provides electrical insulation and protection of the cells from the external environment.

After lamination, the excess EVA and back sheet protruding out from sides are trimmed using a hot knife. This is known as edge trimming process. Anodized aluminium frames are then inserted from all four sides to provide strength to the module and also to make it compatible for easy installation by fixing the modules to the external frames. Double-sided tapes are inserted between the trimmed laminated module and the frame for durability. A more advanced process uses silicone glue for frame fixing. After framing, the junction box is attached to the back side of the module. The junction box connects the cell strings to external cables. It also has by-pass diodes required to optimize the power output of the module due to shading.

Finished module has to undergo detail testing for quality, safety, reliability, and performance. The quality is ensured by several quality check (QC) procedures during and after manufacturing. Reliability test is also done as per stipulated standards. One of the safety tests is the high voltage (HV) test to ensure there is no leakage between cell string and the outside conductor, such as metallic frame [32]. Electrical testing is done by measuring I-V and P-V characteristics and then extracting parameters such as P_{\max} , V_{OC} , I_{SC} , V_m , I_m , fill factor. Electrical testing is carried out using dedicated tester, known as sun simulator. About 1000 W/m^2 irradiance falling perpendicular to the module kept at 25°C is used as standard test condition (STC). The irradiance used must be equivalent to sun spectrum at AM1.5G; G denotes global. The tester must meet specific stipulated criteria such as uniformity, stability and accuracy. Calibration of the sun simulator is also important [33]. Reference modules certified by authorized agencies, such as NREL and

Fraunhofer are used for calibration. The total power obtained from a module is somewhat less than that of the sum of powers of all the cells. This is known as cell to module (CTM) conversion loss [34]. This loss must be as minimum as possible.

5.1.3 Advances in c-Si Solar PV Technology

Cell Technology

Solar PV technology has made significant advancement in last ten years. The improvement of the efficiency and reduction of cost is the hallmark of such advancement. About 10 years ago, the cost was more than $\$4/W_p$ for module. This has come down to less than $\$0.7/W_p$ due to all around advancement.

The continuous improvement of the efficiency of solar cell is one of the prime reasons for rapid progress of the solar PV. It is particularly challenging as the enhancement of the efficiency has to be done keeping the cost in mind. A brief overview of the technology advancement has been discussed next without going into much detail. The improvements of efficiency of the solar cell are achieved by (a) ensuring more light reaching silicon by reducing shading (b) increasing the probability of capturing the photo-generated carriers and (c) reduction of loss of carriers due to surface and bulk defects.

The shading loss is mainly due to the front side metal fingers and bus bars. Bus bar width and numbers are optimized based on the compatibility of the T&S process and final electrical resistance arising due to external connections. Internal series and contact resistances are decided by the widths, heights and numbers of the fingers. The width to height ratio, which is known as aspect ratio, depends on the metal printing process used. It is preferable to have smaller line width with larger height so that lower electrical resistance is achieved along with lesser shading loss. However, the aspect ratio of the conventional metal printing technology is high, requiring higher aspect ratio and results in total shading loss of about 7–9% to maintain acceptable electrical resistance. Double printing (DP) technology has recently been introduced to circumvent this issue. In this, it is possible to reduce the aspect ratio, so that the shading loss is less, typically about 4–6%, without compromising on the electrical resistance. A cross-sectional view of a metal finger-printed in a DP technology is shown in Fig. 23b. DP uses a two-steps printing and requires a special equipment having higher accuracy, particularly for alignment of the two layers. Metal fingerprinted in conventional process is also shown in Fig. 23a for comparison. There are about 60–70 fingers in total in a typical $156\text{ mm} \times 156\text{ mm}$ solar cell.

Shading loss can be reduced by using metal wrap through (MWT) [35] and emitter wrap through (EWT) [36] technologies. In MWT, the bus bars for front contact are placed at the back side of the cells. The shading loss due to the bus bar metal is therefore eliminated. Cross-sectional diagram of MWT process is shown in Fig. 24. Grooves are made using LASER before phosphorus diffusion step. During

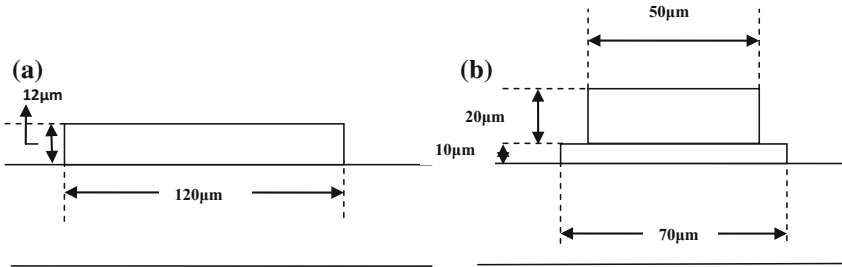
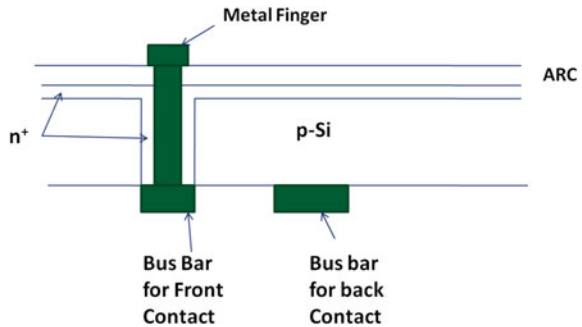


Fig. 23 **a** Conventional printing (single print) and **b** double printing technologies

Fig. 24 Cross-sectional diagram of metal wrap through (MWT) process

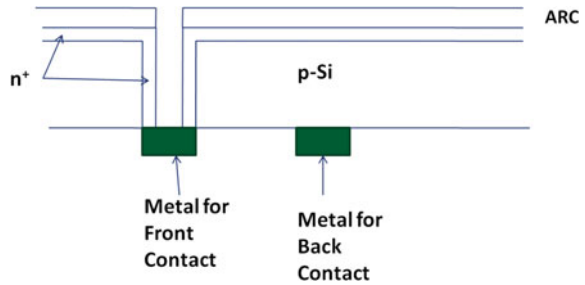


the front side doping for n^+ , the sides of the grooves are also doped as shown in Fig. 24. The metal fingers on the front are connected by bus bar located at the back by metal “wrap through” to the back.

In emitter wrap through (EWT) process, even the fingers are located on the back side. This eliminates the entire shading due to metal. Cross-sectional diagram of EWT process is shown in Fig. 25. Instead of metal finger, the equivalent finger connections are taken to the back side through several LASER grooves. The n^+ regions formed on the front and the sides of the grooves provide electrical connection between fingers (located at the back) and front emitter (n^+). Only one bus bar and finger have been shown in Figs. 24 and 25. There are more than one bus bar and several fingers in a solar cell. MWT and EMT processes are complex, and several details are skipped and not shown in Figs. 24 and 25. The EWT process is more complex than the MWT process.

Defect passivation [37, 38] is another area where improvements are possible. There are mainly two types of defects in crystalline materials. One is due to bulk defects such as impurities and grain boundaries. Impurities can capture active carriers resulting in reduced photocurrent. This type of defects is not very prominent for c-Si solar PV, due to high purity of substrate used to make cells. In multi-crystalline silicon, the grain boundaries are also considered as defects which can capture active carriers reducing the photocurrent. Another prominent surface defect originates due to surface state. The crystal structure is terminated at the

Fig. 25 Cross-sectional diagram of emitter wrap through (EWT) process



surface, and the bond structure remains incomplete for the silicon atoms located at the surface. This results in dangling bonds, which are also called surface states. These surface states can capture active carriers and reduce the photocurrent. The surface states are present both at the front and back surfaces.

The surface states can be deactivated by removing dangling bonds by providing hydrogen atoms to satisfy the incomplete silicon bonds. This technique is known as passivation and is used during several types of semiconductor device fabrication. Front surface passivation automatically happens during ARC deposition. The gasses used, SiH_4 and NH_3 for ARC deposition, contain hydrogen which can passivate incomplete silicon bonds by attaching themselves to the lattice structure. This is very effective technique and also passivates the grain boundary defects to a large extent. The same method is now being extended to back surface passivation. Additional processing steps are required to provide hydrogen to the back side for passivation. Although looks simple, it has some complications. The incorporation of hydrogen at the back silicon interferes with the p^+ doping and reduces its effectiveness. Several versions of the back surface passivation techniques have been recently developed. The simplest one is passivated emitter and rear contact (PERC) [39]. More advance techniques are passivated emitter and rear locally diffused (PERL) [40] and passivated emitter and rear totally diffused (PERT) [40]. A detail description is beyond the scope of this introductory chapter. A cross-sectional diagram of the PERT process is shown in Fig. 26. The front metal is not shown in this Figure.

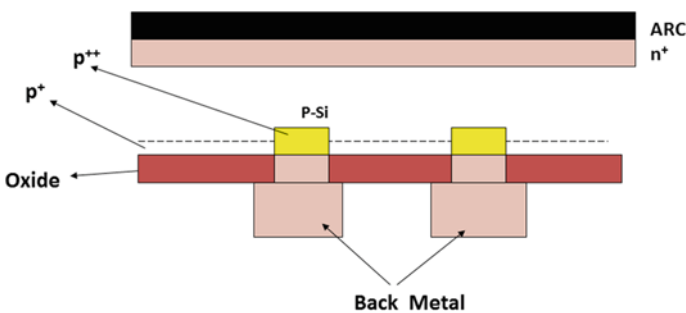


Fig. 26 Cross-sectional diagram of passivated emitter and rear totally diffused (PERT) process

Improvement of the collection efficiency of the carriers can be done by selective emitter process [41, 42]. In the conventional process (see Fig. 17), the entire surface is doped with phosphorus to form the n^+ emitter. Higher doping concentration is required to get lower resistivity and contact resistance which are prerequisite to increase the fill factor and hence the efficiency of the solar cell. However, it is known that higher doping introduces bulk defects, which act as recombination centres. The efficiency of the solar cell is thus reduced. Selective emitter introduces two separate doping regions. The portion which is connected to metal (see Fig. 27) is doped heavily to get lower electrical resistivity and contact resistance. Rest of the portion where the irradiance actually gets absorbed is doped lightly. Bulk defects arising out of doping is therefore reduced to manageable level. A cross-sectional diagram of selective emitter process is shown in Fig. 27 in which heavily doped and lightly doped regions are denoted as n^{++} and n^+ , respectively.

Interdigitated back contact (IBC) [43] process has been developed to manufacture high-efficiency cells. In this, both n^+ and p^+ are formed at the back. Many closely spaced n^+ and p^+ regions are formed using lithography and ion implantation. Metal contacts are taken by opening holes, using lithography and etching, through additionally deposited oxide. The metal connections are then formed using lift-off lithography. A cross-sectional diagram of IBC process is shown in Fig. 28. The topographical pattern of IBC metal connections is shown in Fig. 29. This is a typical interdigitated pattern and hence the name IBC.

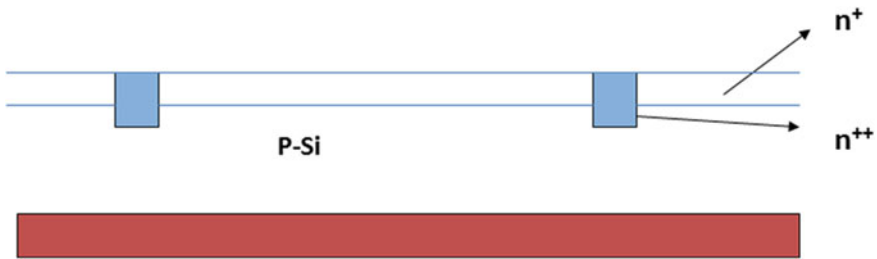
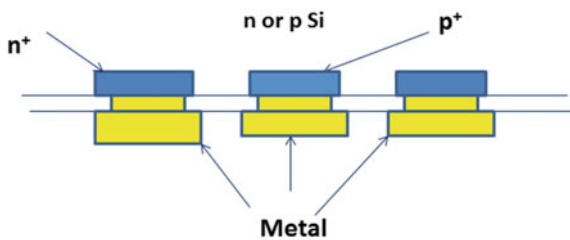


Fig. 27 Cross-sectional diagram of selective emitter process

Fig. 28 Cross-sectional diagram of interdigitated back contact (IBC) process



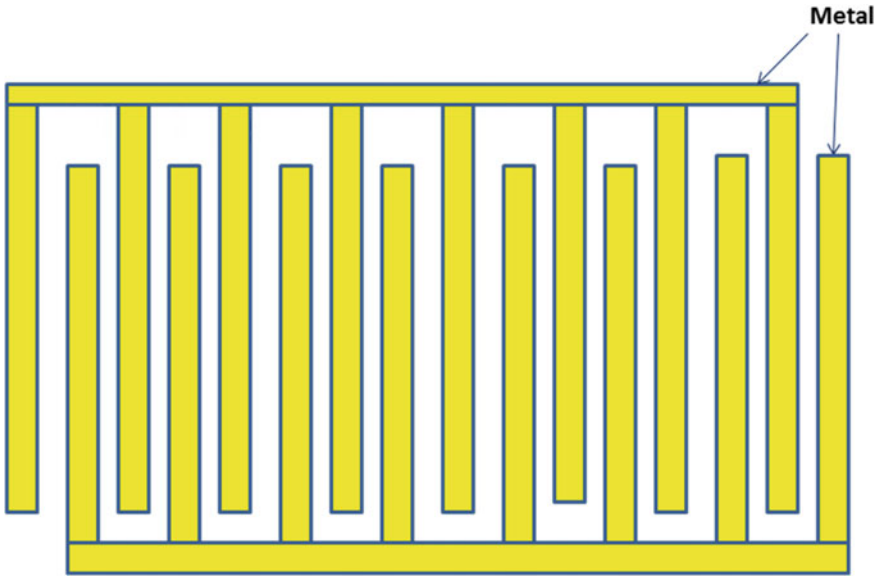


Fig. 29 Topological diagram of interdigitated back contact (IBC). Two separate comb-shaped metals connecting n^+ and p^+

There are some other advanced processes such as buried contact, light-induced electroplating that have also been developed with varying degree of success. Details are not discussed in this chapter.

Module Technology

Advances in module technology are mainly concentrated on developing new materials for cost reduction. Continuous improvement of equipment capabilities in terms of accuracy, stress reduction, and automation are also being done. Lower stress and higher automation resulted in reduction of cell thickness with very small rejection rate. Higher accuracy allows to place the cells more closer during lay-up resulting in reduction of module size giving higher effective efficiency of the module. Textured and anti-reflective-coated (ARC) glass [44, 45] have been introduced in SPV module manufacturing for improvement of the efficiency. There are some attempts for innovative process improvement [46–48] but these are limited and not very successful. Conductive adhesive instead of copper ribbon have been tried so that T&S process is replaced by a more stress-free process. There are attempt to replace the front glass by fibre-reinforced plastic (FRP) to have light-weight module. c-Si Concentrated PV (CPV) module with low level of concentration ($C < 2$) has been developed by modifying the cover glass. Instead of flat

surface, the cover glass has curved surface for concentration. Less silicon is required for producing the same power as compared to conventional module. However, these modules can only be used along with single-axis tracking system.

5.2 Thin Film Technology

5.2.1 a-Si, CdTe and CIGS Thin Film Technologies

Unlike c-Si; a-Si, CdTe and CIGS (Copper Indium Gallium Sulphide), thin film modules are manufactured directly by deposition techniques using transparent conductive oxide (TCO)-coated glass substrate. The process flow of a a-Si manufacturing process is shown in Fig. 30. The cross-sectional diagram of a single-junction a-Si cell is shown in Fig. 31. Plasma-enhanced chemical vapour deposition (PECVD) technique is use to deposit n-i-p layers to form the solar cell. Here, i indicate intrinsic layer. Several LASER scribing steps are used to configure these cells and also to connect, generally in parallel. Lamination step, similar to what is used for c-Si module manufacturing process, is used. However, it is common to use another glass, instead of back sheet, for lay-up and lamination. These types of modules are called glass on glass modules.

a-Si material has large number of dangling bonds. These are passivated using hydrogen, which is present in the gas (SiH_4) used for PECVD deposition of a-Si. Therefore, this material is denoted as c-Si:H. The band gap of a-Si:H is about 1.7 eV. This can be tailored by introducing C (a-Si:C) or Ge (a-Si:Ge) which have higher and lower band gap, respectively, than a-Si. It is understood that H is also present in a-Si:C and a-Si:Ge. Additional gas containing C or Ge is introduced along with main gas such as SiH_4 for formation of a-Si:C or a-Si:Ge. Multiple junction, which is also called tandem junction cells can be made by depositing

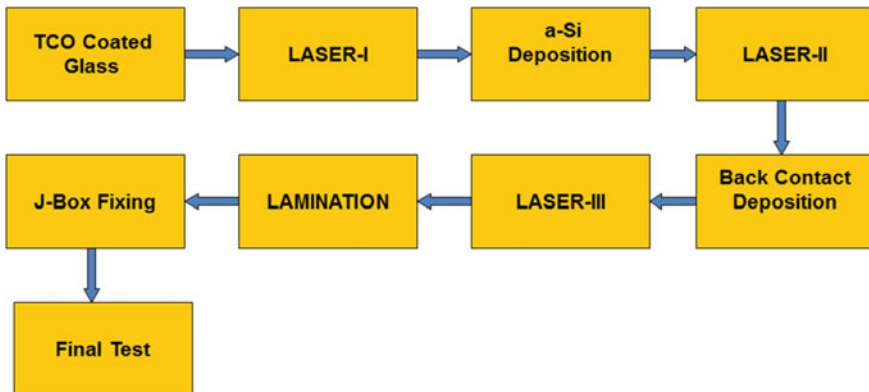
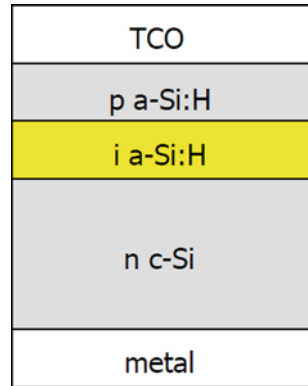


Fig. 30 a-Si thin film process flow

Fig. 31 Cross-sectional diagram of a single-junction a-Si thin-film solar cell



multiple layers as shown in Fig. 9. Layer 3, layer 2 and layer 1 can be made of a-Si: C, a-Si and a-Si:Ge, respectively. Band gaps of a-Si:C and a-Si:Ge can be adjusted by adjusting the amount of C and Ge present in the structure. The a-Si:Ge layer of the tandem cell can be replaced with microcrystalline silicon having band gap of about 1.1 eV. This is known as micromorph a-Si tandem solar cell. Microcrystalline layer can be formed by adjusting the deposition parameter during PECVD.

CdTe is another important thin film technology. Cross-sectional diagram is shown in Fig. 32. The process flow is somewhat similar to the a-Si solar cell. n-CdS, and p-CdTe are used for this solar cell. CdS has large band gap (≈ 2.42 eV) and therefore acts as a window for incoming light. Most of the light spectrum is absorbed in p-CdTe having a band gap of about 1.45 eV which is very close to the ideal band gap (see Fig. 8).

CIGS solar cell is relatively new technology which also uses the similar process as a-Si and CdTe. The cross-sectional diagram is shown in Fig. 33. In this also CdS is used as window layer.

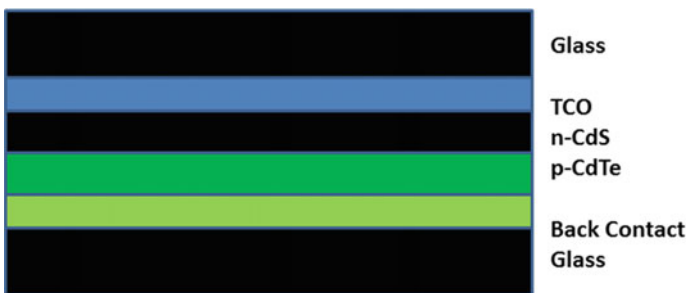


Fig. 32 Cross-sectional diagram of a CdTe thin-film solar cell

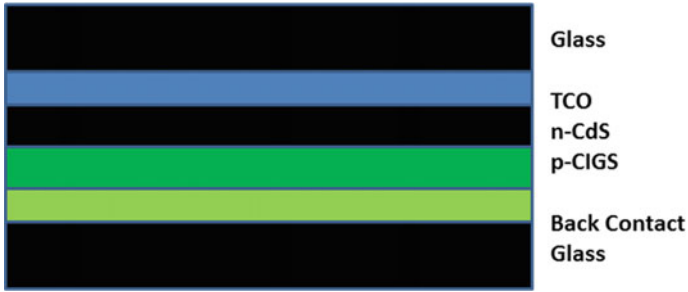


Fig. 33 Cross-sectional diagram of a CIGS thin-film solar cell

5.3 High-Efficiency III–V Solar Cell Technology

High-efficiency III–V cells [49] are used in space and terrestrial CPV applications. It is not preferred in conventional terrestrial application due to higher cost. It is possible to tailor the band gap by using ternary or quaternary compounds as discussed in Sect. 3. A cross-sectional diagram of a triple-junction high-efficiency solar cell is shown in Fig. 34. Germanium, which has close lattice matching with III–V compounds, is used as a substrate. Any III–V compound such as GaAs is a better option, but to reduce the cost Ge is used. High-quality single-crystal thin film

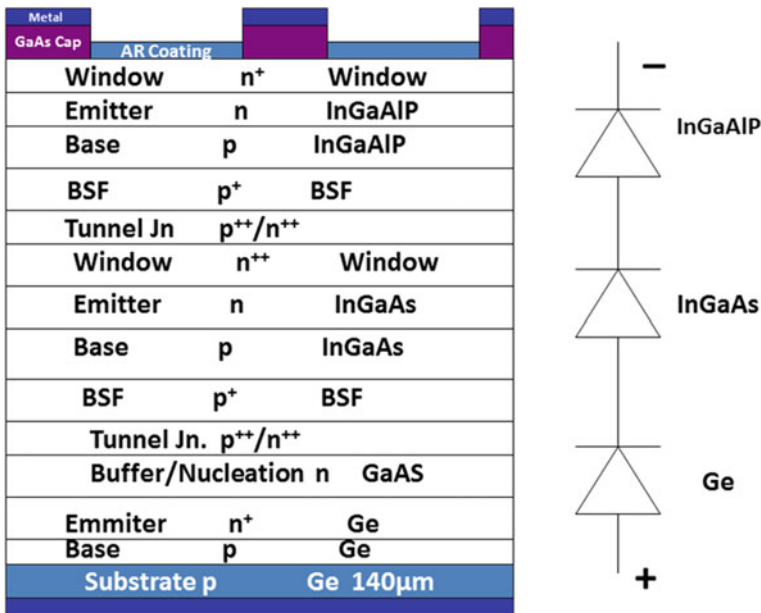


Fig. 34 Cross-sectional diagram of a III–V high-efficiency triple-junction solar cell. The diode representation of this triple-junction cell is also shown on the right

layers are deposited on the substrate usually using metal-organic vapour phase epitaxy (MOVPE) [50]. Figure 34 shows the layer sequence and composition. Other combinations are also possible. Lithography and etching steps are used to define the structure. The gasses and the processes employed are expensive resulting in higher cost of III–V high-efficiency cells. The MOVPE equipment is also very expensive and has lower throughput, adding to the overall cost. The laboratory scale efficiency achieved for triple-junction III–V cell is more than 40%. Commercial cells have achieved maximum efficiency of about 32% at present.

Similar to c-Si technology, III–V cells having diameter of about 100 mm are made first. These cells are then connected together to get a bigger system such as module. In this case, however, there is no standard module size. The cells are assembled directly on the final system such as solar panel for the spacecraft. In terrestrial applications, the cells are cut into small pieces and then assembled along with the concentrator, usually made of large lenses, to configure a CPV system.

5.4 Dye-Sensitized Solar Cell (DSSC)

Details of third-generation cell technologies are not taken up as the focus of this chapter is more on the commercial technologies. A brief description of DSSC is given in this section to bring out some basic understanding of such technologies.

Photosensitive dye such as ruthenium polypyridine dissolved in a suitable solvent is used in DSSC. The dye is coated with TiO_2 nano-particles of about 2 nm in size (diameter). These are immersed in an electrolyte, typically made of compounds of iodine dissolved in solvent such as acetonitrile (Fig. 35). Fluorine-doped Tin Oxide (FTO), which has a high conductivity, is used as one of the electrodes. FTO is transparent and allows the light to enter the cell. The other electrode uses a coating of platinum or carbon which also acts as a catalyst. During exposure with light, photons are absorbed by the dye and electrons and holes are produced as shown in Fig. 36. The electrons are moved to the TiO_2 conduction band (Fig. 36) and travel to the other side of the electrolyte through FTO, load and opposite electrode (Fig. 35). The holes get neutralized by the negative ions in the electrolyte. The negative ions are typically negatively charged iodide (I^-) or tri-iodide (I_3^-). The loss of negative charges in iodide gets compensated by the electrons entering the electrolyte from the opposite side of the transparent electrode. The coating of platinum or carbon acts as a catalyst to help the conversion of iodide or tri-iodide to negative ions. The electron flowing through the load produces current which is similar to short-circuit current (I_{SC}) if $R_{\text{L}} = 0$. The open-circuit voltage (V_{OC}) gets decided by the potential difference between the conduction band of TiO_2 and the negative ion. The negative ion potential is also known as redox potential.

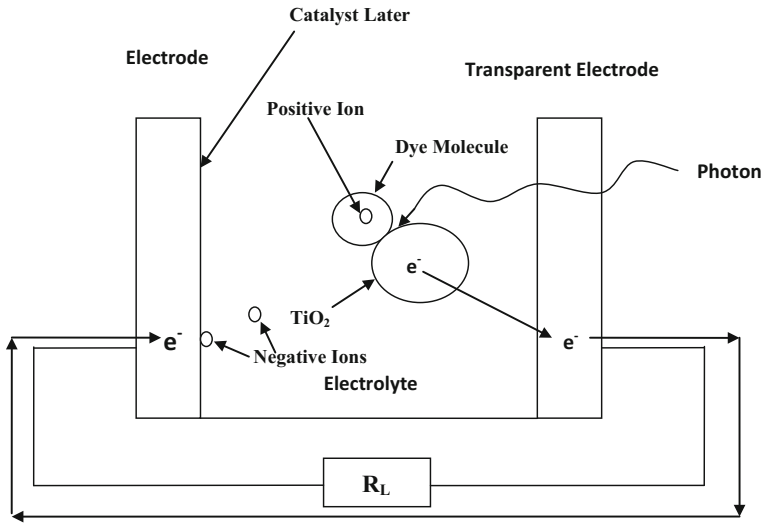


Fig. 35 Representative structure of dye-sensitized solar cell (DSSC)

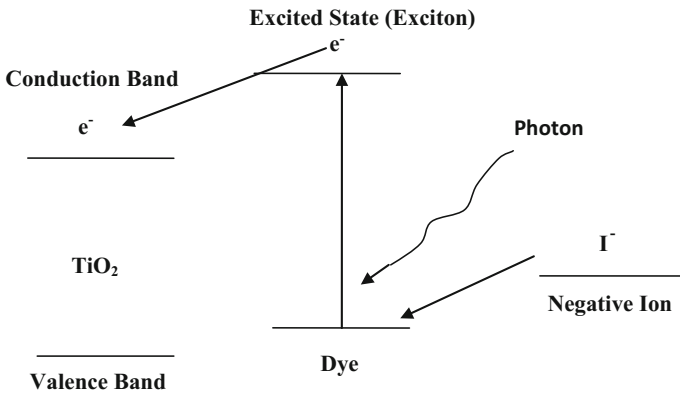


Fig. 36 Energy levels applicable to dye-sensitized solar cell (DSSC)

References

1. Masters GM (2013) Renewable and efficient electric power systems. IEEE Press, Wiley, Hoboken
2. Boyle G (2004) Renewable energy. Oxford University Press, Oxford
3. Nelson V (2011) Introduction to renewable energy. CRC Press, Boca Raton
4. Foster R, Ghassemi M, Cota A (2010) Solar energy, renewable energy and environment. CRC Press, Boca Raton
5. Markvart T, Castaner L (2005) Practical handbook of photovoltaics: fundamentals and applications. Elsevier, Oxford
6. Green MA (1995) Silicon solar cells: advanced principles and practice. Bridge Printery, Sydney
7. Street RA (2005) Hydrogenated amorphous silicon. Cambridge University Press, Cambridge
8. Ahmed G, Mandal S, Barua AK, Bhattacharya TK, Roy JN (2017) Band offset reduction at defect-rich p/i interface through a wide bandgap a-SiO: H buffer layer. *IEEE J Photovoltaics* 7 (2):414–420
9. Staebler DL, Wronski CR (2004) Intrinsic and light induced gap states in a-Si: H materials and solar cells—effects of microstructure. *Thin Solid Films* 451–452:470–475
10. Cusano DA (1963) CdTe solar cells and photovoltaic heterojunctions in II–VI compounds. *Solid State Electron* 6:217
11. Fardi H, Buny F (2013) Characterization and modeling of CdS/CdTe heterojunction thin film solar cell for high efficiency performance. *Int J Photoenergy* 2013. Article ID: 576952
12. Ikegami S (1988) CdS/CdTe solar cells by the screen-printing-sintering technique: fabrication, photovoltaic properties and applications. *Solar Cells* 23(1–2):9–105
13. Ohlsen HJ, Bodegard M, Kylner A, Stolt L, Hariskos D, Ruckh M, Schock HW (1993) ZnO/CdS/Cu(In,Ga)Se₂ thin film solar cells with improved performance. In: *Proceedings of 23rd IEEE photovoltaic specialists conference*, pp 364–371
14. Kronik L, Cahen D, Schock HW (1998) Effects of sodium on polycrystalline Cu (In, Ga)Se₂ and its solar cell performance. *Adv Mater* 10:31–36
15. Gratzel M (2003) Dye sensitized solar cells. *J Photochem Photobiol C Photochem Rev* 4:145–153
16. Nazeeruddin MK, Snaith HK (eds) (2015) Perovskite photovoltaics. *MRS Bull* 40(8)
17. Cui M, Chen N, Yang X, Wang Y, Bai Y, Zhang X (2009) Thermal analysis and test for single concentrator solar cells. *J Semicond* 20:4
18. Sze SM (1985) Semiconductor devices—physics and technology. Wiley, New York
19. Sharps PR, Stan MA, Aiken DI, Clevenger B, Hills JS, Fatemi NS (2003) Multi-junction cells with monolithic bypass diodes. In: *World conference on photovoltaic energy conversion*, pp 626–629
20. Nazeeruddin MK, Snaith HK (eds) (2015) High efficiency tandem solar cells. *MRS Bull* 40 (8):681
21. Taguchi M, Yano A, Tohoda S, Matsuyama K, Nakamura Y, Nishiwaki T, Fujita K, Maruyama E (2014) 24.7% record efficiency HIT solar cell on thin silicon wafer. *IEEE J Photovoltaics*, 4(1):96–99
22. Rob WA, Pollard A, Pearce JM (2013) Photovoltaic system performance enhancement with non-tracking planar concentrators: experimental results and BDRF based modelling. In: *39th IEEE photovoltaic specialists conference*, p 229
23. Sam-Shajing S, Niyazi Serdar S (eds) (2005) Organic photovoltaics: mechanisms, materials, and devices (optical engineering). CRC Press, Taylor & Francis Group, Boca Raton
24. Bose DN (2012) Organic photovoltaics in semiconductor materials and devices. New Age, Delhi, p 743
25. Kojima A, Teshima K, Shirai Y, Miyasaka T (2009) Organometal halide perovskites as visible-light sensitizers for photovoltaic cells. *J Am Chem Soc* 131(17):6040

26. Chuang CHM, Brown P, Bulovic V, Bawendi MG (2014) Improved performance and stability in quantum dot solar cells through band alignment engineering. *Nat Mater* 13:796–801
27. Zemen Y, Schulz SC, Trommler H, Buschhorn ST, Bauhofer W, Schulte K (2013) Comparison of new conductive adhesive based on silver and carbon nanotubes for solar cells interconnection. *Sol Energy Mater Sol Cells* 109:55–159
28. Macdonald DH, Cuevas A, Kerr MJ, Samundsett C, Ruby D, Winderbaun S, Leo A (2004) Texturing industrial multi-crystalline solar cells. *Sol Energy* 76:277–283
29. Campbell P (1990) Light trapping in textured solar cells. *Sol Energy Mater Sol Cells* 21:165–172
30. George M, Chandra H, Morse P, Morris J, Madocks J (2008) Silicon nitride ARC thin films by new plasma enhanced chemical vapour deposition source technology. In: *IEEE photovoltaic specialist conference*, pp 1641–1647
31. Dutttagupta S, Ma F, Hoex B, Mueller T, Aberle AG (2012) Optimized antireflection coating using silicon nitride on textured silicon surfaces based on measurements and multidimensional modelling. In: *International conference on materials for advanced technologies*, vol 15, pp 78–83
32. Roy JN (2015) Modeling of insulation characteristics of Solar Photovoltaic (SPV) modules. *Sol Energy* 120:1–8
33. Roy JN, Gariki GR, Nagalakshmi V (2010) Reference module selection criteria for accurate testing of photovoltaic (PV) panels. *Sol Energy* 84:32–36
34. Roy JN (2016) Comprehensive analysis and modeling of cell to module (CTM) conversion loss during c-Si Solar Photovoltaic (SPV) module manufacturing. *Sol Energy* 130:184–192
35. Magnone P, Rose RD, Tonini D, Frei M, Zanucoli M, Belli A, Galiazzo M, Sangiorgi E, Fiegna C (2014) Numerical simulation on the influence of via and rear emitter in MWT solar cell. *IEEE J Photovolt* 4:1032–1039
36. Kiefer K, Ulzhofer C, Brendemuhl T, Harder NP, Brendel R, Mertens V, Bordihn S, Peters C, Muller JW (2011) High efficiency n-type emitter wrap through silicon solar cells. *IEEE J Photovolt* 1:49–53
37. Fenner DB, Biegelsen DK, Brinquans RD (1989) Silicon surface passivation by hydrogen termination: a comparative study of preparation methods. *J Appl Phys* 66:419–424
38. Wang F, Zhang X, Wang L, Wei C, Sun J, Zhao Y (2014) Role of hydrogen plasma pretreatment in improving passivation of the silicon surface for solar cells applications. *ACS Appl Mater Interfaces* 10:15098–15104
39. Wang ZA, Green MA (1994) Series resistance caused by the localized rear contact in high efficiency silicon solar cells. *Sol Energy Mater Sol Cells* 32:89–94
40. Zhao J, Wang A, Green MA (1999) 24.5% efficiency silicon PERT cells on MCZ substrates and 24.7% efficiency PERL cells on FZ substrate. *Prog Photovolt Res Appl* 7:471–474
41. Roder TC, Eisele SJ, Grabitz P, Wagner C, Kulushish G, Kohler JR, Werner JH (2010) Add-on laser tailored selective emitter solar cells. *Prog Photovolt Res Appl* 18:505–510
42. Antoniadis H, Jiang F, Shan W, Liui Y (2010) All screen printed mass produced silicon ink selective emitter solar cells. In: *Proceedings of photovoltaic specialist conference (PVSC)*, pp 1193–1196
43. Zanucoli M, Magnone P, Sangiorgi E, Fiegna C (2015) Analysis of the impact of geometrical and technological parameters on recombination losses in interdigitated back contact solar cells. *Sol Energy* 116:37–44
44. Bunea G, Xavier G, Rose D, Nelson L, Peurach J (2010) Performance and reliability of modules with antireflective coated glass. In: *Proceedings of 25th EUPVSEC*, pp 4103–4106
45. Wohlgemuth J, Cunningham D, Shaner J, Nguyen A, Ransome S, Artigeo A (2015) Crystalline silicon photovoltaic modules with antireflective coated glass. In: *Proceedings of IEEE Photovoltaic Conference (PVSC)*, pp 1015–1018
46. Mickiewicz RA, Cahill E, Wu PI (2012) Non-destructive determination of degree of cross linking of EVA solar module encapsulation using DMA shear measurements. In: *Proceedings of photovoltaic specialist conference (PVSC)*, pp 710–713

47. Su WS, Chen YC, Liao WH, Huang CH, Liu DC, Huang MY, Wu ZC, Ho SJ (2011) Optimization of the output power by effect of backsheet reflectance and spacing between cell strings. In: Proceedings of IEEE photovoltaic specialist conference (PVSC), pp 3218–3220
48. Poulek V, Strebekor DS, Persie IS, Libra M (2012) Towards 50 years lifetime of PV panels laminated with silicone gel technology. *Sol Energy* 86:3103–3108
49. Geisza JF, Friedmann DJ, Ward JS, Duda A, Olavarria WJ, Moriarty TE, Kiehl JT, Romero MJ, Norman AG, Jones KM (2008) 40.8% efficiency inverted triple-junction solar cell with two independent metamorphic junctions. *Appl Phys Lett* 93:123505-1-3
50. Stringfellow GB (1999) *Organometallic vapor-phase epitaxy: theory and practice*, 2nd.edn. Academic Press, New York

Microgrids

N. K. Kishore, Saroja Kanti Sahoo and A. K. Sinha

Abstract A microgrid is an aggregation of distributed generating units, distributed energy storage, sensitive and non-sensitive loads, smart switches, communication facility, automation capability, and centralized/decentralized control system. It is capable of operating in grid-connected as well as islanded mode. The remotely located load centers are highly benefitted with the development of microgrid at these locations. Solar and wind energy can be harnessed using the power electronics-based converters with an associated control system. Additionally, energy storage devices in the microgrids improve the power supply reliability during generation deficit conditions in the islanded mode of operation. This chapter addresses the attributes of such systems, its architecture, control issues, and developments around the world.

Keywords Distributed generation · Energy storage units · Voltage source converters · Microgrid controllers

1 Introduction

Electricity is perhaps the third most important commodity, next to only air and water. Day by day demand is increasing. Traditionally, the power system forms the centrally controlled network with generators located close to the source of energy and load centers being large cities, very far from power plants. Sources, being predominantly coal, oil, natural gas, and water. Of these, first three are fossil based

A. K. Sinha: Deceased on 31 March, 2017.

N. K. Kishore (✉) · S. K. Sahoo · A. K. Sinha
Department of Electrical Engineering, Indian Institute of Technology
Kharagpur, Kharagpur, India
e-mail: kishor@ee.iitkgp.ernet.in

S. K. Sahoo
e-mail: sarojaksahoo@ee.iitkgp.ernet.in

fuels and polluting, necessitating centralized remote location of power plants. While hydro generation depends on the source and head of water, making it again centrally located. It necessitates transmission over long distances leading to line losses. These inefficiencies, together with pollution and depleting fossil fuels, have increased developments in renewable energy sources based on solar and wind energy predominantly. Global cumulative installed capacity of the wind and solar power in 2014 country-wise is shown in Figs. 1 [1] and 2 [2], respectively.

To improve efficiencies, the renewable sources being clean are being located close to loads giving rise to distributed energy resources or also termed as a dispersed generation (DG) into the fore. This has brought into the development of such localized grids including DG that operates in isolation and also in grid-connected mode being called microgrids. Such an interconnection necessitates suitable control and monitoring techniques for effective delivery of power supply. This article is an attempt at collating state of the art on microgrids an interesting developing trend in the delivery of electric power supply to the readers. A formal definition from the Conseil International des Grands Réseaux Electriques or (CIGRE) states [3].

Microgrids are electricity distribution systems containing loads and distributed energy resources (such as distributed generators, storage devices, or controllable

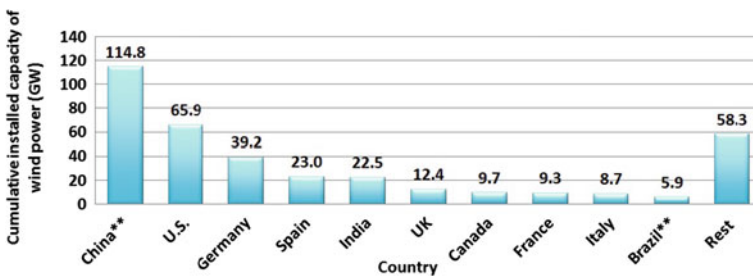
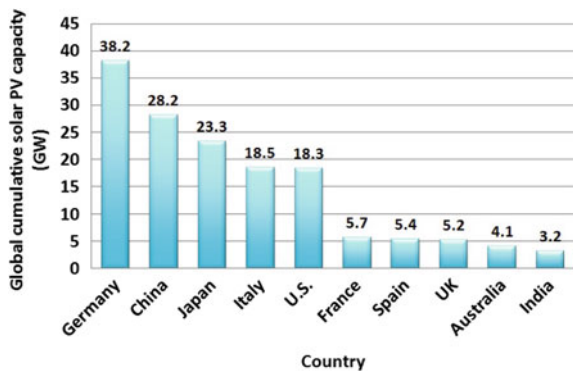


Fig. 1 Global cumulative installed capacity of wind in 2014 (country-wise) [1]

Fig. 2 Global cumulative installed capacity of solar PV in 2014 (country-wise) [2]



loads) that can be operated in a controlled, coordinated way either while connected to the main power network or while islanded.

Although, the definition does not require a mix of different types of Distributed Energy Resource technologies involved, and in fact, many microgrids also include a combination of resources and can take quite complex forms. There is hardly any guidance given on the size of microgrids regarding geographical extent or size. However, the definition does focus on the following two attributes:

- As opposed to centralized control in traditional grid a localized control;
- Ability to operate synchronously with a mega-grid (traditional grid) or in an Islanded manner.

Based on the nature of power, a microgrid can be classified as AC, DC, and hybrid AC–DC microgrid. Since the modern distribution system is AC in nature, AC microgrid is most commonly found experimental test beds around the world. AC microgrid has some advantages over other microgrids, such as its potential to easily transform voltages at various levels, accommodation of AC inertial machines with less power conversion requirement, and its long-distance power transmission capability without power electronics converters. Some issues with an AC microgrid are related to power quality, unbalanced networks/loads, and grid synchronization issues. A DC microgrid has a common DC bus for accommodating DC/AC-based sources, storage units, and loads. It is preferable when the system has a large number of DC loads and generation. In this case, the inverter and transformer losses are reduced. Further, in DC microgrid, loads are free from power quality and grid synchronization issues. However, DC microgrid protection is challenging due to the absence of zero current crossing. A hybrid microgrid combines the advantages of an AC and DC microgrids. An interlinking converter usually connects a DC subgrid with AC subgrid, and flexible power transfer occurs between them by using proper control. This section has brought out the importance of microgrid, a formal definition of microgrid and major attributes. It emphasizes a need for a good control to be able to operate effectively in stand-alone mode as well as when connected to a mega-grid. As a result, of the two major attributes involved, a new here to unseen feature, of bidirectional power flow comes up unlike in traditional grids where power flows from the grid to load. All this calls for a new philosophy of control, monitoring, and protection. Next section discusses microgrid architecture. That is followed by the mathematical modeling of microgrids. Control – a very central focus of the topic is covered in Sect. 4. The article would be incomplete without a survey of efforts made in developing microgrids. Hence, an overview of efforts made is covered in Sect. 5. Summary of the article with takeaways is listed in Sect. 6. Conclusion follows in Sect. 7.

2 Microgrid Architecture

A typical AC microgrid consists of distributed generation (DG) units with power electronic-based converters as interfaces, energy storage devices such as batteries and super capacitors, microgrid controllers, AC or DC loads, static switch, and distribution lines. Figure 3 shows schematic representation and architecture of a typical AC microgrid. The electricity sources other than the utility in the figure are described below:

- Solar photovoltaic (PV) system with DC–DC converter and a voltage source converter as an interface with the grid at the point of interconnection [4];
- Wind energy-based sources such as DFIG with fractional rated back-to-back converter interface [5] and permanent magnet AC generator-based source with fully rated converters;
- Diesel generator is the auxiliary source which is used as an emergency inertial backup source;

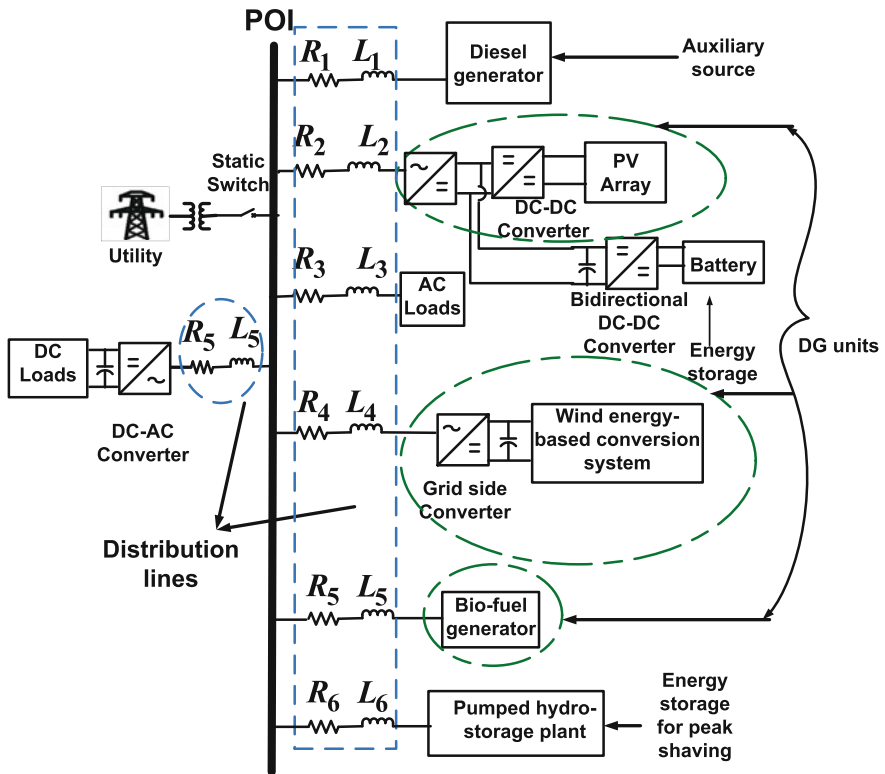


Fig. 3 A typical AC microgrid structure

- Battery as energy storage device for backup generation. It is observed to be connected to the DC bus of the PV source. Depending on excess (more than the threshold) or reduced (less than the threshold) state of charge (SOC), it can supply/consume power. Hence, during surplus generation and less SOC, it acts like a load. A bidirectional DC–DC converter operates in buck/boost mode during charging/discharging of the battery;
- Bio-energy-based sources such as biofuel generator, biomass-based generator, and biogas-based generator;
- Pumped hydro-storage power plant for acting as an energy storage and for the purpose of peak shaving.

In the next subsection, attributes of the AC microgrid components are described.

2.1 Distributed Generation

Distributed generation: DG units are the small-scale generating units with the rated capacity of few kW to MW, installed in the distribution systems at the feeders close to the end user [6, 7]. The DG units can be dispatchable like micro-turbines and diesel generators, whose output power can be controlled by the DNO (distribution network operator) [8]. The non-dispatchable DGs like PV system and wind turbines are stochastic and intermittent generating units. The non-dispatchable DG combined with energy storage can be used as a dispatchable unit. The dispatchable combined heat and power (CHP) units which feed both the electric and thermal loads increase the overall efficiency of the microgrid [8].

Benefits offered by DG integration are as follows:

- **Cogeneration:** Combined heat and power plants are being installed to provide both powers to the local loads and waste heat to the thermal loads. These are commonly located near heat utilizing consumer terminals, such as hotels, hospitals, and large industries which require heat for various operations. These plants replace the need for boiler and furnace arrangements at consumer end and also provide power locally.
- **Peak shaving:** The power requirement and the market price of power increases during peak hours of the daily load profile. DGs can maintain the continuity and reliability of power in the distribution network while reducing the power requirement from the utility side, during peak hours of demand. They reduce the economic burden on the customers by supplying electricity during the peak period.
- **Clean power:** The renewable energy-based DG units reduce the greenhouse gas emissions and hence provide clean power.
- **Ancillary services:** The DG units provide ancillary services by providing voltage and reactive power support, reduction in transmission losses, and as an emergency backup generation.

Disadvantages of DG integration are:

- **Voltage rise effect:** The effect of DG power output on voltage is determined by the amount of power flow from it. If the DG output exceeds the total loads, voltage rise is evident at the point of connection of DG. Centralized voltage control using load ratio control transformer and shunt capacitor is addressed in [9], and coordinated control with under-load tap changer (ULTC) and static synchronous compensator (STATCOM) usage is given in [10]. A probable centralized solution to maintaining voltage magnitude at substation bus is given in [10] by introducing an ANN-based coordination controller whose main objective is to minimize the tap changes of ULTC transformer and STATCOM output. Reactive power control with optimal references tracking for a decentralized solution is employed in [11] for PV-based DG, for voltage regulation, and distribution loss reduction. A comparison of centralized and decentralized voltage control problems can be found in [12].
- **Distribution system issues:** Overall enforcement of distribution grid infrastructure, voltage and reactive power management, improved distribution automation, protection and control is required with the integration of DGs.
- **Power quality:** DG connection in a lightly loaded feeder raises the voltage at the point of connection. The steady state voltage rise depends on X/R ratio, feeder load, and injected power [7, 13, 14]. Variation in load current causes variation in feeder current and voltage. The voltage distortion caused due to harmonics generated by inverter-based DGs deteriorates power quality [15].
- **Protection issues:** Problems associated with protection are the prohibition of automatic reclosing, unsynchronized reclosing, fuse–recloser coordination, islanding problems, blinding of protection, and false tripping [15]. Some of these protection issues are addressed with consideration of load voltage control, use of frequency relays, and adaptive overcurrent protection, respectively.

2.2 *Distributed Energy Storage (DES)*

DES units absorb the temporary mismatch between generation and loads, mainly in autonomous mode of operation. They stabilize and allow the DG units to operate at a constant output power despite load and generation fluctuations, provide peak shaving, smoothen the load profile, and permit DG to operate as a dispatchable unit. Batteries, pumped hydroelectric systems, compressed air energy storage, hydrogen storage, flywheels, supercapacitors, and superconducting magnetic energy storage systems are some examples of energy storage systems [16–18].

The energy storage elements can be classified as capacity-oriented and access-oriented energy storage systems [19]. The capacity-oriented energy storage systems do not have a fast transient response but provide long-term generation and load balancing. For example, batteries, pumped hydroelectric systems, compressed air energy storage, and hydrogen storage are capacity-oriented energy storage systems. The access-oriented energy storage systems have a faster transient response and high power density and are used for mitigating short-term high-frequency power transients. For example, flywheels, supercapacitors, and superconducting magnetic energy storage systems are access-oriented energy storage units [17, 18]. The supercapacitors have a higher power density and faster response compared to other DES units and are used for short-term power balancing during transients in a microgrid [8, 18]. A flywheel has high energy density, is environment-friendly, and can provide energy for an extended period. However, it has high standby loss and large volume [20]. Very high-speed (up to 60,000 r/min) flywheel energy storage with superconducting magnetic bearings has reduced inertia and friction losses for the same amount of energy storage for flywheels with mechanical bearings [21].

2.3 *Microgrid Loads*

The microgrid loads [8, 16, 22] can be classified as:

- **Controllable load:** They can adjust their power consumption according to the operating condition of the microgrid. These loads are capable of supplying power to the microgrid under emergency conditions. In case of generation and load mismatch, the controllable loads absorb or deliver power according to the prevailing surplus or deficit generation conditions in the microgrid. This way, the magnitude and frequency of the terminal voltages of the microgrid are maintained within the required limits. The necessity of these loads is required for smooth and reliable functioning of an islanded microgrid. Energy storage units like batteries, plug-in electric vehicles (PEV), combined cooling, heating, and power (CCHP), and plug-in hybrid electric vehicles (PHEV) are some examples of controllable loads.
- **Critical load:** The critical/sensitive loads need an uninterruptible power supply. They are given highest priority service from the microgrid side. Schools, industry, and hospitals are some examples of critical loads.
- **Sheddable load:** Sheddable loads are the non-critical loads which are the lowest in priority. The load curve can be altered by lowering the load demand. These loads are not capable of injecting power to the microgrid and are hence also known as passive controllable loads [22]. Residential loads such as fridges, washing machines, and water heaters are some examples of these loads.

2.4 Point of Interconnection (POI)

The node at which the DGs are connected to the host grid by a distribution feeder is known as a point of interconnection (POI) [8]. The POI as shown in Fig. 3 is a crucial node as it may be affected by the upstream grid disturbances unless islanded. Further, if unbalanced loads are connected at the POI, voltage unbalance control becomes necessary at the node. Similarly, harmonic compensation is also a requirement under severe voltage distortion, in the presence of large nonlinear loads.

3 Mathematical Modeling of Microgrid

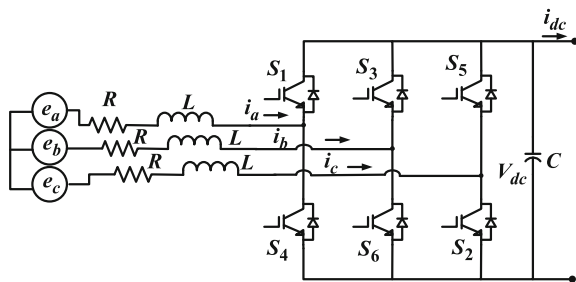
The modeling of a microgrid will involve the source modeling with power electronics-based interfaces, implementation of controllers to regulate DC bus voltage, AC side terminal voltages, output current to allow flexible active and reactive power flow. Voltage source converters (VSCs) and their controllers are the crucial components of an AC microgrid. In the following section, mathematical modeling is commenced from the voltage source converters.

Here, a two-level VSC as shown in Fig. 4 is considered for mathematical modeling and analysis. A single-phase leg of a VSC consists of two switches consisting of a combination of an insulated-gate bipolar transistor (IGBT) switching device and an antiparallel diode at the top (positive terminal) and bottom (negative terminal) of the input side. A switching function of the switch S_{tm} is defined as [23, 24]:

$$sw_{tm} = \begin{cases} 1, & \text{when switch } S_{tm} \text{ is closed} \\ 0, & \text{when switch } S_{tm} \text{ is open} \end{cases} \quad (1.1)$$

where t represents the phase, and variable $m = p, n$ is used to identify the upper and lower elements of the phase leg. In case of a three-phase VSC, $t = a, b, c$. The switch S_{tm} operates whenever IGBT or diode of the upper or lower side is on. There

Fig. 4 Schematic of a grid-connected voltage source converter



is a constraint on the on/off of the switch in each leg, which allows only either of the switch (sw_t) to be on or off. This can be represented by the following relationship.

$$sw_{tp} + sw_{tn} = 1 \quad (1.2)$$

A phase switching function hints about the connection of the output terminal of VSC (point t) to the positive or negative potential of DC link voltage. It can be represented as follows.

$$sw_t = \begin{cases} 1, & \text{when switch } S_t \text{ is connected to point p} \\ -1, & \text{when switch } S_t \text{ is connected to point n} \end{cases} \quad (1.3)$$

Transformation from stationary reference frame ($\alpha - \beta$) to synchronously rotating reference frame ($d - q$) is given below.

$$\bar{x}_{dq} = \bar{x}_{\alpha\beta} e^{-j\theta} \quad (1.4)$$

Applying Kirchoff's current law and voltage law across the DC bus capacitor (C) and filter inductor (L) respectively, as shown in Fig. 4, the equations obtained in complex vector notation for a grid-connected VSC are given as:

$$C \frac{dV_{dc}}{dt} = \frac{3}{2} \operatorname{Re} \bar{i}_{dq} \overline{sw}_{dq} - i_{dc} \quad (1.5)$$

$$L \frac{d\bar{i}_{dq}}{dt} + R\bar{i}_{dq} = \bar{e}_{dq} - V_{dc} \overline{sw}_{dq} \quad (1.6)$$

Separating the above equation in synchronous rotating reference $d - q$ frame:

$$C \frac{dV_{dc}}{dt} = \frac{3}{2} (i_d sw_d + i_q sw_q) - i_{dc} \quad (1.7)$$

$$L \frac{di_d}{dt} + \omega L i_q + R i_d = e_d - V_{dc} sw_d \quad (1.8)$$

$$L \frac{di_q}{dt} - \omega L i_d + R i_q = e_q - V_{dc} sw_q \quad (1.9)$$

Mathematical equations governing operation of an islanded VSC shown in Fig. 5 are given as follows [25]:

$$C_f \frac{d\bar{V}_{C_{dq}}}{dt} = \bar{i}_{dq} - \bar{i}_{L_{dq}} \quad (1.10)$$

Separating the above equations in synchronous reference frame d and q axis separately, are given by:

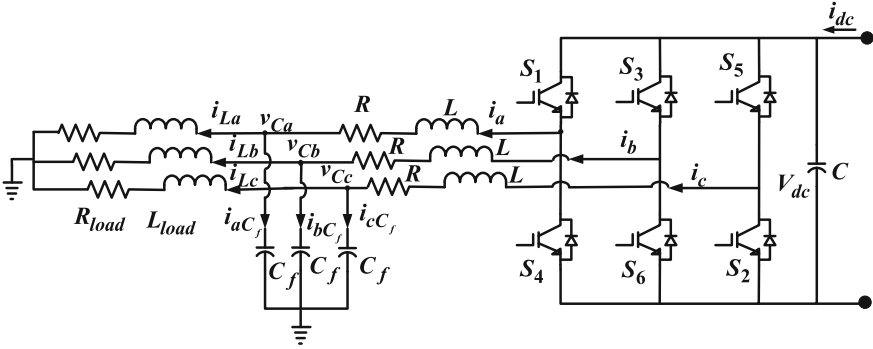


Fig. 5 Schematic of an islanded voltage source converter

$$C_f \frac{dV_{C_d}}{dt} = i_d - i_{L_d} + \omega C_f V_{C_d} \quad (1.11)$$

$$C_f \frac{dV_{C_q}}{dt} = i_q - i_{L_q} - \omega C_f V_{C_q} \quad (1.12)$$

where V_{dc} is the DC bus voltage, e_{dq} , i_{dq} and $V_{C_{dq}}$ are $d - q$ frame transformation of grid voltages (e_{abc}), grid currents (i_{abc}) and filter capacitor voltages ($V_{C_{abc}}$) respectively. C_f is the filter capacitor. sw_{dq} is the switching function in $d - q$ frame.

4 Microgrid Controllers

The control system of a microgrid forms a crucial component of the system. There are primarily three categories of control achieved hierarchically.

They are:

1. Primary level of control;
2. Secondary level of control;
3. Tertiary level of control.

The primary level consists of control of VSC coupling inductor current and maintaining DC bus voltage in grid-connected mode. In the islanded mode, the VSC terminal voltages are regulated based on their droop characteristics. The bandwidth of the current control loop is greater than the bandwidth of the outer voltage control loop. The current control loop bandwidth is usually limited to one-tenth of the switching frequency. A typical primary level control consisting of a power-sharing controller, voltage controller, and current controller is shown in Fig. 6 [26]. Secondary level control restores frequency and magnitude deviations in the output voltage of the VSC. The tertiary level control is used to generate optimal set points for the secondary control level. In the grid-connected mode, the tertiary

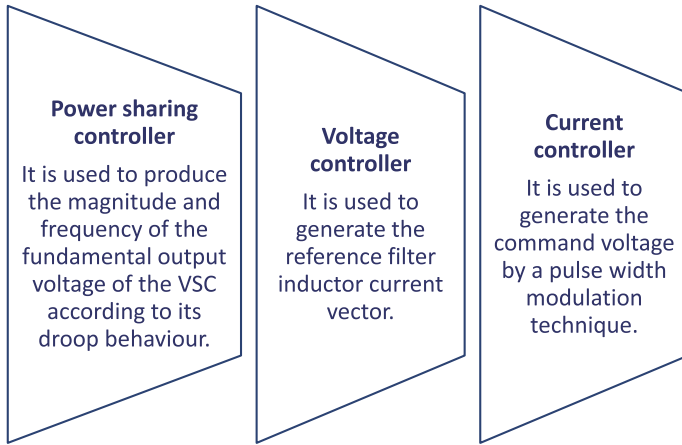


Fig. 6 Primary control of a VSC in a microgrid [26]

control determines the power set points as required by the main grid, for the optimal operation of the microgrid. This is illustrated in the schematic given in Fig. 7 and a schematic illustrating the hierarchical control objectives in Fig. 8. The frequency and magnitude of output voltage of the VSC are determined by the host grid in grid-connected mode. However, they are internally generated in the secondary control loop in islanded mode of operation [27]. Notations used in Fig. 7 can be defined as: P^* and Q^* are the active and reactive power references at the point of interconnection of microgrid, set by the grid, P and Q are the measured active and reactive powers at the POI, ω_{ref} and E_{ref} are the frequency and magnitude references set internally in the secondary control in islanded mode. The compensators $H_p(s)$, $H_q(s)$, $H_f(s)$, and $H_v(s)$ are used to regulate the active power flow, reactive power flow, frequency and voltage control at the microgrid POI.

A block diagram representation of the current control loop is observed in Fig. 9. The gains and time constants incorporated in the block diagram are as follows [25]:

- T_s is the sampling time.
- V_{dis} is the disturbance voltage.
- K_i is the gain of the PI controller.
- T_i is the time constant of the PI controller.
- K_{PWM} is the gain of the pulse width modulator.
- T_{PWM} is the time constant of the pulse width modulator.
- K_{RL} is the gain of the R-L load.
- T_{RL} is the time constant of the R-L load.

The overall control block diagram in grid-connected mode is shown in Fig. 10: The gains and time constants incorporated in the block diagram shown in Fig. 10 are as follows [25]:

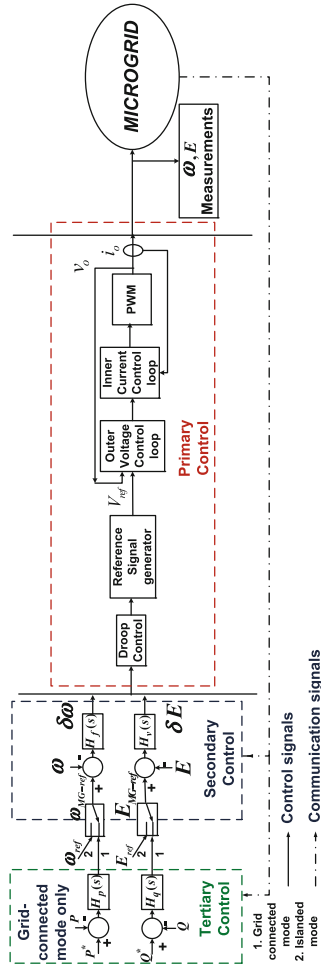


Fig. 7 Hierarchical control system in an AC microgrid [27]

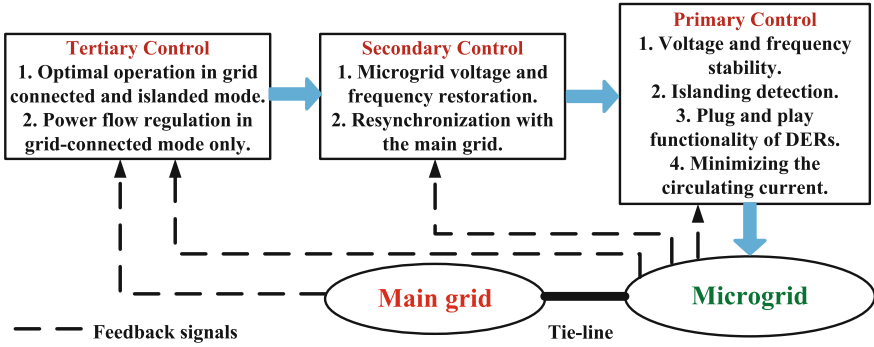


Fig. 8 Schematic of hierarchical control objectives with respect to microgrid and main grid

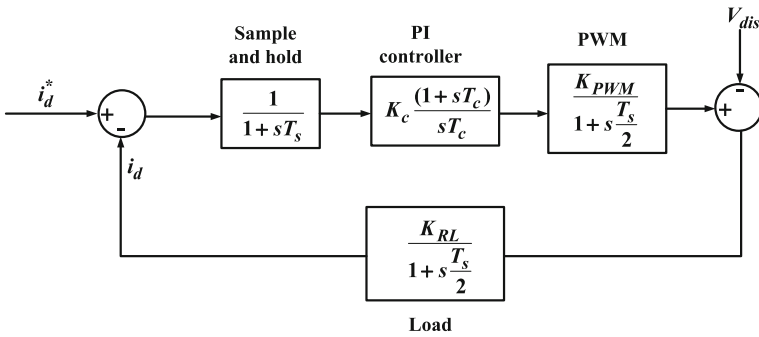


Fig. 9 Block diagram of current control loop [25]

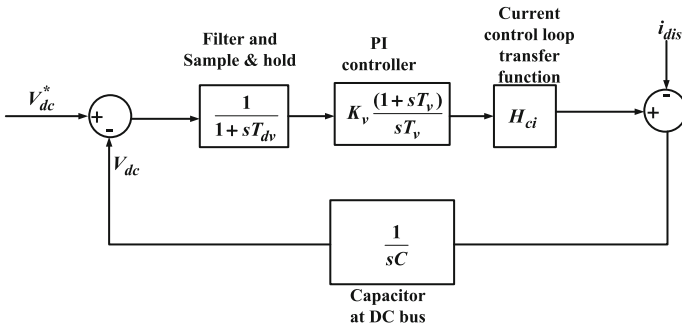


Fig. 10 Block diagram of overall control with DC bus voltage control loop [25]

- T_{dv} is the feedback loop delay due to sampling, operating time, and feedback filter.
- K_v is the gain of the PI controller.
- T_v is the time constant of the PI controller.
- The inner current control loop is represented by the first-order transfer function H_{ci} .

The differences between a typical AC and DC microgrid controller are shown in Table 1.

An overview of the primary controllers consisting of inner current controllers and droop control techniques is discussed in the upcoming Sects. 4.1–4.3, respectively.

4.1 Inner Current Controllers

Inner current control loops form the group of fast controllers with higher bandwidth than the outer voltage control loop. An overview of different inner current controllers is described below.

4.1.1 Proportional–Integral–Derivative (PID) Controller

The family of the proportional–integral–derivative (PID) controllers has been used for control of many industrial processes. The PID controller invention dates back to 1910 as a part of Elmer Sperry’s ship autopilot [28]. They are simple in application and easy to use for a complicated plant. The transfer function of a standard PID controller is given as [28]:

Table 1 Comparison of AC and DC microgrid attributes

Attributes	AC microgrid	DC microgrid
Grid synchronization	Required	Not required
Reactive power control	Required	Not required
Droop characteristics	P - f droop	P - V droop
Protection aspect	Zero current crossing detection possible.	Zero current crossing detection is not possible
Voltage transformation	Transformers	DC–DC converters
Voltage stability	It can be achieved by reactive power control without affecting active power flow	It is dependent on active power flow

$$G(s) = K_p + K_i \frac{1}{s} + K_d s \quad (1.13)$$

where K_p is the proportional gain, K_i is the integral gain, and K_d is the derivative gain. The proportional gain provides an overall control, integral gain reduces steady state error, and derivative gain improves the transient response. Increasing the proportional and integral gain unreasonably may lead to instability, while derivative gain improves the stability of the system. To avoid actuator saturation, anti-windup action can be integrated with PID controllers. Anti-wind up mechanism reduces integrator saturation by feeding it a negative feedback which is obtained as the difference between the control signal before saturation and after saturation through a compensator. Fractional PID ($PI^{\lambda}D^{\mu}$) is an extension of traditional PI and was introduced by I. Podlubny in 1994 [29]. It can achieve iso-damping quite easily and is less sensitive to parameter variation of the controlled system. A typical PID operation with variation in proportional, integral, and derivative gains separately and in combination is illustrated in the [Appendix](#).

4.1.2 Proportional-Resonant (PR) Controllers

The primary objective of a PR controller is to put forward an infinite gain at a chosen resonant frequency to do away with the steady state error [30]. The PR controller is comparable to a generalized AC integrator and is mathematically represented by the transfer function $G_{PR}(s)$ as:

$$G_{PR}(s) = \frac{2K_i \omega_c s}{s^2 + 2\omega_c s + \omega_c^2} \quad (1.14)$$

where K_i is the controller gain, ω_c is the cutoff frequency, and ω is the signal frequency. This when grouped with proportional gain K_p forms a non-ideal PR controller.

4.1.3 Sliding Mode Controllers (SMC)

Sliding mode control is a category of nonlinear control which is primarily developed for the control of variable structure systems. The main purpose for using SMC is to guarantee stability and robustness against parameter variation. The sliding mode controller is realized by using the relay, signum function, and hysteresis functions. Traditional SMC suffered from chattering problem, and this was solved by modifying the SMC in various ways. It is characterized by tracking a trajectory known as sliding manifold in reaching phase, later sliding on the plane, and descending on the stable equilibrium point. The chosen trajectory $S_T(x, t)$ is usually

taken as a linear combination of weighted values of the state variables and is represented as [31]:

$$S_T(x, t) = \sum_{i=1}^n a_i x_i(t) \quad (1.15)$$

4.1.4 Predictive Controller

Predictive control uses the model of the system for predicting the anticipated behavior of the controlled variable [32]. It uses the system model data to obtain optimal control action by solving a predefined optimization problem. The hysteresis-based predictive control keeps the controlled variables inside the range of the hysteresis area. While in trajectory-based control, the controlled variables have an obligatory trajectory to follow. The model predictive control uses cost function minimization as a major objective of the optimization problem [33]. Out of these controllers, deadbeat and model predictive control require a modulator to produce the necessary voltage, resulting in fixed switching frequency [32].

4.2 Conventional Droop Methods

Conventional droop strategies like P - f and Q - V droop methods are employed for controlling frequency and voltage of the islanded microgrid [34, 35]. If $V_{\text{mg}} \angle 0$ and $E \angle \delta$ be grid and converter voltage, respectively, and assuming δ is small, the active and reactive power expressions for an inductive line are proportional to converter output voltage phase angle and magnitude, as shown in (1.16) and (1.17), respectively.

$$P = \frac{V_{\text{mg}} E}{X} \delta \quad (1.16)$$

$$Q = \frac{V_{\text{mg}} E - V_{\text{mg}}^2}{X} \quad (1.17)$$

However, distribution networks are highly resistive in nature, and the conventional droop equations are not valid for them.

The equations for active and reactive powers for resistive lines are given by (1.18) and (1.19), respectively:

$$P = \frac{V_{\text{mg}} E}{R} \cos \delta - \frac{V_{\text{mg}}^2}{R} \quad (1.18)$$

$$Q = -\frac{V_{mg} V_i}{R} \sin \delta \tag{1.19}$$

The P - f droop characteristics permit frequency reduction of the output voltage with the increase in inverter real power output, while Q - V droop reduces the output voltage magnitude with the corresponding increase in [37] reactive power output in an islanded mode of operation of the microgrid as shown in Fig. 11.

The purpose of droop control is to mimic the inertial potential of alternators in conventional power plants to adjust the differences in generation and demand by regulating the frequency [36]. However, due to sudden grid disturbances and loss of utility, the frequency and voltage deviate from its nominal values leading to instability. The VSC output voltage frequency and magnitude reference are set according to [37].

$$w = w_o - D_1 P \tag{1.20}$$

$$V = V_o - D_2 Q \tag{1.21}$$

where w_o and V_o are the nominal angular frequency and rated VSC output voltage, and D_1 and D_2 are droop constants for the P - f and Q - V droop characteristics. D_1 and D_2 are given by (1.22) and (1.23), respectively [36].

$$D_1 = \frac{\omega_{max} - \omega_{min}}{P_{max}} \tag{1.22}$$

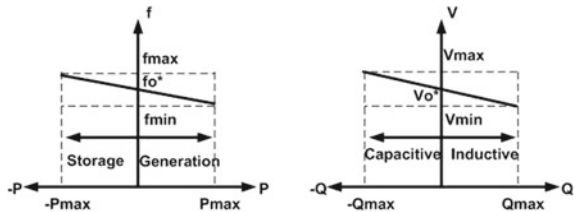
$$D_2 = \frac{V_{max} - V_{min}}{Q_{max}} \tag{1.23}$$

where ω_{max} and ω_{min} are the maximum and minimum system frequency limits imposed on the droop control. V_{max} and V_{min} are maximum and minimum voltage magnitude limits imposed on the droop control. P_{max} and Q_{max} are maximum allowable active and reactive power outputs from the concerned VSC-based distributed energy resource (DER).

The drawbacks of the conventional droop control techniques are [37–39]:

- The droop equations are applicable only for the highly inductive transmission system. They are not suited for low-voltage distribution networks which are highly resistive in systems.

Fig. 11 Conventional droop characteristics of a microgrid [37]



- A compromise has to be there between the time constant of the controller and the frequency regulation.
- Voltage regulation is poor for critical loads under reactive power control.
- It fails for nonlinear and single-phase loads.
- It may be subjected to load-dependent frequency deviation.
- Poor power sharing among the DER units due to unequal output impedance between DER and load.

4.3 Improved Droop Methods

Summary of the improved droop control methods is given in the sequel.

- **Voltage-Real Power Droop/Frequency-Reactive Power Boost (VPD/FQB) Droop Control:**

The VPD/FQB droop control proposed in [40] is applicable to low-voltage resistive distribution lines, where active power and voltage, and reactive power and frequency are coupled as seen in (1.24) and (1.25), respectively.

$$P = \frac{V_{\text{mg}}E - V_{\text{mg}}^2}{R} \quad (1.24)$$

$$Q = -\frac{V_{\text{mg}}E}{R} \delta \quad (1.25)$$

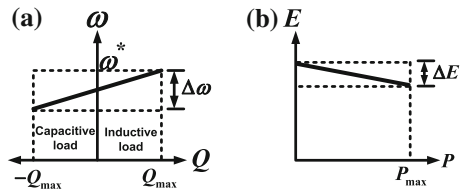
where V_{mg} and E are inverter-based DER output voltage and common AC bus voltage, respectively. V - P droop and F - Q boost characteristics are represented by (1.26) and (1.27), respectively, as shown in Fig. 12.

$$V_i = V_o - D_1 P \quad (1.26)$$

$$w_i = w_o + B_1 Q \quad (1.27)$$

$$B_1 = \frac{\Delta\omega}{2Q_{\text{max}}} \quad (1.28)$$

Fig. 12 Frequency-reactive power boost and voltage-real power droop characteristics



$$D_1 = \frac{\Delta E}{P_{\max}} \quad (1.29)$$

where w_o and V_o are the angular frequency and DER rms output voltage references values, and D_1 and B_1 are droop and boost coefficients for the $P - V$ and $Q - \omega$ droop characteristics. It significantly improves power sharing in low-voltage AC resistive lines, but it depends on system parameters and is unsuitable for nonlinear loads.

- **Reactive Power Differential of Voltage, $Q - V'$ droop Control:**

A $Q - V'$ droop control method is proposed in [41] for reactive power sharing independent of output line impedances. A voltage restoration loop regulates the output voltage by maintaining $V' = 0$. Equations governing the proposed droop control action are as given in (1.30) and (1.31), respectively.

$$V'_i = V'_{oi} - n(Q_{oi} - Q) \quad (1.30)$$

$$V_i = V_o + \int V'_i dt \quad (1.31)$$

where V_i is the output voltage, V' is the time rate of change of output voltage, V'_{oi} is the nominal V' , Q_{oi} is rated reactive power, and n is the droop constant.

- **Angle Droop Control:**

In [42, 43], the authors have proposed an angle droop control which has significantly low-frequency deviation compared to the frequency droop control. The phase angle measurements of the output voltage of the VSC rely upon low-bandwidth GPS-based communication techniques. However, it assumes an inductive impedance between the VSC and microgrid AC bus. A high angle droop gain with a supplementary control loop for a weak system is suggested in [43] for improving the load-sharing accuracy. The angle droop equations are expressed as:

$$\delta_i = \delta_{\text{rated}} - m_i(P_i - P_{i,\text{rated}}) \quad (1.32)$$

$$V_i = V_{\text{rated}} - n_i(Q_i - Q_{i,\text{rated}}) \quad (1.33)$$

where δ_{rated} and V_{rated} are rated VSC output voltage angle and magnitude, respectively; $P_{i,\text{rated}}$ and $Q_{i,\text{rated}}$ are rated active and reactive power outputs of the VSC, respectively; and m_i and n_i are droop coefficients.

- **Virtual Frame Transformation:**

Virtual frame transformation approach uses a linear orthogonal transformation matrix to refer the active and reactive power flow equations to a new reference frame, where they are independent of line impedance [44–46].

$$\begin{bmatrix} P_n \\ Q_n \end{bmatrix} = T_n \begin{bmatrix} P \\ Q \end{bmatrix} = \begin{bmatrix} \sin\theta & -\cos\theta \\ \cos\theta & \sin\theta \end{bmatrix} \begin{bmatrix} P \\ Q \end{bmatrix} \quad (1.34)$$

The transformed P_n and Q_n are replaced in the droop equation in (1.20) and (1.21), respectively. In the same way, frequency and amplitude of VSC output voltage is also transformed with respect to the virtual frame and the transformed variables ω_n and E_n are used for providing voltage magnitude and frequency references to the VSC voltage control loop.

$$\begin{bmatrix} \omega_n \\ E_n \end{bmatrix} = T_\omega \begin{bmatrix} \omega \\ E \end{bmatrix} = \begin{bmatrix} \sin\theta & \cos\theta \\ -\cos\theta & \sin\theta \end{bmatrix} \begin{bmatrix} \omega \\ E \end{bmatrix} \quad (1.35)$$

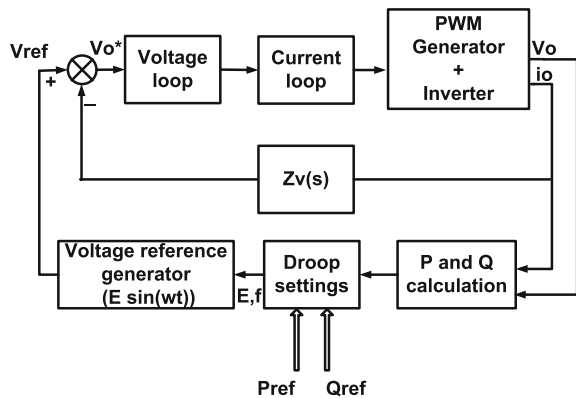
- **Virtual Impedance Method:**

The virtual impedance approach is used in [27, 47] which considers a virtual impedance in the feedback path of the voltage control loop as shown in Fig. 13. In this way, the inverter output voltage is controlled by adjusting the virtual impedance $Z_v(s)$. The VSC output voltage reference is set according to (1.36).

$$v_{\text{ref}} = v_o^* - Z_v(s)i_o \quad (1.36)$$

where v_o^* is the VSC output voltage at no-load, i_o is the output current, and $Z_v(s)$ is the virtual impedance. If $Z_v(s) = sL_v(s)$, the output voltage droops proportional to the derivative of the output current. However, when nonlinear loads are being supplied, the total harmonic distortion (THD) of the VSC output voltage would be high. To overcome this, a high-pass filter is used instead of sL_v as shown in (1.37).

Fig. 13 Primary control of an AC microgrid with virtual impedance in islanded mode [27]



$$v_{\text{ref}} = v_o^* - L_v \frac{s}{s + \omega_c} i_o \quad (1.37)$$

where ω_c is the corner frequency of the high-pass filter.

- **Adaptive Voltage Droop Control:**

In [48], a modified voltage droop is proposed which improves voltage regulation by eliminating the connecting impedances between VSC and point of voltage control. In this method, the voltage drop across the connecting impedances between VSC and common AC bus is included in the conventional Q - V droop control. The modified droop equation is expressed as given in (1.38):

$$V_i = \left(V_{oi} + \frac{r_i P_i}{V_{oi}} \right) - \left(D_q + \frac{x_i}{V_{oi}} \right) Q_i \quad (1.38)$$

where V_i , V_{oi} , and $(r_i + jx_i)$ are VSC drooped output voltage, no-load voltage, and connecting impedance between VSC and common AC bus, respectively. And D_q is the droop coefficient which is a quadratic function of active and reactive power outputs of the VSC.

- **Unbalanced Power Flow Control and Nonlinear Load Sharing:**

The adverse effect of the unbalanced power flow in lines can be overcome by high-frequency signal injection [49]. The proposed method is not influenced by system parameter variations and line impedance mismatches by injecting high-frequency control signal into the power distribution network. The frequency of this control signal is controlled by the quantity to be shared such as real, reactive, and distortion power.

$$\omega_q = \omega_{qo} + BQ \quad (1.39)$$

$$V_i = V_o - D_v p_q \quad (1.40)$$

where ω_{qo} and p_q are the nominal frequency and real power of the injected control signal, V_o is the VSC output voltage at no-load condition, B and D_v are boost and droop coefficients, respectively.

In the presence of nonlinear loads, the distortion power is shared by reducing the frequency of the injected control signal such that the bandwidth of the voltage loop is controlled.

$$BW = BW_o - D_{bw} p_d \quad (1.41)$$

where BW_o is the bandwidth of the outer voltage loop, p_d is the power in the injected signal for distortion power sharing, and D_{bw} is the droop coefficient.

The method proposed in [50] permits harmonic current sharing among paralleled converters without communication. Converter output harmonic voltage is controlled to be leading the output current by 90° . In the method presented in [51],

harmonic voltage derived from harmonic current and VSC output impedance for each harmonic frequency is added to the VSC reference voltage for removing the effect of harmonic voltage from the VSC output voltage. However, this harmonic droop controller needs computation of the harmonic voltage at each harmonic frequency to be compensated.

5 Microgrid Developments Around the World

With the advancement in power electronics technology, the development of microgrid is taking place around the world. Some of the examples of the microgrid test facility are described in the sequel.

5.1 CERTS Microgrid

The Consortium for Electric Reliability Technology Solutions (CERTS) is one of the most well-recognized microgrids operated by the American Electric Power. It is installed in the Dolan Technology Center in Columbus, Ohio, in the USA [16]. Members involved in the establishment of the microgrid include four DOE National Labs, Lawrence Berkeley National Laboratory (LBNL), Sandia National Laboratory (SNL), Oak Ridge National Laboratory (ORNL), and Pacific Northwest National Laboratory (PNNL); NSF's Power Systems Engineering Research Center; and the Electric Power Group [52]. It was formed in 1999 to improve the reliability and efficiency of the US electric power system. The dominant sources present are liquid-cooled natural gas-based permanent magnet generator [53]. The microgrid provides plug and play capability, and it can isolate from the host grid under severe grid disturbances using the fast acting static switch.

5.2 Microgrid Test Facility at University of Texas, Arlington

The researchers at the University of Texas have initiated the development of a microgrid test facility with a hierarchical control system on the campus [54]. The test facility is equipped with vertical axis wind turbines, solar panels, fuel cell, storage systems, diesel generator with grid availability. Embedded control system using National Instrument's (NI) CompactRIO has been used in the UTA microgrid [54]. The test bed consists of three sub-grids with central ring architecture capable of independent operation as a microgrid. It can operate in grid-tied, islanded mode and interconnected mode with the availability of lithium-ion batteries to provide ancillary services to the system.

5.3 Microgrid Test Facility at Illinois Institute of Technology

The Illinois Institute of Technology (IIT), smart grid prototype, is located near Comiskey Park in Chicago, Illinois, USA. The team comprises the IIT (lead organization), Exelon/Commonwealth Edison Company, S&C Electric Company, Intelligent Power Solutions, and the Galvin Electricity [55]. Initiative, and other power industry experts are aiming to build perfect power prototype with main objective as minimum outage (at least three power outages) per year. The campus peak load is around 10 MW, and the distributed energy resources including wind turbines, roof top solar, combined cycle gas units, and energy storage units are coming up to 9 MW [55]. The entire objective is to enhance the reliability of the campus microgrid and to make it operational in fully islanded condition.

5.4 Microgrid Setup at Kythnos Island

Kythnos Island Microgrid is generating power for 12 houses in Kythnos Island in the Cyclades Archipelago, of the Aegean Sea [16] in Greece. The generation system comprises of a 10 kW of PV, a nominal 53-kWh battery bank, and a 5-kW diesel gen set [16]. It is a single-phase residential microgrid having centralized and decentralized controllable features. Further, load management can be incorporated into the supervisory control by monitoring the battery SOC.

5.5 Microgrid Test Facility at University of California, San Diego (UCSD)

The UCSD microgrid project aims to supply power and facilitates heating and cooling for 450-hectare campus with a daily population of 45,000 [56]. It comprises of two 13.5 MW gas turbines, one 3 MW steam turbine, and a 1.2 MW solar cell installation that together caters 85% of campus power needs, 95% of its heating needs, and 95% of its cooling needs [56]. UCSD is installing a novel supervisory controller-Paladin, which will regulate all generation, storage, and loads with hourly computation to optimize the operating situations.

5.6 Microgrids in India

A Bangalore-based, for-profit social enterprise (SELCO Solar Light Private Limited) has installed solar storage remote DC microgrids to supply power in

Baikampady, Mangalore; Neelakantarayanagaddi Village, Mendare Village, and Kalker Sangeet Vidyalaya [57]. A microgrid is being operated by Indian Coast Guard in Andaman Island [57]. Another development is located in Sundarban region and is popularly known as Sagar Island Microgrid [58]. The project is being funded jointly by Ministry of New and Renewable energy (MNRE), Indo-Canadian Environment Facility (ICEF), and West Bengal Renewable Energy Development Agency (WBREDA) [58]. The microsourses in the Sagar Island include solar power of 250 kW and a diesel generator of 400 kW [58]. The Greenpeace India solar microgrid foundation of 100 kW is powering 450 homes of the 2400 residents, 50 commercial operations, two schools, a training center, and a health care facility, at Dharnai Village of Bihar state in India [59]. The Chief Ministers Official Residence in Bihar, India, is also powered by 125 kW solar microgrid [57].

6 Summary

The takeaways from this chapter are enumerated below:

1. The microgrid formation can help the remote load centers where the utility fails to supply power.
2. Solar and wind energy sources are highly intermittent, and hence, they should be installed with battery and auxiliary sources in remote locations.
3. Microgrids are incomplete without the power electronics-based converters such as DC–DC converters and VSCs, which are used as interfaces.
4. The controllers at the three levels of the hierarchy help in maintaining optimality and reliability of the system. Further, flexible active and reactive power supply is possible.
5. In stand-alone/islanded mode of operation, the VSC terminal voltage magnitude and frequency are regulated using conventional and improved droop control characteristics.
6. The hurdles faced in accurate power sharing in islanded mode are due to unknown line impedances between VSC and common AC bus, unbalance and nonlinear loads, and highly resistive lines. Some of the solutions provided in the literature are including virtual resistance/impedance in the feedback output path, harmonic current sharing, and adaptive voltage control.
7. Laboratory level developments of the microgrid are taking place globally for research on the various issues in it. CERTS microgrid is one of the earliest developments of a test facility in Ohio, USA.

7 Conclusion

The rapid depletion of fossil fuel and proliferation of renewable energy sources has led to the development of microgrid. This chapter has attempted to highlight the major issues, control attributes, and developments around the world. A discussion on the structure of the microgrid, which includes DG units and its integration issues, energy storage benefits, and different microgrid loads, is carried out. Since the controllers are the heart of any microgrid system, the discussion is incomplete without it. A comprehensive survey is further carried on them. Major experimental developments around the world are also taking place at a rapid rate due to rapid advancement in power electronics technology and expansion of renewable sources. Hence, the experiments as on date have been mentioned.

Acknowledgements The authors are thankful to Indian Institute of Technology Kharagpur for its support and permission to submit this chapter.

Appendix

The family of PID controllers is the simplest of the controllers. The gains of the controller have different impacts on the closed-loop response of the plant in a microgrid.

Assuming a plant to be represented by a closed-loop transfer function given as:

$$G = \frac{20}{s^4 + 12s^3 + 40s^2 + 55s + 30} \tag{1.42}$$

The effect of the P controller when only K_p is varied independently is shown in Fig. 14. It is observed that the steady state error reduces with increase in K_p . However, the damping reduces and overshoot increases with increase in K_p .

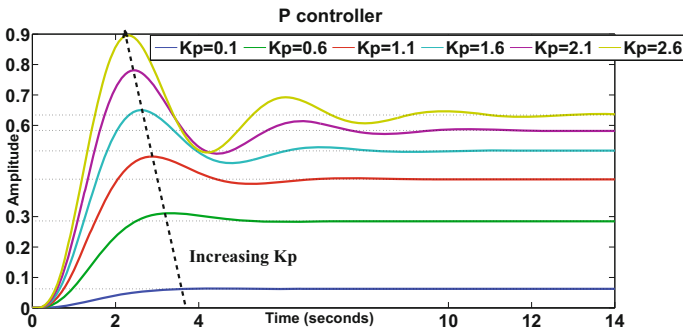


Fig. 14 Typical P controller behavior with increasing proportional gain

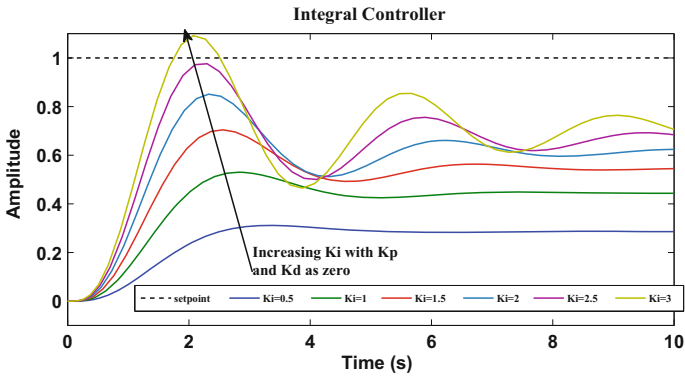


Fig. 15 Typical I controller behavior with increasing integral gain

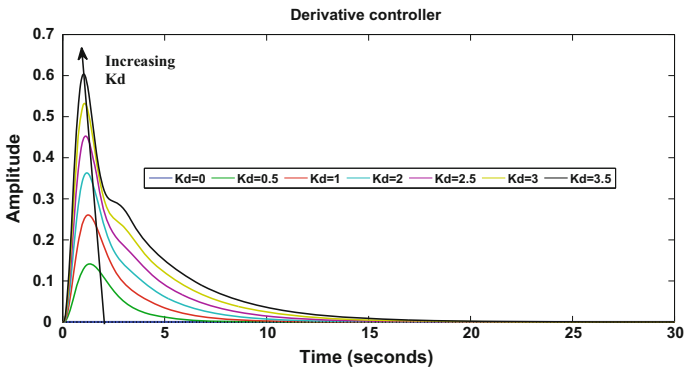


Fig. 16 Typical derivative controller behavior with increasing derivative gain

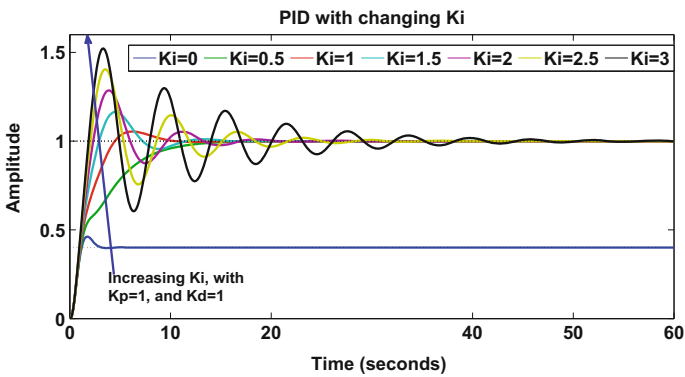


Fig. 17 Typical PID controller behavior with increasing integral gain ($K_p = 1, K_d = 1$)

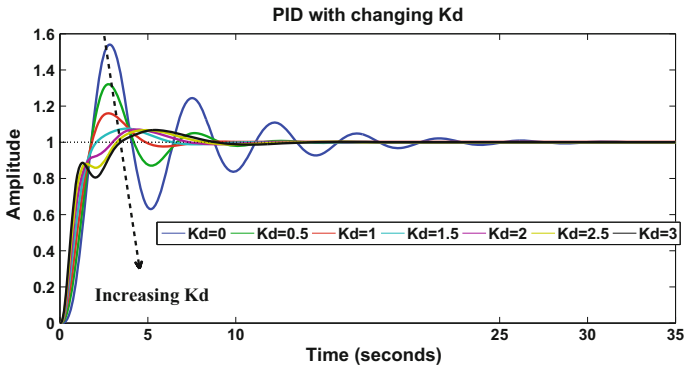


Fig. 18 Typical PID controller behavior with decreasing derivative gain ($K_p = 1, K_i = 1$)

Table 2 Effect of increasing $K_p, K_i,$ and K_d independently in PID controller

Closed-loop response	Rise time	Overshoot	Settling time	Steady state error	Damping
Increasing K_p	Reduces	Increases	Slightly increases	Reduces	Reduces
Increasing K_i	Slightly reduces	Increases	Increases	Eliminates	Reduces
Increasing K_d	Slightly reduces	Reduces	Reduces	Minor change	Increases

The integral gain is separately varied keeping P and D gains as zero, as shown in Fig. 15. The overshoot is seen increasing, and damping reduction is observed with increasing K_i .

The derivative controller alone fails to control the controlled variable when K_p and K_i are zero, as observed in Fig. 16.

The effect of the PID controller with fixed P and D gains but increasing K_i is observed in Fig. 17. The steady state error is almost eliminated with increase in the integral gain. However, the overshoot increases and damping reduces with its increase.

The effect of the PID controller with fixed P and I gains and increasing K_d can be observed in Fig. 18. The derivative gain reduces overshoot significantly.

The overall impact of increasing the gains of the PID controller is illustrated in Table 2.

References

1. International Energy Agency. <http://www.iea.org/topics/renewables/subtopics/wind/>

2. International Energy Agency. <http://www.iea.org/topics/renewables/subtopics/solar/>
3. About microgrids <https://building-microgrid.lbl.gov/about-microgrids>
4. Sahoo SK, Sinha AK, Kishore NK (2015, December) Modeling and real-time simulation of an AC microgrid with solar photovoltaic system. In India conference (INDICON), 2015 Annual IEEE, pp 1–6
5. Sahoo SK, Sinha AK, Kishore NK (2016, December) Low voltage ride-through of a grid-connected doubly-fed induction generator with speed sensorless vector control. In power systems conference (NPSC), 2016 National, pp 1–6
6. Lasseter RH (2007) Microgrids and distributed generation. *J Energy Eng* 133:144–149
7. Ackermann T, Andersson G, Söder L (2001) Distributed generation: a definition. *Electr Power Syst Res* 57:195–204
8. Katiraei F, Iravani R, Hatziargyriou N, Dimeas A (2008) Microgrids management. *IEEE Power Energy Mag* 6
9. Gu Z, Rizy DT (1996) Neural networks for combined control of capacitor banks and voltage regulators in distribution systems. *IEEE Trans Power Deliv* 11:1921–1928
10. Kim GW, Lee KY (2005) Coordination control of ULTC transformer and STATCOM based on an artificial neural network. *IEEE Trans Power Syst* 20:580–586
11. Tanaka K, Oshiro M, Toma S, Yona A, Senjyu T, Funabashi T, Kim CH (2010) Decentralised control of voltage in distribution systems by distributed generators. *IET Gener Transm Distrib* 4:1251–1260
12. Vovos PN, Kiprakis AE, Wallace AR, Harrison GP (2007) Centralized and distributed voltage control: impact on distributed generation penetration. *IEEE Trans Power Syst* 22:476–483
13. Logeshwari V, Chitra N, Kumar AS, Munda J (2013) Optimal power sharing for microgrid with multiple distributed generators. *Procedia Eng* 64:546–551
14. Lopes JP, Hatziargyriou N, Mutale J, Djapic P, Jenkin N (2007) Integrating distributed generation into electric power systems: a review of drivers, challenges and opportunities. *Electric Power Syst Res* 77:1189–1203
15. Coster EJ, Myrzik J, Kruimer B, Kling WL (2011) Integration issues of distributed generation in distribution grids. *Proc IEEE* 99:28–39
16. Hatziargyriou N, Asano H, Iravani R, Marnay C (2007) Microgrids. *IEEE power and energy mag* 5:78–94
17. Burke AF (2007) Batteries and ultracapacitors for electric, hybrid, and fuel cell vehicles. *Proc IEEE* 95:806–820
18. Roberts B (2009) Capturing grid power. *IEEE Power and Energy Mag*, 7
19. Nejabatkhah F, Li YW (2015) Overview of power management strategies of hybrid AC/DC microgrid. *IEEE Trans Power Electron* 30:7072–7089
20. Tan X, Li Q, Wang H (2013) Advances and trends of energy storage technology in Microgrid. *Int J Electr Power Energy Syst* 44:179–191
21. Bernhoff H (2011) Magnetic bearings in kinetic energy storage systems for vehicular applications. *J Electrical Syst* 7:225–236
22. Shen J, Jiang C, Li B (2015) Controllable load management approaches in smart grids. *Energies* 8(10):11187–11202
23. Lee BK, Ehsami M (2001) A simplified functional simulation model for three-phase voltage-source inverter using switching function concept. *IEEE Trans Industr Electron* 48:309–321
24. Itkonen T, Luukko J (2008, November) Switching-function-based simulation model for three-phase voltage source inverter taking dead-time effects into account. In *Industrial Electronics, 2008. IECON 2008. 34th Annual Conference of IEEE*, pp 992–997
25. Blasko V, Kaura V (1997) A new mathematical model and control of a three-phase AC–DC voltage source converter. *IEEE Trans Power Electron* 12:116–123
26. Han H, Hou X, Yang J, Wu J, Su M, Guerrero JM (2016) Review of power sharing control strategies for islanding operation of AC microgrids. *IEEE Trans Smart Grid* 7:200–215

27. Guerrero JM, Vasquez JC, Matas J, De Vicuña LG, Castilla M (2011) Hierarchical control of droop-controlled AC and DC microgrids? A general approach toward standardization. *IEEE Trans Ind Electron* 58:158–172
28. Ang KH, Chong G, Li Y (2005) PID control system analysis, design, and technology. *IEEE Trans Control Syst Technol* 13:559–576
29. Podlubny I (1994) Fractional-order systems and fractional-order controllers. *Inst Exp Phy Slovak Acad Sci Kosice* 12(3):1–18
30. Teodorescu R, Blaabjerg F, Liserre M, Loh PC (2006) Proportional-resonant controllers and filters for grid-connected voltage-source converters. *IEE Proc-Electric Power Appl* 153:750–762
31. Tan SC, Lai YM, Tse CK (2011) Sliding mode control of switching power converters: techniques and implementation. CRC Press
32. Cortés P, Kazmierkowski MP, Kennel RM, Quevedo DE, Rodríguez J (2008) Predictive control in power electronics and drives. *IEEE Trans Industr Electron* 55:4312–4324
33. Rodríguez J, Pontt J, Silva CA, Correa P, Lezana P, Cortés P, Ammann U (2007) Predictive current control of a voltage source inverter. *IEEE Trans Ind Electron* 54:495–503
34. Chandorkar MC, Divan DM, Adapa R (1993) Control of parallel connected inverters in standalone ac supply systems. *IEEE Trans Industry Appl* 29:136–143
35. Katiraei F, Iravani MR (2006) Power management strategies for a microgrid with multiple distributed generation units. *IEEE Trans Power Syst* 21:1821–1831
36. Lopes JP, Moreira CL, Madureira AG (2006) Defining control strategies for microgrids islanded operation. *IEEE Trans Power Syst* 21:916–924
37. Guerrero JM, De Vicuna LG, Matas J, Castilla M, Miret J (2004) A wireless controller to enhance dynamic performance of parallel inverters in distributed generation systems. *IEEE Trans Power Electron* 19:1205–1213
38. Guerrero JM, De Vicuna LG, Matas J, Castilla M, Miret J (2005) Output impedance design of parallel-connected UPS inverters with wireless load-sharing control. *IEEE Trans Ind Electron* 52:1126–1135
39. Bidram A, Davoudi A (2012) Hierarchical structure of microgrids control system. *IEEE Trans Smart Grid* 3:1963–1976
40. Sao CK, Lehn PW (2008) Control and power management of converter fed microgrids. *IEEE Trans Power Syst* 23:1088–1098
41. Lee CT, Chu CC, Cheng PT (2013) A new droop control method for the autonomous operation of distributed energy resource interface converters. *IEEE Trans Power Electron* 28:1980–1993
42. Majumder R, Ghosh A, Ledwich G, Zare F (2009, July) Angle droop versus frequency droop in a voltage source converter based autonomous microgrid. In: Power and Energy Society General Meeting, 2009. (PES'09). IEEE. pp 1–8
43. Majumder R, Chaudhuri B, Ghosh A, Majumder R, Ledwich G, Zare F (2010) Improvement of stability and load sharing in an autonomous microgrid using supplementary droop control loop. *IEEE Trans Power Syst* 25:796–808
44. Vasquez JC, Guerrero JM, Luna A, Rodríguez P, Teodorescu R (2009) Adaptive droop control applied to voltage-source inverters operating in grid-connected and islanded modes. *IEEE Trans Ind Electron* 56:4088–4096
45. De Brabandere K, Bolsens B, Van den Keybus J, Woyte A, Driesen J, Belmans R (2007) A voltage and frequency droop control method for parallel inverters. *IEEE Trans Power Electron* 22:1107–1115
46. Li N, Chen L, Low SH (2011, July) Optimal demand response based on utility maximization in power networks. In Power and Energy Society General Meeting, 2011 IEEE pp 1–8
47. Guerrero JM, Hang L, Uceda J (2008) Control of distributed uninterruptible power supply systems. *IEEE Trans Ind Electron* 55:2845–2859
48. Rokrok E, Golshan MEH (2010) Adaptive voltage droop scheme for voltage source converters in an islanded multibus microgrid. *IET Gener Transm Distrib* 4:562–578

49. Tuladhar A, Jin H, Unger T, Mauch K (2000) Control of parallel inverters in distributed AC power systems with consideration of line impedance effect. *IEEE Trans Ind Appl* 36:131–138
50. Borup U, Blaabjerg F, Enjeti PN (2001) Sharing of nonlinear load in parallel-connected three-phase converters. *IEEE Trans Ind Appl* 37:1817–1823
51. Zhong QC (2013) Harmonic droop controller to reduce the voltage harmonics of inverters. *IEEE Trans Industr Electron* 60:936–945
52. CERTS Microgrid Test Bed Dolan Technology Center. [http://certs.aeptechlab.com/CERTS Microgrid Test Bed](http://certs.aeptechlab.com/CERTS/Microgrid%20Test%20Bed)
53. Lasseter RH, Eto JH, Schenkman B, Stevens J, Vollkommer H, Klapp D, Linton E, Hurtado H, Roy J (2011) CERTS microgrid laboratory test bed. *IEEE Trans Power Deliv* 26:325–332
54. Turner G, Kelley JP, Storm CL, Wetz DA, Lee WJ (2015) Design and active control of a microgrid testbed. *IEEE Trans Smart Grid* 6:73–81
55. Flueck AJ, Nguyen CP (2010) Integrating renewable and distributed resources-IIT perfect power smart grid prototype. In *Power and Energy Society General Meeting, 2010 IEEE* pp 1–4
56. UCSD. <https://building-microgrid.lbl.gov/ucsd>
57. Microgrid Projects. <http://microgridprojects.com/india-microgrids/>
58. Balijepalli VM, Khaparde SA, Dobariya CV (2010, July) Deployment of microgrids in India. In *2010 IEEE Power and Energy Society General Meeting*, pp 1–7
59. VIDEO: Get a closeup view of the solar microgrid village in India. [http://www.greenpeace.org/usa/video-get-closeup-view-solar -micro-grid-village-india/](http://www.greenpeace.org/usa/video-get-closeup-view-solar-micro-grid-village-india/)

Transition of Power Distribution System Planning from Passive to Active Networks: A State-of-the-Art Review and a New Proposal

Shubh Lakshmi and Sanjib Ganguly

Abstract The planning of electrical power distribution systems (DS) is a strategy to meet load demand and to expand the services economically and yet, reliably. The lower energy efficiency of DS, because of the high network power loss and voltage-drop problem, makes the DS planning problem more relevant, even today. Integration of distributed generation (DG) to DS is one of the solutions to improve energy efficiency. The inclusion of DG units in DS planning transformed the traditional passive distribution system (PDS) to active distribution system (ADS). The ADS planning includes the modern communication technique, active energy management technologies and distribution system automation technologies. There are various approaches on ADS planning including various features. These are classified into a three-level tree structure. The first level is based on the type of the planning. The second level is based on the types of load and generation models used. The third level of classification is based on the different types of solution strategies used. Among these approaches, the research gap is identified, and a planning model to optimally convert PDS to ADS is proposed. The model includes a novel strategy to integrate photovoltaic unit in DS along with unified power quality conditioner so as to get simultaneous improvements of power quality and energy efficiency. The proposed model is validated on a 69-bus radial distribution network.

Keywords Distribution system planning · Distributed generation
Energy storage · Power quality · Unified power quality conditioner (UPQC)

S. Lakshmi · S. Ganguly (✉)

Department of Electronics and Electrical Engineering, Indian Institute of Technology Guwahati, Guwahati 781039, India
e-mail: sanjib191@gmail.com; sganguly@iitg.ernet.in

S. Lakshmi

e-mail: shubhlakshmi26@gmail.com; shubh.lakshmi@iitg.ernet.in

© Springer Nature Singapore Pte Ltd. 2018

S. De et al. (eds.), *Sustainable Energy Technology and Policies*, Green Energy and Technology, https://doi.org/10.1007/978-981-10-7188-1_4

Nomenclature and Acronyms

PDS (ADS)	Passive (active) distribution system
MG	Micro-grid
CP (I)	Conversion planning from PDS to ADS (investment planning)
CP (O)	Conversion planning from PDS to ADS (operational planning)
SGP (I)	ADS planning with smart grid features (investment planning)
SGP (O)	ADS planning with smart grid features (operational planning)
MGP (I)	MG planning (investment planning)
MGP (O)	MG planning (operational planning)
IC	Installation cost
OC	Operational cost
MC	Maintenance cost
OMC	Operational and maintenance cost
WT	Wind turbine
PV	Photovoltaic
FC	Fuel cell
DE	Diesel engine
GT	Gas turbine
MT	Micro turbine
HT	Hydro turbine
EL	Electrolyzer
BM	Bio-mass
UPQC	Unified power quality conditioner
PQ	Power quality
DG	Distributed generation
DDG	Dispatchable DG
ESS	Energy storage system
$V_{Se1}^{sag}(V_{Se1})$	Voltage injected by the series inverter of UPQC in voltage sag (healthy) condition
I_R	Line current before the placement of UPQC
$I_{R1}(I_{R2})$	Line current after the placement of UPQC without (with) PV-storage unit
δ_1	Load end voltage phase angle shift after the placement of UPQC
V'_S	Source end voltage of the UPQC
$V_S(V_R)$	Sending end (receiving end) voltage of a distribution line
K_{Se}	Ratio of V_{Se1} to V_R
$I_{Sh1}(I'_{Sh1})$	Shunt compensating current injected by the shunt inverter of UPQC without (with) PV-storage unit
k	Amount of sag in voltage
Q_{total}	Total reactive power demand of the network
I_{St}	Current supplied by the storage unit

K_{St}	Ratio of I_{St} to I_R
$Q_{Se1_{max}}^i \left(Q_{Sh1_{max}}^i \right)$	Maximum reactive power supplied by series (shunt) inverter of UPQC-WPV at bus 'i'
THD_L (THD _{Sh})	Total harmonic distortion of line current I_R (shunt compensating current I'_{Sh1})
C_{UPQC}^m	Investment cost of the UPQC at location 'm' (\$/kVA)
$S_{UPQC}^{WPV_m}$	VA-rating of UPQC at location 'm' (kVA)
C_{INV}^{St}	Investment cost of storage unit (\$/kWh)
$P_{UPQC}^{St_m}$	Size of storage unit at location 'm' (kW)
$C_{O\&M}^{St}$	Annual operation and maintenance cost of storage unit (\$/kW)
C_{INV}^{PV}	Investment cost of PV unit (\$/kW)
$P_{UPQC}^{PV_m}$	Size of PV array at location 'm' (kW)
$C_{O\&M}^{PV}$	Annual operation and maintenance cost of PV array (\$/kW)
T^h	Planning horizon (years)
D^f	Discount factor for planning horizon
C^E	Cost of energy loss (\$/kWh)
t_1 (t_2)	Duration of peak (off-peak) hour in a day (hours)
t_3	Operation hour of PV array (hours)
CUF	Capacity utilization factor of PV array
$P_{loss_mn}^{peak} \left(P_{loss_mn}^{off-peak} \right)$	Peak (off-peak) hour power loss of branch 'mn' after placement of UPQC
$P(m)$	Active power demand of bus 'm'
$Q(m)$	Reactive power demand of bus 'm'
TPC	Cost of placement of UPQC-WPV at bus 'm'

1 Introduction

In last few years, distribution system (DS) planning has attracted attention of power systems planners because it involves a number of conflicting objectives to be simultaneously optimized. The aim of DS planners is to design economical and yet, reliable DS, in such a way that it should supply uninterrupted power to the consumers. The distribution systems planning can be done in two ways: (i) single-stage planning and (ii) multi-stage planning. In single-stage planning, whole planning is performed at one step by considering discount factor for a planning horizon. In the case of multi-stage planning, the planning horizon is divided into multiple steps, and the planning is performed for each step. There are some state-of-the-art review papers reported on DS planning [1–6]. Among these, the papers [1–3] are on review of the passive DS (PDS) planning. In PDS, the power flow is unidirectional. The inclusion of distributed generation (DG) in DS planning converts the PDS to active

Table 1 The planning cost and variables for PDS and ADS planning

Types of cost/ problem variables	PDS planning	ADS planning
Installation/ reinforcement/ replacement cost for:	Substation, transformers, feeders, lines/feeder branches, sectionalizing switches and tie-lines, conventional reactive power compensators, such as voltage regulators, capacitors and on-load tap changers.	DG units, storage units (i.e. battery), advanced protection and communication infrastructure, advanced automation and metering technologies, power electronics devices for reactive power compensation and PQ improvement, etc.
Operational cost:	Cost of energy loss and maintenance cost for each equipment associated with PDS	Cost of energy loss and maintenance cost for each equipment associated with ADS
Planning problem variables:	Size and location for new substation, number of feeders, feeder routing, number and locations for sectionalizing switches and tie-lines, conductor types and sizes, etc.	Sizes and locations for DG units, sizes and locations for battery, appropriate coordination of protection and automation technologies, generation mix among different types of DG units, etc.

distribution system (ADS). The works reported on ADS planning and/or PDS planning till 2015 have been reviewed in [4–6]. The different objectives and planning variables used in the planning of PDS and ADS are shown in Table 1.

The differences between traditional PDS and ADS are categorically shown in [6]. Some typical characteristics of ADS planning, which make it different to the traditional PDS planning are given below.

- The designed network topology/structure is to be flexible, and it can automatically be reconfigured to a different structure, unlike PDS.
- The designed network should reliably work with high penetration of DG.
- The designed network should reliably work with uncertainties of the generation of renewable energy sources, such as PV and WT.
- The operation of the designed network should be automated unlike manual operation of PDS.

The difference in features between PDS and ADS is shown with example networks in Fig. 1. Usually, a typical PDS consists of single or multiple feeders, several sectionalizing switches, tie line(s) and capacitor bank(s) as shown in Fig. 1a. In addition to these, a typical ADS, as shown in Fig. 1b, consists of distributed energy resources (DERs), charging station for electric vehicles, smart metres and distribution management system (DMS), which includes smart communication devices, advanced metering technologies, demand-side management technologies, energy management technologies and smart automation technologies. Traditionally, the tie line and sectionalizing switches in PDS are manually operated, whereas advanced automation technologies are used to operate these in ADS.

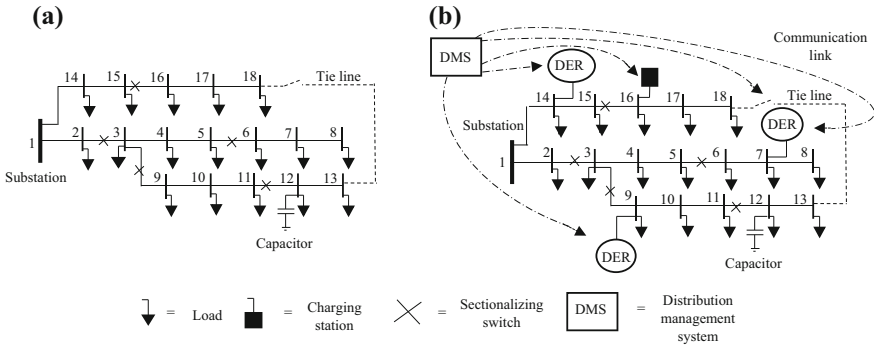


Fig. 1 The different features of typical distribution networks: **a** PDS and **b** ADS

The scheduling for the operation of different DER units and charging station(s) is done using DMS. Hence, there are differences among the objectives and optimizing variables in PDS and ADS planning as summarized in Table 1. Thus, the ADS planning is an involved multi-objective optimization process with a number of objectives, such as (i) minimization of installation/reinforcement/replacement cost for DG units and storage units (if any), (ii) minimization of operational cost (cost of energy loss and maintenance cost), (iii) maximization of reliability, (iv) maximization of capacity of DG penetration, (v) minimization of carbon emission, (vi) determination of optimal operational strategy for DG units and (vii) maximization of power quality (PQ). These objectives are optimized subjected to several technical and operational constraints. In many occasions, these objectives do conflict with each other. For example, the integration of renewable DG unit reduces the carbon emission at the expense of higher investment cost. Hence, to solve the ADS planning problem consisting of several such conflicting objectives, one needs multi-objective optimization approach. There are various multi-objective optimization approaches available in the literature. These are weighted aggregation-based approach, Pareto-based approach, ϵ -constrained approach etc. It is seen that the Pareto-based approach is popularly used in solving most of the multi-objective ADS planning problems.

The power systems researchers around the globe have significantly contributed to ADS planning during last 2–3 years. Hence, the theme of this work is to systematically present these works. Thus, a classification tree is developed for ADS planning, as shown in Fig. 2. It consists of three levels based on different attributes of planning. The different forms of ADS planning are grouped in Level #1 classification. The Level #2 further categorizes the Level #1 based on different load and generation models used. The Level #3 classification is based on the different solution strategies reported to solve the ADS planning optimization problem. The special emphasis is given to identify the inclusion of two important features of modern sustainable energy planning: (i) mitigation of the power quality (PQ) problems and (ii) integration of storage units. Based on the research gap

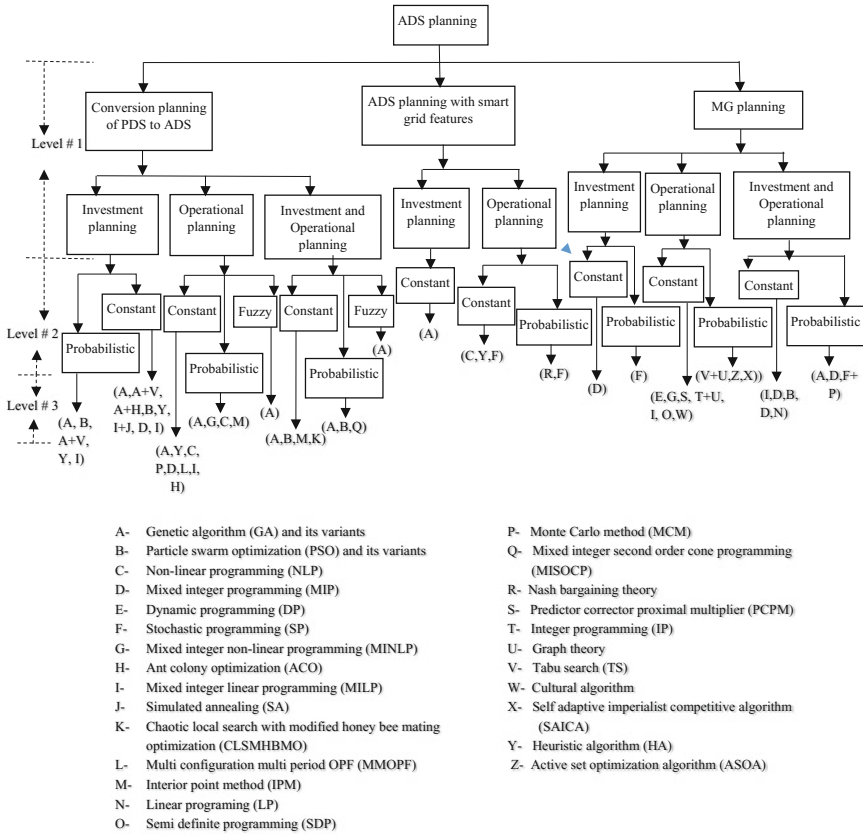


Fig. 2 Classification tree of ADS planning

identified, a planning model, to optimally convert PDS to ADS, is proposed. The contributions of this chapter are summarized as:

- Classification of different ADS planning models in view of type of the planning and load and/or generation models
- Identification whether two important aspects of modern ADS planning, i.e. integration of energy storage and mitigation of PQ problems are considered in the reported models
- Proposal of an ADS planning approach including storage and PQ problem mitigation

This chapter is organized as follows. Section 2 presents a systematic literature review on ADS planning and the research gap. In Sect. 3, a new approach on ADS planning is provided along with simulation results. Section 4 concludes the chapter.

2 Literature Review on ADS Planning

In view of different approaches on ADS planning, a three-level classification tree structure is developed as shown in Fig. 2. The Level #1 classification is based on the type of the planning. There are three different types found, and they are (i) conversion planning (CP) from PDS to ADS, (ii) ADS planning including smart grid (SGP) features and (iii) Micro-grid planning (MGP). In the conversion planning, [7–43], the traditional PDS is converted to ADS with at least one DG unit of either conventional or renewable type. In ADS planning with smart grid features [44–49], the planning approaches consist of smart technologies, such as charging of electric vehicle (EV), fault passage indicator, distribution automation, advanced metering techniques, advanced communication techniques, energy management technologies and demand management technologies. The MG is a kind of low/medium-voltage distribution network consisting of DG units and controllable loads, which can be operated in either islanded or grid-connected mode. The MG planning [50–70] is done to improve system self-adequacy and to design self-sufficient DS. These three types of planning are further divided into three sub-categories based on the objective function formulations. They are: (i) investment planning, (ii) operational planning and (iii) combined investment and operation planning. In investment planning, a planner's job is to find out the amount of fund to be optimally invested for achieving particular objectives within a planning horizon. In the ADS operational planning, the planners are dealing with the objectives to determine the optimal operational strategy for energy management. This is done by maximizing the profit by energy export/import, by finding the optimal power flow, by finding the optimal exchange of power with main grid and by considering different operational parameters of DS, such as power loss, voltage deviation and emission. The combined investment and operation planning are an approach combining both investment and operational planning objectives. The investment planning is long-term planning process, whereas the operational planning is a short-term planning process. The different attributes of individual work are given in Table 2.

The Level #2 further categorizes the Level #1 based on different types of load and generation models. Basically, three types of load and generation models are used in the literature: (i) constant, (ii) probabilistic and (iii) fuzzy set theory-based. The probability-based load models are reported in [9, 11, 13, 16–18, 23, 28, 33, 35, 39, 40, 42, 46, 51, 55, 56, 58, 59, 67, 70]. In [9, 11, 13, 17, 18, 22, 23, 28, 30, 31, 33, 35, 39, 40, 42, 46, 49, 51, 52, 55, 56, 58, 59, 67, 68, 70], probability-based generation models are used. Probabilistic load and generation are usually modelled by using a chosen probability density function (PDF), such as normal distribution, beta PDF, Weibull PDF and Rayleigh PDF. In some of the approaches [8, 10], the fuzzy set theory is used to model the uncertain load and generation. The rest of the works are based on constant load and generation values.

The Level #3 classification is based on the solution strategies used in ADS planning. Several solution strategies are used to solve the planning optimization problems. The reported solution strategies can be categorized into two groups:

Table 2 Different features of different ADS planning approaches

Reference No.	Planning category	Objective functions	Type of DG	Solution strategy	PQ problem mitigation included?	Integration of storage included?
[7]	CP (I)	IC and OC of substation, feeder, DG units, ESS, replacement cost of ESS and cost of outage	Not mentioned	TSGA, GA-ACO and PSO	No	Yes
[8]	CP (O)	Power loss and voltage deviation	Not mentioned	Adaptive GA	No	No
[9]	CP (O)	Energy loss	WT	MINLP	No	No
[10]	CP (I + O)	IC and OC of DG units, cost of energy loss, risk of overloading in substations and line segments, risk of over/under voltage in buses, and economic risk due to electricity price uncertainty	Not mentioned	NSGA-II	No	No
[11]	CP (I + O)	Costs of line up-gradation, cost of energy loss, IC and OMC of DG units, cost of energy produced by DG units, and emission from DG units and for the purchased energy from the grid	PV, WT and GT	NSGA-II	No	No
[12]	CP (I + O)	IC and OC of DG units, costs of substation and feeder reinforcement, cost of purchased energy from the grid, emission cost, and voltage satisfaction	GAS I.C., MT and FC	CLSMHBM0	No	No
[13]	CP (I + O)	Technical constraints dissatisfaction, cost of energy purchase from the grid, reinforcement of substation and feeder, IC and OC of DG units, and total emission from DG units and the grid	WT, GT and MT	Binary PSO	No	No
[14]	CP (I)	IC and OC of DG units, capital cost to upgrade substation and feeders, and cost for import and export of energy	GT	HA	No	No

(continued)

Table 2 (continued)

Reference No.	Planning category	Objective functions	Type of DG	Solution strategy	PQ problem mitigation included?	Integration of storage included?
[15]	CP (I)	IC and OMC of DDG units, capacitors, lines and transformers, cost of energy loss, reliability cost, and cost of the reduction in purchased energy from the grid	DE	Modified discrete PSO	No	No
[16]	CP (I)	IC of substation, feeder and DG units, and OC of DG units and substation	Not mentioned	PSO	No	No
[17]	CP (I)	Costs of energy loss, imported energy from the grid and non-distributed energy, cost of reconfiguration using switches, IC of DG units, cost of conductor replacement and additional lines	Thermal and WT	GA	No	No
[18]	CP (I)	IC, OMC, and capacity adequacy cost of DG units and cost of energy loss	WT, PV and DE	Point estimated GA	No	No
[19]	CP (I)	Costs of new lines, cost of energy losses, cost of undelivered energy due to faults, and cost of production loss of DG units due faults in lines	Not mentioned	MILP & SA	No	No
[20]	CP (O)	Cost of energy not supplied and energy losses	WT and PV	HA	No	Yes
[21]	CP (O)	Maximization of energy export and revenue from energy export	Not mentioned	NLP	No	Yes
[22]	CP (O)	Costs of energy loss	WT, PV and HT	GA	Yes	No
[23]	CP (I)	Costs of energy loss, imported energy and non-distributed energy, cost of reconfiguration using switches, IC of DG units and new lines, and cost of conductor replacement	WT and Thermal	GA	No	No

(continued)

Table 2 (continued)

Reference No.	Planning category	Objective functions	Type of DG	Solution strategy	PQ problem mitigation included?	Integration of storage included?
[24]	CP (O)	Energy loss	WT and PV	MCM	No	Yes
[25]	CP (O)	Load curtailment minimization	Fossil fuel-based DG	MIP	No	No
[26]	CP (O)	DG capacity maximization	WT	MMOPF	No	No
[27]	CP (O)	Cost of energy loss, generation cost of wind energy and cost of ESS	WT	NLP	No	Yes
[28]	CP (I + O)	IC and MC of distributed storage systems and OC of grid (voltage deviation, cost of energy purchase from the grid, energy losses, and load curtailment)	WT, PV and DE	MISOCP	No	Yes
[29]	CP (O)	Network power loss and voltage deviation	Not mentioned	GA	No	No
[30]	CP (I)	IC and OC of DG units and capacitor and cost of purchase energy from the grid	WT	TS and GA	No	No
[31]	CP (I)	IC and OC of substation and lines, cost of energy loss, and fault cost	WT	NSGA-II	No	No
[32]	CP (I + O)	Cost of energy loss, voltage regulation and peak demand, and IC and OMC of ESS	-	IPM	No	Yes
[33]	CP (O)	OC of PV units, cost of reduction in demand with the integration of demand response program, and energy loss	PV	IPM	No	No
[34]	CP (O)	DG hosting capacity maximization	Not mentioned	MILP	No	No

(continued)

Table 2 (continued)

Reference No.	Planning category	Objective functions	Type of DG	Solution strategy	PQ problem mitigation included?	Integration of storage included?
[35]	CP (I)	Cost of substation expansion, IC of substation, DG units, and feeder, replacement cost of feeder, OC of DG units, cost of energy purchase from the grid, cost of energy loss, cost of energy not supplied due to faults, and pollutant emission	WT and DDG	GA and OPF	No	No
[36]	CP (O)	Power loss, voltage improvement, and load balancing of the lines in feeder	PV	ACO and fuzzy	No	No
[37]	CP (I + O)	Profit due to sale of energy, IC of ESS and DG units, and OMC of ESS and DG units	Not mentioned	PSO	No	Yes
[38]	CP (I)	IC of ESS, OC of ESS and lines, cost of conductor replacement, cost of power imported from the substation, outage cost, and value of lost load	-	MIP	No	Yes
[39]	CP (I + O)	Substation expansion cost, IC of substation, feeder and DG units, conductor replacement cost of feeder, OC of DG units, cost of energy purchase from the grid, cost of energy loss, cost of expected energy not supplied, and emission	WT and DDG	GA	No	No
[40]	CP (O)	Cost of energy	WT	NLP	No	No
[41]	CP (I)	IC and OMC of DG units, cost of energy purchase from the grid, cost of unserved energy, cost of energy loss, and emission	WT, PV, HT, GT, Geothermal, Heavy fuel oil turbine, BM	MILP	No	No

(continued)

Table 2 (continued)

Reference No.	Planning category	Objective functions	Type of DG	Solution strategy	PQ problem mitigation included?	Integration of storage included?
[42]	CP (I)	IC and OMC of feeder, transformer, substation and DG units, cost of energy loss, and cost of unserved energy	WT and PV	MILP	No	No
[43]	CP (O)	Active and reactive power losses of the network	PV, MT, etc.	MOEA	No	No
[44]	SGP (I)	IC and OMC of substation, lines, fault passage indicator and parking lot, and expected energy not supplied	-	NSGA-II	No	Yes (EV)
[45]	SGP (I)	Revenue earned from energy export, IC and OMC of substations, feeders, and lines, cost of energy loss, and interruption and fault repairing cost of lines	-	GA	No	No
[46]	SGP (O)	Saving cost for reactive power compensation and the voltage deviation	Not mentioned	Nash Bargaining theory	No	No
[47]	SGP (O)	Economic benefit from load and plug-in EV (PEV), OC of DG units, and cost of energy purchase from the grid	WT and PV	NLP	No	Yes (PEV)
[48]	SGP (O)	Generation curtailment for DG units and load curtailment minimization	WT	HA	No	Yes (EV)
[49]	SGP (O)	OC of DDG unit, cost of import and export of energy, and cost of battery degradation due to vehicle-to-grid connection	WT, PV and DDG	SP	No	Yes (EV)
[50]	MGP (I + O)	IC and OMC of lines and DG units, cost of energy purchase from the grid, and cost of lost load	Not mentioned	MILP	No	No

(continued)

Table 2 (continued)

Reference No.	Planning category	Objective functions	Type of DG	Solution strategy	PQ problem mitigation included?	Integration of storage included?
[51]	MGP (I + O)	IC, OMC, and replacement cost of battery ESS and DG units, fault repairing cost of all equipment, and pollutant emission	WT, DE and PV	NSGA-II	No	Yes
[52]	MGP (I + O)	IC of battery ESS and OC of MG (fuel cost, start-up and shutdown costs of units, and cost of energy purchase)	WT and thermal	MIP	No	Yes
[53]	MGP (I)	IC of DG units, OC of MG, and reliability cost	WT, PV, FC and GT	MIP	No	Yes
[54]	MGP (I + O)	IC, OMC and replacement cost of components, cost of lost load, and costs of purchased energy from the grid, and cost of energy sale to the grid	WT, PV and FC	PSO	No	Yes
[55]	MGP (I)	IC and OMC of DG units, cost of energy sale, and cost of purchased energy from the grid	WT, MT and PV	MIP	No	No
[56]	MGP (I)	IC and OMC of ESS and DG units and interruption cost	WT and DE	SP	No	Yes
[57]	MGP (I + O)	Revenue from electrical and thermal energy sale, IC and OMC of ESS and DG units, cost of energy exchange with the grid, and emission	WT, PV, DE, MT and FC	PSO	No	Yes
[58]	MGP (O)	Energy losses, load and generation balance within MG, and MG self-adequacy	WT, PV and BM	TS and Graph theory	No	Yes
[59]	MGP (O)	MC of ESS, OC of DG units, and cost of energy exchange	Renewable source, MT, DE and FC	ASOA	No	Yes
[60]	MGP (O)	Cost of energy purchase from the grid	WT and PV	DP and Gauss-Seidal	No	Yes

(continued)

Table 2 (continued)

Reference No.	Planning category	Objective functions	Type of DG	Solution strategy	PQ problem mitigation included?	Integration of storage included?
[61]	MGP (O)	Cost of energy purchase from the grid, OC of DG units, cost of peak loading, emission cost, and cost of non-delivered energy	WT, PV and DE	MINLP	No	No
[62]	MGP (O)	OC of DG units, cost of storing energy and energy purchase from the grid, customer dissatisfaction, and power loss	WT, PV and DE	PCPMA	No	Yes
[63]	MGP (O)	Generation-load balance and ESS capacity sharing	Not mentioned	IP and graph theory	No	Yes
[64]	MGP (O)	Start-up cost of DG units, OMC of DG units and battery ESS, cost of energy sale/purchase from the grid, and cost of load curtailment	PV and FC	MILP	No	Yes
[65]	MGP (O)	Power loss, cost of energy purchase from the grid, and cost of energy supplied by DG units	Conventional DG	SDP	No	No
[66]	MGP (O)	IC and OMC of battery ESS and DG units, OC of MG, cost of energy purchase and sale to the grid	Solar, FC and BM	Cultural algorithm	No	Yes
[67]	MGP (O)	Cost of energy purchase from the grid, cost of EVs charging, cost of degradation of battery	WT	SAICA	No	Yes
[68]	MGP (I + O)	Power procurement cost, OC of battery, and IC of DG units	WT and PV	MIP and convex optimization	No	Yes
[69]	MGP (I + O)	IC and OC of DG units and ESS, cost of unserved energy, and cost of energy purchase/sale to the grid	WT, PV and DDG	LP	No	Yes
[70]	MGP (I + O)	IC and OMC of DG units and ESS, and value of lost load	WT and DE	SP and Monte Carlo	No	Yes

(i) classical and enumerative search techniques and (ii) meta-heuristic approaches. Different conventional mathematical approaches and enumerative search techniques used are LP, NLP, MILP, MINLP, MISOCP, SDP, Nash bargaining approach, DP and PCPM. The meta-heuristic methods use problem-independent set of rules to search feasible solutions. Some of the meta-heuristic approaches used are GA and its different variants, PSO and its different variants, HA, ACO, SA, TS, cultural algorithm, etc. In some of the approaches, hybrid solution strategy combining both classical and meta-heuristic approaches is used, for example hybrid MILP and SA, hybrid TS and graph theory, hybrid IP and graph theory, and hybrid MIP and convex optimization. The individual approaches are summarized in Table 2.

2.1 Research Gap and Motivations Behind a New Proposal

The DG integration is one of the solutions to meet increasing load growth with uninterrupted power supply to the consumers. The integration of converter-based DG units such as PV, and WT deteriorates the PQ of distribution networks by injecting harmonics to the distribution system. For example, as shown in Fig. 1b, if the DER unit located at bus 9 is of converter-based unit, it may cause harmonic pollution to its neighbouring buses. The line current harmonics flowing through the system deteriorates the quality of supply voltage as well. The excessive harmonics in line current may result in mal-operation of the sensitive equipment, additional network losses, etc. The single line to ground fault and the presence of arc furnaces cause voltage sag, which may create operational problem for some of the sensitive loads, such as adjustable speed drives, certain medical equipment and data processing centres. For example, if such a sensitive load is located at bus 5 of the example networks shown in Fig. 1 and there is an event of voltage sag at bus 4, this may lead to mal-operation of the sensitive load. This results in production loss for the process industries, loss of data for the data processing centres, etc. Hence, an appropriate measure should be taken to ensure a desired PQ level to all the customers. The installation of the custom power devices [71] can be one of the approaches. Similarly, the power shortage during peak load demand is a common problem for the developing nations, such as India. This results in load curtailment. To avoid this, the energy generated by such renewable sources can be stored in battery so as to utilize during peak hour. In view of the above, the following shortcomings are found in the literature of ADS planning:

- In none of the ADS planning models, the allocation of both DG and custom power devices is found.
- In none of the ADS planning models, both the storage units and PQ features are included.

These are the motivations behind the new proposal for ADS planning. The proposed ADS planning approach includes placement of the storage unit, renewable source, and unified power quality conditioner (UPQC), a custom power device.

3 Proposed Planning Approach with Numerical Simulation

In the proposed planning approach, the conversion of PDS to ADS is planned with the placement of a hybrid energy generation system consisting of PV array and battery. The hybrid system is connected to the DC link of the UPQC as shown in Fig. 3. A UPQC is a type of custom power devices which provides both series and shunt compensations by using series and shunt inverters, respectively. The series inverter of UPQC injects series voltage to mitigate the voltage sag caused by the upstream part of the network. Hence, it can protect the downstream loads from voltage sag. The shunt inverter of UPQC injects shunt compensating current to provide both harmonic and reactive power compensations [72]. These two inverters are interconnected to a DC link as shown in Fig. 3. A state-of-the-art review on UPQC can be found in [73]. The various UPQC models are found in the literature, such as UPQC-P [73], in which series voltage is injected to provide active power compensation, UPQC-Q [73], in which series voltage injected to provide only reactive power compensation, UPQC-S [74], in which both active and reactive power compensations are provided by injecting the series voltage, UPQC-VA_{min} [75], which is designed for the minimization of VA-rating of UPQC, 3-phase 4-wire structure [76], interline UPQC [77], in which different feeders of a network are equipped with the two inverters, open UPQC [78], in which the UPQC series and shunt inverters are not connected to a common DC link, etc. In [79], the minimization of UPQC installation cost is considered as an objective. In [80–82], the UPQC model with distributed generation is provided.

In all the above-mentioned works, UPQC is used to protect the most sensitive load. In [83], a study is reported with the placement of UPQC and its impact on network power loss, line loadability and voltage stability. In [84], a multi-objective

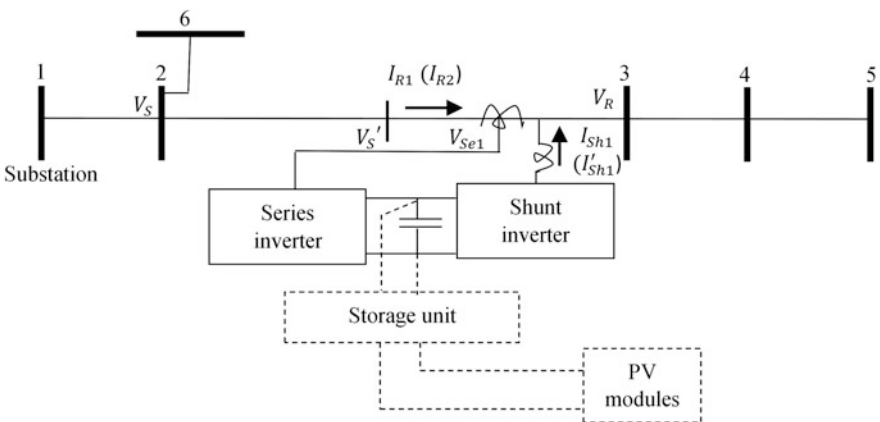


Fig. 3 A 6-bus distribution network with the UPQC-WPV placement at bus 3 {symbols used in bracket are applicable for the UPQC with PV-storage unit}

optimization-based planning approach is provided to find the optimal location(s) and size(s) for UPQC. Both these works show that a UPQC placed at an appropriate location can be used to reduce the network power loss, to mitigate the voltage sag, to eliminate the harmonics, to improve the bus voltages, etc. But, the placement of UPQC along with PV and storage units to study its impact on distribution network parameters is not investigated. Thus, a new UPQC model is proposed, in which PV array and battery are connected to the DC link of UPQC (i.e. UPQC-WPV). A 6-bus radial distribution network is used to demonstrate the model as shown in Fig. 3. In the proposed approach, the UPQC-WPV model is designed to mitigate voltage sag of the upstream network, which is a common PQ problem. The salient features of the proposed planning approach are given below.

- The energy generated by the PV array is stored in the battery, and it is injected into the network during peak hour.
- In voltage sag condition, the series inverter of UPQC-WPV is used to mitigate the voltage sag. Thus, it is used to protect the downstream load from voltage sag. In healthy condition, series inverter provides reactive power compensation.
- The shunt inverter of UPQC-WPV is designed to provide the reactive power and harmonic compensations. In addition, it is also used in active power compensation during peak hour.

3.1 Modelling of UPQC-WPV for Distribution Systems

The modelling of UPQC to improve the energy efficiency of distribution networks is provided in detail in [83, 84]. In this work, it is revised to UPQC-WPV model. The phasor diagram is shown in Fig. 4. In healthy condition, the series inverter

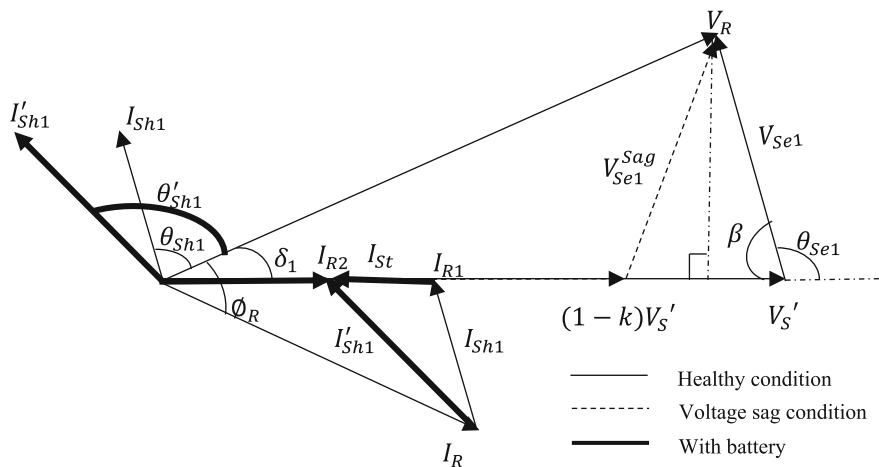


Fig. 4 Phasor diagram of UPQC-WPV

injects a fraction (K_{Se}) of V_R , i.e. V_{Se1} to provide the reactive power compensation by shifting the load end voltage phase angle by δ_1 . The amount of voltage sag (k) to be mitigated by the series inverter depends on the amount of series voltage to be injected, as shown in [84]. Accordingly, the phase angle δ_1 is computed. The reactive power sharing between the inverters is computed as in [84]. The PV-battery unit connected to the UPQC DC link is designed to provide a fraction (K_{St}) of line current I_R , i.e. $I_{St} = K_{St}I_R$.

Assuming lossless inverter configuration, the active power provided to the load is sum of active power delivered by the PV-battery unit and active power drawn from the source [84]. Hence,

$$I_{R2}V'_S + V'_S I_{St} = V_R I_R \cos \varnothing_R \quad (1)$$

$$I_{R2} = I_R (\cos \varnothing_R - K_{St}) \quad [\text{For } V_R = V'_S \text{ and } I_{St} = K_{St}I_R] \quad (2)$$

From Fig. 3,

$$I'_{Sh1} = \sqrt{I_{R2}^2 + I_R^2 - 2I_{R2}I_R \cos(\varnothing_R - \delta_1)} \quad (3)$$

From Eqs. (2) and (3),

$$I'_{Sh1} = I_R \sqrt{1 + (\cos \varnothing_R - K_{St})^2 - 2(\cos \varnothing_R - K_{St}) \cos(\varnothing_R - \delta_1)} \quad (4)$$

The shunt inverter of UPQC-WPV provides harmonic compensation by eliminating the distortion components present in the line current. Thus, the distortion component of the line current ((I_R^{dis})) is nullified by the distortion component of the shunt compensating current ((I'_{Sh1}^{dis})) [83], i.e. $I_R^{dis} = I'_{Sh1}^{dis}$. From the definition of THD (i.e. $THD = I^{dis} / I^{fun}$),

$$THD_L I_R^{fun} = THD_{Sh} I'_{Sh1}^{fun} \quad (5)$$

From Eqs. (4) and (5),

$$THD_{Sh} = \frac{THD_L}{\sqrt{1 + (\cos \varnothing_R - K_{St})^2 - 2(\cos \varnothing_R - K_{St}) \cos(\varnothing_R - \delta_1)}} \quad (6)$$

The RMS value of I'_{Sh1} is calculated as,

$$I'_{Sh1} = I_{Sh1}^{fun} \sqrt{1 + THD_{Sh}^2} \quad (7)$$

From Eqs. (6) and (7),

$$I'_{Sh1} = I_R^{\text{fun}} \sqrt{1 + (\cos \varnothing_R - K_{St})^2 - 2(\cos \varnothing_R - K_{St}) \cos(\varnothing_R - \delta_1) + \text{THD}_L^2} \quad (8)$$

The VA-rating of the shunt inverter is computed as:

$$S_{Sh1}^{\text{WPV}} = V'_S I'_{Sh1} \quad (9)$$

The amount of series voltage injected by the series inverter is computed as:

$$\begin{aligned} V_{Se1} &= \sqrt{V_S'^2 + V_R^2 - 2V_S'V_R \cos \delta_1} \\ &= V_S' \sqrt{2(1 - \cos \delta_1)} \quad [\text{For } V_R = V_S'] \end{aligned} \quad (10)$$

The VA-rating of the series inverter is computed by using Eqs. (2) and (10),

$$S_{Se1}^{\text{WPV}} = V_{Se1} I_{R2} \quad (11)$$

The VA-rating of UPQC-WPV is obtained as:

$$S_{UPQC}^{\text{WPV}} = S_{Se1}^{\text{WPV}} + S_{Sh1}^{\text{WPV}} \quad (12)$$

The size of the battery storage unit is computed as:

$$P_{UPQC}^{\text{St}} = V'_S I_{St} \quad (13)$$

The size of PV is computed as:

$$P_{UPQC}^{\text{PV}} = \frac{t_1 P_{UPQC}^{\text{St}}}{24 \text{CUF}} \quad (14)$$

where CUF is the capacity utilization factor of the PV array. The phase angle θ_{Se1} and θ'_{Sh1} can be derived by following the similar steps as shown in [72].

$$\theta_{Se1} = 90^\circ + \frac{\delta_1}{2} \quad (15)$$

For $((\delta_1 > \varnothing_R)$, θ'_{Sh1} is calculated as,

$$\theta'_{Sh1} = \tan^{-1} \left[\frac{\cos(\delta_1 - \varnothing_R) - \cos \varnothing_R + K_{St}}{\sin(\delta_1 - \varnothing_R)} \right] + 90^\circ - \delta_1 \quad (16)$$

Otherwise,

$$\theta'_{Sh1} = \tan^{-1} \left[\frac{\cos(\varnothing_R - \delta_1) - \cos \varnothing_R + K_{St}}{\sin(\varnothing_R - \delta_1)} \right] + 90^\circ - \delta_1 \quad (17)$$

The active and reactive power of series and shunt inverters can be calculated by using the respective VA-ratings and phase angles.

3.2 Computation of Planning Cost for UPQC-WPV Placement

The cost of placement of UPQC-WPV in any bus, say bus m , is computed by considering: (i) investment cost of UPQC; (ii) investment cost of storage unit (i.e. battery) and PV array; (iii) operational and maintenance cost of storage unit and PV array; and (iv) cost of energy loss during a planning horizon. The unit price of UPQC is taken from [79]. The energy loss is computed for two load levels, i.e. peak hour (assuming 4 h in a day) and off-peak hour load levels. The forward-backward sweep load flow algorithm is used to compute the power loss including the UPQC-WPV model as in [84]. It is to be noted that the energy generated by PV array in off-peak hour is stored so as to provide active power compensation during peak hour. During off-peak hour, UPQC-WPV is designed to provide only reactive power compensation. The computation of the total planning cost for the UPQC-WPV placement is shown in Eq. (18). The total planning cost is sum of six cost components. The first two cost components are the investment costs for UPQC and the battery storage units, respectively. The fourth one is the investment cost for the PV array. The third and fifth cost components are the discounted cost of annual operation and maintenance for the battery storage unit and the PV array, respectively. The sixth one is the cost of energy losses during peak and off-peak hours.

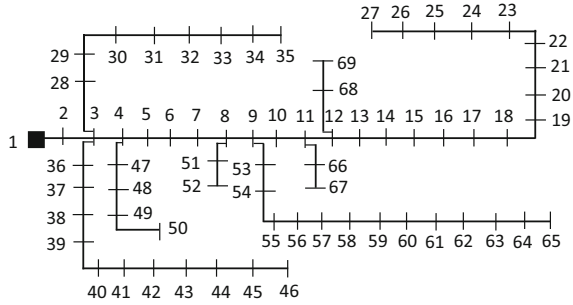
$$\begin{aligned} TPC = & C_{UPQC}^m S_{UPQC}^{WPV-m} + C_{INV}^{St} P_{UPQC}^{St-m} t_1 + T^h D^f C_{O\&M}^{St} P_{UPQC}^{St-m} + C_{INV}^{PV} P_{UPQC}^{PV-m} + T^h D^f C_{O\&M}^{PV} P_{UPQC}^{PV-m} \\ & + 365 C^E T^h D^f \sum_{mm \in [1, \dots, N-1]} \left(t_1 P_{loss_mm}^{peak} + t_2 P_{loss_mm}^{off-peak} \right) \end{aligned} \quad (18)$$

In this work, an exhaustive approach is used to study the impact of UPQC-WPV placement, in each bus of a distribution network similar to [83].

3.3 Simulation Results and Discussions

The 69-bus test network is used to demonstrate the proposed approach of UPQC-WPV placement in radial distribution networks. In this test network, bus 1 is the substation bus and rest are load buses. The single-line diagram for the 69-bus

Fig. 5 Single-line diagram of 69-bus radial distribution network



network is shown in Fig. 5. The network data are available in [85]. The substation bus voltage magnitude is considered as 1.0 p.u. A case study, consisting of five cases based on the variation of the ratio of current provided by the storage unit to the original line current (i.e. K_{St}), is provided in this subsection.

- Case 1: with $K_{St} = 0.1$
- Case 2: with $K_{St} = 0.2$
- Case 3: with $K_{St} = 0.3$
- Case 4: with $K_{St} = 0.4$
- Case 5: with $K_{St} = 0.5$

The cost component used to determine the planning cost is given in Table 3. The UPQC-WPV is designed to mitigate 30% of upstream voltage sag and 20% of load THD.

3.3.1 Power Loss Reduction Due to UPQC-WPV Placement

The impact of the allocation of UPQC-WPV in different locations of the network on the network power loss is shown in Fig. 6a, b for the peak and off-peak hours, respectively. The network power losses of the 69-bus network without compensation are 224.98 and 75.53 kW during peak and off-peak hours, respectively. A significant amount of loss reduction is observed in both peak and off-peak hours. It happens because the UPQC-WPV is designed to provide both active and reactive

Table 3 Different planning parameters

Planning parameters	Cost components
$T_h = 10$ years, rate of interest = 10%, $CUF = 0.2$	$C^E = 0.08$ \$/kWh [82]
$K_{St} = 0.1 - 0.5$, $THD_L = 0.2$, $k = 30\%$	$C_{INV}^{St} = 300$ \$/kWh [86]
Ratio of the off-peak demand to the peak demand = 0.6	$C_{O\&M}^{St} = 10$ \$/kW [87] annually
Duration for peak hour load demand = 4 h	$C_{INV}^{PV} = 2025$ \$/kW [88]
Duration for off-peak hour load demand = 20 h	$C_{O\&M}^{PV} = 16$ \$/kW [88] annually

power compensations in peak hours and reactive power compensation in off-peak hours. The power loss during peak hours is reducing with the increase of K_{St} as shown in Fig. 6a. It is because of the increase in active power compensation provided by the UPQC-WPV with the increase in K_{St} .

3.3.2 Improvement in Bus Voltage Due to UPQC-WPV Placement

Without compensation, the minimum bus voltages for the 69-bus network are 0.9092 p.u. and 0.9476 p.u. during peak and off-peak hours, respectively. From the Fig. 7a, b, it can be seen that the minimum bus voltages of the 69-bus network during peak and off-peak hours are improved. The minimum bus voltage of the network increases with K_{St} because of the higher compensation provided by the UPQC-WPV.

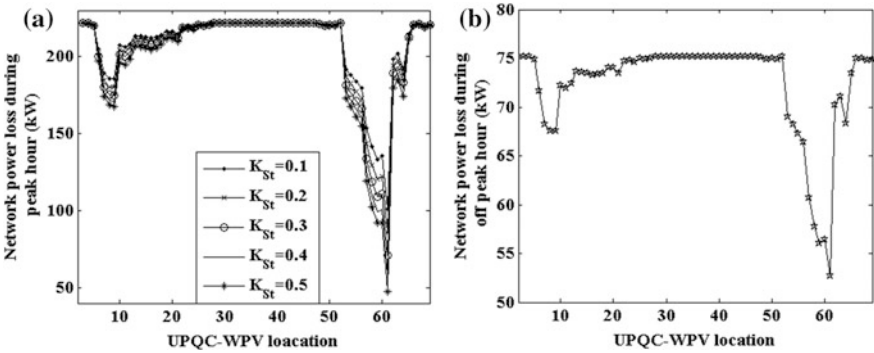


Fig. 6 Impact on network power loss due to UPQC-WPV allocation in different locations/buses of the network during a peak and b off-peak hour load demand

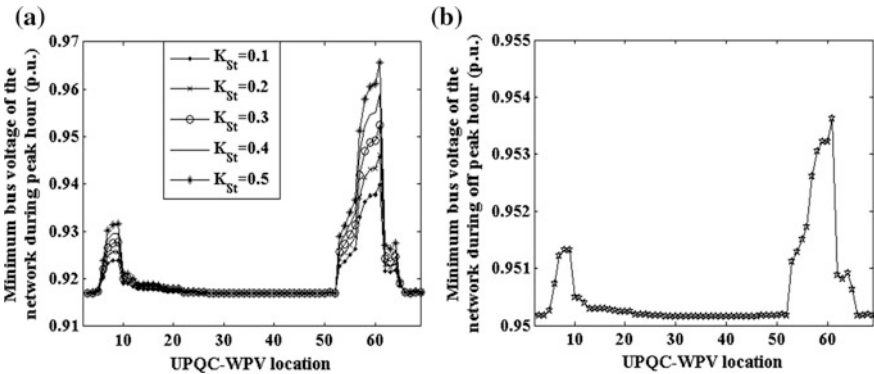


Fig. 7 Impact of UPQC-WPV allocation on network minimum bus voltage during a peak and b off-peak hour load demand

3.3.3 The Rating Requirements for UPQC-WPV, Battery and PV Array

The rating requirement of UPQC-WPV for its placement in different locations of the network for different values of K_{St} is shown in Fig. 8. The VA-rating of the UPQC-WPV is found to be higher when it is placed near the substation. This is because of the higher amount of line current is to be carried by the UPQC-WPV near the substation. The VA-rating of the UPQC-WPV is also found to be increasing with K_{St} . It is obvious because the compensations provided by the UPQC-WPV increases with K_{St} . The rating requirement for the storage unit and PV array due to the UPQC-WPV placement in different locations of the network for different values of K_{St} are shown in Figs. 9 and 10, respectively. Near the substation, the rating requirements for both the battery and PV array are high. The size of the battery storage needs to be increased with K_{St} because it depends on I_{St} ,

Fig. 8 The rating requirement for UPQC-WPV in different locations (bus number) of the network

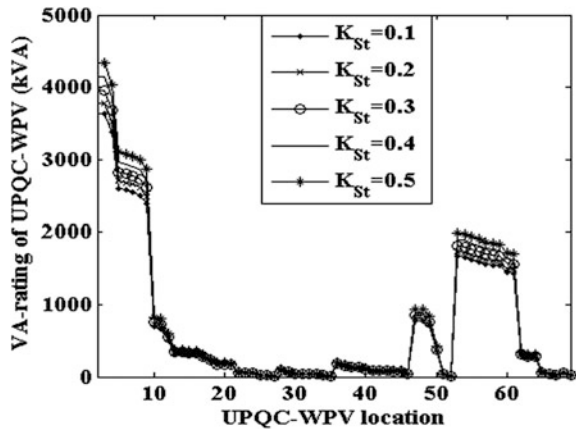


Fig. 9 The rating requirement for the battery for UPQC-WPV in different locations (bus number) of the network

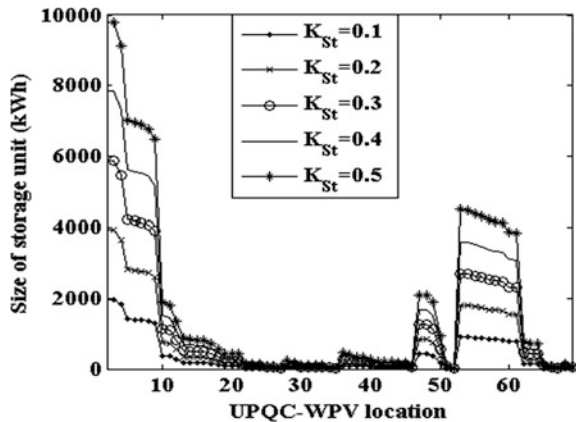
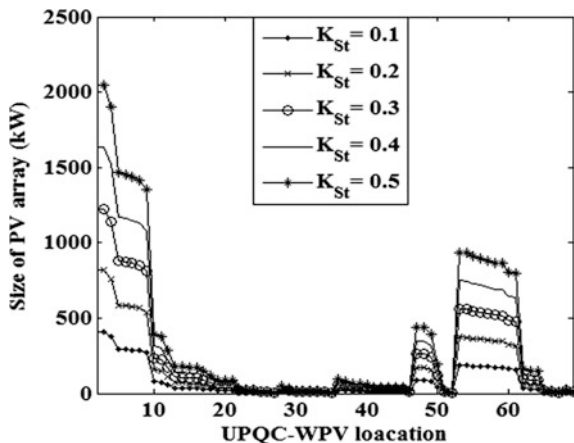


Fig. 10 The size of PV array required in different locations (bus number) of the network

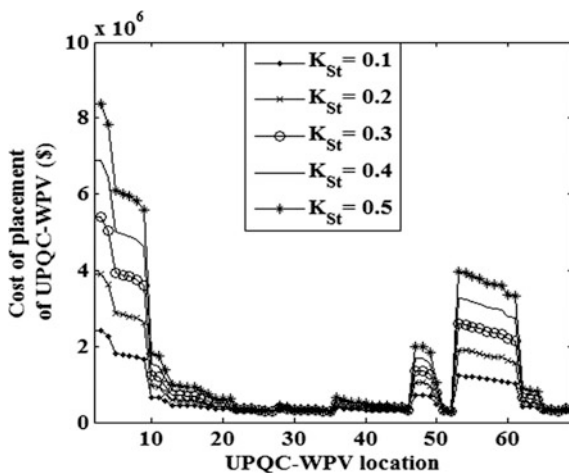


which increases with K_{St} . The size of the PV array depends on the size of storage unit as shown in Eq. (14). Hence, for higher value of K_{St} , the rating requirement for the PV array would be higher.

3.3.4 Cost of UPQC-WPV Placement

The cost of the UPQC-WPV placement in different locations of the network is shown in Fig. 11. The cost of the UPQC-WPV placement is found to be higher near the substation. It is also found to be higher with the increase in K_{St} . These happen because of the increase in rating requirements.

Fig. 11 The cost of placement of UPQC-WPV in different locations (bus number) of the network



3.3.5 Quantitative Comparison among Different Cases

To provide a quantitative comparison among the different cases, the results corresponding to the minimum power losses in each case are shown in Table 4. The location for UPQC-WPV placement is found to be same in each case. It is seen that the VA-rating of the series inverter reduces with the increase in K_{St} . Basically, I_{st} increases with the increase in K_{St} , and this results in reduction of I_{R2} and the series inverter rating (Eq. 11). However, the shunt inverter rating increases with K_{St} because the shunt compensating current I'_{Sh1} increases. The overall rating requirement for the UPQC-WPV increases with the increase in K_{St} , so as the ratings of the battery storage and the PV units. However, the increase in rating requirement for UPQC-WPV from Case 1 to Case 5 is nearly 20%, whereas the ratings for the battery and PV array increase to 5 times. In fact, the ratings of the battery and the PV array are found to be linearly increased with K_{St} . Hence, the percentage of the costs of the PV array and the battery to the total planning cost is significantly increased from Case 1 to Case 5. It is found that more than 50% of the planning cost is due to the installation of PV array in Case 5.

Table 4 Solution for the 69-bus network corresponding to lowest network power loss (in peak hours)

Solution	Case 1	Case 2	Case 3	Case 4	Case 5
UPQC-WPV location (bus number)	61	61	61	61	61
Peak hour power loss (kW)	101.2756	85.5411	71.0109	58.2641	47.6110
Off-peak hour power loss (kW)	52.6891	52.6891	52.6891	52.6891	52.6891
Percentage of energy loss reduction in a year (%)	39.4784	42.0894	44.5005	46.6157	48.3835
Peak hour minimum bus voltage (p.u.)	0.9399	0.9460	0.9524	0.9589	0.9655
Off-peak hour minimum bus voltage (p.u.)	0.9536	0.9536	0.9536	0.9536	0.9536
VA-rating of series inverter (MVA)	0.7509	0.6457	0.5405	0.4354	0.3302
VA-rating of shunt inverter (MVA)	0.6784	0.8406	1.0132	1.1917	1.3740
Total VA-rating of UPQC-WPV (MVA)	1.4293	1.4863	1.5537	1.6271	1.7041
Size of battery (i.e. storage unit) (MWhr)	0.7681	1.5361	2.3042	3.0723	3.8404
Size of PV module (kW)	160.0155	320.0310	480.0465	640.0620	800.0775
Cost of placement of UPQC-WPV ($\times 10^6$ \$)	1.0044	1.5798	2.1576	2.7373	3.3187
The percentage of the cost of storage unit to total cost	23.6788	30.1082	33.0682	34.7532	35.8303
The percentage of the cost of UPQC to total cost	26.7304	17.6700	13.5238	11.1624	9.6414
The percentage of the cost of the PV array to total cost	33.2437	42.2712	46.4266	48.7926	50.3058

Table 5 Solution corresponding to lowest power loss during peak hour

Solution	UPQC-WPV (Case 5)	UPQC-SPAC
Location	61	61
Peak hour power loss (kW)	47.61	80.28
Peak hour minimum node voltage (p.u.)	0.9655	0.9567
VA-rating of UPQC (MVA)	1.7041	1.924
Size of DG unit (MW)	0.8	1
Power factor of the DG unit	Unity	0.8 leading

3.3.6 Performance Comparison with an Existing UPQC Model

Since the planning problem formulated in this chapter is not exactly similar to those reported in the literature, no strong conclusion can be drawn from the comparative results with the already reported UPQC models. However, a performance comparison is provided between the proposed UPQC-WPV model and UPQC sag-based phase angle control model (UPQC-SPAC) reported in [83] to show that the performance of the proposed UPQC-WPV model is comparable with that of the UPQC-SPAC. The 69-bus distribution network is used for this purpose. It is worth noting that there is no DG or storage unit connected to the DC link of UPQC-SPAC as in UPQC-WPV. In UPQC-SPAC model [83], a UPQC is placed in same bus with a DG unit to support the reactive power demand of the DG unit. The result corresponding to the lowest power loss is shown in Table 5 with the placement of UPQC-WPV (Case 5) and UPQC-SPAC with a DG unit. The results show that the power loss and minimum bus voltage of the network are found to be better in case of UPQC-WPV as compared to UPQC-SPAC. The rating requirement for UPQC is also found to be less in case of UPQC-WPV. However, the placement of UPQC-WPV is a costlier option because of the presence of the storage unit.

4 Conclusions

In this chapter, a review on recent approaches on ADS planning has been provided. A three-level classification tree has been developed to provide a comprehensive review on recent advancement in ADS planning. Different important features of different ADS planning approaches have been brought out and discussed. Since the integration of converter-based renewable generation units, such as PV, creates harmonic pollution, there needs a strategy/device to mitigate. This motivates to devise a new proposal on ADS planning. In the proposed approach, PV array and battery storage unit are connected to the DC link of UPQC to provide active power compensation. The battery storage unit is basically used to store energy generated by the PV array so as to inject into the network during peak hours. This eliminates the need of load curtailment due to energy shortage in peak hours. An exhaustive

search is carried out for the allocation of UPQC-WPV in distribution networks. The salient features of the new proposal are:

- The allocation of UPQC-WPV in a distribution network can protect all the downstream loads from a given value of voltage sag. It is also designed to mitigate a given value of THD.
- The allocation UPQC-WPV in a suitable location of a network results in significant reduction of power loss. Hence, the energy efficiency of the network would significantly be improved.
- The amount of compensation to be provided by UPQC-WPV can be controlled by the design parameter K_{St} . With the higher value of K_{St} , UPQC-WPV can capable of providing higher compensation. Obviously, this increases the rating requirements for the storage unit and the PV array.
- The results show that the planning cost primarily governs by the costs of the battery storage unit and the PV array, and these are found to be linearly varying with the design parameter K_{St} .

In future, this study can be extended with the multiple placements of UPQC-WPV and the required coordinated control among different UPQC-WPV units.

References

1. Gonen T, Ramirez-Rosado IJ (1986) Review of distribution system planning models: a model for optimal multi-stage planning. IEE proceedings C-generation, transmission and distribution, vol 133, pp 397–408
2. Temraz HK, Quintana VH (1993) Distribution system expansion models: an overview. *Electr Power Syst Res* 26:61–70
3. Khator SK, Leung LC (1997) Power distribution planning: a review of models and issues. *IEEE Trans Power Syst* 12:1151–1159
4. Ganguly S, Sahoo NC, Das D (2013) Recent advances on power distribution system planning: a state-of-the-art survey. *Energy Syst* 4:165–193
5. Georgilakis PS, Hatziaargyriou ND (2015) A review of power distribution planning in the modern power system era: models, methods and future research. *Electr Power Syst Res* 121:89–100
6. Xiang Y, Liu J, Li F, Yong L, Youbo L, Xu R, Su Y, Ding L (2016) Optimal active distribution network planning: a review. *Electr Power Compon Syst* 44:1075–1094
7. Sedghi M, Ahmadian A, Aliakbar-Golkar M (2016) Assessment of optimization algorithms capability in distribution network planning: review comparison and modification techniques. *Renew Sustain Energy Rev* 66:415–434
8. Ganguly S, Samajpati D (2015) Distributed generation allocation on radial distribution networks under uncertainties of load and generation using genetic algorithm. *IEEE Tran Sustain Energy* 6:688–697
9. Atwa YM, El-Saadany EF (2011) Probabilistic approach for optimal allocation of wind-based distributed generation in distribution systems. *IET Renew Power Gener* 5:79–88
10. Haghifam M-R, Falaghi H, Malik OP (2008) Risk-based distributed generation placement. *IET Gener Transm Distrib* 2:252–260

11. Zidan A, Shaaban MF, El-Saadany EF (2013) Long-term multi-objective distribution network planning by DG allocation and feeders' reconfiguration. *Electr Power Syst Res* 105:95–104
12. Jahromi ME, Ehsan M, Meyabadi AF (2012) A dynamic fuzzy interactive approach for DG expansion planning. *Electr Power Energy Syst* 43:1094–1105
13. Soroudi A, Afrasiab M (2012) Binary PSO-based dynamic multi-objective model for distributed generation planning under uncertainty. *IET Renew Power Gener* 6:67–78
14. Humayd ASB, Bhattacharya K (2013) Comprehensive multi-year distribution system planning using back-propagation approach. *IET Gener Transm Distrib* 7:1415–1425
15. Ziari I, Ledwich G, Ghosh A, Platt G (2013) Optimal distribution network reinforcement considering load growth, line loss, and reliability. *IEEE Trans Power Syst* 28:587–597
16. Hemmati R, Hooshmand R, Taheri N (2015) Distribution network expansion planning and DG placement in the presence of uncertainties. *Electr Power Energy Syst* 73:665–673
17. Martins VF, Borges CLT (2011) Active distribution network integrated planning incorporating distributed generation and load response uncertainties. *IEEE Trans Power Syst* 26:2164–2172
18. Evangelopoulos VA, Georgilakis PS (2014) Optimal distributed generation placement under uncertainties based on point estimate method embedded genetic algorithm. *IET Gener Transm Distrib* 8:389–400
19. Popovic ZN, Kerleta VD, Popovic DS (2014) Hybrid simulated annealing and mixed integer linear programming algorithm for optimal planning of radial distribution networks with distributed generation. *Electr Power Syst Res* 108:211–222
20. Kim S, Kim W, Kim J (2014) Determining the optimal capacity of renewable distributed generation using restoration methods. *IEEE Trans Power Syst* 29:2001–2013
21. Gill S, Kockar I, Ault GW (2014) Dynamic optimal power flow for active distribution networks. *IEEE Trans Power Syst* 29:121–131
22. Carpinelli G, Celli G, Pilo F, Russo A (2003) Embedded generation planning under uncertainty including power quality issues. *Int Trans Electr Energy Syst* 13:381–389
23. Borges CLT, Martins VF (2012) Multistage expansion planning for active distribution networks under demand and distributed generation uncertainties. *Electr Power Energy Syst* 36:107–116
24. Martinez JA, Guerra G (2014) A parallel Monte Carlo method for optimum allocation of distributed generation. *IEEE Trans Power Syst* 29:2926–2933
25. Yuan W, Wang J, Qiu F, Chen C, Kang C, Zeng B (2016) Robust optimization-based resilient distribution network planning against natural disasters". *IEEE Trans Smart Grid* 7:2817–2826
26. Al Kabbi SS, Zeineldin HH, Khadkikar V (2014) Planning active distribution networks considering multi-DG configurations. *IEEE Trans Power Syst* 29:785–793
27. Gabash A, Li P (2012) Active-reactive optimal power flow in distribution networks with embedded generation and battery storage. *IEEE Trans Power Syst* 27:2026–2035
28. Nick M, Cherkaoui R, Paolone M (2014) Optimal allocation of dispersed energy storage systems in active distribution networks for energy balance and grid support. *IEEE Trans Power Syst* 29:2300–2310
29. Ganguly S, Samajpati D (2017) Distributed generation allocation with on-load tap changer on radial distribution networks using adaptive genetic algorithm. *Appl Soft Comput* 59:45–67
30. Pereira BR Jr et al (2016) Optimal distributed generation and reactive power allocation in electrical distribution systems. *IEEE Trans Sustain Energy* 7:975–984
31. Taroco CG, Takahashi RHC, Carrano EG (2016) Multiobjective planning of power distribution networks with facility location for distributed generation. *Electr Power Syst Res* 141:562–571
32. Jayasekara N, Masoum MAS, Wolfs PJ (2016) Optimal operation of distributed energy storage systems to improve distribution network load and generation hosting capability. *IEEE Trans Sustain Energy* 7:250–261
33. Mokryani G (2015) Active distribution networks planning with integration of demand response. *Sol Energy* 122:1362–1370

34. Wang S, Chen S, Ge L, Wu L (2016) Distributed generation hosting capacity evaluation for distribution systems considering the robust optimal operation of OLTC and SVC. *IEEE Trans Sustain Energy* 7:1111–1123
35. Bagheri A, Monsef H, Lesani H (2015) Renewable power generation employed in an integrated dynamic distribution network expansion planning. *Electr Power Syst Res* 127:280–296
36. Tolabi HB, Ali MH, Rizwan M (2015) Simultaneous reconfiguration, optimal placement of DSTATCOM, and Photovoltaic array in a distribution system based on Fuzzy-ACO approach. *IEEE Trans Sustain Energy* 6:210–218
37. Saboori H, Hemmati R (2017) Maximizing DISCO profit in active distribution networks by optimal planning of energy storage systems and distributed generators. *Renew Sustain Energy Rev* 71:365–372
38. Shen X, Shahidehpour M, Han Y et al (2017) Expansion planning of active distribution networks with centralized and distributed energy storage systems. *IEEE Trans Sustain Energy* 8:126–134
39. Bagheri A, Monsef H, Lesani H (2015) Integrated distribution network expansion planning incorporating distributed generation incorporating distributed generation considering uncertainties, reliability, and operational conditions. *Electr Power Energy Syst* 73:56–70
40. Mokryani G, Hu YF, Pillai P, Rajamani H-S (2017) Active distribution network planning with high penetration of wind power. *Renew Energy* 104:40–49
41. Santos SF et al (2017) Novel multi-stage stochastic DG investment planning with recourse. *IEEE Trans Sustain Energy* 8:164–178
42. Munoj-Delgado G, Contreras J, Arroyo JM (2016) Multistage generation and expansion planning in distribution systems considering uncertainty and reliability. *IEEE Trans Power Syst* 31:3715–3728
43. Biswas PP et al (2017) A multiobjective approach for optimal placement and sizing of distributed generators and capacitors in distribution network. *Appl Soft Comput* 60:268–280
44. Nejadfard-Jahromi S, Rashidinejad M, Abdollahi A (2015) Multistage distribution network expansion planning under smart grids environment. *Electr Power Energy Syst* 71:222–230
45. Heidari S, Fotuhi-Firuzabad M, Kazemi S (2015) Power distribution network expansion planning considering distribution automation. *IEEE Trans Power Syst* 30:1261–1269
46. Nguyen HK, Mohsenian-Rad H, Khodaei A, Han Z (2017) Decentralized reactive power compensation using Nash Bargaining solution. *IEEE Trans Smart Grid* 8:1679–1688
47. Xiang Y, Liu J, Liu Y (2016) Optimal active distribution system management considering aggregated plug-in electric vehicles. *Electr Power Syst Res* 131:105–115
48. Zhou L, Li F, Gu C, Hu Z, Blond SL (2014) Cost/benefit assessment of a smart distribution system with intelligent electric vehicle charging. *IEEE Trans Smart Grid* 5:839–847
49. Eajal AA et al (2016) Stochastic centralized dispatch scheme for AC/DC hybrid smart distribution systems. *IEEE Trans Sustain Energy* 7:1046–1059
50. Shen X, Shahidehpour M, Zhu S, Han Y, Zheng J (2016) Multi-stage planning of active distribution networks considering the co-optimization of operation strategies. *IEEE Trans Smart Grid*
51. Guo L, Liu W, Jiao B, Hong B, Wang C (2014) Multi-objective stochastic optimal planning method for stand-alone microgrid system. *IET Gener Transm Distrib* 8:1263–1273
52. Bahramirad S, Reder W, Khodaei A (2012) Reliability-constrained optimal sizing of energy storage system in microgrid. *IEEE Trans Smart Grid* 3:2056–2062
53. Lofti H, Khodaei A (2017) AC versus DC microgrid planning. *IEEE Trans Smart Grid* 8:296–304
54. Hakimi SM, Moghaddas-Tafreshi SM (2014) Optimal planning of a smart microgrid including demand response and intermittent renewable energy resources. *IEEE Trans Smart Grid* 5:2889–2900
55. Wang Z, Chen B, Wang J, Kim J, Begovic MM (2014) Robust optimization based optimal DG placement in microgrids. *IEEE Trans Smart Grid* 5:2173–2182

56. Hajipour E, Bozorg M, Fotuhi-Firuzabad M (2015) Stochastic capacity expansion planning of remote microgrids with wind farms and energy storage. *IEEE Trans Sustain Energy* 6: 491–498
57. Moradi MH, Eskandari M, Hosseini SM (2015) Operational strategy optimization in an optimal sized smart microgrid. *IEEE Trans Smart Grid* 6:1087–1095
58. Arefifar SA, Mohamed YAI, EL-Fouly THM (2013) Comprehensive operational planning framework for self-healing control actions in smart distribution grids. *IEEE Trans Power Syst* 28:4192–4200
59. Xiang Y, Liu J, Liu Y (2016) Robust energy management of microgrid with uncertain renewable generation and load. *IEEE Trans Smart Grid* 7:1034–1043
60. Levron Y, Guerrero JM, Beck Y (2013) Optimal power flow in microgrids with energy storage. *IEEE Trans Power Syst* 28:3226–3234
61. Ross M, Abbey C, Bouffard F, Joos G (2015) Multi-objective optimization dispatch for microgrids with a high penetration of renewable generation. *IEEE Trans Sustain Energy* 6:1306–1314
62. Shi W, Xie X, Chu C, Gadh R (2015) Distributed optimal energy management in microgrids. *IEEE Trans Smart Grid* 6:1137–1146
63. Che L, Zhang X, Shahidehpour M, Alabdulwahab A, Al-Turki Y (2017) Optimal planning of loop-based microgrid topology. *IEEE Trans Smart Grid* 8:1771–1781
64. Parisio A, Rikos E, Glielmo L (2014) A model predictive control approach to microgrid operation optimization. *IEEE Trans Control Syst Technol* 22:1813–1827
65. Dall’Anese E, Zhu H, Giannakis GB (2013) Distributed optimal power flow for smart microgrids. *IEEE Trans Smart Grid* 4:1464–1475
66. Som T, Chakraborty N (2014) Studies on economic feasibility of an autonomous power delivery system utilizing alternative hybrid distributed energy resources. *IEEE Trans Power Syst* 29:172–181
67. Yang H et al (2017) Operational planning of electric vehicles for balancing wind power and load fluctuations in a microgrid. *IEEE Trans Sustain Energy* 8:592–604
68. Wang H, Huang J (2016) Cooperative planning of renewable generations for interconnected microgrids. *IEEE Trans Smart Grid* 7:2486–2496
69. Khodaei A, Bahramirad S, Shahidehpour M (2015) Microgrid planning under uncertainty. *IEEE Trans Power Syst* 30:2417–2425
70. Hajipour E, Bozorg M, Fotuhi-Firuzabad M (2015) Stochastic capacity expansion planning of remote microgrids with wind farms and energy storage. *IEEE Trans Sustain Energy* 6:491–498
71. Ghosh A, Ledwith G (2009) *Power quality enhancement using custom power devices*. Springer, Berlin
72. Khadkikar V, Chandra A (2008) A new control philosophy for a unified power quality conditioner (UPQC) to coordinate load-reactive power demand between shunt and series inverters. *IEEE Trans Power Deliv* 23:2522–2534
73. Khadkikar V (2012) Enhancing Electric Power Quality Using UPQC: A Comprehensive Overview. *IEEE Trans Power Electron* 27:2284–2297
74. Khadkikar V, Chandra A (2011) UPQC-S: A novel concept of simultaneous voltage sag/swell and load reactive power compensations utilizing series inverter of UPQC. *IEEE Trans Power Electron* 26:2414–2425
75. Kisk DO, Navrapescu V, Kisk M (2007) Single-phase unified power quality conditioner with optimum voltage angle injection for minimum VA requirement. *IEEE international symposium on industrial electronics*, pp 2443–2448
76. Khadkikar V, Chandra A (2009) A novel structure for three-phase four-wire distribution system utilizing unified power quality conditioner (UPQC). *IEEE Trans Ind Appl* 45:1897–1902
77. Jindal AK, Ghosh A, Joshi A (2007) Interline unified power quality conditioner. *IEEE Trans Power Deliv* 22:364–372

78. Brenna M, Faranda R, Tironi E (2009) A new proposal for power quality and custom power improvement: OPEN UPQC. *IEEE Trans Power Deliv* 24:2107–2116
79. Heydari H, Moghadasi AH (2011) Optimization scheme in combinatorial UPQC and SFCL using normalized simulated annealing. *IEEE Trans Power Deliv* 26:1489–1498
80. Han B, Bae B, Kim H, Baek S (2006) Combined operation of unified power-quality conditioner with distributed generation. *IEEE Trans Power Deliv* 21:330–338
81. Jayanti NG, Basu M, Conlon MF, Gaughan K (2009) Rating requirements of the unified power quality conditioner to integrate the fixed speed induction generator-type wind generation to the grid. *IET Renew Power Gener* 3:133–143
82. Sarker J, Goswami SK (2016) Optimal location of unified power quality conditioner in distribution system for power quality improvement. *Electr Power Energy Syst* 83:309–324
83. Ganguly S (2014) Impact of unified power quality conditioner allocation on line loading, losses, and voltage stability of radial distribution systems. *IEEE Trans Power Deliv* 29:1859–1867
84. Ganguly S (2014) Multi-objective planning for reactive power compensation of radial distribution networks with unified power quality conditioner allocation using particle swarm optimization. *IEEE Trans Power Syst* 29:1801–1810
85. Savier JS, Das D (2007) Impact of network reconfiguration on loss allocation of radial distribution systems. *IEEE Trans Power Deliv* 22:2473–2480
86. DiOrio N, Dobos A, Janzou S (2015) Economic analysis case studies of battery energy storage with SAM. National Renewable Energy Laboratory Technical Report, NREL/TP-6A20-64987
87. Manuel WG (2014) TURLOCK Irrigation District Energy storage study 2014. California Energy Commission Report
88. http://www.nrel.gov/analysis/tech_lcoe_re_cost_est.html (last Accessed on July 2017)

Solar Dish Micro Gas Turbine Technology for Distributed Power Generation

Davide Iaria, Jafar Alzaili and Abdalnaser I. Sayma

Abstract To enable renewable distributed power generation with minimum reliance on the grid, it is essential to develop systems that are able to operate in stand-alone mode. Advances in the development of parabolic dish systems powering a micro gas turbine coupled to thermal energy storage offer this possibility through being able to operate without the need for backup power except when there are days with lengthy periods of clouds. Further backup can be provided through hybridisation with fossil fuels which could allow the system to operate completely in stand-alone mode (dispatchable). Although such systems are still in the development stage, they potentially offer a substantial advantage over photovoltaic cells that create significant grid instability if operated without local backup. The alternative is to provide battery storage which is very expensive or to provide diesel engines' backup which has adverse environmental impact. This chapter describes recent developments in dispatchable parabolic dish solar concentrator systems powering a micro gas turbine operated by a single dish that tracks the sun on two axes. System arrangement and component design options are discussed. A bespoke micro gas turbine design is required with the aim to minimise the overall cost of the system which is dominated by the dish. The mechanical arrangement poses significant challenges compared to conventional micro gas turbines due to the potentially wide operating range and the interconnected thermal management requirements of the micro gas turbine, high-speed alternator, recuperator and solar receiver. Solar receiver system design is of importance when the system is to be integrated with high-temperature thermal energy storage depending on the storage technology used. Safe and efficient operation requires the development of suitable operation and control strategies that will also be discussed in this chapter.

D. Iaria · J. Alzaili · A. I. Sayma (✉)
City University of London, London, UK
e-mail: a.sayma@city.ac.uk

D. Iaria
e-mail: Iaria.Davide@city.ac.uk

J. Alzaili
e-mail: Jafar.Alzaili@city.ac.uk

Keywords Concentrated solar power • Solar dish • Micro gas turbine

1 Introduction

Concentrated solar power (CSP) systems use mirrors arranged to focus the direct sunlight onto a receiver to raise the temperature of a working fluid. The working fluid then transfers its energy to a prime mover. Parabolic dish and solar towers have the potential to increase the temperature of the working fluid in excess of 800 °C which is needed for certain types of prime movers such as gas turbines [1]. However, the solar towers are not suitable for low power range of tens of kilo-Watts [2]; hence, parabolic solar dish concentrators are the most suitable for such applications. Internal combustion (IC) reciprocating engines are not a suitable contender because of inherent features in their basic engine cycle and design principles. Stirling engines have been proposed as a possible choice. These are piston-type reciprocating engines that operate with an external heat source, and thus, they are suited for CSP. Stirling engines use hydrogen as the working fluid at high pressure. Mainly because of this feature, they suffer from a number of technical problems affecting life and reliability, such as issues with cylinder seals, hydrogen leakage, hot spots in the heater and difficulties with part-load control. Such problems lead to system complexity and increased weight and cost.

Gas turbines are used extensively in power generation as well as in aero applications. Micro gas turbines (MGTs) are a term loosely used for gas turbines producing power from several hundred Watts to about 1 MW. Nowadays, they are commercially available in the power range from 30 kW up to 1 MW. Small MGTs producing less than 10 kW are not commercially available yet. However, there is a growing interest in MGTs in this power range for various applications, including domestic combined heat and power (CHP), range extenders in hybrid vehicles, auxiliary power units in heavy vehicles, portable power generation, marine auxiliary power and standby power units and small unmanned air vehicles (UAVs). Compared with IC engines that currently dominate the market below 10 kW, MGTs offer the potential for lower emissions, superior fuel flexibility (including renewable fuels), higher reliability, longer engine life, lower noise and vibrations and reduced maintenance costs. The focus of this chapter is on MGT application for concentrated solar power generation systems.

The first attempt to use a MGT in a CSP prime mover seems to be the work done by at NASA during the 1980s [3]. However, the work has not been continued. Six and Elkins [4], among others, attempted the concept by adopting turbochargers technology. More recently, purpose-designed MGT engine was adopted to examine the performance of the CSP systems based on MGT [5]. It is worth noting that some projects for Stirling engine-based CSP failed mainly because the cost of the prime mover hardware was too high [6]. On the other hand, MGTs have the potential to be more reliable and robust alternative and have been the subject of recent development of a demonstration system (www.omspo.eu).

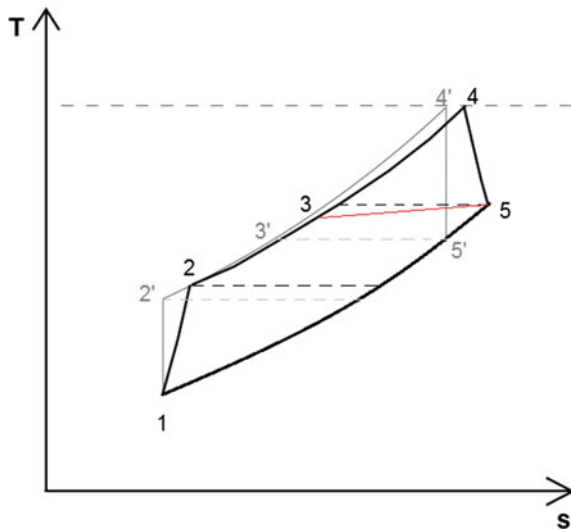
For CSP systems, the MGT presents relatively small part of the overall capital cost compared to the solar dish [7, 8]. Thus, optimising the MGT for high efficiency and the related increase in production cost could be outweighed by the reduction in the dish size and thus overall cost of the system. The variable solar insolation requires the MGT to operate efficiently at a much wider range than conventional technology. This has a significant impact on the rotor dynamic design of the shaft-bearing arrangement and mechanical design. The control strategy of the MGT needs to take into account that thermal input to the system cannot be used as a control parameter. The main challenge with thermal storage is to provide high-temperature output from thermal storage systems usually in excess of 800 °C. There are technical challenges facing hybridisation of MGT-CSP systems mainly related to the combustor design in order to operate efficiently over a wide range of loading. In addition to providing continuous power, hybridisation of the system will improve controllability of the MGT.

2 Micro gas Turbine Solar Dish Systems

2.1 Thermodynamic Cycle

MGTs in the power range below 100 kW typically use recuperated Brayton–Joule cycle. Relatively low-pressure ratios are used, and hence, efficiency can be enhanced by partial recovery of the exhaust heat using a heat exchanger (recuperator). Figure 1 shows the main thermodynamic transformations characterising a recuperated Brayton–Joule cycle. The ideal cycle is characterised by an isentropic compression ($1 - 2'$), an isobaric heat recovery ($2' - 3'$), isobaric heating ($3' - 4'$) and an isentropic expansion ($4' - 5'$). In real cycles however, due to irreversibility in the processes, there is a deviation from ideal behavior. This is shown on the Entropy ($T-S$) diagram of the cycle from 1 to 5 in Fig. 1.

Fig. 1 $T-S$ thermodynamic diagram representing a recuperated Brayton–Joule cycle



The thermodynamic transformations are subject to irreversibility, and all the components are characterised by losses which lead to deviation from the ideal behaviour of the plant. Moreover, the recuperator is not able to fully recover the exhaust heat and is usually characterised by effectiveness around 85–90%. For this reason, the real behaviour of the plant can be represented on the T–S thermodynamic plane by the cycle from 1 to 5 as shown in Fig. 1. The open cycle uses air as the working fluid, where its pressure is increased by the compressor before it enters the recuperator, where a partial recovery of the exhaust heat occurs. Subsequently, air enters the solar receiver to absorb the energy coming from the concentrated solar irradiation. Air is finally expanded in the turbine to provide power necessary to sustain the system and generate electricity (Fig. 2).

The OMSoP project, funded by the European 7th framework, has been investigating the feasibility of a concentrated solar-powered micro gas turbine. A demonstration plant was built and tested in Italy. A schematic of the system is shown in Fig. 2, which incorporates a recuperated cycle micro gas turbine rated at 6 kWe. The main micro gas turbine parameters are given in Table 1.

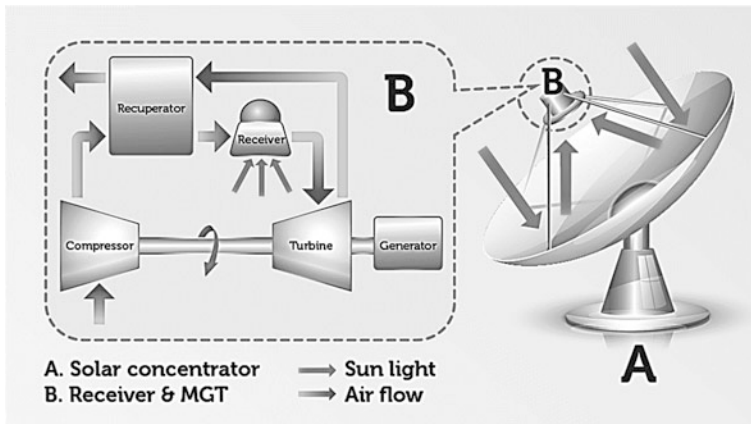


Fig. 2 OMSoP plant scheme (www.omspo.eu)

Table 1 OMSoP plant's main specifications

Parameter	Value
Turbine inlet temperature	800 °C
Compressor efficiency	74%
Turbine efficiency	80%
Recuperator effectiveness	85%
Dish area	42 m ²
Rotational speed	130 krpm
Thermal efficiency	22.3%

2.2 Hybridisation with Combustion and Thermal Storage

A significant complication with the utilisation of solar thermal power as a primary source of energy is the intermittency of solar irradiation. DNI is characterised by a high-frequency daily fluctuation as well as low-frequency seasonal variations. Hybrid operation, where the solar energy is integrated with a fuel backup, allows the system to operate continuously. Moreover, the high exhaust temperature of the micro gas turbine also admits the feasibility of supplying additional services, such as heating, cooling and water purification and desalination.

Hybridisation presents a number of technological challenges, especially for Stirling engines where heat pipes integrated with the receiver are typically required. Hybrid solar MGT (Fig. 3), however, has advantages over Sterling engines as the combustor can be installed separately from the receiver either in parallel or serial arrangements.

Another opportunity to increase the plant dispatchability is thermal storage. The receiver maximum operating temperature imposes a strict limit on the maximum amount of solar energy that can be transferred to electricity and may result in a high amount of wasted solar energy. Thermal storage systems can absorb the excess thermal power increasing the annual solar share of the plant, reducing fuel consumption during hybrid operation and consequently emissions. Current dish CSP systems do not include thermal storage; this is due to the technological issue that the storage system must be incorporated into the receiver to reduce thermal energy losses in transmission pipes, and hence, innovative arrangements are required.

The solar energy that would have been wasted otherwise can be used to generate electricity, increasing the annual power output. These storage systems have also the advantage of smoothing power output fluctuations caused by the solar irradiation variability. A typical dispatching of a thermal storage system for solar application is represented in Fig. 4.

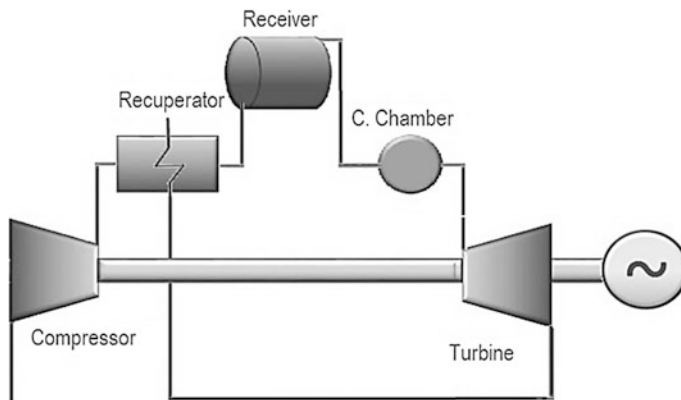


Fig. 3 Hybrid solar micro gas turbine plant schematic

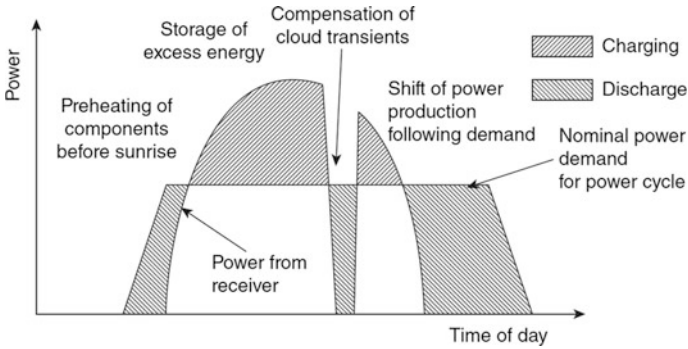


Fig. 4 Typical thermal storage dispatching for solar application [9]

There are three main thermal energy storage systems. The first is sensible energy storage (SES), where the variation of the stored energy is dependent on the temperature difference, the mass (m) of the storage material and its specific heat, $C(T)$. (Eq. 1).

$$\Delta Q = m \int_{T_1}^{T_2} C(T) dT \quad (1)$$

The thermal capacity and the heat release rate are the most important parameters for SES systems as it dictates the selection of materials. Concrete and castable ceramics are the most used materials for this application, due mainly to their low prices and high heat storage capacity.

The most promising materials are molten salts, a mixture of salts with a low freezing temperature $\cong 220$ °C. At these temperatures, molten salts are attractive candidates due to their relatively high heat capacity, density, thermal stability and relatively low cost and low operating pressure. Nevertheless, complexity and cost of such systems increase due to the need to external heating to prevent freezing during low solar irradiation periods. Moreover, at high temperatures, salt stabilities and corrosion aspects play a major role reducing storage expected lifetime and therefore cost.

The second storage option is the latent heat storage (LHS). These systems store and release the heat by changing a material from a phase to another. The biggest advantage of this kind of storage is the option to store energy within a narrow temperature range characterised by a high latent heat released during the transition. These features potentially enable a smaller and cheaper storage system compared to the SES systems. Moreover, phase changes at a constant temperature and thus takes some time to complete its transition with the consequent benefits of smoothing temperature variations [9]. However, a majority of them do not satisfy the criteria required for an adequate storage media. Indeed, some storage systems are characterised by an insufficient long-term stability of materials and containers.

The third energy system is the thermochemical energy storage (TCES). TCES systems use the energy stored in the enthalpy change of a reversible chemical reaction, resulting in a very high energy density compared to the other storage systems and potentially admitting a long-term storage within a small volume. The basic concept of chemical energy storage is to absorb energy that comes from an endothermic reaction, and during the discharge process, the reaction products are recombined exothermically generating heat. In general, TCES systems are characterised by a high-energy density kW/m^3 and a theoretically unlimited discharge time when operating at ambient temperature. Nevertheless, the technology is still in an early stage of development.

3 Issues of Detailed Machinery and Devices

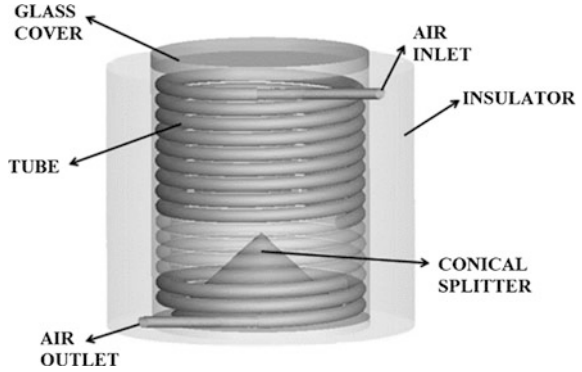
The main components of a solar hybrid MGT are as follows: compressor, recuperator, receiver, combustor and turbine. In the present section will be discussed the main design criteria and issues related to each component.

Compressor Centrifugal compressors are composed of an impeller, a diffuser, either vaned or vaneless, and a volute and are usually used in small MGTs. For solar applications, the machine works most of the time in off-design conditions, due to the solar fluctuations along the day. For this reason, it is important to have a wide range of efficient operations. Studies conducted by the authors [10] demonstrate that optimised vaneless diffusers could guarantee a wider range of efficient operations compared to vaned ones, with consequent benefits for the whole plant.

Recuperator Usually for solar dish applications, the micro gas turbine is mounted on the front side of the dish. For this reason, weight and volume of the machine must be kept as low as possible and compact heat exchangers seem to be then the most attractive option. Different arrangements and designs are available on the market depending on the required compactness and materials. The recuperator is one of the most expensive components of the MGT, and an accurate selection of layout and materials is required to achieve a competitive cost of energy. On the other hand, the heat exchanger must be able to withstand the high temperature of the working fluid, for this reasons the most suitable choice must be found in a trade-off between these two objectives.

Receiver A solar receiver is a device that can capture the solar energy coming from the dish and transfers it to the working fluid. Unlike Stirling engines and other concentrated solar power arrangements, for micro gas turbine solar dish application the air can be directly heated inside the receiver without having to resort to another heat transfer fluid. Different layouts can be conceptualised; one of the most promising arrangements is the air tube cavity receiver. As shown in Fig. 5, an air tube cavity receiver is mainly composed of a cylindrical cavity surrounded by an insulator. At the bottom of the cavity, an optical splitter can be present to readdress

Fig. 5 Air tube cavity receiver components

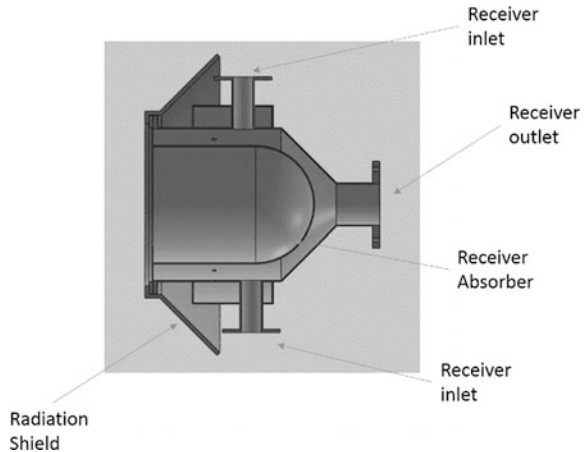


incident sun rays, and at the top of the cavity, a quartz glass can be present to minimise heat transfer between the receiver and the ambient, reducing losses.

Another concept that can be used by this application is the one adopted by the OMSoP project, called volumetric receiver. In this arrangement, the inlet air is heated impinging on the absorber surface. This arrangement is pipeless and then able to minimise the thermal stresses that characterise other arrangements (Fig. 6).

Combustor MGT’s combustor operating conditions could be significantly different from those of a larger gas turbine. The low value of pressure ratio, the low mass flow rate and the relatively low turbine inlet temperature cause non-negligible technological issue. During the day, solar fluctuation forces the machine to work mainly in off-design conditions. High variations in operating conditions have direct consequence on the emissions level and the flame stability inside the combustor can. Recently, special focus has been placed on the development of combustor operating by the Flameless Oxidation (FLOX[®]) principle. In comparison with conventional flame regime, this concept enables increased efficiency, while

Fig. 6 Volumetric cavity receiver schematic



simultaneously reducing pollutant emissions, especially NO_x . Moreover, a further advantage is the low risk of flashback, meaning that a high level of fuel flexibility can be achieved and it is possible to use fuels containing hydrogen [11].

Turbine Radial turbine is typically used which is mainly composed of the impeller, nozzle vanes and the volute. The turbine must be able to provide good performances in off-design conditions. Although these machines usually have relatively high efficiency in a wide range of operating points, there is still room for further improvements. An option to improve off-design performances of the turbine is adopting variable nozzle guide vanes. The variation of the inclination angle of the nozzle can significantly improve the performances of the turbine in part-load condition.

4 Mechanical Arrangement and Dynamic Stability

A challenge is associated with the variable solar insolation requiring the MGT to operate efficiently at a much wider range than conventional technology. This has a significant impact on the rotor dynamic design of the shaft-bearing arrangement and mass distribution. At least three different mechanical arrangements can be considered for the MGT components (compressor, bearings, turbine and the electricity generator). These are as follows: cantilevered design, generator-in-middle design and coupled shaft design. The main features of each are summarised below:

Cantilevered arrangement This is the most common set-up in small-scale micro gas turbines. In this arrangement, the assembly of the turbine and compressor is hanged from one end of the rotor. The main advantage of this design is that no significant cooling arrangement is required for the high-speed generator (HSG). Practically, incoming air to the compressor can act as cooling subsystem for the HSG. Although this could affect the efficiency of the MGT, it can reduce the size and cost of the accessories. Alternatively, a separate cooling system can be integrated to the MGT. The main disadvantage of this arrangement is that this design suffers from rotor dynamic issues. For the range of power concerned with an MGT powered by a single dish (below 20 kWe), it is not practical to have a stable cantilevered design for the wide range of operating speeds needed for the solar application.

Coupled shaft arrangement In this design, two separate shafts are coupled, using flexible coupling that does not transmit bending moment; one contains the rotor and the HSG and the other shaft will contain the compressor and turbine impellers. The rotor dynamics of this arrangement is improved compared to the cantilevered design. This allows moving all bending modes out of the operating range, and no excessive cooling is required for the HSG as it sits on a separate shaft and far from the turbine. However, this results in the additional expense of more bearings and

associated costs. Also, this raises technical difficulties with the high-speed coupling design and reliability.

Generator-in-middle arrangement The HSG rotor is located between the compressor and turbine wheels in this design. It provides a simpler mechanical design with improved dynamic stability. Similar to the coupled shaft design, it is possible to move all bending modes out of the extended range of operation required for the solar application. However, a more significant cooling is required for the HSG as it is sitting in the vicinity of the turbine wheel, but it has also the advantage that the compressor, particularly its inlet, is far from the hot section. Although the cooling system can be integrated with the lubrication system of the bearings, it is considered as a disadvantage for this design.

A study was undertaken as part of OMSoP project showed that the generator-in-middle design could potentially fit better for the solar-powered MGT [12]. The study has taken into account different factors such as cost, reliability and losses. It was concluded that generator-in-middle arrangement could be more suitable for solar-only-powered micro gas turbine.

Another aspect of the rotor dynamic for MGTs is the choice of bearings. The rolling angular contact ball bearings, oil film bearings, floating ring bearings, magnetic bearings and air/foil bearings are different options for the MGTs. The ball bearings are the most common type particularly in smaller MGTs. The technology is well known; however, it requires an oil system. Recent advancement in the development of high-speed ball bearing makes this technology a viable option for the MGTs. For CSP-based MGTs, some form of damping is required to reduce the vibrations caused by passing through or running close to the critical modes. Squeeze film damping (SFD) is a feasible option to be integrated with this type of bearing. Oil film bearings have been the most common type in automotive turbochargers. Despite their robustness, their high friction loss is a big disadvantage for MGT applications, where the efficiency is a critical issue. More work in larger engines was done on magnetic bearings; however, their development and implementation cost for MGTs prevented them from being used despite their advantage of oil-free operation and the inherent ability to control vibrations. Foil air bearings have made significant progress recently due to their high reliability and their oil-free operation. However, there is still much work to be done for the smaller machines in the lower power range to make them a feasible option. The main technical challenges related to the bearings for CSP-based MGT are the robustness of the bearings and their ability to work efficiently for a wide operating range of both rotational speed and loading. They are also required to operate in a more hostile environment, as the most appropriate location is near the focal point of the dish, which typical MGTs would not operate efficiently.

5 Electrical Arrangements and Control Strategies

The control strategy of the MGT needs to be adapted to the fact that the thermal input to the system cannot be used as a control parameter. In a conventional MGT, the fuel (or heat input for the external fired MGTs) is used to control the MGT, namely the rotational speed, turbine inlet temperature (TIT) and turbine exit temperature (TET). For CSP-based MGTs, this option is not possible as the incoming solar power to the receiver cannot be practically controlled [13]. For example, controlling the dish position in order to adjust the amount of thermal input power would not be an option due to the much slower dynamic response of the dish movement mechanism than that of the MGT dynamic response that is orders of magnitude apart. A feasible option to control the MGT in such system is by adjusting the power taken (or given) to the HSG. This would result in controlling the TIT, TET and rotational speed.

A different power electronic architecture can be considered for the CSP-based MGT. As mentioned before, the power electronics would be responsible for controlling the MGT alongside its primary function to convert the power to and from the grid; this would happen in the electronic power conversion system (EPCS). At least two different architectures can be considered for the power conversion system: single converter architecture and double converter architecture. All designs involve an active inverter to control the power output, as this is essential for solar-based MGT.

Single convertor architecture By using electronic components such as IGBTs, the conversion system can act as bidirectional converter. The insulated-gate bipolar transistor (IGBT) acts as passive rectifier during the generating mode, while they will function as variable frequency converter during the motoring mode. The later function controls the speed of the MGT during the start-up process. The MGT control unit will be integrated with this convertor. The technology is not commercially available for the power range of concern of this work. The main challenges are to design an efficient conversion system for higher speed as the speed will be higher for the lower power range.

Double convertor architecture A simple option is to have two separate convertors for the two modes of operation, motoring and generation modes. The conversion system will form of a passive rectifier during generation modes and a grid-tie inverter to feed the power into the grid. For the motoring mode, another passive rectifier and variable frequency inverter are used to run the HSG as motor during the start-up. The design is less complex than the single convertor architecture but it increases the number of components in the system and subsequently the size. The need to alternating between the two separate circuits would also increase the electrical losses. Furthermore, using the passive rectifier (basically a set of diodes) will introduce more power losses compared to IGBTs. Although using IGBTs will increase the complexity of both the conversion system and the control system but it will increase the robustness of the system and decreases the power losses in the

power electronic circuits. Different components of the double converter architecture system are widely available commercially with more optimisation required for the lower power range, where the speed is higher.

Another option is to adopt active rectifiers in the EPCS. An active rectifier can control the speed of the HSG (and subsequently the speed of the MGT) along with a primary function to convert the AC to DC. This potentially can act as controller for the speed of the MGT although the power output of the system still needs to be controlled in order to keep the TIT and TET within the acceptable range. The main disadvantage for the active rectifier is the relatively higher losses compared to the passive rectifier. To have adequate control over the speed, the switching frequency of the active rectifier could be as high as 50 kHz. The switching frequency in other components of the system is usually about 16 kHz.

Although power electronics and control technology are well-developed fields, the challenge is to provide a robust and cost-effective design for the CSP-based MGT giving high rotational speed, wide range of rotational speeds in generation mode and the need for more frequently alternating between the motoring and generation modes than in conventional MGTs. Other challenges are also associated with the electrical and electronic components' design and performance due to the more frequent need to alternate between motoring and generation modes of the high-speed motor/generator which require adequate addressing.

6 Conclusions

This chapter described the main features of a parabolic solar dish concentrator powering a micro gas turbine for distributed power applications. The main features of the system components were described and differences from conventional power plants were highlighted, in particular, those related to compressor and turbine designs, solar receiver, combustor and recuperator. The issues of mechanical arrangement affecting the rotor dynamic stability and system control and electrical scheme have also been described. It can be concluded that significant design features of micro gas turbines need to be adapted for solar applications compared to conventional micro gas turbines.

References

1. Pavlovic TM, Radonjic I, Milosavljevi D, Pantic L (2012) A review of concentrating solar power plants in the world and their potential use in Serbia. *Renew Sustain Energy Rev* 16 (6):3891–3902
2. Buck R, Bräuning T, Denk T, Pfänder M, Schwarzbözl P, Téllez F (2002) Solar-hybrid gas turbine-based power tower systems (REFOS). *J Solar Energy Eng* 124(1):2–9
3. English RE (1986) Technology for Brayton-cycle space power plants using solar and nuclear energy. NASA-TP-2558

4. Six L, Elkins R (1981) Solar Brayton engine/alternator set. In: Parabolic dish solar thermal power annual program review, pp 23–36
5. Dickey B. (2011) Test results from a concentrated solar Microturbine Brayton cycle integration, ASME GT2011-45918
6. Sinai J, Sugarmen C, Fisher U. (2005) Adaptation and modification of gas turbines for solar energy applications, ASME GT2005 (68122)
7. Alzaili J, Sayma A (2016) Challenges in the development of micro gas turbines for concentrated solar power systems. In: 8th International gas turbine conference, Belgium, Brussels
8. Gavagnin G, Sánchez D, Martínez GS, Rodríguez JM, Muñoz A (2017) Cost analysis of solar thermal power generators based on parabolic dish and micro gas turbine: manufacturing, transportation and installation. *Appl Energy* 194:108–122
9. Lovegrove K, Stein W (2012) Concentrating solar power technology. Woodhead Publishing
10. Iaria D, Kader M, Alzaili J, Sayma A (2017) Multi-objective optimisation of a centrifugal compressor for a micro gas turbine operated by concentrated solar power. In: GPPF conference 2017
11. Zornek T, Monz T, Aigner M (2015) Performance analysis of the micro gas turbine Turbec T100 with a new FLOX-combustion system for low calorific fuels. *Appl Energy* 159:276–284
12. Arroyo A, McLorn M, Fabian M, White M, Sayma A. (2016) Rotor-dynamics of different shaft configurations for a 6 kW micro gas turbine for concentrated solar power, ASME, GT2016-56479
13. Ghavami M, Alzaili J, Sayma A (2017) A comparative study of the control strategies for pure concentrated solar power micro gas turbines, Turbo Expo 2017, TE2017-63987

Distributed Energy Solution for India: Exploring the Possibilities

Kuntal Jana and Sudipta De

Abstract Distributed generation is emerging as a possible energy solution from the viewpoint of energy access, energy security and climate change. To use the scattered and intermittent renewable energy resources efficiently, distributed generation is an effective option. About 237 million population of India is living without access to electricity, though India has huge potential for renewable-based distributed generation. Hence, to increase the energy access in rural areas, Government of India is developing and implementing various policies to promote renewable energy and distributed generation. At the same time, development of new and improved technology is making the renewable energy more attractive. However, to be a sustainable energy solution, distributed generation should be economically affordable, environmentally and socially acceptable.

Keywords Distributed energy systems • Renewable energy resources
Sustainable energy solution • Indian context

1 Introduction

Energy sector of India is facing many formidable challenges. Instead of economic growth, a large number of populations in India are facing lack of energy access to electricity and clean cooking [1]. More than 230 million population of India do not have access to electricity. At the same time, high dependency on the imported petroleum and degradation of coal quality reduces the energy security of India. On the other hand, due to coal-based power generation, power sector of India is highly carbon intensive [2]. However, as per ‘Paris Agreement’ along with other countries,

K. Jana

Centre for Energy, Indian Institute of Technology Guwahati, Guwahati 781039, India

S. De (✉)

Department of Mechanical Engineering, Jadavpur University, Kolkata 700032, India
e-mail: de_sudipta@rediffmail.com; sde@mech.jdvu.ac.in

© Springer Nature Singapore Pte Ltd. 2018

S. De et al. (eds.), *Sustainable Energy Technology and Policies*, Green Energy and Technology, https://doi.org/10.1007/978-981-10-7188-1_6

India is also committed to reduce the greenhouse gas emission [3]. To increase the electricity access, high-voltage transmission line may not be economically viable. Sometimes grid connection is not feasible due to geographically remote location and transmission and distribution loss [4]. Conversely, India has a huge potential of renewable energy resources [5]. However, to use the scattered and low-dense renewable energy resource, suitable technology is an imperative need. It is one of the suitability criteria selected from the economic viewpoint. The cost of produced utility should be affordable. Also, initial investment cost should be less as the energy access to be provided is mostly in rural areas [6]. Simultaneously, suitable renewable energy-based technology reduces the life cycle greenhouse gas emission and hence, reduces the carbon intensity of India's energy sector.

In this context, distributed energy generation plays an important role [7, 8]. Distributed generation (DG) may be defined as small-scale power generation and supplied directly to distribution network (low-voltage) for local use, without employing the high-voltage transmission network. It is designated to cater to the secondary energy need of locality only. Electricity is supplied to the locality without high-voltage transmission only through low voltage distribution. However, other utilities are also consumed in the local areas only without long-distance transportation and transmission. Hence, transmission and distribution losses can be minimized through distributed generation. Thus, distributed generation increases the energy security in rural areas. Various advantages of distributed generation are discussed in subsequent section. Distributed energy generation is mainly developed by using locally available energy resource. Hence, assessment of renewable energy resources is necessary for sustainable and uninterrupted operation. The distributed generation should cater to the needs of local population efficiently. Hence, proper design with suitable planning is necessary. For this purpose, distributed polygeneration with locally available energy resources may be possible sustainable solution [9]. However, to implement 'distributed generation' successfully, financial and policy support from government are necessary to be a competitive option with fossil-fuel-based energy [6].

In this chapter, various options of distributed generation with Indian perspective are discussed. Present scenario of the energy sector of India is reviewed for electricity supply and demand and transport sector. Then, challenges regarding to distributed generation and policies of Indian Government are discussed. Then, advantages of distributed generation and its technological aspects are shown. Mapping of renewable energy resources in India and its potential is estimated. Distributed generation for multi-utility generation is explored. Potential of a specific biomass-based polygeneration in India is estimated through a case study. Finally, the sustainability aspects of distributed generation are discussed.

2 Review of Indian Energy Sector

To maintain the present economic growth, India is increasing its electricity generation capacity. As on 31 March 2016, installed generation capacity of power utilities in India was 298 GW, and the gross generation in 2015/16 was 1102 billion units [2]. Out of this, maximum electricity was generated from thermal power plants. Sharing of total electricity generation (in 2014) by different sources is shown in Fig. 1a. From the figure, it is noted that thermal power dominates mostly though a significant amount of hydro-electricity and renewable-based electricity available in Indian electricity mix. Coal is the main primary energy source to the thermal power plants. Coal contributes more than 60% of the total capacity addition during the year of 2015/16. Hence, Indian power sector is carbon intensive and at the same time, facing the challenges of ‘Paris Agreement’. In Fig. 1b, electricity demand in different sector is shown. It is noted that the maximum electricity is consumed in domestic sector followed by industrial sector. Hence, reliable and affordable electricity access for the domestic purpose is important. Distributed generation may play an important role for this purpose.

In Fig. 2, the state-wise installed capacity of electricity generation is shown. From the Fig. 2, it is noted that the Western part of the country produces maximum electricity and Eastern part produces less; though the maximum electricity is generated from coal-based power plant, and Eastern region produces most of the Indian coal. Hence, long-route freight transportation is required for coal, which needs additional investment and consumption of diesel oil. Electricity production with local resources may reduce these burdens.

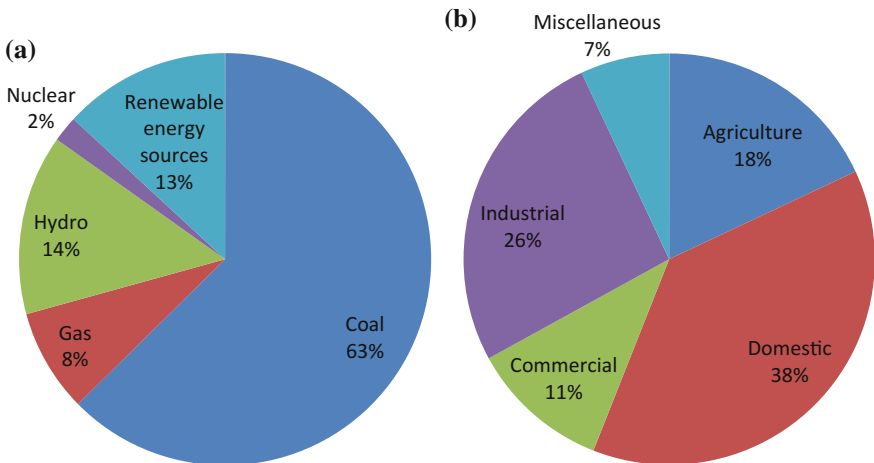


Fig. 1 a Sharing of total electricity generation by different sources [10], b sharing of total electricity demand by different sectors [11]

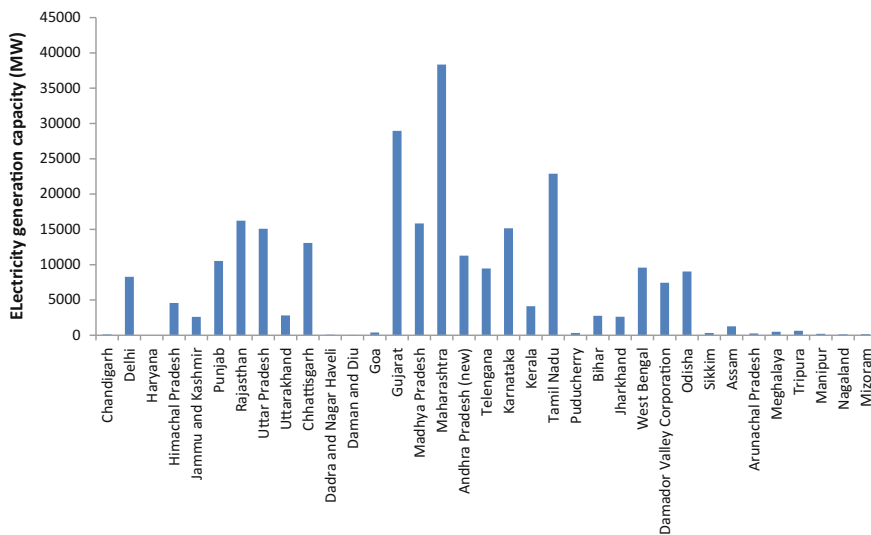


Fig. 2 State-wise total installed electricity generation capacity (2015) in MW [2]

After the power sector, the transportation sector is another major area. In this sector, most of the imported petroleum is consumed. India’s gross domestic product (GDP) largely depends upon the transport sector. It shares 4.8% of total GDP [11]. There are four kinds of transportation system available, e.g. (a) road transport, (b) aviation, (c) shipping and (d) railways. These transportation systems largely depend on imported petroleum from middle-east countries. The consumption of high-speed diesel in the transport sector is shown in Fig. 3. It is noted that both railways and road transport consume a significant amount of imported oil. Hence, it reduces the energy security of India. Due to a large amount of fossil fuel use, the transportation sector is carbon intensive also. Thus, alternative options are necessary for low-carbon transport sector with indigenous fuel. Hence, use of local resources (say, biomass) for alternative option of fuel is necessary.

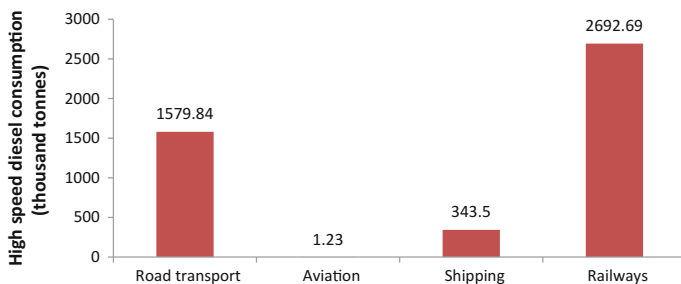


Fig. 3 Consumption (in thousand tonnes) of high-speed diesel oil in the transport sector (2014/15) [12, 13]

Domestic sector is another area of energy demand. It consumes 38% of electricity as shown in Fig. 1a. According to the 68th National Sample Survey, 72.7% of rural and 96.1% of urban households depend on electricity for lighting [14]. Liquefied petroleum gas (LPG) used widely for cooking in 68% of urban and 15% of rural households. Still, significant parts of the rural area face lack of access to electricity and clean cooking [12, 13].

A significant amount of electricity (18%) is consumed in the agriculture sector also. About 168 TWh of electricity is consumed by the agricultural sector. Fertilizer industry for agriculture is another area of significant energy consumption. This is mainly due to urea production. On the other hand, this sector is the third major consumer of diesel (13%), as the maximum amount of diesel is consumed due to water pumping for irrigation [11].

Industrial demand for electricity is the second after the domestic demand. Due to the present economic growth, the capacity of the industry is increasing. In the first half of 2015/16, a growth of 4% in the index of industrial production (IIP) was registered compared to the growth of 2.9% in the first half of 2014/15 [15]. At the same time, energy demand in this sector is increasing due to the energy-intensive industry like cement, iron and steel, aluminium, fertilizers and pulp and paper.

3 Challenges and Policy

India faces a shortage of secondary energy as stated earlier. The electricity shortage was 2.1%, and the peak deficit was 3.2% during 2015/16. Hence, capacity addition is required to maintain the present economic growth. Another important challenge is to increase the 'energy access' all over the country. More than 230 million of people have no access to electricity. About 841 million populations rely on traditional use of biomass for cooking. Clean cooking is not available for a large population. 'Energy security' is also a significant challenge to India. India strongly depends on imported crude oil. Domestic production of oil and gas declined continuously in 2015/16. Imports of crude oil increased significantly to 199 million tonnes in 2015/16 [12, 13]. Hence, India needs to search an alternative option to increase energy access and to reduce the dependency on imported oil.

The Government of India has taken a few policies to deal with these challenges as follows [11].

- (i) In Twelfth Five-year Plan, a capacity addition target of 88,537 MW (excluding renewables) was fixed. Of this target, 38,448 MW was achieved till 31 March 2014. Thermal power accounted for 36,889 MW, which was 96% of the total capacity addition. This will help to reduce the power deficit.
- (ii) The Government of India has launched various programmes for the electrification of rural areas in the country, including the Pradhan Mantri Gramodaya Yojana in 2001/02, Accelerated Rural Electrification

Programme in 2003/04 and Accelerated Electrification of One Lakh Villages and One Crore Households in 2004/05.

- (iii) Rural Electrification Policy, 2006: This policy emphasized on the usage of green technologies for electrification in areas that were very remote or where installing centralized grid infrastructure was technically or financially not feasible.
- (iv) Remote Village Electrification Programme: This programme was launched advance basic lighting facilities in un-electrified villages and hamlets that were out of the Rajiv Gandhi Grameen Vidyutikaran Yojana (RGGVY) and where grid extension was technically/financially not feasible for electricity. Presently, it is discontinued, and new scheme started named as Deendayal Upadhyaya Gram Jyoti Yojana (DDUGJY).
- (v) National Biogas and Manure Management Programme: This scheme is for setting up of family-type biogas plants, mainly for rural and semi-urban households.
- (vi) Jawaharlal Nehru National Solar Mission: The Jawaharlal Nehru National Solar Mission (JNNSM) or the National Solar Mission is under the National Action Plan on Climate Change. In this mission, the target is to deploy 20,000 MW of grid-connected solar power by 2022. Reducing the cost of solar power generation in the country is one of the aims of this mission. In 2015, the government revised the overall JNNSM target to 100 GW.
- (vii) National Biomass Cookstove Programme: The government launched the National Biomass Cookstove Programme for implementation in the Twelfth Five-year Plan period.
- (viii) National Electricity Policy, 2005: This policy recognized electricity as a critical infrastructure for the socio-economic development of the country.

Apart from these, other important policies are Solar City, Akshay Urja Shops, Unnat Chulha Abhiyan, Deendayal Upadhyaya Gram Jyoti Yojana, Pradhan Mantri Ujjwala Yojana, Rajiv Gandhi Gramin LPG Vitaran Yojana etc.

4 Distributed Generation and India

As indicated earlier, India is facing the problem of ‘energy access’ to a large number of populations. The limited capacity of electricity generation is another barrier for meeting the secondary energy demand. Apart from generation, loss of electricity in transformation, transmission and distribution (including unaccounted electricity) was 23% of the total available electricity in 2012/13 [14]. This is a major disadvantage of the centralized power plant. Also, large capital investment is required for the centralized power plant. Water demand for power generation is also high. Apart from the technological and economical viewpoint, greenhouse gas emission is also an inevitable fact of coal-based centralized plant. In case of the large hydropower plant, uprooting of local people and damage in ecosystem

become the strong barrier for capacity addition in electricity generation through large hydel power.

Considering the above difficulties, distributed energy generation may become a sustainable solution for India. Distributed generation (DG) may be defined as small-scale power generation and supplied directly to distribution network (low-voltage) for local use, without the high-voltage transmission network as shown in Fig. 4 [16, 8]. Apart from power generation, there are possibilities for other secondary energy supply like heating, cooling, biofuels and potable water through distributed multi-generation or polygeneration [9]. Distributed generation is also possible where grid connection is not economically viable, or the place is remote and inaccessible. Several advantages of distributed generation are as follows:

- (a) *Reduces peak load demand*: If consumer produces electricity through distributed generation, it reduces the dependency on central grid. Hence, reduces the peak load demand.
- (b) *Negligible transmission and distribution loss*: In distributed generation, long-route transmission is not required. It also reduces the unaccounted loss of distribution.
- (c) *Easy and fast installation*: Easy and quicker installation is possible by using pre-fabricated standardized components.
- (d) *Less capital investment*: As the capacity of distributed generation is low; it requires less capital investment.
- (e) *Environment friendly*: Most of the distributed generation technology uses renewable energy. Hence, it is more environment friendly than fossil-fuel-based centralized plant.
- (f) *Less complex and create job*: Distributed generation is lesser complex. Hence, user-operator participation is possible. So it creates jobs in the locality.

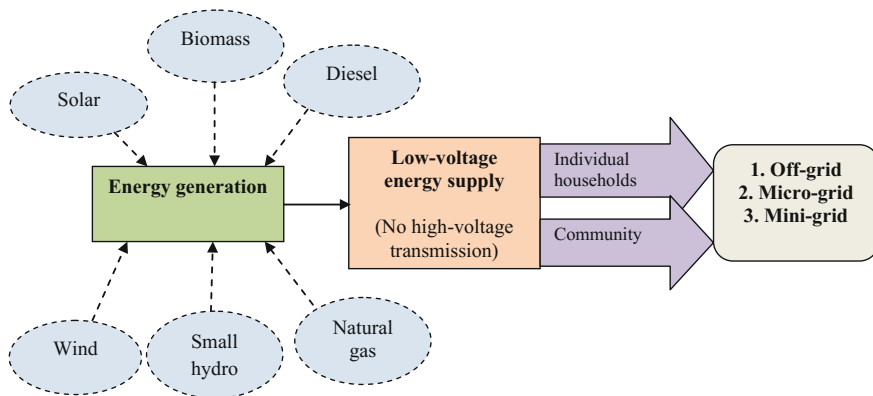


Fig. 4 Input-output of distributed energy solution

- (g) *Easy for capacity addition*: The scale of distributed generation is small, and the gestation period is also low. Hence, it enables faster and easy capacity additions when required.
- (h) *Better energy and load management*: Distributed generation systems offer the possibility of combining energy storage and management systems.

However, there are several challenges regarding the successful commercialization of distributed generation. The technology should be well established. The cost is to be competitive with large-scale power generation. Distributed generation also requires more number of semi-skilled personnel for operation at the community level or for individual house. Also, the supply of resource should be uninterrupted. Emission and noise at locality due to combustion engine or micro-turbines may create negative impacts.

There are several options available for distributed generation based on energy resources and prime movers for power generation as shown in Fig. 5. Energy input to the distributed generation may be renewable or non-renewable. For renewable resources, energy system should be designed according to locally available resources because it is dispersed in nature, and energy density is less. Long-route transportation (say, biomass) may not be economically feasible. Among the renewable resources, from biomass syngas, producer gas, biogas, liquid biofuels can be produced. These products may be used in the gas engine, combustion engine or micro-turbines. Heat and/or electricity can be obtained by solar thermal/photovoltaic system. Power can be generated by wind turbines and small hydro turbines by utilizing the kinetic/potential energy of wind and water. For non-renewable resources like diesel, natural gas, kerosene and suitable technologies are already commercially available combustion engine, gas turbine, etc. [17].

Biomass	<ul style="list-style-type: none"> • Gasifier- gas engine, micro-turbine • Digester - gas engine, micro-turbine • Liquefaction - direct combustion engine
Solar	<ul style="list-style-type: none"> • Solar thermal heat/power • Solar photo-voltaic
Wind	<ul style="list-style-type: none"> • Wind turbine • Aero-generator
Hydro	<ul style="list-style-type: none"> • Small hydro • Micro-hydro
Diesel	<ul style="list-style-type: none"> • Direct combustion engine
Natural gas	<ul style="list-style-type: none"> • Direct combustion engine • Micro-turbine
Kerosene	<ul style="list-style-type: none"> • Direct combustion engine

Fig. 5 Technology options for distributed generation

In Table 1, energy conversion technologies for distributed generation is given with their fuel input, application range, electric conversion efficiency, investment cost of per kW electricity and specific CO₂ emission. From the table, it is noted that investment cost for per kW_e is lower for gas turbine though its scale is much higher than other options. For small-scale application with gaseous fuel, micro-turbine is suitable. Solar PV is suitable for scaling up and down. From the viewpoint of efficiency, the fuel cell is the best option. The specific CO₂ emission greatly depends on fuel input. It is the minimum for the case of renewable inputs. For renewable energy, there is an indirect emission associated with manufacturing and logistics of modules and fuels, respectively.

With the implementation of new policies and technologies, India is increasing the sharing of distributed generation. The policies taken by Indian Government are given in the previous section. Under Deendayal Upadhyaya Gram Jyoti Yojana (DDUGJY-RE), Ministry of Power of India has sanctioned 921 projects to electrify 1,21,225 un-electrified villages, intensive electrification of 592 thousand partially electrified villages and provide free electricity connections to 39.7 million rural households with below poverty level. As on 30 June 2015, works in 110 thousand un-electrified villages and intensive electrification of 320 thousand partially

Table 1 Issues related to distributed generation technologies [4, 8, 19]

Energy conversion technology	Fuel	Application range	Electric conversion efficiency	Investment cost per kW _e (INR)	Specific CO ₂ emissions (g/kWh)
Combustion engine	Diesel	20 kW _e –10 MW _e	36–43%	100,000–170,000	650 (Diesel), 500–620 (Gas)
	Gas	5 kW _e –5 MW _e	28–48%		
Gas turbine	Gas, kerosene	1–20 MW _e	21–40%	7000–90,000	580–680
Micro-turbines	Natural gas, biogas, producer gas	30–200 kW _e	25–30%	100,000–140,000	720, ~0 (for biogas)
Fuel cell: MCFC, PEMFC, SOFC, DMFC	Methanol, H ₂ , natural gas	MCFC: 50 kW _e –1 MW _e , PEMFC: 1–250 kW _e , SOFC: 1 kW _e –5 MW _e	MCFC: 50–55%, PEMFC: 35%, SOFC: 50–55%	310,000–1,400,000	Depends largely on fuel used
Photovoltaic	The sun	Easy to scale up and down	–	35,000–480,000	200–250 (indirect)
Wind	Wind	200 W–3 MW	–	55,000–700,000 (for onshore), 140,000 (for offshore)	13–34 (indirect), depends on wind speed

Table 2 Number of electrified and un-electrified villages of India [23]

State	Total un-electrified villages	Electrified	To be electrified	Under progress
Arunachal Pradesh	1578	349	1229	1224
Assam	2892	2224	558	554
Bihar	2747	2323	424	416
Chhattisgarh	1080	759	321	320
Himachal Pradesh	35	28	0	0
Jammu & Kashmir	134	32	102	49
Jharkhand	2525	1892	579	487
Karnataka	39	14	25	22
Madhya Pradesh	472	373	52	43
Manipur	276	199	77	76
Meghalaya	912	682	230	230
Mizoram	58	40	18	18
Nagaland	82	76	4	4
Odisha	3474	2404	555	553
Rajasthan	495	426	1	1
Tripura	26	26	0	0
Uttar Pradesh	1529	1470	6	6
Uttarakhand	76	23	53	37
West Bengal	22	17	5	3

electrified villages have been completed, and 22 million free electricity connections have been released to BPL households [18]. In Table 2, state-wise electrified, un-electrified and to be electrified villages are shown.

5 Mapping and Present Status of Renewable Energy in India

India has a target of 175 GW of electricity from renewable energy by 2022 [20]. Distributed generation will have great role to achieve this target. However, distributed energy generation greatly depends on input energy resources. Technology is selected for DG according to the available energy resources. For a distributed generation, renewable resources are selected mainly because of its availability in local areas, and it also increases the energy security in rural and remote areas. Hence, mapping of renewable energy resources is necessary for planning and long-term operation of distributed generation.

5.1 Solar Energy

India targets 100 GW of electricity by 2022 from solar energy through utility-scale, distributed off-grid and mini-grid. To achieve this target, mapping of solar resource is important for solar installation. In Fig. 6a, b, direct normal irradiance (DNI) and global horizontal irradiance (GHI) are shown [21]. From the figure, it is noted that the maximum DNI is available at Western part of India (Gujarat, Rajasthan) and a

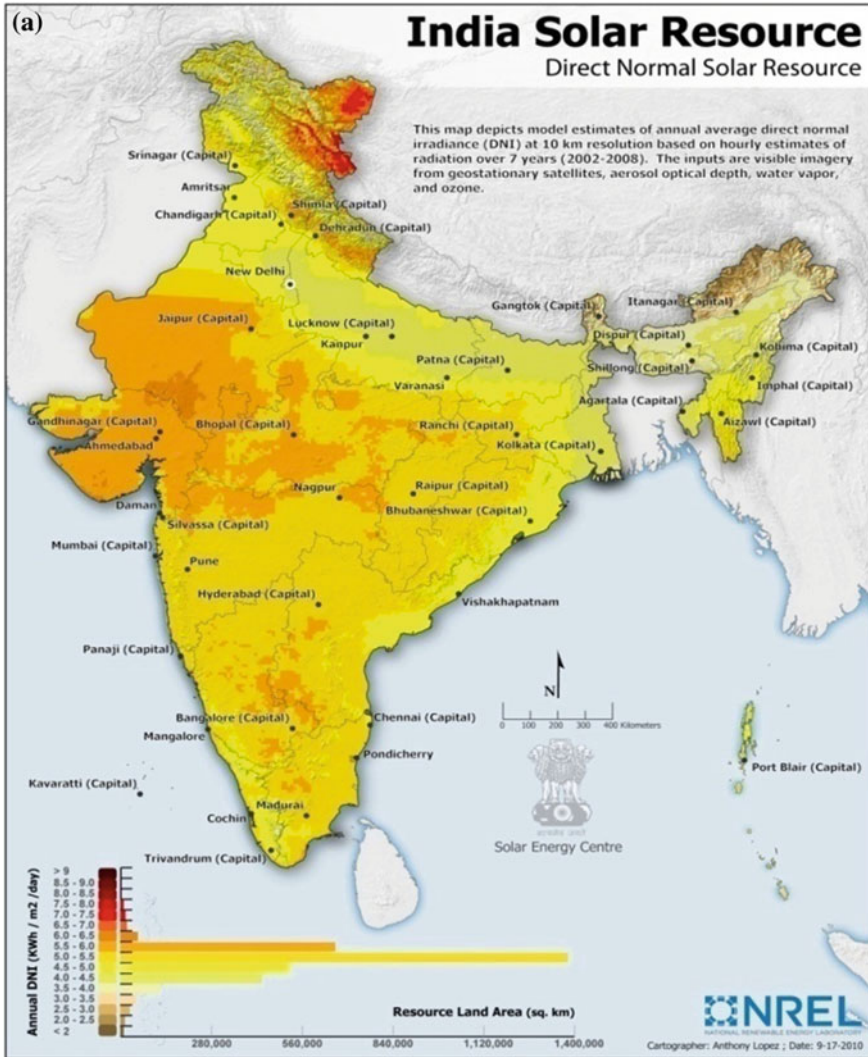


Fig. 6 Annual average of a direct normal irradiance (DNI) and b global horizontal irradiance (GHI) [21, 22]

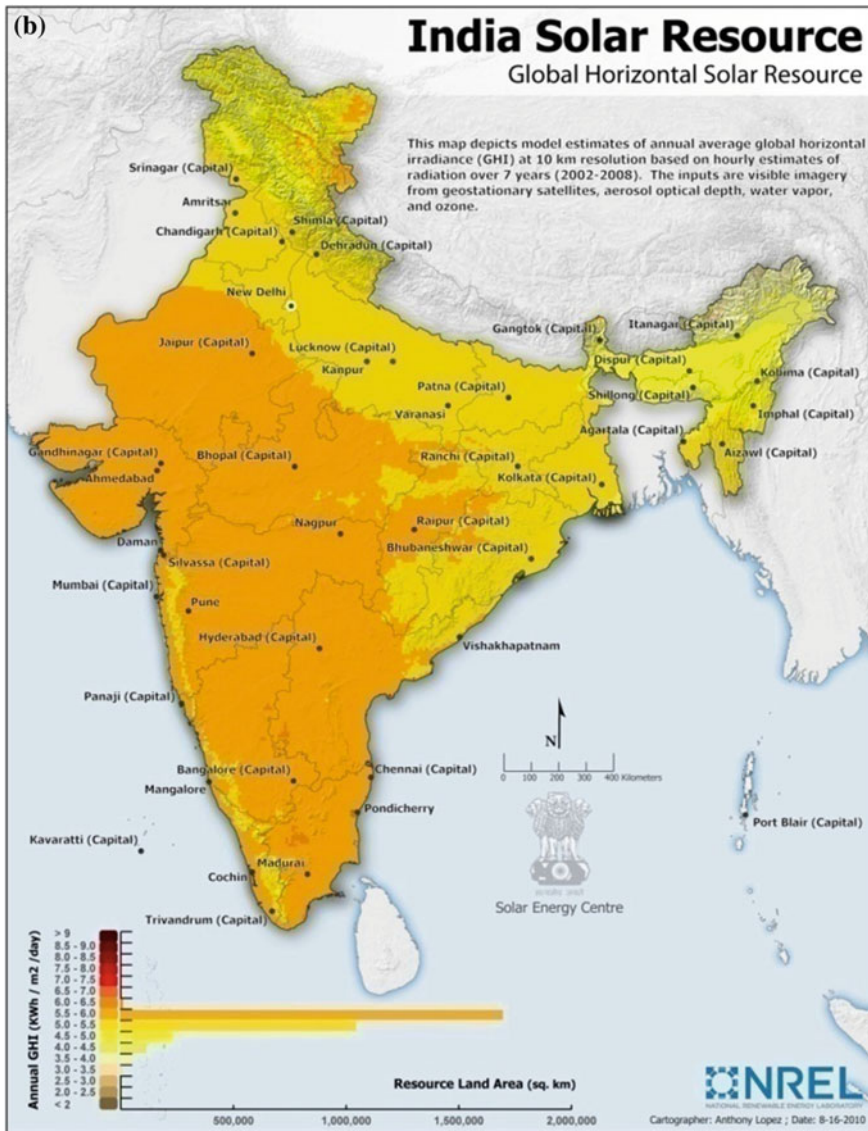


Fig. 6 (continued)

part of the Jammu & Kashmir. However, the maximum GHI is available all over the Western and Southern part of India. For an off-grid solar application, MNRE has various schemes like off-grid solar PV, solar water pumping systems for irrigation and drinking water, solar water heating system, solar cooking, concentrated solar thermal systems and solar air heating. Under these schemes, various subsidies are available from Government of India [11].

5.2 Biomass

Biomass is one of the most abundantly available resources in India. As biomass has good calorific value, it can be used as solid fuel for secondary energy generation. Also, biomass to liquid/gaseous fuel is an attractive option to replace the petroleum oil. Hence, it increases the energy security. Conversion of biomass to secondary energy can be done in two ways, i.e. thermo-chemical conversion and bio-chemical conversion. Apart from conversion technologies, availability and logistics of biomass are also important to ensure long-run operation of the plant. State-wise availability of biomass in India is given in Table 3. According to the Ministry of New and Renewable Energy (MNRE) of India, estimated potential of

Table 3 State-wise availability of biomass in India [5]

State	Area (kha)	Crop production (kt/y)	Biomass generation (kt/y)	Biomass surplus (kt/y)
Andhra Pradesh	2540.2	3232.0	8301.7	1172.8
Assam	2633.1	6075.7	6896.3	1398.4
Bihar	5833.1	13817.8	20441.8	4286.2
Chattisgarh	3815.5	6142.8	10123.7	1907.8
Goa	156.3	554.7	827.2	129.9
Gujarat	6512.9	20627.0	24164.4	7505.5
Haryana	4890.2	13520.0	26160.9	9796.1
Himachal Pradesh	710.3	1329.2	2668.2	988.3
Jammu & Kashmir	368.7	648.7	1198.7	237.7
Jharkhand	1299.8	1509.0	2191.2	567.7
Karnataka	7277.3	38638.5	23766.8	6400.6
Kerala	2041.7	9749.7	9420.5	5702.6
Madhya Pradesh	9937.0	14166.9	26499.6	8033.3
Maharashtra	15278.3	51343.3	36804.4	11803.9
Manipur	72.6	159.4	318.8	31.9
Meghalaya	0.8	14.0	42.0	8.4
Nagaland	27.1	87.6	149.2	27.2
Orissa	2436.6	3633.3	5350.4	1163.4
Punjab	6693.5	27813.7	46339.8	21267.0
Rajasthan	12537.5	93654.8	204887.6	35531.1
Tamil Nadu	2454.0	24544.6	15976.6	6658.7
Uttar Pradesh	12628.2	46800.8	50416.7	11725.9
Uttaranchal	66.4	135.8	159.9	51.6
West Bengal	5575.6	21062.8	23316.0	2959.7
Total	105786.8	399262.1	546422.6	139355.8

biomass-based power and bagasse cogeneration is shown in the Fig. 7. From these estimations, it is noted that potential of biomass as an energy resource is reasonable, and biomass may play a crucial role for India’s sustainable energy future.

5.3 Wind

Wind energy has significant potential in India. State-wise wind power potential of India is shown in Fig. 8. It is noted that the maximum wind power is available in Gujarat, Andhra Pradesh, Tamil Nadu and Karnataka. Total installed capacity of onshore wind power in India is 28,082 MW as on 30.10.2016. India has significant potential of offshore wind also as it has very large coastal area. India has an added advantage due to its annual manufacturing capacity of wind turbine of 9.5 GW [24].

5.4 Other Energy Resources

India has significant potential of small hydropower (SHP) (19,759 MW) as shown in Fig. 9 [24]. Karnataka and Himachal Pradesh have the maximum potential for small hydropower. SHP projects are classified based on the capacity as: micro-hydro (up to 100 kW), mini-hydro (101–2000 kW) and small hydro (2001–25,000 kW). The focus of the SHP programme is to decrease equipment cost, increase reliability and capacity utilization.

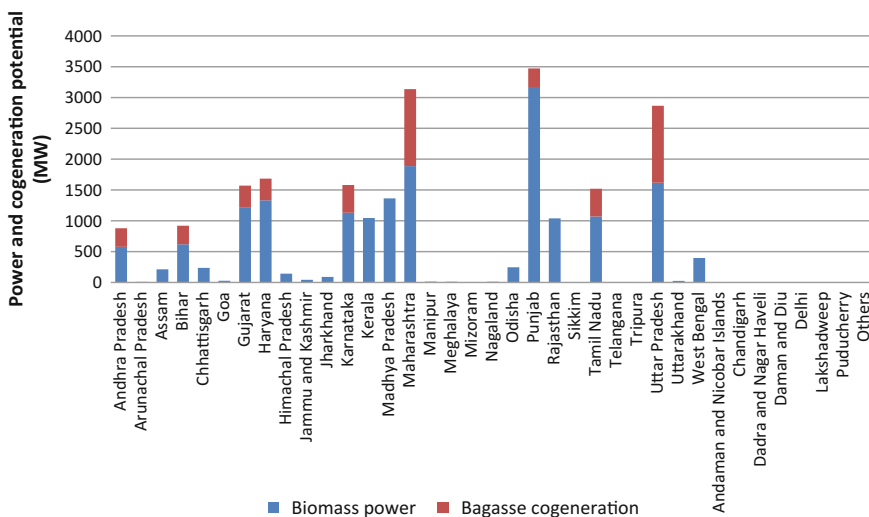


Fig. 7 State-wise potential of biomass-based power and bagasse-based cogeneration (MW) [24]

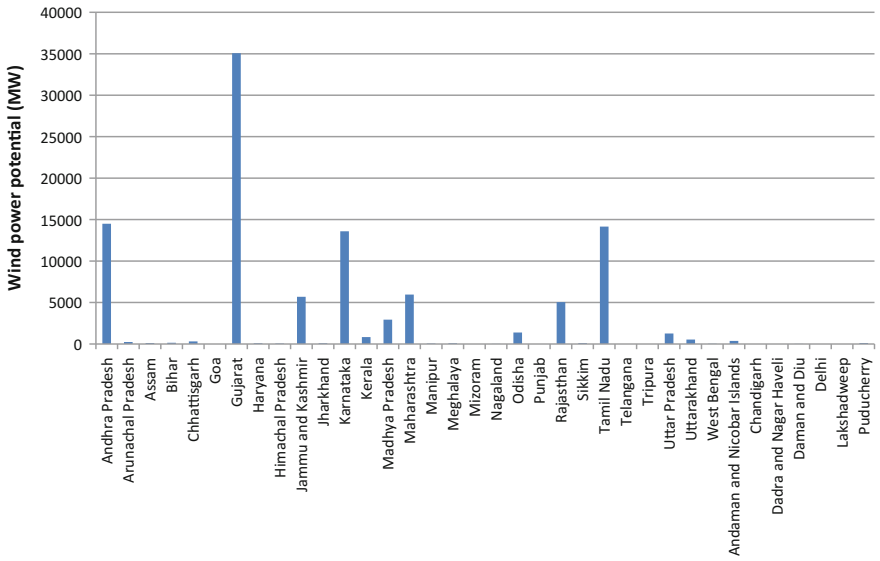


Fig. 8 State-wise potential of wind power (MW) [24]

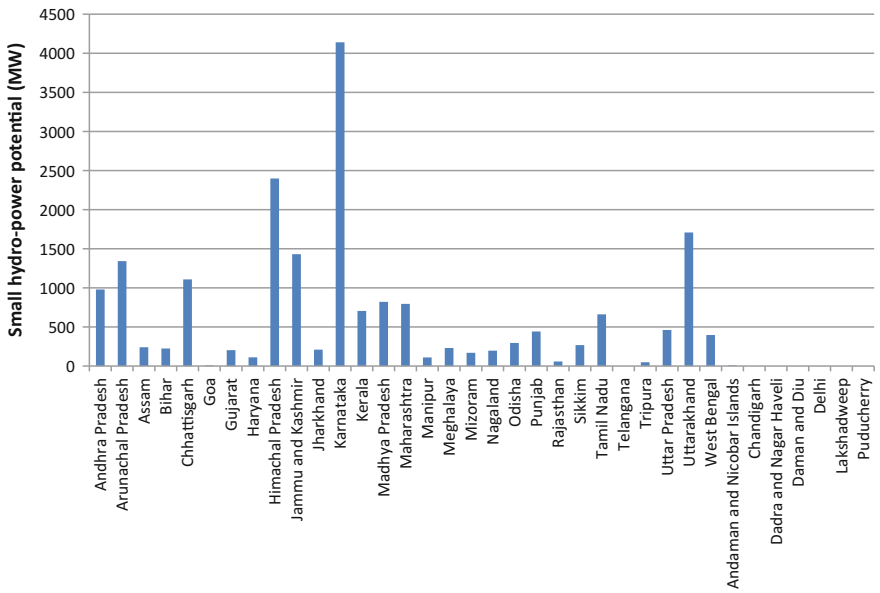


Fig. 9 State-wise potential of small hydropower (MW) [24]

Waste-to-energy has also significant potential. The state-wise potential of waste-to-energy is shown in Fig. 10. Maharashtra has the highest capability in this technology. Other states like Uttar Pradesh, West Bengal have also significant potential. India has the potential of geothermal energy about 10,000 MW. Fuel cell, ocean thermal energy, tidal energy are different options for renewable energy in India.

6 Distributed Polygeneration

In a locality or community, secondary energy-utility demands are in different form say, lighting, heating, cooling, fuels for transportation, etc. However, polygeneration or multi-generation may cater to these demands in addition to electricity. It is an energy conversion system for producing multiple utilities in a single unit by efficient system integration [9]. As a result, its thermodynamic, economic and environmental performances are better than the stand-alone units. However, the design of distributed polygeneration should be according to locally available resources and demands. Hence, specific planning with proper governance is required. As it caters to local demands, it has good social acceptability also. Another advantage of distributed polygeneration is that it can reduce the problem associated with the intermittency of renewable resources (solar, wind). Proper matching of multiple inputs and multiple outputs according to demand is possible by distributed polygeneration. Thus, distributed polygeneration can be a future sustainable option specifically for poor and rural people of India.

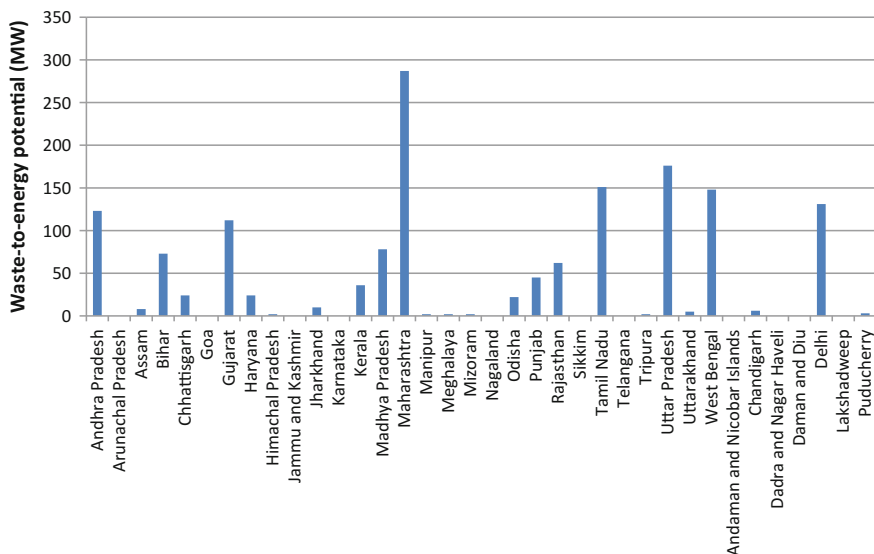


Fig. 10 State-wise potential of waste-to-energy (MW) [24]

7 Biomass-Based Polygeneration: Case Study

A polygeneration with locally available biomass was conceptualized in a previous study [25]. This case study shows the potential of a specific polygeneration fuelled by local biomass to cater to the local demands. Three typical biomasses are used for this study, i.e. rice straw, sugarcane bagasse and coconut fibre. Rice straw is seasonally available agricultural waste. Sugarcane bagasse is available at sugar mills in a concentrated way. Coconut fibre is available from plantation crop at constant rate in coastal areas.

Four basic utilities can be obtained from this polygeneration, i.e. electricity, ethanol, cooling and heating. As this polygeneration is designed for the decentralized application, electricity can be used mainly in domestic or small commercial purpose. Ethanol is an established biofuel. It may be used directly in a combustion engine for transportation or for agricultural machinery. Cooling may be used for food storage or storage of agro-products in rural areas. Utility heat is a by-product of this system. It may be used for food processing. Schematic of the polygeneration is shown in Fig. 11. This polygeneration is based on gasification of biomass. About 60% of produced syngas is used for power generation, and rest is used for ethanol production. As ethanol is easy to store, this distribution may be varied according to utility demand. Power is generated by combined cycle gas turbine, i.e. by a gas turbine and steam turbine. Ethanol is produced in the thermo-chemical process, and heat is a by-product of this process. Cooling may be obtained by vapour absorption cooling where the waste heat of syngas cooling process is utilized. Sensible heat of this process may be used for the heating purpose as shown in Fig. 11. Detailed simulation and thermodynamic analysis of this polygeneration are previously published. Based on this result and availability of biomass, the state-wise potential of power generation and ethanol production of rice straw, sugarcane bagasse and coconut fibre is given in Table 4. Heating and cooling potential of India through this polygeneration is shown in Table 5 (Fig. 12).

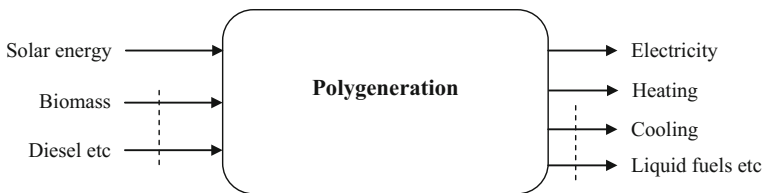


Fig. 11 Concept of polygeneration

Table 4 Power generation and ethanol production potential of a polygeneration using three generic biomasses

	Power generation (GWh/y) potential			Ethanol production (kt/y) potential		
	Rice straw	Sugarcane bagasse	Coconut fibre	Rice straw	Sugarcane bagasse	Coconut fibre
Andhra Pradesh	14008	3749	618	1386	368	64
Arunachal Pradesh	136	0	0	13	0	0
Assam	6446	210	123	638	20	12
Bihar	6779	1239	0	671	121	0
Chhattisgarh	7098	0	0	702	0	0
Goa	255	0	183	25	0	19
Gujarat	1622	2647	144	160	260	14
Haryana	3217	1985	0	318	195	0
Himachal Pradesh	144	0	0	14	0	0
Jammu & Kashmir	6	0	0	0.6	0	0
Jharkhand	1845	0	0	182	0	0
Karnataka	6057	7174	2565	599	705	265
Kerala	1050	0	5174	103	0	536
Madhya Pradesh	2898	441	0	286	43	0
Maharashtra	3891	9600	138	385	943	14
Manipur	171	0	0	17	0	0
Meghalaya	179	0	0	17	0	0
Mizoram	0	0	0	0	0	0
Nagaland	288	0	0	28	0	0
Orissa	12,331	136	0	1220	13	0
Punjab	10,531	1880	0	1042	184	0
Rajasthan	243	0	0	24	0	0
Sikkim	8	0	0	0.8	0	0
Tamilnadu	3371	7731	2098	333	759	217
Tripura	0	0	43	0	0	4
Uttar Pradesh	12,955	24,716	0	1282	2429	0
Uttaranchal	643	1607	0	63	157	0
West Bengal	22,473	420	485	2224	41	50
Total	118,659	63,539	11,576	11,745	6245	1199

Table 5 Heating and cooling potential of India through a polygeneration using three generic biomasses

Biomass	Heating (GWh/y)	Cooling (GWh/y)
Rice straw	40,632	26,740
Sugarcane bagasse	19,352	13,207
Coconut fibre	3444	2337

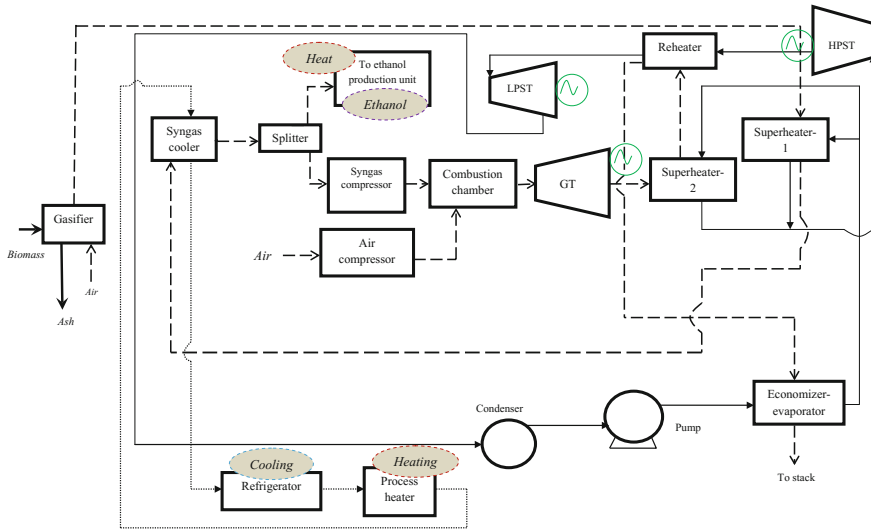


Fig. 12 Schematic of a biomass-based polygeneration [25]

8 Sustainability Aspects of Distributed Generation

The sustainability of energy system is grossly measured by the definition of ‘sustainable development’. Sustainable development is defined as ‘development that meets the needs of the present generation without compromising the ability of future generations to meet their own needs’ by the Brundtland Commission in 1987 (United Nation 1987). Hence, it has three dimensions, i.e. economic, environmental and social. Thus, to be a sustainable energy solution, distributed generation should be economically viable, environmentally and socially acceptable. However, there are several issues associated with the planning of sustainable distributed generation in India as shown in Fig. 13. The efficiency and the plant load factor of distributed generation should be reasonable. The starting and installation time is to be minimized. Lifetime of the plant should be good with less maintenance. As the distributed generation is targeted for rural off-grid areas, investment cost and operation and investment cost should be less to supply output utilities (e.g. electricity) at a low price. Apart from these, environmental issues are also critical from the viewpoint of sustainability and climate change.

Technical issues	Economic issues	Environmental issues
<ul style="list-style-type: none"> • Efficiency • Plant load factor • Starting time • Installation time • Maintenance • Life time 	<ul style="list-style-type: none"> • Investment cost • O&M cost including fuel cost • Utility cost 	<ul style="list-style-type: none"> • CO₂ • SO₂ • NO_x • PM₁₀ • HC • Noise etc.

Fig. 13 Issues related to planning of distributed generation in India

9 Conclusion

In the present context of energy access, energy security, climate change and sustainability of energy system, distributed energy generation is emerging as a possible sustainable energy solution. Presently, India's energy sector is highly dependent on the large capacity fossil-fuel-based plant, and produced electricity is transmitted through grid transmission. However, in off-grid rural areas, distributed generation may be the solution for increasing energy access. For distributed energy generation, input energy is mainly renewable, and India has very good potential of renewable energy in the form of solar, biomass, hydro, wind, etc. Several technologies are available for distributed generation. Design and planning of distributed energy supply by utilizing local resources are very crucial. In this regard, polygeneration may be a possible option for catering multiple utility demand using local renewable resources efficiently. However, present challenges of distributed energy are supplying energy utilities at low cost with less environmental impacts and through socially acceptable technology.

Acknowledgements Dr. Kuntal Jana gratefully acknowledges to the Science and Engineering Research Board (SERB, DST), India for awarding National Post-Doctoral Fellowship.

References

1. OECD/IEA (2015) India energy outlook: world energy outlook special report. International Energy Agency, France
2. CEA (2016) Executive summary power sector. Central electricity authority. Available at www.cea.nic.in/reports/monthly/executivesummary/2016/exe_summary-03.pdf
3. UNFCCC (2014) The Paris Agreement. United Nations framework convention on climate change. Available at http://unfccc.int/paris_agreement/items/9485.php. Accessed on 30 June 2017
4. IEA (2002) Distributed Generation in Liberalised Electricity Markets, Paris

5. MNRE (2016) State-wise potential of various renewable energy technologies. data.gov.in/catalog/state-wise-potential-various-renewable-energy-technologies. Accessed 31 July 2016
6. Brass JN, Carley S, MacLean LM, Baldwin E (2012) Power for development: a review of distributed generation projects in the developing world. *Annu Rev Environ Resour* 37:107–136
7. Hiremath RB, Kumar B, Balachandra P, Ravindranath NH, Raghunandan BN (2009) Decentralised renewable energy: scope, relevance and applications in the Indian context. *Energy Sustain Dev* 13:4–10
8. Pepermans G, Driesenb J, Haeseldonckx D, Belmans R, D’haeseleer W (2005) Distributed generation: definition, benefits and issues. *Energy Policy* 33: 787–798
9. Jana K, Ray A, Majoumerd MM, Assadi M, De S (2017) Polygeneration as a future sustainable energy solution—a comprehensive review. *Appl Energy* 202:88–111
10. CEA (2015) Annual report 2014/2015, Central Electricity Authority, Ministry of Power, Government of India
11. TERI (2016) TERI energy and environment data diary and yearbook 2015/16 (Updated Edition)
12. MoPNG (2016) Ministry of Petroleum and Natural Gas. Government of India. Annual Report 2015–2016. New Delhi: MoPNG
13. MoPNG (2016) State-wise LPG domestic consumers. Ministry of Petroleum and Natural Gas. Available at http://ppac.org.in/content/148_1_Marketing.aspx. Accessed on 4 June 2016
14. MoSPI (2015) Ministry of Statistics and Programme Implementation. Energy Statistics 2015. New Delhi: MoSPI, Government of India
15. DIPP (2016) Annual report 2015–2016. Department of Industrial Policy and Promotion New Delhi: DIPP
16. Mukhopadhyay S, Singh B (2009) Distributed generation—basic policy, perspective planning, and achievement so far in India. Available at <http://ieeexplore.ieee.org/stamp/stamp.jsp?arnumber=5275741>
17. Banerjee R (2006) Comparison of options for distributed generation in India. *Energy Policy* 34:101–111
18. MoP (2017) Rural electrification—status of rural electrification (RE) under DDUGJY, Ministry of Power. <http://powermin.nic.in/en/content/rural-electrification>
19. Ackermann T, Andersson G, Soder L (2001) Distributed generation: a definition. *Electr Power Syst Res* 57:195–204
20. NITI Aayog (2015) Report of the expert group on 175 GW RE by 2022. Available at http://niti.gov.in/writereaddata/files/writereaddata/files/document_publication/report-175-GW-RE.pdf
21. NREL (2016) India solar resource maps & data (updated March 2016), National Renewable Energy Laboratory, USA. www.nrel.gov/international/ra_india.html. Accessed 30 June 2017
22. SEC (2017) India solar resource maps. Solar Energy Centre, Ministry of New and Renewable Energy, Government of India. Accessed on 30 June 2017
23. REC (2017) Rural Electrification Corporation. <https://garv.gov.in/garv2/dashboard>. Accessed on 01 July 2017
24. MNRE (2016) Ministry of New and Renewable Energy. Annual Report 2015/16. New Delhi: MNRE, Government of India
25. Jana K, De S (2015) Polygeneration using agricultural waste: thermodynamic and economic feasibility study. *Renew Energy* 74:648–660

Synthesis of Cogeneration, Trigeneration, and Polygeneration Systems Using Target-Oriented Robust Optimization

Charlle L. Sy, Kathleen B. Aviso, Aristotle T. Ubando and Raymond R. Tan

Abstract Simultaneous generation of heat, cooling, and other secondary products along with electricity can be more efficient than stand-alone production of these individual streams, due to the opportunities for process integration that naturally arise in such systems. Various cogeneration, trigeneration, and polygeneration schemes can also be configured to achieve operational flexibility to cope with a variable supply of fuels and feedstocks, as well as fluctuating product demand. However, techno-economic risks resulting from long-term uncertainties in the prices of both inputs and outputs can be a barrier to investing in these efficient systems. Hence, this chapter presents a target-oriented robust optimization (TORO) approach for dealing with parametric uncertainties in the synthesis of cogeneration, trigeneration, and polygeneration systems. The model is formulated as a mixed-integer nonlinear program (MINLP), and candidate designs at different levels of robustness can be assessed using Monte Carlo simulation. The methodology is illustrated with a case study on the synthesis of a cogeneration plant.

Keywords Cogeneration · Trigeneration · Polygeneration · Energy efficiency
Target-oriented robust optimization · Uncertainty

C. L. Sy
Industrial Engineering Department, De La Salle University,
2401 Taft Avenue, 0922 Manila, Philippines

K. B. Aviso · R. R. Tan (✉)
Chemical Engineering Department, De La Salle University,
2401 Taft Avenue, 0922 Manila, Philippines
e-mail: raymond.tan@dlsu.edu.ph

A. T. Ubando
Mechanical Engineering Department, De La Salle University,
2401 Taft Avenue, 0922 Manila, Philippines

1 Introduction

The impact of anthropogenic greenhouse gas (GHG) emissions is widely considered to have exceeded safe limits [1]. Since the bulk of these emissions are associated with energy use, mitigation of these GHG emissions can be achieved through various strategies involving low-carbon energy [2]. For example, improvements in the energy efficiency of industrial processes through the application of systematic process integration (PI) techniques can in turn reduce carbon intensity [3]. In particular, high levels of efficiency can be achieved through the simultaneous production of electricity with secondary product streams via polygeneration [4]. Polygeneration is a natural extension of combined heat and power (CHP) or cogeneration systems and is generally more efficient than stand-alone production of individual streams in separate facilities, as it takes advantage of PI opportunities that occur on site. The concept of polygeneration dates back to the early 1980s [5], and a recent review paper outlines the key developments [6]. Alternative terms include multi-energy systems (MES) [7]; the term trigeneration is used for the special case of systems with three products, as in the case of combined cooling, heating, and power (CCHP) systems [8]. When biomass is the primary feedstock, the concept of polygeneration also overlaps with that of the biorefinery [6]. In addition to higher thermodynamic efficiency, polygeneration systems also have other potential advantages, such as the operational flexibility to use multiple fuels and feedstocks [9].

Different process systems engineering (PSE) or computer-aided process engineering (CAPE) tools have been developed for the optimal synthesis and operation of polygeneration and related energy systems. For example, Lozano et al. [10] proposed a linear programming (LP) model for trigeneration plants. The generic mixed-integer linear programming (MILP) formulation first proposed by Grossmann and Santibanez [11] has been applied to the case of polygeneration systems by assuming fixed technical parameters [12, 13]. Alternatively, a mixed-integer nonlinear programming (MINLP) formulation can first be developed and subsequently linearized to allow globally optimal solutions to be determined more easily [14, 15]. In addition, multiple objective optimization models have also been developed to allow environmental aspects to be incorporated along with economic considerations [13, 16, 17]. Other models have been developed to address system robustness or reliability aspects. Andiappan et al. [18] developed a MINLP model that considers unit redundancy to improve operational reliability. Models for the synthesis of robust systems have also been formulated for biorefineries [19] and MES [20]. While most of the models focus on the problem of process synthesis, PSE approaches have also dealt with operational issues. For example, an algebraic approach to debottlenecking was proposed by Tan et al. [21]. Kasivisvanathan et al. [22] developed a MILP model to optimize abnormal operations to minimize economic losses resulting from partial inoperability of process units. Also, in addition to mathematical programming approaches, process graph models have been developed both for synthesis [23] and operation problems [24].

This chapter presents a target-oriented robust optimization (TORO) approach for the synthesis of highly efficient cogeneration, trigeneration, and polygeneration systems under uncertainty. TORO was originally developed as a generic optimization framework [25, 26] and has recently been applied to the design of energy systems [27]. The latter work is based on a MILP formulation, which upon introduction of robustness aspects results in a mixed-integer nonlinear program (MINLP). Monte Carlo simulation is then used to generate and evaluate a range of solutions, from which a decision-maker can select a final choice depending on the associated level of risk aversion; a tutorial treatment of the latter paper is given in this work. The rest of the chapter is organized as follows. First, a formal problem statement is given in the next section. Then, the MILP and MINLP formulations are given for the deterministic and TORO models, respectively; the corresponding LINGO code for the models is also given in the Appendix A, and pedagogical cogeneration system example is then solved to illustrate the methodology. Finally, conclusions and prospects for further development are given.

2 Problem Statement

The formal problem statement can be stated as follows:

- Given that cogeneration, trigeneration, or polygeneration system has m process units and n streams including fuel and other feedstocks, intermediates, and products;
- Given that the technological characteristics (e.g., efficiency or yield) of each process unit is defined by a set of fixed input–output parameters;
- Given that the capital cost of each process unit is described by a piecewise linear cost function with fixed and variable cost components;
- Given that there is a demand range for product streams of interest and a range of the availability of resource streams of interest with intermediate product streams completely consumed;
- Given that there is a range for the unit price of products (including fuel and feedstocks).

The assumptions used, which are necessary to maintain the linearity of the model, are as follows:

- Constant efficiency or coefficient of performance (COP) of the component units;
- Piecewise linear capital cost function of the component units;
- Steady-state operation of the entire system.

The problem is to design the polygeneration system for maximizing its profit, while at the same time, considering uncertainties from demand and prices of the product outputs and raw materials.

3 Conventional Model Formulation

The basic deterministic MILP model for general process synthesis was first proposed by Grossmann and Santibanez [11]. A simplified form of their model is given here:

$$\max \mathbf{c}_1^T \mathbf{y} - AF(\mathbf{c}_2^T \mathbf{x} + \mathbf{c}_3^T \mathbf{b}) \quad (1a)$$

subject to:

$$\mathbf{A} \mathbf{x} = \mathbf{y} \quad (1b)$$

$$\mathbf{y}_L \leq \mathbf{y} \leq \mathbf{y}_U \quad (1c)$$

$$\mathbf{x} \leq M \mathbf{b} \quad (1d)$$

$$b_i \in \{0, 1\} \quad \forall i \quad (1e)$$

where \mathbf{A} is the process matrix, \mathbf{c}_1 is the price vector of process streams, \mathbf{c}_2 is the variable cost coefficient vector for process unit capital costs, \mathbf{c}_3 is the fixed cost vector for process unit capital costs, AF is the annualizing (or capital recovery) factor, M is an arbitrary large number, \mathbf{y}^L is the net output lower limit vector for process streams, \mathbf{y}^U is the net output upper limit vector for process streams, \mathbf{b} is the binary variable vector indicating the presence or the absence of the process units, \mathbf{x} is the process unit capacity vector, and \mathbf{y} is the net output vector for process streams. In this formulation, the elements of \mathbf{y} corresponding to inputs, intermediates, and products are negative, zero, and positive, respectively. The LINGO code for this deterministic MILP model is given in Appendix A. The code can be readily modified to accommodate larger data sets, which can be transferred directly from spreadsheets into the relevant data sections. This model can be readily solved to global optimality with conventional branch-and-bound solvers.

4 Robust Model Formulation

Equations 1a and 1b in the previously described model can be modified to integrate uncertainties in various parameters. Equations 2a and 2b for example, integrate uncertainties in the demand and unit price of each product.

$$\max \tilde{\mathbf{c}}_1^T \tilde{\mathbf{y}} - AF(\mathbf{c}_2^T \mathbf{x} + \mathbf{c}_3^T \mathbf{b}) \quad (2a)$$

subject to:

$$\mathbf{Ax} = \tilde{\mathbf{y}} \quad (2b)$$

Where $\tilde{\mathbf{c}}_1$ and $\tilde{\mathbf{y}}$ represent the uncertain unit price and demand, respectively, which are further defined in Eqs. 2c and 2d. $\bar{\mathbf{c}}_1$ and $\bar{\mathbf{y}}$ are the nominal values for unit price and demand while $\delta\mathbf{c}_1$ and $\delta\mathbf{y}$ represent the perturbations for the unit price and the demand, respectively, which follow the conditions given in Eq. 3.

$$\tilde{\mathbf{c}}_1 = \bar{\mathbf{c}}_1 - \delta\mathbf{c}_1 \quad (2c)$$

$$\tilde{\mathbf{y}} = \bar{\mathbf{y}} - \delta\mathbf{y} \quad (2d)$$

$$Z_\theta = \left\{ \delta\mathbf{c}_1, \delta\mathbf{y} \in \mathbb{R}^N \mid 0 \leq \delta c_{1i} \leq \widehat{\delta c_{1i}}(\theta), 0 \leq \delta y_i \leq \widehat{\delta y_i}(\theta), \forall i = 1, \dots, N \right\} \quad (3)$$

The largest perturbation occurs when $\delta c_{1k} = \widehat{\delta c_{1k}}$ and $\delta y_k = \widehat{\delta y_k}$, for all $k = 1, 2, \dots, N$. Furthermore, these perturbations are parameterized by the robustness index, $\theta \in [0, 1]$ where a higher value of θ implies a larger degree of perturbation for the uncertain parameters. A decision-maker with a risk-averse attitude will prefer a higher value of θ while someone who is risk seeking will prefer a lower value. The model is then further reformulated so that the objective function is to maximize the robustness of the system with the constraint of achieving a defined target (τ).

$$\max_{\theta \in [0,1]} \theta \quad (4a)$$

subject to:

$$\left(\bar{\mathbf{c}}_1^T \mathbf{Ax} - \theta \widehat{\delta c_1} z_1 \right) - \text{AF}(\mathbf{c}_2^T \mathbf{x} + \mathbf{c}_3^T \mathbf{b}) \geq \tau \quad (4b)$$

$$\mathbf{Ax} \leq \left(\bar{\mathbf{y}} - \theta \widehat{\delta \mathbf{y}} z_2 \right) \quad (4c)$$

$$\mathbf{z}_1 \geq \mathbf{Ax} \quad (4d)$$

$$\mathbf{z}_2 \geq \mathbf{1} \quad (4e)$$

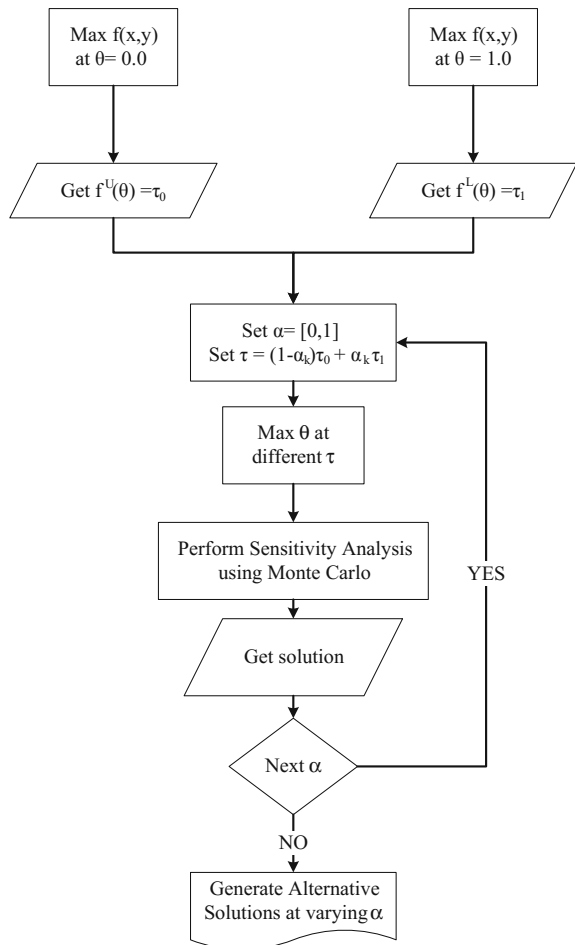
$$\mathbf{x}, \mathbf{z}_1, \mathbf{z}_2 \geq 0, \mathbf{b} \in \{0, 1\} \quad (4f)$$

The model is implemented by finding the highest (Profit^U) and lowest (Profit^L) possible profit. The highest profit is obtained for the most optimistic scenario when the unit price (\mathbf{c}_1) of the products is at the upper limit, the unit cost of raw materials at the lowest limit, and the product demand (\mathbf{y}) does not exceed the upper demand limit. Alternatively, the lowest profit happens during the most pessimistic scenario

when the unit price of the products is at the lowest level, the unit cost of the raw materials is at the highest level, and the product demands do not exceed the lowest demand limit. The maximum robustness index that maximizes the profit at different profit targets is then determined using Eqs. 5a and 5b, by taking different levels of α_k within the interval of 0–1 (Eq. 5d). The profit target is obtained by using Eq. 5c. The constraints defined in Eqs. 5e, 5f, 5g and 5h should also be satisfied. In the event that multiple objectives are considered; it is possible to carry out the TORO model using different parameter targets (or objectives) and generating a robustness index for various optimization scenarios. The flowchart for implementing the model is illustrated in Fig. 1.

$$\max \theta \tag{5a}$$

Fig. 1 Flowchart of TORO model



subject to:

$$\text{Profit} \geq \tau \quad (5b)$$

$$\tau_k = (1 - \alpha_k)\text{Profit}^U + \alpha_k\text{Profit}^L \quad (5c)$$

$$\alpha_k \in [0, 1] \quad (5d)$$

$$\text{Profit} = (\mathbf{c}_1^T \mathbf{A} \mathbf{x}) - \text{AF}(\mathbf{c}_2^T \mathbf{x} + \mathbf{c}_3^T \mathbf{b}) \quad (5e)$$

$$\mathbf{A} \mathbf{x} \leq (1 - \theta) \mathbf{y}^U + \theta \mathbf{y}^L \quad (5f)$$

$$\mathbf{c}_1 = (1 - \theta) \mathbf{c}_1^U + \theta \mathbf{c}_1^L \quad (5g)$$

$$\mathbf{b} \in \{0, 1\} \quad (5h)$$

Note that the resulting model is an MINLP due to the presence of quadratic terms. In this work, the global solver toolbox in LINGO is used to ensure that the global optimum is found. This solver is based on a branch-and-bound algorithm described by Gau and Schrage [28]. The corresponding LINGO code of this TORO model is given in Appendix B. As with the previous model, this code can also be readily modified to handle larger problems. However, the user needs to activate the global solver toolbox in LINGO in order to determine the correct solutions.

5 Pedagogical Case Study

This case study considers a cogeneration plant for producing electricity, steam at 1.2 bar, and hot water at 75 °C using natural gas (NG) as fuel. The scenario presented here is purely illustrative in nature. Assumptions used are based on parameters used in the literature [13, 27]. The plant consists of four candidate process units:

- Cogeneration module—consists of a gas turbine (GT) generator to produce electricity, with a heat recovery steam generator (HRSG) to produce steam from the waste heat of the GT.
- Boiler—generates steam from NG.
- Hot water generator—generates hot water directly from NG.
- Steam/hot water heat exchanger—generates hot water from steam.

The process units are illustrated separately in Fig. 2a, b, c, and d. For each process unit, all streams normalized per one unit of the main output. These process units can also be combined into a superstructure, as shown in Fig. 3. Based on the information in Fig. 2, the process matrix (\mathbf{A}) can be generated as shown in Table 1. The parameters denote the relative ratio of stream magnitudes. The fixed and

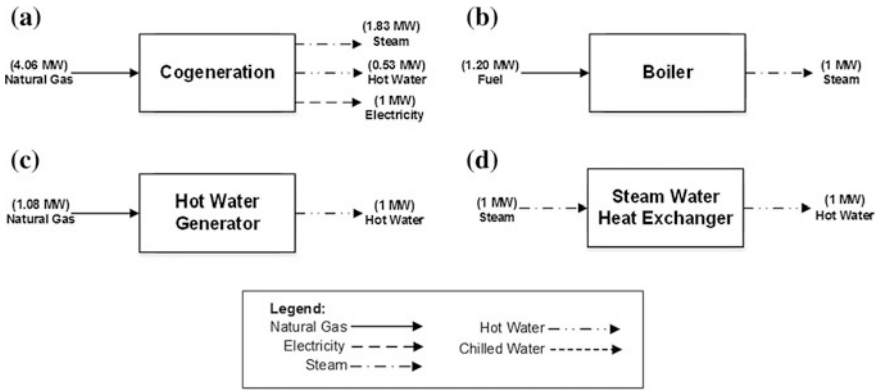


Fig. 2 Process units in the cogeneration case study adapted from Refs. [13, 27]

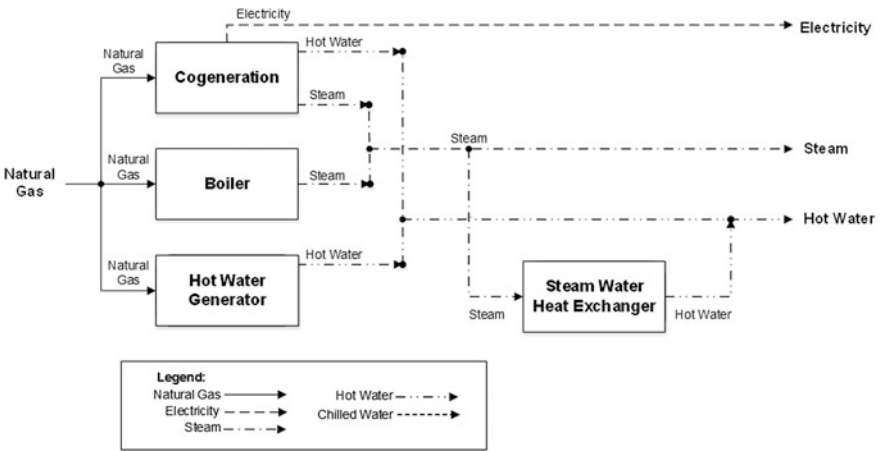


Fig. 3 Superstructure for the cogeneration case study

Table 1 Process matrix of cogeneration plant adapted from Refs. [13, 27]

	CHP module	Boiler	Hot water generator	Heat exchanger
Natural gas (MW)	-4.06	-1.2	-1.08	0
Steam (MW)	1.83	1	0	-1
Hot water (MW)	0.53	0	1	1
Electricity (MW)	1	0	0	0

Table 2 Trigeneration plant process unit cost parameters adapted from Refs. [13, 27]

	CHP module	Boiler	Hot water generator	Heat exchanger
Fixed cost (€)	382,500	45,500	7500	625
Variable cost coefficient (€/MW)	948,347	175,000	39,474	4688

variable cost parameters for the four process units are given in Table 2. The polygeneration plant is assumed to operate 8000 h per year. It is also assumed that the annualizing or capital recovery factor is 0.08/y. Meanwhile, the ranges of values of both demand parameters and price parameters are shown in Tables 3 and 4, respectively.

Solving the deterministic MILP model results in an optimal design shown in Fig. 4. Note that the design requires a 12 MW CHP module, a 3.04 MW boiler, and a 1.64 MW hot water generator; no steam/hot water heat exchanger is required. This design gives an annual profit of €8.905 million and produces 25 MW of steam, 8 MW of hot water, and 12 MW of electricity. However, this nominal optimum is best suited for a deterministic scenario which, in practice, may not materialize. Thus, it has been argued that the availability of multiple solutions can facilitate in identifying good solutions to practical engineering problems [27, 29].

The uncertainties are then integrated by using the TORO formulation. The first step is to identify the profits for the most optimistic ($\theta = 0.00$) and the most pessimistic ($\theta = 1.00$) scenarios. The most optimistic scenario is obtained by setting the unit price for the products at the upper limit, the unit cost of raw materials at the lowest limit, and setting the product demands not exceeding the upper demand limit. Alternatively, the most pessimistic scenario is obtained by setting the unit price of the products at the lowest level, the unit cost of the raw materials at the highest level, and the demands not exceeding the lowest demand limit. The deterministic model is solved for these two scenarios, and the results are as summarized in Table 5. In Scenario 2, it is also important to note that the hot water

Table 3 Product demand ranges in the cogeneration case study adapted from Ref. [27]

	Lower limit	Upper limit
Steam (MW)	20	25
Hot water (MW)	6	8
Electricity (MW)	10	12

Table 4 Price ranges in the cogeneration case studies adapted from Ref. [27]

	Lower limit	Upper limit
Natural gas (€/MWh)	20	30
Steam (€/MWh)	40	50
Hot water (€/MWh)	30	40
Electricity (€/MWh)	90	130

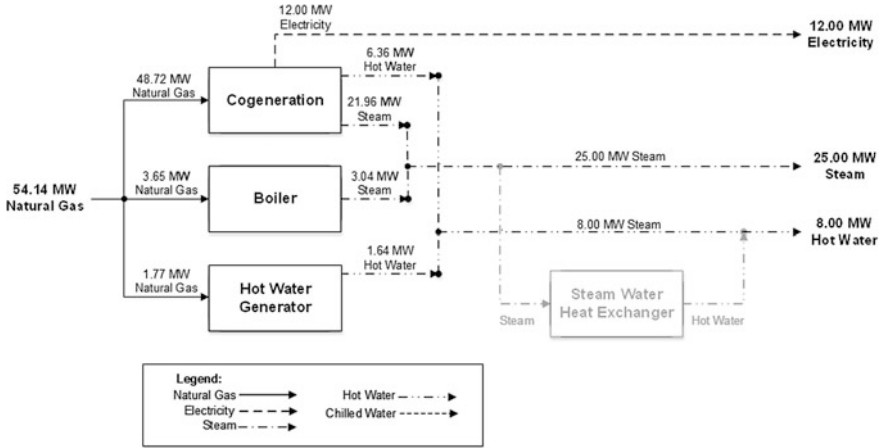


Fig. 4 Optimal configuration of the cogeneration plant using deterministic MILP model

Table 5 Results of the most optimistic and most pessimistic scenarios

	θ	CHP module (MW)	Boiler (MW)	Hot water generator (MW)	Heat exchanger (MW)	Profit (€ million/y)
Scenario 1	0.00	12.00	3.04	1.64	0.00	15.385
Scenario 2	1.00	10.00	1.70	0.00	0.00	3.822

generated is only 5.3 MW and is less than the lower demand limit of 6 MW. The resulting profits for these two scenarios are then used to evaluate the degree of robustness for various realizations of profit target using Eqs. 5c and 5d, where Profit^U and Profit^L are the highest and lowest profits obtained from Scenario 1 and Scenario 2, respectively. Eleven (11) different targets are identified by taking α_k in increments 0.1 within the interval of 0–1.

In addition, Monte Carlo simulation was performed with each target to evaluate the performance of each design. A summary of the system design for different profit targets is given in Table 6; the results of the Monte Carlo simulation are found in Table 7. The different profit targets all revealed the same design, which recommends the installation of the CHP module, boiler, and hot water generator for α value from 0.00 to 0.80 while only the CHP module and boiler are recommended for α equal to 0.90 and 1.00. In addition, results from the Monte Carlo simulation reveal that the mean profit is less than the target profit for α from 0.00 to 0.50. It can also be shown that for α of about 0.70 or above, the mean profit minus one standard deviation already matches or exceeds the target profit. These results show that a conservative decision-maker will favor less ambitious profit targets, coupled with simpler, and less expensive plant configurations.

Table 6 Summary of cogeneration system design for different profit targets

α	τ (10^6 €/y)	θ	CHP module (MW)	Boiler (MW)	Hot water generator (MW)	Heat exchanger (MW)
0.00	15.385	0.00	12.00	3.04	1.64	0.00
0.10	14.229	0.09	11.83	2.92	1.56	0.00
0.20	13.072	0.17	11.65	2.81	1.48	0.00
0.30	11.916	0.26	11.47	2.69	1.39	0.00
0.40	10.760	0.36	11.28	2.56	1.30	0.00
0.50	9.603	0.46	11.09	2.43	1.21	0.00
0.60	8.447	0.56	10.89	2.30	1.12	0.00
0.70	7.291	0.66	10.68	2.16	1.02	0.00
0.80	6.134	0.77	10.47	2.01	0.92	0.00
0.90	4.978	0.88	10.24	1.86	0.00	0.00
1.00	3.822	1.00	10.00	1.70	0.00	0.00

Table 7 Results of the Monte Carlo simulation at different profit targets

α	τ (10^6 €/y)	θ	Mean (10^6 €/y)	Standard deviation (10^6 €/y)	Minimum (10^6 €/y)	Maximum (10^6 €/y)
0.00	15.385	0.00	9.976	1.901	4.797	15.225
0.10	14.229	0.09	9.821	1.870	4.727	14.985
0.20	13.072	0.17	9.663	1.838	4.655	14.738
0.30	11.916	0.26	9.499	1.806	4.581	14.484
0.40	10.760	0.36	9.331	1.773	4.505	14.222
0.50	9.603	0.46	9.157	1.738	4.426	13.952
0.60	8.447	0.56	8.978	1.702	4.344	13.673
0.70	7.291	0.66	8.791	1.665	4.259	13.382
0.80	6.134	0.77	8.597	1.627	4.171	13.080
0.90	4.978	0.88	8.345	1.568	4.085	12.654
1.00	3.822	1.00	8.136	1.528	3.986	12.335

6 Conclusions

A TORO approach for the synthesis of cogeneration, trigeneration, and polygeneration systems under uncertainty was presented in this chapter. This framework uses a MINLP formulation to generate a range of solutions of different levels of robustness; candidate solutions are then analyzed using Monte Carlo simulation. The methodology has been illustrated with a pedagogical case study of a cogeneration system. It is shown in this case that robust designs can be generated to ensure a higher probability of meeting the profit targets. In practice, the interplay between

such factors depends on the degree of risk aversion of the decision-maker. The TORO model simply provides the means for generating a range of such options.

The TORO approach has been demonstrated to be useful for generating a range of solutions to facilitate the design of cogeneration, trigeneration, and polygeneration systems under uncertainty. The methodology can potentially be applied to a wider range of energy systems at different scales and in consideration of multiple objectives. Potential applications include the design of robust heat exchanger networks and planning of robust renewable energy supply chains.

APPENDIX A: LINGO Code for Deterministic MILP Model

```
!MILP MODEL FOR POLYGENERATION ;
```

```
SETS:
```

```
STREAM: PRICE, YL, Y, YU;
```

```
PROCESS: FC, VC, B, X;
```

```
AMATRIX (STREAM, PROCESS) :A;
```

```
ENDSETS
```

```
DATA:
```

```
STREAM = FUEL STEAM
```

```
HOTWATER
```

```
ELECTRICITY;
```

```
PROCESS = P1
```

```
P2
```

```
P3
```

```
P4;
```

```
A =
```

-4.06	-1.2	-1.08	0
1.83	1	0	-1
0.53	0	1	1
1	0	0	0;

```
!USE THIS CONSTRAINT FOR MILP MODEL WITHOUT UNCERTAINTY;
```

```
PRICE =
```

20	40	30	90;
----	----	----	-----

!USE THIS CONSTRAINT IN FINDING LOWER LIMIT OF PROFIT, PROFIT(L);

!PRICE =

30	40	30	90;
----	----	----	-----

!USE THIS IN FINDING FOR UPPER LIMIT OF PROFIT, PROFIT(U);

!PRICE =

20	50	40	130;
----	----	----	------

FC, VC =

382500	948347
45500	175000
7500	39474
625	4688;

YL, YU =

,	,
20,	25,
6,	8,
10,	12;

ENDDATA

MAX = PROFIT;

```

@FOR(STREAM(I) : Y(I) = @SUM(PROCESS(J) : A(I,J)*X(J));
PROFIT = 8000*@SUM(STREAM(I) : PRICE(I)*Y(I)) - CAPCOST;
CAPCOST = 0.08* @SUM(PROCESS(J) : B(J)*FC(J) + VC(J)*X(J));
@FOR(PROCESS(J) : @BIN(B(J)); X(J) <= B(J)*100000);
@FREE(Y(1));
!USE THIS CONSTRAINT FOR MILP MODEL WITHOUT UNCERTAINTY;
@FOR(STREAM(I) | I#GT#1 : Y(I) <=YU(I); Y(I) >=YL(I));

!USE THIS CONSTRAINT WHEN FINDING LOWER LIMIT OF PROFIT,
PROFIT(L);
!@FOR(STREAM(I) | I#GT#1 : Y(I) <= YL(I));
!USE THIS CONSTRAINT WHEN FINDING UPPER LIMIT OF PROFIT,
    
```

```
PROFIT(U);
!@FOR(STREAM(I) | I#GT#1: Y(I) <= YU(I));
```

APPENDIX B: LINGO Code for TORO Model

```
SETS:
STREAM: PRICE, YL, Y, YU, PRICEU, PRICEL;
PROCESS: FC, VC, B, X;
AMATRIX (STREAM, PROCESS):A;
```

```
ENDSETS
```

```
DATA:
```

```
STREAM = FUEL          STEAM          HOTWATER          ELECTRICITY;
PROCESS =      P1              P2              P3              P4;
```

```
A =
```

-4.06	-1.2	-1.08	0
1.83	1	0	-1
0.53	0	1	1
1	0	0	0;

```
PRICEL =
```

20	40	30	90;
----	----	----	-----

```
PRICEU =
```

30	50	40	130;
----	----	----	------

```
FC, VC =
```

382500	948347
45500	175000
7500	39474
625	4688;

YL, YU =

,	,
20,	25,
6,	8,
10,	12;

```

PU = 15385920; !MAXIMUM PROFIT THAT CAN BE ACHIEVED WITH
                THE MOST OPTIMISTIC SCENARIO;
PL = 3821690; !MINIMUM PROFIT THAT CAN BE ACHIEVED WITH
                THE MOST PESSIMISTIC SCENARIO;
ALPHA = 0.9; !VARIED FROM 0 - 1.0 IN INCREMENTS OF 0.1;
ENDDATA

MAX = THETA;
PROFIT >=TARGET;
TARGET = (1-ALPHA)*PU + ALPHA*PL;
THETA < ALPHA;
@FOR(STREAM(I) : Y(I) = @SUM(PROCESS(J) : A(I,J)*X(J)));
PROFIT = 8000*@SUM(STREAM(I) : PRICE(I)*Y(I)) - CAPCOST;
CAPCOST = 0.08* @SUM(PROCESS(J) : B(J)*FC(J) + VC(J)*X(J));
@FOR(PROCESS(J) : @BIN(B(J)); X(J) <= B(J)*100000);
@FREE(Y(1));

@FOR(STREAM(I) | I#GT#1 : Y(I) <= (1-THETA)*YU(I) + THETA*(YL(I)));
PROFITB = (1-ALPHA)*PU + ALPHA*PL;
@FOR(STREAM(I) | I#GT#1 : PRICE(I) = ((1-THETA)*PRICEU(I)) + (THETA*PRICEL
(I)));
PRICE(1) = (1-THETA)*PRICEL(1) + (THETA*PRICEU(1));
    
```

References

1. Rockström J, Steffen W, Noone K, Persson A, Chapin FS, Lambin EF, Lenton TM, Scheffer M, Folke C, Schellnhuber HJ, Niykvist B, De Wit CA, Hughes T, Van der Leeuw S, Rodhe H, Sorlin S, Snyder PK, Constanza R, Svedin U, Falkenmark M, Karlberg L, Corell RW, Fabry VJ, Hansen J, Walker B, Liverman D, Richardson K, Crutzen P, Foley JA (2009) A safe operating space for humanity. *Nature* 461:472–475
2. Obama B (2017) The irreversible momentum of clean energy. *Science* (<https://doi.org/10.1126/science.aam6284>)
3. Klemeš JJ, Varbanov PS, Kravanja Z (2013) Recent developments in process integration. *Chem Eng Res Des* 91:2037–2053

4. Serra LM, Lozano MA, Ramos J, Ensinas AV, Nebra SA (2009) Polygeneration and efficient use of natural resources. *Energy* 34:575–586
5. Burns RK, Staiger PJ, Donovan RM (1982) Integrated gasifier combined cycle polygeneration system to produce liquid hydrogen. Report No. NASA-TM-82921 (ntrs.nasa.gov/archive/nasa/casi.ntrs.nasa.gov/19820022837.pdf). Accessed 15 Mar 2016
6. Adams TA, Ghouse JH (2015) Polygeneration of fuels and chemicals. *Curr Opin Chem Eng* 10:87–93
7. Mancarella P (2014) MES (multi-energy systems): an overview of concepts and evaluation models. *Energy* 65:1–17
8. Wu DW, Wang (2006) Combined cooling, heating and power: a review. *Prog Energy Combust Sci* 32:459–495
9. Hemmes K, Zachariah-Wolf JL, Geidl M, Andersson G (2007) Towards multi-source multi-product energy systems. *Int J Hydrogen Energy* 32:1332–1338
10. Lozano MA, Carvalho M, Serra LM (2009) Operational strategy and marginal costs in simple trigeneration systems. *Energy* 34:2001–2008
11. Grossmann IE, Santibanez J (1980) Application of mixed integer linear programming in process synthesis. *Comput Chem Eng* 4:2015–2214
12. Carvalho M, Serra LM, Lozano MA (2011) Optimal synthesis of trigeneration systems subject to environmental constraints. *Energy* 36:3779–3790
13. Carvalho M, Lozano MA, Serra LM (2012) Multicriteria synthesis of trigeneration systems considering economic and environmental aspects. *Appl Energy* 91:245–254
14. Liu P, Gerogriorgis DI, Pistikopolous EN (2007) Modeling and optimization of polygeneration energy systems. *Catal Today* 127:347–359
15. Liu P, Pistikopolous EN, Li Z (2009) A mixed-integer optimization approach for polygeneration energy systems design. *Comput Chem Eng* 33:759–768
16. Liu P, Pistikopolous EN, Li Z (2010) A multi-objective optimization approach to polygeneration energy systems design. *AIChE J* 56:1218–1234
17. Ng KS, Hernandez EM (2016) A systematic framework for energetic, environmental and economic (3E) assessment and design of polygeneration systems. *Chem Eng Res Des* 106:1–25
18. Andiappan V, Tan RR, Aviso KB, Ng DKS (2015) Synthesis and optimisation of biomass-based tri-generation systems with reliability aspects. *Energy* 89:803–818
19. Tay DHS, Ng DKS, Tan RR (2013) Robust optimization approach for synthesis of integrated biorefineries with supply and demand uncertainties. *Environ Prog Sustain Energy* 32:384–389
20. Kasivisvanathan H, Ubando AT, Ng DKS, Tan RR (2014) Robust optimisation for process synthesis and design of multi-functional energy systems with uncertainties. *Ind Eng Chem Res* 53:3196–3209
21. Tan RR, Lam HL, Kasivisvanathan H, Ng DKS, Foo DCY, Kamal M, Hallale N, Klemeš JJ (2012) An algebraic approach to identifying bottlenecks in linear process models of multifunctional energy systems. *Theor Found Chem Eng* 46:642–650
22. Kasivisvanathan H, Barilea IDU, Ng DK, Tan RR (2013) Optimal operational adjustment in multi-functional energy systems in response to process inoperability. *Appl Energy* 102:492–500
23. Varbanov P, Friedler F (2008) P-graph methodology for cost-effective reduction of carbon emissions involving fuel cell combined cycles. *Appl Therm Eng* 28:2020–2029
24. Tan RR, Cayamanda CD, Aviso KB (2014) P-graph approach to optimal operational adjustment in polygeneration plants under conditions of process inoperability. *Appl Energy* 135:402–406
25. Ng TS, Sy C (2014) An affine adjustable robust model for generation and transmission network planning. *Electr Power Energy Syst* 60:141–152
26. Ng TS, Sy CL (2014) A resilience optimization approach for workforce-inventory control dynamics under uncertainty. *J Sched* 17:427–444
27. Sy CL, Aviso KB, Ubando AT, Tan RR (2016) Target-oriented robust optimization of polygeneration systems under uncertainty. *Energy* 116:1334–1347

28. Gau C-Y, Schrage LE (2004) Implementation and testing of a branch-and-bound based method for deterministic global optimization: operations research applications. In: Floudas CA, Pardalos P (eds) *Frontiers in global optimization*, vol 74. Springer, Boston
29. Voll P, Jennings M, Hennen M, Shah N, Bardow A (2015) The optimum is not enough: a near-optimal solution paradigm for energy systems synthesis. *Energy* 82:446–456

Detoxification of Crude Oil

Aysar T. Jarullah, Iqbal M. Mujtaba and Alastair S. Wood

Abstract Petroleum contributes significantly to our lives and will continue to do so for many years to come. Petroleum derivatives supply more than 50% of the world's total supply of energy (Jarullah Kinetic modelling simulation and optimal operation of trickle bed reactor for hydrotreating of crude oil. University of Bradford, UK, 2011 [20]). Traditionally, crude oil goes through fractional distillation to produce different grades of fuel such as gasoline, kerosene, and diesel oil providing fuel for automobiles, tractors, trucks, aircraft, and ships. Catalytic hydrotreating (HDT) is used to detoxify the oil fractions produced by fractional distillation in the petroleum refining industries which involve removal of pollutants such as sulfur, nitrogen, metals, and asphaltene in trickle-bed reactors. Recently, Jarullah and co-workers proposed detoxification of whole crude oil a priori before the crude oil enters further processing in a fractionating column. This chapter highlights this new technology.

Keywords Crude oil · Hydrotreatment · Trickle-bed reactor · Pilot plant Modeling · Simulation

1 Toxic Compounds in Crude Oil

Crude oil contains different hydrocarbon compounds in addition to several toxic compounds such as sulfur, nitrogen, oxygen, and some metallic compounds containing nickel, vanadium, iron, and copper. The presence of these compounds not only has severe and many detrimental effects (such as health problems and catalyst poisoning) but also dictates the quality of oil products.

A. T. Jarullah
Department of Chemical Engineering, Tikrit University, Tikrit, Iraq

I. M. Mujtaba (✉) · A. S. Wood
School of Engineering, University of Bradford, Bradford BD7 1DP, UK
e-mail: I.M.Mujtaba@bradford.ac.uk

Sulfur pollutes the environment through the formation of sulfur dioxides, which can be further oxidized with ultraviolet rays to SO_3 resulting in the formation of sulfuric acid that can cause lung diseases such as asthma and shortness of breath. In addition, these impurities cause catalyst poisoning and reduce the catalyst activity. Therefore, environmental regulations have enforced significantly low amounts of sulfur compounds in fuels [3, 5, 14, 33, 36, 42].

The nitrogen compounds in crude oil or oil fractions can severely affect refining industries. They are responsible for dye formation causing catalyst poisoning and reduced catalyst activity in addition to the environmental pollution [2, 14, 42].

The metallic compounds in crude oil and its fractions can plug the pores of catalysts causing rapid deactivation of the catalyst [1, 9, 40]. Also, particularly vanadium in the fuel used in high-power machines such as gas turbines, these compounds lead to the formation of sediment on the turbine, which can lead to a change in the balance of the rotating parts of the turbine [3, 15].

Asphaltenes are the most complex mixture of high-boiling, high-molecular weight compounds and consist of condensed polynuclear aromatics carrying alkyl and cycloalkyl. They are highly undesirable compounds as they are responsible for high density and viscosity of crude oils and heavy oils, which leads to transport problems [6, 10, 11, 43, 46].

The contents of these toxic compounds for Kirkuk crude oil (Iraq) and its physical properties are shown in Table 1 [20].

2 Traditional Industrial Refinery Practice

A petroleum refinery is a complex chemical processing unit, producing a number of refined fuel products from crude oil feedstock with varying properties. Fractional distillation of crude oil leads to such products based on the boiling ranges of these

Table 1 Kirkuk crude oil (Iraq) properties

Chemical specification	Units	Value
Sulfur content	wt%	2.0
Vanadium content	ppm	26.5
Nickel content	ppm	17
Nitrogen content	wt%	0.1
Asphaltenes content	wt%	1.2
Ash content	wt%	0.008
Specific gravity at 15.6 °C	–	0.8558
API	–	33.84237
Viscosity at 37.8 °C	cSt	5.7
Pour point	°C	–36
Molecular weight	kg/kg mole	227.5
Mean average boiling point	°C	291

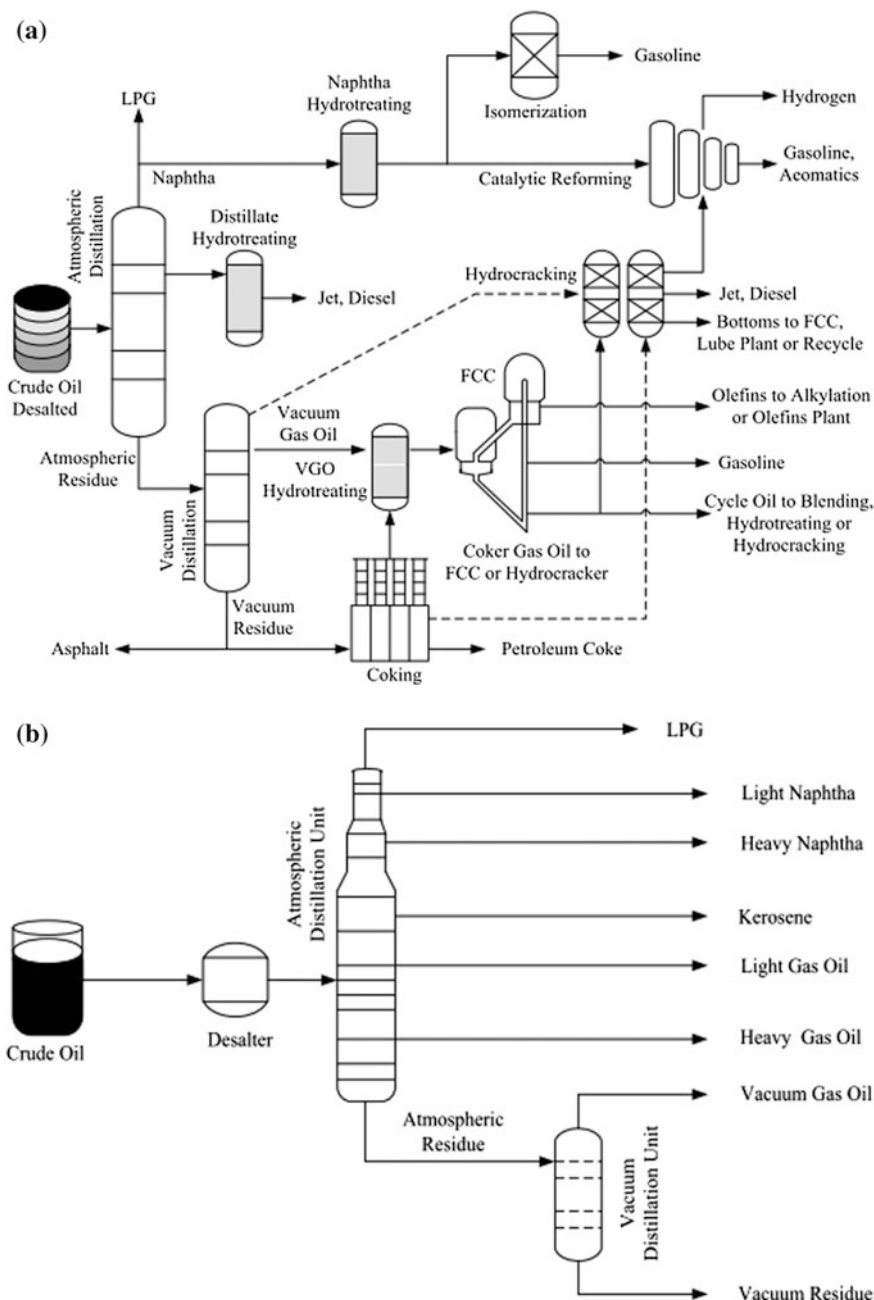


Fig. 1 a Typical layout for an oil refinery showing hydrotreating/hydrocracking. b Simple layout of atmospheric and vacuum fractional distillation (adapted from Refs. [4, 19])

products. Figure 1a shows a typical layout for an oil refinery. Figure 1b is a simplified version of Fig. 1a where the atmospheric column produces the lighter fuels. The residue (high boiling) of the first column then goes to vacuum distillation column to produce further fuels.

Crude oil contains water, salts, and suspended solids. These materials are removed from crude oil before the distillation process in order to reduce corrosion, plugging, and fouling in crude heaters and towers, and in order to prevent the poisoning of catalysts in downstream units by a process called desalting (as shown in Fig. 1b). Either chemical or electrostatic methods are commonly used for desalting. In the chemical method, water and surfactants are added to the crude oil, which is heated in order to dissolve salts and other contaminants and is then sent to a settling tank where the water and oil separate. In the electrostatic method, strong electrostatic charge is used to drive the separation of water from oil [3].

Modern operation of crude oil distillation columns can process 200,000 barrels of oil per day [19]. These towers can be up to 50 m high and contain 20–40 fractionation trays. Before entering the distillation column, desalted crude oil passes through a network of pre-heat exchangers in order to heat it, initially with hot material drawn from the bottom of the distillation tower to raise its temperature up to 232 °C and then to a heating furnace that brings the temperature up to about 343 °C (Fig. 2). This is linked to heat recovery and energy saving [8]. In the distillation column, products are collected from the top, bottom, and side of the column. Side-drawn products are taken from trays at which the temperature corresponds to the boiling point range for a desired product. In modern towers, a portion of each side-drawn stream is returned (pump around) to the tower to control tray temperatures and further enhance separation. Part of the top product is also returned; this “reflux” plays a major role in controlling the temperature at the top of the tower (Fig. 2).

The reduced crude residue, RCR (the part remaining at the bottom of the atmospheric distillation—above 350 °C), will be sent to a vacuum distillation tower, which recovers additional liquid at 4.8–10.3 kPa. The vacuum, which is created by a vacuum pump, is pulled from the top of the tower. The overhead stream (light vacuum gas oil) can be utilized as a lube base stock, heavy fuel oil, or as feed to a conversion unit. Heavy vacuum gas oil is pulled from a side draw. The remaining part at the bottom of the vacuum distillation column is called vacuum residue (VR). This part is taken to the deasphalted (DAO) and De-wax Units in order to remove the asphaltenes and wax, respectively. The oil product is called bright-stock. The vacuum residue can be sent to a coking or visbreaking unit for further processing. After leaving the tower, products go to the downstream process units where each compound (such as light naphtha (LN), heavy naphtha (HN), heavy kerosene (HK), diesel oil, light gas oil (LGO), vacuum gas oil (VGO) or bright-stock) will be sent to the hydrotreating units (Fig. 1a) in order to remove the impurities (mainly sulfur, nitrogen, metals, and asphaltene). Table 2 shows some of the oil fractions destinations and ultimate products with their boiling ranges.

The most valuable products from crude oil are gasoline, kerosene (jet fuel), and diesel oil. In order to enhance the amount of these fractions, heavier streams are

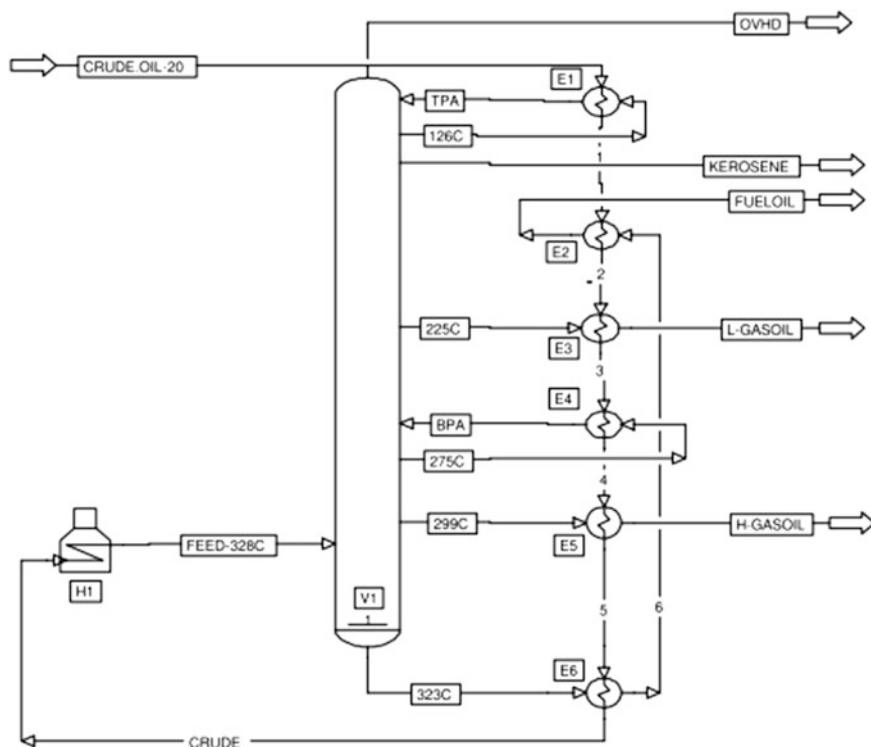


Fig. 2 Distillation column with pump around (Adapted from Ref. [7])

cracked down into smaller molecules by a fluid catalytic cracking (FCC) unit [30]. The profitability of the FCC operation depends mainly on the type of catalyst used in the FCC unit and upon the kind of feedstock being processed. FCC generally uses a solid acid zeolite catalyst. The larger molecules are broken into smaller molecules in order to create additional material in the naphtha range for producing more valuable product, gasoline [21].

Catalytic hydrotreating (HDT) is one of the methods used to detoxify the oil fractions produced by fractional distillation, which involves removal of pollutants such as sulfur, nitrogen, metals, and asphaltene in trickle-bed reactors [20] by reacting with hydrogen. HDT reactions include hydrodesulfurization (HDS), hydrodenitrogenation (HDN), hydrodeasphaltenization (HDAs), hydrodemetallization (HDM), hydrodeoxygenation (HDO), and hydrocracking (HDC) and are carried out in trickle-bed reactors (TBRs) (Fig. 3). These reactors in which three phases, liquid (oil), gas (mostly hydrogen), and solid catalyst particle are frequently preferred due to ease of control and used for different feedstocks.

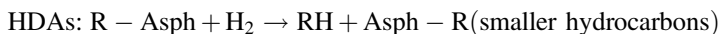
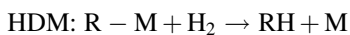
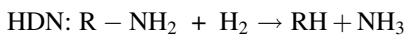
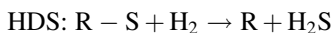
There are other methods employed especially to remove sulfur such as oxidative desulfurization [31, 32, 37–39].

Table 2 Oil fractions destinations and ultimate products with their boiling ranges (adapted from Ref. [19])

Oil fractions	Boiling ranges (°C)	From distillation column to	Final products
LPG	-40 to 0	Sweetener	Propane fuel
Light naphtha	IBP-85	Hydrotreating	Gasoline
Heavy naphtha	85-200	Cat. reformer	Gasoline, aromatics
Kerosene	170-270	Hydrotreating	Jet fuel, diesel No. 1
Gas oil	180-240	Hydrotreating	Heating oil, diesel No. 2
Vacuum gas oil	340-566	FCC	Gasoline, LGO, gases
		Hydrotreating	Fuel oil, FCC, feed
		Lube plant	Lube base stock
		Hydrocracking	Gasoline, jet fuel, diesel, FCC feed, base stock
Vacuum residue	>540	Coker	Coke, coker gas oil,
		Visbreaking	Visbreaker gas oil, resid
		Asphalt unit	Deasphalted oil, asphalt
		Hydrotreating	FCC feed

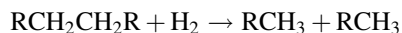
3 Hydrotreating Reactions and Process Parameters

The general hydrotreating reactions can be expressed as follows [6, 34, 35]:



R represents the hydrocarbon molecule.

Other reactions may take place in the HDT of heavy oils such as hydrocracking and hydrogenation of aromatics rings. At high temperatures in the hydrotreating process, hydrocracking reactions that include the breaking of the C-C bonds are most likely to happen (also a reduction of molecular weight is noticed), e.g.,



or

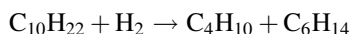
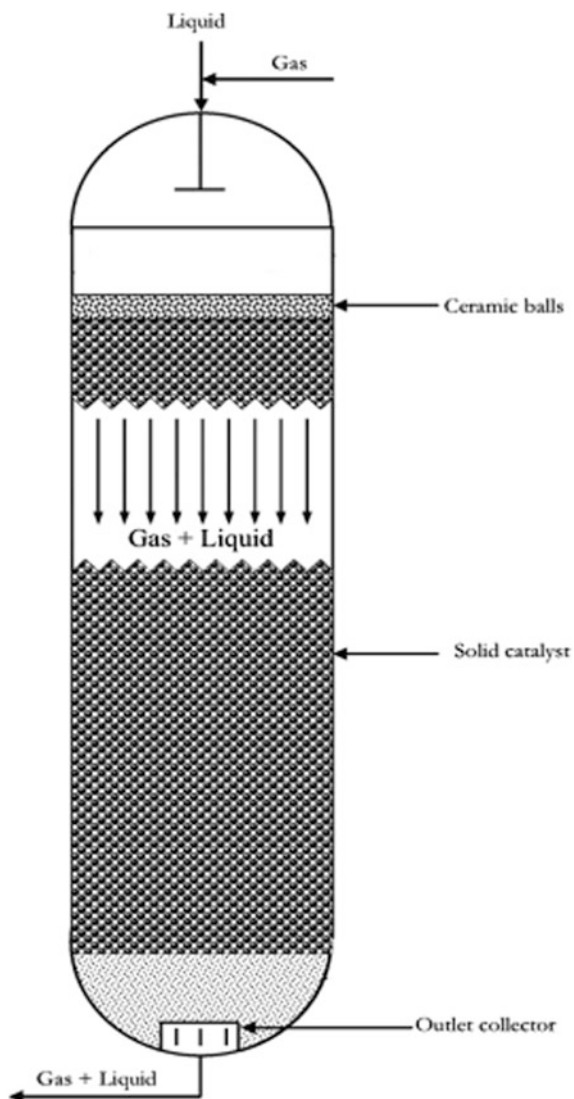
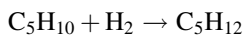


Fig. 3 Trickle-bed reactor with co-current downflow (adapted from Ref. [20])



Hydrogenation of unsaturated hydrocarbons is also a significant class of reactions happening through the HDT operation, e.g., Gully and Ballard [17] and Girgis and Gates [16].



The range of operating conditions that are used in hydrotreating is very wide. The choice of operating conditions is determined by the feedstock type, the required product level, and the purity and availability of hydrogen in addition to economic

considerations [45]. In conventional processes, the range of operating conditions for HDT of different petroleum fractions is summarized in Table 3 [44].

There are four process variables frequently reported in the literature as the most important in hydrotreating operations: reaction temperature, liquid hourly space velocity (LHSV), hydrogen partial pressure, and hydrogen to oil ratio (H_2/Oil) ratio. In general, for a specific feedstock and catalyst, the degree of impurities removal and conversion increases with increasing severity of the reaction, that is, increasing pressure, temperature, or H_2/Oil ratio, and decreasing space velocity. The effect of these parameters on the HDT process is briefly discussed below.

3.1 Effect of Temperature

Temperature plays a significant role in the HDT process. An increase in reaction temperature can substantially enhance the rate of catalytic reaction and hence enhance the sulfur, nitrogen, asphaltene, and metal removal. Higher temperature will increase the rate of diffusion inside the active site of the catalyst, and as a result, the rate of reaction will be increased [18, 41]. In addition, high temperature can significantly enhance the thermal cracking. The best range of temperature used in the refineries lies between 553 and 683 K, except heavy vacuum residue where under 553 K, the reaction rates tend to be slow, and above 683 K, there is undesirable side reaction. At temperatures above 683 K, the activity of the catalyst used will decrease due to coke deposits that form on the catalyst [18, 42].

3.2 Effect of Pressure

Hydrogen partial pressure mainly affects the rate of reaction by promoting the reaction between hydrogen and feedstock compounds. Generally, when the boiling range of feedstock increases from naphtha through to vacuum residue, the impurities compounds such as sulfur, nitrogen, and other heteroatoms become more complex and require higher partial pressure to cause them to react with these

Table 3 Typical process conditions for various hydrotreatment on oil fractions

Oil fractions	Temperature (K)	Pressure (MPa)	LHSV (h^{-1})
Naphtha	593	1.5–3.0	3–8
Kerosene	603	3.0–4.5	2–5
Atmospheric gas oil	613	3.8–6.0	1.5–4
Vacuum gas oil	633	7.5–13.5	1–2
Atmospheric residue	643–683	12.0–19.5	0.2–0.5
Vacuum residue	673–713	15.0–22.5	0.2–0.5

compounds [4, 18]. In addition, the system pressure impacts on both the degree of hydrogenation of unsaturated compounds in the feedstock as well as the reaction rate of hydrocarbon cracking. Refinery experience indicates that the HDT processes conducted at higher partial pressure of hydrogen will produce products with lower sulfur, nitrogen, and aromatics contents [2].

3.3 Effect of Liquid Hourly Space Velocity

Liquid hourly space velocity (LHSV) is the inverse of residence time, which impacts on the hydroprocessing efficiency and also upon the life of the catalyst. With the volume of catalyst being constant, the LHSV will vary directly with the rate of feedstock. A decrease in the LHSV will generally bring an increase in the extent of the HDS, HDN, HDM, HDAs, and HDC processes and as a result, increase the reaction severity and the efficiency of hydrotreating processes [12]. The residual sulfur, metals, nitrogen, and other impurities from any catalytic hydrotreating process are proportional to the LHSV utilized. Thus, the heavier residue cuts require longer residence time for the reaction to go to completion compared with the lighter residue cuts [18].

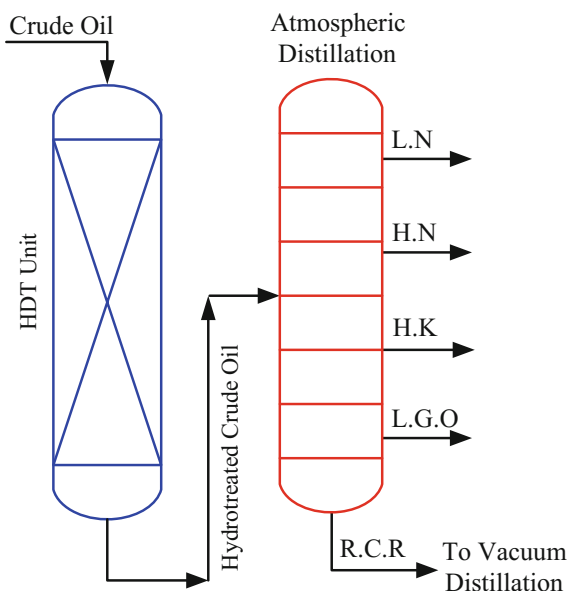
3.4 Effect of Gas Oil Ratio

The choice of gas flow rate is governed by economic considerations. Recycling is utilized to maintain the H₂ partial pressure and the physical contact of the hydrogen with the catalyst and hydrocarbon for ensuring adequate conversion and impurities removal. To make the process economically feasible, the unused hydrogen is recycled back to the reactor. Thus, for diesel oil, residue from atmospheric column and other heavy feedstock, it is normal to have a gas compressor to recycle gas back through the reactor [2, 18, 42].

4 Whole Crude Oil Fractionation then Hydrotreating or Whole Crude Oil Hydrotreating then Fractionation?

As described in the section above, in all existing refineries, the hydrotreating processes are implemented upon oil fractions followed by distillation and not on the whole crude oil before the distillation. Recently, Jarullah and co-workers proposed detoxification of whole crude oil a priori before the crude oil enters into further processing in a fractionating (distillation) column (Fig. 4). This new development is highlighted in the next few sections.

Fig. 4 Whole crude oil hydrotreating before fractionation (Adapted from Ref. [24])



5 Pilot Plant Experiments for Whole Crude Oil Hydrotreating

Jarullah [20] and Jarullah et al. [22–27] considered the pilot plant shown in Fig. 5 for hydrotreating whole crude oil. The detailed description of this plant can be found in original references.

In brief, the feed tank is a cylindrical tank with a capacity of 2 l. The feedstock and hydrogen pass through the reactor in a downward concurrent flow mode. The reactor tube is made of stainless steel with an inside diameter of 2 cm and a length of 65 cm. The length of the reactor is divided into three parts. The first part, of 20 cm, was packed with inert particles (glass beads of 4 mm diameter). This entrance section was employed to heat up the mixture to the required temperature, to ensure homogeneous flow distribution of gas and liquid and to avoid end effects. The following section of length 27.8 cm contained a packing of 60.3 g catalyst. The bottom section (17.2 cm) was packed with inert particles in order to ensure as serve as disengaging section. The reactor was operated in isothermal mode by independent temperature control of five zone electric furnaces, which provided an isothermal temperature along the active reactor section. The product section consists of low and high gas-liquid separators and a products storage tank.

The product from the storage tank is fed to the distillation unit at atmospheric and vacuum pressure for fractionation. This unit consists mainly of the (a) bottom flask in which the feedstock is shipped (capacity of 5 l), (b) electric heating mantle, (c) thermocouple (to measure the temperature of the raw material during the

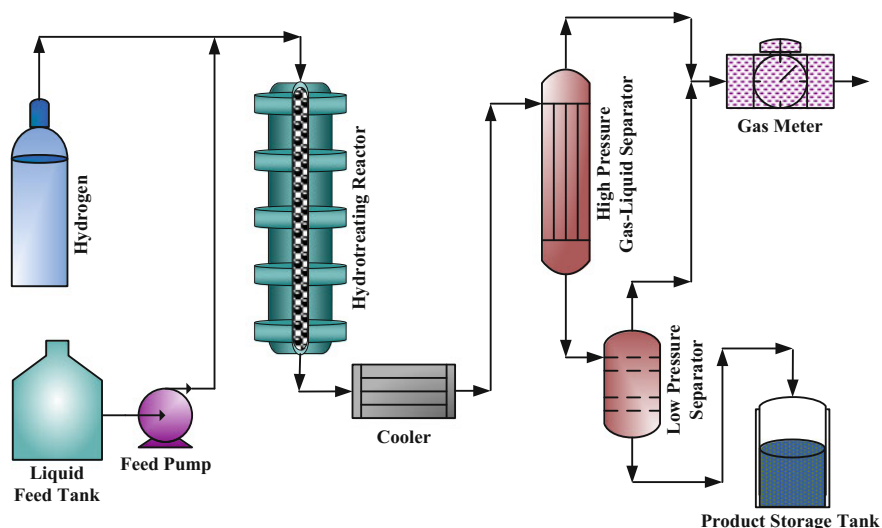


Fig. 5 Whole crude oil hydrotreating pilot plant (adapted from Ref. [20])

distillation process, (d) Oldershaw (15 trays), (e) condenser, (f) reflux regulator, and (g) vacuum pump. The distillation column used in this work is shown in Fig. 6.

6 The Experiments

Details of the experimental procedures are outlined in Jarullah [20] and Jarullah et al. [24]. In brief, the catalyst used for the hydrotreating (HDT) processes was commercial cobalt–molybdenum on alumina ($\text{Co-Mo}/\gamma\text{-Al}_2\text{O}_3$), similar to the type used in the industrial reactor in the Baiji Refinery (North Oil Company—Iraq). The properties of the catalyst are shown in Table 4.

6.1 Operating Conditions

Of note, there are many limitations in operating an HDT process. Reactor temperatures above $410\text{ }^\circ\text{C}$ can result in hydrocracking reactions producing not only undesirable compounds but also reducing the catalyst life. Hydrogen pressure beyond 10 Mpa ($\sim 100\text{ atm}$) does not necessarily increase the partial pressure required for improved conversion [13, 28, 29]. LHSV dictates the plant capacity, and lower LHSV will require larger hydrotreating reactors in order to keep a desired production capacity. Based on a full factorial three-level three-factor DoE, we carried out 27 experiments in the pilot plant, and the ranges of operating conditions

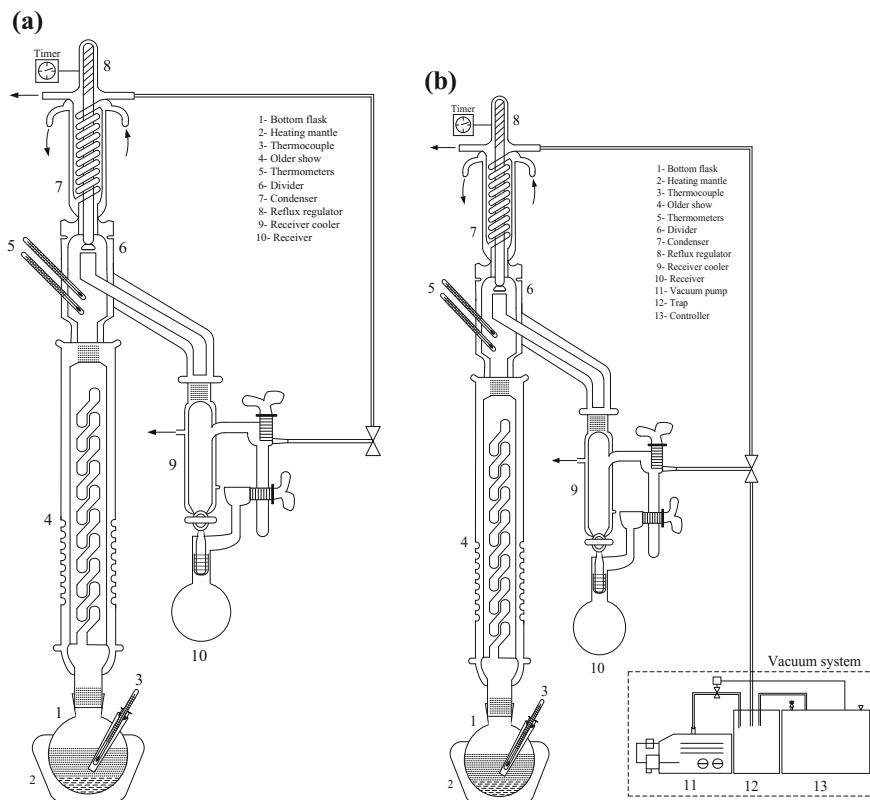


Fig. 6 a Atmospheric distillation column. b Vacuum distillation column

Table 4 Catalyst properties (adapted from Ref. [24])

Chemical composition	Units (%)	Value
Al ₂ O ₃	wt%	78.79
MoO ₃	wt%	15
NiO	wt%	3
SO ₂	wt%	2
SiO ₂	wt%	1.1
Na ₂ O	wt%	0.07
Fe	wt%	0.04
Physical properties		
Surface area	m ² /g	180
Mean particle length	mm	4
Mean particle diameter	mm	1.8
Pore volume	cm ³ /g	0.5
Bulk density	g/cm ³	0.67

Table 5 Operating conditions used in the HDT process [20]

Run	LHSV (h^{-1})	P (Mpa)	T ($^{\circ}\text{C}$)
1	0.5	4	335
2	1.0	4	335
3	1.5	4	335
4	0.5	4	370
5	1.0	4	370
6	1.5	4	370
7	0.5	4	400
8	1.0	4	400
9	1.5	4	400
10	0.5	7	335
11	1.0	7	335
12	1.5	7	335
13	0.5	7	370
14	1.0	7	370
15	1.5	7	370
16	0.5	7	400
17	1.0	7	400
18	1.5	7	400
19	0.5	10	335
20	1.0	10	335
21	1.5	10	335
22	0.5	10	370
23	1.0	10	370
24	1.5	10	370
25	0.5	10	400
26	1.0	10	400
27	1.5	10	400

used in this study are given in Table 5. In all cases, hydrogen to oil ratio used was 250L/L.

7 The Results

7.1 Trickle-Bed Reactor

The results for the HDT operation in the pilot plant for the 27 experiments under various operating conditions (outlined in Table 5) are shown in Table 6. Conditions at which the maximum conversion ($X\%$) of all the toxic compounds took place are highlighted in Table 6. These conditions are obviously the highest temperature and pressure and longest residence time and may not necessarily be the optimum conditions. Further details are given in Jarullah [20].

Table 6 Experimental results for the HDT operation in the pilot plant

RUN	Sulfur (wt%)	X (%)	Nitrogen (wt%)*10 ⁴	X (%)	Vanadium (ppm)	X (%)	Nickel (ppm)	X (%)	Asphaltene (wt%)	X (%)
1	0.670	66.50	526.9	47.31	8.33	68.57	2.01	88.18	0.639	46.75
2	1.110	44.50	713.2	28.68	14.34	45.89	4.80	71.76	0.868	27.67
3	1.360	32.00	783.5	21.65	17.79	32.87	6.80	60.00	0.966	19.50
4	0.430	78.50	327.9	67.21	5.54	79.09	1.11	93.47	0.335	72.08
5	0.880	56.00	512.7	48.73	11.70	55.85	3.10	81.76	0.610	49.17
6	1.150	42.50	618.9	38.11	15.50	41.51	4.95	70.88	0.760	36.67
7	0.229	88.50	203.7	79.63	3.21	87.89	0.73	95.70	0.153	87.25
8	0.640	68.00	362.8	63.72	8.40	68.30	2.28	86.59	0.355	70.42
9	0.930	53.50	485.3	51.47	12.10	54.34	3.85	77.35	0.510	57.50
10	0.520	74.00	472.5	52.75	5.60	78.87	1.15	93.23	0.560	53.33
11	1.010	49.50	649.0	35.10	11.80	55.47	3.22	81.06	0.790	34.17
12	1.260	37.00	738.1	26.19	15.10	43.02	5.10	70.00	0.910	24.17
13	0.280	86.00	261.0	73.90	3.15	88.11	0.62	96.35	0.262	78.16
14	0.710	64.50	449.1	55.09	8.66	67.32	2.02	88.12	0.512	57.33
15	1.001	49.95	571.9	42.81	12.50	52.83	3.50	79.41	0.660	45.00
16	0.135	93.25	155.3	84.47	1.59	94.00	0.36	97.88	0.116	90.33
17	0.500	75.00	305.5	69.45	5.46	79.40	1.33	92.18	0.295	75.42
18	0.761	61.95	418.6	58.14	9.13	65.55	2.48	85.41	0.440	63.33
19	0.430	78.50	424.9	57.51	3.84	85.51	0.81	95.23	0.520	56.67
20	0.900	55.00	605.3	39.47	9.42	64.45	2.50	85.29	0.750	37.50
21	1.200	40.00	687.9	31.21	13.23	50.00	4.07	76.06	0.860	28.33
22	0.196	90.20	234.2	76.58	1.98	92.53	0.42	97.53	0.236	80.33
23	0.597	70.15	418.5	58.15	6.63	74.98	1.48	91.29	0.475	60.42

(continued)

Table 6 (continued)

RUN	Sulfur (wt%)	X (%)	Nitrogen (wt%)*10 ⁴	X (%)	Vanadium (ppm)	X (%)	Nickel (ppm)	X (%)	Asphaltene (wt%)	X (%)
24	0.898	55.10	518.3	48.17	10.27	61.24	2.71	84.06	0.620	48.33
25	0.082	95.90	130.5	86.95	0.891	96.64	0.24	98.59	0.089	92.58
26	0.376	81.20	274.4	72.56	3.95	85.10	0.93	94.53	0.255	78.75
27	0.640	68.00	387.1	61.29	6.89	74.00	1.87	89.00	0.398	66.83

Adapted from Ref. [20]

The temperature of the reactor influences the mass velocity of the gases and liquids, the diffusivities of the components, the mass transfer coefficient at the gas–liquid and liquid–solid interfaces, the solubility, and Henry’s coefficients of hydrogen and hydrogen compound in addition to viscosity and density of the compounds. Increasing the reaction temperature leads to an increase in reaction rate constants defined by the Arrhenius equations [22–26]. As a result, the reaction rates of these reactions will increase.

The hydrogen partial pressure has an effect on the reactions used in this study. The mechanisms utilized to describe HDS, HDN, HDAs, HDV, and HDNi reactions used a kinetic equation with the order of the hydrogen concentration at the catalyst surface set at a value less than 1 [22–26]. Therefore, conversion of S, N, Asph, V, and Ni compounds increases with pressure. The effect of pressures above 10 MPa can be neglected due to the fact that the viscosity of the oil feedstock increases with pressure, and the diffusivity and mass transfer coefficient decrease with pressure. The liquid hourly space velocity (LHSV) is also a significant operational factor that determines the severity of reaction and the efficiency of hydrotreating, as described earlier.

7.2 Fractionation

The hydrotreated crude oil at these conditions was distilled into the following fractions:

- Light naphtha (IBP–90 °C).
- Heavy naphtha (90–150 °C).
- Heavy kerosene (150–230 °C).
- Light gas oil (230–350 °C).
- Reduced crude residue (350 °C+).
- Gases [100–(naphtha + heavy kerosene + light gas oil + reduced crude residue)].

Table 7 shows the experimental results for product compositions. It is clearly observed that the conversion of high boiling point molecules (such as those contained in the residue fraction) into lighter molecules increases when the reaction temperature is increased, and LHSV is decreased. This behavior can be attributed to the severity of the reaction at high operating conditions. At a low temperature of 335 °C (with different LHSV), there is no conversion of product compositions and they are almost unchanged, which means that the conversion of large molecules can be achieved at high operating conditions. The highest conversion from RCR to oil distillates is seen at a high reaction temperature and low LHSV. Figure 7 clearly captures these and compares against the base case.

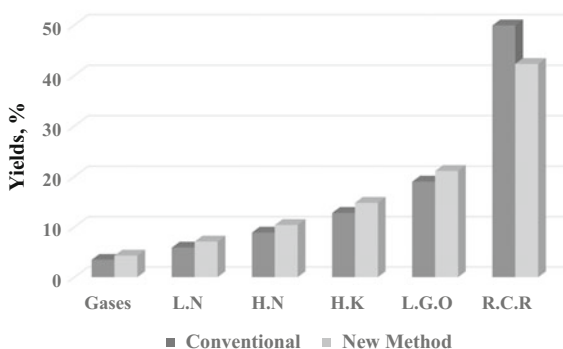
Figure 7 shows the comparison between the yields of different fractions from the hydrotreated crude oil at 400 °C and 0.5 h⁻¹ LHSV and those yielded by the conventional method. Clearly, the yield of LN, HN, HK, and LGO increases with

Table 7 Fractionation column yield results

Yields by conventional method (fractionation before HDT) %							
Base case		Gases	L.N	H.N	H.K	L.G.O	R.C.R
		3.47	5.9	8.9	12.8	19.0	49.93
Yields by new method (fractional after HDT) %							
HDT temperature (°C)	LHSV (1/h)	Gases	L.N	H.N	H.K	L.G.O	R.C.R
335	0.5	3.6	5.93	8.97	12.9	19.20	49.40
	1.0	3.48	5.91	8.92	12.82	19.02	49.85
	1.5	3.48	5.91	9.91	12.81	19.01	49.88
370	0.5	4.00	6.80	9.90	13.80	20.00	45.50
	1.0	3.80	6.40	9.50	13.50	19.50	47.30
	1.5	3.70	6.00	9.20	13.30	19.20	48.60
400	0.5	4.30	7.10	10.4	14.80	21.10	42.30
	1.0	4.00	6.70	9.80	14.00	20.50	45.00
	1.5	3.80	6.20	9.40	13.60	19.90	47.10

Adapted from Ref. [20]

Fig. 7 Comparison of yields by conventional and proposed methods (adapted from Ref. [24])



the proposed method but with a decrease in RCR yield. The increase in the yield is due to conversion of heavy compounds and long molecules present in heavy fractions (like RCR) to light compounds.

7.3 Quality of the Fuel: Conventional Method Versus New Method

Table 8 presents the quality of different grades of fuel by the conventional and new method (the hydrotreating conditions were as follows: 400 °C reaction temperature,

0.5 h⁻¹ LHSV, and 10 MPa hydrogen pressure). The quality of each fraction has improved using the proposed method (method B) where the specific gravity (sp gr) of oil cuts produced by method B is less than the sp gr of the same fractions produced by conventional methods (method A), which gives a clear indication of incremental productivity improvement of these fractions.

The reduced crude residue (RCR) from the bottom of the atmospheric distillation has a boiling range above 350 °C. RCR is mainly used as a feedstock to vacuum distillation units to produce base oils, in addition to producing vacuum gas oil and lubricating oils under certain conditions. Also, it is utilized as a component of fuel oil used in power plants, as fuel for furnaces, and as a component of diesel oil [36]. During hydrotreating of whole crude oil, it was observed that the properties of RCR produced via hydrotreating of crude oil directly are better than the properties of RCR produced by conventional processes, as shown in Table 8. The sulfur content, nitrogen content, metals content, and asphaltene content are much lower compared with these contents of RCR produced by conventional methods, thus producing a good fuel oil as shown in Table 9.

Table 8 Properties of oil fractions produced by conventional (A) and new (B) methods

Property	Oil fractions							
	Light naphtha (L.N)		Heavy naphtha (H.N)		Heavy kerosene (H.K)		Light gas oil (L.G.O)	
	A	B	A	B	A	B	A	B
Sp gr @ 15.6 °C	0.6625	0.6513	0.7385	0.7311	0.7918	0.7723	0.8389	0.8324
Distilled (vol.)	°C	°C	°C	°C	°C	°C	°C	°C
I.B.P	40	30	100	91	171	159	220	218
5%	45	36	105	95	176	166	230	227
10%	48	40	107	101	181	171	240	236
20%	50	43	110	107	188	179	252	243
30%	52	45	113	111	193	184	264	255
40%	54	49	116	114	196	188	272	262
50%	58	54	119	116	199	191	280	271
60%	60	59	123	120	204	199	289	279
70%	65	64	127	125	209	206	295	288
80%	70	70	132	131	216	215	305	297
90%	78	75	139	137	225	223	317	314
95%	87	83	146	141	232	234	326	322
Ep%	89	85	149	144	245	237	338	335
T.D%	98.0	98.0	99.0	99.0	99.0	99.5	97.0	98.5
Loss%	2.0	2.0	0.5	1	0.0	0.0	0.0	0.0
Rest%	0.0	0.0	0.5	0.0	1.0	0.5	3.0	1.5

Adapted from Ref. [20]

Table 9 Properties of reduced crude residue (RCR) produced by new and conventional methods

Specifications	Units	By conventional method	By new method
Sulfur content	wt%	4.0	0.811
Vanadium content	ppm	59.88	16.42
Nickel content	ppm	37.47	10.16
Nitrogen content	wt%	0.1763	0.04122
Asphaltenes content	wt%	5.9	0.91
Specific gravity @ 15.6 °C	–	0.9540	0.9392
API	–	16.82	19.16
Viscosity @ 50 °C	cSt	236.8	191.4
Pour point	°C	+14	+2

Adapted from Ref. [24]

It is also noted that the viscosity and density of RCR are less than those found in RCR produced by conventional methods, which makes flow easy at low temperatures and gives an indication of increasing the light cuts. The bottom residual fuel oil produced by a conventional method is less useful due to the fact that it is very viscous and that it has to be heated with a special heating system before use. In addition, it contains high amounts of contaminants in comparison with the new study. The decrease in the viscosity and density during the hydrotreating process facilitates its direct use as a fuel. Also, there is a conversion of a large part of it into light compounds due to the cracking of the bonds of heavy compounds with long chain and high density and viscosity [1, 3, 6, 36].

8 Process Economics

Jarullah [20] and Jarullah et al. [27] studied the process economics of the conventional and the new process in terms of overall cost (both capital and operating costs) for an industrial scale process (10,000 bbl/day). They have reported a total yearly cost savings of more than 16%. Also, significant savings in H₂ consumption are reported for the new process.

9 Conclusions

This chapter reviewed details of pilot plant experiments that involve hydrotreating reactions at different operating conditions (HDS, HDN, HDAs, HDV, and HDNi reactions), and the distillation process (light naphtha (LN), heavy naphtha (HN), heavy kerosene (HK), light gas oil (LGO), and reduced crude residue (RCR)). Also, this chapter presented and discussed results obtained via experimental work.

The effects of different operation parameters such as temperature, pressure, and liquid hourly space velocity (LHSV) upon the quality of crude oil are presented. It has been observed that the whole crude oil hydrotreating before fractionation leads to better grades fuels due to better removal of the impurities (S, N, V, Ni, and Asph).

The oil fractions produced by distillation after the HDT process are compared with those produced by conventional methods in terms of yields of light naphtha (LN), heavy naphtha (HN), heavy kerosene (HK), light gas oil (LGO), and reduced crude residue (RCR). The middle distillates showed greater yield compared with the middle distillates produced by conventional methods. This consequently not only reduces the yield of RCR yield but produces better quality RCR in terms of the contents of sulfur, nitrogen, metals, and asphaltene. This leads to the production of good lighter fuel oils expecting to reduce catalyst deactivation rate, pumping costs, etc.

References

1. Abbas AS (1999) Low sulfur feedstock from basrah reduced crude oil for coke production. MSc thesis, University of Baghdad
2. Al-Humaidan FS (2004) Modelling hydrocracking of atmospheric residue by discrete and continuous lumping. MSc thesis, Kuwait University
3. Ali LH, Abdul-Karim E (1986) The oil, origin. Iraq, AlMosul University, Composition and Technology
4. Ancheyta J, Speight JG (2007) Hydroprocessing of heavy oils and residua. CRC Press, USA
5. Andari MK, Behbehani H, Stanislaus A (1996) Sulfur compound type distribution in Naphtha and gas oil fractions of Kuwaiti crude. *Fuel Sci Technol Int* 14:939
6. Areff HA (2001) The effect of operating conditions on vacuum gas oil hydrotreating on sulfur and aromatics content. MSc thesis, University of Tikrit
7. Ashaibani AS (2002) Modelling, simulation and optimisation of refinery processes with energy conservation. PhD thesis, University of Bradford, UK
8. Ashaibani AS, Mujtaba IM (2007) Minimisation of fuel energy wastage by improved heat exchanger network design-an industrial case study. *Asia-Pac J Chem Eng* 2:575
9. Bartholdy J, Cooper BH (1993) Metal and coke deactivation of resid hydroprocessing catalysts. ACS Symposium on Resid Upgrading Denver, USA, p 386
10. Benito AM, Callejas MA, Martínez MT (1997) Kinetics of asphaltene hydroconversion: 2. Catalytic hydrocracking of a coal residue. *Fuel* 76:907
11. Callejas MA, Martínez MT (2000) Hydroprocessing of a maya residue. 1. Intrinsic kinetics of asphaltene removal reactions. *Energy Fuel* 14:1304
12. Chung SYK (1982) Thermal hydroprocessing of heavy gas oils. MSc thesis, University of Alberta
13. Fogler HS (1999) Elements of chemical reaction engineering, 2nd edn. Prentice-Hall, New Jersey
14. Gajardo P, Pazos JM, Salazar GA (1982) Comments on the HDS, HDM and HDN activities of commercial catalysts in the hydrotreating of heavy crude oils. *Appl Catal* 2:303
15. Gary JH, Handwerk GE (1994) Petroleum refining: technology and economics, 3rd edn. Marcel Dekker, New York
16. Girgis MJ, Gates BC (1991) Reactivities, reaction networks, and kinetics in high-pressure catalytic hydroprocessing. *Ind Eng Chem Res* 30:2021

17. Gully AL, Ballard WP (1963) *Advances in petroleum chemistry and refining*. Wiley, New York
18. Hobson GD (1984) *Modern petroleum technology*. 5th edn. Wiley, New York
19. Hsu ChS, Robinson PR (2006) *Practical advances in petroleum processing*. Springer, New York
20. Jarullah AT (2011) Kinetic modelling simulation and optimal operation of trickle bed reactor for hydrotreating of crude oil. PhD Thesis. University of Bradford, UK
21. Jarullah AT, Awad NA, Mujtaba IM (2017) Optimal design and operation of an industrial fluidized catalytic cracking reactor. *Fuel* 206:657
22. Jarullah AT, Mujtaba IM, Wood AS (2011) Kinetic parameter estimation and simulation of trickle-bed reactor for hydrodesulfurization of crude oil. *Chem Eng Sci* 66:859
23. Jarullah AT, Mujtaba IM, Wood AS (2011) Kinetic model development and simulation of simultaneous hydrogenation and hydrodemetallization of crude oil in trickle bed reactor. *Fuel* 90:2165
24. Jarullah AT, Mujtaba IM, Wood AS (2011) Improvement of the middle distillate yields during crude oil hydrotreatment in a trickle-bed reactor. *Energy Fuels* 25:773
25. Jarullah AT, Mujtaba IM, Wood AS (2011) Whole crude oil hydrotreating from small-scale laboratory pilot plant to large-scale trickle-bed reactor: analysis of operational issues through modeling. *Energy Fuels* 26:629
26. Jarullah AT, Mujtaba IM, Wood AS (2012) Improving fuel quality by whole crude oil hydrotreating: a kinetic model for hydrodeasphaltenization in a trickle bed reactor. *Appl Energy* 94:182
27. Jarullah AT, Mujtaba IM, Wood AS (2012a) Economic analysis of an industrial refining unit involving hydrotreatment of whole crude oil in trickle bed reactor using gPROMS. In: Bogle IDL, Fairweather M (eds) *Computer aided chemical engineering- 30*, vol 30. Elsevier, pp 652–656
28. Jimenez F, Nunez M, Kafarov V (2005) Study and modelling of simultaneous hydrodesulfurization, hydrogenation and hydrodearomatization on vacuum gas oil hydrotreatment. *Comput Aided Chem Eng* 20:619
29. Jimenez F, Ojeda K, Sanchez E, Kafarov V, Filho RM (2007) Modeling of trickle bed reactor for hydrotreating of vacuum gas oils: effect of kinetic type on reactor modelling. *Comput Aided Chem Eng* 24:515
30. John YM, Patel R, Mujtaba IM (2017) Maximization of gasoline in an industrial fluidized catalytic cracking unit. *Energy Fuels* 31:5645–5661
31. Khalfalla HA (2009) Modelling and optimization of oxidative desulfurization process for model sulfur compounds and heavy gas oil. PhD Thesis. University of Bradford
32. Khalfalla HA, Mujtaba IM, El-Garni M, El-Akrami H (2007) Experimentation, modelling and optimisation of oxidative desulphurization of heavy gas oil: energy consumption and recovery issues. *Chem Eng Trans* 11:53–58
33. Kim LK, Choi KS (1987) Hydrodesulfurization over hydrotreating catalysts. *Int chem Eng* 27:340
34. Leprince P (2001) Conversion processes. Institute Francais du Petrole, Paris
35. Leyva C, Rana MS, Trejo F, Ancheyta J (2007) On the use of acid-base-supported catalysts for hydroprocessing of heavy petroleum. *Ind Eng Chem Res* 46:7448
36. Mahmood Sh, Abdul-Karim R, Hussein EM (1990) *Technology of oil and gas*. Baghdad, Oil Training Institute
37. Nawaf AT, Jarullah AT, Ghani SA, Mujtaba IM (2015) Development of kinetic and process models for the oxidative desulfurization of light fuel, using experiments and the parameter estimation technique. *Ind Eng Chem Res* 54:12503
38. Nawaf AT, Jarullah AT, Ghani SA, Mujtaba IM (2015) Optimal design of a trickle bed reactor for light fuel oxidative desulfurization based on experiments and modeling. *Energy Fuels* 29:3366

39. Nawaf AT, Jarullah AT, Gheni SA, Mujtaba IM (2015) Improvement of fuel quality by oxidative desulfurization: design of synthetic catalyst for the process. *Fuel Process Technol* 138:337
40. Pereira CJ, Cheng JW, Suarez WC (1990) Metal deposition in hydrotreating catalyst. *Ind Eng Chem Process Des Dev* 29:520
41. Scherzer J, Gruia AJ (1996) *Hydrocracking science and technology*. Marcel Dekker, New York
42. Speight JG (2000) *The desulfurization of heavy oils and residua*, 2nd edn. Marcel Dekker, New York
43. Ting PD, Hirasaki GJ, Chapman WG (2003) Modeling of asphaltene phase behavior with the SAFT equation of state. *Pet Sci Technol* 21:647
44. Topsøe H, Clausen BS, Massoth FE (1996) *Hydrotreating catalysis*. Germany, Springer-Verlag, Berlin Heidelberg, Science and Technology
45. Turaga UT (2000) MCM-41-supported cobalt-molybdenum catalysts for deep hydrodesulfurization of diesel and jet fuel feedstocks. PhD Thesis. Pennsylvania State University
46. Wauquier JP (1995) *Crude oil: petroleum products*. Process Flowsheets, Paris, Editions Technip

The Sustainable Option of Power from Fossil Fuels with Carbon Capture and Storage: An Overview of State-of-the-Art Technology

Maria Elena Diego, Karen N. Finney and Mohamed Pourkashanian

Abstract To limit the global rise in temperature to 1.5–2 °C, considerable reductions in greenhouse gas emissions, especially CO₂, are needed—challenging because of the continuous increases in energy demand and the large contribution from fossil fuels. Gas-fired power plants will be a significant part of power generation over the next few decades, and whilst CO₂ emissions are significantly lower than for coal, they must still be addressed to lower carbon intensity. This can be achieved through carbon capture and storage (CCS) as a key enabling technology. This chapter aims to summarize the key research on state-of-the-art gas turbine technologies for enhanced post-combustion capture and oxy-turbine gas-CCS cycles, including the technical challenges and opportunities. For post-combustion systems, supplementary firing, humidification, exhaust gas recirculation and selective exhaust gas recirculation will be assessed, which outline the CO₂ increases and electrical efficiencies achievable when considering the capture penalty. An alternative to post-combustion capture is the use of oxy-turbine cycles, where the relative merits are assessed. Lastly, this chapter discusses the impacts of the technical, policy, financial and social challenges on scaling-up these technologies for full-chain commercial-level deployment. Overcoming these will be a necessity to enable CCS to decarbonize energy for a sustainable future.

Keywords Carbon capture and storage · CCS · Natural gas · Gas-CCS
Post-combustion capture · Oxy-turbine cycles

M. E. Diego (✉) · K. N. Finney · M. Pourkashanian
Energy 2050, Faculty of Engineering, University of Sheffield, Sheffield S10 2TN, UK
e-mail: m.diegodepaz@sheffield.ac.uk

K. N. Finney
e-mail: k.n.finney@sheffield.ac.uk

M. Pourkashanian
e-mail: m.pourkashanian@sheffield.ac.uk

1 Introduction

The global energy demand is expected to increase significantly in the near future as a result of economic growth and population increases worldwide, with the power sector predicted to account for 47% of the total primary energy consumption by 2035 [1]. Current predictions indicate that more than half of the electricity demand will be provided by fossil fuels in the next few decades [1, 2], therefore making it challenging to achieve the necessary reductions in CO₂ emissions to tackle climate change [3]. It is clear that any efficiency improvements and the current trend to switch to less carbon-intensive fossil fuels (i.e. natural gas) will contribute to lowering the amount of CO₂ emitted into the atmosphere. However, these alone are not enough to achieve the profound emission cuts required to keep global average temperature rises below 1.5–2 °C, and further actions are thus required [1–3]. No stand-alone solution is possible for this purpose, but the integration of several options will be key to ensure a transition to a fully integrated, low-carbon economy. This includes both efficiency improvements and fuel switching, as mentioned above, but also an increase in the share of nuclear and renewable energy, as well as the use of CO₂ capture and storage (CCS) technologies [4].

In this decarbonization context, carbon capture and storage is expected to play an important role within the solution portfolio, accounting for up to 14% of the total cumulative effort in CO₂ emissions reduction through to 2050 [4]. The importance of CCS relies on its ability to decouple CO₂ emissions from fossil fuel sources, thus securing the supply of an increased energy demand whilst still attaining the CO₂ emission targets associated with the most demanding scenarios [4]. It has a large importance in the industrial sector (such as, cement, iron and steel, chemical and refinery plants), where CCS is one of the few options that can provide substantial cuts in CO₂ emissions here. CCS is also relevant in the power sector, where flexible, reliable, fossil-fuelled backup utilities are widely required in spite of the increasing penetration of renewables (which are inherently intermittent), in order to guarantee the security of supply and ensure a precise match between the instantaneous electricity generation and demand at all times. Although the high costs are at present a limiting factor to deployment, further advantages of CCS could come from an economic perspective, as it can contribute to limiting the mid- and long-term costs of the transition towards a sustainable, low-carbon model. This is the case of the electricity sector, where it has been estimated that excluding CCS from the solution portfolio will increase investment costs by 40% if the same CO₂ reduction targets are to be achieved [4].

Focusing on the power sector, large efforts have been initially devoted to the development of CCS technologies for coal applications. However, coal is very carbon-intensive and a move towards fuels with a lower carbon footprint will mean that CCS technologies will also have to be utilized with these other resources. This is the case of natural gas, which has experienced rapid growth in the last few

decades due to its lower carbon emissions per unit of energy generated (less than 400 kg/MWh vs. approximately 800 kg/MWh for coal), in addition to the more flexible operation and lower capital costs of gas-fired systems with respect to coal-fired power plants [4]. Given the increasing importance of those systems [1, 2], this chapter aims to discuss the implementation of CCS in natural gas-fired power plants, with a focus on the capture step. For this purpose, a summary of the different capture systems and the current status of CCS commercialization are covered in Sects. 1.1 and 1.2, respectively. Moreover, Sect. 2 is dedicated to adapting post- and oxy-combustion capture options to best suit natural gas combustion, focusing on state-of-the-art technologies and discussing the main technical challenges. Pre-combustion systems using natural gas are not considered in detail herein due to the less attractive economics at present, although alternatives are currently being studied to improve the competitiveness of these systems [5, 6]. Political, financial and social factors affecting the deployment of CCS are also commented on in Sect. 3, where a final discussion on the opportunities of these systems is included. The conclusions of this chapter are then presented in the last section.

1.1 Overview of Carbon Capture Systems

Carbon capture and storage technologies aim to separate the CO₂ generated from industrial processes and generate a CO₂-concentrated stream that can be then purified, compressed and permanently stored. The CO₂ capture stage is key in CCS systems, as it is responsible for reducing the CO₂ emissions of a specific process and accounts for the largest cost share of the entire CCS chain (i.e. capture, transportation and storage) [7, 8]. Three systems can be distinguished depending on where the separation step happens, namely post-combustion, oxy-combustion and pre-combustion capture [7]. These are briefly discussed here.

Post-combustion systems separate the CO₂ contained in a gaseous stream (i.e. the flue gas) as a result of a fossil fuel or biomass combustion process, leading to a CO₂-rich stream that can be ultimately stored. This separation step can be carried out using solvents, solid sorbents, membranes or cryogenic processes. Post-combustion technologies are suitable for its implementation in existing plants (retrofitting), as they are placed downstream of the plant thus hardly affecting the production process.

Oxy-combustion systems burn the fuel using an oxygen-rich flow instead of air. A gaseous stream that mainly contains CO₂ and H₂O is obtained after combustion, leading to a CO₂-rich flow after water condensation. Therefore, the gas separation stage takes place in this system before combustion, i.e. O₂ separation from N₂ in air. Cryogenic methods are often considered for this purpose, although the use of chemical looping combustion systems or membranes has been proposed to reduce the often high energy penalty and costs.

Pre-combustion processes separate CO_2 prior to combustion. In these systems, a CO/H_2 stream (syngas) is produced after gasification or reforming of the fuel using air or oxygen and/or steam. The syngas then undergoes a water–gas shift reaction, where the CO reacts with steam to obtain a CO_2/H_2 mixture. The CO_2 is then separated by physical absorption or using some of the post-combustion processes referred to above, leading to a highly concentrated H_2 flow that can be used as energy source.

The systems discussed above are mainly focused on energy generation processes. Nevertheless, an area of great importance is CO_2 capture from industrial sources (e.g. in the cement or the iron and steel industry). Separation of CO_2 from industrial gas streams has been routinely carried out with purposes different from CCS, such as to reduce the CO_2 content in natural gas or to separate CO_2 from H_2 during ammonia production [7]. Nevertheless, the study of technologies aimed at capturing CO_2 from a range of industrial sources has received increasing attention recently, as it is one of the few options to achieve deep cuts in CO_2 emissions in these systems.

1.2 Current Status of Commercial CCS Deployment in the Power Sector: Carbon Capture from Coal

A number of large-scale CCS projects with individual CO_2 capture capacities in the range of 0.4–8.4 MtCO_2/yr are currently operational [9]. Many of them are related to CO_2 separation in the natural gas processing industry, but there are dedicated projects in the power generation sector as well. Others are also related to industrial sectors like the iron and steel industry and the production of fertilizers, synthetic natural gas, hydrogen and ethanol [9]. The resulting CO_2 stream is employed for enhanced oil recovery (EOR) in most of these projects, as this is an economic driver for the development of CO_2 capture initiatives in some regions (e.g. USA and Canada). Nevertheless, there are also CCS projects that target the geological storage of CO_2 . Some have been running for several years, thus injecting considerable amounts of CO_2 underground and providing valuable information for control and monitoring purposes (see, for example, the ongoing Sleipner, Weyburn-Midale and Snøvit projects [9] and the In Salah project (injection suspended in 2011) [10]).

In the power sector, the recent deployments of full-chain CCS demonstrations have primarily focused on coal-fired generation as mentioned in Sect. 1, with two fully operational plants at large scale coming online in the past few years. This is the case of Boundary Dam, which was the first power station in the world to implement the technology at scale [11]. In this project, located in Saskatchewan (Canada), one of the units (139 MW) of the existing power plant was retrofitted with post-combustion CO_2 capture at 90% efficiency using the Shell CANSOLV's combined CO_2 and SO_2 capture process, with a capture capacity of 1 MtCO_2/yr [12]. It became operational in 2014, and the captured CO_2 is mainly transported via

pipeline to be used for EOR in the Weyburn oil field [12], although a small fraction is taken for geological storage under the framework of the Aquistore project [13]. More recently, Petra Nova in the USA has become the largest post-combustion carbon capture plant worldwide. It also uses solvent-based technologies—specifically, a proprietary KS-1 solvent—and can capture up to 1.4 MtCO₂/yr with ~90% efficiency from a slipstream (equivalent to 240 MW) of flue gas from the associated coal-fired power plant. The CO₂ is then used for EOR purposes at the West Ranch oil field [14].

The projects mentioned above show that CCS in the power sector is already a reality. These are important assets for the future of CCS, providing valuable information and operational experience that can be employed to optimize these processes and reduce risks, uncertainties and costs for future plants. Nevertheless, more projects are required at demonstration and commercial scale to prove and optimize the more mature and also novel emerging capture technologies from a variety of sources and gain additional knowledge. To this end, further potential CCS projects at large scale are at different stages of development, including capture projects dedicated to the industrial sector, as well as post-, pre- and oxy-combustion options for power generation [9]. Current and future demonstration activities are essential to reduce the costs of CO₂ capture, improve system performance and gain confidence in the entire CCS chain, which could facilitate a more rapid deployment of CCS in the near future if adequate policies and incentives are in place. This is discussed in detail in Sect. 3.

2 Carbon Capture from Natural Gas-Fired Power Plants: Gas-CCS

Widespread deployment of carbon capture and storage in gas-fired power plants (gas-CCS) requires adaptation of the capture technologies and/or the turbomachinery and other process units to the specific characteristics of these systems. This section focuses on post- and oxy-combustion gas-CCS applications, highlighting the main challenges and opportunities with a view to its commercial deployment.

2.1 Post-combustion CO₂ Capture

Conventional gas-fired power plants use very high excess air ratios to limit the temperature in the combustion chamber and protect the gas turbine from damage occurring when working at very high inlet temperatures. This operating strategy results in large flows of flue gas with a CO₂ content of just 3–4 vol%—much lower than that of coal-fired power plants (around 12–15 vol% CO₂)—which negatively affects the performance of any CO₂ capture process placed downstream [15, 16]. As

a result, coupling post-combustion carbon capture systems with gas-fired plants is particularly challenging, and large capture reactors are required to cope with the increased flows, which should also capture CO₂ efficiently under restricted driving force conditions. Therefore, higher penalties and capture costs can be expected in gas-CCS systems [15, 16]. In addition, the flue gas also contains large amounts of oxygen (of the order of 12–13 vol%), which can increase oxidative solvent degradation in those systems using amines as the capture technology [17], thus increasing operating costs. A number of options have been proposed in order to enhance the CO₂ content in the flue gases generated in gas-fired systems, which lead to lower oxygen levels and can also reduce the flue gas flow to be treated in some cases. These therefore have a range of benefits for the capture system, as they can potentially reduce the size, energy penalty and costs associated with the post-combustion plant. These are:

- Supplementary firing
- Humidification
- Exhaust gas recirculation
- Selective exhaust gas recirculation.

These schemes are explained in detail in Sects. 2.1.1, 2.1.2 and 2.1.3. The discussion in these sections is mainly focused on the use of amine scrubbing (usually employing monoethanolamine (MEA) as the solvent) in gas-CCS systems, especially in terms of electrical efficiencies, as they are the most mature post-combustion capture systems as indicated in Sect. 1.2, and much information is available on these systems. Nevertheless, it is important to highlight that all post-combustion capture technologies could potentially benefit from the increase in the flue gas CO₂ content attained through the gas turbine configurations described in the next sections.

In addition to the specific characteristics of the flue gas to be treated, further challenges of gas-CCS systems are related to the need for flexible operation of the post-combustion CO₂ capture plant. Gas-fired power plants have the ability to quickly respond to changes in demand and are often employed for backup purposes at varying loads [18]. Therefore, any capture plant coupled to these systems will also need to operate flexibly, exhibiting reliable and effective performance under a wide range of conditions. Dynamic operation of capture systems is not fully understood at the moment for any of the capture technologies proposed in the literature, and it is currently an active R&D area. Another topic of research is related to process optimization and intensification. There is still scope for specific improvements in the capture systems for all of the proposed technologies, with large efforts devoted to finding new optimized configurations that can improve the energy penalties and costs of these systems. However, it is important to point out that alternative layouts can often lead to increased complexity/costs of the power plant and/or the capture system, and their effects on the overall performance of the integrated plants and their flexibility should be carefully evaluated, especially for gas-fired systems.

2.1.1 Supplementary Firing

Supplementary firing consists of burning additional fuel downstream the gas turbine (see Fig. 1) by taking advantage of the high oxygen content remaining in the exhaust gas of gas-fired systems (around 12–13 vol% O₂ as discussed in Sect. 2.1). This option was initially proposed to increase the power output of natural gas combined cycle (NGCC) systems during periods of peak electricity demand, since extra power can be generated in the steam cycle as a result of the higher temperature of the flue gas entering the heat recovery steam generator (HRSG) after the supplementary firing stage [19]. This idea can be also exploited to compensate for the adverse effect of ambient conditions on gas turbines (e.g. an increase in ambient temperature), which reduce the power output of the plant [20]. Additionally, supplementary firing has been investigated for gas-CCS applications because of its associated benefits, namely (i) a higher CO₂ content in the flue gas, which increases the driving force in the CO₂ capture stage; (ii) a reduction in the flue gas O₂ concentration, which can lead to lower rates of solvent degradation in amine CO₂ capture systems; (iii) a decrease in NO_x emissions; and (iv) the potential use of biomass in the supplementary firing unit, which can lead to a further reduction in CO₂ emissions linked to the concept of negative emissions [15, 16, 21–25]. Moreover, some authors have claimed that further advantages can be obtained if the power plant is designed to continuously operate under supplementary firing conditions, as the flue gas flowrate arriving at the capture plant could be reduced with respect to that of a reference NGCC plant (without supplementary firing) with the same power output [24], thus reducing the cost of the downstream CO₂ capture system.

NGCC plants using supplementary firing are available at commercial scale—see, for example [26]. However, there are specific challenges and limitations that need to be considered when coupling those systems with CCS. This is certainly the case of the maximum CO₂ increase that can be achieved in the flue gas as a result of supplementary firing, which is related to the energy consumption in the post-combustion capture system (see [16] for amine scrubbing plants) and depends on the amount of fuel that can be burnt in this stage. This is usually limited by material considerations, i.e. by the maximum temperature of the flue gas at the inlet

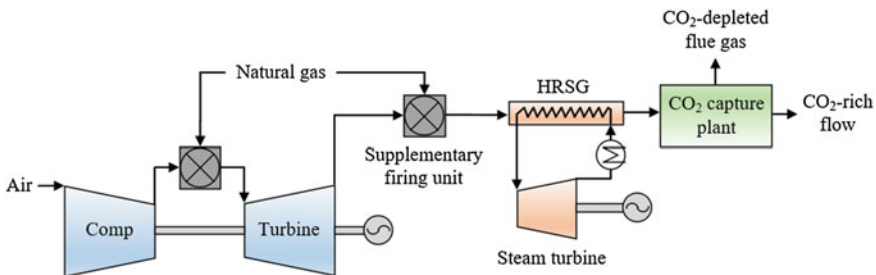


Fig. 1 Representation of a natural gas combined cycle with supplementary firing and CO₂ capture

of the HRSG. A limit of 800 °C is often considered [24, 27], but higher temperatures can be employed if insulated casings (up to 900 °C) or water-cooled furnaces (up to 1300 °C) are employed in the HRSG [28]. Concentrations around 7 vol% CO₂ can be achieved assuming the supplementary firing process operates at ~1300 °C, although this can theoretically increase up to ~11 vol% CO₂ under stoichiometric conditions (which imply much higher temperatures) [16]. Alternatively, sequential supplementary firing can be used, thus allowing for high CO₂ concentrations in the flue gas whilst keeping temperatures in the HRSG at moderate values [24]. In this case, the supplementary fuel is distributed into a number of firing stages throughout the HRSG, as opposed to the system seen in Fig. 1. As a result, the flue gas achieves a more limited temperature increase in each stage, and therefore, more supplementary fuel can be burnt (leading to higher CO₂ concentration) without compromising material performance. The maximum flow of fuel that can be burnt is then limited by the flue gas oxygen concentration in the last firing stages. Concentrations close to 11 vol% CO₂ have been calculated at the inlet of the absorber reactor in NGCC systems using sequential supplementary firing with maximum temperatures in the HRSG of 820 °C, assuming complete and stable combustion can be performed at very low oxygen levels in the last firing stage (around 1 vol% O₂ at the exit of the last stage) [24].

Moreover, the use of supplementary firing can increase the mass flowrate of the flue gas to be treated in the capture plant in those cases where no exhaust gas condensation is applied, thus offsetting the benefits of an increased CO₂ concentration [16, 25]. Another important limitation is the associated reduction in the net electrical efficiency of the power plant, as the fuel fed to the supplementary firing unit is only used to produce power in the Rankine steam cycle, unlike the main fuel stream. This cycle is less efficient than the combined Rankine and Brayton cycles, which together with the higher temperature difference in the HRSG results in a reduced efficiency [25]. Therefore, the potential benefits of supplementary firing in CO₂ capture applications depend on two opposite effects that impact the overall system efficiency: the efficiency loss in the power plant versus the decrease in the energy consumption of the capture process as a result of the higher flue gas CO₂ content. This has been studied in NGCC power plants that make use of a supplementary firing stage and incorporate an amine CO₂ capture plant downstream (MEA-based). Electrical efficiencies between 42 and 48% have been calculated for these systems, which can be up to 7–8 net percentage points lower than those of a NGCC without supplementary firing coupled to an amine capture plant [16, 24]. Similar trends were also reported in a recent study that investigates the use of supplementary firing in NGCC plants with CO₂ capture in order to compensate for the power reduction experienced by these systems when the ambient temperature increases [29]. Results obtained also indicate a substantial efficiency drop of around 5 net percentage points with respect to the system without supplementary firing [29]. The efficiency drop associated with the system of Fig. 1 can be partially compensated with the use of supercritical steam cycles in the HRSG [16, 24]. Nevertheless, this comes at the expense of a more complex system, thus affecting its cost and flexibility [25, 30].

More complex supplementary firing configurations have been evaluated for its application in NGCC plants equipped with amine scrubbing CO₂ capture in order to investigate further performance improvements [25]. One of these options consists of the use of supplementary firing together with exhaust gas reheating, which can raise the electrical efficiency by 15% compared to the conventional supplementary firing case, but the CO₂ concentration is also reduced [25]. Another alternative is based on combining supplementary firing and exhaust gas recirculation, the latter of which is explained in detail in Sect. 2.1.3. In this case, the effect on efficiency is more moderate (~4% increase with respect to the conventional supplementary firing configuration), but it largely reduces the mass flow and increases the CO₂ content of the flue gas, which will reduce the costs of the CO₂ capture plant. However, there is a substantial decrease in the oxygen available in the supplementary firing stages [25]. The use of a NGCC system that incorporates supplementary firing, exhaust gas reheating and recirculation, as well as a supercritical HRSG design, has also been analysed, leading to an efficiency penalty of just ~3 net percentage points with respect to the NGCC system without CO₂ capture [25]. Nonetheless, it is important to highlight that the alternative configurations mentioned here have substantially more complex process schemes than that of Fig. 1. Therefore, this has implications in terms of operational flexibility and costs, as discussed in Sect. 2.1, which are sensitive areas for power plants incorporating CCS systems and should be carefully evaluated.

2.1.2 Humidification of Gas Turbine Cycles

Humidified turbines introduce moisture to a conventional gas turbine cycle so that the working fluid is changed from air to an air–H₂O mix. Such systems have previously been utilized to: (i) improve electrical efficiencies, since the mass flowrate of working fluid through the turbine is increased whilst keeping the compressor power unchanged (moisture is added after compression), therefore increasing the power output [31–39], and (ii) to control emissions, particularly of NO_x, as peak flame temperatures in the primary combustion zone are reduced by the higher heat capacity of the working fluid [16, 35, 40, 41]. Furthermore, humidification has also been reported to improve the specific output [42] and specific work [43].

More recently, humidified turbine cycles have been evaluated as a means of augmenting the CO₂ level in the exhaust to aid carbon capture. Humidified cycles increase the CO₂ content of the flue gas, since the moisture replaces some of the air and can be condensed out [16, 40, 44]. The amount of CO₂ augmentation, however, depends on a range of factors related to the various operating parameters/conditions, but mainly on the degree of humidification. This water–air ratio is also a key defining parameter for efficiency improvements [16]. Various maximum CO₂ concentrations have been reported for the flue gas generated in humidified gas turbine cycles—although often these are around 5 vol% [16, 45]. This is equivalent to an increase in the flue gas CO₂ content of ~25–30%, which could enable large

reductions in the reboiler duty of amine capture systems [16, 46]. As the degree of humidification or water–air ratio is such an important parameter, the moisture addition needs to be finely balanced, even though the amount of water/steam required to achieve performance improvements is often substantial. High water–fuel ratios are often needed, but at such levels, increases in emissions relating to incomplete combustion are found—specifically CO and unburned hydrocarbons due to the lower oxygen availability and reduced system temperatures in the primary combustion zone [16, 47]. Takahashi et al. [42] state that each system has a different optimal point for efficiency maximization, which is often in the region of 12–14 vol% of moisture inclusion in the inlet oxidizer (water/air ratio)—this has been corroborated by Li et al. [16]. Others have suggested that much lower levels of humidification in the region of 5–6 vol% are sufficient [32, 33, 48].

Wet turbine cycles are classified depending on the way the moisture is introduced, and there are a range of possible configurations. Methods exist for both the injection of water in its liquid form, either directly or with evaporative cycles using humidification towers, and as steam [40]. Humid air turbines (HAT) and steam injected gas turbines (STIG) are considered in turn below. These are recuperative cycles that recover the heat to use again, which means the efficiency and outputs are increased, whilst the specific investment costs decrease [40, 49]. This can be beneficial to mitigate, at least in part, some of the energy penalty caused by adding carbon capture to an electricity generation process. Part-load performance is also better than that of a combined cycle [40], and as a result, they are classed as higher performance gas turbine technologies.

Humid air turbine systems, also referred to as evaporative gas turbines (EvGT), utilize a saturator or humidification tower to add moisture downstream of the compressor [44, 50], as shown in Fig. 2 in its simplest configuration. The inclusion of heat recovery components (e.g. an economizer) means that the thermal energy in the flue gases and in the compressor outlet gas can be recovered by using it to heat and evaporate water, which is then used to saturate the air exiting the compressor. This gives a single phase mixture, which can be further heated with the heat recovered from the turbine exit stream before entering the combustor, as depicted in Fig. 2 [49]. By recovering and reusing this heat, considerably higher thermal efficiencies can be achieved for a specific system. Moreover, the increased mass flow of the working fluid through the turbine (due to the addition of moisture to the air) results in a higher specific power output and greater electrical efficiencies, as the power consumption in the compressor remains unchanged [44, 51–53]. This is equivalent to arguing that the compressor power demand decreases in HAT systems with respect to a non-humidified gas turbine if the same power output is to be achieved, since humidification occurs after the compressor [44, 54, 55]. HAT systems can achieve maximum electrical efficiencies in the region of 50–52% [35, 56, 57], and decrease significantly with the addition of a post-combustion capture system downstream, to ~42% using a MEA-based scrubbing plant [16]. HAT systems can start up faster and have a higher availability than non-humidified combined cycles and could therefore play a valuable role in a future with significant amounts of intermittent renewables in the grid mix [58].

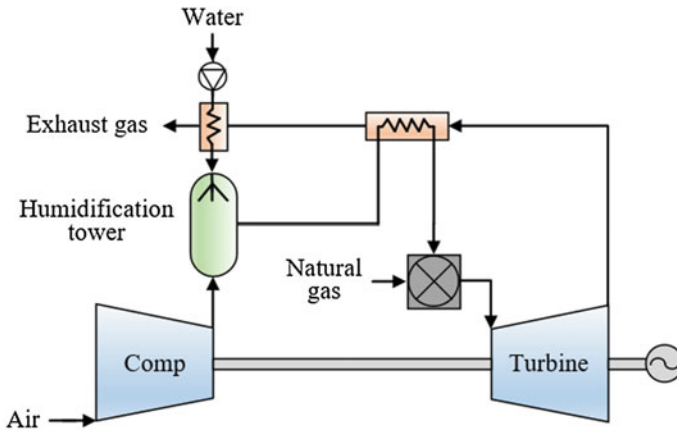


Fig. 2 Schematic of a humidified gas turbine operating under HAT conditions

Another humidification option is based on steam injected gas turbine systems. These integrate a HRSG, where the heat contained in the flue gas is recovered to generate steam after the turbine, which is then injected into the combustion chamber, as delineated in Fig. 3 [40, 51–53]. Additional recuperation can be included by heating the compressed air prior to combustion [52]. As in the case of HAT cycles, a fraction of the air is replaced by steam, which increases the mass flowrate of the working fluid through the turbine without increasing the power consumption in the compressor, thus leading to higher electrical efficiencies [40, 51, 53]. For STIGs in combined cycles, a single HRSG can be used, with a bleed-off to feed steam to the combustor. Horlock [52] reports that the work output of the turbine increases linearly with the quantity of the steam injected, and the optimum steam quantity corresponds to the maximum steam exit temperature, along with the minimum pinch point temperature difference. This also has limitations based on the compressor surge and maximum steam flowrate [59]. STIG cycles typically have much lower electrical efficiencies than HAT systems by comparison—which peak at up to 48%, but are generally lower at around 37–41% [16, 31, 53, 60–62]. This, together with the limited increase in the CO₂ content that can be achieved in the flue gas, makes the option of coupling STIG systems with post-combustion CO₂ capture unattractive. Advances and modifications to standard STIGs can further improve performance up to 50% though [51].

In addition to these two main modifications (HAT and STIG), a range of other more complex cycles and altered configurations have been proposed. These include, but are not limited to, the inclusion of an inverted Brayton cycle, integrated bottoming cycles, recuperative heating of the flue gas after the condenser, part-flow evaporative gas turbines, recuperated and intercooled-recuperated cycles, semi-closed humidified cycles, multi-effect thermal vapour compression, chemically recuperated cycles, spray intercooling/aftercooling, humid air water injected turbines and regenerated water injected cycles, as well as CHENG, FLECS,

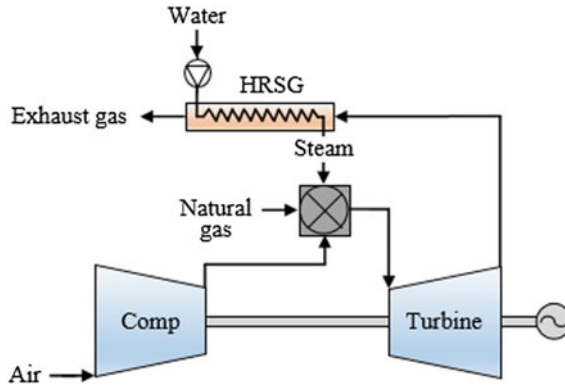


Fig. 3 Schematic of a humidified gas turbine operating under STIG conditions

REVAP and advanced-HAT turbines [35, 38, 42, 43, 57, 61–65]. Hybrid systems have also been considered, which primarily focus on the integration of low-carbon energy sources, such as renewables (solar and biomass) or fuel cells into humidified systems [66–70]. Whilst these have shown a range of additional benefits to the traditional humidification technologies, such as further improvements in efficiency, their considerable complexity can substantially increase the costs and reduce the flexibility of such systems, and are therefore not considered viable at present.

Moreover, there are a number of common issues with humidified gas turbine cycles. Water consumption for all ‘wet’ gas turbine cycles can be problematic, specifically adding significant cost. Water utilization rates for STIG designs though can be up to three times greater than for HAT systems [37, 49]. Condensing out the moisture from the flue gas to reuse is vital to ensure the operational costs are not excessive. Choosing the most appropriate condenser can have significant impacts on the plant footprint and costs [71]. However, reusing the water can also lead to problems. Demineralization of the recycled water is often required to stop build-up of species that can cause deposition and corrosion within the system [35, 47]. Furthermore, extra components are required for all these systems to achieve the humidification. These, and the necessary ancillary equipment, add notably to their complexity as well as their costs. Minimizing the moisture inclusion in the cycle is therefore necessary in terms of water consumption, but there are other reasons to ensure an optimal moisture–air ratio is used: (i) excessive moisture addition lowers the oxygen content of the oxidizer stream and can negatively impact flame stability, and (ii) excess water in the outlet flue gas stream can further dilute the solvent used for amine scrubbing carbon capture, increasing the reboiler duty [16, 56]. Moreover, modifications are sometimes required to the gas turbine system components, which have to cope with a mismatch in the compressor and turbine flows. Increases in the pressure ratio are often needed in optimized humidified systems, and thus, higher-grade materials could be needed [51, 53]. Additionally, blade cooling optimization may also be required, which presents new opportunities (or challenges!) in the field of blade and disc cooling architecture [72].

The general consensus then is that gas turbine humidification can result in considerable performance benefits when looking at the gas turbine itself (no CO₂ capture); however, the improvements in performance are more pronounced for systems operating with HAT than STIG. Nevertheless, these systems can only provide a limited increase in the CO₂ content of the flue gas (up to ~5 vol%), and the calculated electrical efficiencies when coupled with amine-based capture technologies are lower than those of other available options (e.g. a conventional NGCC using amine scrubbing for CO₂ capture with or without exhaust gas recirculation or supplementary firing) [16]. This limits the interest of humidified turbine cycles for gas-CCS applications.

2.1.3 Exhaust Gas Recirculation and Selective Exhaust Gas Recirculation

Both exhaust gas recirculation (EGR) and selective exhaust gas recirculation (S-EGR) can increase the CO₂ partial pressure in the turbine flue gases that are sent to the post-combustion capture plant by concentrating the CO₂ into a smaller flowrate of gas. In the EGR case depicted in Fig. 4, this is achieved by recirculating a proportion of the flue gases back to the compressor after passing through a flue gas cooler and a water knockout unit [73]. The recirculated flow contributes to control temperatures in the combustor and replaces a fraction of the inlet air, thus reducing the exhaust flowrate and increasing the back-end CO₂ levels, which facilitates effective post-combustion capture in a plant with a reduced size and energy penalty. Several studies report that using EGR decreases the volumetric flue gas flowrate by an equivalent amount [18, 74–77]—e.g. the flue gas flow can be halved by using recirculation ratios of ~50%. At this level, the CO₂ content in the flue gas increases from ~4 to ~8 vol% CO₂, with the specific reboiler duty of an associated MEA capture plant decreasing by ~8% [77]. Other benefits can also be found when deploying EGR into gas-CCS systems. NO_x reductions have been extensively reported for EGR operation [16, 78–81]. Whilst this is primarily due to the decrease in the peak combustion and flame temperatures [82], since the CO₂ has a higher heat capacity, the reduced oxygen availability may also play a role [77].

Despite the beneficial impacts of EGR, there are also limitations, as considered herein. The recirculation ratio is the defining parameter for the CO₂ increase [16], which is related to the efficiency gains attained in the NGCC plant with CO₂ capture. The overall consensus on EGR from both experimental and theoretical studies is that EGR ratios of 40% are the most ideal, although an absolute maximum recirculation rate, which is under much debate, of 50% could be used with small system modifications [83].

This key defining factor needs to be chosen carefully to ensure that the maximum potential CO₂ concentration is achieved, with minimal negative consequences, such as increases in other emissions resulting from combustion instabilities due to oxygen depletion in the oxidizer and/or lower peak temperatures. The recirculation ratios reported vary widely, although typical maximum EGR

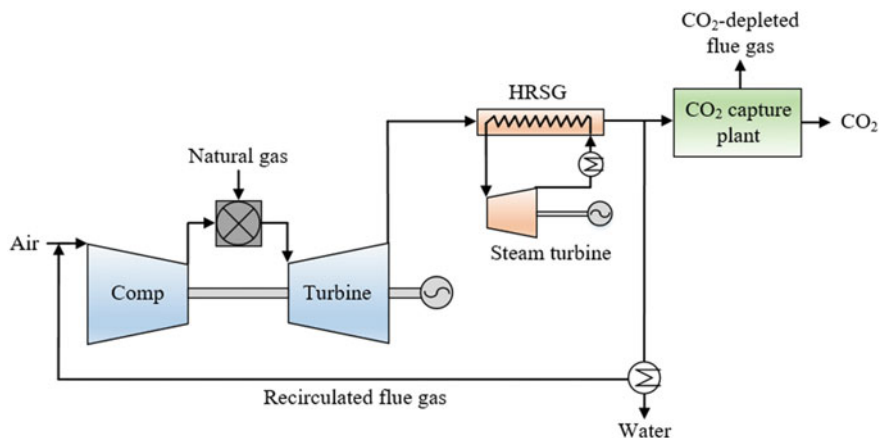


Fig. 4 Schematic of a gas turbine operating with exhaust gas recirculation

ratios employed are usually in the region of 35–40%, leading to up to 6.5 vol% CO₂ in the resulting flue gas [16]. At these values, the oxygen concentration at the inlet of the combustor is of ~ 16 –17 vol%, which ensures stable combustion and low emissions [84, 85] without the need for major combustor redesign [16, 73, 75, 84]. High overall electrical efficiency of the NGCC (above 50%) using EGR at those levels and with CO₂ capture (amine-based) has also been reported, reducing the energy penalty associated with the amine scrubbing system by 0.3–0.7 net percentage points with respect to an equivalent system without EGR [18, 75, 77]. Others though, such as Peeters et al. [83], Evulet et al. [80] and Li et al. [77], have reported higher optimal EGR ratios of up to 50%, suggesting this is where the electrical efficiency peaks. Whilst this is able to increase the CO₂ content of the flue gas further, up to ~ 8 vol% [76, 80, 84, 85], as indicated above, issues associated with depleted oxygen conditions in the combustor can start to arise, such as instabilities in combustion and in the flame, resulting in poor burnout [77]. This is due to the narrower flame stability limits when combusting in an air–CO₂ environment [84]. In extreme cases, where the EGR ratio is too high, this can even lead to lean blowout [81]. EGR ratios of 60% result in excess oxygen of just around 1 vol%, with the O₂ content of the oxidizer less than 10 vol% [16]. These combustion and flame instabilities, as well as the limited O₂ availability in the combustor at high EGR ratios, can increase pollutant formation, in particular CO and unburned hydrocarbons [76–78, 83, 85–87]. At low air–fuel ratios and altered oxidizer compositions, variations in heat transfer, reductions in temperatures and slower chemical kinetic reaction rates also result in more incomplete combustion [84, 85].

The techno-economics of such configurations has also been considered [18, 75]. As well as benefitting the efficiency, EGR is advantageous for the economics. A more compact design is possible for the absorber by the use of EGR because of the reduced gas flowrates with a higher CO₂ content, thus lowering the capital costs of the capture unit [18, 75]. Although carbon capture significantly increases the

overall costs of power generation, the integration of EGR can lower these compared to a standard gas turbine facility with CCS. Therefore, EGR can reduce the cost of electricity of an NGCC with an amine-based capture system from \$84.3/MWh (no EGR) to \$81.9/MWh (EGR), leading to a cost of CO₂ avoided ~9% lower than without EGR [75].

In addition to conventional EGR, more recent studies have started to look at selective EGR (S-EGR), where a fraction of the CO₂ from the flue gas is selectively recycled (not all the other species), which mitigates some of the drawbacks explored above [79, 88–91]. These configurations use a membrane (or another CO₂ separating device, such as a rotary wheel [90]), where the combustion air flows counter-currently with the flue gas (richer in CO₂ due to S-EGR). The CO₂ passes through the CO₂-selective membrane and enriches the oxidant before going to the compressor, with this CO₂ separation mainly driven by the difference in partial pressure between the permeate and retentate streams (without the need for energy consumption due to compression/vacuum) [88]. As a result, such studies consider higher levels of CO₂ in the inlet stream to the capture plant than EGR systems. Nevertheless, the final CO₂ concentration attained in the flue gas depends on the individual capture efficiencies of the capture plant and the selective membrane.

Series configurations, where all the flue gas is treated in the capture plant and subsequently in the CO₂ separator (as outlined in Fig. 5a), can result in CO₂ concentrations in the flue gas of up to 13–14 vol% if the capture plant and the selective membrane (or CO₂ separator) operate at ~30 and ~95% capture efficiency, respectively, to ensure an overall CO₂ capture efficiency of ~90% [88, 90]. However, higher CO₂ levels (well above 20 vol%) can be attained if the selective membrane is forced to work at increased CO₂ separation efficiencies [88, 92]. For parallel arrangements, where the flue gas is split into two streams that go to the CO₂ separator and CO₂ capture plant (shown in Fig. 5b), flue gas CO₂ levels in excess of 18 vol% have been reported if the capture plant and the CO₂ selective separator are able to operate at very high capture efficiencies between 96 and 98% [88, 90]. However, they diminish to around 8 vol% CO₂ if these individual capture efficiencies are of 95% [89]—with an overall capture efficiency of 90% in all cases.

As can be seen, parallel configurations require high capture efficiencies in both the CO₂ separator and the CO₂ capture plant to ensure overall capture rates remain high, whereas for the series design, capture efficiencies in the capture unit can be considerably lower, whilst still maintaining high overall levels of capture [88]. If these are balanced successfully, potential capital and operational cost savings (CAPEX and OPEX) in the capture unit can be achieved, due to (i) the higher CO₂ content in the flue gas and (ii) the greatly reduced size of the capture plant, due to the significantly lower volumetric flue gas flowrates [88–90]. However, the overall efficiency and cost benefits of a parallel S-EGR plant regarding the integrated gas-CCS system (not just the capture plant) are very sensitive to the auxiliary energy consumption and the costs associated with the selective membrane [89]. There also is potential here for process intensification and improvements in the overall cycle efficiency.

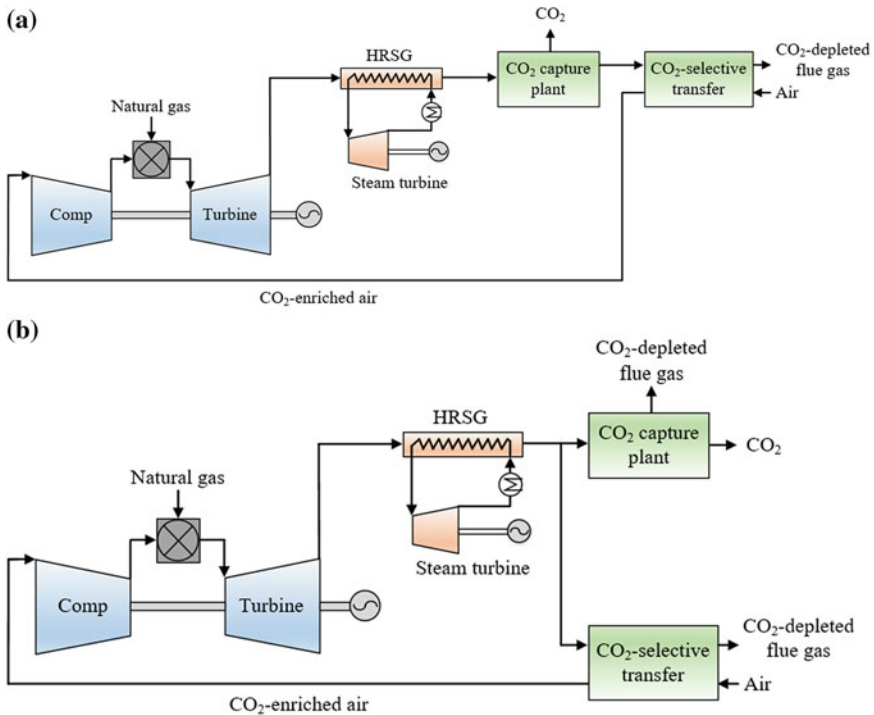


Fig. 5 Schematics of gas turbines operating with selective exhaust gas recirculation, showing (a) the series configuration and (b) the parallel configuration

Moreover, the use of S-EGR increases the CO₂ and reduces the O₂ content in the inlet oxidizer, which can have detrimental impacts on combustion performance and therefore emissions release. This is particularly true for unburned and incompletely combusted species, like CO and unburned hydrocarbons, as with EGR [79, 91]. These emissions are caused by flame instabilities and the reduction in flame temperatures. If the level of O₂ in the combustor becomes too low and the instabilities too great, blow-off and flame extinction can occur, which would necessitate changes to the operating regime—notably the air–fuel ratio to allow stable combustion [91]—and/or combustor redesigns to avoid those effects. Ensuring sufficient oxygen availability in the combustor is key for S-EGR, as with EGR above. However, with S-EGR, much more CO₂ can be recirculated without approaching stoichiometric conditions [88].

At present, preliminary economic analyses suggest that such configurations would still be more costly than a simple EGR system. Whilst the CO₂ capture system would cost less, other plant systems, namely the selective membrane set-up, would increase the total plant costs and therefore negatively impact on the cost of electricity according to a recent analysis of the parallel configuration [89]. The effect of the auxiliary consumption in S-EGR systems could also be substantial

[89]. Nevertheless, S-EGR configurations could show better competitiveness against conventional NGCCs coupled with amine capture plants only (without EGR or S-EGR) [88, 89, 92]. Additional cost reductions for membranes in the future though can help in this area and are likely to be due to material advancements. Improvements in CO₂ permeance, and to a lesser extent CO₂ selectivity, will reduce the costs of the selective membrane and also make the units much more compact and should thus be explored [88].

2.1.4 Comparison of Advanced Cycles

A brief comparison of the benefits and potential of the cycles discussed above is carried out in this section. According to the discussion in Sects. 2.1.1, 2.1.2 and 2.1.3, simple humidified cycles, without the complexities of the bottoming cycle, are seen to cost less than other system modifications; however, the least benefits are observed for these when coupled with CCS systems [16, 45]. This is because they offer lower levels of electrical efficiency than any of the other gas-fired power plant configurations with CO₂ capture (around 9 net percentage points lower than NGCCs using MEA scrubbing), and thus, these seem a less attractive option for gas-CCS applications [16]. NGCC power plants incorporating supplementary firing and amine scrubbing for CO₂ capture can achieve higher concentrations of CO₂ in the flue gas than EGR configurations, depending on the maximum combustion temperature allowed, but their electrical efficiency is lower [16]. The use of NGCCs with EGR and amine capture systems generally shows the greatest electrical efficiency when compared to supplementary firing, humidified gas-fired plants [16] and conventional NGCC schemes with amine scrubbing [18, 75]. The economics of the EGR option in NGCCs with an amine capture plant is also better compared to conventional NGCC+amine systems, in terms of CAPEX, cost of electricity and CO₂ avoided [18, 75]. However, careful design of the exhaust recycle control system is required to avoid affecting the turbine performance (back-pressure) [18]. Moreover, the impacts of EGR on turbomachinery when targeting moderate EGR ratios appear to be fairly manageable [16, 76]. Finally, S-EGR options have the potential to significantly increase the CO₂ content in the flue gas, and they could be competitive against conventional NGCC+MEA plants [88–90, 92]. The performance and economics of these systems are very sensitive to the assumptions considered though [89], and the effects of the CO₂-rich working fluid on the turbomachinery should be considered [92]. S-EGR systems are under study and further benefits against EGR are still under discussion [89, 90].

2.2 *Oxy-Turbine Cycles*

Oxy-combustion gas turbines burn the fuel using an oxygen-rich flow instead of air in the combustion chamber, thus leading to a flue gas that contains nearly pure CO₂

after H₂O condensation (see Sect. 1.1). The oxygen used as oxidizer is usually supplied by an air separation unit (ASU), which delivers a high-purity O₂ stream after separation from air. Combustion in oxy-fired systems takes place at close to stoichiometric conditions to minimize the costs and energy penalty associated with the ASU, as well as the requirements for subsequent purification of the CO₂-rich stream prior to storage or use (EOR). Under these conditions, extremely high temperatures can be achieved in the combustor, and therefore, these systems usually employ recycled CO₂ or water in order to control combustion temperatures. As a result, oxy-fired gas turbine cycles are often classified as CO₂- or water-based cycles. These differ depending on the main component in the working fluid, i.e. CO₂ (semi-closed oxy-combustion combined cycle (SCOC-CC), MATIANT cycle and NET Power/Allam cycle) or H₂O (CES and Graz cycles) [93, 94]. In addition to these configurations (which make use of an ASU), alternative cycles have been proposed incorporating O₂ separation from air by means of high-temperature membranes (AZEP and ZEITMOP cycles). Chemical looping combustion of gaseous fuels has also been proposed, where oxygen from air is transferred to oxidize the fuel using an oxygen carrier. However, substantial development of these systems is required to achieve efficiencies competitive with NGCCs, requiring the use of pressurized fluidized beds and high temperatures [5, 95, 96].

A summary of the main oxy-cycles investigated so far is shown in Table 1, which has been recently published by the International Energy Agency [93]. This presents the cycle efficiency (used as a performance indicator), together with the degree of development of key components for each cycle, which allows the classification of the systems on the basis of their current potential [93].

As can be seen in Table 1, the most promising cycles are the semi-closed oxy-combustion combined cycle, the NET Power/Allam cycle, as well as the Graz and CES water-based cycles [93, 94]. Therefore, these will be described in Sects. 2.2.1, 2.1.2, 2.1.3 and 2.2.4.

Table 1 Summary of the main oxy-fired gas turbine cycles (adapted from [93])

Cycle	Efficiency (%)	Efficiency score	Development index penalty	Total cycle score
SCOC-CC	45–49 ^a	7	1	6
MATIANT	40–49	7	4	3
E-MATIANT	46–47	7	2	5
NET Power/Allam cycle	55–59	10	4	6
CES	45–50	8	2	6
Graz	49–54	9	2	7
AZEP	49–53	9	6	3
ZEITMOP	46–51	8	9	–1

^aMaximum value according to [94]

2.2.1 Semi-closed Oxy-Combustion Combined Cycle

The semi-closed oxy-combustion combined cycle is represented in Fig. 6. In this system, a recycle stream that contains mainly CO₂ is compressed and sent to the combustion chamber, where natural gas is combusted using oxygen from an ASU. The resulting flue gas at elevated temperature and pressure is expanded in the gas turbine to generate electricity. The hot gases leaving the turbine are subsequently fed to the HRSG, thus recovering heat in a steam cycle to generate additional electricity. Water is then knocked out from the flue gas stream that exits the HRSG—composed of CO₂ and H₂O mainly—after cooling, leading to a highly CO₂-concentrated flow. Most of this stream will be recycled back to the compressor to initiate a new cycle, whereas the remaining fraction is taken to the compression and purification unit before finally being stored or used (i.e. EOR) [15, 73, 93, 94].

The configuration of the SCOC-CC cycle of Fig. 6 is similar to that of air-combustion NGCCs, but using a CO₂-rich stream as the working fluid in the gas turbine. No major design changes are expected in the HRSG with respect to conventional combined cycles, whereas the gas turbine section (compressor, combustor and turbine) requires some modifications to accommodate the new characteristics of the working fluid [93, 94]. This is the case of the lower specific heat ratio of CO₂ compared to air, which requires SCOC-CC systems to operate with higher pressure ratios of around 30–40 (for a turbine inlet temperature of 1300–1400 °C) to achieve optimum cycle efficiencies in the range of 45–49%, as shown in Table 1 [93, 94]. Considerations related to cooling of the turbine blades and the optimum temperature of the recycled CO₂-rich stream are also important when designing SCOC-CC systems [93, 94].

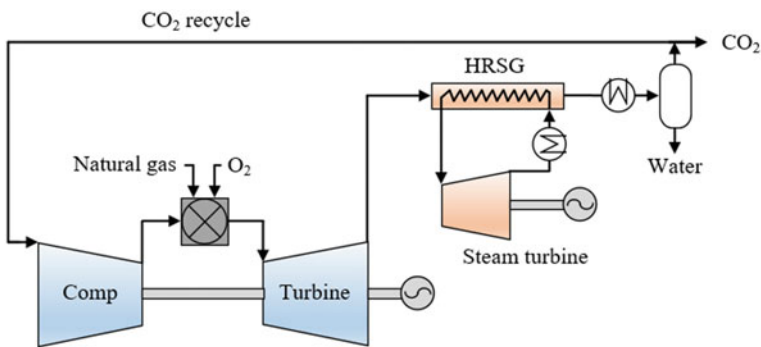


Fig. 6 Schematic representation of the semi-closed oxy-combustion combined cycle

2.2.2 NET Power/Allam Cycle

The NET power cycle, also named the Allam cycle, is represented in Fig. 7. It characterizes by using supercritical CO_2 as the working fluid in a semi-closed, recuperated Brayton cycle that employs a single gas turbine operating at high pressure (inlet pressure ~ 300 bar) and low pressure ratio (~ 10) [97, 98]. The turbine is driven by the CO_2 -rich flue gas generated in the high-pressure combustor, where natural gas is burnt under oxy-firing conditions at close to $1100\text{--}1200$ °C [98]. After expanding in the turbine, the flue gas enters an economizer heat exchanger where heat is recovered and transferred to the recycled high-pressure CO_2 stream before it enters the combustor. The low-temperature flue gas that exits the economizer is further cooled to near ambient conditions, and water is separated and taken out of the cycle. The resulting CO_2 -rich stream is then initially compressed in an intercooled compressor, followed by subsequent cooling and pumping steps (up to ~ 300 bar). A fraction of this flow exits the system (at ~ 100 bar) [97]. The remaining CO_2 is heated in the economizer up to $700\text{--}750$ °C prior to entering the combustor.

The main benefit of the Allam cycle is the very high efficiencies that can be achieved, which are between 55 and 59% (see Table 1) with nearly zero CO_2 emissions. Additional advantages include compact designs and reduced footprint, as well as predicted competitive costs with respect to other capture options [97, 98]. There are, however, a number of challenges related to the operating conditions in the cycle. This is the case of the turbine design, which has characteristics of both steam and gas turbines due to its high pressure and temperature of operation. The combustor also requires a novel design due to the high pressures and the working

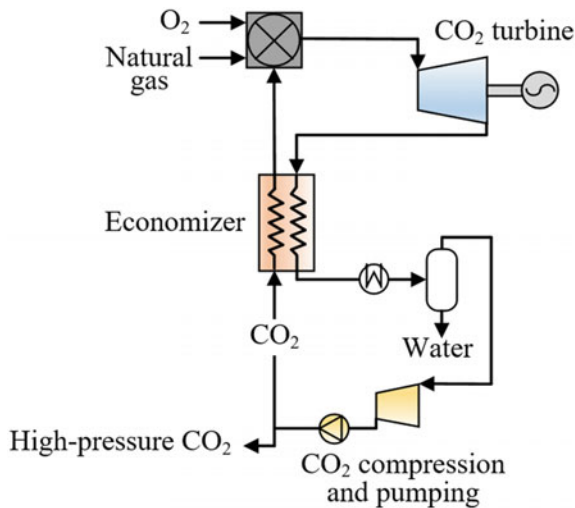


Fig. 7 Representation of the Allam cycle

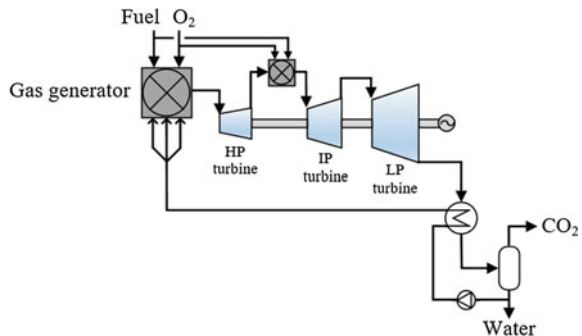
fluid employed, and it has been recently tested at reduced scale during a limited time of operation [99]. Moreover, the economizer heat exchanger is a key part of the cycle that requires development and careful design, as it needs to cope with large flows of CO₂ and substantially different pressures and temperatures [93, 94, 97, 98]. Nevertheless, rapid progress is being made in all these areas [97], and a 50 MW_{th} demonstration plant is being built in La Porte, Texas, to continue these investigations. This plant will test the performance of the key components mentioned above and the process itself, thus allowing valuable operational experience to be gained and providing essential information for the development of the technology [97].

2.2.3 CES Cycle

The CES cycle uses steam as the main working fluid, as depicted in Fig. 8 following the configuration presented by Anderson et al. [100]. In this scheme, natural gas is combusted using oxygen from an ASU in the gas generator, which operates at 50–100 bar. Liquid water is injected and evaporated in the combustor to control temperature, leading to a flue gas with around 90% steam content. This flue gas is expanded in a high-pressure turbine that operates with a pressure ratio of ~5, and it is further reheated in a second oxy-fired gas combustor. The temperatures considered for the reheating stage are between 760 and 1760 °C, depending on the development stage of the subsequent intermediate-pressure turbine (first, second and third generation turbines have been anticipated) [101]. After final expansion in a low-pressure turbine, the flue gas is sent to a vacuum condenser. A CO₂-rich stream is then recovered for storage/use (i.e. EOR) purposes, and water is pumped, preheated (using heat from the flue gas that leaves the low-pressure turbine) and sent back to the gas generator.

The efficiency of the CES cycle is highly dependent on the temperature at the inlet of the intermediate-pressure turbine, with values close to 50% for the more advanced designs [93, 94]. Therefore, a major technical challenge is the design of the intermediate-pressure turbine capable of working under very high inlet

Fig. 8 Representation of the CES cycle



temperatures with a steam-rich flow [102]. Less challenging is the design of the high- and low-pressure turbines due to the much more limited temperatures of operation [93, 94, 101, 102]. Tests have been performed at the 20 and 200 MW_{th} scale to reduce the uncertainties associated with the gas generator equipment [103].

2.2.4 Graz Cycle

The S-Graz cycle, a high-efficiency modification of the Graz cycle that uses a steam-rich working fluid, is represented in Fig. 9. In this system, natural gas is burnt at ~ 40 bar in an oxy-fired combustor that uses two streams with high steam concentrations to moderate temperature [104, 105]. The flue gas leaving the combustor is expanded in a high-temperature turbine to atmospheric pressure and passed through a HRSG. A fraction of the cooled gas is expanded in a low-pressure turbine to vacuum conditions and sent to a condenser, where CO₂ is separated from steam and is then further compressed and subsequently stored. The condensed water is then pumped and taken to the HRSG, thus recovering heat from the flue gas exiting the high-temperature turbine and generating steam at high pressure and temperature (~ 180 bar and 550 °C) [93]. This stream is then expanded in a high-pressure turbine to ~ 40 bar and enters the combustor to control temperature (a fraction is also used to cool the high-temperature turbine). The remaining fraction of the flue gas exiting the HRSG is also used to limit temperatures in the combustor after passing through an intercooled compressor [104, 105]. This configuration has been further improved in the modified S-Graz cycle, where condensation takes place at higher pressure [104].

The Graz cycle can achieve efficiencies up to 54% (see Table 1), using a combustor that operates at 40–50 bar and 1400–1500 °C [93, 94, 105, 106]. The main limitation of this cycle is the need for a new design suitable for the high-temperature turbine, capable of withstanding corrosion and operating at very high temperatures similar to steam turbines and moderate pressures close to gas turbines [93, 94].

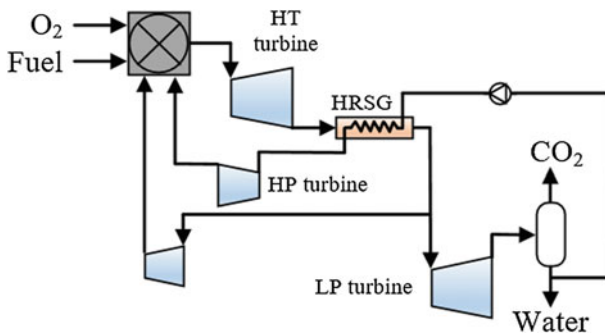


Fig. 9 Representation of the S-Graz cycle

3 Scaling-up: Deployment at a Commercial Scale and the Challenges of Decarbonization

The challenges of decarbonization via gas-CCS at a commercial level are not just technical and policy based but also financial—which are all interconnected and heavily dependent on each other. As the technologies develop, are scaled up and become more commercially viable, the economic aspects should also become more favourable, and therefore, extensive policy support will be required to bring them from the brink of commercialization to actual full-scale deployment. All these aspects need to be addressed in order to derisk the market and allow gas-CCS to be deployed, whether these are integrated into new builds or retrofitted into existing infrastructure. Much of the policy and financial aspects considered herein apply to the CCS industry as a whole and are not necessarily specific issues to deploying just gas-based power with carbon capture. These various barriers are therefore examined in the wider context of CCS, as well as for gas-CCS specifically.

One of the key challenges that covers all of these aspects—technical, political and financial—is the potentially disruptive nature of CCS technologies to the power and industry sectors [107]. To implement carbon capture is not an easy task, neither for new-built plant nor considering retrofits. Developing these to higher levels of technology maturity and commercial readiness and producing the supporting regulatory and policy frameworks to surround this will go a long way to convincing companies that not only is the technology sound, but is also vital.

3.1 Technical Aspects

Technology developments are needed to ensure that the optimized options and configurations of gas-CCS plants are ready to be utilized reliably at the large-scale, centralized facilities. Furthermore, knowledge transfer from demonstration projects and their vast operational experience will go a long way to contribute to the commercial-scale deployment of these technologies. The technical challenges for different NGCC options have been highlighted throughout the previous sections. Advances in the key areas will alleviate some of the issues currently seen with demonstrating these technologies and scaling them up for deployment at a commercial scale. This includes material advancements and developments for many configurations, including humidification, EGR and S-EGR, as well as the selective membranes that are often used with the latter. Comparative studies of the different options considered in Sect. 2.1 have shown that whilst all these pursue improvements in the overall electrical efficiency of the power plant with CCS, not all of these options would necessarily be suitable for up-scaling—although the reasons for these are not always technical. NGCC systems incorporating humidification and CCS, for example, have been shown not to be competitive against other options in terms of electrical efficiency (see Sect. 2.1). However, they may be better suited to

other applications at a smaller scale where NGCCs are not an option [51, 53, 108], providing a CCS hub and cluster approach is followed. This leaves the other configurations—EGR/S-EGR and supplementary firing—to be considered for implementation in full-scale commercial plants with CCS. In fact, supplementary firing is already used at such scales, and thus, other considerations are needed to evaluate in detail its compatibility with CCS, related to the reduction in process efficiency, as discussed in Sect. 2.1.1. The limited data availability, however, for some of these options, especially S-EGR for enhanced carbon capture, at both pilot or larger scales, means that at present it is difficult to consider which may be preferable in terms of scaling-up and developing to a commercial level of deployment. Consequently, these require much research into all aspects of the technology to advance their progress from pilot-scale testing through to full-scale demonstrations.

Moreover, the progress in the development and understanding of the different capture technologies itself is a key. The technology readiness levels of these vary widely, from those more mature (e.g. post-combustion amine scrubbing) to others that only exist as a concept or at very small scales. It is important to continue the optimization of the more mature technologies, but equally essential is the development of second and third generation technologies. This could potentially improve the energy penalties, costs and environmental aspects of the mature systems, and find different application niches. Nevertheless, up-scaling any technology is fairly challenging and scaling factors are vast. Scaling-up from laboratory to pilot scale often involves factors of 10 or more, and when pilot to full, commercial-scale systems are considered, these factors can be in the order of thousands to tens of thousands [109]. Whilst the risks are high when it comes to dramatically increasing the size of the technology process, these up-scaling risks can be notably reduced through comprehensive process designing and extensive modelling, which all need to be reinforced by in-depth laboratory and pilot-scale experiments, in particular for the most key controlling parameters. This is true for both the operation of individual system components and the complete integrated plant [109]. Moreover, optimization and process intensification will need to be tailored specifically for individual deployments, with a view for flexible operation.

3.2 Policy Challenges

Technical developments in this area are required to inform policy and regulation on natural gas utilization and CCS applications in the future, especially where these are integrated into gas-CCS systems. Strong policy drivers and regulatory framework development are much needed to create a favourable CCS market and facilitate its deployment in all forms, across power and industry, not just with natural gas [110]. There appears to be a ‘chicken and egg’ situation in this regard though—with full-chain demonstration projects at scale being required to gain policy acceptance for CCS [111], whilst full policy support being needed to diminish the risks and get

to large-scale projects in the first place. Which will come first? There is need for risk minimization, and thus, policies where governments can underpin investment will be of great benefit to getting ‘first of a kind’ projects of the ground. Whilst this is already happening for coal, mainly on the North American continent (such as at Petra Nova [112] and Boundary Dam [11], considered in Sect. 1.2), there has been considerably less interest in natural gas. Often the technologies cannot be used directly, and other sectors and disciplines further afield may have to be looked to, in order to gain the knowledge and experience required to develop the relevant integrated system infrastructure. In the UK, for example, the ‘buy, not build’ mentality means that it is not developing its own technologies specifically for the UK market, as the requisite policy framework is currently still not in place. Furthermore, it is a necessity for the relevant policies to be stable and developed over time with the technologies as their deployment progresses—only this can build the long-term confidence required for this industry. An established and secure policy environment, among other factors, is essential to ensure the future of the emerging CCS sector.

Other gas emissions than CO₂ have been successfully minimized due to extensive legislation being passed to limit their release. Technologies were developed and then deployed on all qualifying plants to ensure environmental safeguarding and regulatory bodies were formed to monitor this. As more technology was developed and deployed, the costs were reduced (learning curve)—many similar stories can be found for technologies in all industry sectors. Dealing with CO₂ emissions, however, is especially challenging and costly (not only at a capture level, but also for the transportation and storage stages). Therefore, the progress from feasibility studies and laboratory-/pilot-scale demonstrations of the basic principles for proof of concept to full-scale, full-chain commercial CCS operation is taking a significant period of time—highlighting the complexities of the technologies and the surrounding issues.

Industries are needed, and expected, to take the knowledge and technical developments to the next stage, by providing business-level and business-led development. However, if the necessary incentives, directives and regulations are not in place, this will be increasingly difficult to achieve. The inconsistent and conflicting messages coming from government in this respect, with regard to the policy disconnect, are making this increasingly difficult. This is most notably in the UK with the cancellation of yet another CCS demonstration competition [113]. It is not just the *policy*, but also the *politics* that play a role here—recognizing that climate change mitigation is vital and that CCS options can have an important contribution is one thing, but actually developing the political willingness to invest and form pertinent policy support and specific regulations is another, and not yet forthcoming [114]. The UK, however, is not the only country to abandon or postpone projects, with many examples across the rest of Europe and North America particularly, where once-promising projects have been cancelled or remain dormant [115]. In Europe, an effective policy structure to encourage the commercialization of CCS still remains elusive after years of stagnation in the industry [116]. CO₂ emissions do not have borders, and therefore, the policy framework

cannot either—connectivity here between the national and international is imperative.

Policy instruments need to be clear in their aims and objectives, and be broad enough to comprehensively regulate all aspects of CCS. This will need to look at not only the technologies and financial aspects, but also strategic procedures for permitting, liability and monitoring activities by the relevant competent authority [110]. The temporal issues with consistently postponing the decision-making on CCS—or ‘kicking the can down the road’ as Karimi [117] terms it—are just delaying the inevitable, whatever that might be.

A greater awareness and general public support should also be gained through continued dissemination, and therefore, also hopefully public (and private!) investment and acceptance could be attained [114]. CCS remains largely unknown in the public domain, and consequently, effective communication, engagement and outreach are essential to demonstrate to the general population that CCS is a needed and safe technology—especially in geographical areas that may be directly impacted by its implementation and where extensive phased consultations will likely be compulsory [111, 118].

Even though public acceptability is something that may not be considered as an essential requirement for CCS advancement and deployment, corporate perception is something that cannot be ignored. Braunreiter and Bennett [107] and Karimi [117] report that there is a lack of interest among key stakeholders as fossil fuel companies have not shown a great deal of interest in CCS. They are the most likely ‘consumers’ of the technology though, and as something that will inform and thus directly influence their decision-making on CCS investment, their views need to be taken into account. Business models and strategies in this area will need to be developed with input from the relevant policy-making bodies. Kapetaki and Scowcroft [119] assessed the risks and enablers for CCS demonstration project business models. Whilst the financial implications are by far the most dominant factor, a range of other aspects play a key role and are often impacted by the overall economics. They suggest that the efficiency of permitting processes, protracted stakeholder engagement and clarity of regulatory frameworks, considered in detail further along in this section, are all needed to deliver a successful project [119]. Worldwide government engagement with academia and industry for knowledge sharing is hence vital. And this appears to be one of the best ways to engage, along with taking advantage of previous ‘lessons learned’ from other projects, nationally and internationally [120].

3.3 Financial Issues

The financial implications of integrating CCS into natural gas power plants and also the wider context can only lessen over time if the above issues are addressed. The technical challenges need to be overcome (and are currently being extensively researched), and policy is certainly required for it to become more favourable for

investment to enable the widespread deployment of such technologies. However, it would seem that costs (or perceived costs) are the primary driver of both development and deployment, and therefore, to get this fledging industry off the ground, funding and other incentives (both financial and non-financial) may be needed [116]. Coordination is required between different financing schemes, particularly those operating on different regional, national and international levels—greater connectivity and complementarity are essential to incentivize interest and thus investment [110]. It is to be expected that subsidies will be needed for many if not all of the early CCS plants [121].

Further to this, the deployment of post-combustion CCS and other capture systems is required to demonstrate the technologies, and this will also lead to notably reductions in overall costs, as the majority of the derisking processes will have already been undertaken for an ‘*n*th of a kind’ plant. Cost reductions here arise through analysing the real-world experience of planning and building an actual project and then using it to identify the potential improvements and key cost saving opportunities [111]. Economies of scale will also be imperative to minimize implementation costs over time, especially when it comes to geological storage of CO₂.

Temporal aspects of both projects and policies have a part in defining the way forward [117]. Though renewables (including wind, geothermal, solar, biomass and waste) are experiencing continued rapid growth rates [122], the delays, postponements and cancellations in developing and deploying CCS mean that there is a much reduced prospect of achieving our 2050 greenhouse gas emissions reductions.

In the UK, reports such as that of the Parliamentary Advisory Group on CCS [113] have stated that although the use of carbon capture technologies is vital to ensure the lowest cost of decarbonization, a system of economic regulation is still needed. This means that in addition to the regulatory framework considered above, an economic framework is also required to aid deployment. These need to be in place as soon as possible to enable CCS technologies to be used in the near future. Most decarbonization scenarios for the UK do not have unabated gas power still on the grid in the future (by 2050), and thus, any new builds will need to have CCS integrated at this stage, or at least be capture-ready when they are built [113]. Without this, they are susceptible to becoming stranded assets with a limited life, especially if/when carbon pricing comes into force and emission limits are more severe. Moreover here, investment in new gas power is inherently risky at this point with the deficiencies in current CCS and climate policy [113]. This is making it increasingly difficult to form and maintain a dedicated CCS industry. The cost of the overall system is as much dependent on the gas price as it is for the CCS technology [123]. Carbon pricing will also have significant impacts of all aspects of CCS deployment, and this CO₂ tax could be used to incentivize investment on the technologies [110], especially for natural gas with its lower inherent carbon intensity than coal.

3.4 *Additional Considerations*

In the broader context, gas-CCS should more likely be deployed where domestic natural gas resources are used. This protects investments, allowing the continued use of the resources to generate power whilst still addressing the energy trilemma issues [114]. However, it is the Middle East, Europe and Eurasia which account for almost 75% of proven reserves [122], and although there are some gas-CCS projects in these areas, they are not yet at the scale they are required to be [115]. Demands for natural gas in the global primary energy consumption remain high and are increasing, whilst the use of oil and coal is declining and is predicted to continue to do so [122]. Overall, it can be seen that many of the technical, political and financial issues of implementing carbon capture are not just specific to gas. Developing a transport and storage infrastructure that is fully integrated with all sources of CO₂ will invariably do much to enable the deployment of CCS technologies with natural gas, as it will for coal and industrial CO₂ capture. Moreover, derisking investments, specifically the areas that others do not want to, needs to be considered strategically by governments to ensure their climate targets are met.

Billson and Pourkashanian [116] outline the three main issues that have arisen in Europe in particular and have resulted in the current situation for CCS deployment in general. This essentially summarizes much of the previous discussion. These are: (i) poor engagement and communication of the key message to the relevant stakeholders; (ii) a market that compels industry to depend on government funding and subsidies, which results in considerable vulnerabilities to political forces, as seen with the UK commercialization programme; and (iii) governments not willing to help in financing the initial CCS projects, which does nothing to bolster industrial support [116].

It is only by addressing all of the various challenges—the technological, policy and financial issues considered above—that we can get to a point where the deployment of these technologies on a large scale is both feasible and favourable. Focusing on just one of these will not be sufficient. Whilst many aspects of these systems have been demonstrated, often at scale, integrating these different components to form a full-chain gas-CCS system will be the only way to start to derisk investment. Combining carbon capture with fossil fuel-based energy can realize a number of benefits in decarbonizing the power sector, which will clearly be needed to meet the climate change targets for emissions limits. Much research is still evidently required here though to make this a reality and for gas-CCS to ‘catch-up’ with the developments in capture from coal.

4 Conclusions

With global energy demand increasing and the power sector needing to be rapidly decarbonized, disruptive technologies, such as carbon capture, will be required. This can enable energy to be produced within the confines of the energy trilemma—of being sustainable, secure and affordable. This is the case of power generation using natural gas as a fuel, which although significantly less carbon intense than coal still necessitates profound emission cuts. Considerable efforts have been seen for coal-CCS, and substantial knowledge and experience have been and are still being gained in this sector. Nevertheless, these CCS technologies will need to be adapted and optimized to be used with gas-fired plants.

Post-combustion systems for CO₂ capture are at present the most developed and advanced, with several operational plants online. However, separating the CO₂ from the flue gas of a NGCC is difficult and costly without further adaptations. High excess air ratios used in gas-fired systems result in large flows of flue gas with low CO₂ and high O₂ levels that can negatively affect downstream capture performance. A range of options have been proposed to enhance the CO₂ content generated by gas-fired systems to ensure high capture efficiencies are achieved with potentially reduced energy penalties and cost—supplementary firing, humidified turbine cycles, EGR and S-EGR have been discussed in this chapter.

Promising oxy-combustion gas turbine systems are also being researched, still requiring significant developments. These include SCOC-CC, NET Power/Allam, CES and Graz cycles, amongst others. It is the NET Power/Allam cycle which at present results in the highest achievable efficiencies, using supercritical CO₂ as the working fluid. Although the compact designs and reduced plant footprint are favourable, the challenges related to the extreme operating conditions need addressing and further technology development is required—ongoing at present.

Particularly important for gas-fired power plants is the need to be flexible in order to balance a grid with increasing proportions of intermittent renewables. Therefore, any gas-CCS option will also need to be flexible by definition. At a more general level, the technical barriers to the large-scale implementation of CCS require knowledge transfer between the existing infrastructure to enable the scale-up, demonstration and commercial roll-out of these options. The lessons learned from these are needed to support and be supported by the regulatory framework to deliver the strong policy drivers and the consequent favourable CCS market that are required by industry. Risk minimization through the underpinning of investments will certainly be essential to getting ‘first of a kind’ projects of the ground. Greater engagement with key industry stakeholders, and to a lesser extent, also the public, will also go a long way to facilitating the wider-scale utilization of CCS on a scale to help in mitigating climate change. However, to achieve this, conflicting and inconsistent government messages need to be prevented, to allow projects to develop, rather than be abandoned, postponed or cancelled altogether. The financial challenges can only lessen over time if the technology and policy issues are overcome. Investment needs to be incentivized, but this must be

coordinated on regional, national and international levels. Other factors, as well as the technology and commercial readiness levels, effect the costs; these are also impacted by economies of scale, carbon pricing/tax, ‘1st of a kind’ versus ‘*n*th of a kind’ plants and a system of economic regulation, which is invariably is still needed. This is a prerequisite for a dedicated CCS industry to mature and become sustainable.

References

1. BP (2017). BP Energy Outlook
2. IEA (2016) World energy outlook 2016
3. United Nations Framework Convention on Climate Change (2017) The Paris Agreement. Retrieved September 2017, Available from: http://unfccc.int/paris_agreement/items/9485.php
4. IEA (2013) Technology roadmap. Carbon capture and storage
5. Abanades JC, Arias B, Lyngfelt A, Mattisson T, Wiley DE, Li H, Ho MT, Mangano E, Brandani S (2015) Emerging CO₂ capture systems. *Int J Greenhouse Gas Control* 40: 126–166
6. Jansen D, Gazzani M, Manzolini G, Ev Dijk, Carbo M (2015) Pre-combustion CO₂ capture. *Int J Greenhouse Gas Control* 40:167–187
7. IPCC (2005) IPCC Special report on carbon dioxide capture and storage. In: Prepared by working group III of the intergovernmental panel on climate change, Cambridge University Press, Cambridge
8. ZEP (2011) The costs of CO₂ capture: post-demonstration CCS in the EU
9. Global CCS Institute. (2017) Large Scale CCS Projects. Retrieved September 2017, Available from: <https://www.globalccsinstitute.com/projects/large-scale-ccs-projects>
10. Ringrose PS, Mathieson AS, Wright IW, Selama F, Hansen O, Bissell R, Saoula N, Midgley J (2013) The In Salah CO₂ storage project: lessons learned and knowledge transfer. *Energy Procedia* 37:6226–6236
11. SaskPower (2017) SaskPower CCS: Boundary Dam Carbon Capture Project. Available from: saskpower.com/our-power-future/carbon-capture-and-storage/boundary-dam-carbon-capture-project/
12. Stéphanne K (2014) Start-up of world’s first commercial post-combustion coal fired CCS project: contribution of Shell Cansolv to SaskPower Boundary Dam ICCS Project. *Energy Procedia* 63:6106–6110
13. Worth K, White D, Chalaturnyk R, Sorensen J, Hawkes C, Rostron B, Johnson J, Young A (2014) Aquistore project measurement, monitoring, and verification: from concept to CO₂ injection. *Energy Procedia* 63:3202–3208
14. NRG (2017) NRG Energy, JX nippon complete world’s largest post-combustion carbon capture facility on-budget and on-schedule. Retrieved September 2017, Available from: <http://investors.nrg.com/phoenix.zhtml?c=121544&p=irol-newsArticle&ID=2236424>
15. Diego ME, Akram M, Bellas J-M, Finney KN, Pourkashanian M (2017) Making gas-CCS a commercial reality: the challenges of scaling up. *Greenhouse Gases: Sci Technol* 7:778–801
16. Li H, Ditaranto M, Berstad D (2011) Technologies for increasing CO₂ concentration in exhaust gas from natural gas-fired power production with post-combustion, amine-based CO₂ capture. *Energy* 36:1124–1133
17. Gouedard C, Picq D, Launay F, Carrette PL (2012) Amine degradation in CO₂ capture. I. A review. *Int J Greenhouse Gas Control* 10:244–270
18. IEAGHG (2012) CO₂ capture at gas fired power plants. Cheltenham, UK

19. Kehlhofer R (1991) Combined-Cycle gas & steam turbine power plants. Pennwell Books, Lilburn, GA
20. Arrieta FRP, Lora EES (2005) Influence of ambient temperature on combined-cycle power-plant performance. *Appl Energy* 80:261–272
21. Bhattacharya A, Datta A (2013) Effects of supplementary biomass firing on the performance of combined cycle power generation: a comparison between NGCC and IGCC plants. *Biomass Bioenergy* 54:239–249
22. Biliyok C, Yeung H (2013) Evaluation of natural gas combined cycle power plant for post-combustion CO₂ capture integration. *Int J Greenhouse Gas Control* 19:396–405
23. Datta A, Mondal S, Gupta SD (2008) Perspectives for the direct firing of biomass as a supplementary fuel in combined cycle power plants. *Int J Energy Res* 32:1241–1257
24. González Díaz A, Sánchez Fernández E, Gibbins J, Lucquiaud M (2016) Sequential supplementary firing in natural gas combined cycle with carbon capture: a technology option for Mexico for low-carbon electricity generation and CO₂ enhanced oil recovery. *Int J Greenhouse Gas Control* 51:330–345
25. Li H, Ditaranto M, Yan J (2012) Carbon capture with low energy penalty: supplementary fired natural gas combined cycles. *Appl Energy* 97:164–169
26. Ansaldo Energia (2014) Open and combined cycles
27. Biliyok C, Canepa R, Hanak DP (2015) Investigation of alternative strategies for integrating post-combustion CO₂ capture to a natural gas combined cycle power plant. *Energy Fuels* 29:4624–4633
28. Ganapathy V (1996) Heat-recovery steam generators: understand the basics. *Chem Eng Progress* 92:32
29. González-Díaz A, Alcaráz-Calderón AM, González-Díaz MO, Méndez-Aranda Á, Lucquiaud M, González-Santaló JM (2017) Effect of the ambient conditions on gas turbine combined cycle power plants with post-combustion CO₂ capture. *Energy* 134:221–233
30. Zhang W, Magee J, Singh H, Ruchti C, Selby G (2012) HRSG development for the future. PowerGen Europe, Cologne
31. Carapellucci R, Milazzo A (2007) Repowering combined cycle power plants by a modified STIG configuration. *Energy Convers Manag* 48:1590–1600
32. De Paepe W, Delattin F, Bram S, De Ruyck J (2012) Steam injection experiments in a microturbine—A thermodynamic performance analysis. *Appl Energy* 97:569–576
33. De Paepe W, Delattin F, Bram S, De Ruyck J (2013) Water injection in a micro gas turbine—Assessment of the performance using a black box method. *Appl Energy* 112:1291–1302
34. Delattin F, Bram S, Knoops S, De Ruyck J (2008) Effects of steam injection on microturbine efficiency and performance. *Energy* 33:241–247
35. Gallo WLR (1997) A comparison between the hat cycle and other gas-turbine based cycles: Efficiency, specific power and water consumption. *Energy Convers Manag* 38:1595–1604
36. Lee JJ, Jeon MS, Kim TS (2010) The influence of water and steam injection on the performance of a recuperated cycle microturbine for combined heat and power application. *Appl Energy* 87:1307–1316
37. Poullikkas A (2005) An overview of current and future sustainable gas turbine technologies. *Renew Sustain Energy Rev* 9:409–443
38. Traverso A, Massardo AF (2002) Thermo-economic analysis of mixed gas-steam cycles. *Appl Therm Eng* 22:1–21
39. Wang FJ, Chiou JS (2002) Performance improvement for a simple cycle gas turbine GENSET—A retrofitting example. *Appl Therm Eng* 22:1105–1115
40. Jonsson M, Yan J (2005) Humidified gas turbines—A review of proposed and implemented cycles. *Energy* 30:1013–1078
41. Kayadelen HK, Ust Y (2017) Thermodynamic, environmental and economic performance optimization of simple, regenerative, STIG and RSTIG gas turbine cycles. *Energy* 121: 751–771

42. Takahashi T, Koda E, Mimaki T (2002) A systematic analysis of the effect of air humidification to gas turbine systems. *Jpn Soc Mech Eng Int Journal—Ser B* 45:530–535
43. Yari M, Sarabchi K (2005) Modelling and optimization of part-flow evaporative gas turbine cycles. *Proc Inst Mech Eng, Part A: J Power Energy* 219:533–548
44. Gabriëlsson R, Toriïsson T (2003) Research and development for turbo machinery-based electric generation in a sustainable energy system. Lund (Sweden)
45. Rao AD, Day WH (1996) Mitigation of greenhouse gases from gas turbine power plants. *Energy Convers Manag* 37:909–914
46. Akram M, Ali U, Best T, Blakey S, Finney KN, Pourkashanian M (2016) Performance evaluation of PACT pilot-plant for CO₂ capture from gas turbines with exhaust gas recycle. *Int J Greenhouse Gas Control* 47:137–150
47. Cohen H, Rogers GFC, Saravanamuttoo HIH (1996) *Gas turbine theory*. Longman Group Limited, Harlow, England
48. Wei C, Zang S (2013) Experimental investigation on the off-design performance of a small-sized humid air turbine cycle. *Appl Therm Eng* 51:166–176
49. Heppenstall T (1998) Advanced turbine cycles for power generation: a critical review. *Appl Therm Eng* 18:837–846
50. Abdallah H, Harvey S (2001) Thermodynamic analysis of chemically recuperated gas turbines. *Int J Therm Sci* 40:372–384
51. Chiesa P (2012) Chapter 5: Novel cycles: humid air cycle systems combined cycle systems for near-zero emission power generation. Woodhead Publishing (Elsevier), Cambridge
52. Horlock JH (2003) *Advanced gas turbine cycles*. Elsevier Science Ltd, Oxford, UK
53. Rao A (2015) *Evaporative Gas Turbine (EvGT)/Humid Air Turbine (HAT) Cycles*. Handbook of Clean Energy Systems, Wiley, Hoboken
54. Montero Carrero M, De Paepe W, Bram S, Parente A, Contino F (2017a). Does humidification improve the micro Gas Turbine cycle? Thermodynamic assessment based on Sankey and Grassmann diagrams. *Appl Energy* <https://doi.org/10.1016/j.apenergy.2017.05.067>
55. Montero Carrero M, De Paepe W, Magnusson J, Parente A, Bram S, Contino F (2017) Experimental characterisation of a micro Humid Air Turbine: Assessment of the thermodynamic performance. *Appl Therm Eng* 118:796–806
56. Li H, Flores S, Hu Y, Yan J (2009) Simulation and optimization of evaporative gas turbine with chemical absorption for carbon dioxide capture. *Int J Green Energy* 6:527–539
57. Manfrida G (1999) Opportunities for high-efficiency electricity generation inclusive of CO₂ capture. *Int J Appl Thermodyn* 2:165–175
58. Nyberg B, Thern M (2012) Thermodynamic studies of a HAT cycle and its components. *Appl Energy* 89:315–321
59. Zhang C, Wang X, Yang C, Yang Z (2017) Control strategies of steam-injected gas turbine in CCHP system. *Energy Procedia* 105:1520–1525
60. De Paepe W, Montero Carrero M, Bram S, Parente A, Contino F (2017) Advanced humidified gas turbine cycle concepts applied to micro gas turbine applications for optimal waste heat recovery. *Energy Procedia* 105:1712–1718
61. Ghazikhani M, Passandideh-Fard M, Mousavi M (2011) Two new high-performance cycles for gas turbine with air bottoming. *Energy* 36:294–304
62. Han W, Jin H, Zhang N, Zhang X (2007) Cascade utilization of chemical energy of natural gas in an improved CRGT cycle. *Energy* 32:306–313
63. Desideri U, Di Maria F (1997) Water recovery from HAT cycle exhaust gas: A possible solution for reducing stack temperature problems. *Int J Energy Res* 21:809–822
64. Wan K, Zhang S, Wang J, Xiao Y (2010) Performance of humid air turbine with exhaust gas expanded to below ambient pressure based on microturbine. *Energy Convers Manag* 51:2127–2133
65. Wang Y, Lior N (2007) Performance analysis of combined humidified gas turbine power generation and multi-effect thermal vapor compression desalination systems—Part 2: The evaporative gas turbine based system and some discussions. *Desalination* 207:243–256

66. Chacartegui R, Blanco MJ, Muñoz de Escalona JM, Sánchez D, Sánchez T (2013) Performance assessment of molten carbonate fuel cell-humid air turbine hybrid systems. *Appl Energy* 102:687–699
67. Kuchonthara P, Bhattacharya S, Tsutsumi A (2003) Combinations of solid oxide fuel cell and several enhanced gas turbine cycles. *J Power Sources* 124:65–75
68. Layi Fagbenle R, Oguaka ABC, Olakoyejo OT (2007) A thermodynamic analysis of a biogas-fired integrated gasification steam injected gas turbine (BIG/STIG) plant. *Appl Therm Eng* 27:2220–2225
69. Livshits M, Kribus A (2012) Solar hybrid steam injection gas turbine (STIG) cycle. *Sol Energy* 86:190–199
70. Zhang X, Chan SH, Li G, Ho HK, Li J, Feng Z (2010) A review of integration strategies for solid oxide fuel cells. *J Power Sources* 195:685–702
71. De Paepe M, Dick E (2001) Technological and economical analysis of water recovery in steam injected gas turbines. *Appl Therm Eng* 21:135–156
72. Cleeton JPE, Kavanagh RM, Parks GT (2009) Blade cooling optimisation in humid-air and steam-injected gas turbines. *Appl Therm Eng* 29:3274–3283
73. Bolland O, Sæther S (1992) New concepts for natural gas fired power plants which simplify the recovery of carbon dioxide. *Energy Convers Manag* 33:467–475
74. Ali U, Agbonghae EO, Hughes KJ, Ingham DB, Ma L, Pourkashanian M (2016) Techno-economic process design of a commercial-scale amine-based CO₂ capture system for natural gas combined cycle power plant with exhaust gas recirculation. *Appl Therm Eng* 103:747–758
75. DOE/NETL (2013) Current and future technologies for Natural Gas Combined Cycle (NGCC) Power Plants. U. S. Department of Energy
76. Jonshagen K, Sipöcz N, Genrup M (2011) A novel approach of retrofitting a combined cycle with post combustion CO₂ capture. *J Eng Gas Turbines Power* 133:011703
77. Li H, Haugen G, Ditaranto M, Berstad D, Jordal K (2011) Impacts of exhaust gas recirculation (EGR) on the natural gas combined cycle integrated with chemical absorption CO₂ capture technology. *Energy Procedia* 4:1411–1418
78. Best T, Finney KN, Ingham DB, Pourkashanian M (2016) Impact of CO₂-enriched combustion air on micro-gas turbine performance for carbon capture. *Energy* 115: 1138–1147
79. Best T, Finney KN, Santis AD, Ingham DB, Pourkashanian M (2016) Exhaust gas recirculation and selective exhaust gas recirculation on a micro-gas turbine for enhanced CO₂ capture performance. In: *The future of gas turbine technology: 8th International gas turbine conference, Brussels, Belgium*. Paper ID Number (31-IGTC16)
80. Evulet AT, ElKady AM, Brand AR, Chinn D (2009) On the performance and operability of GE's dry low NO_x combustors utilizing exhaust gas recirculation for post-combustion carbon capture. *Energy Procedia* 1:3809–3816
81. Røkke PE, Hustad JE (2005) Exhaust gas recirculation in gas turbines for reduction of CO₂ emissions: Combustion testing with focus on stability and emissions. *Int J Thermodyn* 8:167–173
82. De Santis A, Ingham DB, Ma L, Pourkashanian M (2016) CFD analysis of exhaust gas recirculation in a micro gas turbine combustor for CO₂ capture. *Fuel* 173:146–154
83. Peeters ANM, Faaij APC, Turkenburg WC (2007) Techno-economic analysis of natural gas combined cycles with post-combustion CO₂ absorption, including a detailed evaluation of the development potential. *Int J Greenhouse Gas Control* 1:396–417
84. ElKady AM, Evulet A, Brand A, Ursin TP, Lyngghjem A (2009) Application of exhaust gas recirculation in a DLN F-class combustion system for postcombustion carbon capture. *J Eng Gas Turbines Power* 131:034505
85. Jansohn P, Griffin T, Mantzaras I, Marechal F, Clemens F (2011) Technologies for gas turbine power generation with CO₂ mitigation. *Energy Procedia* 4:1901–1908
86. Ditaranto M, Hals J, Bjørge T (2009) Investigation on the in-flame NO reburning in turbine exhaust gas. *Proc Combust Inst* 32:2659–2666

87. Elkady AM, Evulet A, Brand A, Ursin TP, Lynghjem A (2008) Exhaust gas recirculation in DLN F-class gas turbines for post-combustion CO₂ capture. ASME Turbo Expo 2008: Power for Land, Sea and Air, Berlin, Germany. 847–854
88. Merkel TC, Wei X, He Z, White LS, Wijmans JG, Baker RW (2013) Selective exhaust gas recycle with membranes for CO₂ capture from natural gas combined cycle power plants. *Ind Eng Chem Res* 52:1150–1159
89. Diego ME, Bellas J-M, Pourkashanian M (2017) Process analysis of selective exhaust gas recirculation for CO₂ capture in natural gas combined cycle power plants using amines. *J Eng Gas Turbines Power* 139:121701–121710
90. Herraiz L (2016) Selective exhaust gas recirculation in combined cycle gas turbine power plants with post-combustion carbon capture
91. Marsh R, Giles A, Runyon J, Pugh D, Bowen P, Morris S, Valera-Medina A, Best T, Finney KN, Pourkashanian M (2016) Selective exhaust gas recycling for carbon capture applications: combustion and operability measurement. In: The future of gas turbine technology: 8th international gas turbine conference. Paper ID Number (32-IGTC16)
92. Turi DM, Ho M, Ferrari MC, Chiesa P, Wiley DE, Romano MC (2017) CO₂ capture from natural gas combined cycles by CO₂ selective membranes. *Int J Greenhouse Gas Control* 61:168–183
93. IEAGHG (2015) Oxy-combustion turbine power plants
94. Stanger R, Wall T, Spörl R, Paneru M, Grathwohl S, Weidmann M, Scheffknecht G, McDonald D, Myöhänen K, Ritvanen J, Rahiala S, Hyppänen T, Mletzko J, Kather A, Santos S (2015) Oxyfuel combustion for CO₂ capture in power plants. *Int J Greenhouse Gas Control* 40:55–125
95. Adanez J, Abad A, Garcia-Labiano F, Gayan P, de Diego LF (2012) Progress in chemical-looping combustion and reforming technologies. *Prog Energy Combust Sci* 38:215–282
96. Boot-Handford ME, Abanades JC, Anthony EJ, Blunt MJ, Brandani S, Mac Dowell N, Fernandez JR, Ferrari M-C, Gross R, Hallett JP, Haszeldine RS, Heptonstall P, Lyngfelt A, Makuch Z, Mangano E, Porter RTJ, Pourkashanian M, Rochelle GT, Shah N, Yao JG, Fennell PS (2014) Carbon capture and storage update. *Energy Environ Sci* 7:130–189
97. Allam R, Martin S, Forrest B, Fetvedt J, Lu X, Freed D, Brown GW, Sasaki T, Itoh M, Manning J (2017) Demonstration of the Allam Cycle: an update on the development status of a high efficiency supercritical carbon dioxide power process employing full carbon capture. *Energy Procedia* 114:5948–5966
98. Allam RJ, Palmer MR, Brown GW, Fetvedt J, Freed D, Nomoto H, Itoh M, Okita N, Jones C (2013) High efficiency and low cost of electricity generation from fossil fuels while eliminating atmospheric emissions, including carbon dioxide. *Energy Procedia* 37:1135–1149
99. Iwai Y, Itoh M, Morisawa Y, Suzuki S, Cusano D, Harris M (2015) Development approach to the combustor of gas turbine for oxy-fuel, supercritical CO₂ cycle. In: ASME Turbo Expo 2015: Turbine technical conference and exposition. Montreal, Canada
100. Anderson RE, MacAdam S, Viteri F, Davies DO, Downs JP, Paliszewski A (2008) Adapting gas turbines to zero emission oxy-fuel power plants. ASME Turbo Expo 2008: Power for Land, Sea and Air, Berlin, Germany pp 781–791
101. Anderson R, Viteri F, Hollis R, Keating A, Shipper J, Merrill G, Schillig C, Shinde S, Downs J, Davies D, Harris M (2010) Oxy-fuel gas turbine, gas generator and reheat combustor technology development and demonstration pp 733–743
102. Anderson R, Hustad C, Skutley P, Hollis R (2014) Oxy-fuel turbo machinery development for energy intensive industrial applications. *Energy Procedia* 63:511–523
103. Pronske K (2013) Oxy-turbine technology update Available from: https://ukccsrc.ac.uk/sites/default/files/documents/blog/gasccsmay2013/christian_biebuyck.pdf
104. Jericha H, Sanz W, Göttlich E (2008) Design concept for large output Graz cycle gas turbines. *J Eng Gas Turbines and Power* 130:011701–011710

105. Sanz W, Jericha H, Moser M, Heitmeir F (2005) Thermodynamic and economic investigation of an improved Graz cycle power plant for CO₂ capture. *J Eng Gas Turbines Power* 127:765–772
106. Jericha H, Sanz W, Göttlich E, Neumayer F (2008) Design details of a 600 MW Graz cycle thermal power plant for CO₂ capture. pp 507–516
107. Braunreiter L, Bennett SJ (2017) The neglected importance of corporate perceptions and positions for the long-term development of CCS. *Energy Procedia* 114:7197–7204
108. Parsons EL, Shelton WW (2002) Advanced fossil power systems comparison study. Final Report
109. Reichl AE, Schneider R, Ohligschläger A, Rogalinski T, Hauke S (2014) Process development and scale-up for post combustion carbon capture—validation with pilot plant operation. *Energy Procedia* 63:6379–6392
110. Kapetaki Z, Hetland J, Guenan TL, Mikunda T, Scowcroft J (2017) Highlights and lessons from the EU CCS demonstration project network. *Energy Procedia* 114:5562–5569
111. Spence B, Horan D, Tucker O (2014) The Peterhead-Goldeneye gas post-combustion CCS project. *Energy Procedia* 63:6258–6266
112. Inc. NE (2017) Petra Nova. Available from: nrg.com/generation/projects/petra-nova/
113. Oxburgh R (2016) Lowest cost decarbonisation for the UK: The critical role of CCS—Report to the Secretary of State for Business, Energy and Industrial Strategy from the Parliamentary Advisory Group on Carbon Capture and Storage (CCS). Available from: sccs.org.uk/images/expertise/reports/oxford/oxburgh_report_the_critical_role_of_ccs.pdf
114. Lipponen J, McCulloch S, Keeling S, Stanley T, Berghout N, Berly T (2017) The politics of large-scale CCS deployment. *Energy Procedia* 114:7581–7595
115. SCCS (2016) Scottish Carbon Capture and Storage: Expertise—Global CCS Map. Available from: sccs.org.uk/expertise/global-ccs-map
116. Billson M, Pourkashanian M (2017) The evolution of European CCS policy. *Energy Procedia* 114:5659–5662
117. Karimi F (2017) Timscapes of CCS projects: Is deferring projects and policies just kicking the can down the road? *Energy Procedia* 114:7317–7325
118. Vercelli S, Lombardi S, Modesti F, Tartarello MC, Finioia MG, Angelis DD, Bigi S, Ruggiero L, Pirrotta S (2017) Making the communication of CCS more “human”. *Energy Procedia* 114:7367–7378
119. Kapetaki Z, Scowcroft J (2017) Overview of carbon capture and storage (CCS) demonstration project business models: risks and enablers on the two sides of the Atlantic. *Energy Procedia* 114:6623–6630
120. O’Connor C, Chalmers H, Wright S, Adderley B, Gibbins J (2017) Developing CCS in the UK and beyond: insights from the UK CCS Research Centre. *Energy Procedia* 114
121. Osmundsen P, Emhjellen M (2010) CCS from the gas-fired power station at Kårstø? A commercial analysis. *Energy Policy* 38:7818–7826
122. BP (2017) BP statistical review of world energy June 2017. Available from: bp.com/content/dam/bp/en/corporate/pdf/energy-economics/statistical-review-2017/bp-statistical-review-of-world-energy-2017-full-report.pdf
123. CCSA HM Treasury consultation—carbon capture & storage: a consultation on barriers to commercial deployment, response by the Carbon Capture & Storage Association (CCSA). Available from: ccsassociation.org/docs/2006/CCSA%20submission%20to%20HM%20Treasury%20Consultation.doc

CO₂ Capture and Utilization (CCU) in Coal-Fired Power Plants: Prospect of In Situ Algal Cultivation

Ranjana Chowdhury, Sumona Das and Shiladitya Ghosh

Abstract Coal-fired plants, presently sharing 90% of Indian thermal power, are the main point sources of anthropogenic emission of CO₂. Although there is a prediction of significant decline in the share of coal by 2040, it will remain the obvious choice as power plant fuels due to economic constraints and natural abundance. Therefore, from the perspective of environmental protection, immediate measures for the mitigation of CO₂ emission are necessary. Micro- and macroalgae are the photoautotrophs which naturally sequester atmospheric CO₂ through photosynthesis. The captured inorganic carbon derived from CO₂ is stored as carbohydrates in the algal cells. On the other hand, under nitrogen stress, many algae store oil along with carbohydrates. Therefore, from a microalgal cultivation facility, oil can be extracted by solvent extraction process and can be utilized in pharmaceutical sector, and the residual oil can be converted to biodiesel. Valuable biochemicals can be recovered from the algal solid, and the process residue can be ultimately pyrolyzed to generate pyro-oil, pyro-gas, and biochar. Pyro-oil and pyro-gas can be utilized as fuels, and the biochar can be utilized for the amendment of soil. Therefore, an algal cultivation unit, either a raceway pond or a closed reactive system, can be integrated with coal-based power plants for their environmental and financial sustainability through the CO₂ capture and utilization (CCU) and for the creation of revenue through the generation of biofuels and valuable biochemicals. This chapter has assessed the prospect of application of different algal strains for the CCU in Indian power plants with special focus on *Rhizoclonium hieroglyphicum* JUCHE 1, *Pithophora varia* JUCHE 2, *Leptolyngbya subtilis* JUCHE 1, the native algae isolated from water handling units (cooling water forebay, clarifier water tank, and cooling tower) of Indian power plants by the present group.

Keywords CO₂ emission from coal-fired power plants · CCU · Biofuels and biochemicals · Power plant algae · Integration of algal refinery with power plant

R. Chowdhury (✉) · S. Das · S. Ghosh
Chemical Engineering Department, Jadavpur University, Kolkata 700032, India
e-mail: ranjana.juchem@gmail.com

© Springer Nature Singapore Pte Ltd. 2018
S. De et al. (eds.), *Sustainable Energy Technology and Policies*, Green Energy and Technology, https://doi.org/10.1007/978-981-10-7188-1_10

231

1 Introduction

Presently, elevated emission of prime greenhouse gases (GHGs) into the atmosphere is receiving harsh criticism for their substantial contribution to the global warming phenomenon [1, 2]. Among the GHGs, anthropogenic CO₂ emission has been given special attention and is considered to be the single most deleterious factor for global warming [1, 3]. CO₂ emission is largely caused by combustion of hydrocarbon fossil fuels such as coal, oil, and natural gas in thermal power plants as primary sources of energy to produce the more easily utilizable secondary energy sources, namely heat and electricity [4]. Presently, the thermal power plants, particularly, the coal-fired ones, are adversely regarded as one of the major point sources of extensive emission of anthropogenic CO₂ throughout the world [5, 6]. In India, coal-based thermal power plants, perhaps, are responsible for majority of the country's huge CO₂ emission footprint [7–9]. Average low calorific value, high levels of non-organic impurities, and high-ash content of Indian coals further worsen the CO₂ emission scenario of coal-fired power plants by manifolds [10]. Estimation of recent statistics of the annual CO₂ emission from the coal-fired thermal power plants is necessary to understand the necessity of taking urgent action in this area. Immediate remedial measures should be undertaken for reduction of the CO₂ emission from coal combustion as well as post-combustion CO₂ capture from the atmosphere to notably cut down the current CO₂ emission loads of the country [10, 11]. Joint administration of clean coal technologies (CCTs), carbon capture and storage (CCS), and/or carbon capture and utilization (CCU) techniques as mitigation strategies to lower the emission of CO₂ from coal-fired thermal power plants is viewed as necessary action plans for India [10, 11].

Although several physical- and chemical-based processes are commonly used for CCS, their impacts are not always certain, regarding several technical, economic, and environmental barriers [12–14]. Particularly, the geological storage capacity of most of the leading CO₂-emitting countries is not sufficient, and further, the storage itself is just a 'stopgap' management, not completely 'leakage-proof' yet [5, 12]. Therefore, utilization of the captured carbon in place of storing it is grabbing a lot of interest worldwide, paving the way for CCU as a complementing technology for CCS [11, 13]. Biological CCU using microalgae offers an eco-friendly route of capturing post-combustion CO₂ and its further utilization through conversion to various value-added products [13]. Major aim of this chapter is to provide: (1) updated information on the present CO₂ emission from the Indian coal-fired thermal power plants on a state-wise basis, (2) overview of probable strategies for mitigation of CO₂ emission from thermal power plants, (3) identification of the capacity of algae as candidate CCU agents, (4) assessment of the potential of native power plant algae for on-site administration of biological CCU technology.

2 Coal-Fired Power Plants in India: Locations and Capacity

It is a well-reported fact that coal is the single most reliable source of energy for India [10, 15, 16]. About 90% of the thermal power generated in India is based on coal. According to the most recent documentation presented by ministry of power, it is observed that coal accounts for 194,553 MW ($\approx 88\%$ of total) thermal power generation in India in 2017 [17]. As reported by NTPC, in the year 2016, the coal-based thermal power generation was 167,707 MW [18]. Coal is used in the thermal power plants for conversion to heat and electricity to back up the Indian power sector and sustain the domestic as well as commercial sectors [15]. There are over 100 major coal-fired thermal power plants in India, situated in 17 states [18]. The power plants vary in total capacity of power generation (GW), ranging from below 5–20 GW [18]. As per the representation of Fig. 1, the highest coal-based thermal power generating states are Maharashtra (17.72 GW) and Madhya Pradesh (15.77 GW) [18]. Gujarat, Uttar Pradesh, Odisha, West Bengal, Chhattisgarh, Tamil Nadu, and Bihar fall in the range of 10–15 GW total power generation [18]. Andhra Pradesh is the only state with a total power generation capacity lying between 5 and 10 GW [18]. Rest of the seven states produce thermal power in small amounts (<5 GW); they are Rajasthan, Telangana, Jharkhand, Karnataka, Punjab, Haryana, and Delhi [18]. The trend of distribution can be explained by the energy demand and abundance of coal in that particular region [18]. In Fig. 1, state-wise distribution of total power generation capacity (GW) of coal-fired thermal power plants has been illustrated [18].

3 CO₂ Emission Loads of Thermal Power Plants

From the analysis of the Fig. 2, it is notable that capacity and distribution of the thermal power plants in different states are not uniform [18]. Due to this fact, sometimes, the CO₂ flux of a large state is smaller than that of a small state, as represented in Fig. 2. From the presentation of Fig. 2, it can be seen that among the Indian states, Delhi, the smallest one, has the highest value of CO₂ flux. For the smaller states with large CO₂ flux values, the local air quality becomes poor and unhealthy. The worst case is seen in Delhi, which is recently been tagged as a city with heavily polluted air (according to a survey by WHO) [15]. The annual CO₂ emission has been estimated using reported data for GHG emission from Indian thermal power plants as following: 0.75 kg CO₂/kWh for Mundra power plants and 1.259 kg CO₂/kWh for other coal-fired thermal power plants [10]. For the representation of CO₂ flux range in Fig. 2, the values for each state have been calculated by dividing the total annual CO₂ emission from coal-fired power plants of particular state by the total area of respective state [10, 18, 19].

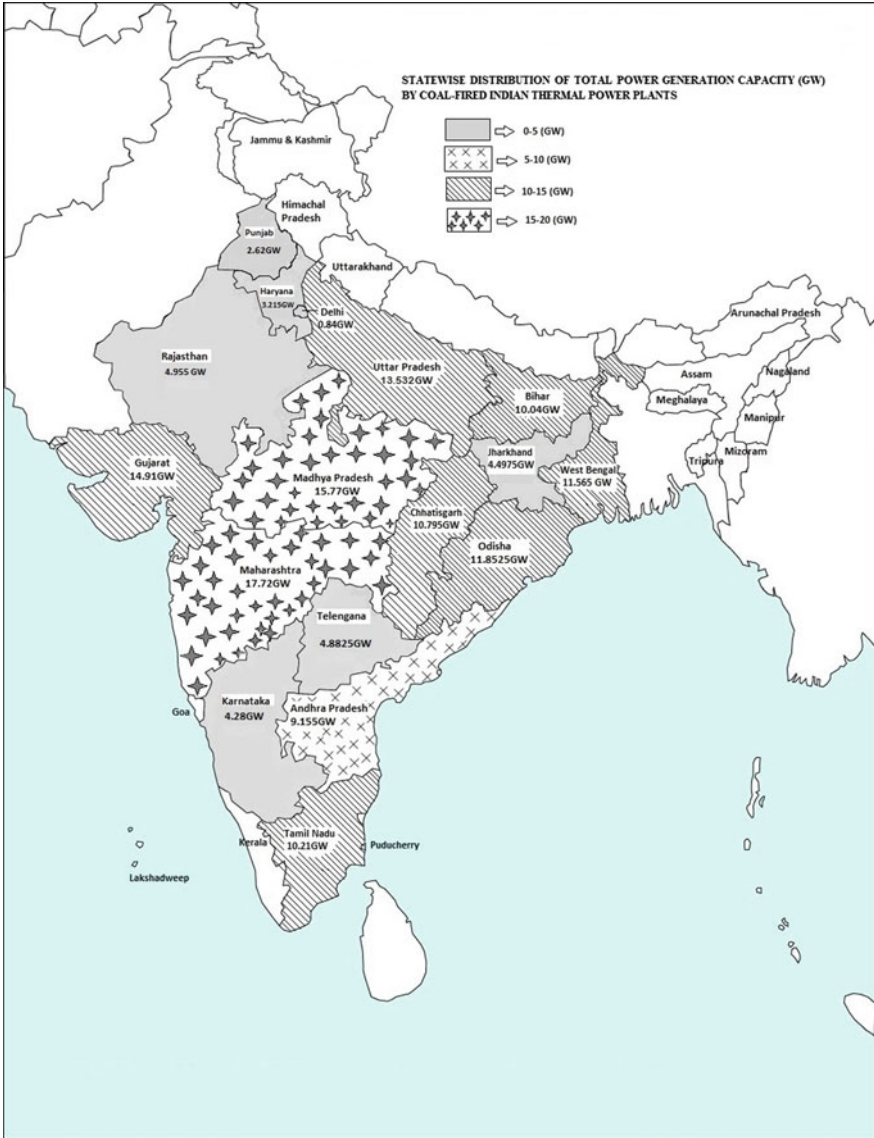


Fig. 1 Coal-fired thermal power plants in different states of India with total power generation capacity, calculations have been done as per the data reported by NTPC [18]

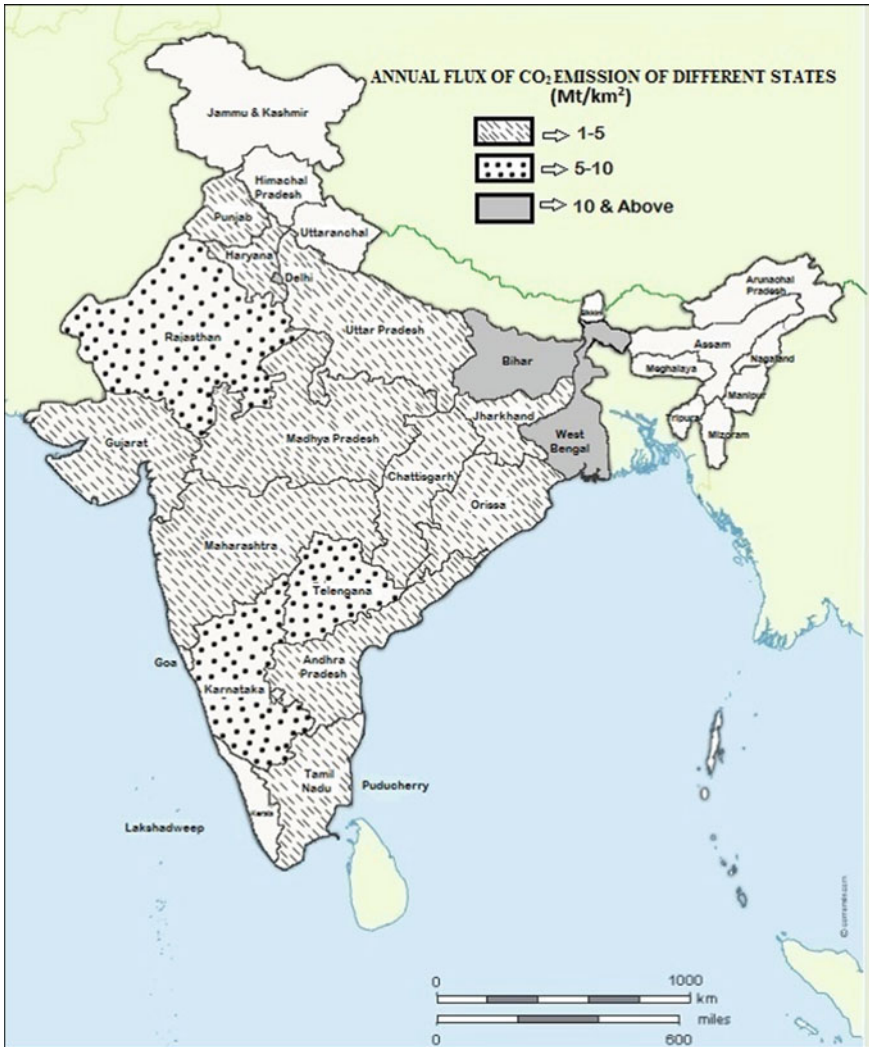


Fig. 2 Coal-fired thermal power plants in different states of India along with total annual CO₂ flux

4 Technology Options for Mitigation of CO₂

In the preceding section, it has been clearly highlighted that coal-fired thermal power plants are the large emitters of CO₂, directly contributing to the escalation of the threat of global warming [5, 6]. Hence, mitigation of CO₂ from these power plants through administration of modern technologies is a primary concern for India. Particularly, to keep the voluntary commitment of the country to United Nation’s Framework Convention on Climate Change (UNFCCC) for significant

reduction of total emissions by 2020 [20]. Globally practiced carbon/CO₂ capture technologies can be generally categorized into three major classes, namely pre-combustion capture, post-combustion capture, and oxy-fuel combustion [13, 20–22]. Basic features of these three processes have been provided in Table 1. Among the available technologies for mitigation of CO₂ from the targeted sites, clean coal technology (CCT) and carbon capture and utilization (CCU) are appearing to be the most potent as well as eco-friendly options.

4.1 Clean Coal Technology (CCT)

CCT is a cluster-term, comprising several different technologies specifically designed to enable more environmentally benign usage of coal for power generation [10, 20–22]. While some of the CCTs are based on direct combustion of coal, integrated with efficient combustion processes, the rest uses advanced gasification technology for cleaner conversion of coal [20–22]. According to the recent reports, the most fitting CCT options for implementation in India are as follows.

In the cluster of advanced CCTs, CCS is the latest addition, which possesses better eco-friendly attributes compared to the other routes. CCS significantly differs from other CCTs at its point of application. However, more recently, a few bottlenecks of CCS technology have been observed, most of which are either technical or economical. Huge initial capital investment and problems of CO₂ leakage from the storage sites as well as the risk of earthquakes are the major constraints associated with large-scale CCS [12].

4.2 Carbon Capture and Utilization (CCU)

Both in CCS and CCU, the carbon capture part is same and is conducted applying common technical processes worldwide. Most commonly employed carbon capture techniques, namely physical or chemical adsorption/absorption and membrane-based or cryogenic separation, have been mentioned in Table 1 [12, 13, 20–22]. A variety of different liquid solvents and solid sorbents, as well as different type of membranes, are available for chemical/physical CCS [12, 13]. CCS and CCU mainly differ from each other in their end step. The former technology tries to store the captured CO₂ at any natural (geological or ocean) site. While in the latter technology, the CO₂ is utilized in a commercial process either directly or after conversion to chemical/fuels/heat/electricity via different routes [13]. Among these, sequestration of CO₂ using microalgae and its conversion to fuels and chemicals can be considered as a promising CCU platform.

Algal CO₂ biosequestration is a completely eco-friendly green route for carbon capture. Operation at ambient temperature and pressure makes the process less energy intensive, although indoor operations require energy investment for

Table 1 Technical options for carbon/CO₂ capture and clean coal technology (CCT) options for Indian coal-based power generation sector

Carbon/CO ₂ capture options	Technologies involved	Basic features
Pre-combustion	Gasification–separation–combustion	<ul style="list-style-type: none"> • N₂ is separated from air and mixed with fuel (coal/other fossil fuel) in a gasifier to produce syngas • CO₂ is separated from the syngas using physical/chemical/porous organic adsorbents prior to the combustion stage • Energy penalty and cost of capture is less
Post-combustion	Combustion–separation	<ul style="list-style-type: none"> • Fuel (coal/other fossil fuel) and air are mixed and combusted to produce a flue gas • CO₂ is separated from the flue gas using chemical absorbents/solid adsorbents/membranes or cryogenic separation techniques • Energy penalty and cost of capture is high (varies with separation techniques used)
Oxy-fuel combustion	Separation–combustion	<ul style="list-style-type: none"> • Fuel (coal/other fossil fuel) is combusted in presence of 100% O₂ (separated from air) to produce flue gas (CO₂/H₂O) • CO₂ content of the produced flue gas is very high (up to 90%) • H₂O is separated using condensation, and residual CO₂ is compressed and send for transport and storage
<i>CCT option</i>	<i>Used technical routes</i>	<i>Basic features</i>
1. Supercritical power generation	Combustion	<ul style="list-style-type: none"> • Employs thermodynamic cycles to enhance thermal efficiency of coal combustion • Operated using a steam cycle at pressure >226 bars and temperature >537 °C
2. Ultra-supercritical power generation	Combustion	<ul style="list-style-type: none"> • Same as supercritical, operating pressure and temperature are 357 bar and 625 °C, respectively
3. Circulating fluidized bed combustion (CFBC)	Combustion	<ul style="list-style-type: none"> • Combustion of air-suspended fine coal particles (0.07–0.3 mm) in a fluidized bed with fluidization velocity of 5–10 m/sec • Enables rapid transfer of heat and efficient burning • Used for high-ash, high-moisture, and low-grade coals
4. Pressurized fluidized bed combustion (PFBC)	Combustion	<ul style="list-style-type: none"> • Combustion of crushed coal along with a sorbent (limestone suspension) to capture sulfur • Operating pressure and temperature are 16–20 bars and 850 °C, respectively • Used for high-sulfur-containing coals.

(continued)

Table 1 (continued)

Carbon/CO ₂ capture options	Technologies involved	Basic features
5. Integrated gasification combined cycle (IGCC)	Gasification	<ul style="list-style-type: none"> • Gasification of coal is conducted in an oxygen/air atmosphere in a pressurized (30 bars) gasifier at or above 1000 °C • Coal-gas is burnt in a gas turbine for power generation • Process heat (gasifier, hot gases) is recovered and used in a combined cycle to run the steam turbine • High overall efficiency and less pollution
6. Carbon capture and storage (CCS)	Physical, chemical, or biochemical	<ul style="list-style-type: none"> • Employs different technical means to capture emitted CO₂ from atmosphere • Adsorption is traditionally used in both physical and chemical routes, other than solvent absorption, membrane, and cryogenic separation • Biochemical CCS is mainly conducted using micro/macroalgae • Efficiency varies among physical, chemical, or biochemical methods

providing illumination to the photobioreactor [23]. Since it holds the prospect of production of low-emission renewable biofuels from the algal biomass, the overall process can become CO₂ neutral/negative [24]. On the economical front, most of the biochemicals derived from the algal cells are high-value products, which will compensate the high cost of algal biodiesel in comparison to conventional petro-fuels. Hence, as the focal point of discussion of the present chapter, detail of biochemical CCU through microalgae cultivation has been provided in the subsequent sections. The fundamentals of algal CCU have been covered starting from the biochemical route of CO₂ capture to the conversion of carbon-enriched biomass to an array of biofuels, biochemicals, and biomaterials.

5 CO₂ Sequestration Through Photosynthetic Pathway by Algae: The Capture of Carbon

Photoautotrophic algae, both micro and macro, conduct oxygenic photosynthesis alike the terrestrial plants [23, 25, 26]. While the photobiochemical process is mainly driven by the energy obtained from light (in nature sunlight), CO₂ serves as an important inorganic reactant for the biosynthesis of several biomolecules and biomass [23, 26]. Like the terrestrial plants, algae conduct oxygenic photosynthesis in which the inorganic CO₂ is converted to organic compounds and molecular

oxygen is produced as an end product [26]. The general biochemical reaction of photosynthesis process can be represented as the following equation:



Photosynthesis in algae is divided into two distinct stages, i.e., light-dependent and light-independent. Light-dependent stage is the primary one in which the light energy is captured by the antenna complexes of chlorophyll and other carotenoids present in Photosystem I or Photosystem II of chloroplast [23]. At the expense of the captured light energy, ADP and NADP⁺ are, respectively, converted to the energy carriers, ATP and NADPH, through the transfer of electrons via the electron transport chain (ETC), and oxygen is produced as the end product [23, 26]. CO₂ is used in the light-independent phase of photosynthesis. CO₂ enters the algal cells as either HCO₃⁻ or as CO₂ through the transporters present in the cell membrane and chloroplast membrane [23]. The biofixation or the sequestration of the inorganic carbon from CO₂ is conducted via the redox reactions of the Calvin–Benson cycle [27]. In Calvin–Benson cycle, each molecule of CO₂ gets condensed with ribulose 1,5-bisphosphate (a 5 carbon compound) to produce two molecules of 3 carbon compound 3-phosphoglycerate through the action of the enzyme ribulose 1,5-bisphosphate carboxylase-oxygenase (Rubisco) using the ATP and NADPH produced in the light-dependent stage [23, 26, 27]. From the produced 3-phosphoglycerate, the starting compound ribulose 1,5-bisphosphate is cyclically regenerated through a series of intermediate compounds [23, 26]. 3-phosphoglycerate also serves as the precursor for the biosynthesis of biomass in form of glucose [23]. The produced glucose is transported to the cytoplasm and gets stored in form of starch molecules. This is the overall procedure of the sequestration of carbon of CO₂ via assimilation into organic biomass of algae. The stored carbohydrates of algae can be harnessed and used for the production of several biofuels through specific conversion routes.

6 CO₂ Capture Potential of Different Algal Strains

Due to the inherent photobiochemical CO₂ capture potential of algae, several studies have used them as carbon capture agents for sequestration of atmospheric CO₂ [28–35]. The rate or capacity of CO₂ capture hugely varies among the algal strains, depending on their source of origin and adaptation to atmospheric conditions. CO₂ capture and fixation obtained by some species of algae, as reported in recent literatures, have been presented in Table 2 for comparative assessment of their potential. CO₂ fixation rate, a major assessment factor, is the measure of mass (g) of CO₂ photosynthetically up-taken per unit time by the algal cells for the ultimate conversion to cellular carbohydrate. The CO₂ tolerance level of algal strains signifies the highest concentration of feed concentration of CO₂ up to which the algal growth is sustained. Above this limiting value, the inhibition of algal growth is encountered [36].

Table 2 CO₂ biocapture and fixation potential of different algal strains

Algal strain	Inlet CO ₂ concentration (%v/v)	Light intensity ($\mu\text{mol m}^{-2} \text{s}^{-1}$)	Cultivation system	Biomass productivity (g/L/d)	CO ₂ fixation rate (g/L/d)	Refs.
<i>Chlorella kessleri</i>	6	105	2-L conical flask PBR	0.087	0.163 ^a	[28]
<i>Scenedesmus obliquus</i>	12	105	2-L conical flask PBR	0.076	0.142 ^a	[28]
<i>Spirulina</i> sp.	6	105	3-stage 2-L serial tubular PBR	0.22	0.413	[29]
<i>Scenedesmus obliquus</i>	12	105	3-stage serial tubular PBR	0.14	0.26 ^a	[29]
<i>Chlorella</i> sp. UK001	15	112	Flat culture vessel	1.67	0.8183	[30]
<i>Scenedesmus obliquus</i> CNW- \bar{N}	2.5	250	10-L PBR	0.32	0.495	[31]
<i>Chlorella vulgaris</i>	4	–	15-L PBR	0.1 \pm 0.07	0.14	[32]
	8	–	15-L PBR	0.08 \pm 0.07	0.073	[32]
<i>Nannochloropsis gaditana</i>	4	–	1.5-L plastic bottle	0.07 \pm 0.08	0.112	[32]
	8	–	1.5-L Plastic bottle	0.06 \pm 0.08	0.10	[32]
<i>Scenedesmus obliquus</i>	2	180–250	1-L tubular PBR	0.46–0.49	0.855–0.910	[33]
<i>Scenedesmus obliquus</i>	2.5	180–250	1-L single PBR	1.030	1.782	[33]
<i>Chlorella</i> sp.	1	136	250-ml Erlenmeyer flask	0.87 \pm 0.05	1.538 \pm 0.093	[34]
<i>Pseudochlorococcum</i> sp	1	136	250-ml Erlenmeyer flask	0.81 \pm 0.04	1.18 \pm 0.062	[34]
<i>Nannochloropsis</i> sp.	1	120	5-L bubble-column PBR	0.38 \pm 0.03	0.46 \pm 0.09	[34]
<i>Scenedesmus</i> sp.	4	–	18-L IIPBR	0.401	0.733	[34]
<i>Nannochloropsis salina</i>	1	–	18-L IIPBR	0.104	0.191	[35]
<i>Rhizoclonium hieroglyphicum</i> JUCHE1	15	398.71	1.8-L flat-plate photobio-bubble-reactor	0.52	0.561	[36]
<i>Leptolyngbya subtilis</i> JUCHE1	40	250	1.8-L flat-plate photobio-bubble-reactor	0.252	0.3237	Authors own data

^aCalculated from the biomass productivity according to equation, CO₂ fixation rate (Pco₂) = 1.88 \times biomass productivity (P), g/L/d which is derived from the typical molecular formula of microalgal biomass, CO_{0.48}H_{1.83}N_{0.11}P_{0.01} [37]

From the tabulated information, it can be seen that a variety of algal strains have been used in laboratory-scale (small to medium) studies using different PBRs (Table 2). Both freshwater and marine algal species have been used for CO₂ biocapture which exhibited distinct difference in the CO₂ tolerance as well as rate of CO₂ fixation. Apparent CO₂ tolerance is reflected in the amount of CO₂ concentration used for cultivation of the algae. Some of the algal strains have been cultivated using lower inlet concentration of CO₂ in the range of 1–8%V/V [28, 29, 31–35], whereas a few have tolerated moderately higher inlet concentrations (12–15%V/V) of CO₂ [28–30, 36]. *Scenedesmus obliquus*, *Chlorella* sp. UK001, and *Rhizoclonium hieroglyphicum* JUCHE1 belong to the high CO₂-tolerant group of algae [28–30, 36]. *Leptolyngbya subtilis* JUCHE 1, a very recently isolated strain of algae, shows much higher CO₂ tolerance up to 40%V/V of inlet concentration. Among these, *Rhizoclonium hieroglyphicum* JUCHE 1 and *Leptolyngbya subtilis* JUCHE 1 are isolated from local coal-fired thermal power plants [36]. Another algal strain, namely *Chlorella kessleri*, is also isolated from a thermoelectric power plant and used for CO₂ sequestration [28]. However, the CO₂ tolerance and CO₂ fixation capacities of algal strains cannot be correlated directly, because the latter is dependent on several operational factors.

Different trends of CO₂ fixation rate and biomass productivity have also been reported for different algae. CO₂ fixation rate varies from a low value of 0.073 g/L/d to values as high as 1.782 g/L/d [32, 33]. *Chlorella* sp. UK001, *Scenedesmus obliquus*, *Chlorella* sp., *Pseudochlorococcum* sp. have been reported to exhibit high rates of CO₂ fixation [33, 34]. Among the algal strains, *Chlorella* sp. UK001 has exhibited highest biomass productivity of 1.67 g/L/d [30]. *Scenedesmus obliquus*, *Chlorella* sp., *Pseudochlorococcum* sp. are some other algal strains with high biomass productivity in the range of 0.8–1 g/L/d [33, 34]. However, it is understandable that the performances of different algal strains are not directly comparable due to the differences in the cultivation conditions, photobioreactor (PBR) configuration, and illumination. Therefore, the CO₂ capture performance and biomass productivity of the algal strains may be significantly enhanced through optimization of bioprocesses.

7 Prospect of Generation of Specialty Biochemicals and Biofuels from Algae

7.1 Biochemicals from Algae

By using photosynthesis process, algae efficiently convert solar energy into chemical energy and store it in the cells. Other than biofuels, algal biomass is a potential source of different type of biochemicals [38–47]. The major biochemicals are mainly categorized as polyunsaturated omega 3 fatty acids, namely docosahexaenoic acid (DHA), docosapentaenoic acid (DPA), eicosapentaenoic acid

(EPA), α -linolenic acid (ALA), and stearidonic acid (SDA) and pigments such as chlorophyll, carotenoids (lutein, β -carotene), xanthophyll, astaxanthin [38, 46, 47]. Polyunsaturated fatty acids (PUFAS) are mainly present in algal oil/lipid [14]. Among all the PUFAS, DHA is the most crucial due its medicinal properties [48]. Mostly marine species of algae are rich in DHA content, which is very beneficial for human health. Its consumption as a food additive may lower the risk of cancer, cardiovascular diseases (reduces the high blood pressure and stimulates blood circulation), Alzheimer's disease, etc. [48]. Due to its high utility in pharmaceutical industries, these biochemicals are very expensive [48, 49]. EPA is a biochemical with proven anti-inflammatory activity and enhances lipid metabolism and overall neural health [50]. DPA also helps in the storage of EPA and DHA in human body. According to Table 3, it has been observed that many of the algal strains produce DHA, ALA, SDA, EPA, and DPA as fractions of the product omega 3 fatty acids [38]. Among all the algal strains, the contents of DHA and SDA of *Isochrysis T-iso* are maximum, i.e., 46 ± 4 mg/g of oil and 43 ± 2 mg/g of oil, respectively [38]. Highest concentration of ALA is present in *Tetraselmis suecica* (68 ± 4 mg/g of oil) and *Rhodomonas salina* (92 ± 5 mg/g of oil) [38]. The *Nannochloropsis gaditana* and *Nannochloropsis oculata* contain the highest quantity of EPA, as high as 175 ± 12 and 193 ± 24 mg/g oil, respectively [38]. Very few strains of algae produce only a little quantity of DPA in the order of 1–2 mg/g of oil, which is comparatively less than other PUFAS [38]. As per the data of Table 3, only two algal species, namely *Phaeodactylum tricorutum* and *Thalassiosira pseudonana*, contain 1.08 ± 0.01 and 1.82 ± 0.01 mg DPA/g of oil, respectively [38].

Other categories of biochemicals extracted from algae are pigments, namely chlorophyll (chl a and chl b), carotenoid (carotene, lutein), etc. Algal strains contain chlorophyll a, chlorophyll b, and chlorophyll c, depending on the species [46, 47]. Green algae mostly contain chlorophyll a and chlorophyll b, red algae contain chlorophyll a only, and diatoms mainly contain chlorophyll c [46]. Due to its use in food and cosmetic industries, chlorophyll is a valuable biochemical. Carotenoids, which are tetra-terpenoids in nature, are pigments of red, orange, and yellow colors. Different carotenoids are lutein, beta-carotene, xanthophylls, astaxanthin, etc., are found in algal biomass [40, 47]. Table 3 presents that most algal strains contain chlorophyll a, as it is the most common photosynthetic pigment of algal photo-systems. Maximum concentration of chlorophyll a is found in *Isochrysis galbana*, *Chaetoceros calcitrans*, *Isochrysisaff galbana (T-Iso)*, and *Thalassiosira pseudonana* [47]. Maximum carotene production of 8.6 ± 1.9 mg/g of biomass is reported in *Tetraselmis suecica* [38]. Among eight algal strains, *Neosporiococcus gelatinosum* produces lutein in highest concentration, i.e., 7.6 mg/g of dry cell weight [45]. Similarly, the maximum carotenoid content of 2.6 mg/g of dry cell weight is obtained from *Chaetoceros calcitrans* [47].

The price lists (Table 4) of some commercially available biochemicals, which are also produced by different algal strains, clearly show that they are very highly priced [49]. It is noteworthy that the high cost of algal biochemicals includes the investment incurred for algal cultivation as well as the rigorous downstream processing for the separation of the chemicals in highly pure forms. If the biochemicals

Table 3 Production of various biochemicals from different algal strains

Biochemicals	Algal strains	Concentration range (mg/g)	Refs.
^a DHA (C22:6n-3)	<i>Tetraselmis suecica</i>	>1	[38]
	<i>Phaeodactylum tricorutum</i> , <i>Rhodomonas salina</i> , <i>Thalassiosira pseudonana</i>	1–25	[38]
	<i>Pavlova lutheri</i> , <i>IsochrysisT-iso</i>	25–50	[38]
^a ALA (C18:3n-3)	<i>Nannochloropsis gaditana</i> , <i>Nannochloropsis oculata</i> , <i>Phaeodactylum tricorutum</i>	>1	[38]
	<i>Pavlova lutheri</i> , <i>Thalassiosira pseudonana</i> , <i>Porphyridium cruentum</i>	1–25	[38]
	<i>IsochrysisT-iso</i>	25–50	[38]
	<i>Tetraselmis suecica</i> , <i>Rhodomonas salina</i>	50 and above	[38]
^a SDA (C18:4N-3)	<i>Nannochloropsis gaditana</i>	>1	[38]
	<i>Phaeodactylum tricorutum</i> , <i>Pavlova lutheri</i> , <i>Tetraselmis suecica</i> , <i>Thalassiosira pseudonana</i>	1–25	[38]
	<i>IsochrysisT-iso</i> , <i>Rhodomonas salina</i>	25–50	[38]
^a EPA (C22:5N-3)	<i>IsochrysisT-iso</i> , <i>Tetraselmis suecica</i> , <i>Rhodomonas salina</i> , <i>Porphyridium cruentum</i>	1–50	[38]
	<i>Thalassiosira pseudonana</i> , <i>Pavlova lutheri</i>	50–100	[38]
	<i>Phaeodactylum tricorutum</i>	100–150	[38]
	<i>Nannochloropsis gaditana</i> , <i>Nannochloropsis oculata</i>	150–200 and above	[38]
^a DPA (C22:5N-3)	<i>Phaeodactylum tricorutum</i> , <i>Thalassiosira pseudonana</i>	1–2	[38]
^a Carotene	<i>Porphyridium cruentum</i>	>1	[38]
	<i>Phaeodactylum tricorutum</i> , <i>IsochrysisT-iso</i> , <i>Pavlova lutheri</i> , <i>Nannochloropsis oculata</i> , <i>Nannochloropsis gaditana</i> , <i>Thalassiosira pseudonana</i>	1–5	[38]
	<i>Rhodomonas salina</i>	5–10	[38]
	<i>Tetraselmis suecica</i>	10 & above	[38]
^b Lutein (C ₄₀ H ₅₆ O ₂)	<i>Chlorella protothecoides</i> , <i>Chlorella zofingiensis</i>	1–5	[39, 40]
	<i>Desmodesmus</i> sp., <i>Chlorella sorokiniana MB-I</i> , <i>Scenedesmus almeriensis</i> , <i>Muriellopsis</i> sp., <i>Chlorococcum citrifforme</i> , <i>Neosporangiococcus gelatinosum</i>	5–10	[41, 42, 43, 44, 45]
^b Chlorophyll a	<i>Chlorella vulgaris</i> sp.	1–5	[46]
	<i>Chaetoceros</i> sp., <i>Tetraselmis suecica</i>	5–10	[47]
	<i>Isochrysis galbana</i> , <i>Chaetoceros calcitrans</i> , <i>Isochrysisaff galbana (T-Iso)</i> , <i>Thalassiosira pseudonana</i>	10 & above	[47]

(continued)

Table 3 (continued)

Biochemicals	Algal strains	Concentration range (mg/g)	Refs.
^b Chlorophyll b	<i>Chlorella vulgaris</i> sp., <i>Tetraselmis suecica</i>	1–5	[46, 47]
^b Chlorophyll c	<i>Chaetoceros</i> sp., <i>Thalassiosira pseudonana</i> , <i>Isochrysis galbana</i> , <i>Isochrysisaff Galbana (T-Iso)</i> , <i>Chaetoceros calcitrans</i>	1–5	[47]
^b Carotenoids	<i>Tetraselmis suecica</i> , <i>Chaetoceros</i> sp., <i>Thalassiosira pseudonana</i> , <i>Isochrysis galbana</i> , <i>Isochrysisaff galbana (T-Iso)</i> , <i>Chaetoceros calcitrans</i>	1–5	[47]

^amg chemicals/g of oil, ^bmg chemicals/g of algal biomass

Table 4 Price lists of some biochemicals which can be produced by algae

Name of the biochemical	Quantity	Price (INR)
Lutein	1 mg	31,413.53
β-Carotene	5 mg	3415.96
Chlorophyll	2 ml	7935.66
Docosapentaenoic acid (DPA)	10 mg	26,694.04
Linolenic acid (LA)	1 ml	14,090.52
Eicosapentaenoic acid (EPA)	100 mg	11,558.89
Stearidonic acid (SDA)	1 mg	8289.53
Docosahexaenoic acid (DHA)	10 mg	6420.32

^aFrom Sigma Aldrich, India [49]

are efficiently extracted, the revenue generated from them will be able to offset the expenditure of algal harvesting and processing cost for the generation of biofuels from algae.

7.2 Biofuels from Algae

Algae are considered as a potential renewable resource for biofuel production. As a part of their metabolism, some algae can produce high amount of lipids/fats in their cells as storage materials. This ‘oil fraction’ can be separated from the algal biomass using particular solvent extraction method [51]. After extracting the oil-soluble biochemicals (the omega 3 fatty acids), the residual algal oil is converted to bio-diesel through transesterification process [51]. The oil-extracted solid biomass fraction, rich in storage carbohydrates (mainly algal starch of the cell wall), can serve as feedstock for production of different other biofuels. Absence of lignin in

algal biomass makes it a favorable substrate for conversion to biofuels via biochemical routes [52]. Besides biochemical routes, algal biomass has been considered as an attractive feedstock in thermochemical bioenergy process as shown in Table 5 [53–73]. Algal biomass can be directly fed to anaerobic digestion process for its conversion to biomethane/biogas [69]. The mixed microbes of the anaerobic digestion process can efficiently perform the necessary hydrolysis of the biomass and subsequent conversion to biogas [67]. The algal biomass, after mild chemical treatment to facilitate release of simple sugars, can be converted to ethanol or hydrogen through fermentative routes conducted by dedicated microbes [58]. Biodiesel, biomethane, bio-ethanol, and biohydrogen are greatly valued as promising renewable energy vectors. Production of these biofuels from algal biomass is classified under third generation of biofuels, which is free from the constraints of the first-generation (food vs. fuel) and second-generation (recalcitrance of lignin) biofuel platforms. Production of biodiesel from residual algal oil is also a third-generation process due to the non-edibility.

Recently, the algal biomass has been popularly used in the thermochemical processes such as pyrolysis and gasification [66]. In these processes, the residual algal biomass, after deriving the oil and biochemicals, is used as feedstock. In pyrolysis, the algal biomass is converted to pyro-oil, pyro-gas, and pyro-char [56, 57]. The pyro-oil is considered as a promising blend-in option for petro-fuels for the transportation sector. In Table 5, production of various biofuels from algal oil/biomass has been presented to clearly depict the overall usage of algae in the 3G platform.

From Table 5, it can be seen that all the algal strains are efficiently used for different biofuels through various routes. In case of bio-oil production through pyrolysis of algal biomass, it has been found that all the algal strains have high bio-oil production capacity, varying in the range of 39–58% [53–57]. Among the reported strains, *Chlorella protothecoides*, *Blue green algae (BGAB)*, and *Chlorella vulgaris* exhibit maximum bio-oil yield of 57.9, 54.97, and 52.7% of dry algae weight, at a pyrolysis temperature of 500 °C [53–55]. Another product of pyrolysis of algal biomass is the biochar, which is used as adsorbent and soil amender. The biochar can be considered as a biofuel, since it can be further gasified to produce syngas. From the pyrolysis of algal biomass of different algae, biochar yield of 28–33 g/100 g of dry algae has been reported [56, 57]. The biodiesel yield varies among 56.31–91.6% of TAG in algal oil in different algae [62–65]. Maximum biodiesel yield has been obtained from the alga *Scenedesmus* sp. [62]. Using the biomass of three different algae in a two-step thermochemical process (pyrolysis followed by steam gasification), hydrogen yields of 413, 937, and 1036 mL have been obtained per gram of dry algae [66]. Algal biomass can be used as feedstocks in fermentative processes for production of biohydrogen, with mild pretreatment [67]. Dilute-acid-pretreated biomass of *Gelidium amansii*, a species of red algae, has been used in a mixed-culture-driven dark fermentation process for production

Table 5 Production of several 3G biofuels from different algae

Biofuel	Basis of yield calculation	Algal strains	Process	Yield	Refs.
Bio-oil	100 g dry algae	<i>Chlorella protothecoides</i>	Fast pyrolysis at 500 °C	57.9	[53]
		<i>Blue green algae (BGAB)</i>	Pyrolysis at 500 °C	54.9	[54]
		<i>Chlorella vulgaris</i>	Fast pyrolysis at 500 °C	52.7	[55]
		<i>Saccharina japonica</i>	Pyrolysis at 450 °C	47	[56]
		<i>Spirulina</i> sp.	Slow pyrolysis at 550 °C	46	[57]
		<i>Spirogyra</i> sp.	Slow pyrolysis at 550 °C	43	[57]
		<i>Cladophora</i> sp.	Slow pyrolysis at 550 °C	39	[57]
Bio-ethanol	1 g dry algae	<i>Chlorococcum infusionum</i>	Fermentation	0.26	[58]
		<i>Scenedesmus dimorphus</i>	Fermentation	0.266	[59]
		<i>Porphyridium cruentum</i>	Fermentation	0.059	[60]
		<i>Desmodesmus</i> sp. FG	Fermentation	0.134	[61]
Biodiesel	100 g TAG In algal oil	<i>Scenedesmus</i> sp.	Two-step catalytic conversion	96.6	[62]
		<i>Nannochloropsis</i> sp.	Two-step catalytic conversion	91.6	[62]
		<i>Spirulina-platensis</i>	Acid-catalyzed in situ Transesterification	84.7	[63]
		<i>Chrysophyta</i>	Transesterification	56.31	[64]
		<i>Chlorella</i> sp.	Transesterification	63.78	[64]
		<i>Spirulina</i> sp.	Transesterification	79.50	[65]
Biohydrogen	1 g dry algae	<i>Fucus serratus</i>	Two-step thermochemical process	1036 mL	[66]
		<i>Laminaria digitate</i>	Two-step thermochemical process	937 mL	[66]
		<i>Nannochloropsis oculata</i>	Two-step thermochemical process	413 mL	[66]
		<i>Gelidium amansii</i>	Dilute-acid hydrolysis and fermentation	37 mL	[67]
		<i>Chlorella sorokiniana</i>	Thermophilic dark fermentation	958 mL	[68]

(continued)

Table 5 (continued)

Biofuel	Basis of yield calculation	Algal strains	Process	Yield	Refs.
Biomethane	1 g dry algae	<i>Spirulina</i> sp.	Anaerobic digestion	0.32–0.31 L CH ₄	[69,70]
		<i>Dunaliella</i> sp.	Anaerobic digestion	0.44–0.45 L CH ₄	[69,70]
		<i>Chlorella vulgaris</i>	Anaerobic digestion	0.31–0.35 ^a L CH ₄	[71]
		<i>Spirulina maxima</i>	Anaerobic digestion	0.26 L CH ₄	[72]
Biochar	100 g dry algae	<i>Chlorella vulgaris</i>	Fast pyrolysis at 500 °C	31	[73]
		<i>Saccharina japonica</i>	Pyrolysis at 450 °C	33	[56]
		<i>Spirulina</i> sp.	Slow Pyrolysis at 550 °C	31	[57]
		<i>Spirogyra</i> sp.	Slow pyrolysis at 550 °C	28	[57]
		<i>Chladophora</i> sp.	Slow pyrolysis at 550 °C	31	[57]

^aCalculated from data given in L CH₄ gCOD⁻¹ using a COD/VS ratio of 1.5 (where COD is the chemical oxygen demand)

of biohydrogen [67]. In another study, mild-acid-pretreated biomass of *Chlorella sorokiniana* has been used in thermophilic dark fermentation process for production of biohydrogen [68]. In the thermophilic process, hydrogen yield of 958 mL H₂/g of dry algae was obtained, which was much higher than (37 mL H₂/g of dry algae) obtained from the mesophilic process [67, 68]. Biomass of different algal strains has been used in many studies for the production of biogas/biomethane through anaerobic digestion process. The yield of biomethane obtained in those studies varied from 0.26 L CH₄ to 0.45 L CH₄ per gram of algal biomass used [69–72].

From the information provided in Table 5, it is evident that algae or biomass of algae is an excellent source of different 3G biofuels. The promise of integrating the algal cultivation with CO₂ capture from different industrial plants can significantly enhance the eco-friendliness of the total process. Among this, integration of the algal units with thermal power plants is a great way of achieving CCU in a totally green way with significant reduction in CO₂ emission from these point sources.

7.3 Complexities of Algal Cultivation

For algal biomass cultivation process, there are some important optimum parameters for the regulation of algal growth. These are nutrients, mainly the nitrogen, phosphorous, and potassium sources, CO₂, light, pH, salinity, temperature, etc. From the reported studies, it is evident that mostly the growth regulating optimum parameters are specific with respect to algal strains [38, 39, 45–47]. Therefore, the following precautions should be taken during algal cultivation: (1) The light penetration length should be short; (2) the algal biomass should be removed at regular intervals to avoid the shading effect on light caused by overgrowth of algal biomass; (3) the temperature should be maintained near the optimum value; (4) the concentration of nutrients should be maintained at their optimal levels.

8 Indian Power Plant Algae and Their CCU Potential: Preliminary Assessments

In tropical countries, like India, algal blooms are commonly observed in almost any and every open water bodies, where plenty of sunlight is available. Interestingly, algae can even grow in any moist place where limited amount of sunlight is available. They even grow in the process water and wastewater handling units of several industries upon utilizing the CO₂ generated from the concerned processes. Very recently, few algal strains, namely *Rhizoclonium hieroglyphicum* JUCHE 1, *Pithophora varia* JUCHE 2, and *Leptolyngbya subtilis* JUCHE 1, have been isolated from different water handling units of coal-fired thermal power plants of West Bengal, India. These algae, macro/micro by nature, exhibit higher CO₂ tolerance, higher CO₂ uptake and sequestration, and greater biomass productivities. These attributes of Indian power plant algae need more in-depth research attention, which is the current focus of the present group or authors of this chapter. Cultivation of the isolated power plant algae, assessment of their CCU potential through performance of photobioreactor operation, extraction of algal oil and biochemicals from the algal biomass and pyrolysis of the residual algal biomass for the production of pyro-oil, pyro-gas, and pyro-char are currently underway.

CO₂ biosequestration by *R. hieroglyphicum* JUCHE 1 has already been studied in a flat-plate photobioreactor. The strain was cultivated using varying inlet CO₂ concentrations from 5 to 25% under illumination of 398.71 μmolm⁻²s⁻¹ light intensity [36]. At 15% inlet CO₂ concentration, *R. hieroglyphicum* JUCHE 1 resulted in 0.52 g/L/d biomass productivity along with 0.561 g/L/d of CO₂ biofixation rate [36]. From preliminary studies on *Leptolyngbya subtilis* JUCHE 1, the strain was observed to be very highly CO₂ tolerant, which is a reflection of its adaptation to high CO₂-laden areas inside the thermal power plant. At 40% inlet CO₂ concentration, the strain showed a CO₂ fixation rate of 0.3237 g/L/d, which is moderately low. It is expected that the high CO₂ fixation capacity of this algal strain

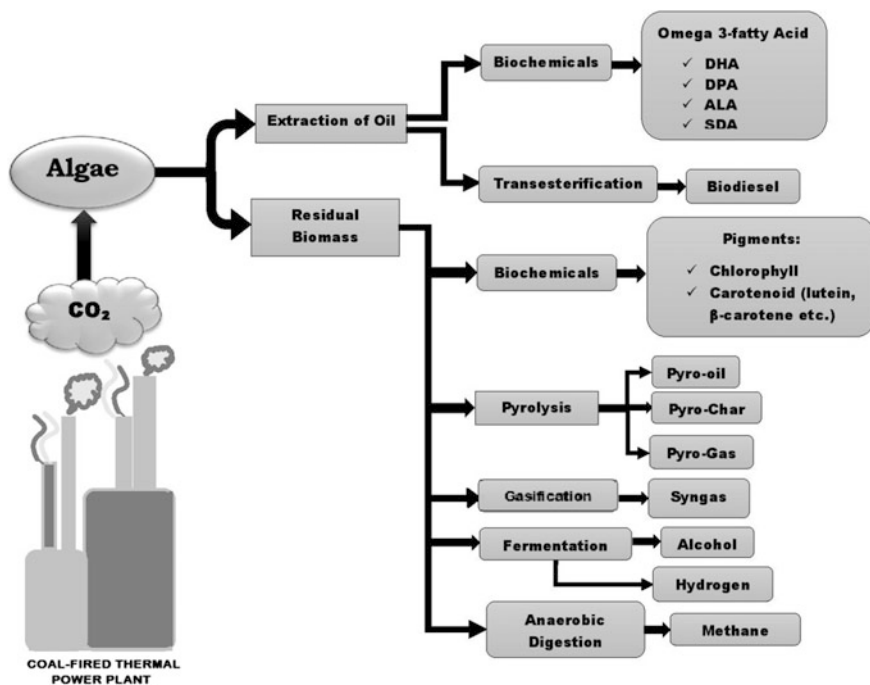


Fig. 3 Integrated scheme of a coal-fired thermal power plant with algal cultivation unit followed by generation of biofuels and biochemicals

will be fully understood in near future through performance of more detailed studies. *Pithophora varia* JUCHE 2 was found to be an oil-producing strain of algae, with prospect of producing valuable biochemicals and biodiesel. Oil productivity of *P. varia* JUCHE 2 was experimentally found to be 28.4% (unpublished data). Extraction of different biochemicals, namely omega 3 fatty acids, chlorophyll, and carotenoids from these algal strains is currently being conducted to enhance the overall economic feasibility of the process. Upon maximization of the CO₂ biosequestration by these algal strains through process optimization, they may be endorsed as native ‘on-site CCU’ agents for Indian coal-fired thermal power plants. The promising scheme has been illustrated in Fig. 3.

9 Integration of Algal Refinery with Coal-Fired Thermal Power Plants: Present Status

Very recently, the prospect of integration of algal refinery with power plants is attracting the interest of bioenergy researchers worldwide. Gutierrez-Arriaga et al. [74] have investigated an integrated energy system combining algal CO₂

sequestration units of open raceway ponds with a 400 MW thermoelectric power plant operating in Mexico [74]. The model algal cultivation unit has a dimension of 100 m × 10 m × 0.3 m. The study also designed sequential units for harvesting of algal biomass, extraction of algal oil, conversion of algal oil to biodiesel to complete the algae-to-biodiesel chain. The used algal strain was *Chlorella vulgaris*. The rationale of supplied CO₂ to algal biomass was 1.83 tonne CO₂ per tonne of algal biomass for 12 h/d [74]. The algal unit has successfully captured CO₂ at 70% efficiency [74]. Very high lipid recovery yield of 80% was achieved in the oil extraction unit using hexane as the extraction solvent [74]. Finally, 1 g of biodiesel was produced from 1 g of triglyceride through transesterification. Lipid-extracted algal biomass was co-combusted in the boiler to reduce the load on the fossil fuel usage [74]. Results of this study affirmatively underlined the practicality of CCU using microalgae for on-site CO₂ mitigation in power plants and use of algal oil for biodiesel production as an attractive revenue-generating process. A few industrial endeavors on the integration of algal cultivation units with power plants for the purpose of CO₂ capture and biofuel generation have been reported by Schmidt, 2012 [75]. Although the success of CO₂ mitigation has been highlighted by most of the industries, the requirement of large cultivation area has been indicated as a great concern. Moreover, it is not clear from the review whether the revenue generated through the marketing of algal biofuels can offset the cost of chemicals and land required for algal cultivation. However, it is understandable that better designing of cultivation units, increase of light conversion efficiency, etc., and the derivation of algal biochemical, as discussed in the previous section (Table 5), can significantly brighten the economic status of the overall process to further extents. As reported by Baral et al. [76], some initiatives of introducing algal CO₂ capture units are being considered for application in coal-fired thermal power plants, namely Angul, Orissa, and Kolaghat, West Bengal [76]. Converting these CO₂ capture units to CCU is promising due to the expected profitability of the setups. Regarding this, the power plants algae may be the best choice for their inherent adaptability to the plant environment. More research and development endeavors will play the crucial role in this regard.

10 Conclusion

In this article, an attempt has been made to project the state-wise CO₂ emission threat of coal-based thermal power plants in India. Discussing on different possible mitigation routes, the advantages of algal CCU have been highlighted. The present status of biomass growth, CO₂ capture potential, and the capacity of generating different biofuels as well as biochemicals by several algal strains has been revisited. Special attention has been given for the first time on Indian power plant algae indicating their characteristics of high CO₂ capture and oil content. Although constrained by scanty database, an attempt has also been made to reflect on the present status of integration of algal cultivation units with coal-based thermal power

plants. It is expected that the knowledge base presented in the article will be useful for the future endeavors on integration of algal refineries generating fuels and biochemicals with coal-fired power plants for their greenness.

Acknowledgements The authors are highly thankful to UPEII, Jadavpur University, funded by University Grant Commission (UGC), New Delhi, for extending the financial assistance required to conduct the studies on power plant algae.

References

1. Intergovernmental Panel on Climate Change (2015) *Climate change 2014: mitigation of climate change*, vol 3, Cambridge University Press
2. Wallington TJ, Srinivasan J, Nielsen OJ, Highwood EJ (2009) Greenhouse gases and global warming. *Environ Ecol Chem* 1:36
3. Ajmi AN, Hammoudeh S, Nguyen DK, Sato JR (2015) On the relationships between CO₂ emissions, energy consumption and income: the importance of time variation. *Energy Econ* 49:629–638
4. Vernon C, Thompson E, Cornell S (2011) Carbon dioxide emission scenarios: limitations of the fossil fuel resource. *Procedia Environ Sci* 6:206–215
5. Rahman FA, Aziz MMA, Saidur R, Bakar WAWA, Hainin MR, Putrajaya R, Hassan NA (2017) Pollution to solution: capture and sequestration of carbon dioxide (CO₂) and its utilization as a renewable energy source for a sustainable future. *Renew Sustain Energy Rev* 71:112–126
6. Board CIA (2010) Power generation from coal: measuring and reporting efficiency performance and CO₂ emissions. CIAB International Energy Agency, Paris, Report: OECD/IEA2010, pp 1–114
7. Sethi M (2015) Location of greenhouse gases (GHG) emissions from thermal power plants in India along the urban-rural continuum. *J Clean Prod* 103:586–600
8. Mittal ML, Sharma C, Singh R (2012) Estimates of emissions from coal fired thermal power plants in India. In: 2012 International emission inventory conference, pp 13–16
9. Ito O (2011) Emissions from coal fired power generation. In: Workshop on IEA high efficiency low emissions coal technology roadmap, vol 29
10. www.teriin.org/projects/green/pdf/India-CCT.pdf, 2015. Greengrowth and cleancoal technologies in India. The Energy and Resources Institute, New Delhi
11. Goel M (2017) CO₂ Capture and utilization for the energy industry: outlook for capability development to address climate change in India. In: Carbon utilization, Springer, Singapore, pp 3–33
12. Leung DY, Caramanna G, Maroto-Valer MM (2014) An overview of current status of carbon dioxide capture and storage technologies. *Renew Sustain Energy Rev* 39:426–443
13. Cuéllar-Franca RM, Azapagic A, (2015) Carbon capture, storage and utilisation technologies: a critical analysis and comparison of their life cycle environmental impacts. *J CO₂ Utilization* 9:82–102
14. Viebahn P, Vallentin D, Höller S (2014) Prospects of carbon capture and storage (CCS) in India's power sector—an integrated assessment. *Appl Energy* 117:62–75
15. Cully M (2015) Coal in India. Australia Government Office of the Chief Economist, June
16. Guttikunda SK, Jawahar P (2014) Atmospheric emissions and pollution from the coal-fired thermal power plants in India. *Atmos Environ* 92:449–460
17. <http://powermin.nic.in/en/content/power-sector-glance-all-india>
18. <http://cbrienvs.nic.in/Thermal%20Power%20Station%20in%20India%202016.pdf>
19. https://en.wikipedia.org/wiki/List_of_states_and_union_territories_of_India_by_area

20. Mishra MK, Khare N, Agrawal AB (2015) Scenario analysis of the CO₂ emissions reduction potential through clean coal technology in India's power sector: 2014–2050. *Energy Strategy Rev* 7:29–38
21. Chang S, Zhuo J, Meng S, Qin S, Yao Q (2016) Clean coal technologies in China: current status and future perspectives. *Engineering* 2:447–459
22. Goel M (2010) Implementing clean coal technology in India
23. Zhao B, Su Y (2014) Process effect of microalgal-carbon dioxide fixation and biomass production: a review. *Renew Sustain Energy Rev* 31:121–132
24. Moreira D, Pires JC (2016) Atmospheric CO₂ capture by algae: negative carbon dioxide emission path. *Biores Technol* 215:371–379
25. Aresta M, Dibenedetto A, Barberio G (2005) Utilization of macro-algae for enhanced CO₂ fixation and biofuels production: development of a computing software for an LCA study. *Fuel Process Technol* 86:1679–1693
26. Cardol P, Forti G, Finazzi G (2011) Regulation of electron transport in microalgae. *Biochimica et Biophysica Acta (BBA)-Bioenerg* 1807:912–918
27. Jablonsky J, Bauwe H, Wolkenhauer O (2011) Modeling the Calvin-Benson cycle. *BMC Syst Biol* 5:185
28. de Morais MG, Costa JAV (2007) Isolation and selection of microalgae from coal fired thermolectric power plant for biofixation of carbon dioxide. *Energy Convers Manag* 48:2169–2173
29. de Morais MG, Costa JAV (2007) Biofixation of carbon dioxide by *Spirulina* sp. and *Scenedesmus obliquus* cultivated in a three-stage serial tubular photobioreactor. *J Biotechnol* 129:439–445
30. Murakami M, Yamada F, Nishide T, Muranaka T, Yamaguchi N, Takimoto Y (1998) The biological CO₂ fixation using *Chlorella* sp. with high capability in fixing CO₂. *Stud Surf Sci Catal* 114:315–320
31. Chen CY, Chang HW, Kao PC, Pan JL, Chang JS (2012) Biosorption of cadmium by CO₂-fixing microalga *Scenedesmus obliquus* CNW-N. *Biores Technol* 105:74–80
32. Adamczyk M, Lasek J, Skawińska A (2016) CO₂ biofixation and growth kinetics of *Chlorella vulgaris* and *Nannochloropsis gaditana*. *Appl Biochem Biotechnol* 179:1248–1261
33. Ho SH, Lu WB, Chang JS (2012) Photobioreactor strategies for improving the CO₂ fixation efficiency of indigenous *Scenedesmus obliquus* CNW-N: statistical optimization of CO₂ feeding, illumination, and operation mode. *Biores Technol* 105:106–113
34. Taher H, Al-Zuhair S, Al-Marzouqi A, Haik Y, Farid M (2015) Growth of microalgae using CO₂ enriched air for biodiesel production in supercritical CO₂. *Renew Energy* 82:61–70
35. Pegallapati AK, Nirmalakhandan N (2013) Internally illuminated photobioreactor for algal cultivation under carbon dioxide-supplementation: performance evaluation. *Renew Energy* 56:129–135
36. Pradhan L (2014) Studies on carbon sequestration through microalgal culture in photobioreactor (Doctoral dissertation)
37. Ho SH, Chen CY, Lee DJ, Chang JS (2011) Perspectives on microalgal CO₂-emission mitigation systems—a review. *Biotechnol Adv* 29:189–198
38. Ryckebosch E, Bruneel C, Termote-Verhalle R, Goiris K, Muylaert K, Foubert I (2014) Nutritional evaluation of microalgae oils rich in omega-3 long chain polyunsaturated fatty acids as an alternative for fish oil. *Food Chem* 160:393–400
39. Wei D, Chen F, Chen G, Zhang X, Liu L, Zhang H (2008) Enhanced production of lutein in heterotrophic *Chlorella protothecoides* by oxidative stress. *Sci China, Ser C Life Sci* 51:1088–1093
40. Del Campo JA, Rodriguez H, Moreno J, Vargas MA, Rivas J, Guerrero MG (2004) Accumulation of astaxanthin and lutein in *Chlorella zofingiensis* (Chlorophyta). *Appl Microbiol Biotechnol* 64:848–854
41. Yeh TJ, Tseng YF, Chen YC, Hsiao Y, Lee PC, Chen TJ, Lee TM (2017) Transcriptome and physiological analysis of a lutein-producing alga *Desmodesmus* sp. reveals the molecular mechanisms for high lutein productivity. *Algal Res* 21:103–119

42. Chen CY, Hsieh C, Lee DJ, Chang CH, Chang JS (2016) Production, extraction and stabilization of lutein from microalga *Chlorella sorokiniana* MB-1. *Biores Technol* 200:500–505
43. Sánchez JF, Fernández JM, Acien FG, Rueda A, Pérez-Parra J, Molina E (2008) Influence of culture conditions on the productivity and lutein content of the new strain *Scenedesmusalmeriensis*. *Process Biochem* 43:398–405
44. Del Campo JA, Rodríguez H, Moreno J, Vargas MA, Rivas J, Guerrero MG (2001) Lutein production by *Muriellopsis* sp. in an outdoor tubular photobioreactor. *J Biotechnol* 85:289–295
45. Fernández-Sevilla JM, Fernández FA, Grima EM (2010) Biotechnological production of lutein and its applications. *Appl Microbiol Biotechnol* 86:27–40
46. Molnár É, Rippel-Pethő D, Bocsi R (2013) Solid-liquid extraction of chlorophyll from microalgae from photoautotroph open-air cultivation. *Hung J Ind Chem* 41:119–122
47. Whyte JN (1987) Biochemical composition and energy content of six species of phytoplankton used in mariculture of bivalves. *Aquaculture* 60:231–241
48. Tang S, Qin C, Wang H, Li S, Tian S (2011) Study on supercritical extraction of lipids and enrichment of DHA from oil-rich microalgae. *J Supercrit Fluids* 57:44–49
49. <http://www.sigmaaldrich.com/india.html>
50. Swanson D, Block R, Mousa SA (2012) Omega-3 fatty acids EPA and DHA: health benefits throughout life. *Adv Nutr: Int Rev J* 3:1–7
51. Johnson MB, Wen Z (2009) Production of biodiesel fuel from the microalga *Schizochytrium limacinum* by direct transesterification of algal biomass. *Energ Fuels* 23:5179–5183
52. Welker CM, Balasubramanian VK, Petti C, Rai KM, DeBolt S, Mendu V (2015) Engineering plant biomass lignin content and composition for biofuels and bioproducts. *Energies* 8:7654–7676
53. Miao X, Wu Q (2004) High yield bio-oil production from fast pyrolysis by metabolic controlling of *Chlorella protothecoides*. *J Biotechnol* 110:85–93
54. Hu Z, Zheng Y, Yan F, Xiao B, Liu S (2013) Bio-oil production through pyrolysis of blue-green algae blooms (BGAB): product distribution and bio-oil characterization. *Energy* 52:119–125
55. Thangalazhy-Gopakumar S, Adhikari S, Chattanathan SA, Gupta RB (2012) Catalytic pyrolysis of green algae for hydrocarbon production using H + ZSM-5 catalyst. *Biores Technol* 118:150–157
56. Suh DJ, Choi JH, Woo HC (2014) Pyrolysis of seaweeds for bio-oil and bio-char production. *Chem Eng Trans* 37:121–126
57. Chaiwong K, Kiatsiriroat T, Vorayos N, Thararax C (2012) Biochar production from freshwater algae by slow pyrolysis. *Maejo Int J Sci Technol* 6
58. Harun R, Jason WSY, Cherrington T, Danquah MK (2011) Exploring alkaline pre-treatment of microalgal biomass for bioethanol production. *Appl Energy* 88:3464–3467
59. Chng LM, Lee KT, Chan DJC (2017) Synergistic effect of pretreatment and fermentation process on carbohydrate-rich *Scenedesmus dimorphus* for bioethanol production. *Energy Convers Manage* 141:410–419
60. Kim HM, Oh CH, Bae HJ (2017) Comparison of red microalgae (*Porphyridium cruentum*) culture conditions for bioethanol production. *Biores Technol* 233:44–50
61. Rizza LS, Smachetti ME, Do Nascimento M, Salerno GL, Curatti L (2017) Bioprospecting for native microalgae as an alternative source of sugars for the production of bioethanol. *Algal Res* 22:140–147
62. Chen L, Liu T, Zhang W, Chen X, Wang J (2012) Biodiesel production from algae oil high in free fatty acids by two-step catalytic conversion. *Biores Technol* 111:208–214
63. El-Shimi HI, Attia NK, El-Sheltawy ST, El-Diwani GI (2013) Biodiesel production from *Spirulina-platensis* microalgae by in-situ transesterification process. *J Sustain Bioenergy Syst* 3:224

64. Zhou D, Qiao B, Li G, Xue S, Yin J (2017) Continuous production of biodiesel from microalgae by extraction coupling with transesterification under supercritical conditions. *Biores Technol* 238:609–615
65. Nautiyal P, Subramanian KA, Dastidar MG (2014) Production and characterization of biodiesel from algae. *Fuel Process Technol* 120:79–88
66. Duman G, Uddin MA, Yanik J (2014) Hydrogen production from algal biomass via steam gasification. *Biores Technol* 166:24–30
67. Park JH, Cheon HC, Yoon JJ, Park HD, Kim SH (2013) Optimization of batch dilute-acid hydrolysis for biohydrogen production from red algal biomass. *Int J Hydrogen Energy* 38:6130–6136
68. Roy S, Kumar K, Ghosh S, Das D (2014) Thermophilic biohydrogen production using pre-treated algal biomass as substrate. *Biomass Bioenergy* 61:157–166
69. Sialve B, Bernet N, Bernard O (2009) Anaerobic digestion of microalgae as a necessary step to make microalgal biodiesel sustainable. *Biotechnol Adv* 27:409–416
70. Chen PH (1987) Factors influencing methane fermentation of micro-algae. PhD thesis, University of California, Berkeley, CA, USA
71. Hernández ES, Córdoba LT (1993) Anaerobic digestion of *Chlorella vulgaris* for energy production. *Resour Conserv Recycl* 9:127–132
72. Samson R, Leduy A (1982) Biogas production from anaerobic digestion of *Spirulina maxima* algal biomass. *Biotechnol Bioeng* 24:1919–1924
73. Wang K, Brown RC, Homsy S, Martinez L, Sidhu SS (2013) Fast pyrolysis of microalgae remnants in a fluidized bed reactor for bio-oil and biochar production. *Biores Technol* 127:494–499
74. Gutiérrez-Arriaga CG, Serna-González M, Ponce-Ortega JM, El-Halwagi MM (2014) Sustainable integration of algal biodiesel production with steam electric power plants for greenhouse gas mitigation. *ACS Sustain Chem Eng* 2:1388–1403
75. Schmidt M (ed) (2012) *Synthetic biology: industrial and environmental applications*. Wiley
76. Baral SS, Singh K, Sharma P (2015) The potential of sustainable algal biofuel production using CO₂ from thermal power plant in India. *Renew Sustain Energy Rev* 49:1061–1074

Sustainability of Coal as a Source of Energy in India

Partha S. Bhattacharyya

Abstract Indian dependence on coal as a source of commercial energy is primarily attributed to the abundance of coal resources, unlike other fossil fuels such as oil or natural gas. Close to 60% of power generation capacity and 80% of actual power generation are coal-based. The aggregate coal resources—proven, inferred and indicated have risen from around 70 bt at the time of coal nationalization in the early 1970s to over 300 bt currently. The capability of exploration and drilling for faster proving of coal resources has increased manifold. Indian coal has typically high ash and low moisture. However, through a process of continuous innovation in boiler design, adequate capability of using such coal has been created. As a result, almost all capacities for power generation created in main heartland are based on such a low-grade coal. Responding to the fast growth in demand, coal production and consumption in the country have increased manifold since nationalization. This has raised significant issues of environmental and social sustainability around coal mining as well as coal consumption in the power stations. Degradation of a vast tract of land, uprooting local tribal population leading to erosion of their culture and traditional impacts on forest cover are some of the impacts of coal mining that need to be mitigated, if not eliminated. Similarly, inadequate management of fly ash in power stations, emission of obnoxious gases, presence of particulate matter beyond acceptable norms, besides the problems associated with resettlement, and rehabilitation of local populace are the challenges at the point of coal consumption in power stations. Of late, in response to bidding the renewable tariff has reduced to levels not far away from the coal-based tariff. This is fast emerging as a major issue impacting sustainability of coal-based power in the country. However, considering affordability as a key policy determinant, it will still be necessary to focus on improvement in PLF of existing coal-based capacities for which substantial scope exists. Such improvement in PLF will lead to substantially higher generation of coal-based power reinforcing additional demand for coal. However, while creating new capacity, coal-based power is likely to lose out to solar on consideration of

P. S. Bhattacharyya (✉)
Former Chairman
Coal India Ltd, Kolkata, India
e-mail: partha3020@gmail.com

economics. The article proposes to deal with the interplay of these complex and conflicting issues and suggests an appropriate sustainable road map in keeping with Indian commitment at COP21.

Keywords Energy sustainability · Coal · Indian context · Environmental impact Research needs

1 Preamble

Nationalization of coal in the 1970s happened under trying circumstances. An oil price shock triggered a process of evaluating energy options for the country by a high-powered committee with Dr. Sukhomoy Chakrabarti, an eminent economist and a member of planning commission in the Chair. This led to an identification of coal as the mainstay in the energy scenario. The growth in coal sector in 1960s was less than 2% CAGR, clearly inadequate to fuel the then aspired GDP growth rate of 5%. The low growth was primarily due to inadequate private investments caused by unattractive returns arising from low-administered price of coal. To set the coal price at a remunerative level was equivalent to a political harakiri since coal was widely used as domestic fuel in kitchens. The only option was to inject massive public funds to the coal sector. This made nationalization imperative. This also became imperative to redress the significant exploitative gap in the wages and benefits of coal workers with other industrial workers. Post-nationalization of coking coal in 1971 and non-coking coal in 1973 followed by a phase of reorganization, Coal India Limited was formed as a holding company with five subsidiaries in Nov 1975. The company dependent on budgetary support from the government for the first two decades and became financially self-reliant since 1997.

Coal in India is remained as the key provider of energy security. The production has increased manifold from less than 100 mtpa in the 1970s to over 600 mtpa currently, 80% of which is contributed by CIL. During this period, coal consumption increased even faster to over 800 mtpa; currently, the gap is being met through imports. In the mean while, the number of subsidiaries increased from five to eight.

At present, the share of coal in power generation is over 60% in terms of capacity and over 80% in terms of actual generation. Among fossil fuels, coal is far ahead of oil and gas not only in power generation but also in overall commercial fuel businesses. The primary reason for this is ostensibly the relative abundance of the fuel. Coal resources in the country are estimated at over 300 billion tonnes, of which, over 125 billion tonnes are in the proven category, rest being classified as inferred or indicated. At the current rate of consumption growing at 6% CAGR, the proven reserves alone, assuming conservatively 60% extractability, should suffice for over 40 years. With a steady shift of inferred and indicated resources to proven reserves through systematic drilling and exploration, the known reserves should be in a position to support coal consumption till the end of the current century.

Despite steady growth in the use of coal, India remains substantially lower than the comparable China both in terms of per capita power consumption and emission of green house gas. Indian share in global GHG emission is around 7% against a share in population of 16%. In contrast, China shares nearly 30% of global GHG emission with a population share of 17%. Not surprisingly, the per capita consumption of power in India is 1030 units low per year as compared to over 2800 units for China.

Availability of better quality of coal with low ash and high GCV is restricted in India to the coalfields of Rani Gunj and a part of Jharia in the eastern part of the country and Korea Rewa in central India, mainly from underground mines. The coal production from these mines/coalfields has stagnated or in most cases declined due to difficult geo-mining conditions and high cost. Post-nationalization, the growth in coal production has arisen mostly from Talcher, Korba and Rajmahal (lower grade) as well as North Karanpura and Singrauli (medium grades). However, the boiler design evolved over the period acquiring capability of running on such low-grade coal. The inferior quality of coal in India is a constraint arising from the coal formation being largely based on 'drift' as opposed to 'insitu'

The ability of the generators to use inferior grade coal due to improved boiler technology has significantly diluted the demand for coal washing so far. The rather poor state of coal washing in India is attributable to reluctance of the consumers to accept the cost of coal washing consequently disincentivize the coal producer to set up washeries. The gains arising from cost savings on account of extending boiler life, lesser ash disposal and handling need to be weighed against the cost of washing, and a net advantage to consumer established before coal washing gets the much-needed policy push.

Most Indian mines are not gassy. Only 4% of the mines are gassy. This restricts the scope of CBM in India, unless technological breakthrough in terms of microbial enhancement of CBM gas becomes a reality. This is a long-drawn research project that needs to bring together outcome of research happening globally in this field. Serious efforts are yet to commence in this direction.

2 Power for All 24 * 7

India is pursuing an inclusive development agenda—power for all 24 * 7 by 2020. At present, around 25% of Indians lack access to electricity. Another 35–40% access electricity for sometime in a day but not 24 * 7. Correcting these aberrations alone will require the per capita consumption to move from current levels to at least 1800 units per year. The additional consumption arising from higher intensity of white goods usage expected in a developing economy may get partly offset through the use of LED bulbs and energy efficient devices in replacement of older devices. In other words, a doubling of per capita consumption of power as soon as possible is necessary to percolate down the fruits of development to the common man.

In order to arrive at a sustainable solution to reach the aforesaid goal, the country has embarked on a multipronged strategy. Renewable power—both wind and solar—has been receiving greater attention. The drastic fall in tariff of power from these sources as revealed through successive bids has been added to the momentum. The wind power tariff has fallen to a low of Rs. 3.46 per unit whereas the latest solar power bid has discovered a tariff of Rs. 2.44 per unit. These rates are lower than the expected tariff from a newly constructed coal-based power station. Placed in this situation, the feasibility of adding fresh coal-based capacity in power generation, besides those in the pipeline, is clearly questionable.

Placed in this situation, it is normal to suspect the future of coal as a sustainable source of energy over a longer term. Nevertheless, a 360° understanding of the complexities involved may lead to a different conclusion.

Of overriding importance is AFFORDABILITY of power generated. The limited paying capacity of the marginal power consumers coupled with the stressed financial situation of the Discoms makes it imperative for power to be generated at the least possible cost and a mechanism to ensure that the resultant savings in cost is passed on to the Discoms and the ultimate consumer to the extent possible.

While the lowest bids for solar and wind powers in the range of Rs. 2.44–3.46 are possibly lower than the expected tariff from a new coal-based power station, it needs to be appreciated that:

- (a) the coal-based tariff will still be lower if the capital and other subsidies for renewable power are accounted for, and
- (b) even without accounting for these subsidies, the lowest solar/wind tariff is distinctly higher than the marginal cost of coal-based power from existing power stations that entail only the variable cost of coal. The cost differential is of the order of INR 0.60–1.00 with reference to the lowest offer of solar tariff.

In other words, the least-cost power is the one that the existing coal-based plants can generate by improving the plant load factor (PLF).

3 Improving PLF of Existing Coal-Based Plants—A Compelling Step Forward

An assessment of the potential for additional generation from these plants can be made based on the trend of past average PLF of coal-based plants. The highest PLF witnessed so far is around 79% in 2007–08. Since then, by 2011–12, the PLF had witnessed a modest fall to around 75%, largely due to faster addition of coal-based capacity without linkage to the required quantity of coal. However, in recent times, arising from increased focus to push renewable power into the system, the PLF of coal-based capacity fell to around 60% in 2016–17 and to an even lower level of around 55% during the current year. The problem is partly due also to mechanically complete power stations not receiving coal due to absence of a regular power

purchase agreement (PPA). In any case, it is policy-level hindrances to generation of least-cost power—that needs to be addressed as soon as possible.

The low PLF, well below the level considered at the time of estimating financial viability of the investment in the power plants is causing financial distress to the Gencos. It is, in effect, fuelling the process of conversion of bank loans to Gencos into non-performing assets (NPA). The collective exposure of the banks to Gencos is of the order of a few lakh crores of rupees. The inability of the Gencos to service the loans will eventually impact the tax payers of this country to meet the consequential recapitalization needs of the nationalized banks and/or the consequential rise in fees and charges levied by the banks, particularly the private ones, to stay afloat. Conversely, enhancing the PLF to the levels considered at the feasibility stage of the power plants will enable the Gencos service their debts and save the common man from being required to bear the financial consequences of non-servicing of bank loans.

The quality of coal-based capacity has improved significantly over the last decade partly due to phasing out of inefficient plants, though at a lesser rate than desirable, and partly due to introduction of plants with high-efficiency low-emission (HELE) technology. Hence, the average PLF unconstrained by policy bottlenecks can safely move to a level 6–7% higher than the best level of 79% witnessed a decade ago. In other words, the potential for the average unconstrained PLF may be estimated at around 85%.

A systematic debottlenecking can, therefore, lead to the PLF of existing plants improving from the current 55% to say 85% over the next few years injecting the least-cost power into the system. The current coal-based generation is around 950 bn units. The additional generation possible through PLF improvement is, therefore, around 500 bn units. The resultant cost saving estimated at an average tariff differential of INR 0.8 works out to INR 40,000 crores. The mechanism to ensure that a substantial part of this cost saving gets passed on to the ultimate consumer through Discoms is discussed subsequently.

A direct consequence of the aforesaid strategy is to create additional coal demand of around 300 million tonnes estimated at a conservative specific consumption of 0.6 kg/unit. Assuming a 5-year period for implementing the aforesaid strategy, the existing players including Coal India Ltd can be expected to regain growth of around 6% CAGR leading to an incremental production of around 200 mtpa 5 years hence. This leaves a gap of 100 mtpa. In addition, the efforts to replace the import of thermal coal by domestic production are expected to create further demand for another 100 mtpa of domestic coal. The resultant gap of 200 mtpa needs to be bridged through commercial mining. Measures are already initiated to bring in commercial mining needs to be pursued with vigour to attain this target. More importantly, at the average clean environment cess of INR 400 per tonne, the additional contribution to the fund from this strategy will work out to INR 16,000 crores that can be utilized to push the renewable and clean environment agenda even harder!

Successful introduction of mining companies with proven experience with focus on best practices in mining and environment management holds the key to bring

competition in the coal mining space. This, in effect, will help the coal-based power companies to source coal at competitive price and thus become cost-competitive helping sustainability. In order to achieve this objective, the bidding process of the blocks for commercial mining needs to be different from the bidding process adopted so far for auction of blocks to captive users. The blocks should be large enough to sustain coal production at a commercial scale of say 30–50 million tonnes for a 20–30-year period. The selection should focus more on core competence in coal mining and proven experience than on the price offer. A quality and cost-based system (QCBS), which is widely practised and no less transparent, may be the preferable mode to identify the successful bidder.

The success of the suggested approach will essentially depend on creating an institutional mechanism to ensure pass through of the cost savings realised by the power generators to the ultimate consumers via Discoms. In the current context, generators are expected to sell power by executing long-term PPAs, where tariff is discovered through a bidding mechanism. In order to ensure competitiveness vis a vis the falling solar power tariff, it is suggested that such biddings are carried out seeking discount to weighted average solar tariff (WAST) over a period of 1 year prior to the month of bidding. The WAST is expected to gradually fall over time as technological breakthrough occurs. Setting this as a cap to the bidding process will ensure that the cost advantage accruing to the existing power plants from additional generation through improvement in PLF is passed on to the Discoms through the bidding process. In other words, the gain arising to the generators from all round efficiency in procurement of coal competitively and improvement in PLF is compellingly shared with the Discoms through a transparent market-driven process.

It needs to be highlighted in this context that even the benchmark WAST carries a built-in discount of roughly INR 0.50 per unit on account of the levy of clean environment cess of INR 400 per mt, since this adds to the cost of coal-based generation to the tune INR 0.25, and its use in subsidizing solar power has the effect of reducing solar tariff by another INR 0.25. Any discount provided by the successful bidder over WAST will be an additional benefit.

4 Meeting Multiple Nationally Desirable Objectives

The strategy as aforesaid meets multiple objectives of:

- (a) Encouraging additional generation of the least-cost coal-based power through the improvement of PLF of existing plants thereby relieving the country from the burden of huge cost of idle capacity.
- (b) Enhancing debt service capability of the Gencos and thereby avoid the adverse fallout on the average tax payer arising from non-servicing of bank loans.
- (c) Laying down a mechanism for sharing of the cost advantage gained by the generator with Discoms/consumers.

- (d) Enabling substantial growth in coal production to continue with consequential additional contribution to clean environment fund thereby supporting pursuit of clean agenda.
- (e) Creating a space for commercial coal mining to usher in successfully.
- (f) Reaping above benefits without hindering the systematic growth and development of solar and other forms of renewable power.
- (g) On the contrary, it makes effective use of the positive developments in the renewable space to drive down the coal-based power tariff through a bidding system benchmarked to WAST.
- (h) With a fast-rising generation of coal-based power, a breathing space gets created for calibrated infusion of renewable power drawing full advantage of the downward cost spiral in this field arising from disruptive technological innovation happening at a frantic pace.

The strategy outlined as aforesaid will lead to the coal production growing from the current level of around 650 mtpa to a sustainable level of 1050 mtpa in five years time. By that time, the existing coal-based capacity will be generating at optimum PLF, and no further coal demand is expected from this segment. The addition to coal-based capacity beyond those in the pipeline is questionable given the levels to which solar and wind tariff has fallen. The trigger for sustaining further growth in coal demand can, therefore, arise only from sectors other than power.

Beyond power generation, thermal coal finds use as feedstock in certain industries and also for conversion to liquid fuels and chemicals. The Sasol plant in South Africa is case to highlight. The plant came into operation long back mainly due to sanctions imposed on the country. It converts around 40 mtpa of coal, mined captively, to oil and more than 100 chemicals. It meets more than 25% of oil demand in SA. Because of backward and forward integration—coal mining on the back end and diverse range of downstream chemicals, the company has weathered the volatility of global oil prices over the decades very well and held its ground staying profitable.

The other example is China where substantial quantity of coal is converted to ammonia for use in manufacture of fertilizers. The technology developed in-house is fairly robust and cost-effective.

Indian dependence on import is substantial for both oil and ammonia/fertilizers. In fertilizers, while domestic production of urea, largely based on LNG, is close to 75% of demand, the share is substantially lower in case of complex fertilizers (NPK). Also, a large complement of ammonia required to produce NPK is imported. Availability of domestic gas for NPK is meagre and priority for allocation is low. Large Indian imports of ammonia and complex fertilizers are known to fuel cartelization creating an adverse impact on the price of such commodities. Fertilizer being a critical input to ensure food security, it is imperative that a strategy to reduce import dependence be implemented at the least possible time.

The aforesaid imperative can be squarely met by creating substantial capacity for the conversion of coal into oil, ammonia and chemicals based on proven technology long in use in other countries. As a result, the demand for coal as feedstock shall

continue to increase in the longer term supporting thereby a sustained growth in coal production.

It is important to contain the growth in coal production within the boundary conditions laid down by our commitments under COP21 at Paris. The two principal commitments to be achieved by 2030 are:

- (a) Renewable energy to have a minimum share of 40% in power generation capacity, increasing from the current level of 28%. With the implementation of the ambitious 175 GW power programme by 2022 based on renewable, this condition is expected to be achieved well ahead of time.
- (b) The emission intensity of GDP to be 33% lower than the corresponding number on the base year of 2005.

The GDP in 2030 is expected to be 5.8 times the GDP of 2005 assuming a CAGR of 7%. In order to meet the condition at b) the fossil fuel consumption in 2030 should be contained with 67% of 5.8, i.e. 3.9 times of 2005 consumption. Applying the factor on coal justifies a consumption of 1500 mtpa in 2030. Subtraction of 1050 mtpa of domestic coal and 100 mtpa of imported coal for power generation leaves a balance of up to 350 mtpa of coal for alternate uses as feedstock for production of oil and ammonia. In other words, the strategy described earlier is fully consistent with COP 21 commitments.

The suggested growth in coal production from the current level of 650 mtpa to a maximum of 1500 mtpa by 2030, though consistent with COP 21 commitments, will call for more aggressive handling of the resultant issues of social and environmental sustainability. This is not to suggest that these are not being handled currently. The statutory requirements are being generally met, particularly with coal mining being predominantly in the government sector. The focus on addressing these issues acquired renewed thrust in 2009–10 as Coal India Ltd commenced preparation for its stake sale through initial public offer (IPO) that eventually turned out to be the largest Indian IPO so far and one of the top 3 globally in 2010. A landmark effort was a GIS application to determine the adequacy or otherwise of the restoration and reclamation activities in opencast mines through annual satellite surveillance. It established in no uncertain terms the adequacy of restoration and reclamation in the top 50 opencast mines. This eventually led to these mines securing ISO 14001 certification. Incidentally, this GIS application won global recognition at a function held at Netherlands in 2012.

The other highlight was the practice adopted for afforestation of large OB dumps post-biological reclamation. Most of these mines required diversion of forest land and hence afforestation was a binding imperative. It transpired that over the decades for every hectare of forest land subsumed in coal mining, roughly 2.5 hectares of land have been afforested! Any doubt on the quality of forest created was dispelled by the exercise carried out by the ministry of environment and forest (MOEF) through the Forest Research Institute of India using satellite imagery. This was to identify high-density forests for designating those as NO GO zones. Quite a few of these afforested areas got listed as NO GO areas!!

While the aforesaid are instances of well-meaning practices to address the environmental sustainability issues, there are good instances of managing the social issues as well. Creation of rehabilitation villages for displaced persons, mostly tribals, with modern amenities including healthcare and education are fairly commonplace, particularly for large projects. Care is also taken to enable the community preserve their heritage and culture despite exposure to modern amenities. Employment or indirect engagement of project affected persons (PAP) to create more livelihood and income opportunities as compared to the scenario before the project is taken up, holds the key to securing community buy-in for the project.

Coal mining in India is mostly in backward areas with a preponderance of BPL and Tribal population. The livelihood opportunities are in most cases grossly inadequate. The benefits of resettlement and rehabilitation, as well as direct and indirect employment centring on the mines, make a significant addition to decent livelihood opportunities. Viewed in this context, coal mining promotes sustainability of human life in some of the backward areas for the underprivileged section of the population. Besides, the aggressive focus of mining companies on afforestation creates avenues for harnessing forest produce to help create more livelihood opportunities among tribals and backward classes.

Nevertheless, it needs to be acknowledged that the current practices do leave scope for further improvement in these areas. The restoration of land in large opencast mines usually implies creating a biologically well-reclaimed afforested hillock out of the over burden dump which originally was a levelled piece of land. Thus, coal mining alters the land use, impairing the usefulness of mined-out areas significantly. The global best practice of restoring land to its original form is largely absent, even in cases where the strip ratio is not much enough to impede such practice. Further, in the area of dust suppression by use of water sprinklers, the domestic practice is yet to catch up with global best. In the later case, water is used to create a fine spray that settles the dust to the soil without creation of watery mud. India needs to encourage manufacture and use of such high-quality sprinklers. In quite a few cases, extensive use of water sprinklers often leads to creation of muddy areas with the resultant inconvenience to people making place in the print media with pictures!

However, the coal producers alone cannot be blamed for this state of affairs. Domestic coal in India has to bear a significant burden of state royalty besides the clean environment cess. It stands to reason that states plough back a portion of the cess collected to improve the quality of life of people around the mines. Sharing the financial costs by the state in part will help the coal producer to stay cost-competitive.

The convergence of domestic practices for social and environmental sustainability to global best practices is expected with India opening up coal mining to global majors through a transparent bidding process.

The low-cost coal-based development strategy intensively pursued by China over five decades has transformed it into a giant superpower capable of meeting consumption needs of not only its own people but also the global population. Its per capita income is substantially higher and the economy is cost-competitive. Its

balance of trade is highly in its favour with exports exceeding imports by a wide margin. The strategy has triggered a rethink today due to its share in global emission exceeding its share of population by a wide margin. The situation in India is reverse. It should, therefore, allow us to comfortably pursue the low-cost coal-based development strategy intensively for at least two decades, allowing at the same time the renewable sector to grow in a calibrated manner to gain out of continuous technological innovation happening in that sector. This is expected to bring in faster least cost-inclusive growth.

5 Conclusions

Availability of better quality of coal with low ash and high GCV is restricted in India to the coalfields of Rani Gunj and a part of Jharia in the eastern part of the country and Korea Rewa in central India, mainly from underground mines. The coal production from these mines/coalfields has stagnated or, in most cases, are declined due to difficult geo-mining conditions and high cost. Post-nationalization, the growth in coal production has arisen mostly from Talcher, Korba and Rajmahal (lower grade) as well as North Karanpura and Singrauli (medium grades). However, the boiler design evolved over the period acquiring capability of running on such low-grade coal. The inferior quality of coal in India is a constraint arising from the coal formation being largely based on 'drift' as opposed to 'insitu'

The ability of the generators to use inferior grade coal due to improved boiler technology has significantly diluted the demand for coal washing so far. The rather poor state of coal washing in India is attributable to reluctance of the consumers to accept the cost of coal washing consequently disincentivize the coal producer to set up washeries. The gains arising from cost savings on account of extending boiler life, lesser ash disposal and handling need to be weighed against the cost of washing, and a net advantage to consumer established before coal washing gets the much-needed policy push.

Most Indian mines are not gassy. Only 4% of the mines are gassy. This restricts the scope of CBM in India, unless technological breakthrough in terms of microbial enhancement of CBM gas becomes a reality. This is a long-drawn research project that needs to bring together outcome of research happening globally in this field. Serious efforts are yet to commence in this direction.

Gas Hydrates as a Potential Energy Resource for Energy Sustainability

Vishnu Chandrasekharan Nair, Pawan Gupta and Jitendra S. Sangwai

Abstract Energy is an essential commodity for the survival and socioeconomic development of the human race. The energy supply sector primarily comprises of industrial, commercial, and domestic applications. The foremost challenges faced by the energy supply sector are growing consumption levels, limited accessibility, environmental concerns, viz-a-viz, climate change, and pollution of water and air resources. As conventional resources of energy have started to decline and are expected to get exhausted by 2040, the main focus has been shifted to unconventional sources [1]. In this category, natural gas resources such as gas hydrate, shale gas, coal bed methane will provide tremendous potential for meeting the demand. Gas hydrates are ice-like crystalline substance formed by a framework of water and natural gas molecules. Recent exploration programs by various agencies such as United States Geological Survey (USGS), National Gas Hydrate Program (India), Japanese Methane Gas Hydrate R&D have proved that massive amount of gas hydrate deposits lying across marine settings and permafrost environments. Hydrate deposits are currently estimated to be $5 \times 10^{15} \text{ m}^3$ of methane gas [2]. If this untapped resource of energy becomes feasible for the economic production, it could increase natural gas reserves to multifold. Moreover, this would be considerably greater than the total amount of all fossil fuels together. As reported by USGS, gas hydrates hold more than 50% of the entire world's carbon. It has been estimated that commercial production of methane from 15% of natural gas hydrate can fulfill the energy requirement of the entire world for next 200 years [3]. Hence, natural gas hydrates are considered to be the vital sustainable energy resource. Many pilot production tests have been completed and are underway to recover methane from gas hydrate deposit across the world [4]. Preliminary studies and pilot tests have shown promising results in terms of methane recovery from natural gas hydrates by employing methods such as thermal stimulation, depressurization, inhibitor injection. Ongoing gas hydrate research programs throughout the world and advances in technology will certainly help to cater any technical challenges in

V. C. Nair · P. Gupta · J. S. Sangwai (✉)

Gas Hydrate and Flow Assurance Laboratory, Petroleum Engineering Program, Department of Ocean Engineering, Indian Institute of Technology Madras, Chennai 600036, India
e-mail: jitendrasangwai@iitm.ac.in

order to potentially harness the huge amount of energy stored in the form of natural gas hydrates.

Keywords Gas hydrates · Gas hydrate occurrence · Natural gas production Storage · Sustainable future energy

1 Introduction

1.1 Energy and Future Challenges

Energy is one of the main drivers of the economic and social development of the nation. A major chunk of energy today is derived from conventional fossil fuel such as coal and oil. Rapid growth and improving prosperity is the reason behind the growth in energy demand. Rising energy demands, uncertainty in supply, and the need to reduce release of greenhouse gases lead to an uncertain energy prospect. Just a few years ago, uncertainty in energy supplies rose the prices of oil and gas. The rate of growth of non-conventional resources of energy such as hydropower, solar energy, and wind power is much slower than expected. Solar power still accounts for just 1% of electricity generation worldwide while oil, coal, and natural gas still account for more than 80% of the primary energy need. It is predicted that by 2050, the energy demand is likely to get doubled [1]. However, the major contributors to the energy basket will still be the same, viz., coal, oil, and natural gas. The burden on fossil energy resources may rise to the threshold limit and contribute to more uncertainty on energy future and rise in pollution [5]. Energy prices and its highly related volatility certainly will lead to an unclear path for the future. A faster change in politics, consumer anticipation, and technological improvement is making energy market more and more complex. The Paris agreement on climate change brings together nations to reduce the greenhouse gas emissions and use energy efficiently. This also represents the determination of nations to cut down the level of pollution by moving to a clean energy system. Several countries have started to recognize the importance of alternate energy sources with lowest greenhouse gas emission [6].

1.2 Natural Gas and Its Sources

Natural gas composed mainly of methane. It is colorless, odorless, and shapeless. It releases about 1000 btu/ft³ of energy when burned [7]. It is now widely used in domestic applications like water heating, coking, space heating, power generation and as a chemical feedstock for making fertilizer [7]. New discoveries of conventional reservoirs and development of unconventional reservoir and their associated gas resources have opened up fresh gas frontiers. This resulted in more

widespread presence of gas around the world geography. Gas trade has now been dominated by gas pipeline transportation, and long-distance trade has increased significantly in a recent decade. The usage of natural gas has been increased with the development of transportation concepts, viz, gas liquefaction, gas compression, and regasification. Power generation has now been the main driver of natural gas consumption. Natural gas is likely to play a vital role in the transition from carbon-constrained economy to closed carbon-free economy by replacing the coal and by compensating the shortfall in output of the present source of energy. For these reasons, there has been a significant increase in exploration, field development, and gas production activities.

Natural gas hydrates (NGH) have gained a huge attention nowadays among unconventional resources of energy [8]. Methane is the main constituent in the gas hydrates and an important component in natural gas. The gas hydrate can hold enormous amounts of methane into its structure [9]. Recent exploration programs by various agencies such as United States Geological Survey (USGS), National Gas Hydrate Program (India), Japanese Methane Gas Hydrate R&D suggest that enormous deposits of gas hydrates occur in marine settings and permafrost environments. Hydrate deposits are currently estimated to be $5 \times 10^{15} \text{ m}^3$ of methane gas [2]. If this untapped resource of energy becomes feasible for economic production, it could increase natural gas reserves to multifold. Moreover, this would be considerably greater than the total amount of all fossil fuels together. As reported by USGS, gas hydrates hold more than 50% of the entire world's carbon. Commercial production of methane from 15% of natural gas hydrate is able to fulfill the energy requirement of the entire world for next 200 years; hence, natural gas hydrates are considered to be a vital sustainable energy resource [3, 10].

2 Gas Hydrates

Gas hydrate was discovered by Sir Humphrey Davy in 1810. After the discovery, gas hydrate was only an educational inquisitiveness for more than centuries because there was no practical application discovered for these laboratory-made hydrates. Only after 1934, it was noticed that an ice-like substance was plugging the oil- and gas-transporting pipelines. Hammerschmidt [11] first discovered that this ice-like substance is nothing but gas hydrate. Until the 1950s, the chemical structure of gas hydrate was unknown [9]. Use of X-ray diffraction has revealed that gas hydrates does not have fixed chemical composition. They are the crystalline structure of water in which small guest gas molecules are trapped within a host lattice structure of water. The physical conditions (stability) necessary to form gas hydrates have been put forward by Makogon [12]. He predicted that gas hydrates exist few hundred meters below the surface. The drilling programs conducted in permafrost region in Arctic have confirmed this hypothesis. Since then several drilling programs and expeditions have established the presence of vast resource in the form of gas hydrate around the world.

2.1 Structural Information of Gas Hydrate

Gas hydrates resemble like crystalline ice structure formed by a framework of host molecules and guest molecules under low-temperature and high-pressure environment. Different types of structures emerge during the interaction of water and gas framework, such as sI, sII, and sH, constituting of small and large cages. The ratio of free cage diameter to the size of guest molecules decides the structure. The cages formed by water molecules in methane hydrate should be partially filled (>70%) to form a stable hydrate [13]. The percentage occupancy of the small and large cages can fluctuate, depending on the pressure, temperature, and the types of guest gas. As a consequence, these structures categorize as non-stoichiometric compounds. It is found that methane hydrate has a configuration of $8\text{CH}_4 \cdot 46\text{H}_2\text{O}$. Various guest gas molecules which form hydrate structure are methane, ethane, propane, carbon dioxide, nitrogen, etc. Methane is the most common gas that forms hydrate naturally. Figure 1 shows different types of hydrate structures. The most common clathrate structure sI forms in the presence of methane and any other guest

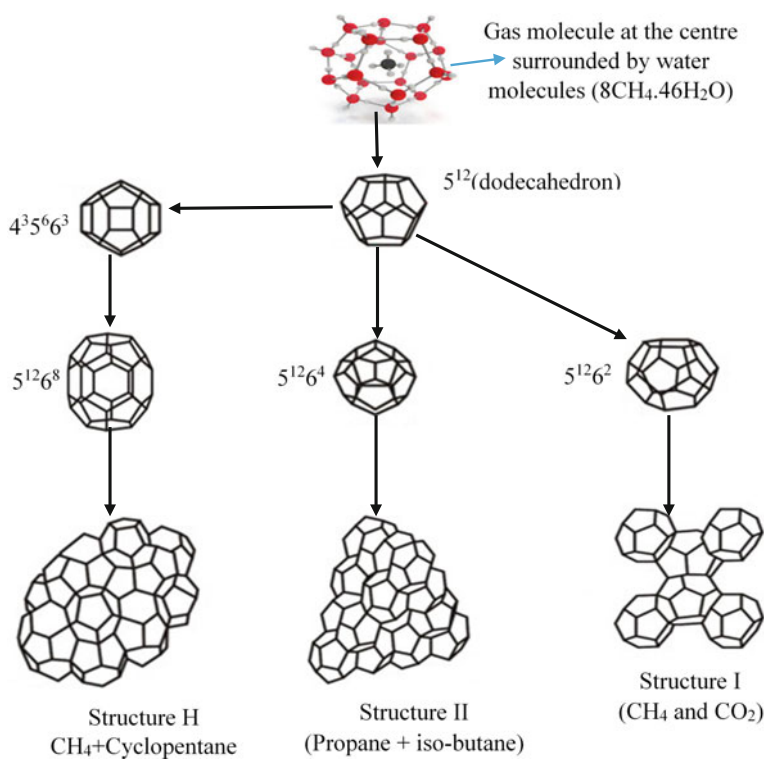


Fig. 1 Typical gas hydrate structure (Example: $4^3 5^6 6^3$ cavity signifies, 3 square faces, 6 pentagonal faces, and 3 hexagonal faces [61])

molecules with diameters lying between 4 and 6 Angstroms (Å). A unit cell, of the Structure I hydrate lattice consists two smaller cavities and six larger cavities enclosed by 46 water molecules. When the size of gas molecules (such as ethane, propane) increases beyond 6 Å, another structure sII may form. A unit cell of the Structure II hydrate lattice consists of 16 smaller cavities and eight larger cavities enclosed by 136 water molecules. Another bigger structure sH has also been noticed when the size of gas molecules are larger than 7 Å. Typically, the formation of structure sH has been seen for the molecules with size lying between 7 and 9 Å. Field studies suggest that the most common structure found naturally are structure sI and sII. The occurrence of structure sH is extremely uncommon [9].

2.2 Energy Density of Gas Hydrates

The energy density of gas hydrate is enormous. A unit volume of hydrate contains almost 172 m³ of methane in its structure. The storage capacity calculation for pure methane hydrate is discussed below. Method 1 is used to calculate the storage capacity of pure methane hydrate using the information on the density of hydrate, while method 2 uses the structural information to calculate the storage capacity of pure methane hydrate. It can be observed that both the approaches resulted in similar hydrate storage capacity.

2.2.1 Method 1

The storage capacity is defined as the volume of methane that can be accommodated in unit volume of hydrate. The storage capacity of hydrate was calculated earlier [14] and has subsequently been used by other researchers [15] to find out storage capacity of clathrate hydrate.

$$V_{gh} = \frac{1000 \cdot V_g \cdot \rho}{M_h} \quad (1)$$

where V_{gh} is the volume of gas in the unit volume of hydrate at hydrate formation temperature and pressure; V_g is the molar volume of the gas; ρ is the density of the hydrate; M_h is the molecular weight of molar hydrate.

Density of hydrate can be calculated as follows [9]:

$$\rho = \frac{N_w \cdot MW_{H_2O} + \sum_{j=1}^c \sum_{i=1}^N \theta_{ij} \cdot \vartheta_i \cdot MW_j}{N_{ava} \cdot V_{cell}} \quad (2)$$

where N_w is the number of water molecules per unit cell; N_{ava} is the Avogadro number; MW_j is the molecular weight of component j ; θ_{ij} is the fractional occupancy of cavity i by gas component j ; i is the cavity type; j represents the

component in hydrate; v_i is the number of type i cavity per water molecule in unit cell; V_{cell} is the volume of unit cell; N is the number of cavity type in unit cell; c is the number of component in hydrate phase.

Density of pure hydrate for structure I, fully occupied by methane gas is calculated by Eq. (2). Following data is taken from the literature [9]; $N_w = 46$; $V_{\text{cell}} = (12 \text{ \AA})^3$; $\Theta_{ij} = 1$ (for both the cavity); $v_{i=1} = 2$; and $v_{i=2} = 6$

$$\begin{aligned}\rho &= (48 \times 18 + 2 \times 16 + 6 \times 16) / \left(6.023 \times 10^{23} \times (12 \times 10^{-8})^3 \right) \\ &= 0.91854 \text{ g/cm}^3\end{aligned}$$

$M_h =$ molecular weight of methane + $18.02 \times$ hydration number = $16 + 18.02 \times 5.75 = 119.615 \text{ g}$.

Using Eq. (1) (considering STP conditions),

$$V_{\text{gh}} = (1000 \times 22.4 \times 0.91854) / 119.615 = 172 \text{ m}^3 \text{ (STP)} / \text{m}^3 \text{ of hydrate}$$

For pure methane hydrate, storage capacity value turned out to be $172 \text{ m}^3 \text{ (STP)} / \text{m}^3$ of hydrate (V/V) for a hydrate density of 0.91845 g/cm^3 . It is also found to be 182 m^3 at $60 \text{ }^\circ\text{F}$ and 1 atm using above equation.

2.2.2 Method 2

The storage capacity can also be calculated if the structure of hydrate forming species is known. With the advent of new technologies such as NMR and Raman Spectrometry [16], it has become possible to know the structure of hydrate. The storage capacity for the cubic-structured pure methane hydrate is calculated below [17]. For structure I cubic hydrate, there are total eight cages where methane gas can be trapped [9]. The volume of the unit cubic cell of hydrate with 12 \AA as the side of the cube having full occupancy is $(12 \times 10^{-10} \text{ m})^3 = 1.73 \times 10^{-27} \text{ m}^3$.

Number of gas molecules in 1 m^3 of hydrate = $8 / (1.73 \times 10^{-27} \text{ m}^3) = 4.63 \times 10^{27}$ molecules.

It is also known that there are 6.023×10^{23} molecules in 1 g mole of gas (Avogadro number).

Therefore, g mole gas in 1 m^3 of hydrate = $(4.63 \times 10^{27}) / (6.023 \times 10^{23}) = 7.69 \times 10^3 \text{ g moles}$.

The volume of gas occupied by 1 g mole gas is 22.4 L at STP conditions (273 K and 1 atm).

Hence, the volume of gas stored in 1 m^3 hydrates = $(7.69 \times 10^3) \times (22.4) = 172,179 \text{ L} = 172 \text{ m}^3$. Therefore, one m^3 of gas hydrates can store 172 m^3 of gas at STP conditions (same as method-1).

Tables 1 and 2 shows the parameters used for calculating hydrate volume. Additionally, this method of calculation can be utilized to find the storage capacity in the presence of other gases, inhibitors, and promoters in hydrate structure [17].

Table 1 Details of parameter for method 1

Structure of hydrate	8CH ₄ .46H ₂ O
Type of hydrate	Pure water hydrate
Number of water molecules in unit cell	46
Molecular mass of water	18.02
Fractional occupancy	1
Number of small and large cavity	2, 8
Molecular mass of component in small and large	16(CH ₄), 16(CH ₄)
Volume of unit cell in cm ³	1.728×10^{-21}
Avogadro number	6.023×10^{23}
Mass of hydrate(1 mol of CH ₄)	119.615
Density of hydrate	0.9185
Volume/volume(storage capacity)	172.01

Table 2 Details of parameter for method 2

Structure of hydrate	8CH ₄ .46H ₂ O
Type of hydrate	Pure water hydrate
Number of methane gas molecules in unit cell volume of hydrate	8
Volume of unit cell in m ³	1.728×10^{-27}
Molecules of gas stored in 1 m ³ of hydrate	4.62963×10^{27}
Number of molecules in 1 g moles	6.023×10^{23}
Gram moles of gas in 1 m ³ of hydrate	7686.58
1 g moles of gas occupies liter at STP condition	22.4
Gram moles of gas in 1 m ³ of hydrate will occupy in liters	172179.5
1 m ³ of hydrate will occupy in m ³ of methane gas	172.18
Volume/volume(storage capacity)	172.18

3 Worldwide Occurrence of Hydrate

Gas hydrates are found worldwide below seafloor and permafrost regions. More than 230 natural gas hydrate deposits were identified worldwide with the majority in marine settings [18]. The existence of natural gas hydrate is basically dependent on factors, such as pressure, temperature, nature, and composition of the gas, and the environment. There is a huge amount of natural gas preserved in the form of natural gas hydrate. The estimates on methane gas preserved as natural gas hydrate vary from $1.4 \times 10^{13} \text{ m}^3$ [19] to $3.4 \times 10^{16} \text{ m}^3$ [20] in permafrost regions and from $3.1 \times 10^{15} \text{ m}^3$ [19] to $7.6 \times 10^{18} \text{ m}^3$ [20] in marine settings. This amount surpasses the combined amount of all other fossil fuels. Figures 2 and 3 show the detailed world map and Indian subcontinent map of gas hydrate inferred and recovered locations. From Fig. 2, it is clear that countries like USA, India, China, Japan, and Canada are having good amount of known hydrate reserves. The temperature, pressure, and surrounding environmental conditions influence the existence of gas hydrates. Figure 4 shows the depth-temperature zones at permafrost and marine environment where natural gas hydrates are stable. From the figure, it can be inferred that hydrates can be possibly found 200–1100 m deep in permafrost and 1200–1500 m below sea level in the marine environment [21, 22]. However, in certain regions like Arctic, the hydrate occurrence depth ranges from 200 to 1100 m below the sea level. Also, in Antarctica, it ranges from 300 to 700 m [22, 23].

Though the quantity of natural gas hydrate is huge, the numbers of technically recoverable reserves (TRR) are limited so far. The main reason attributed to this limited TRR is the low capability of current technologies for the hydrate dissociation and the recovery of methane from the natural gas hydrate reservoir. Figure 5 shows a simplified hydrate resource pyramid with current TRR to understand the importance of the development of technology for tapping this huge energy reserve for the future energy sustainability. Collet et al. [21] demonstrated a hydrate

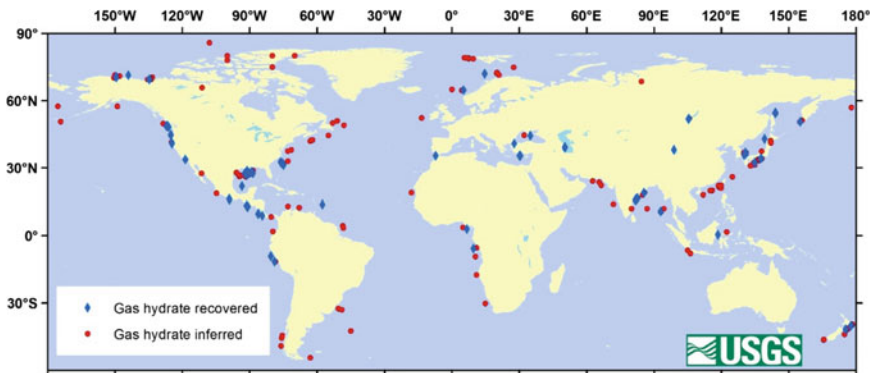


Fig. 2 World map of gas hydrate inferred and recovered locations (courtesy, USGS Gas Hydrates Project)

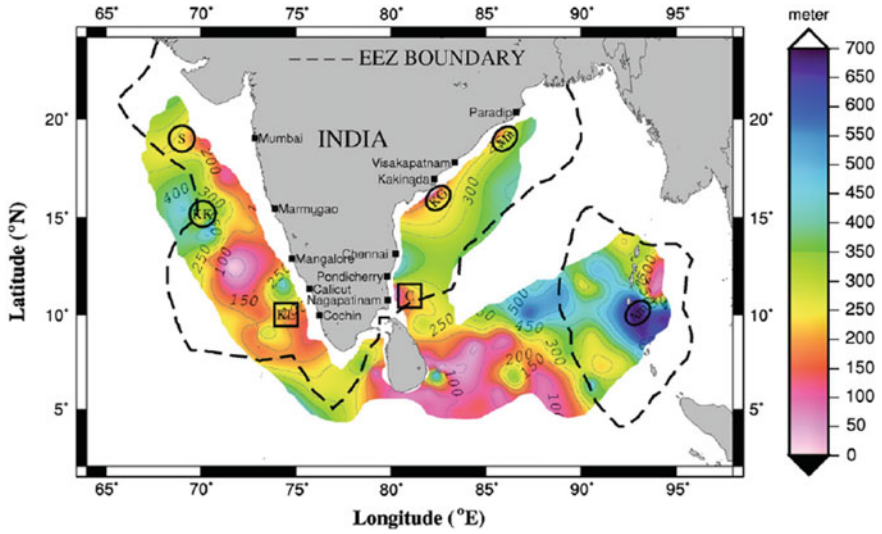


Fig. 3 Gas hydrate accumulation in Indian subcontinent [62]

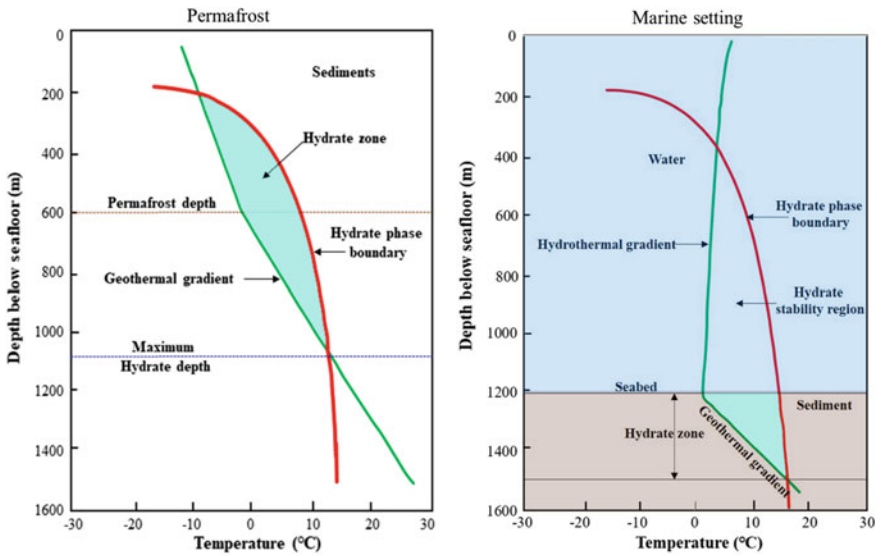


Fig. 4 Depth-temperature zones at permafrost and marine environment where natural gas hydrate is stable [63]

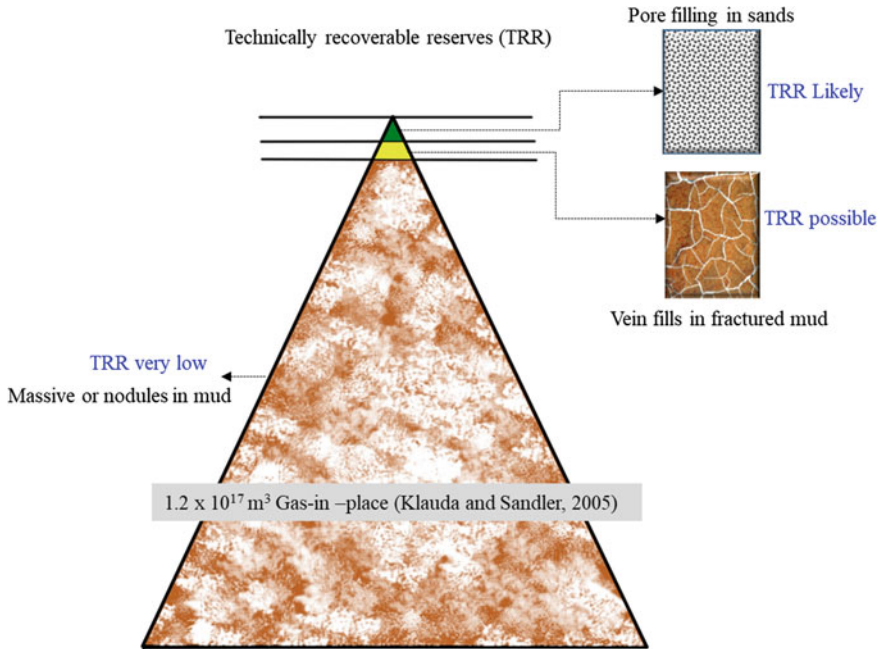


Fig. 5 Simplified hydrate resource pyramid with current TRR

resource pyramid by arranging the natural gas hydrate deposits according to the gas-in—place and reservoir quality. Figure 6 shows resource pyramid of the different types of hydrate accumulations.

3.1 Gas Hydrate Petroleum System

Similar to the conventional petroleum system, natural gas hydrate petroleum system has been proposed for a better understanding of natural gas reservoir [21]. The gas hydrate petroleum system includes the following components:

- (1) Gas hydrate stability conditions
- (2) Gas source
- (3) Availability of water
- (4) Migration of gas
- (5) Reservoir rocks
- (6) Timing

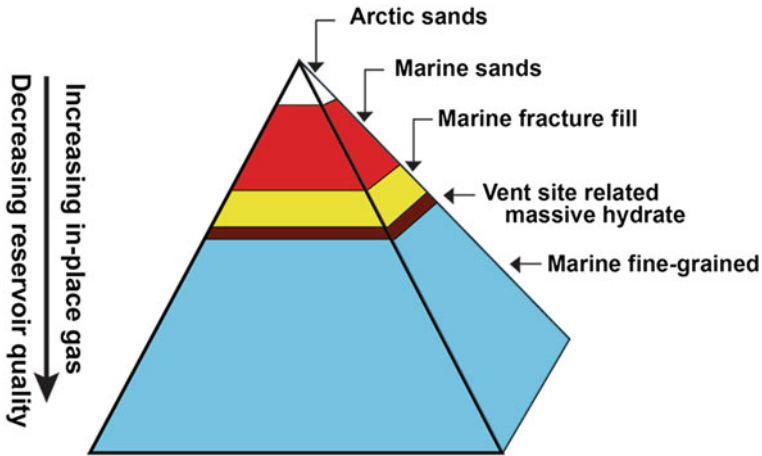


Fig. 6 Resource pyramid of the different types of hydrate accumulations [64]

3.1.1 Gas Hydrate Stability Conditions

Natural gas hydrate is stable within certain conditions as per the hydrate phase equilibrium. The favorable conditions for the hydrate formation are low temperature, high pressure, low pore-water salinity, and presence of higher molecular weight hydrocarbon gases.

3.1.2 Gas Source

The gas source for the formation of natural gas hydrate is microbial and thermogenic origin. A lot of hydrocarbon gases from these sources are a primary requisite for a gas hydrate reservoir. It has been experimentally shown that the availability of huge quantities of gas from both thermogenic and microbial origin plays an important role in controlling the formation and distribution of gas hydrates [24–26].

3.1.3 Availability of Water

As hydrate formed by the entrapment of gas molecule inside the water cages, availability of water is essential for the hydrate formation. The gas/water ratio of sI and sII gas hydrate is 8:46 and 24:136, respectively [21].

3.1.4 Migration of Gas

After the gas generation (thermogenic/biogenic origin), methane and other hydrocarbon gases migrate within the sediments depending on the formation type and structure. Migration occurs mainly by three processes [21, 27]:

- (1) Dissolved gas in water and migrating with it
- (2) Diffusion
- (3) Buoyancy.

3.1.5 Reservoir Rocks

Hydrate found in nature associated with fine-grained muds to coarse-grained sands. The gas hydrate reservoir rock can be of (1) Coarse-grained rocks; (2) Hydrate nodules dispersed in fine-grained rocks; (3) Fractured rocks; or (4) Massive hydrate mounts with a minimum amount of sediments [9, 21].

3.1.6 Timing

Unlike in petroleum system, gas hydrate forms its own trap. The timing of gas generation and time of trap formation are not affecting much in the accumulation of natural gas hydrate.

3.2 Classification of Reserves

3.2.1 Classification Based on Sediment Type

Gas hydrate reservoirs are classified on the basis of sediments types, in which three types of gas hydrate accumulations are observed. Clay dominated, such as in Blake plateau lying in the western Atlantic Ocean [28], sand dominated, like the Eileen Tarn gas hydrate petroleum system in Northern Alaska [25, 29] and complex gas hydrate reservoirs (clay with limited silt/sand) like in KG basin of offshore continental margin of the Indian Peninsula [30].

3.2.2 Classification Based on Initial Reservoir Conditions

Based on initial reservoir condition, gas hydrate reservoirs are classified into four classes. Class 1 consists of two zones, a hydrate-bearing zone and an underlying two-phase fluid zone with mobile gas and liquid water. Class 2 entails hydrate-bearing layer overlying a mobile water zone. Class 3 has a single

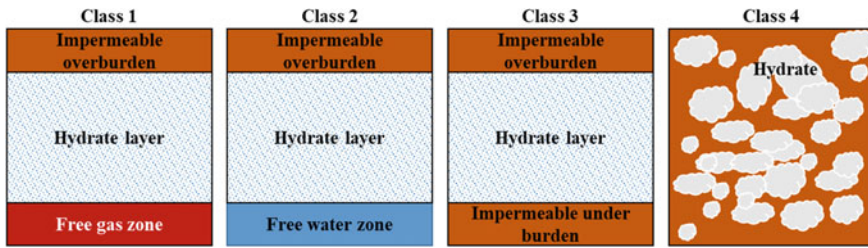


Fig. 7 Hydrate reservoir classification based on initial reservoir conditions

hydrate-bearing layer, which has no underlying mobile fluid zone. Class 4 has many oceanic accumulations consisting of dispersed low-saturation natural gas hydrate deposits which lacks confining geologic strata and may not be a desirable system for gas production. Figure 7 shows the schematic representation of all classes of gas hydrate reservoirs [31, 32].

3.2.3 Classification Based on Geological Features

Another classification of gas hydrate reservoirs is based on their geological features. This can be of (a) pore filling in the pore spaces of sediments; (b) fracture filled with hydrate in the natural fractures of formation; and (c) massive or nodules of hydrate in fine-grained sediments [32].

4 Gas Production Methods Form Hydrates

At the initial reservoir condition, the in situ pressure and temperature falls within the methane hydrate stability region. By shifting the phase toward the unstable region (low pressure high temperature), hydrate can be dissociated into water and natural gas [9]. There are many methods proposed for the dissociation of natural gas hydrate and production of methane from the hydrate reservoir. The most common approaches for the natural gas production from hydrates are thermal stimulation, depressurization, inhibitor injection, and gas replacement/exchange. All these methods primarily depend on the phase stability alteration of hydrate. In thermal stimulation, the hydrate reservoir temperature increases above the phase equilibrium temperature of the methane hydrate, while depressurization decreases the hydrate reservoir pressure below the methane hydrate equilibrium pressure. During inhibitor injection, a hydrate inhibitor is injected into the reservoir to dissociate hydrate. The injection of inhibitor shifts the phase equilibrium condition toward the low-temperature and high-pressure region. In gas replacement/exchange, a gas (such as carbon dioxide) which forms hydrate under high temperature and low pressure compared to methane is injected into the reservoir to exchange the

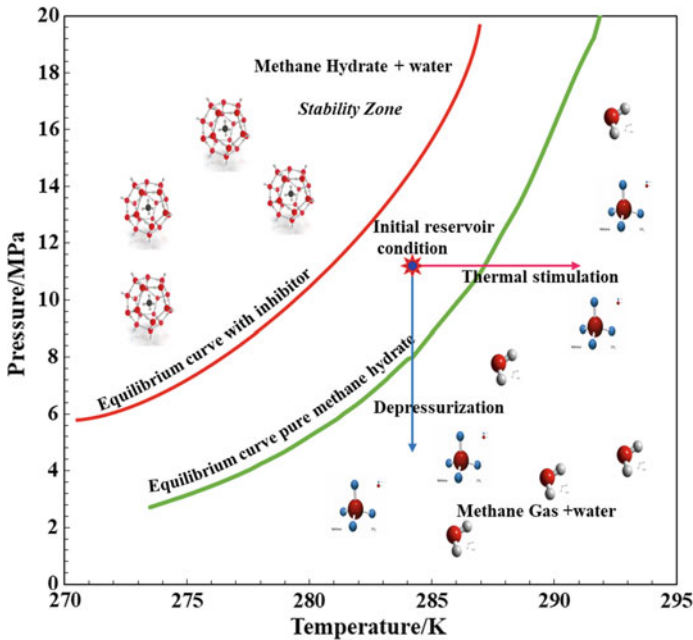


Fig. 8 Different methane production methods from the gas hydrate reservoir

methane with the injected gas, so as to release the natural gas. The combination of these methods can also be employed for the production of methane from the gas hydrate reservoir. Figure 8 shows the different methane production methods from the gas hydrate reservoir.

4.1 Thermal Stimulation

Thermal stimulation can be employed by the injection of hot water/gas into the hydrate reservoir to promote methane hydrate dissociation by means of increasing reservoir temperature. As illustrated in Fig. 8, thermal stimulation method aims to increase the temperature in the vicinity of a well. It includes hot water/gas circulation method in which the bottomhole temperature is raised by circulating hot water inside the wellbore. In wellbore heating method, heaters are installed in the downhole to increase the near wellbore temperature, and in hot water huff'n'puff method, injection of hot water into the reservoir is provided from a well (huff). The heat from the water is then transferred to the reservoir (soak) by shutting the well for a certain period of time, and then the well is opened for production (puff). In thermal flooding, hot water is injected from the injection well and flooded toward production wells to increase the temperature and thereby dissociating the hydrate between these wells. On applying hot water circulation and wellbore heating

methods, the reservoir temperature exceeds the phase equilibrium temperature of natural gas hydrate and hydrate dissociation thereafter [33–36]. The first ever successful methane gas production from a hydrate reservoir was conducted at the Mallik site in Canada in the year 2002 which applied hot water circulation method [37]. However, the application of the thermal methods is under dispute in terms of energy efficiency since these methods require a large supply of energy.

4.2 *Depressurization*

In the depressurization method, dissociation of gas hydrate is induced by reducing the bottomhole pressure using a pump installed in the downhole and transferring this low pressure to the reservoir to propagate the dissociation front thereby dissociating the hydrate. Due to the high energy efficiency of depressurization method, it has gained huge attention among other production methods [38, 39]. The energy required for the hydrate dissociation during depressurization derives from the energy contained in surrounding formation [40]. The methane production decreases after the sensible heat in the reservoir is exhausted [41]. Besides, during depressurization, the formation of ice and the reformation of hydrate may occur due to the endothermic hydrate dissociation which hinders the methane production [9, 42, 43].

4.3 *Inhibitor Injection*

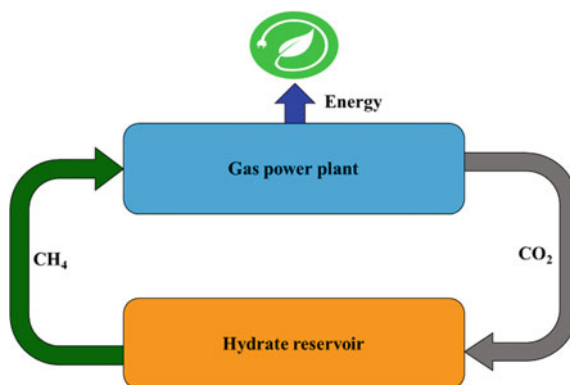
Thermodynamic hydrate inhibitors such as salts, alcohols, glycols are injected into the hydrate reservoir to dissociate the hydrate and produce the natural gas. It shifts the hydrate equilibrium curve toward the high-pressure and low-temperature region. Due to the small shift in the equilibrium curve, significant hydrate dissociation may not be achieved. Also, there are practical limitations in the injectivity of inhibitors into the low permeable hydrate reservoirs [44–46]. Table 3 shows different inhibitors used by the industry for gas hydrate dissociation.

4.4 *CO₂ Sequestration*

CO₂ sequestration is another viable method for the production of natural gas from a gas hydrate reservoir. As CO₂ hydrate forms at much lower pressure and higher temperature, injection of CO₂ into the methane hydrate reservoir will replace the methane with CO₂ [47, 48]. This method can be very effective in places where the availability of CO₂ is not a concern or it can be connected to a gas power plant nearby [49, 50]. The CO₂ produced from the power plant can be injected into the hydrate reservoir, and the produced methane gas can be used for the energy production from the power plant (Fig. 9).

Table 3 Various inhibitor used by the industry for dissociation of hydrate

Sl. no.	Methane hydrate inhibition at 10 wt%	Average freezing temperature depression (approx.) (K)	References
1	Methanol	3.05	Sloan and Koh [9]
2	Ethylene Glycol	1	Sloan and Koh [9]
3.	Tri-ethylene Glycol	1.1	Sloan and Koh [9]
4.	Sodium Chloride solution	1	Sloan and Koh [9]
5.	Ionic liquids	0.9	Xiao et al. [65]

**Fig. 9** Closed carbon cycle: Methane production, energy generation, and CO₂ sequestration

4.5 Combined Methods

Depending on environmental conditions and reservoir features like permeability and saturation, single production method may not be a viable option for the production of methane from a natural gas hydrate reservoir. So, in these circumstances, a combination of the common production methods may be feasible. For example, in case of low-temperature reservoirs, depressurization combined with thermal stimulation can be a feasible option [51]. This will help to avoid ice formation or hydrate reformation during depressurization [43].

4.6 Unconventional Methods

For the dissociation of natural gas hydrates, many unconventional methods are gaining research interest nowadays. Electrothermal heating, gas lift, ultrasonic wave irradiation method, mining are some of the examples (Table 4).

Table 4 Major production methods with their advantages and limitations

Sl. No.	Production method	Basic principle	Advantages	Limitations
1	Thermal stimulation	Increasing the temperature above hydrate phase equilibrium temperature	Best suitable for low-temperature high-permeable reservoirs	High energy loss to the surrounding formation
2	Depressurization	Decreasing the pressure below the hydrate equilibrium pressure	High energy efficiency ratio	Ice formation/hydrate reformation may happen to hinder the dissociation front propagation
3	Gas injection/ CO ₂ sequestration	Replace/exchange of gas with methane	Least impact on the formation	Availability of huge quantities of exchange-gas/CO ₂ is a concern
4	Inhibitor injection	Shifts the equilibrium curve to high-pressure and low-temperature region	Very effective, when combined with thermal flooding methods	By inhibitor injection alone, significant hydrate dissociation cannot be expected due to the small shift of the phase equilibrium. Environmental concern related to the manufacturing, handling, and disposal of chemicals
5	Electro-Thermal heating	Increasing the temperature above hydrate phase equilibrium temperature	Easily implemented and can be operated remotely	Limited depth of penetration
6	Combined methods	Simultaneously increasing the temperature and decreasing the pressure	Reducing the limitations of individual methods	Good amount of reservoir data is a prerequisite
7	Mining	Mining hydrate out of the reservoir	Best suitable for unconfined highly saturated reservoirs	Not a viable option for hostile and deep sea environments

5 Gas Hydrate Production Initiatives and Field Tests

With the collaboration of US Department of Energy (DOE) and the US Geological Survey (USGS), investigation on gas hydrate as a energy resource has begun in the 1980s. USGS in 1995 estimated a total 9×10^{15} cubic meters (STP) of domestic hydrate resource, which was the first systematic and scientific assessment on a hydrate resource. Encouraged by this statistics, under the direction of Department of

Energy and USGS, the Methane Hydrate Research and Development (MHR&D) has been enacted in the year of 2000. The main objective of MHR&D is to reveal the geographical features, economic potential, and environmental role of natural gas hydrate reserves. There has been a tremendous development in the field of gas hydrate, which can be mainly attributed to the improvements in the laboratory work, numerical simulation analyses, and national and international collaborative field experiments [21, 52].

Onshore- and offshore-based field studies done by US researchers mainly focus on Alaska and Gulf of Mexico. Furthermore, investigations are done via laboratory experiments and simulation studies. In both the Gulf of Mexico and on the Northern Slope of Alaska, several public–private partnership firms were formed for the production of natural gas. Due to the significant availability of pipeline capacity and market accessibility, Gulf of Mexico also has the possibility of witnessing the first US domestic production through offshore operations which are substantially complex in nature. Recently, on the North Slope of Alaska, methane was produced by hydrate dissociation using $\text{CO}_2 + \text{N}_2$ with CH_4 exchange [53]. Canada, a country having a large amount of hydrate reserve is very active in exploration and production of methane from its hydrate reservoirs. Both thermal stimulation (in the year 2002) and depressurization (in the year 2008) tests were carried out in Mallik field at the northwest territories of Canada [37].

Japan, another important player, started the exploration and production testing early in the first decade of this century. In March 2003, first offshore natural gas production test from natural gas hydrate was carried out at Eastern Nankai trough of Japan using depressurization [54]. In March 2013, Japan has become the first country to produce natural gas from an offshore hydrate reservoir, Eastern Nankai Trough. From April to June 2017, the second offshore production test was conducted in the same sea area with the aim of consecutively extracting natural gas for a longer period than in the first test, which was terminated for six days due to an accident caused by sand entering into a well [55].

To fulfill the current and future energy requirements, the government of India has been supporting financially to its national gas hydrate program. A scientific expedition was done in the summer of 2006 owing to the discovery of gas hydrates in the Indian continental margin. The hydrate discovery is revealed by seismic studies as well as samples that were found accidentally during conventional oil and gas drilling. A vast number of hydrate-bearing cores were found in the four offshore locations thus confirming the presence of gas hydrate deposits in the country. The most notable hydrate deposit is 130-m-thick fractured-shale occurrence in the Krishna Godavari basin [30].

Research and development of gas hydrate production studies in China has the history of more than a decade. The expedition conducted by China in the South China Sea in the year 2007 has found gas hydrate occurrences with hydrate saturation up to 40% in the clay-dominated sediments at many locations [56]. Recently, China successfully extracted natural gas from hydrate reservoir for the first time in

the Shenhu area of the South China Sea on May 8, 2017. Therefore, China has become the first country in the world to produce steady gas continuously from hydrate reservoirs [57].

Korean research programs are mainly focused to quantify the potential hydrate resources in the Korean East Sea. From the surveys conducted by the Korea Institute of Geoscience and Mineral Resources between 2000 and 2004 and numerical simulation studies, Ulleung basin of Korea was found to have rich gas hydrate deposits, and the possibilities of the production potential from these deposits are under investigation. The drilling and coring programs in Korea's East Sea reported several 100-m-thick occurrences which are similar to the thick fractured-shale deposit discovered in India in 2006 [21, 58].

Government-funded research programs are being conducted in several other countries (e.g., Taiwan, Vietnam, and Malaysia) to investigate about the viability of gas production from hydrate deposit. Research programs like Hydratech and Hydramed conducted in Europe make use of funds available via various sources of the European Union. The list of countries with hydrate occurrences and that started production is hence expanding [21].

6 Applications: Storage and Transportation

The global consumption of natural gas is increasing rapidly. Gas markets are usually very far away from natural gas-producing areas. There are different know-hows of transporting gas from production area to petrochemical plants and finally to consumer. Gas can be transported in the form of pipeline natural gas, liquefied natural gas (LNG), compressed natural gas (CNG), and maybe as natural gas hydrate (NGH) [17]. Natural gas storage and transportation in the form of LNG or CNG is very expensive and less energy efficient. It is thus required to develop alternative technologies in the area of natural gas transportation and storage. The natural gas can be converted to gas hydrates which are used for gas storage and transportation [59]. To improve the storage capacity of hydrate and cost associated with it, the methane hydrate formation conditions should be shifted to moderate environment conditions (toward the right) with the help of thermodynamic promoters as shown in Fig. 10. Further, to recover the gas from hydrate, the temperature is increased or the pressure is decreased. This can be achieved by the use of chemical inhibitors. Since the natural gas hydrates are stable at high-pressure and low-temperature settings, their use for effective transportation and storage is limited. Hence, a different type of hydrates known as semiclathrate hydrates can be explored for such applications [60]. Semiclathrate hydrates are analogous to gas hydrates, but structurally different compared to gas hydrates. This structural dissimilarity occurs because semiclathrate hydrates are formed specifically in the presence of some thermodynamic promoter. Use of Tetra-Butyl-Ammonium-Bromide (TBAB) in gas hydrate storage and transportation saves a lot of energy and time; thereby, it is seen as the primary agent for such application. Gas transportation

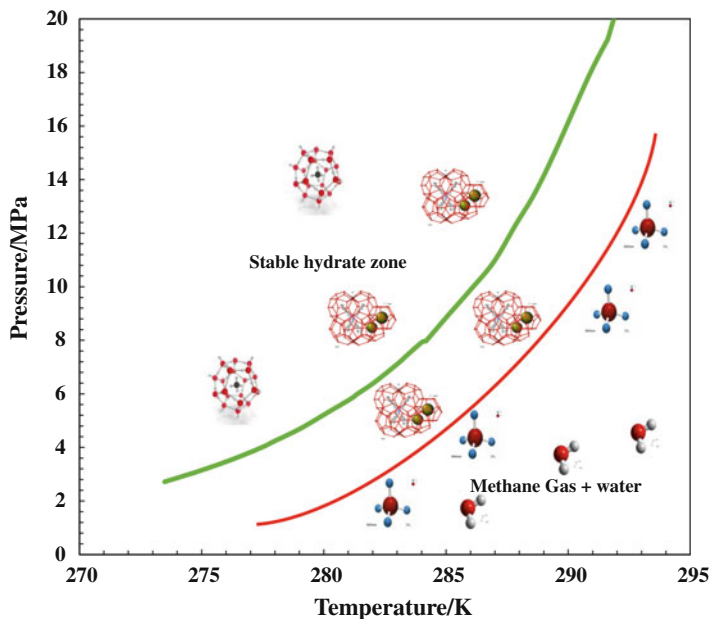


Fig. 10 Thermodynamic phase equilibrium of pure methane hydrate (green) and methane hydrate in presence of promoter (red)

in the form of gas hydrate technology is an idea under investigation, and its operative settings and procedure are not well established.

7 Conclusion and Future Direction

A massive amount of methane is delineated in the form of gas hydrates. Research is in progress to estimate the regions around the world that are probable to contain gas hydrates using seismic acquisitions, cores, well logs details, temperature information, and gas compositions. A minor fraction of this huge untapped energy resource can fulfill the energy necessities of the world. If explored and produced appropriately, the gas hydrates have the potential to be a sustainable source of energy in the near future. Several pilot production tests have been completed and are underway to recover methane from gas hydrate deposit. In addition, production tests have been executed and are also planned in near future by Japan, USA, India, and China to establish the sustainability of various production technologies for methane recovery. Gas hydrate research programs throughout the world and advances in technology will certainly help to cater technical challenges in order to harness enormous energy stored in the form of natural gas hydrates.

References

1. U.S. Energy Information Administration (2016) International Energy Outlook 2016
2. Konno Y, Masuda Y, Hariguchi Y, Kurihara M, Ouchi H (2010) Key factors for depressurization-induced gas production from oceanic methane hydrates. *Energy Fuels* 24:1736–1744
3. Ip W-H, Gan J (2010) *Advances in geosciences*, vol 18. Ocean science (OS). World Scientific
4. Siazik J, Malcho M (2017) Accumulation of primary energy into natural gas hydrates. *Procedia Eng* 192:782–787
5. Dell R (2001) Energy storage, a key technology for global energy sustainability. *J Power Sources* 100:2–17
6. Rogelj J, Den Elzen M, Höhne N, Fransen T, Fekete H, Winkler H, Schaeffer R, Sha F, Riahi K, Meinshausen M (2016) Paris Agreement climate proposals need a boost to keep warming well below 2 °C. *Nature* 534:631–639
7. Wang X, Economides M (2013) *Advanced natural gas engineering*. Gulf Publishing Company, Houston, TX
8. Kvenvolden KA (1993) Gas hydrates—geological perspective and global change. *Rev Geophys* 31(2):173–187
9. Sloan ED, Koh CA (2008) *Clathrate hydrates of natural gases*, 3rd edn. CRC Press, FL, USA
10. Lu SM (2015) A global survey of gas hydrate development and reserves: specifically in the marine field. *Renew Sustain Energy Rev* 41:884–900
11. Hammerschmidt EG (1934) Formation of gas hydrates in natural gas transmission lines. *Ind Eng Chem* 26:851–855
12. Makogon YF (1965) A gas hydrate formation in the gas saturated layers under low temperature. *Gas Ind* 5:14–15
13. Holder GD, Hand JH (1982) Multiple-phase equilibria in hydrates from methane, ethane, propane and water mixtures. *AIChE J* 28:440–447
14. Makogon YF (1997) *Hydrates of hydrocarbons*. PennWell Books
15. Sun ZG, Wang R, Ma R, Guo K, Fan S (2003) Natural gas storage in hydrates with the presence of promoters. *Energy Convers Manage* 44:2733–2742
16. Sum AK, Burruss RC, Sloan ED (1997) Measurement of clathrate hydrates via Raman spectroscopy. *J Phys Chem B* 101:7371–7377
17. Mech D, Gupta P, Sangwai JS (2016) Kinetics of methane hydrate formation in an aqueous solution of thermodynamic promoters (THF and TBAB) with and without kinetic promoter (SDS). *J Nat Gas Sci Eng* 35:1519–1534
18. Vedachalam N, Ramesh S, Jyothi VBN, Prasad NT, Ramesh R, Sathianarayanan D, Ramadass GA, Atmanand MA (2015) Evaluation of the depressurization based technique for methane hydrates reservoir dissociation in a marine setting, in the Krishna Godavari Basin, east coast of India. *J Nat Gas Sci Eng* 25:226–235
19. Meyer RF (1981) Speculations on oil and gas resources in small fields and unconventional deposits. In: Meyer RF, Olson JC (eds) *Long-term energy resources*. Pitman, Boston, pp 49–72
20. Dobrynin VM, Korotajev Yu P, Plyushev DV (1981) Gas hydrates—a possible energy resource. In: Meyer RF, Olson JC (eds) *Long-term energy resources*. Pitman Publishers, Boston, pp 727–729
21. Collett TS, Johnson AH, Knapp CC, Boswell R (2009) Natural gas hydrates: a review, pp 146–219
22. Zhao J, Song Y, Lim XL, Lam WH (2017) Opportunities and challenges of gas hydrate policies with consideration of environmental impacts. *Renew Sustain Energy Rev* 70:875–885
23. Wadham JL, Arndt S, Tulaczyk S, Stibal M, Tranter M, Telling J, Lis GP, Lawson E, Ridgwell A, Dubnick A, Sharp MJ (2012) Potential methane reservoirs beneath Antarctica. *Nature* 488:633–637

24. Collett TS (1993) Natural gas hydrates of the Prudhoe Bay and Kuparuk river are, North Slope, Alaska. *AAPG Bull* 77:793–812
25. Collett TS (2002) Energy resource potential of natural gas hydrates. *AAPG Bull* 86:1971–1992
26. Kvenvolden KA (1993) A primer in gas hydrates. *The Future of Energy Gases* 1570:279–292
27. Xu W, Ruppel C (1999) Predicting the occurrence, distribution, and evolution of methane gas hydrate in porous marine sediments. *J Geophys Res Solid Earth* 104:5081–5095
28. Collett TS, Ladd J (2000) Detection of gas hydrate with downhole logs and assessment of gas hydrate concentrations (saturations) and gas volumes on the Blake Ridge with electrical resistivity log data. In: *Proceedings of the Ocean drilling program. Scientific Results*, vol 164, pp 179–191
29. Hunter RB, Collett TS, Boswell R, Anderson BJ, Digert SA, Pospisil G, Baker R, Weeks M (2011) Mount Elbert gas hydrate stratigraphic test well, Alaska North Slope: overview of scientific and technical program. *Marine Petrol Geol* 28:295–310
30. Collett TS, Boswell R, Cochran JR, Kumar P, Lall M, Mazumdar A, Ramana MV, Ramprasad T, Riedel M, Sain K, Sathe AV (2014) Natural gas hydrates of the Prudhoe Bay and Kuparuk river area: results of the national gas hydrate program expedition 01. *Marine Petrol Geol* 58:3–28
31. Mordis GJ, Collet TS, Boswell R, Kurihama M, Reagan MT, Koh C, Sloan ED (2008) Toward production from gas hydrate: current status, assessment of resources, and simulation based evaluation of technology and potential. In: *SPE unconventional reservoirs conference*, pp 10–12, February, Keystone, Colorado, USA
32. Kurihara M, Ouchi H, Narita H, Masuda Y (2011) Gas production from methane hydrate reservoirs. In: *Proceedings of the 7th International Conference on Gas Hydrates (ICGH)*, vol 1721. Edinburgh, UK
33. Tang LG, Xiao R, Huang C, Feng ZP, Fan SS (2005) Experimental investigation of production behaviour of gas hydrate under thermal stimulation in unconsolidated sediment. *Energy Fuels* 19:2402–2407
34. Cranganu C (2009) In-situ thermal stimulation of gas hydrates. *J Petrol Sci Eng* 65:76–80
35. Liu Y, Strumendo M, Arastoopour H (2008) Simulation of methane production from hydrates by depressurization and thermal stimulation. *Ind Eng Chem Res* 48:2451–2464
36. Wang Y, Li XS, Li G, Zhang Y, Li B, Chen ZY (2013) Experimental investigation into methane hydrate production during three-dimensional thermal stimulation with five-spot well system. *Appl Energy* 110:90–97
37. Yamamoto K, Dallimore S (2008) Aurora-JOGMEC-NRCan Mallik 2006-2008 gas hydrate research project progress. *Nat Gas & Oil* 304:285–4541
38. Ji C, Ahmadi G, Smith DH (2001) Natural gas production from hydrate decomposition by depressurization. *Chem Eng Sci* 56:5801–5814
39. Kono HO, Narasimhan S, Song F, Smith DH (2002) Synthesis of methane gas hydrate in porous sediments and its dissociation by depressurizing. *Powder Technol* 122:239–246
40. Bai Y, Yang H, Du Y, Zhao Y (2013) The sensitivity analysis of scaling criteria in gas hydrate reservoir physical simulation. *Energy Convers Manage* 67:138–144
41. Konno Y, Jin Y, Shinjou K, Nagao J (2014) Experimental evaluation of the gas recovery factor of methane hydrate in sandy sediment. *RSC Adv* 4:51666–51675
42. Pang WX, Xu WY, Sun CY, Zhang CL, Chen GJ (2009) Methane hydrate dissociation experiment in a middle-sized quiescent reactor using thermal method. *Fuel* 88:497–503
43. Song Y, Cheng C, Zhao J, Zhu Z, Liu W, Yang M, Xue K (2015) Evaluation of gas production from methane hydrates using depressurization, thermal stimulation and combined methods. *Appl Energy* 145:265–277
44. Dong F, Zang X, Li D, Fan S, Liang D (2009) Experimental investigation on propane hydrate dissociation by high concentration methanol and ethylene glycol solution injection. *Energy Fuels* 23:1563–1567
45. Sung W, Lee H, Lee C (2002) Numerical study for production performances of a methane hydrate reservoir stimulated by inhibitor injection. *Energy Sources* 24:499–512

46. Mech D, Pandey G, Sangwai JS (2015) Effect of molecular weight of polyethylene glycol on the equilibrium dissociation pressures of methane hydrate system. *J Chem Eng Data* 60:1878–1885
47. Chong ZR, Yang SHB, Babu P, Linga P, Li XS (2016) Review of natural gas hydrates as an energy resource: prospects and challenges. *Appl Energy* 162:1633–1652
48. Koh D-Y, Kang H, Lee J-W, Park Y, Kim S-J, Lee J, Lee JY, Lee H (2016) Energy-efficient natural gas hydrate production using gas exchange. *Appl Energy* 162:114–130
49. Goel N (2006) In situ methane hydrate dissociation with carbon dioxide sequestration: current knowledge and issues. *J Petrol Sci Eng* 51:169–184
50. Mekala P, Busch M, Mech D, Patel RS, Sangwai JS (2014) Effect of silica sand size on the formation kinetics of CO₂ hydrate in porous media in the presence of pure water and seawater relevant for CO₂ sequestration. *J Petrol Sci Eng* 122:1–9
51. Wang B, Dong H, Fan Z, Zhao J, Song Y (2017) Gas production from methane hydrate deposits induced by depressurization in conjunction with thermal stimulation. *Energy Procedia* 105:4713–4717
52. Collett TS (2004) Gas hydrates as a future energy resource. *Geotimes* 49:24–27
53. Schoderbek D, Martin KL, Howard J, Silpngarmert S, Hester K (2012) North Slope hydrate field trial: CO₂/CH₄ exchange. In: OTC Arctic Technology Conference. Offshore Technology Conference. 3rd December, Houston, Texas, USA
54. Yamamoto K, Terao Y, Fujii T, Ikawa T, Seki M, Matsuzawa M, Kanno T (2014) Operational overview of the first offshore production test of methane hydrates in the Eastern Nankai Trough. In: Offshore Technology Conference. Offshore Technology Conference, 5–8 May, Houston, TX
55. Reuters (2017) Japan reports successful gas output test from methane hydrate (online). Available at: <http://www.reuters.com/article/japan-methane-hydrate-idUSL4N1IA35A>. Accessed 20 Jun 2017
56. Zhang HQ, Yang SX, Wu NY, Su X, Holland M, Schultheiss P (2007) China's first gas hydrate expedition successful. *Fire Ice Newslett* 7(2):1
57. News.cgtn.com (2017) China's first gas hydrate extraction successful (online). Available at: https://news.cgtn.com/news/3d67544f786b7a4d/share_p.html. Accessed 10 Jun 2017
58. Park KP (2006) Gas hydrate exploration in Korea. In: Proceedings of the 2nd international symposium on gas hydrate technology, November. Daejeon, Korea, pp 1–2
59. Mech D, Sangwai JS (2014) Phase stability of hydrates of methane in tetrahydrofuran aqueous solution and the effect of salt. *J Chem Eng Data* 59:3932–3937
60. Sangwai JS, Oellrich L (2014) Phase equilibrium of semiclathrate hydrates of methane in aqueous solutions of tetra-n-butyl ammonium bromide (TBAB) and TBAB–NaCl. *Fluid Phase Equilib* 367:95–102
61. Nago A, Nieto A (2011) Natural gas production from methane hydrate deposits using clathrate sequestration: state-of-the-art review and new technical approaches. *J Geol Res* 2011:1–6
62. Sain K, Gupta H (2012) Gas hydrates in India: potential and development. *Gondwana Res* 22:645–657
63. Kvenvolden KA (1988) Methane hydrate—a major reservoir of carbon in the shallow geosphere? *Chem Geol* 71:41–51
64. Boswell R, Collett TS (2006) The gas hydrates resource pyramid: fire in the ice. Methane hydrate newsletter, US Department of Energy, Office of Fossil Energy, National Energy Technology Laboratory, Fall Issue, pp 5–7
65. Xiao C, Wibisono N, Adidharma H (2010) Dialkylimidazolium halide ionic liquids as dual function inhibitors for methane hydrate. *Chem Eng Sci* 65:3080–3087

Current Advances in Bio-Oil Upgrading: A Brief Discussion

Anand Mohan Verma and Nanda Kishore

Abstract Conventional fuels being on their verge of depletion and regularly increasing air pollution demand a robust need of a promising energy resource to meet the present energy demand and diminish the pollution concerns. The renewable energy resources, for instance, wind energy, tidal energy, solar energy, geothermal energy, biomass are presently being employed widely across the globe. However, out of all renewable energy resources, only biomass ensures the sustainability of carbon element for existing transportation vehicles. There have been enormous amount of research regarding the biomass and its conversion into bio-oil, but the suitable and economical bio-oil upgradation technology is still challenging. The raw bio-oil derived from the thermochemical conversion of lignocellulosic biomass comprises of a huge number of oxy-compounds which vitiate its quality as biofuel; therefore, the research regarding the upgradation of raw bio-oil is emerging as one of the fastest and exciting research field amongst researchers across the globe. In this chapter, a comprehensive review of types of biomass, available methods of conversion, bio-oil chemistry, and the bio-oil upgradation is carried out. In addition, single component-wise upgradation of raw bio-oil components, e.g. glucose, fructose, acetic acid, furfural, glycerol, over various catalysts is reviewed. Along with the experimental works, this article also aims for the review of several contemporary theoretical works which are carried out for the investigations of the reaction mechanisms behind the conversion of various bio-oil components. Currently, the density functional theory (DFT) is widely applied as a computational tool for the accurate investigation of reaction mechanisms of various bio-oil components; therefore, numerous studies based on the DFT methods are also included.

Keywords Biomass · Bio-oil · Sustainable energy · Catalytic upgrading Kinetics · Density functional theory

A. M. Verma · N. Kishore (✉)
Department of Chemical Engineering,
Indian Institute of Technology Guwahati, Guwahati 781039, India
e-mail: nkishore@iitg.ernet.in; mail2nkishore@gmail.com

Abbreviations

Glu	Glucose
Fru	Fructose
LA	Levulinic Acid
HMF	5-hydroxymethylfurfural
Fur	Furfural
FAL	Furfuryl Alcohol
THFAL	Tetrahydrofurfuryl Alcohol
THF	Tetrahydrofuran
DHF	Dihydrofuran
MF	2-Methylfuran
Xyl	Xylose
Sor	Sorbitol
AA	Acetic Acid
Acde	Acetaldehyde
Gly	Glycerol
PD	1,2-propanediol
HP	1-hydroxypropan-2-one
PA	Propanoic Acid

1 Introduction

Due to significant surge in global population and socio-economic factors, the energy demand has been increased enormously compared with past few decades. According to World Energy Council (2016) [1], global electricity demand is projected to be doubled by year 2060. Particular to India, annual per capita consumption of electricity has seen rise by nearly twice in last decade, 2005–2006 to 2015–2016 [2]. However, a huge population of India (and world) still lives in the absence of electricity; an assessment by World Energy Outlook (2016) estimates that around 244 million people (1186 million in world) are without electricity in India [3]. It also advocates that 63% population of India (38% of world) is still primarily dependent on biomass as fuel for cooking. It can be seen that global energy demand is at its peak, and it will further foresee a huge escalation due to increasing demands by developing nations like India, China, Brazil, etc. Currently, a huge fraction of energy demand is targeted through non-renewable energy resource, particularly fossil fuels which are on their verge of depletion and regularly increasing air pollution caused by them is not effectively controllable; therefore, a robust need of a promising energy resource is required to meet the present energy demand and diminish the pollution concerns. In the recent past, the application of clean and renewable energy resources is increased due to limited availability of conventional fuels, increasing pollution, and increasing energy demand.

2 Biomass

The share of renewable energy resource (other than hydro power) in total primary energy supply, surveyed by World Energy Resources (2013) [4], has been documented as 11% in 2011 which is further projected to achieve 16% in 2020. The renewable energy resources such as hydropower, wind energy, geothermal energy, tidal energy, biomass, solar energy are regularly increasing their share in global energy demand; however, the sustainability of carbon element for transportation fuels and value-added chemicals is ensured by only biomass as renewable energy resource [5]. This unique feature of biomass queue itself out from other potential renewable energy resources and has become a hot topic for research across the globe. Biomass, a plant material, is derived from photosynthesis reaction between CO₂ and water in the presence of sunlight to produce carbohydrates to form various fractions, i.e. building blocks, of biomass [6]. The storage of energy in biomass is in the form of chemical bonds, and these stored chemical energies release when bonds between carbon, oxygen, and hydrogen break due to combustion, digestion, or decomposition [6]. It is regarded as one of the most promising alternative energy resource to fossil fuel and if it is exploited properly then the net rise in CO₂ level in the atmosphere will be zero (see Fig. 1) [7]. Biomass is abundantly available in most of countries and also an inexpensive renewable energy resource, therefore, in the recent past, a major fraction of research is devoted towards biomass. Lignocellulosic biomass belongs to most abundant class of biomass and is a persuasive candidate for biofuel production because of no ‘food or fuel’ concerns which is a major issue with first generation biofuels. There are three main building blocks of lignocellulosic biomass, viz. cellulose, hemicellulose, and lignin (see Fig. 2). Cellulose (40–50%) is a polymer composed of C₆ glucose monomers connected via β-glycosidic bonds, whereas hemicellulose (25–35%) is a polymer composed of five different monomers, namely D-xylose, L-arabinose, D-galactose, D-glucose, and D-mannose [7]. On the other hand, lignin (15–20%) is three-dimensional structure (see Fig. 2) composed of three main units, i.e. coniferyl alcohol, sinapyl alcohol, and *p*-coumaryl alcohol [7]. The fractions of building blocks of lignocellulosic biomass differ with different types of biomass [5, 6, 8, 9].

In this review work, various types of biomass, its conversion to bio-oil, characteristics of bio-oil, problems to bio-oil, bio-oil upgradation as a whole, and component-wise bio-oil upgradation are discussed. Various bio-oil components such as glucose, fructose, acetic acid, glycerol, furfural are reviewed for their reduction into lower fraction products in the presence of numerous catalysts.

2.1 Biomass Species and Their Compositions

A general biomass species is composed of various components, e.g. celluloses, hemicelluloses, lignins, extractives (starches, terpenes), and ash [5]. Other

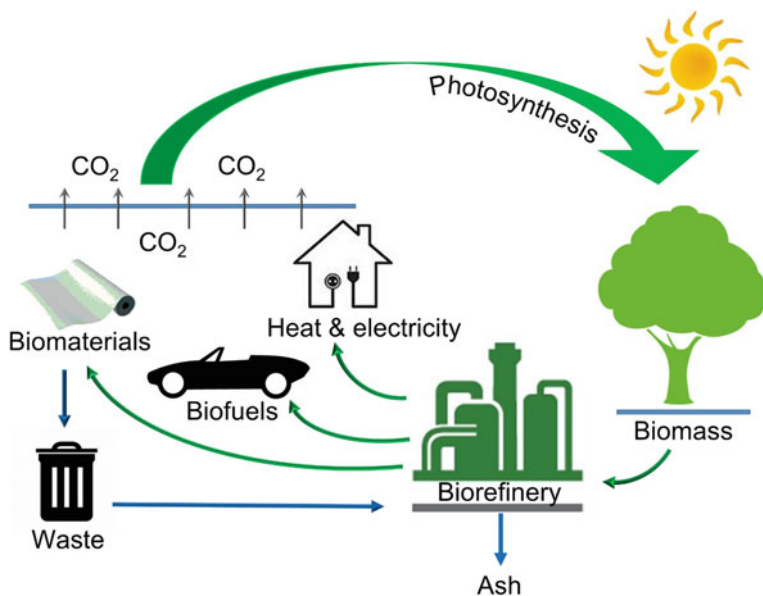


Fig. 1 CO₂ cycle in biomass growth and its utilization *via* different approaches [5, 7]

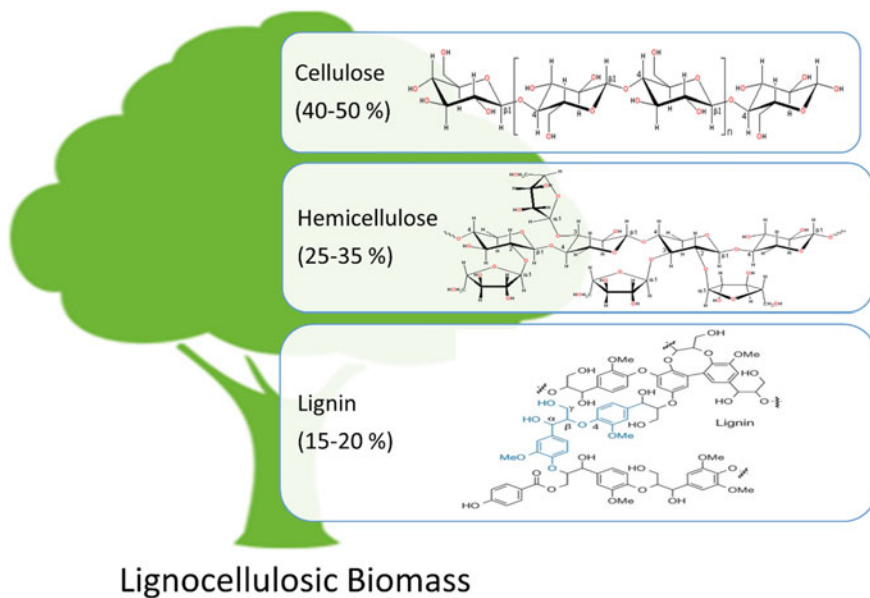


Fig. 2 Building blocks of lignocellulosic biomass [5, 10]

Table 1 Various types of biomass with their chemical compositions [5, 6, 8, 9]

Composition	Biomass type				
	Switchgrass	Pine	Eucalyptus	Corn grain	Corn stover
Lower heating value (MJ/dry kg)	~ 17	18.6	18.1	17	17.5
<i>Components (dry wt%)</i>					
Cellulose	40–45	46–50	48	3	36
Hemicellulose	31–35	19–22	14	6	23
Lignin	6–12	21–29	29	2	17
Extractives (terpenes, starches)	0	3	2	72	6
Ash	5–6	0.3	1	–	10

components of biomass such as triglycerides, resins, pigments, sterols, waxes are present in minute portions [5]. Although the composition of various components depends on numerous factors such as climate, soil quality, precipitation; therefore, each biomass species can represent different component and elemental compositions [5–7]. Table 1 depicts a few types of biomass species with their chemical compositions and energy contents [5, 6, 8, 9]. The fractions of cellulose are higher in eucalyptus and pine biomass species compared to corn grain and corn stover. Low ash content, high fractions of representative components (cellulose, hemicellulose, and lignin), and high ‘lower heating values’ of eucalyptus and pine biomass species present them as desirable biomass species. On the other hand, corn grain is majorly composed of extractives which include starches and terpenes compared to cellulose, hemicellulose, and lignin fractions (see Table 1).

2.2 Conversion Routes of Biomass into Bio-Oil

The conversion of biomass into lower fraction products is mainly performed via three primary routes, namely gasification, liquefaction or pyrolysis, and hydrolysis [5, 10]. In Fig. 3, all three main routes and post-processing methods are shown.

2.2.1 Gasification

In gasification process, solid or liquid carbonaceous materials, e.g. biomass, coal, oil convert into *syn gas* or producer gas upon reacting with air, steam and/or oxygen. The product gases contain CO, H₂, CH₄, CO₂, and N₂ in different fractions [6]. A complex combination of chemical reactions occur in different stages of gasification tower during biomass gasification such as partial oxidation, water–gas shift, pyrolysis, steam gasification, and methanation reactions [5]. Pyrolysis process

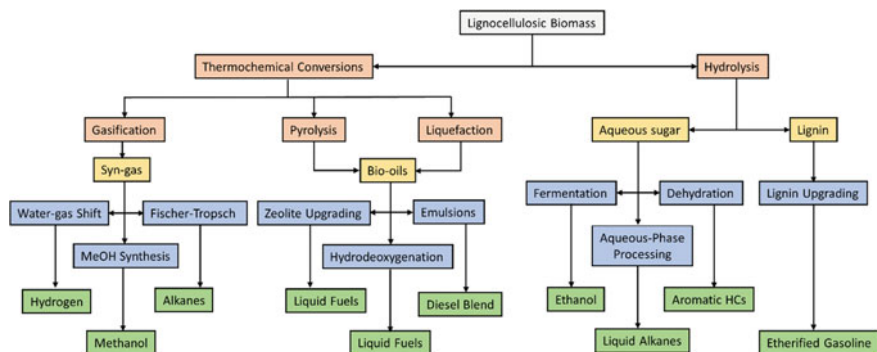
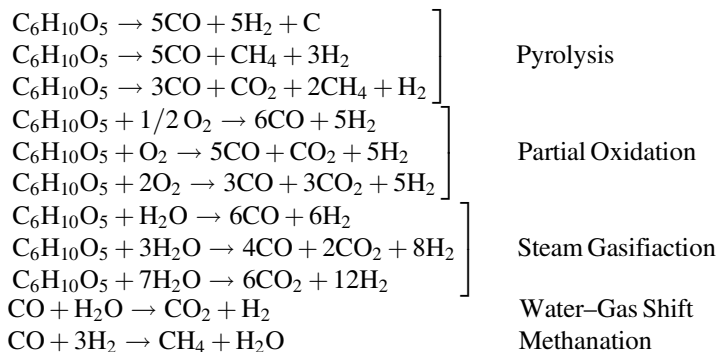


Fig. 3 Various routes for biomass conversion into unprocessed bio-oils followed by their upgradation routes [5, 7]

decomposes biomass into lower fractions and occurs in the absence of oxygen, whereas partial oxidation involves less amount of oxygen for combustion compared to stoichiometric requirement. Steam gasification involves the reaction of biomass components with water to produce CO, H₂, and CO₂; in water–gas shift reaction, CO and water react to produce CO₂ and H₂. The temperature conditions vary in the ranges of 700–800 °C and 900–1000 °C for conventional and high-temperature steam gasification processes, respectively [5]. On the other hand, methanation involves the production of methane and water from reaction of CO and H₂. The stoichiometric chemical equations of cellulose gasification chemistry are as following [5, 6]:



The composition of product gases is dependent of composition of biomass species, gasifier type, etc. Nevertheless, the produced *syn gas*, i.e. CO and H₂, can be employed in several ways, [11] such as in the production of hydrogen via water–gas shift reactions, in the production of methanol via methanol synthesis, and in the production of alkanes via Fischer-Tropsch process (see Fig. 3). Furthermore, the utilization of *syn gas* can be in the productions of isobutane via isosynthesis, ethanol via fermentation, aldehydes and alcohols via oxosynthesis, etc. [11].

Methanol, on the other hand, which is produced during methanol synthesis from *syn gas* can be utilized in the production of dimethyl ether (DME), H₂, methyl *tert*-butyl ether (MTBE), etc. [11].

The clogging of tars in exit pipes is very problematic; therefore, primary aim of gasification should be to reduce the tar formation [5]. In order to achieve low tar formation, various catalysts such as noble metals (Pt, Pd, etc.), CeO₂/SiO₂ supported Ni in gasifiers have been tested by researchers [12]. Few researches have also been performed using the addition of alkali metals with the biomass feedstocks to reduce tar formations [13].

2.2.2 Pyrolysis and Liquefaction

Bio-oils from pyrolysis process are produced by the heating of lignocellulosic biomass in the absence of air/oxygen at elevated temperature of 450–550 °C [14, 15]. At such elevated temperature, the decomposition of lignocellulosic biomass occurs and produces vapour phase products which can be subsequently condensed into liquid phase upon cooling. The unprocessed bio-oils from pyrolysis of lignocellulosic biomass are comprised of high oxygen content, low carbon content, and high moisture content [16]. The pyrolysis-derived bio-oil contains over hundreds of oxy-compounds in various oxy-catalogues such as, acids, ketone, esters, aldehydes, sugars, phenols, miscellaneous oxygenates [10]. A general reaction scheme 1 for biomass pyrolysis can be given as:

On the other hand, liquefaction of biomass produces a water-insoluble bio-oil at high pressure (50–200 atm) and low temperature (250–450 °C) [18]. The bio-oil produced from liquefaction of biomass contains less amount of oxygen and high amount of carbon content than pyrolysis [16]. In addition, liquefaction oils have higher heating values compared to pyrolysis oils because of high carbon content. Although the high pressure requirement for liquefaction causes an increase in capital cost and so the technical problems [5]. Table 2 comprises of the properties of unprocessed bio-oils from pyrolysis, liquefaction oil and heavy fuel oil in percentages [5, 19]. Liquefaction-derived bio-oils appear beneficial compared to pyrolysis-derived bio-oils (see Table 2) but liquefaction process involves various technical difficulties and economic problems due to high-pressure operation, that is, why pyrolysis-derived bio-oil draws more attention than liquefaction-derived bio-oils.

Scheme 1 A general mechanism for biomass pyrolysis [17]

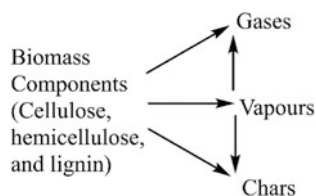


Table 2 Properties of bio-oils from pyrolysis, liquefaction, and heavy fuel oil

Property	Pyrolysis oil	Liquefaction oil	Heavy fuel oil
Moisture content, wt%	15–30	5.1	0.1
pH	2.5	–	–
Specific gravity	1.2	1.1	0.94
<i>Elemental compositions (wt%)</i>			
Carbon	54–58	73	85
Hydrogen	5.5–7.0	8	11
Oxygen	35–40	16	1.0
Nitrogen	0–0.2	–	0.3
Ash	0–0.2	–	0.1
Higher heating value, MJ/kg	16–19	34	40
Viscosity (50 °C), cP	40–100	15,000 (at 61 °C)	180
Solids, wt%	0.2–1	–	1
Distillation residue, wt%	Up to 50	–	1

The data are taken from Czernik and Bridgwater [19] and Elliott and Schiefelbein [33]

2.2.3 Hydrolysis

Hydrolysis reaction converts cellulose into sugar monomers reacting with water molecules. However, hydrolysis of starches is less complicated compared to the hydrolysis of cellulose because the latter is in crystalline structure with hydrogen bonding [5]. Figure 3 depicts the conversion of biomass via hydrolysis which degrades it into sugars and lignin. The utilization of lignin remains challenging because of its complex structure; however, it undergoes upgradation process to produce etherified gasoline, while the monomers of sugar undergo fermentation, aqueous phase processing, and dehydration to form ethanol, liquid alkanes, and aromatic hydrocarbons, respectively [5, 20]. Ethanol as first generation biofuels is already being used as blend or primary fuel to transportation vehicles in countries like Brazil. Aqueous phase processing of sugars involves various reactions, for instance, dehydration, hydrogenation, hydrogenolysis, aldol condensation and produces long alkane chains for liquid fuels [20, 21]. On the other hand, dehydration of sugars involves elimination of water molecules from sugar to produce various intermediate products such as 5-hydroxymethylfurfural (5-HMF) which further undergoes in production of intermediates, e.g. levulinic acid, dimethylfuran [22]. The productions of by-products such as 5-hydroxymethylfurfural (HMF), levulinic acid (LA) are also achieved by acid-catalyzed decomposition of sugars.

3 Characteristics of Bio-Oil

Bio-oils, having a distinctive odour, are free-flowing liquid with appearance of dark brown colour. During the conversion of biomass into bio-oil, various reactions take place such as dehydration, hydrolysis, isomerization, dehydrogenation, aromatization, condensation, coking [5, 7, 16]. Branca et al. [23] in their experiment of biomass pyrolysis obtained more than 400 oxy-compounds in unprocessed bio-oil which are classified into acids, esters, alcohols, aldehydes, sugars, miscellaneous oxygenates, furans, phenols, guaiacols, etc. Although the composition of bio-oil differs with different feedstock and it depends on following factor [5, 24]:

- (a) the feedstock,
- (b) nitrogen and protein contents,
- (c) heat transfer rate and final char temperature during pyrolysis,
- (d) water content of the feedstock,
- (e) storage issues, etc.

Bio-oil components are derived from cellulose, hemicellulose, and lignin building blocks. For instance, guaiacols are generally formed from lignin portion, whereas cellulose and hemicellulose parts give rise to sugars, miscellaneous oxygenates, furans, etc. Other oxy-components such as esters, alcohols, ketones, acids, and aldehydes generate from the decomposition reaction of miscellaneous oxygenates, sugars, and furans. Table 3 demonstrates the major oxy-compounds found in unprocessed bio-oil [10]. Sugars contain levoglucosan and glucose as major

Table 3 Major functionals of bio-oil and corresponding major components [10]

Functionals	Major compounds
Water	Water
Simple oxygenates	Acetic acid, formic acid, propanoic acid, methyl-propionic acid, butanoic acid, methyl acetate, methyl formate, methyl propionate, butane-2,3-diol, methanol, ethanol, ethylene glycol, acetone, 2-butanone, 2-butenal, 2,3-butanedione, cyclopentanone, glyoxal, formaldehyde, acetaldehyde, 2-propenal, pentanal, etc.
Miscellaneous oxygenates	Glycoaldehyde, 1-hydroxyl-2-propanone, etc.
Sugars	Levoglucosan, glucose, fructose, D-xylose, etc.
Furans	Furan, 2-methylfuran, dimethylfuran, furfural, 2-furanone, 4-methyl-2-furanone, furfuryl alcohol, etc.
Hydrocarbons	Hexane, methyl-propene, toluene, xylene, ethyl benzene, naphthalene, etc.
Phenolics	Phenol, methylphenols, dimethylphenol, anisole, methyl anisole, ethyl anisole, catechol, methylcatechol, ethylcatechol, guaiacol, methylguaiacol, ethylguaiacol, syringol, methysyringol, ethylsyringol, vanillin, vanillic acid, sinapaldehyde, syringaldehyde, etc.
High-MW species	Dimmer, trimmer, and oligomer of cellulose, hemicellulose, and lignin

compounds. Furans contain furan, furfural and 2-furanone as primary model compounds, whereas phenolics are classified into several phenols such as catechols, guaiacols, syringols.

4 Snags to Raw Bio-Oil and Its Upgradation

As it is aforementioned in the 'Characteristics of Bio-Oil' section that the raw bio-oil from pyrolysis contains more than 400 oxy-organic compounds, unprocessed bio-oil does not display desired characteristics of a good fuel. Therefore, bio-oils obtained from fast pyrolysis cannot be used as transportation fuel directly because it contains a significant amount of oxy-compounds which degrade its quality as transportation fuel in terms of low heating value, low pH, high viscosity, less stability, etc. [5, 10, 19, 25]. The problem occurs with bio-oil subjected to diesel engine is that it is difficult to start ignition because of corrosiveness and coking. It has to be channelized through upgradation processes. Bio-oils must be upgraded before being subjected as an alternative to transportation fuel such as diesel and gasoline fuels. Bio-oils can be upgraded by three primary promising routes, namely (1) zeolite upgrading, (2) forming emulsions with the diesel fuel, and (3) hydrodeoxygenation using hydrotreating catalysts [5].

4.1 Zeolite Upgrading

Zeolite catalysts are widely used catalysts in the petroleum industries for oil refining, production of special and fine chemical and for petrochemistry inside the petroleum fuel [26]. These are crystalline microporous materials with 5–10 Å pore structures and bio-oils can be upgraded using zeolite to reduce oxy-functionals [26]. The products from the reaction contain hydrocarbons, water-soluble organics, gases, and coke. A number of reactions occur during zeolite upgrading such as dehydration, cracking, deoxygenation, aromatization, and polymerization. Advantages to zeolite upgrading are that it does not require additional hydrogen, operates at atmospheric pressure, and temperatures are also same as of bio-oil production [5, 26]. But some disadvantages such as poor hydrocarbon yields and high yield of coking brand this process less suitable in bio-oil upgradation processes [5, 26].

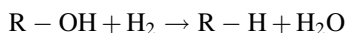
4.2 Forming Emulsion with the Diesel Fuel

Because of high water content in raw bio-oil derived from pyrolysis or liquefaction of lignocellulosic biomass, it is not solvable in petroleum-derived fuel; however, it

can be blended with diesel fuel employing the use of appropriate surfactants [27–29]. Bio-oil emulsion depicts constructive ignition characteristics, though it becomes costly because of addition of surfactant in emulsification process. Nonetheless, corrosion process is still a challenging task in the engine upon the application of bio-oil emulsions [29].

4.3 Hydrodeoxygenation (HDO)

Hydrodeoxygenation (HDO) is a process of cleavage of C–O bonds using hydrogen in the presence of appropriate catalysts; the oxygen atoms in the bio-oil react with H₂ to form water [30, 31]. The hydrodeoxygenation process for upgrading the unprocessed bio-oil occurs at moderate temperature of 300–600 °C and at high pressure of hydrogen. The energy density and the stability of the bio-oil increase after HDO [5]. A general chemical reaction involving HDO reaction mechanism can be shown as:



Here, in the above chemical reaction, R is the organic or oxygenated organic functional group, e.g. CH₃, C₆H₅, C₆H₅(OH), C₄H₃O(CH₂). The additional hydrogen atoms cleave the C–O bonds and produce water as side product along with hydroxyl group reduced primary product. A comprehensive review about the hydrodeoxygenation process and its chemistry is written by Furimsky [30, 31]. Various types of catalysts have been used in HDO process such as sulfided NiMo and CoMo-based catalysts, mono metallic catalysts, noble metal catalyst and transition metal oxide catalysts [32]. Sulfided NiMo and CoMo-based catalysts are very popular in the petroleum industries because these are used to remove sulphur, oxygen and nitrogen-based functionals from petroleum feedstocks. In petroleum feedstocks, the oxygen content is very less compared to bio-oils; therefore, petroleum feedstocks do not involve with much water formation during refining. Sulfided NiMo and CoMo-based catalysts show poisonous behaviour if the reaction involves water formation or reaction itself is in water phase [32]. Since bio-oil contains a large amount of oxy-compounds and during upgradation, the product stream would contain water; therefore, sulfided NiMo and CoMo-based catalysts may not be appropriate. On the other hand, noble metal catalysts such as Pt, Pd show exceptional characteristics of HDO in both cases but are very costly [32]. The disadvantage to HDO process is that it requires a large amount of hydrogen in high pressure. Table 4 depicts the properties and elemental analyzes of raw bio-oil from liquefaction and pyrolysis and upgraded bio-oil from HDO [33, 34]. It is seen in Table 4 that wt% of carbon is increased to 85.3–89.2% when bio-oils were subjected to hydrodeoxygenation compared to the carbon content of unprocessed

Table 4 Analysis of properties of bio-oils and upgraded bio-oils

Elemental analysis	High-pressure liquefaction [33]	Pyrolysis Bio-oil		Hydrodeoxygenated bio-oil [33]
		[33]	[34]	
Carbon (wt%)	72.6	43.5	46.5	85.3–89.2
Hydrogen (wt%)	8.0	7.3	7.2	10.5–14.1
Oxygen (wt%)	16.3	49.2	46.1	0.0–0.7
Sulphur (ppm)	<45	29.0	–	50
H/C atom ratio	1.21	1.23	–	1.40–1.97
Density (g/mL)	1.15	24.8	–	0.796–0.926
Moisture (wt%)	5.1	24.8	18.9	0.001–0.008
HHV (MJ/kg)	35.7	22.6	18.7	42.3–45.3
Viscosity (cP)	15,000 (61 °C)	59 (40 °C)	–	1.0–4.6 (23 °C)

bio-oils due to pyrolysis (43.5–46.5%) and liquefaction (72.6%). Similarly, the oxygen content decreased to 0.0–0.7 wt% upon HDO of raw bio-oil and, therefore, the higher heating value (HHV) increased to 42.3–45.3 MJ/kg. Consequently, HDO process is able to upgrade the unprocessed bio-oil to a higher end biofuel which can be useful to transportation vehicles.

5 Decomposition of Cellulose and Hemicellulose

The decomposition of cellulose and hemicellulose at elevated temperature produces various oxygenated compounds including acids, aldehydes, esters, ketones, miscellaneous oxygenates. Few major oxy-compounds from the pyrolysis of cellulose and hemicellulose are depicted in Fig. 4. The unit cells of structures of cellulose (C₆ sugars) and hemicellulose (C₅ sugars) are depicted in Fig. 4 which produce their monomers, glucose and xylopyranose, respectively. Various oxygenated structures (see Fig. 4) make unprocessed bio-oil unstable because of frequent spontaneous reactions upon its storage. Furthermore, due to these several oxy-structures, the liquid bio-oil suffers from low heating value, highly corrosive, high viscosity, etc. Therefore, further upgradation of these oxy-structures into lower fractions or alkanes is required to enhance the carbon content. Table 5 comprises of various experimental and numerical studies carried out by several researchers based on few model compounds produced from cellulose and hemicellulose fractions along with catalyst, support, and major products.

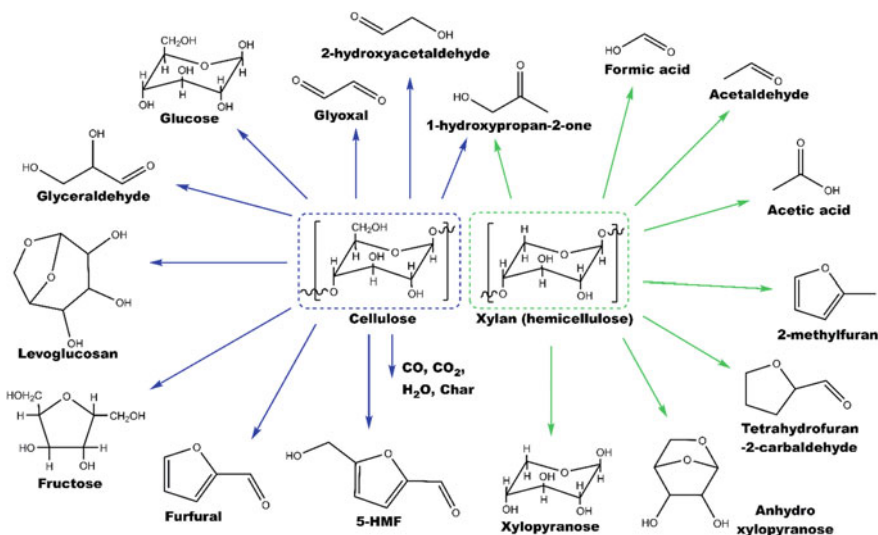


Fig. 4 Few major bio-oil model compounds due to cellulose and hemicellulose fractions of lignocellulosic biomass [10]

5.1 Glucose and Fructose

Depolymerization of cellulose polymer reduces to sugar monomers containing six carbon atoms; however, due to high oxygen content, glucose component undergoes dehydration reactions which produce water as side product. Glucose can be a very important candidate for the production of platform chemicals such as 5-HMF, levulinic acid. The production of 5-HMF first involves isomerization reaction of glucose to fructose followed by dehydration reactions of fructose (see Fig. 5b); however, it may also be produced directly from glucose but its production from fructose often reports favourability. Assary et al. [22] numerically investigated the thermochemistry at 298 and 448 K for the formation of levulinic acid from glucose with 5-HMF as an intermediate product. They observed that higher temperature favours thermodynamic properties of the reactions. They also assessed various functionals of density functional theory based on G4 energies reported that DFT functionals such as PBE, PW91, and B3PW91 perform accurately with 2–5 kcal/mol of energy differences. Along with the thermochemical analyzes, Assary et al. [35] also presented the reaction networks based on glucose and fructose compounds to platform chemicals such as 5-HMF, levulinic acid, and fufuryl alcohol in aqueous phase. In an experimental work, Binder and Raines [36] presented the mechanism of formation of 5-HMF from fructose which itself was yielded from cellulose in the presence of chlorides of chromium and copper catalysts. Their experiments reported 42% of transformation of dry cellulose to 5-HMF. Li et al. [37] carried out the conversion of glucose into 5-HMF via dehydration in the

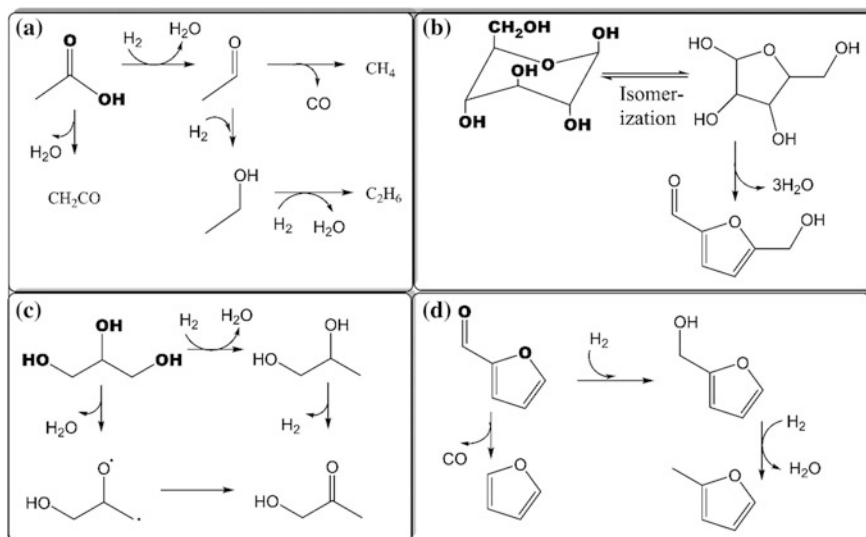
Table 5 Upgradation studies based on several bio-oil model compounds derived from cellulose and hemicellulose fractions of lignocellulosic biomass

Authors	Feed	Catalyst	Support	Major products
Assary et al. [22]	Glu	–	–	LA
Assary et al. [35]	Glu	–	–	HMF, FAL
Assary et al. [35]	Fru	–	–	HMF, FAL
Assary et al. [64]	Fru	–	–	HMF
Binder and Raines [36]	Fru	CrCl ₂ , CuCl, etc.	–	HMF
Li et al. [37]	Glu	C ₄ SO ₃ HmimCl	–	HMF
Huber et al. [20]	Glu	Pt	SiO ₂ –Al ₂ O ₃	C ₇ –C ₁₅ alkanes
Verma and Kishore [21]	Glu	–	–	C ₉ , C ₁₂ , and C ₁₅ alkanes
Xing et al. [38]	Xyl	Ru, Pt	C, SiO ₂ –Al ₂ O ₃	Tridecane
Huber et al. [39]	Sor	Pt	SiO ₂ –Al ₂ O ₃	Hexane, CH ₄ , C ₂ H ₆ , C ₃ H ₈ , H ₂ O
		Pd	SiO ₂ –Al ₂ O ₃	
		Pt	Al ₂ O ₃	
Pallassana and Neurock [40]	AA	Pd(111)	–	Ethanol
		Re(0001)	–	
		PdRe	–	
Rachmady and Vannice [41]	AA	Pt	TiO ₂	Acde, ethanol, ethane
		Pt	SiO ₂	
		Pt	η -Al ₂ O ₃	
		Pt	Fe ₂ O ₃	
Basagiannis and Verykios [42]	AA	Ru	Al ₂ O ₃ , MgO/Al ₂ O ₃	H ₂ , CH ₄ , CO, CO ₂ , C ₃ H ₆ O
Yang et al. [65]	AA	Ni	MgO	H ₂ , CH ₄ , CO, CO ₂ , CH ₂ CO
Pham et al. [43]	AA	Ru	TiO ₂	Acetone, CO ₂ , H ₂ O
Shangguan et al. [44]	AA	Ru	C	Ethanol
Alcala et al. [45]	AA	Pt-Sn	SiO ₂	Ethanol, Acde
		Pt(111)	–	CH ₄ , CO
Zhang et al. [46]	AA	Cu(111)	–	Ethanol
Pallassana and Neurock [40]	Acde	Pd(111)	–	Ethanol
		Re(0001)	–	
		PdRe	–	
Verma and Kishore [56]	Acde	Gas & Aqueous	–	Ethanol
Sato et al. [47]	Gly	Cu	Al ₂ O ₃	PD
Sato et al. [48]	Gly	Ag	SiO ₂	HP

(continued)

Table 5 (continued)

Authors	Feed	Catalyst	Support	Major products
D'Hondt et al. [49]	Gly	Pt	NaY	PD
			γ -Al ₂ O ₃	
			C	
			H-Beta	
Verma and Kishore [58]	HP	–	–	Acetone
Behtash et al. [57]	PA	Pd(111)	–	C2 alkenes and alkanes
		Pd(211)	–	
Bhogeswararao and Srinivas [50]	Fur	Pd	γ -Al ₂ O ₃	FAL, THFAL
		Pt	γ -Al ₂ O ₃	FAL
Sitthisa et al. [51]	Fur	Ni–Fe	SiO ₂	MF
Vorotnikov et al. [52]	Fur	Pd(111)	–	Furan, FAL, MF
Fellah [53]	Fur	Pt-graphene	–	Furan
Jeness and Vlachs [54]	FAL	RuO ₂ (110)	–	MF
Wang et al. [55]	Furan	Pd(111)	–	Butanol, THF, DHF, propene

**Fig. 5** Decomposition mechanisms of acetic acid (a), glucose (b), glycerol (c), and furfural (d) [35, 41, 48, 49, 52]

presence of SO_3H -functionalized ionic liquids. They presented two possible pathways for 5-HMF production from glucose with activation energies of 32.9 and 31.0 kcal/mol. They observed that the produced water compounds from dehydration of glucose take part in the reaction by transferring protons. On the other hand, Huber et al. [20] synthesized various long-chain liquid alkanes from glucose compound using several reactions such as dehydration, hydrogenation, hydrogenolysis, aldol condensation reactions. They reported that produced long-chain liquid alkanes are significantly appropriate for transportation fuels and contain 90% of energy of carbohydrate and hydrogen feeds. Numerical counterpart of experimental analyzes due to Huber et al. [20] is carried out by Verma and Kishore [21] under density functional theory (DFT) framework for thermochemical analyzes in gas and aqueous phases. They reported aqueous phase reactions as more stable compared to gas phase and in particular, hydrodeoxygenation reactions in aqueous phase showed higher thermodynamic favourability compared to gas phase because of contribution of produced water compound in proton transfer. On the other hand, Xing et al. [38] presented an experiment for the production of jet and diesel range fuels from hemicellulose-derived compounds. They followed similar approach as of Huber et al. [20] and reported 76% yield for overall process.

Further, Huber et al. [39] presented the conversion of sorbitol over $\text{SiO}_2\text{-Al}_2\text{O}_3$ supported Pd and Pt catalysts. They described the formation of alkanes from sorbitol employing various reactions such as C–C cleavage, methanation, dehydration, hydrogenation with 90% of heating value compared to the feedstock. In addition, the selectivity of C_6 alkane was recorded in between 30 and 55% over Pt–SiAl catalyst and different reaction parameters.

It is seen that the conversion of glucose and fructose is normally carried out for the formation of 5-HMF which is a very important intermediate to produce long-chain alkanes. However, further conversion of 5-HMF may lead to the production of 5-methylfurfural, furfural, furan, methylfuran, etc. On the other hand, the fermentation of glucose leads to the production of ethanol as biofuel which itself is a good candidate for fuel or blend to fuel.

5.2 Acetic Acid

Acetic acid (AA) component represents ‘acids’ catalogue of oxy-groups and it is found extensively in raw bio-oil [10]. Various experimental and numerical works have been performed on acetic acid decomposition, ketonization, etc., in the presence of several catalysts. Though it is an important product in daily use, but its decomposition to non-oxygenated or less oxygenated structure is highly encouraging in the context of bio-oil upgradation. A decomposition mechanism of acetic acid into several lower fractions is shown in Fig. 5a. The hydrodeoxygenation of AA leads to the formation of acetaldehyde which can itself undergo hydrogenation and decarbonylation reactions to produce ethanol and methane, respectively. The elimination of OH group of AA as water compound without additional H_2 may lead

to the formation of ethenone (CH_2CO), whereas the ethanol component from hydrogenation of acetaldehyde may further reduce to ethane compound upon HDO.

Pallassana and Neurock [40] carried out a numerical study based on acetic acid feedstock over Pd(111), Re(0001), and PdRe alloy. Most favourable reaction path is reported as the formation of acetyl which subsequently gets hydrogenated to form acetaldehyde. Further, the formation of end product ethanol is achieved via hydrogenation of acetaldehyde component. The bond dissociation of C–OH is highly favourable at Re(0001), whereas the hydrogenation of acetyl favours Pd (111) surface. Rachmady and Vannice [41], on the other hand, performed experiments on conversion of acetic acid in the presence of Pt supported SiO_2 , TiO_2 , Fe_2O_3 , and $\eta\text{-Al}_2\text{O}_3$ catalysts. Each support with Pt metal showed different selectivity towards product, for instance, Pt/ SiO_2 showed 50% methane production, Pt/ $\eta\text{-Al}_2\text{O}_3$ favoured 40% methane formation, Pt/ Fe_2O_3 produced 80% acetaldehyde, and Pt/ TiO_2 showed 50% ethanol formation. Basagiannis and Verykios [42] carried out steam reforming of acetic acid over ruthenium supported with Al_2O_3 and $\text{MgO}/\text{Al}_2\text{O}_3$. They observed various products, e.g. H_2 , CH_4 , CO , CO_2 , and $\text{C}_3\text{H}_6\text{O}$, and reported that Ru supported with $\text{MgO}/\text{Al}_2\text{O}_3$ showed higher activity and higher rate of carbon deposition compared to Ru/ Al_2O_3 . On the other hand, Pham et al. [43] studied the reaction kinetics for ketonization of acetic acid over Ru/ TiO_2 catalyst. They also tested other supports such as C and SiO_2 with Ru but both of these supports showed negligible ketonization activity; however, Ru/ TiO_2 catalyst showed higher ketonization activity. The major products were observed as acetone, water, and CO_2 . Shangguan et al. [44] carried out acetic acid conversion over Ru/C in aqueous phase and observed that Ru/C led to form ethanol as major product unlike the case of Ru/ TiO_2 due to Pham et al. [43]. Alcalá et al. [45] carried out experiments and computations for the conversion of acetic acid over Pt and PtSn-based catalysts. They reported that Pt-based catalysts are responsible for acetic acid decomposition into methane, carbon mono oxide, and ethane; however, the addition of Sn into Pt undergoes for the production of acetaldehyde and ethanol. On the other hand, Zhang et al. [46] carried out the conversion of acetic acid over Cu(111) and they also found ethanol as end product.

5.3 Glycerol

Glycerol component is one of the oxy-compounds present in unprocessed bio-oil in considerable amount. There have been various studies based on glycerol component in the context of bio-oil upgradation, for instance, Sato et al. [47, 48] carried out experiments for the conversion of glycerol over Cu/ Al_2O_3 and Ag/ SiO_2 catalysts. For both of catalytic systems, they observed different products, i.e. Cu/ Al_2O_3 led to the production of 1,2-propanediol (PD) and Ag/ SiO_2 was selective towards the production of 1-hydroxypropan-2-one (HP). In addition, D'Hondt et al. [49] carried out the conversion of glycerol over platinum catalyst supported with NaY, $\gamma\text{-Al}_2\text{O}_3$, C, and HBeta. Reported products were 1,2-propanediol, ethanol, *n*-propanol,

1-hydroxypropan-2-one. Pt/NaY catalysts showed higher selectivity towards 1,2-propanediol, whereas Pt/ γ -Al₂O₃, Pt/HBeta, and Pt/C undergo for major productions of *n*-propanol, ethanol, and *n*-propanol, respectively. The formation of PD from glycerol occurs due to the HDO reaction at the terminal hydroxyl group, whereas the production of HP from glycerol involves OH cleavage followed by hydrogen migration reactions. On the other hand, the formation of HP from PD may also occur due the dehydrogenation reaction (see Fig. 5c).

5.4 Furfural and Furfuryl Alcohol

Furfural is usually obtained from cellulose fraction upon dehydration reactions of glucose or fructose. However, further reduction of furfural leads to the production of furan using decarbonylation reaction, whereas furfuryl alcohol (FAL) can be obtained using hydrogenation reactions of furfural (see Fig. 5d). In addition, the HDO of FAL produces 2-methylfuran component. Furfural has been quite a popular compound amongst researchers in bio-oil field because of its ability to produce various specialty chemicals; therefore, numerous studies based on this component are carried out in recent past. For instance, Bhogeswararao and Srinivas [50] performed experiments based on furfural component over γ -Al₂O₃ supported with 2, 5, and 10% Pd and Pt noble metals. They observed that at 298 K, both metal supported catalysts underwent hydrogenation of furfural; however, at higher temperature 453 K, Pd supported catalysts underwent decarbonylation reaction of furfural to produce furan, whereas Pt supported catalysts were selective for the production of 2-methylfuran and furan ring-opened products. Sitthisa et al. [51] carried out furfural conversion over silica supported Ni and Ni-Fe. Over silica supported Ni catalysts, they observed the formation of furan and furfuryl alcohol which further underwent for the production of C₄ products and 2-methylfuran, respectively. However, silica supported Ni-Fe favours the production of 2-methylfuran in greater extent via furfural hydrogenation and furfuryl hydrogenolysis compared to C₄ products. Vorotnikov et al. [52], on the other hand, carried out computational analyzes for the conversion of furfural to furan, furfuryl alcohol, and 2-methylfuran in the presence of Pd(111) catalyst using density functional theory. Their thermodynamic analysis showed favourability for the formation of furan with CO from furfural via decarbonylation reaction. Similarly, Fellah [53] also carried out decarbonylation study of furfural but in the presence of platinum-doped graphene sheet. They calculated the rate determining step as the association of hydrogen atom to form furan component.

On the other hand, Jenness and Vlachos [54] carried out a computational study for the conversion of furfuryl alcohol over RuO₂(110) catalyst. They concluded that direct C–O bond scission is highly kinetic demanding; however, the insertion of a hydrogen atom to the furan ring followed by scission of C–O bond could significantly reduce the kinetic barrier. Wang et al. [55] performed a numerical study on ring hydrogenation and ring opening of furan ring over Pd(111) catalyst surface.

They concluded that the ring opening reaction as high activation barrier demanding; however, hydrogenation at the α -carbon of furan ring followed by ring opening is facile. They observed 1-butanol component as major product at high temperature while tetrahydrofuran as major product at lower temperature.

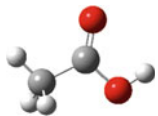
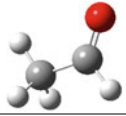
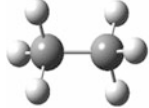
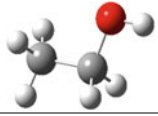
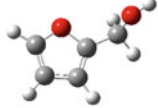
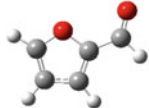
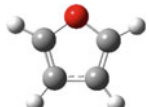
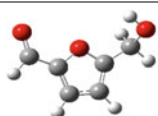
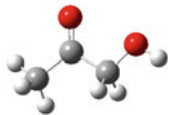

5.5 Other Model Compounds

There has been extensive research over other bio-oil model compounds derived from cellulose and hemicellulose fractions apart from above-mentioned model compounds, e.g. acetaldehyde, 1-hydroxypropan-2-one, 5-HMF, levoglucosan. as shown in Fig. 4. For instance, in the conversion of acetic acid to ethanol numerically, Pallassana and Neurock [40] found acetaldehyde as one of the intermediate product which reduced to ethanol component via ethoxy intermediate. On the other hand, Verma and Kishore [56] carried out numerical study on the conversion of acetaldehyde into ethanol in gas and aqueous milieus. They reported aqueous phase reactions as more favourable compared to gas phase conversions. Behtash et al. [57] carried out the conversion of propanoic acid computationally over Pd(111) and Pd(211) catalyst surfaces using decarbonylation and decarboxylation reactions. They suggested that C–OH and C–H bond scissions are overall rate controlling reaction steps over both catalyst surfaces; however, C–C bond dissociation reaction step over Pd(211) is partially rate controlling. Verma and Kishore [58] carried out another numerical study with 1-hydroxypropan-2-one as bio-oil model compound. They showed the formation of acetone using hydrodeoxygenation of feed component under density functional theory perspective. They opted M05-2X/6-31 + g(d,p) level of theory for single point energy over B3LYP/6-311 + g(d,p) optimized geometry for which the activation barrier was reported as 97.27 kcal/mol.

6 Application of Density Functional Theory in Bio-Oil

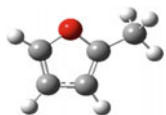
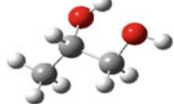
Density functional theory (DFT) [59, 60] is a computational quantum mechanical tool for investigating and predicting the atomic and molecular properties using electronic structure method. Unlike wavefunction methods, DFT depends on electron density which itself is dependent on only three spatial variables (x , y , and z). Here, the electronic energies of few molecular structures such as acetic acid, ethane, ethanol, HMF, furan involved in this study are shown in Table 6 for providing a preliminary idea about their ground-state energetics. Optimizations of all molecular structures using Gaussian 09 [61] software package are performed under DFT framework and at B3LYP (Becke-3-parameters-Lee-Yang-Parr) functional [62] with the basis set of 6–31g(d) [63].

Table 6 Electronic energy added with zero-point vibrational energy (ZPVE), i.e. E_{Total} , and ZPVE of few molecular structures involved in this work. The electronic energies of optimized structures are obtained at B3LYP/6-31g(d) level of theory under DFT framework

Component	Molecular structure	E_{Total} (hartree)	ZPVE (hartree)
AA		-229.019760	0.062027
Acde		-153.774301	0.055820
Ethane		-79.755182	0.075236
Ethanol		-154.953482	0.080319
FAL		-344.439473	0.102980
Fur		-343.266537	0.079804
Furan		-229.950386	0.070196
HMF		-457.759070	0.112738
HP		-268.263107	0.088865
Methane		-40.473159	0.045230

(continued)

Table 6 (continued)

Component	Molecular structure	E_{Total} (hartree)	ZPVE (hartree)
MF		-269.245658	0.098059
PD		-269.446887	0.113868

DFT is one of the most successful and promising computational tool for providing a reliable information of a particular molecule. Its extensive applicability in computational physics and chemistry allows one to investigate and study the chemistry behind the conversion and upgradation of lignocellulosic biomass and unprocessed bio-oil, respectively. In the recent period, the DFT tool has been applied extensively in bio-oil upgradation research area by analyzing the dominating reaction mechanisms to reduce high non-volatiles into low non-oxygenated fractions. Various such computational studies are already cited earlier in this review, and it has been seen that the computational means for analyzing the reaction mechanisms are dominating because of their accuracy, preliminary idea about reaction's favourability, energy requirements, etc.

7 Conclusion and Future Perspective

Various issues are discussed under this review for instance biomass, biomass species, conversion of biomass to bio-oil, glitches to bio-oil, bio-oil upgradation, and component-wise upgradation. Out of various upgradation processes, hydrodeoxygenation occurs as a consistent and reliable process. However, it does require high-pressure hydrogen for upgradation of bio-oil component. On the other hand, various bio-oil components derived from cellulose and hemicellulose fractions are reviewed over various catalysts and supports, be it experimental or numerical work. Cellulose depolymerization gives rise to glucose component which further can be converted to fructose and other specialty chemicals. Various studies suggest fructose as a potential intermediate and easy to dissociate compared to glucose. Fructose also gives rise to various value-added products, e.g. 5-HMF, levulinic acid. On the other hand, acetic acid is one of the bio-oil model components, representing carboxylic acid, which is extensively studied because of its higher fraction in unprocessed bio-oil. It produces lower fraction products such as CH_4 , CO , CO_2 upon its decomposition; also, it is often converted to ethanol as product using hydrogenolysis and hydrogenation reactions over Ru/C , Pt/SiO_2 , PtSn/SiO_2 , $\text{Pd}(111)$, etc. It is observed that few supports such as TiO_2 over Ru

favour ketonization of acetic acid, whereas Ru/C leads to ethanol component. Furfural is another bio-oil model compound which is studied extensively in the presence of various catalysts. It produces several products upon its upgradation such as furan via decarbonylation, furfuryl alcohol via hydrogenation, 2-methylfuran via hydrogenolysis of furfuryl alcohol.

There are various potential bio-oil model compounds which are considered less during upgradation of bio-oil such as 1-hydroxypropan-2-one, butan-2,3-diol, butan-2,3-dione representing miscellaneous oxygenates, alcohol, ketone groups, respectively. These components can be equally valuable to understand the bio-oil upgradation phenomena compared to other discussed bio-oil model compounds. However, apart from model compounds, the synthesis of appropriate catalyst is one of the most challenging tasks in bio-oil upgradation because each catalyst/support combination leads to different selectivity percentage towards desired product. In this case, bimetallic catalysts may lead to interesting results because of two different characteristics due to each metal. In addition, selection of appropriate support is another possibility to achieve desirable product.

References

1. World Energy Scenario 2016 (2016)
2. Government Of India Ministry of Power Central Electricity Authority New Delhi (2016)
3. World Energy Outlook 2016 (2016) Int Energy Agency. doi:http://www.iea.org/publications/freepublications/publication/WEB_WorldEnergyOutlook2015ExecutiveSummaryEnglishFinal.pdf
4. World Energy Council (2013) World Energy Resources: 2013 survey. doi:http://www.worldenergy.org/wp-content/uploads/2013/09/Complete_WER_2013_Survey.pdf
5. Huber GW, Iborra S, Corma A (2006) Synthesis of transportation fuels from biomass: chemistry, catalysts, and engineering. *Chem Rev* 106:4044–4098
6. Klass DL (2004) Biomass for renewable energy and fuels. *Environ Energy* 1:193–212
7. Alonso DM, Bond JQ, Dumesic JA (2010) Catalytic conversion of biomass to biofuels. *Green Chem* 12:1493–1513
8. Towler GP, Oroskar AR, Smith SE (2004) Development of a sustainable liquid fuels infrastructure based on biomass. *Environ Prog* 23:334–341
9. Lynd LR, Wyman CE, Gerngross TU (1999) Biocommodity engineering. *Biotechnol Prog* 15:777–793
10. Wang H, Male J, Wang Y (2013) Recent advances in hydrotreating of pyrolysis bio-oil and its oxygen-containing model compounds. *ACS Catal* 3:1047–1070
11. Spath PL, Dayton DC (2003) Preliminary screening—technical and economic assessment of synthesis gas to fuels and chemicals with emphasis on the potential for biomass-derived syngas. *Natl Renew Energy Lab*. <https://doi.org/10.2172/15006100>
12. Tomishige K, Asadullah M, Kunitomi K (2004) Syngas production by biomass gasification using Rh/CeO₂/SiO₂ catalysts and fluidized bed reactor. *Catal Today* 89:389–403
13. Sutton D, Kelleher B, Ross JRH (2001) Review of literature on catalysts for biomass gasification. *Fuel Process Technol* 73:155–173
14. Mohan D, Pittman CU, Steele PH (2006) Pyrolysis of wood/biomass for bio-oil: a critical review. *Energy Fuels* 20:848–889

15. Evans RJ, Milne TA (1987) Molecular characterization of pyrolysis of biomass. 1. Fundamentals. *Energy Fuels* 1:123–138
16. Stöcker M (2008) Biofuels and biomass-to-liquid fuels in the biorefinery: catalytic conversion of lignocellulosic biomass using porous materials. *Angew Chemie Int Ed* 47:9200–9211
17. Danaei Kenarsari S, Zheng Y (2014) Fast pyrolysis of biomass pellets using concentrated solar radiation: a numerical study. *J Sol Energy Eng* 136:41004–1–41004–7
18. Moffatt JM, Overend RP (1985) Direct liquefaction of wood through solvolysis and catalytic hydrodeoxygenation: an engineering assessment. *Biomass* 7:99–123
19. Czernik S, Bridgwater A (2004) Overview of applications of biomass fast pyrolysis oil. *Energy Fuels* 18:590–598
20. Huber GW, Chheda JN, Barrett CJ, Dumesic JA (2005) production of liquid alkanes by aqueous-phase processing of biomass-derived carbohydrates. *Science* (80-) 308:1446–1450
21. Verma AM, Kishore N (2016) Thermochemistry analyses for transformation of C6 glucose compound into C9, C12 and C15 alkanes using density functional theory. *Mol Phys* 4:413–423
22. Assary RS, Redfern PC, Hammond JR, Greeley J, Curtiss LA (2010) Computational studies of the thermochemistry for conversion of glucose to levulinic acid. *J Phys Chem B* 114:9002–9009
23. Branca C, Giudicianni P, Di Blasi C (2003) GC/MS characterization of liquids generated from low-temperature pyrolysis of wood. *Ind Eng Chem Res* 42:3190–3202
24. Diebold JP (2000) A review of the chemical and physical mechanisms of the storage stability of fast pyrolysis bio-oils. *Natl Renew Energy Lab*. <http://doi.org/NREL/SR-570-27613>
25. Mu W, Ben H, Ragauskas A, Deng Y (2013) Lignin pyrolysis components and upgrading—technology review. *BioEnergy Res* 6:1183–1204
26. Corma A (2003) State of the art and future challenges of zeolites as catalysts. *J Catal* 216:298–312
27. Ikura M, Stanculescu M, Hogan E (2003) Emulsification of pyrolysis derived bio-oil in diesel fuel. *Biomass Bioenergy* 24:221–232
28. Chiamonti D, Bonini M, Fratini E, Tondi G, Gartner K, Bridgwater AV, Grimm HP, Soldaini I, Webster A, Baglioni P (2003) Development of emulsions from biomass pyrolysis liquid and diesel and their use in engines—part 1: emulsion production. *Biomass Bioenergy* 25:85–99
29. Chiamonti D, Bonini M, Fratini E, Tondi G, Gartner K, Bridgwater AV, Grimm HP, Soldaini I, Webster A, Baglioni P (2003) Development of emulsions from biomass pyrolysis liquid and diesel and their use in engines—part 2: tests in diesel engines. *Biomass Bioenergy* 25:101–111
30. Furimsky E (1983) Chemistry of catalytic hydrodeoxygenation. *Catal Rev* 25:421–458
31. Furimsky E (2000) Catalytic hydrodeoxygenation. *Appl Catal A Gen* 199:147–190
32. Saidi M, Samimi F, Karimipourfard D, Nimmanwudipong T, Gates BC, Rahimpour MR (2014) Upgrading of lignin-derived bio-oils by catalytic hydrodeoxygenation. *Energy Environ Sci* 7:103–129
33. Elliott DC, Schiefelbein GF (1989) Liquid hydrocarbon fuels from biomass. *Am Chem Soc Div Fuel Chem Prepr* 34:1160–1166
34. Diebold JP, Czernik S (1997) Additives to lower and stabilize the viscosity of pyrolysis oils during storage. *Energy Fuels* 11:1081–1091
35. Assary RS, Kim T, Low JJ, Greeley J, Curtiss LA (2012) Glucose and fructose to platform chemicals: understanding the thermodynamic landscapes of acid-catalysed reactions using high-level ab initio methods. *Phys Chem Chem Phys* 14:16603–16611
36. Binder JB, Raines RT (2009) Simple chemical transformation of lignocellulosic biomass into furans for fuels and chemicals. *J Am Chem Soc* 131:1979–1985
37. Li J, Li J, Zhang D, Liu C (2015) Theoretical elucidation of glucose dehydration to 5-hydroxymethylfurfural catalyzed by a SO₃H-functionalized ionic liquid. *J Phys Chem B* 119:13398–13406

38. Xing R, Subrahmanyam AV, Olcay H, Qi W, van Walsum GP, Pendse H, Huber GW (2010) Production of jet and diesel fuel range alkanes from waste hemicellulose-derived aqueous solutions. *Green Chem* 12:1933
39. Huber GW, Cortright RD, Dumesic JA (2004) Renewable alkanes by aqueous-phase reforming of biomass-derived oxygenates. *Angew Chemie Int Ed* 43:1549–1551
40. Pallassana V, Neurock M (2002) reaction paths in the hydrogenolysis of acetic acid to ethanol over Pd(111), Re(0001), and PdRe alloys. *J Catal* 209:289–305
41. Rachmady W, Vannice M (2000) Acetic acid hydrogenation over supported platinum catalysts. *J Catal* 192:322–334
42. Basagiannis AC, Veykios XE (2008) Influence of the carrier on steam reforming of acetic acid over Ru-based catalysts. *Appl Catal B Environ* 82:77–88
43. Pham TN, Shi D, Resasco DE (2014) Kinetics and mechanism of ketonization of acetic acid on Ru/TiO₂ catalyst. *Top Catal* 57:706–714
44. Shangquan J, Olarte MV, Chin YH (2016) Mechanistic insights on C-O and C-C bond activation and hydrogen insertion during acetic acid hydrogenation catalyzed by ruthenium clusters in aqueous medium. *J Catal* 340:107–121
45. Alcalá R, Shabaker JW, Huber GW, Sanchez-Castillo MA, Dumesic JA (2005) Experimental and DFT studies of the conversion of ethanol and acetic acid on PtSn-based catalysts. *J Phys Chem B* 109:2074–2085
46. Zhang M, Yao R, Jiang H, Li G, Chen Y (2017) Insights into the mechanism of acetic acid hydrogenation to ethanol on Cu(111) surface. *Appl Surf Sci* 412:342–349
47. Sato S, Akiyama M, Inui K, Yokota M (2009) Selective conversion of glycerol into 1,2-propanediol at ambient hydrogen pressure. *Chem Lett* 38:560–561
48. Sato S, Sakai D, Sato F, Yamada Y (2012) Vapor-phase dehydration of glycerol into hydroxyacetone over silver catalyst. *Chem Lett* 41:965–966
49. D'Hondt E, Van de Vyver S, Sels BF, Jacobs PA (2008) Catalytic glycerol conversion into 1,2-propanediol in absence of added hydrogen. *Chem Commun*: 6011–6012
50. Bhogeswararao S, Srinivas D (2015) Catalytic conversion of furfural to industrial chemicals over supported Pt and Pd catalysts. *J Catal* 327:65–77
51. Sithisa S, An W, Resasco DE (2011) Selective conversion of furfural to methylfuran over silica-supported NiFe bimetallic catalysts. *J Catal* 284:90–101
52. Vorotnikov V, Mpourmpakis G, Vlachos DG (2012) DFT study of furfural conversion to furan, furfuryl alcohol, and 2—methylfuran on Pd (111). *ACS Catal* 2:2496–2504
53. Fellah MF (2017) Direct decarbonylation of furfural to furan: a density functional theory study on Pt-graphene. *Appl Surf Sci* 405:395–404
54. Jenness GR, Vlachos DG (2015) DFT study of the conversion of furfuryl alcohol to 2-methylfuran on RuO₂ (110). *J Phys Chem C* 119:5938–5945
55. Wang S, Vorotnikov V, Vlachos DG (2014) A DFT study of furan hydrogenation and ring opening on Pd(111). *Green Chem* 16:736–747
56. Verma AM, Kishore N (2016) DFT study on hydrogenation reaction of acetaldehyde to ethanol in gas and water phase. *Int J Res Eng Technol* 5:53–57
57. Behtash S, Lu J, Williams CT, Monnier JR, Heyden A (2015) Effect of palladium surface structure on the hydrodeoxygenation of propanoic acid: identification of active sites. *J Phys Chem C* 119:1928–1942
58. Verma AM, Kishore N (2015) DFT study on hydrogenation reaction of 1-hydroxypropan-2-one. In: *Proceedings of 30th Indian Engineering Congress 21st Century Engineering. The Make India Pathway*, pp 9–15
59. Hohenberg P, Kohn W (1964) Inhomogeneous electron gas. *Phys Rev* 136:B864–B871
60. Kohn W, Sham L (1965) Self-consistent equations including exchange and correlation effects. *Phys Rev* 385:A1133–A1138
61. Frisch MJ, Trucks GW, Schlegel HB, Scuseria GE, Robb MA, Cheeseman JR, Scalmani G, Barone V, Petersson GA, Nakatsuji H, Li X, Caricato M, Marenich AV, Bloino J, Janesko BG, Gomperts R, Mennucci B, Hratchian H P, Ortiz JV, Izmaylov AF, Sonnenberg JL, Williams-Young D, Ding F, Lipparini F, Egidi F, Goings J, Peng B,

- Petrone A, Henderson T, Ranasinghe D, Zakrzewski VG, Gao J, Rega N, Zheng G, Liang W, Hada M, Ehara M, Toyota K, Fukuda R, Hasegawa J, Ishida M, Nakajima T, Honda Y, Kitao O, Nakai H, Vreven T, Throssell K, Montgomery JA Jr, Peralta JE, Ogliaro F, Bearpark MJ, Heyd JJ, Brothers EN, Kudin KN, Staroverov VN, Keith TA, Kobayashi R, Normand J, Raghavachari K, Rendell AP, Burant JC, Iyengar SS, Tomasi J, Cossi M, Millam JM, Klene M, Adamo C, Cammi R, Ochterski JW, Martin RL, Morokuma K, Farkas O, Foresman JB, Fox DJ (2009) Gaussian 09, Revision B.01. Gaussian 09, Revis. B.01. Gaussian, Inc., Wallingford CT
62. Becke AD (1993) Density-functional thermochemistry. III. The role of exact exchange. *J Chem Phys* 98:5648–5652
 63. Ditchfield R, Hehre WJ, Pople JA (1971) Self-consistent molecular-orbital methods. IX. An extended gaussian-type basis for molecular-orbital studies of organic molecules. *J Chem Phys* 54:724–728
 64. Assary RS, Redfern PC, Greeley J, Curtiss LA (2011) Mechanistic insights into the decomposition of fructose to hydroxy methyl furfural in neutral and acidic environments using high-level quantum chemical methods. *J Phys Chem B* 115:4341–4349
 65. Yang X, Wang Y, Li M, Sun B, Li Y, Wang Y (2016) Enhanced hydrogen production by steam reforming of acetic acid over a Ni catalyst supported on mesoporous MgO. *Energy Fuels* 30:2198–2203

A Succinct Review on Upgrading of Lignin-Derived Bio-oil Model Components

Anand Mohan Verma and Nanda Kishore

Abstract Increasing energy demand and depleting non-renewable energy resources have centred the researcher's cognition to develop a sustainable technology that can exploit renewable energies. Renewable energies include solar energy, wind energy, tidal energy, hydropower, biomass but leaving a snag there that only biomass, as the renewable energy resource, could be the sustainable alternative for transportation fuels because it delivers sustainable carbon. Biomass comprises of three main units, i.e. cellulose, hemicellulose, and lignin. In the recent past, cellulose and hemicellulose have acquired much attention but, on the other hand, lignin scuffled to get proper consideration. However, earlier it has been used to produce a less effective heat and electricity by combustion. Currently, lignin is magnanimous amongst researchers because of its higher energy density, great source for phenolic fine chemicals, etc. Bio-oils derived from fast pyrolysis of lignocellulosic biomass comprise of more than 300 oxy-compounds which vitiate its quality in the form of low pH value, less stable, highly viscous, and low heating value for the application as transportation fuel. Therefore, it needs the proper upgradation technology to make it exploitable for transportation fuels. Here in this chapter, a succinct review is carried out for the lignin-derived bio-oil model compounds such as phenol, guaiacol, anisole, vanillin, and eugenol. Guaiacol component is one of the key components in phenolic fraction of bio-oil because its presence in bio-oil is often higher and, in addition, other higher molecular weight phenolic model compounds such as vanillin and eugenol reduce to guaiacol majorly. Furthermore, guaiacol component can successfully represent a higher fraction of lignin structure because of attachment of hydroxyl and methoxy groups in its molecular structure.

Keywords Lignin · Bio-oil · Lignocellulosic biomass · Kinetics
Guaiacol · Sustainable energy

A. M. Verma · N. Kishore (✉)

Department of Chemical Engineering, Indian Institute of Technology Guwahati,
Guwahati 781039, India

e-mail: nkishore@iitg.ernet.in; mail2nkishore@gmail.com

Abbreviations

PHE	Phenol
BEN	Benzene
CYHA	Cyclohexane
CYHN	Cyclohexanone
CYHL	Cyclohexanol
CYHD	Cyclohexan-2,4-dione
ANI	Anisole
<i>o</i> -Cr	<i>o</i> -cresol
<i>m</i> -Cr	<i>m</i> -cresol
<i>p</i> -Cr	<i>p</i> -cresol
TOL	Toluene
MXCYHA	Methoxycyclohexane
GUA	Guaiacol
CAT	Catechol
MXCYHL	2-methoxycyclohexanol
MCAT	Methylcatechol
SAL	Salicylaldehyde
MXCYHDL	6-methoxycyclohexa-1,5-dien-1-ol
CYHDN	Cyclohexan-1,2-dione
CYHDDL	Cyclohexa-2,6-dien-1,2-diol
CYPTN	Cyclopentanone
DHBZD	3,4-dihydroxybenzaldehyde
VAN	Vanillin
<i>p</i> -HBZD	4-hydroxybenzaldehyde
MXBZD	3-methoxybenzaldehyde
<i>m</i> -HBZD	3-hydroxybenzaldehyde
EUG	Eugenol
ALCAT	4-allylcatechol
ALPHE	4-allylphenol
PLPHE	4-propylphenol
PLBEN	Propylbenzene
PLGUA	4-propylguaiacol
PLCAT	4-propylcatechol
ALANI	3-allylanisole
ALPHE	3-allylphenol

1 Introduction

The exploration of an alternative energy resource other than fossil reserves in the twenty-first century is at its peak because of declining fossil resources, increasing energy demand, and increasing pollution occurred by fossils. Fossil fuels are the main reason for growth in the pollution levels in urban and suburban regions across the world because it releases the oxides of carbon (carbon monoxide and carbon dioxide), sulphur, and nitrogen which cause serious impacts on habitats [1]. Declining fossil reserves (especially petroleum fuels) and increasing energy demands at the same time have attracted researchers' concerns to develop a socio-economic and green fuel technology to surpass this hurdle. In this scenario, renewable energies are the best possible alternative to diminish the environmental and depletion concerns due to non-renewable energy resources. Renewable energy resources include tidal energy, solar energy, hydropower, geothermal energy, biomass; however, out of all renewable energy resources, only biomass has the potential to provide sustainable carbon element for transportation fuel and specialty or platform chemicals [1, 2]. Due to this remarkable feature, biomass, as renewable energy resource, is favourite amongst researchers compared to other non-conventional energy resources. In addition, biomass is inexpensive, abundant, and easily available in most of the nations; therefore, the research based on biomass has been increased remarkably in the last decade [1, 3, 4]. Furthermore, the net rise in CO₂ level in the atmosphere due to biomass consumption is zero if exploited properly [5, 6]. Lignocellulosic biomass, a class of biomass, is mainly composed of three building blocks, viz. cellulose, hemicellulose, and lignin [1, 7]. Cellulose is polymer of D-glucose monomers linked together via β -1,4-glycoside linkages, and it contributes 40–80 wt% in total biomass composition [1, 7]. Hemicellulose which covers 15–30 wt% of total biomass comprises of five different monomers, namely xylose, mannose, galactose, rhamnose, and arabinose [1, 5, 7]. Lignin, on the other hand, is a complex three-dimensional polymer of different phenylpropane units linked via ether and carbon–carbon bonds (see Fig. 1). It accounts for 15–30 wt% of total biomass. Earlier, due to its complex structure, it used to be scrapped off or combusted to produce low-quality heat or electricity but in the recent past, research based on lignin fraction of lignocellulosic biomass is increased enormously irrespective of its very complex structure because: (a) it has high energy density compared to other two building blocks of lignocellulosic biomass, (b) it is by-product in pulp and paper industries, (c) it can withstand at high temperature during pyrolysis compared to other two fractions of lignocellulosic biomass, (d) it is an excellent platform for generation of various phenolic specialty chemicals, etc. [3, 8]. This review work focuses on chemistry of lignin, model compounds due to lignin-derived bio-oil components, and their upgradation processes.

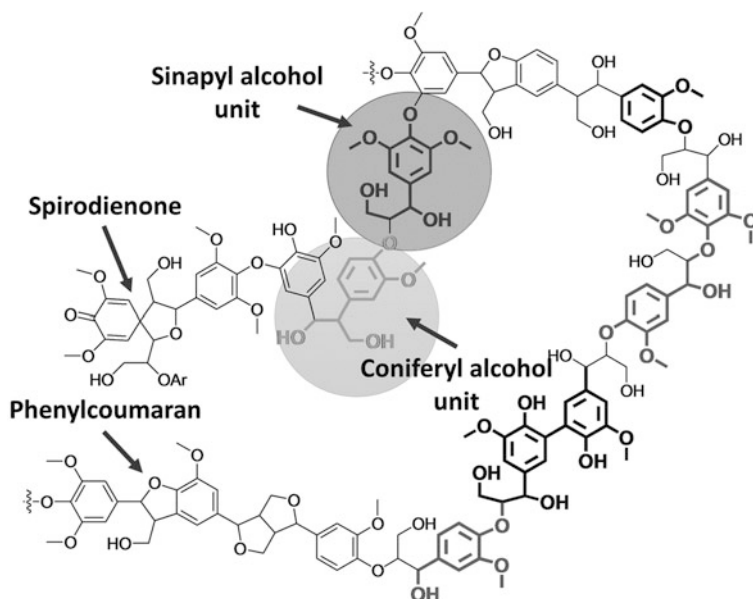


Fig. 1 Three-dimensional structure of lignin [53]

2 Lignin

Lignin (see Fig. 1) is highly complex three-dimensional copolymer of mainly three phenylpropane units, namely *p*-coumaryl alcohol, sinapyl alcohol, and coniferyl alcohol. All these three monomers of lignin are depicted in Fig. 2. Precise structure of lignin is still unclear to researchers; however, it is found that monomers form lignin polymer via various reported bond linkages such as β -O-4-aryl ether, α -O-4-aryl ether, 4-O-5-diaryl ether, β -5-phenylcoumaran, 5-5-biphenyl,

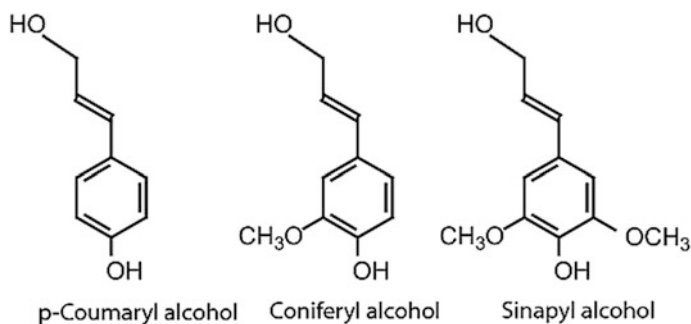


Fig. 2 Structure of lignin monomers: *p*-coumaryl alcohol, coniferyl alcohol, and sinapyl alcohol [1]

β -1-(1,2-diarylpropane), β - β -(resinol). [9]. Out of all these linkages, β -O-4-aryl ether linkage is found to be most frequent type of coupling linkage amongst others in both softwood and hardwood lignins [9]. The lignocellulosic biomass generally comprises lignin fraction from 15 to 30%; however, the amount of lignin depends on type of feedstock, e.g. softwoods contain higher fraction of lignin compared to hardwoods followed by grasses [1, 5, 9].

The isolation of lignin from lignocellulosic feedstocks can be achieved by various mechanical and chemical methods [9]. The isolation of lignin based on solubilizing agent is quite popular; however, there are two approaches in the solubilizing process. First approach dissolves cellulose and hemicellulose fractions of lignocellulosic biomass only and leaves lignin as residue, e.g. by-production of lignin from ethanol fuel biorefinery, while second approach dissolves lignin only and leaves cellulose and hemicellulose fractions as residues, e.g. kraft and sulphate pulping in pulp and paper industries [9, 10]. The cellulose and hemicellulose parts of biomass have got a considerable amount of attention and so the components representing both building blocks in unprocessed bio-oil. But lignin part was not majorly touched by researchers since last decade due to its complex 3D structure. Lignins are also found as the by-product from pulp and paper industries, though they were used to be either scrapped off or to produce low efficiency heat and electricity. However, as it is described earlier that lignins are 3D structure of phenylpropane units, they are a major source for obtaining phenolic platform chemicals. On the other hand, the upgraded phenolic fraction of bio-oil, as a blend to the transportation fuel, is a great source of aromatic hydrocarbons which are well known to enhance the octane number of gasoline.

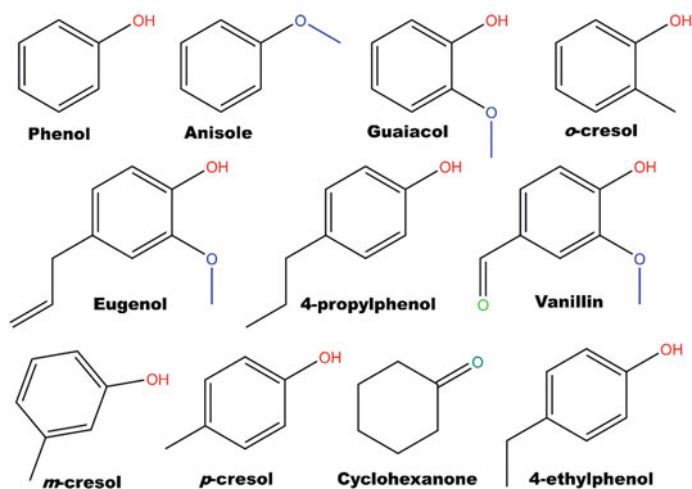
3 Decomposition of Lignin

A major disadvantage of lignin fraction is that it is little complicated to decompose and produces huge amount of solid chars compared to other two building blocks of lignocellulosic biomass. Nevertheless, the conversion of lignin can be carried out primarily via pyrolysis, gasification, thermolysis, hydrogenolysis, hydrolysis, oxidation, and combustion [1, 3, 8, 9]. Pyrolysis process of lignin occurs in the absence of oxygen or steam/air at elevated temperature, while gasification process involves oxygen content to break down heavy molecular weight species. On the other hand, thermolysis is process of breakdown of lignin in the presence of heat; pyrolysis is a type of thermolysis. Under hydrogenolysis, the C–C or C–O bonds are cleaved with hydrogen, while hydrolysis process involves the presence of water to assist in breaking bonds. Furthermore, the conversion of lignin through oxidation and combustion processes is also considered by various researchers due to the presence of oxy-functional groups [11, 12]. These conversion processes convert lignin into four forms of products, namely gases, liquid oils, chars, and heat [1, 5, 8, 9]. The products from different decomposition processes of lignin are listed in Table 1 [13]. Chars and heat can be utilized in the production of electricity. Gaseous products

Table 1 Different decomposition processes of lignin and their products [13]

Process	Feed	Products from lignin
Combustion	Lignin	Flue gases
Gasification		Syngas
Pyrolysis		Bio-oil, char
Hydrolysis		Char

include CO, H₂, CO₂, and CH₄, while liquid oils include phenols, aldehydes, and aliphatic components. The utilization of gaseous products can be in the production of methanol by methanol synthesis, H₂ by water–gas shift reaction, and alkanes by Fisher–Tropsch process. On the other hand, the liquid unprocessed bio-oils which include a huge range of phenolic oxy-compounds such as phenol, anisole, guaiacol, vanillin, eugenol suffer from various drawbacks, e.g. low heating value, low pH, low stability, high viscosity, due to these oxy-compounds. A pyrolytic experiment is carried out by Jiang et al. [14], and they have reported a huge range of major phenolic components. A few major phenolic bio-oil model compounds due to pyrolysis of lignin are depicted in Fig. 3. Furthermore, the presence of major phenolic model compounds is also reviewed by Mu et al. [8]. The unprocessed liquid bio-oils due to various conversion processes of lignin feedstocks cannot be applied to the transportation vehicles due to high amount of oxygen containing compounds; therefore, it must be channelized to upgradation processes. There are various chemical processes for the upgradation of unprocessed bio-oil derived from pyrolysis and/or liquefaction of lignocellulosic biomass, for instance, upgradation on zeolite catalysts, emulsification, hydrodeoxygenation (HDO). Corma [15]

**Fig. 3** Major phenolic bio-oil model compounds derived from lignin fraction of lignocellulosic biomass [54]

carried out a comprehensive review regarding the zeolite catalysts and their applications in bio-oil and petroleum refineries. Zeolite catalysts, however, present advantage of no additional hydrogen requirement for bio-oil upgradation but lack with disadvantage of coking over pores of the catalyst surface which reduces their catalytic activities [1]. Emulsification of bio-oils with appropriate surfactants may show the similar characteristics of diesel fuel but the corrosion process inside vehicle engine due to high water content is still challenging [1]. On the other hand, hydrodeoxygenation process for bio-oil upgradation is reviewed to be the best technique by far; however, this process requires high pressure of hydrogen [1, 3, 8].

4 Hydrodeoxygenation (HDO)

Hydrodeoxygenation is a chemical process of cleaving C–O bonds using hydrogen gas over appropriate catalytic system. In 1983, Furimsky [16] first published the review paper on the catalytic hydrodeoxygenation in which he pointed out the chemistry of hydrodeoxygenation, catalyst behaviour, mechanism, and kinetic study related to HDO process in crude oil upgrading. At that time, a very limited information was available due to the novelty of the subject and also because the hydrodeoxygenation process was not attracting the attention that time. The main reason of unfamed hydrodeoxygenation process earlier in 1980 and 1990s was that in crude petroleum oil, the oxygen content is very less and sulphur content is high; therefore, hydrosulphurization (HDS), hydrodenitrogenation (HDN), etc., are major processes in petroleum refining industries [3]. However, because of declining fossil fuels, increasing pollution, and energy demand, researchers diverted their concerns towards biomass to bio-oil process. The case with raw bio-oil from pyrolysis or liquefaction is quite reverse with the petroleum fuel because, in the raw bio-oil, oxygen content is quite high and sulphur appears as trace amounts; therefore, hydrodeoxygenation process is dominating in the bio-oil upgradation era [1, 3]. In 2000, Furimsky [17] reviewed another catalytic hydrodeoxygenation process with further extended range. This time, more detailed information was included about the components such as phenol, furan, ether, and other bio-oil components. Further, Huber et al. [1] presented a thorough review on synthesis of transportation fuels from biomass. They reported the chemistry of biomass, routes of transformation of biomass to bio-oil, and catalysis in bio-oil upgradation. They also reported transformation of biomass, feedstock types, production of bio-oil, upgrading routes, and their processes. Mu et al. [8] reviewed the upgradation of lignin-derived bio-oil components from pyrolysis. They gave a detailed phenomenon of various catalysts and their deactivation along with supports and promoters for the catalyst. Saidi et al. [3] also reported a review about the upgradation of lignin-derived bio-oils by catalytic hydrodeoxygenation. They reviewed the catalytic upgradation of the lignin-derived model compounds such as guaiacol, phenol, and anisole with their reaction networks and mechanisms. Catalytic behaviours have been reported for

mono-metallic, bimetallic, metal sulphides, metal phosphides, metal nitrides catalysts along with the promoters and supporters to the catalyst.

There are several phenolic bio-oil model compounds present in the lignin-derived bio-oil (see Fig. 3) such as phenol, guaiacol, anisole, vanillin, eugenol which are great source of generating platform chemicals and can be decomposed to obtain various aromatic hydrocarbons. Considerable amount of experimental works is available on phenol, guaiacol, anisole, etc., in the presence of various catalysts; however, research based on theoretical studies involving these model compounds is lacking. Nevertheless, the discussion on various reaction mechanisms and catalytic works based on five phenolic bio-oil model compounds, i.e. phenol, anisole, guaiacol, vanillin, and eugenol, derived from pyrolysis or liquefaction of lignin is presented below.

4.1 Phenol

Phenol component is a very good representation for phenolic fraction of unprocessed bio-oils derived from pyrolysis of lignin feedstock because of hydroxyl group attached with phenyl ring [3]. In fact, the structure of *p*-coumaryl alcohol which is one of the three monomers of lignin represents one hydroxyl group attached to aromatic ring; however, there is another hydroxyl group in *p*-coumaryl alcohol but that is attached with chain (see Fig. 2). Therefore, upgradation study of phenol can be very important in order to understand the cleavages of C_{aromatic}-OH bonds in lignin structures. Figure 4 depicts the conversion mechanism of phenol. Phenol can be upgraded via various routes such as hydrodeoxygenation of phenol yielding benzene, keto-enol tautomerization of phenol to convert the C-O single bond into ketone group by migrating the hydrogen to aromatic carbon followed by two molecular hydrogenation reactions to saturate the ring to produce cyclohexanone, three molecular hydrogenation reactions to saturate the phenyl ring to produce cyclohexanol. The production of cyclohexanol can also be achieved via hydrogenation of C=O double bond of cyclohexanone. On the other hand, the elimination of water compound via HDO of cyclohexanol produces cyclohexane structure. However, the production of cyclohexane can also be achieved via ring saturation of benzene (see Fig. 4). Various experimental and computational studies have been performed for HDO of phenol component (see Table 2); for instance, Şenol et al. [18] in their experiment of phenol conversion observed the production of benzene over γ -Al₂O₃-supported CoMo catalytic system; however, NiMo/ γ -Al₂O₃ catalyst showed major production of cyclohexane. On the other hand, silica-supported Ni catalyst showed higher selectivities of cyclohexanone, cyclohexanol, and benzene in the phenol conversion experiment carried out by Shin and Keane [19] in the temperature range of 423–573 K. However, the production of benzene was observed only at higher temperature cases. Furthermore, the Pd/C and HZSM-5 catalysts showed the formation of cycloalkanes instead of aromatics in the experiments performed by Zhao and Lercher [20]. The HY zeolite catalysts for the

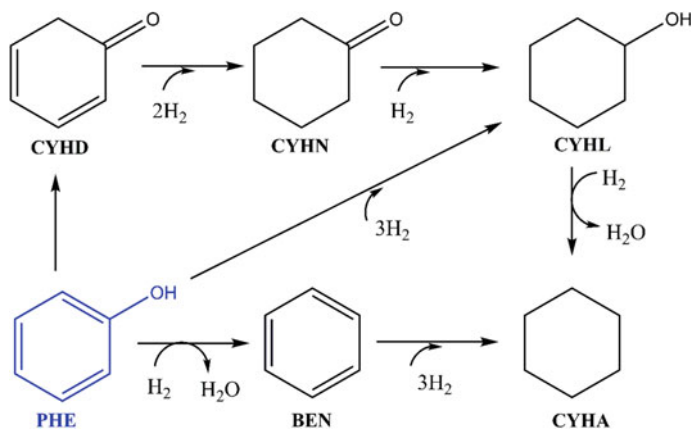


Fig. 4 Conversion mechanisms of phenol

Table 2 Upgradation of lignin-derived bio-oil model compounds over various catalysts and supports

Authors	Feed	Catalyst	Support	Major products
Şenol et al. [18]	PHE	CoMo	$\gamma\text{-Al}_2\text{O}_3$	BEN
		NiMo		CYHA
Shin and Keane [19]	PHE	Ni	SiO_2	CYHA, CYHL, BEN
Zhao and Lercher [20]	PHE	Pd	C, HZSM-5	Cycloalkanes
Hong et al. [21]	PHE	–	HY zeolite	
		Pt	HY, H β , HZSM-5	CYHA
Huuska and Rintala [27]	ANI	CoMo	$\gamma\text{-Al}_2\text{O}_3$	PHE, cresols
		NiMo		
Zhu et al. [23]	ANI	Pt	H β -zeolite	BEN, xylene, toluene
			SiO_2	BEN
Hurff and Klein [24]	ANI	CoMo	Al_2O_3	CYHA, PHE, BEN
Huuska [26]	ANI	Mo	$\gamma\text{-Al}_2\text{O}_3$	PHE, cresol, 2,6-dimethylphenol
		Ni	$\gamma\text{-Al}_2\text{O}_3$, SiO_2	PHE, BEN
Olcese et al. [28]	GUA	Fe	SiO_2	BEN, CYHA
Bykova et al. [31]	GUA	Ni–Cu	SiO_2	CYHA, CYHN
			Al_2O_3	
Lee et al. [33]	GUA	Pt(111)	–	Catechol
Lu et al. [34]	GUA	Pt(111)	–	Catechol

(continued)

Table 2 (continued)

Authors	Feed	Catalyst	Support	Major products
Lu et al. [36]	GUA	Ru (0011)	–	Phenol
Bindwal and Vaidya [37]	VAN	Ru	C	Creosol
Jiang et al. [42]	VAN	Pd	Carbon nitride	Creosol
Nimmanwudipong et al. [46]	EUG	Pt	γ -Al ₂ O ₃	PLGUA
		HY zeolite	–	GUA, isoeugenol
Zhang et al. [47]	EUG	Pd	C	2-methoxy-4-propylcyclohexanol
		HZSM-5	–	
Chen et al. [50]	EUG	Ru	CNT	Propylcyclohexane

conversion of phenol were not reported to be suitable by Hong et al. [21], though HY zeolite upon impregnation of Pt metal showed very high conversion of phenol to cyclohexane. On the other hand, noble metal Pt supported with silica and alumina separately is reported to be favourable for the production of cyclohexanol. Along with dispersion of Pt over HY zeolite, Hong et al. [21] also tested their experiments on H β and HZSM-5-supported Pt catalytic systems and testified cyclohexane as major product. The conversion of phenol, an intermediate in the conversion of guaiacol, in the production of cyclohexanone component is studied recently by Verma and Kishore [22]. They carried out two competitive reaction schemes to produce cyclohexanone numerically in the gas phase and in the absence of catalyst employing the framework of density functional theory (DFT). Under first route, phenol was subjected for a partial ring saturation followed by keto-enol tautomerization reaction and a molecular hydrogenation reaction to completely saturate the ring and produce cyclohexanone. Under second route, phenol underwent keto-enol tautomerization reaction followed by two molecular hydrogenation reactions to produce cyclohexanone component. They concluded latter reaction mechanism as a favourable reaction from thermo-chemical point of view.

4.2 Anisole

Unlike the component phenol, anisole comprises of methoxy functional attached with phenyl ring which is often repeated oxy-functional in three-dimensional lignin structure (see Fig. 1). The research based on conversion of anisole as a representation of lignin fraction-derived bio-oil has got numerous attractions in past [23–27]. Various conversion reaction mechanisms are demonstrated in Fig. 5. For instance, demethylation reaction of anisole using a hydrogen molecule gives rise to

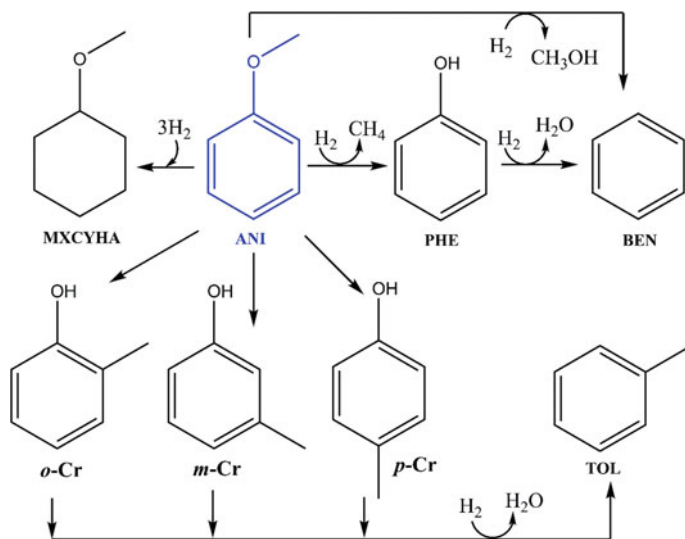


Fig. 5 Conversion mechanisms of anisole to various products

phenol and methane molecules, followed by conversion of phenol to benzene and water molecules via hydrodeoxygenation reaction. The production of benzene can also be achieved by direct demethoxylation reaction of anisole which produces methanol as side product. The conversion of phenol into cyclohexanol and cyclohexane, and conversion of benzene into cyclohexane component follow similar reaction mechanisms as of shown in Fig. 4. On the other hand, ring saturation reaction of anisole using three hydrogen molecules produces methoxycyclohexane as product which further can be decomposed into cyclohexane, cyclohexanone, and cyclohexane components. Various literatures [26, 27] have shown the possibility of formation of cresols (*o*-, *m*-, and *p*-cresol) from anisole which can probably be achieved by alkylation reactions upon the formation of phenol. The productions of phenol and *o*-cresol from anisole are studied by Huuska and Rintala [27] over γ -Al₂O₃-supported CoMo and NiMo catalysts in fixed bed reactor at 573 K and 50 bar reaction conditions (see Table 2). Figure 5 depicts the formations of all three isomers of cresols from anisole which further reduce to toluene upon hydrodeoxygenation reaction. However, Huuska and Rintala [26] did not advocate the formation of toluene but Zhu et al. [23] have reported the formation of toluene along with the productions of benzene and xylene from conversion of anisole over Pt/H β -zeolite catalyst. However, at Pt/SiO₂ catalyst, Zhu et al. [23] observed only benzene as major product. Hurff and Klein [24] also carried out an experiment of anisole conversion over CoMo catalyst but with Al₂O₃ support, and they observed the productions of cyclohexane along with phenol and benzene. On the other hand, Huuska [26] carried out another experiment for anisole conversion over Mo/ γ -Al₂O₃ and Ni metal supported with two different supports γ -Al₂O₃ and SiO₂.

The Ni catalyst with both supports showed selectivities for phenol and benzene as major products, whereas Mo/ γ -Al₂O₃ underwent the formations of phenol, cresol, and 2,6-dimethylphenol as main products.

4.3 Guaiacol

Guaiacol component, in recent past, has acquired various attentions amongst researchers because of representing two oxy-functionals, hydroxyl and methoxy groups, in its molecular structure. Because of this representation, guaiacol component is most preferred model compound for the study of lignin-derived bio-oils [3, 22, 28, 29]. Therefore, numerous studies on conversion of guaiacol component have been devoted in the presence of several catalysts, e.g. Ru/C [30], Fe/SiO₂ [28], Ni/SiO₂ and Ni supported with SiO₂ and Al₂O₃ [31], CoMoS/ γ -Al₂O₃ [32]. Figure 6 depicts various conversion mechanisms of guaiacol model compound. For instance, demethylation reaction of guaiacol converts into catechol intermediate which further reduces to phenol upon hydrodeoxygenation reaction, whereas water elimination from guaiacol component produces anisole component which further reduces to various products via reaction mechanisms as shown in Fig. 5. The demethoxylation reaction of guaiacol directly produces phenol component which

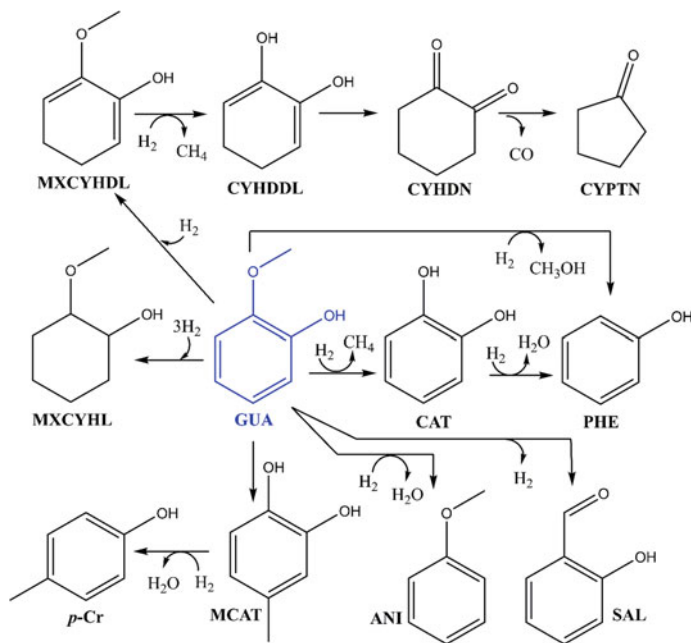


Fig. 6 Various reaction mechanisms for the conversion of guaiacol

can further undergo into formations of several products using reaction mechanisms shown in Fig. 4. The methyl transfer reaction of guaiacol produces 4-methylcatechol which could be utilized for the production of 4-methylphenol by water removal. Various catalytic systems show the favourability of ring saturation reactions prior to cleavage of C–C or C–O bonds; therefore, a reaction route is devoted to the formation of 2-methoxycyclohexanol which can be converted into cyclohexane, cyclohexanol, and cyclohexanone upon cleavages of functionals. On the other hand, Gao et al. [29] showed the possibility of formation of cyclopentanone as product (see reaction mechanism in Fig. 6) which is numerically investigated in the absence of catalyst by Verma and Kishore [22] in gas phase under the framework of density functional theory. The production of cyclopentanone from guaiacol initiates with partial ring saturation of guaiacol followed by demethylation and keto-enol tautomerization reactions; further, the ring opening of cyclohexane-1,2-dione, in order to eliminate CO, produces cyclopentanone. Further conversion mechanisms of phenol and anisole are not included in Fig. 6, and they can be obtained in Figs. 4 and 5, respectively.

Olcese et al. [28] carried out experiments of HDO of guaiacol over Fe/SiO₂ catalyst, and according to their observations, guaiacol favoured demethoxylation route to produce phenol and methanol which is followed by the production of benzene and water. Further hydrogenation reaction of benzene produces cyclohexane. The formations of cyclohexane and cyclohexanone as major products are also observed by Bykova et al. [31] in their experiments on kinetic studies of guaiacol HDO over Ni–Cu bimetallic catalyst using SiO₂ and Al₂O₃ supports. On the other hand, Lee et al. [33] carried out guaiacol conversions over Pt(111) catalyst numerically and they reported that the conversion of guaiacol component proceeds through dehydrogenation reactions of methoxy functional instead of direct dehydroxylation, demethylation, and demethoxylation routes. They observed catechol as major product. Furthermore, the guaiacol conversion study using computations is also carried out by Lu et al. [34] over Pt(111) catalyst and they also affirmed catechol as major product. Chiu et al. [35], on the other hand, performed guaiacol HDO in the presence of Ru(0001) catalyst numerically under DFT framework. Their computations involved the formation of benzene as end product with intermediates catechol and phenol; however, catechol production was observed as favourable product because further conversions of catechol into lower fractions were kinetically demanding. In addition to the work of Chiu et al. [35], Lu et al. [36] performed a microkinetic modelling study for HDO of guaiacol over Ru(0001) catalyst and they observed phenol as major product.

The experimental work using guaiacol is considered by various researchers in past but the numerical works are very limited. However, the numerical works can provide a very good preliminary idea about the favourability of products and their kinetics over different catalysts. Though few computational works are carried out for conversion of guaiacol over bulk catalysts such as Pt(111) and Ru(0001), there is huge information gap in the literature; for example, authors have not found any numerical work employing catalyst support to the metal catalyst for guaiacol model compound.

4.4 Vanillin

The presence of vanillin (4-hydroxy-3-methoxybenzaldehyde) component is often reported by researchers, and it is one of the chief model components of phenolic fractions of bio-oil [14, 37, 38]. For instance, Peng et al. [39] performed pyrolysis experiment of rice husk and observed 2.37 area % of vanillin in raw bio-oil. It possesses three oxy-functionals, viz. hydroxyl, methoxy, and formyl groups; therefore, it is considered as one of the important representations of lignin-derived bio-oil [37, 40, 41]. Major conversion mechanisms of vanillin into lower fraction products are displayed in Fig. 7. The conversion of vanillin is shown in Fig. 7 via four reaction routes: (i) demethylation reaction of vanillin to produce 3,4-dihydroxybenzaldehyde which is further converted to 4-hydroxybenzaldehyde, (ii) HDO of vanillin to produce 3-methoxybenzaldehyde followed by the productions of 3-hydroxybenzaldehyde and benzaldehyde, (iii) decarbonylation reaction of vanillin to produce guaiacol which is further converted into catechol and phenol using aforementioned mechanisms in subsection of ‘Guaiacol’, and (iv) direct demethoxylation reaction of vanillin to produce 4-hydroxybenzaldehyde. The intermediate 3,4-dihydroxybenzaldehyde further undergoes to two more pathways, apart from production of 4-hydroxybenzaldehyde, for the productions of catechol and 3-hydroxybenzaldehyde via decarbonylation and hydrodeoxygenation reactions, respectively. Similarly, the structure 4-hydroxybenzaldehyde follows two

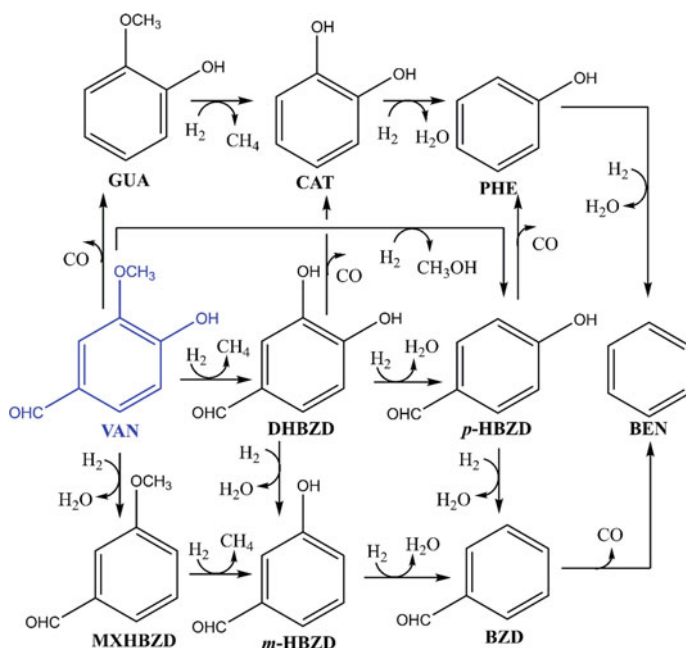


Fig. 7 Conversion mechanisms of vanillin into several lower fractions

reaction possibilities for the productions of phenol and benzaldehyde via decarbonylation and hydrodeoxygenation reactions, respectively. Further, phenol and benzaldehyde convert to benzene via hydrodeoxygenation and decarbonylation reactions, respectively. The formation of anisole, however, not included in Fig. 7, is also possible via decarbonylation reaction of 3-methoxybenzaldehyde. It is to be noted that further conversion mechanisms of phenol, anisole, and guaiacol can be obtained in Figs. 4, 5, and 6, respectively.

Various catalytic systems for vanillin conversion show hydrogenation of vanillin to vanillyl alcohol instead of its decomposition; for instance, Bindwal and Vaidya [37] carried out an experiment of vanillin in the presence of Ru/C catalyst and 313–338 K temperature range. They observed vanillyl alcohol as an intermediate, while creosol as the end product; using temperature dependence analysis, they deduced the reaction as second-order reaction kinetics with 9.84 kcal/mol of activation energy. Similarly, Jiang et al. [42] also observed creosol as major product with 98% yield in their experiment of vanillin conversion over mesoporous carbon nitride modified Pd at 363 K; however, they also observed that formation of creosol occurs with vanillyl alcohol as intermediate product. On the other hand, Shin et al. [43] performed experiments on pyrolysis of vanillin and reported a range of products, for instance, phenol, benzene, guaiacol, 3,4-dihydroxybenzaldehyde. Similarly, Liu et al. [44] carried out an experimental analysis on pyrolysis of vanillin for a temperature range of 673–873 K. They observed major production of guaiacol with other detected components such as catechol, phenol, hydroxybenzaldehyde, carbon monoxide, 5-formylsalicylaldehyde. Recently, Verma and Kishore [38] carried out a numerical study on the pyrolysis of vanillin and they performed theoretical counterparts for the formations of almost all observed products by Liu et al. [44] in their vanillin pyrolysis experiment such as phenol, CO, guaiacol, 2-hydroxybenzaldehyde.

Since various experiments have suggested the formation of creosol from vanillin, its reaction mechanism is also explained here. For the formation of creosol, the vanillin component first undergoes hydrogenation reactions to convert C=O double bond to C–O single bond which converts vanillin into vanillyl alcohol. Further, the vanillyl alcohol intermediate undergoes to OH group removal using hydrodeoxygenation reaction which removes OH in the form of water with additional hydrogen molecule. This reaction step forms creosol as the product.

4.5 Eugenol

Out of various components observed in phenolic fraction of bio-oil derived from pyrolysis or liquefaction of lignin, eugenol component is also detected to be one of the most appropriate model components because of possession of two oxy-groups, viz. hydroxyl and methoxy groups, and an alkenyl group [45–48]. Eugenol component is also found as one of the major products in many pyrolytic studies of lignocellulosic biomass [8, 14, 49]. Therefore, eugenol can also be considered as

Several experimental works have been devoted in recent past for the conversion of eugenol over various catalysts; for instance, Nimmanwudipong et al. [46] performed experiments for the conversion of eugenol over Pt/ γ -Al₂O₃ and HY zeolite catalysts. They observed several products such as phenol, guaiacol, 4-propylguaiacol, *p*-cresol, 4-propylphenol. However, they observed guaiacol and isoeugenol as major products in the presence of HY zeolite catalyst, while 4-propylguaiacol as major product in the presence of Pt/ γ -Al₂O₃ catalyst. Similarly, Zhang et al. [47] performed experimental analyses for hydrogenation/deoxygenation of eugenol over Pd/C and HZSM-5 catalytic systems. Their observations suggest that eugenol favours allyl hydrogenation first instead of decomposition of eugenol followed by the production of 2-methoxyl-4-propylcyclohexanol using ring saturation reactions. Furthermore, Deepa and Dhepe [51] performed HDO experiments of phenol, guaiacol, and eugenol over noble metals and similar to the work of Zhang et al. [47], they also concluded that eugenol proceeds through saturation of allyl to propyl followed by ring saturation reactions. Similarly, Horáček et al. [45] carried out eugenol conversion experiments over zeolite-supported platinum catalyst and they too suggested that eugenol proceeds through allyl hydrogenation of eugenol. On the other hand, Chen et al. [50] carried out HDO of eugenol in the presence of Ru/CNT catalyst and observed propylcyclohexane as end product with intermediate products as 4-propylguaiacol and 4-propylcyclohexanol.

5 Concluding Remarks and Future Perspectives

The upgradation of liquid bio-oils derived from pyrolysis or liquefaction of lignin-derived biomass feedstocks is reviewed here using commonly found phenolic bio-oil model compounds such as phenol, anisole, guaiacol, vanillin, and eugenol. Because of higher content and a wide range of oxy-compounds in lignin-derived bio-oils, the upgradation of bio-oil as a whole is very challenging; therefore, most research works are carried out using a model compound which can successfully represent a range of oxy-groups in the molecular structure of feedstock. However, the presence of higher amount of oxy-compounds in bio-oil also features its ability to deliver various phenolic specialty chemicals. In this review work, various reaction mechanisms based on five phenolic bio-oil model compounds, i.e. phenol, anisole, guaiacol, vanillin, and eugenol, are discussed. Furthermore, several experiments based on aforementioned phenolic bio-oil model compounds are reviewed for their catalysts, supports, reaction conditions, selectivity towards desired product, etc. Guaiacol component is one of the key components in phenolic fraction of bio-oil because its presence in bio-oil is higher, and in addition, other higher molecular weight phenolic model compounds such as vanillin and eugenol reduce to guaiacol majorly. Furthermore, guaiacol component can successfully represent a higher fraction of lignin structure because of attachment of hydroxyl and methoxy groups in its molecular structure.

Recent computational advancements employing density functional theory tool for understanding reaction mechanisms based on aforementioned model compounds are also discussed. Computational models are reported to be very successful for achieving accurate preliminary knowledge of any reaction, e.g. favourability of product, reaction conditions, suitable catalytic systems. Presently, there has been a very little work in bio-oil upgradation using computational means compared to experiments; however, the research based on upgradation of phenolic bio-oil model compounds is also in the early phase and there is a huge information gap regarding synthesis of suitable catalytic system which can show higher catalytic activity and selectivity towards desired product. Till now, no successful technological advancement regarding commercialization is achieved which can be utilized in order to accomplish optimum bio-oil upgradation.

Apart from aforementioned phenolic bio-oil model compounds such as phenol, anisole, guaiacol, the research based on even heavier molecular weight fractions of lignin compounds such as compounds with β -O-4, α -O-4, and 4-O-5 linkages is very limited; therefore, a wide research analysis is needed to unravel and understand complete bio-oil upgradation process. The integration of biorefinery to present petroleum refineries needs a complete catalytic analysis because of utilization of different hydrotreating catalysts in the latter. Also because of differences in feedstocks as petroleums contain trace water content and unprocessed bio-oils comprise a huge fraction of water content.

References

1. Huber GW, Iborra S, Corma A (2006) Synthesis of transportation fuels from biomass: chemistry, catalysts, and engineering. *Chem Rev* 106:4044–4098
2. Wang Y, He T, Liu K, Wu J, Fang Y (2012) From biomass to advanced bio-fuel by catalytic pyrolysis/hydro-processing: hydrodeoxygenation of bio-oil derived from biomass catalytic pyrolysis. *Bioresour Technol* 108:280–284
3. Saidi M, Samimi F, Karimipourfard D, Nimmanwudipong T, Gates BC, Rahimpour MR (2014) Upgrading of lignin-derived bio-oils by catalytic hydrodeoxygenation. *Energy Environ Sci* 7:103–129
4. Klass DL (2004) Biomass for renewable energy and fuels. *Encycl Energy* 1:193–212
5. Alonso DM, Bond JQ, Dumesic JA (2010) Catalytic conversion of biomass to biofuels. *Green Chem* 12:1493–1513
6. Alonso DM, Wettstein SG, Dumesic JA (2012) Bimetallic catalysts for upgrading of biomass to fuels and chemicals. *Chem Soc Rev* 41:8075
7. Stöcker M (2008) Biofuels and biomass-to-liquid fuels in the biorefinery: catalytic conversion of lignocellulosic biomass using porous materials. *Angew Chemie Int Ed* 47:9200–9211
8. Mu W, Ben H, Ragauskas A, Deng Y (2013) Lignin pyrolysis components and upgrading—technology review. *BioEnergy Res* 6:1183–1204
9. Pandey MP, Kim CS (2011) Lignin depolymerization and conversion: a review of thermochemical methods. *Chem Eng Technol* 34:29–41
10. Kanaujia PK, Sharma YK, Garg MO, Tripathi D, Singh R (2014) Review of analytical strategies in the production and upgrading of bio-oils derived from lignocellulosic biomass. *J Anal Appl Pyrolysis* 105:55–74

11. Crestini C, Crucianelli M, Orlandi M, Saladino R (2010) Oxidative strategies in lignin chemistry: a new environmental friendly approach for the functionalisation of lignin and lignocellulosic fibers. *Catal Today* 156:8–22
12. Collinson SR, Thielemans W (2010) The catalytic oxidation of biomass to new materials focusing on starch, cellulose and lignin. *Coord Chem Rev* 254:1854–1870
13. Azadi P, Inderwildi OR, Farnood R, King DA (2013) Liquid fuels, hydrogen and chemicals from lignin: a critical review. *Renew Sustain Energy Rev* 21:506–523
14. Jiang G, Nowakowski DJ, Bridgwater AV (2010) Effect of the temperature on the composition of lignin pyrolysis products. *Energy Fuels* 24:4470–4475
15. Corma A (2003) State of the art and future challenges of zeolites as catalysts. *J Catal* 216:298–312
16. Furimsky E (1983) Chemistry of catalytic hydrodeoxygenation. *Catal Rev* 25:421–458
17. Furimsky E (2000) Catalytic hydrodeoxygenation. *Appl Catal A Gen* 199:147–190
18. Şenol Oİ, Ryymin E-M, Viljaja T-R, Krause AOI (2007) Effect of hydrogen sulphide on the hydrodeoxygenation of aromatic and aliphatic oxygenates on sulphided catalysts. *J Mol Catal A Chem* 277:107–112
19. Shin EJ, Keane MA (2000) Gas-phase hydrogenation/hydrogenolysis of phenol over supported nickel catalysts. *Ind Eng Chem Res* 39:883–892
20. Zhao C, Lercher JA (2012) Selective hydrodeoxygenation of lignin-derived phenolic monomers and dimers to cycloalkanes on Pd/C and HZSM-5 catalysts. *ChemCatChem* 4:64–68
21. Hong D-Y, Miller SJ, Agrawal PK, Jones CW (2010) Hydrodeoxygenation and coupling of aqueous phenolics over bifunctional zeolite-supported metal catalysts. *Chem Commun* 46:1038–1040
22. Verma AM, Kishore N (2016) DFT analyses of reaction pathways and temperature effects on various guaiacol conversion reactions in gas phase environment. *ChemistrySelect* 1:6196–6205
23. Zhu X, Lobban LL, Mallinson RG, Resasco DE (2011) Bifunctional transalkylation and hydrodeoxygenation of anisole over a Pt/HBeta catalyst. *J Catal* 281:21–29
24. Hurff SJ, Klein MT (1983) Reaction pathway analysis of thermal and catalytic lignin fragmentation by use of model compounds. *Ind Eng Chem Fundam* 22:426–430
25. Li K, Wang R, Chen J (2011) Hydrodeoxygenation of anisole over silica-supported Ni₂P, MoP, and NiMoP catalysts. *Energy Fuels* 25:854–863
26. Huuska MK (1986) Effect of catalyst composition on the hydrogenolysis of anisole. *Polyhedron* 5:233–236
27. Huuska M, Rintala J (1985) Effect of catalyst acidity on the hydrogenolysis of anisole. *J Catal* 94:230–238
28. Olcese RN, Bettahar M, Petitjean D, Malaman B, Giovanella F, Dufour A (2012) Gas-phase hydrodeoxygenation of guaiacol over Fe/SiO₂ catalyst. *Appl Catal B Environ* 115–116:63–73
29. Gao D, Xiao Y, Varma A (2015) Guaiacol hydrodeoxygenation over platinum catalyst: reaction pathways and kinetics. *Ind Eng Chem Res* 54:10638–10644
30. Elliott DC, Hart TR (2009) Catalytic hydroprocessing of chemical models for bio-oil. *Energy Fuels* 23:631–637
31. Bykova MV, Ermakov DY, Kaichev VV, Bulavchenko OA, Saraev AA, Lebedev MY, Yakovlev V (2012) Ni-based sol-gel catalysts as promising systems for crude bio-oil upgrading: guaiacol hydrodeoxygenation study. *Appl Catal B Environ* 113–114:296–307
32. Bui VN, Laurenti D, Afanasiev P, Geantet C (2011) Hydrodeoxygenation of guaiacol with CoMo catalysts. Part I: promoting effect of cobalt on HDO selectivity and activity. *Appl Catal B Environ* 101:239–245
33. Lee K, Gu GH, Mullen C, Boateng A, Vlachos DG (2015) Guaiacol hydrodeoxygenation mechanism on Pt(111): insights from density functional theory and linear free energy relations. *ChemSuschem* 8:315–322
34. Lu J, Behtash S, Mamun O, Heyden A (2015) Theoretical investigation of the reaction mechanism of the guaiacol hydrogenation over a Pt(111) catalyst. *ACS Catal* 5:2423–2435

35. Chiu C, Genest A, Borgna A, Rösch N (2014) Hydrodeoxygenation of guaiacol over Ru (0001): a DFT study. *ACS Catal* 4:4178–4188
36. Lu J, Behtash S, Mamun O, Heyden A (2015) Theoretical investigation of the reaction mechanism of the hydrodeoxygenation of guaiacol over a Ru(0001) model surface. *J Catal* 321:39–50
37. Bindwal AB, Vaidya PD (2014) Reaction kinetics of vanillin hydrogenation in aqueous solutions using a Ru/C catalyst. *Energy Fuels* 28:3357–3362
38. Verma AM, Kishore N (2017) Molecular modelling approach to elucidate the thermal decomposition routes of vanillin. *New J Chem* 41:8845–8859
39. Peng J, Chen P, Lou H, Zheng X (2008) Upgrading of bio-oil over aluminum silicate in supercritical ethanol. *Energy Fuels* 22:3489–3492
40. Shen DK, Gu S, Luo KH, Wang SR, Fang MX (2010) The pyrolytic degradation of wood-derived lignin from pulping process. *Bioresour Technol* 101:6136–6146
41. Walton NJ, Mayer MJ, Narbad A (2003) Vanillin. *Phytochemistry* 63:505–515
42. Jiang H, Yu X, Peng X, Zhang H, Nie R, Lu X, Zhou D, Xia Q (2016) Efficient aqueous hydrodeoxygenation of vanillin over a mesoporous carbon nitride-modified Pd nanocatalyst. *RSC Adv* 6:69045–69051
43. Shin EJ, Nimlos MR, Evans RJ (2001) A study of the mechanisms of vanillin pyrolysis by mass spectrometry and multivariate analysis. *Fuel* 80:1689–1696
44. Liu C, Deng Y, Wu S, Mou H, Liang J, Lei M (2016) Study on the pyrolysis mechanism of three guaiacyl-type lignin monomeric model compounds. *J Anal Appl Pyrolysis* 118:123–129
45. Horáček J, Štřábová G, Kelbichová V, Kubička D (2013) Zeolite-Beta-supported platinum catalysts for hydrogenation/hydrodeoxygenation of pyrolysis oil model compounds. *Catal Today* 204:38–45
46. Nimmanwudipong T, Runnebaum RC, Ebeler SE, Block DE, Gates BC (2012) Upgrading of lignin-derived compounds: reactions of eugenol catalyzed by HY zeolite and by Pt/ γ -Al₂O₃. *Catal Lett* 142:151–160
47. Zhang C, Xing J, Song L, Xin H, Lin S, Xing L, Li X (2014) Aqueous-phase hydrodeoxygenation of lignin monomer eugenol: influence of Si/Al ratio of HZSM-5 on catalytic performances. *Catal Today* 234:145–152
48. Verma AM, Kishore N (2017) Gas phase conversion of eugenol into various hydrocarbons and platform chemicals. *RSC Adv* 7:2527–2543
49. Nowakowski DJ, Bridgwater AV, Elliott DC, Meier D, de Wild P (2010) Lignin fast pyrolysis: results from an international collaboration. *J Anal Appl Pyrolysis* 88:53–72
50. Chen M-Y, Huang Y-B, Pang H, Liu X-X, Fu Y (2015) Hydrodeoxygenation of lignin-derived phenols into alkanes over carbon nanotube supported Ru catalysts in biphasic systems. *Green Chem* 17:1710–1717
51. Deepa AK, Dhepe PL (2014) Function of metals and supports on the hydrodeoxygenation of phenolic compounds. *ChemPlusChem* 79:1573–1583
52. Ledesma EB, Hoang JN, Nguyen Q, Hernandez V, Nguyen MP, Batamo S, Fortune CK (2013) Unimolecular decomposition pathway for the vapor-phase cracking of eugenol, a biomass tar compound. *Energy Fuels* 27:6839–6846
53. Dutta S, Wu KC-W, Saha B (2014) Emerging strategies for breaking the 3D amorphous network of lignin. *Catal Sci Technol* 4:3785–3799
54. Wang H, Male J, Wang Y (2013) Recent advances in hydrotreating of pyrolysis bio-oil and its oxygen-containing model compounds. *ACS Catal* 3:1047–1070

Sustainability of Microalgal Biorefinery: Scope, Challenges, and Opportunities

Geetanjali Yadav and Ramkrishna Sen

Abstract The potential of microalgae as a source of renewable energy is of considerable interest. During recent initiatives being taken at the 2015 United Nations Climate Change Conference (COP21) held in Paris, about 196 attending nations have set goals to limit global warming to less than 2 degrees Celsius (°C) compared to pre-industrial levels and move toward attaining zero net anthropogenic greenhouse gas emissions by the second half of the twenty-first century. This necessitates curtailing the usage of non-renewable resources, primarily fossil fuels, which are one of the biggest contributors of GHGs and explore more bio-based alternatives, such as microalgae. A key attraction of algae as biofuel feedstock lies in the potential for high annual oil productivity per unit of area. Due to the wide availability and potential of cultivation or occurrence in naturally occurring habitats including harsh environments such as extreme temperatures, salinity, pH, multiple products could be obtained from a variety of algal species. This multi-product paradigm makes it a suitable candidate for the biorefinery concept. An algal biorefinery aims to increase value from green biomass by recovering every component for its use as feedstock in myriad applications such as biofuels, food and feed, fertilizer, and pharmaceuticals. However, existing biorefinery methods have to be duly modified, improved, and widely adapted for the sustainable production of microalgal biomass and its associated benefits. Thus, this chapter presents a framework to analyze sustainability as cultivation, harvesting, and processing of microalgal biomass and use of bioenergy/refinery has a large range of associated sustainability issues. The process economics of biomass facility production, carbon sequestration, and waste mitigation have been discussed to comply various sustainability criteria for the successful implementation of algal-based biorefinery at commercial scale.

Keywords Algal biorefinery · Sustainability · Bioenergy · Co-culture
Life cycle assessment

G. Yadav · R. Sen (✉)

Department of Biotechnology, Indian Institute of Technology Kharagpur,
Kharagpur, West Bengal 721302, India
e-mail: rksen@yahoo.com

© Springer Nature Singapore Pte Ltd. 2018

S. De et al. (eds.), *Sustainable Energy Technology and Policies*, Green Energy and Technology, https://doi.org/10.1007/978-981-10-7188-1_15

335

1 Introduction

The first and second generation of bioenergy strategies involved biofuel production from edible resources viz. sugar, starch, vegetable or animal oils, and non-edible resources such as waste vegetable oils and agricultural wastes, respectively [20]. However, these technologies were based on deriving energy from terrestrial feedstocks; thus, concerns related to indirect emissions, food vs. fuel debate, carbon debt due to land requirement, etc., were raised. Subsequently, third generation bioenergy feedstock algae became popular with researchers worldwide due to their excellent characteristics. Microalgae are fast-growing photosynthetic microorganisms that exhibit greater CO₂ fixation rates, can utilize waste flue gases and wastewater streams as inexpensive growth medium [30]. Moreover, they accumulate sufficient quantity of lipids, proteins, carbohydrates, pigments, etc., which can be suitably converted into multiple products. Various conversion techniques such as thermochemical, biochemical, direct conversion, transesterification, and electrochemical routes lead to different kinds of products that widen the market opportunities of microalgal products [4].

The microalga exists in a variety of habitats and can yield multiple coproducts in biorefinery approach. They can be cultivated in open ponds like circular or raceways or closed systems (column, flat panel, helical, tubular, horizontal photobioreactors) that involve mixing and/or aeration and provide controlled environmental conditions. An open system is cheaper to construct, less energy intensive, and feasible for commercial scale production, whereas closed systems provide better process control, enables attaining higher cell density and avoids contamination [11]. Microalgal lipids can be utilized for biodiesel production. Carbohydrates can be used as carbon source in fermentation industries to produce bioethanol. In addition to this, microalgal pigments, carotenoids, and certain bioactive exopolymeric molecules have important functions in immune responses, health care, and act as food supplements. Microalgal proteins are a good source of nutrients which can be used for animal feeding and as a source of crop fertilizer. In this chapter, we discuss sustainability of microalgal biorefinery from economic, environmental, and social dimensions. In order to qualify the sustainability criteria, a biorefinery must satisfy these three dimensions. For the same, strategies have been discussed in brief which can help to establish ways that will make the process of microalgal production sustainable.

2 Microalgal Biorefinery

2.1 *The Concept of Biorefinery*

The concept of biorefinery came from “refinery” which refers to the conversion of a raw product into several other value-added products. A microalgal biorefinery is

essentially similar to the traditional petroleum refinery, where microalgal biomass, unlike crude petroleum, is converted into a variety of products like biofuels, food and feed supplements, fertilizer, pharmaceuticals, and other products (Fig. 1). The only significant difference between the two lies in the type of raw material (biomass or crude oil) and the technology employed for the conversion [33]. It is a promising way to mitigate CO₂ emissions, wastewater remediation, and establish an alternate bioenergy pathway for sustainable production of biofuels and bioproducts.

2.2 Routes of Biomass Conversion: “Waste-to-Value”

2.2.1 Thermochemical Conversion

Thermochemical conversion involves the thermal decomposition of algal biomass so that the organic components in the biomass are decomposed to yield fuel products such as bio-crude oil. It is an energy-intensive process. There are three different types of thermochemical conversion: (1) hydrothermal liquefaction (HTL), (2) pyrolysis, and (3) gasification. HTL involves heating the biomass to high temperature of about 250–350 °C and pressure (5–15 MPa). Pyrolysis is a process of decomposition of biomass to form volatile matter at very high temperature (400–600 °C) in absence of oxygen [4]. As the volatile matters re-condenses into the aqueous phase, bio-oil is formed which could be used as a fuel. On the other hand,

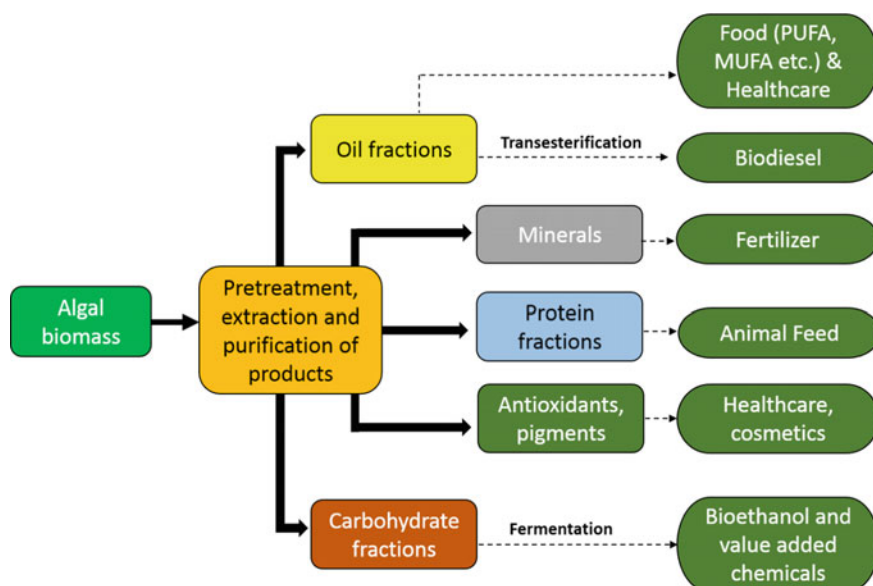


Fig. 1 Microalgal biorefinery and its applications in various sectors

the solid fraction consisting of solid carbon is separated out as bio-char which is used as fertilizer. Gasification is a process that converts biomass or any carbonaceous materials into carbon monoxide, hydrogen, carbon dioxide and traces of methane that forms syngas. This is achieved at higher temperatures of 700 °C with limited oxygen environment. Syngas can be used directly as a fuel or intermediate for making wide range of fuels.

2.2.2 Biochemical Conversion

Biochemical conversion of biomass encompasses the biological processing of biomass into bioenergy. This mainly includes fermentation, anaerobic digestion, and photo-fermentative hydrogen production. Fermentation or alcoholic fermentation involves the conversion of organic substrates into their mono or dimeric forms by the action of enzymes released from microorganisms. Anaerobic digestion involves the conversion of organic substrates into biogas. Photo-fermentative H₂ production entails conversion of water to hydrogen ions and oxygen by the help of algae [27].

2.2.3 Direct Utilization

Microalgae cells have the ability to bioadsorb chemicals and charged moieties due to its surface property. They also release certain compounds like exopolysaccharides which are charged moieties that help in coagulation. This property is exploited for clearing of certain dyes and colors from the industrial effluents. Many industries discharge color bearing dyes in the waste effluent that pollute the water bodies where it is released and affect aquatic flora and fauna. Defatted algal biomass is used to remove such dyes from the wastewater effluents because it contains more exposed sites after cell rupture and has more contact surface area for charged species. Thus, it helps in coagulation and removal by flocculation by an eco-friendly method. Marzbali et al. [18] studied the adsorption of direct yellow dye (DY 12) by *Spirulina* and recorded the maximum absorption capacity of 714 mg g⁻¹ of the dye by the alga, which is highest among previous works.

2.2.4 Transesterification

Transesterification is the process whereby lipids (triglycerides) extracted from microalgal biomass is reacted in the presence of alcohol and acid/base catalyst into fatty acid methyl esters (FAME), i.e., biodiesel. Several factors play a role in this process, mainly reaction time and temperature. Along with FAME (biodiesel), glycerol as a by-product is formed which has many industrial applications [8].

2.2.5 Bioelectrochemical Conversion

Microbial fuel cells are bioelectrochemical devices that use bacteria as the catalysts to oxidize organic and inorganic matter. The oxidation leads to generation of electrons that are transferred to anode and flow to cathode via external circuit. Recently, researchers have been exploiting biological organisms such as algal at the cathode to steer cathode reduction. Microalgae are photosynthetic organisms that capture CO₂ and release O₂. Thus, this property is being exploited to enhance cathode reduction reactions and “green electricity” production [24]. This synergistic action helps to treat biodegradable wastes at the anode and CO₂ fixation at the cathode with concomitant electricity and algal biomass production.

3 Applications of Microalgal Biorefinery

3.1 Bioenergy and Biofuel

In recent years, microalgae are seen as potential biofuel feedstock as it contains significant quantities of lipids (20–70%) and carbohydrates (10–30%) [12]. Lipids and carbohydrates can be converted into biodiesel and bioethanol by transesterification and fermentation reactions. Microalgal-derived fuels have been considered as safe and carbon neutral and are found to meet the International Biodiesel Standard for Vehicles (EN14214) [26]. Lipid accumulation takes place as a response when microalgal administers some kind of stress viz. environmental (temperature, salinity, pH etc.), nutrient limitation (nitrogen and phosphorous) etc. The composition of fatty acids and its profile, however, could depend upon genetic makeup and phenotypic factors such as medium composition, temperature, aeration rate, influence of photoperiod, and light intensity [26].

As the microalgae have high light conversion efficiency, it accumulates greater amounts of carbohydrates. Algal carbohydrates are composed of glucose, starch, cellulose, and various kinds of polysaccharides. Conventionally, microalgal starch or glucose is the main precursor for biofuel production.

3.2 Food and Feed

Microalgae constitute PUFA in their cell accumulated in complex polar lipids (i.e., glycolipids and phospholipids) while TAGs are predominantly constituted of saturated (SFA) and monounsaturated (MUFA) fatty acids. PUFA or polyunsaturated fatty acids are essential nutritional components having nutraceutical and pharmaceutical applications [2]. Potential therapeutic applications of omega-3 long-chain polyunsaturated fatty acids such as docosahexaenoic acid (DHA), eicosapentaenoic acid (EPA), and arachidonic acid (AA) have been demonstrated in recent clinical

and epidemiological studies [22]. Generally, maximum levels of PUFA are synthesized during early stationary phase, decreasing throughout the stationary phase and increasing proportions of SFA and MUFA especially 14:0, 16:0, and 16:1 fatty acids [10]. However, a study is the first to show that a high light intensity combined with N replete conditions could synchronously maximize the yield of biomass ($34.14 \text{ mg L}^{-1} \text{ h}^{-1}$), neutral lipids ($11.83 \text{ mg L}^{-1} \text{ h}^{-1}$), the high value C20 (AA plus EPA, $1.50 \text{ mg L}^{-1} \text{ h}^{-1}$), and C14–C18 FAs in the NLs ($12.38 \text{ mg L}^{-1} \text{ h}^{-1}$) obtained from *N. oceanica* IMET1. The defatted algal biomass constitutes protein and carotenoids fraction which finds suitable application for animal feeds. Microalgal polysaccharides such as exo- (EPS) or endo-polysaccharides have certain biological functions as storage, protection, and structural moieties. It also has some role in immune functions and pharmaceutical applications in cosmetic industries [18].

3.3 Fertilizer

In order to develop a successful microalgal-based biorefinery, it is required to use every component of biomass for deriving value out of it. It is found that the de-oiled algal biomass is rich in protein, minerals, and elements such as magnesium, iron, and other nutritional components such as phosphorous. The basic need of the crop is nitrogen, phosphorus, and potassium, (NPK) as major elements and minerals as microelements. Thus, it is a critical nutritional source for crops and exploited as a source of green fertilizer. Microalgal-bacterial (MaB) flocs were used to treat aquaculture wastewater and at the same time as organic fertilizer to cultivate tomato. It was found that microalgal fertilizer improved the fruit quality by increasing sugar and carotenoid content [6]. Thus, microalgae offer the potential to recover nutrients from waste streams and its subsequent usage as slow-release fertilizer.

4 Sustainability of Microalgal Biorefinery

According to the classic definition of sustainability, “sustainable development is a development that meets the needs of the present without compromising the ability of future generations to meet their own needs.” The typical microalgal biorefinery consists of algae cultivation, harvesting, pre-treatment, metabolites extraction, and its conversion (i.e., transesterification, fermentation, etc.). Microalgal biorefineries are considered to be inherently sustainable due to their property of being renewable in nature. However, this may not essentially be true because 70% of the total production cost (PC) of algal biofuels on a commercial scale goes into algal cultivation, harvesting, and dewatering [14] which have associated economic and environmental constraints. Sustainable production of biomass should protect the

environment and reduce wastage of resources. Sustainable development of an algal biorefinery requires embracing green measures during the upstream and downstream processes such as:

- selection of robust algal strains having enhanced growth characteristics and lipid productivity;
- cultivation strategy with an optimized photosynthetic and nutrients use efficiency;
- use of the co-location strategy to take advantage of the industrial wastes of energy, CO₂, water, and nutrients;
- extraction of valuable chemicals from the biomass that can increase the whole value of microalgae biomass;
- adopting green ways to pretreat, extract, and process the valuable metabolites for its applications in various energy and non-energy sectors.

For the sustainable development of a biorefinery project, it is necessary to establish a balance along three dimensions of sustainability viz. social, environmental, and economic. These three are inter-linked among each other in a way that the poor performance of one may hinder that of others [19].

Thus, it is necessary to develop processes where all dimensions of sustainability are taken into account in a single analysis. In case of a microalgal biorefinery, the valorization of each and every component of a biomass can significantly leverage the total value of the biomass and solve many of today's world problems. It should be able to protect the environment by not causing any kind of irreversible change, should be economically viable and beneficial to the society. This is illustrated in the Fig. 2. The environmental dimension includes mainly use of natural resources, pollution prevention, biodiversity conservation, and maintenance of ecological health. The social pillar includes standards of living, availability of education and jobs, and equal opportunities for all members of society. The economic factors are drivers for growth, profit, reducing costs, and investments into research and development [1].

Fig. 2 Interplay of the environmental, economic, and social aspects of sustainable development



4.1 Sustainable Practices of a Microalgal Biorefinery

4.1.1 Economic Sustainability

In the design of microalgal biorefinery projects, the dimension of economic sustainability is considered mostly through assessing profitability or techno-economic analysis (TEA) where technical aspects of engineering projects are analyzed in terms of process economics. There are numerous indicators which are used to define economic analyses viz. actual sequestration cost (ASC), capital cost (CC), operating cost (OC), production cost (PC), transportation cost (TC), total savings (TS), gross operating margin (GOM), credited gross operating margin (GOM cr), gross profit (GP), internal rate of return (IRR), minimum selling price (MSP), net present value (NPV), payback time (PBT), return on investment (ROI), stakeholder value (SKV), total economic (TEV).

In order to produce a particular product by comparing various biorefinery alternatives, economic performance is evaluated by costs indicators. For example, Coleman et al. [5] have compared the PC of different microalgal fuel production systems and locations combining biomass assessment and logistics models [5]. However, costs metrics per se do not reflect the actual economic performance of the project since expected revenues are not considered for their calculation. Therefore, another measure should be included in the calculations to derive maximum benefits. Profit is an indicator based on costs and revenues and can thus be used for comparisons of systems with different products. Many researchers have used different abovementioned indicators to describe the economics of process [5]. These economic metrics generally reflect the performance of a project on microeconomic terms, mostly to analyze costs and profits related to the project. Some authors have not considered these as true parameters for economic sustainability since they do not add value to the economy [16, 32]. Gheewala et al. [9] have suggested the increase in gross domestic product and tax revenues as the quantifying criteria for addressing human development and assessment of a biorefinery project.

4.1.2 Environmental Sustainability

Environmental sustainability consists of methods that indicate environmental burden of a product or process, and an indication of social impacts through the analysis of damage on human health, climate, ecosystem resources, etc., is included in the analysis. Calculating the environmental impact of microalgal cultivation, harvesting, dewatering, extraction, and conversion into valuable products is necessary [25]. In order to call a microalgal biorefinery sustainable, all three dimensions of sustainability (Fig. 2) must be satisfying the criteria. The production of multiple coproducts in the form of high-value products and biofuel promotes the sustainability of this process when designing biorefinery projects. Eco-Indicator 99 (EI99)

is the most widely used impact assessment method in life cycle assessment (LCA). It is the successor of Eco-indicator 95, the first endpoint impact assessment method, which allowed the environmental load of a product to be expressed in a single score [21]. However, the major limitation with this method lies with its modeling that is mainly based on European situations and not global categories like climate change, ozone depletion. Thus, it may not be really helpful for cases present in other geographical locations.

4.1.3 Social Sustainability

Generally, the social dimension of sustainability is not so common in the design of biorefinery projects in contrast to economic and environmental sustainability. This may be due to lack of engagement between social and the natural and engineering sciences. The social impact of a process must be included while designing any biorefinery project. For example, while allocating lands and infrastructure, the food and energy security must be checked in addition to education and life expectancy at the entry level. Few indicators of social sustainability are energy security index (ES), food price increase (FPI), sustainability factor (SF), human exposure risk (R_HE), employment creation (EC), labor requirements (L). Food and energy security among other indicators have a strong economic and political importance in bioeconomy [28]. More and more reports encourage the inclusion of feedstocks that do not create food versus fuel debate or food insecurity especially in a developing nation like India. Microalgal-based biorefineries are suitable candidates in these scenarios since they do not really require fresh lands or water, CO₂ source and have a diverse range of habitats, growth conditions to thrive. Although, there is going to be acute shortage of non-renewable fuel sources in future, need is to look for alternate energy generating sources. Because “fuel only” option is economically unviable due to overwhelming capital and operation costs, microalgae appear as an excellent candidate to explore in a biorefinery. Thus, high-value coproducts should be produced from microalgal biorefinery to improve the economics of a microalgal biorefinery and maintain sustainability.

4.2 Incorporation of Sustainability in Design Activities

There has been a rise in the inclusion of sustainability criteria during the design of biorefineries by including different methods, indicators, and impact categories. Generally, most of the case studies, publications, and scientific reports consider only economic and environmental dimensions of sustainability and do not focus on social sustainability. All three sustainability criteria (economic, environmental, and social) should be considered in the design stage per se. It has a potential to result in alternate design options as well as significantly influence the overall performance of a microalgal biorefinery.

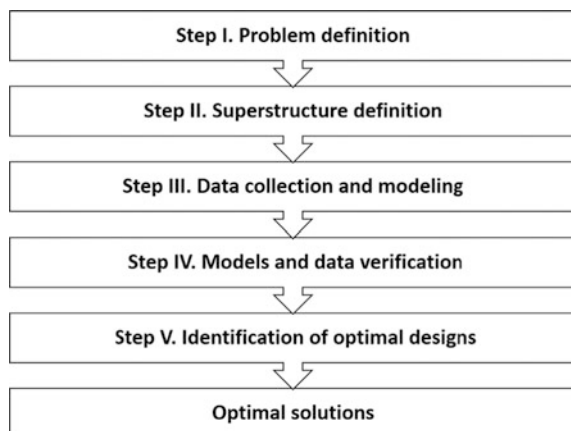
Cheali et al. [3] have presented a framework for sustainable design of algal biorefineries with respect to economic and environmental objectives. They have identified a challenge that refers to the availability of significant number of processing alternatives of algal biomass as it can generate wide variety of products and therefore difficulty in selecting the most suitable processing alternative. Thus, a systematic framework that uses super-structure-based optimization for synthesis and design was developed to create the processing network of an algal biorefinery using verified database (Fig. 3). First, database and design space for all the processes are generated. Secondly, the identification of optimal designs is done by techno-economic criteria and life cycle analysis. This leads to creation of a super-structure that represents the design space of an algal biorefinery containing various alternatives in terms of choice of microalgal species, pre-treatment steps, conversion, and purification or separation technologies to produce multiple products.

Consequently, the database consisting of process specific parameters is integrated with the formed super-structure. Subsequently, the optimization problem is solved using mathematical formulations to identify the most optimal designs with respect to techno-economic criteria and life cycle analysis-related constraints.

4.3 Strategies Toward Achieving Sustainable Microalgal Biomass Cultivation, Harvesting, and Processing

For the successful development of a microalgal-based biorefinery industry, it is important to have a continuous flow of feedstocks, nutrients, raw materials, water, and energy that should derive from inexpensive sources and generate value-added products from the processed biomass. Additionally, it is desirable to choose most efficient options for cultivation, harvesting, and dewatering. This can be achieved if

Fig. 3 Flowsheet of data management and identification for optimal design networks framework



the choices are made judiciously. For example, raceway ponds which are less expensive cultivation systems could be used. Instead of expensive nutrients for biomass cultivation, different effluent streams (municipal, industrial, or agricultural run offs) could be exploited [31]. Microalgae are known to grow phototrophically, heterotrophically, and mixotrophically utilizing the waste organic and inorganic carbon sources. The waste gaseous CO₂ from various point sources could also be utilized to feed microalgal cultures, and in return, microalga can capture CO₂ and reduce the effect caused by greenhouse gases on climate. Following section describes various strategies by which a sustainable microalgal biorefinery can be aimed.

4.3.1 Waste Mitigation and Waste-to-Wealth Conversion

Microalgae can grow under a broad range of environmental conditions. It can utilize waste resources present in water and air efficiently, thus is considered to be a suitable candidate for mitigation of environmental load caused due to over-exploitation of non-renewable resources in world. Different industries daily emit pollutants in their liquid effluent streams which are treated to safe limit before their disposal in water streams (industrial wastewater). Municipal and domestic sectors release effluents that contain lot of organic contaminants. Agricultural water from runoff is a rich source of nutrients such as N, P, and K which are preferred nutrients for microalgal growth. Several reports have been published where microalgae have been cultivated in different kinds of wastewater streams [15]. Additionally, presence of toxicants and some nutrient limitation not only limits biomass growth, but leads to accumulation of lipid and carbohydrates as part of their defense mechanism. Lipids and/or carbohydrates from the microalgal biomass is extracted and converted into biofuel derivatives. The gaseous pollutants of various industrial units as well as thermal power plants which use non-renewable fuel sources to produce electricity emit huge amounts of CO₂. It is reported that microalgae can utilize concentrated forms of CO₂ efficiently to produce biomass rich in metabolites of significant industrial applications [30]. Further, these two individual approaches can also be coupled which can result in zero waste emission and add no environmental footprint.

4.3.2 Co-location of the Biomass Production Facility to an Industry

For the sustainable production of microalgal biorefinery, it is believed to use resources that are inexpensive and do not pollute environment. Availability of those resources at the biomass production facility is not always possible. Thus, there are huge TCs involved in bringing the resources near the production facility. However, for the utilization of waste resources, it is essential to avoid these TC and develop biomass production facilities near wastewater collection or treatment plants and/or CO₂ emitting point sources. Co-location of algal production facilities with power

plants and/or wastewater treatment plants can result in substantial construction cost savings and environmental benefits relative to stand-alone facilities with dependence on fresh water intakes. This approach will help provide nutrients and energy from one facility to be used up by another, thus working in tandem and coherent. It will also result in reducing atmospheric emissions significantly and improve the wastewater effluent discharges. For example, the waste heat generated by thermal power plants during electricity production could be used to dry algae [13]. The waste energy from the plant can also be used to control the temperature of algal reactors during winter seasons. Similarly, algae could be co-fired along with coal to reduce load on non-renewable fuels and move toward green economy. Lohrey et al. in their case study integrated algal biodiesel production with cane sugar production due to the easy availability of flue gas CO₂ from combustion of bagasse, water, and energy at the sugar mill. Upon simulation of the process using the program *Sugars*TM, it was found that utilization of available waste resources from a 10,000 ton/d cane sugar mill may lead to a 530 ha algae farm that can produce 5.8 million L of biodiesel/year and reduce CO₂ emissions of the mill by 15% [17]. Seambiotic (www.seambiotic.com) produces algae which are colocated with a 4 GW fossil fuel burning electricity generation plant for high value dietary supplements at its ~1000 m² facility in Ashkelon, Israel. As a result of co-location, many costs related to transportation, energy, pipelines, nutrients, etc., could be avoided as compared to a stand-alone facility.

4.3.3 Nutrients Recycling

Nutrient recycling is required especially in those cultures where initial medium nutrient concentration is low, and a supplementation is desired for maximizing growth and product formation. An effective strategy should be formulated wherein nutrients from external sources are included which again is not cost intensive. There could be several sources (i) unused nutrients from a previous experiment systems (ii) nutrients remaining in the media after product recovery (iii) exploiting rich nutrient sources from inexpensive and waste resources such as poultry litter, pig-gery waste, aquaculture waste [14, 15].

4.3.4 Co-culture

Harvesting/dewatering of biomass is conventionally being done by centrifugation which incurs lot of energy and cost. In order to operate the microalgal biorefinery at larger scales, the idea of using centrifuges or costly chemicals such as flocculants and coagulants is not wise. Efforts have been made time to time to devise new techniques. Recently, co-culturing of algae with bacteria is gaining tremendous attention due to their high phycoremediation potential and biomass yield. In case of microalgal biorefinery, it has great potential to be used for improving microalgal cultivation and subsequent dewatering. According to a study by Gonzalez and

Bashan, green microalga *Chlorella vulgaris* was co-immobilized and then co-cultured with a plant growth promoting bacteria (*A. brasilense*). *A. brasilense* boosted the growth of green algae and also improved its harvesting by releasing bio-flocculants from its biomass [7]. Co-cultivation of fungi (*A. fumigatus*) cells with algae showed synergistic on wastewater bioremediation, biomass production, and lipid yield efficiency [29]. Such reports pave path for future researches to be focusing on such alternatives in order to make the microalgal biorefinery truly sustainable.

4.4 Techno-economic Analysis and Life Cycle Assessment (LCA)

To determine the economic viability of process technologies for a microalgal biorefinery in the research and development stage, it is desired to perform an overall TEA of the system. TEA helps to predict the PC of a given process technology. Microalgal biorefinery comprises of various products from a single efficient feedstock which has promising characteristics of high lipid yields, better photosynthetic efficiency, potential to utilize waste resources of water, and gaseous CO₂ from industrial effluents. In this scenario, TEA along with LCA has been used as fundamental tools in evaluating the feasibility of microalgae biorefinery for commercial scale. These tools have the capability to analyze alternative processing technologies for the sustainable production of product. For example, microalgal cultivation is carried out in open systems (raceway ponds, circular ponds) as well as closed photobioreactor (PBR). A satisfactory biorefinery system should include an inexpensive cultivation system such as raceway pond and utilize the algal oil free cake for other uses such as fermentation into bioethanol and/or use for animal feeds in order to satisfy economic, environmental, and social performance. Generally, open raceway ponds are relatively inexpensive, easier to construct, and feasible option for the commercial microalgal cultivation as compared to closed PBR that are costly but have better process control, ability of reaching higher culture density and productivity.

According to ISO 10440, LCA is a “compilation and evaluation of the inputs and outputs and the potential environmental impacts of a product system throughout its life cycle” [23]. It is a significant tool for assessing the environmental aspect of a product or process for its sustainable production. Outcome of LCA study depends on the system boundaries such as level of biomass and lipid/protein/carbohydrates content that can be achieved during the cultivation process (Fig. 4). When compared with closed photobioreactors, raceway ponds appear as an economical and feasible alternative for large-scale microalgal cultivation for biofuel and bioproduct production. However, there still are scope of improvements of microalgal feedstock to create a more economically viable and sustainable system which can be done by carrying out a thorough analysis of environmental analysis by LCA methodology.

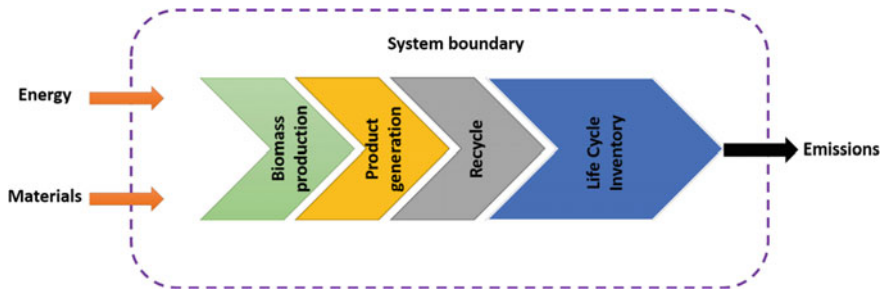


Fig. 4 System boundaries of life cycle assessment for microalgal biorefinery. The studied system includes biomass cultivation, algae oil extraction, conversion into biodiesel (product generation), and its life cycle assessment where all the system inputs such as energy and materials and emissions are evaluated

5 Challenges, Scope, and Opportunities of a Sustainable Microalgal Biorefinery

Despite several advantages of microalgal-based biorefinery approaches toward meeting demands related to supply of biofuels, food, feed, pharmaceuticals, microalgal biorefinery suffers a major challenge associated with its sustainability in larger and futuristic context. There is usually large cost associated with microalgal cultivation, raw materials, and techniques employed during downstream processing of the biomass for extraction of value-added products. These costs sometimes surpass the benefit or costs derived from the product. As a result, there is net CO₂ emission from the process, although microalgal-based technology is considered to be renewable and carbon neutral. The present techniques of biomass conversion are not lucrative and sustainable due to higher biomass PC and low market price of biofuels. For obtaining desired benefits, the choice of the microalgal strain is important. In order to address these issues, an integrated approach is required where a biorefinery is designed by keeping all three dimensions of sustainability. Never should any dimension be compromised which would otherwise make the process unsustainable. Thus, there is a need for the incorporation of sustainability right at the design step of biorefinery projects. Also, more and more of tools, such as mathematical programming, simulation tools, and database, should be referred before starting on any biorefinery-based project. Further, genetically transformed microalgal strains with improved performance in terms of enhanced lipid content, improved light utilization efficiency, accumulation of pigments, etc., should be included in designing step of the algal-based biorefinery.

The declining prices of crude oil in recent times and high capital and investment costs in algal production have a marked negative impact on the market of algae-based products. Innovative strategies should be devised for cost-effective dewatering, harvesting, and lipid recovery. Co-location of flue gas emitting industrial units with algal production and co-culturing seems to be promising

strategies of biomass harvesting and production of renewable resource with additional advantages of phytoremediation and CO₂ mitigation. The lower biomass productivities at higher production scales is a major challenge which needs to be addressed by incorporating cheaper sources of nutrients (waste resources), innovative PBR designs, and lighting strategies as well as different nutrients feed approaches. At last, biorefinery enthusiasts must integrate social and sustainability sciences in their future developments toward the establishment of a high-volume microalgae-based biorefinery industry.

Acknowledgements Geetanjali Yadav acknowledges the financial support provided by Council of Scientific and Industrial Research (CSIR), Government of India, during her doctoral studies. Authors thankfully acknowledge their institute IIT Kharagpur for providing library and computer facilities.

References

1. Becker CU (2012) The structural dimension of sustainability ethics. In: Sustainability ethics and sustainability research. Springer, Netherlands, Dordrecht, pp 83–108. doi:https://doi.org/10.1007/978-94-007-2285-9_10
2. Bumbak F, Cook S, Zachleder V, Hauser S, Kovar K (2011) Best practices in heterotrophic high-cell-density microalgal processes: achievements, potential and possible limitations. *Appl Microbiol Biotechnol* 91:31–46. <https://doi.org/10.1007/s00253-011-3311-6>
3. Cheali P, Posada JA, Gernaey KV, Sin G (2015) Upgrading of lignocellulosic biorefinery to value-added chemicals: sustainability and economics of bioethanol-derivatives. *Biomass Bioenerg* 75:282–300. <https://doi.org/10.1016/j.biombioe.2015.02.030>
4. Chew KW, Yap JY, Show PL, Suan NH, Juan JC, Ling TC, Lee D-J, Chang J-S (2017) Microalgae biorefinery: high value products perspectives. *Bioresour Technol* 229:53–62. <https://doi.org/10.1016/j.biortech.2017.01.006>
5. Coleman AM, Abodeely JM, Skaggs RL, Moeglein WA, Newby DT, Venteris ER, Wigmosta MS (2014) An integrated assessment of location-dependent scaling for microalgae biofuel production facilities. *Algal Res* 5:79–94. <https://doi.org/10.1016/j.algal.2014.05.008>
6. Coppens J, Grunert O, Van Den Hende S, Vanhoutte I, Boon N, Haesaert G, De Gelder L (2016) The use of microalgae as a high-value organic slow-release fertilizer results in tomatoes with increased carotenoid and sugar levels. *J Appl Phycol* 28:2367–2377. <https://doi.org/10.1007/s10811-015-0775-2>
7. De-Bashan LE, Bashan Y (2008) Joint immobilization of plant growth-promoting bacteria and green microalgae in alginate beads as an experimental model for studying plant-bacterium interactions. *Appl Environ Microbiol* 74:6797–6802. <https://doi.org/10.1128/AEM.00518-08>
8. Demirbas A (2008) Comparison of transesterification methods for production of biodiesel from vegetable oils and fats. *Energy Convers Manag* 49:125–130. <https://doi.org/10.1016/j.enconman.2007.05.002>
9. Gheewala SH, Bonnet S, Prueksakorn K, Nilsalab P (2011) Sustainability assessment of a biorefinery complex in Thailand. *Sustainability* 3:518–530. <https://doi.org/10.3390/su3030518>
10. Guihéneuf F, Stengel DB (2013) LC-PUFA-enriched oil production by microalgae: accumulation of lipid and triacylglycerols containing n-3 LC-PUFA is triggered by nitrogen limitation and inorganic carbon availability in the marine haptophyte *Pavlova lutheri*. *Mar Drugs* 11:4246–4266. <https://doi.org/10.3390/md11114246>

11. Harun R, Singh M, Forde GM, Danquah MK (2010) Bioprocess engineering of microalgae to produce a variety of consumer products. *Renew Sustain Energy Rev* 14:1037–1047. <https://doi.org/10.1016/j.rser.2009.11.004>
12. Ho SH, Kondo A, Hasunuma T, Chang JS (2013) Engineering strategies for improving the CO₂ fixation and carbohydrate productivity of *Scenedesmus obliquus* CNW-N used for bioethanol fermentation. *Bioresour Technol* 143:163–171. <https://doi.org/10.1016/j.biortech.2013.05.043>
13. Hosseinizand H, Lim CJ, Webb E, Sokhansanj S (2017) Economic analysis of drying microalgae *Chlorella* in a conveyor belt dryer with recycled heat from a power plant. *Appl Therm Eng* 124:525–532. <https://doi.org/10.1016/j.applthermaleng.2017.06.047>
14. Karemore A, Sen R (2015) RSC advances municipal and industrial liquid and solid waste synthesis for biodiesel. *RSC Adv* 5:70929–70938. <https://doi.org/10.1039/C5RA11670H>
15. Karemore A, Sen R (2015) Green integrated process for mitigation of municipal and industrial liquid and solid waste mixes for enhanced microalgal biomass and lipid synthesis for biodiesel. *RSC Adv* 5:70929–70938. <https://doi.org/10.1039/C5RA11670H>
16. Keller H, Rettenmaier N, Reinhardt GA (2015) Integrated life cycle sustainability assessment—a practical approach applied to biorefineries. *Appl Energy* 154:1072–1081. <https://doi.org/10.1016/j.apenergy.2015.01.095>
17. Lohrey C, Kochergin V (2012) Biodiesel production from microalgae: co-location with sugar mills. *Bioresour Technol* 108:76–82. <https://doi.org/10.1016/j.biortech.2011.12.035>
18. Marzbali MH, Mir AA, Pazoki M, Pourjamshidian R, Tabeshnia M (2017) Removal of direct yellow 12 from aqueous solution by adsorption onto spirulina algae as a high-efficiency adsorbent. *J Environ Chem Eng* 5:1946–1956. <https://doi.org/10.1016/j.jece.2017.03.018>
19. Mitra M, Patidar SK, George B, Shah F, Mishra S (2015) A euryhaline *Nannochloropsis gaditana* with potential for nutraceutical (EPA) and biodiesel production. *Algal Res* 8:161–167. <https://doi.org/10.1016/j.algal.2015.02.006>
20. Moreno-Garcia L, Adjallé K, Barnabé S, Raghavan GSV (2017) Microalgae biomass production for a biorefinery system: recent advances and the way towards sustainability. *Renew Sustain Energy Rev* 76:493–506. <https://doi.org/10.1016/j.rser.2017.03.024>
21. Parada MP, Osseweijer P, Duque JAP (2017) Sustainable biorefineries, an analysis of practices for incorporating sustainability in biorefinery design. *Ind Crops Prod* 106:105–123. <https://doi.org/10.1016/j.indcrop.2016.08.052>
22. Patil V, Reitan KI, Knutsen G, Mortensen LM, Källqvist T, Olsen E (2005) Microalgae as a source of polyunsaturated fatty acids for aquaculture. *Curr topics Plant biol* 6:57–65
23. Pfromm PH, Amanor-Boadu V, Nelson R (2011) Sustainability of algae derived biodiesel: a mass balance approach. *Bioresour Technol* 102:1185–1193. <https://doi.org/10.1016/j.biortech.2010.09.050>
24. Salar-Garcia MJ, Gajda I, Ortiz-Martinez VM, Greenman J, Hanczyc MM, de los Rios AP, Ieropoulos IA (2016) Microalgae as substrate in low cost terracotta-based microbial fuel cells: Novel application of the catholyte produced. *Bioresour Technol* 209:380–385. <https://doi.org/10.1016/j.biortech.2016.02.083>
25. Subramanian G, Yadav G, Sen R (2016) RSC advances rationally leveraging mixotrophic growth of microalgae in different photobioreactor configurations for reducing the carbon footprint of an algal biorefinery : a techno-economic perspective. *RSC Adv* 72897–72904. <https://doi.org/10.1039/C6RA14611B>
26. Trivedi J, Aila M, Bangwal DP, Kaul S, Garg MO (2015) Algae based biorefinery—how to make sense? *Renew Sustain Energy Rev* 47:295–307. <https://doi.org/10.1016/j.rser.2015.03.052>
27. Viswanathan B (2017) Chapter 15—biochemical routes for energy conversion. In: Viswanathan B (ed) *Energy sources*. Elsevier, Amsterdam, pp 357–368. <http://dx.doi.org/10.1016/B978-0-444-56353-8.00015-0>
28. Wellisch M, Jungmeier G, Karbowski A, Patel MK, Rogulska M (2010) Biorefinery systems—potential contributors to sustainable innovation. *Biofuels Bioprod Biorefin* 4:275–286. <https://doi.org/10.1002/bbb.217>

29. Wrede D, Taha M, Miranda AF, Kadali K, Stevenson T, Ball AS, Mouradov A (2014) Co-cultivation of fungal and microalgal cells as an efficient system for harvesting microalgal cells, lipid production and wastewater treatment. *PLoS One* 9. <https://doi.org/10.1371/journal.pone.0113497>
30. Yadav G, Karemore A, Dash SK, Sen R (2015) Performance evaluation of a green process for microalgal CO₂ sequestration in closed photobioreactor using flue gas generated in-situ. *Bioresour Technol* 191:399–406. <https://doi.org/10.1016/j.biortech.2015.04.040>
31. Yadav G, Sen R (2017) Microalgal green refinery concept for biosequestration of carbon-dioxide vis-à-vis wastewater remediation and bioenergy production: recent technological advances in climate research. *J CO₂ Util* 17:188–206. <https://doi.org/10.1016/j.jcou.2016.12.006>
32. Zamagni A, Pesonen H-L, Swarr T (2013) From LCA to life cycle sustainability assessment: concept, practice and future directions. *Int J Life Cycle Assess* 18:1637–1641. <https://doi.org/10.1007/s11367-013-0648-3>
33. Zhu L (2015) Biorefinery as a promising approach to promote microalgae industry: an innovative framework. *Renew Sustain Energy Rev* 41:1376–1384. <https://doi.org/10.1016/j.rser.2014.09.040>

Indian Agro-wastes for 2G Biorefineries: Strategic Decision on Conversion Processes

Ranjana Chowdhury, Shiladitya Ghosh, Biswajit Debnath
and Dinabandhu Manna

Abstract Biorefineries are globally contemplated as the viable platforms for the highly anticipated substitution of fossil-based economy by the bio-based economy. A biorefinery offers the advantage of converting a remarkable variety of biomass feedstocks to different types of biofuels and biochemicals. A great extent of rigorous effort is currently being made for the upgrading of existing biorefinery frameworks to fully attain the sustainability standards required to warrant their full-scale implementation. As a consequence of the mandatory inclusion of the sustainability goals into the biorefinery concept and the escalating concern on the ‘food-fuel conflict’, the second generation (2G) of biorefineries are garnering quick popularity over their first-generation counterparts. In India, there exist huge prospects of development of 2G biorefineries exploiting the abundant resources of the lignocellulosic agro-wastes. Indian agro-wastes display an extraordinary variety of lignocellulosic biomass and round-the-year availability in copious amounts. Unfortunately, due to lack of awareness and poor valorization, these valuable agro-wastes are often destroyed in mass scale for waste management instead of being utilized in a productive way. The major focus of the present chapter is to present a categorical classification of Indian agro-wastes based on their appearance in the supply chain. The adaptability of Indian agro-wastes towards 2G biorefinery has been assessed using their availability, thermochemical properties and composition of a few specific feedstocks, namely, rice straw, rice husk, wheat straw, oil seed press cakes, sugarcane bagasse, coconut shell, banana peels and stems. The analytic hierarchy process (AHP) has been used to decide on the strategy of application of stand-alone biochemical or thermochemical processes and their hybrids for the conversion of different candidate feedstocks in the 2G biorefineries with respect to sustainability parameters.

Keywords Agro-wastes · Abundance in India · Energy potential
2G biorefineries analytic hierarchy process (AHP) · Guideline on strategic decision on conversion route

R. Chowdhury (✉) · S. Ghosh · B. Debnath · D. Manna
Chemical Engineering Department, Jadavpur University, Kolkata 700032, India
e-mail: ranjana.juchem@gmail.com

1 Introduction

Notable attempts for the switch over from ‘fossil-dominated’ to ‘bio-based’ economy have already been initiated worldwide [1, 2]. Rapid decline in fossil fuel reserves and consequent tremendous future energy insecurity, rapid environmental deterioration due to GHG emission, progressive global warming and threatening issues of stagnation of socio-economic growth are the prime drivers of this paradigm shift [1–3]. The utilization of renewable resources (biofuels, biochemicals, biomaterials) in place of exhaustible non-renewables (petro-fuels and petrochemicals) bears the vital significance in this particular context and should be made compulsory worldwide through governmental enforcements. As envisioned by the international energy agency (IEA), this will require the ultimate diversification of primary energy sources by the countries around the world as an immediate measure [4]. Biomass, more specifically the solid lignocellulosic ones, originated from different natural resources can become the dependable alternatives of petro-based fuels as the primary energy source upon proper planning and implementation [5–7]. Significant technological progress made in the past few decades in the conversion of solid biomass to different liquid and gaseous biofuels has incremented the efficacy of end use of the biomass to several folds [8–13]. However, the current status of biofuels regarding competition with the conventional fossil fuels is far behind the baseline required to replace their usage as primary energy source. The major barriers are absence of proper categorization and poor valorization of biomass, unplanned use in non-compatible conversion processes resulting in incomplete recovery of energy and waste of valuable by-products due to lack of planning. It is apparent that the biofuels can never attain a competitive space with the crude-oil fuels if the high cost of production is not scaled down to significant extents [14, 15]. To achieve this particular goal, IEA has brought the focus of bioenergy planners on the concept of ‘bio-refining of biomass’ to facilitate the simultaneous production of (bio)chemicals, heat, power, food, feed and (bio)materials along with (bio)fuels from different variety of biomass in a single facility combining multi-step processes, popularly known as a ‘biorefinery’ [4]. The biorefinery concept has quickly garnered widespread acceptance all over the world and now exhibits a myriad of conceptual, technological and regional variants.

The developing countries with dynamically emerging industrial and economic growth, like the BRICS (Brazil, Russia, India, China and South Africa), display massive requirements of energy in form of oil and other fossil-based fuels to sustain the pace of rapid development [15, 16]. Demand of energy and security of energy availability differ significantly among these countries. Regarding energy security, India portrays a precarious nature, reflected from a history of continually increasing dependence (roughly 30% of energy demand) on imported sources of primary energy vectors [17]. According to the latest report by MPNG, India imports 14, 70 and 30% of its primary energy demand, respectively, in terms of coal, oil and natural gas, totalling in almost worth 150 billion USD [17]. It is being envisaged that cost of this energy import will reach a soaring 3.6 trillion USD by 2030 if

alternative measures are not administered urgently [17]. In this context, the conversion of varieties of Indian lignocellulosic biomass, often mistreated as just waste materials, to energy efficient biofuels has become a supreme concern of Indian bioenergy researchers as well as energy policy makers [18, 19]. India is largely known as an agriculture-based country with huge land coverage of productive agricultural fields spread throughout the country's vast rural expanse. Naturally, enormous quantities of agro-residues are annually generated in India as by-products of the crop cultivation and crop-processing sectors [19, 20]. Besides year-round availability, most of these agro-residues possess suitable biochemical composition and excellent energy content to be utilized as potential candidate feedstocks for the development of agro-waste-based biorefineries [21, 22]. Strategic planning and successful implementation of such biorefineries hold great promise in lessening of the country's forthcoming energy insecurity and existing wide gap between the energy demand and supply.

2 Classification of Biorefineries

As already mentioned in the preceding section, biorefineries currently display myriads of variants based on different basis of classification. Biorefineries have been majorly classified based on the sources of feedstock, generation technology and biomass conversion routes used and/or product/s targeted [23, 24]. Cherubini et al. classified the biorefineries based on four selected features namely platforms, products, feedstocks and processes in a recently published article [25]. In the article, they clearly stated that 'classification approach is flexible' for biorefineries, as new subgroups are continually appearing from the rapid progress of the emerging field. Taking advantage of this flexibility of classification, a simplistic approach of classifying the biorefineries has been adopted keeping direct accordance with the well-known generations of biofuels based on feedstock sourcing [23, 26, 27]. On the basis of origin and type of feedstock to be handled, we have simply classified the biorefineries into three major 'generations' as the following: (1) first-generation (1G) biorefinery, (2) second-generation (2G) biorefinery and (3) third-generation (3G) biorefinery. The classification of biorefineries is schematically represented in Fig. 1.

The 1G biorefineries use different simple sugar, cereal starch, vegetable oils and animal fats as feedstocks for production of biofuels and biochemicals [23]. The 2G biorefineries, also referred as the advanced biorefineries, will particularly use several lignocellulosic feedstocks including agro-wastes, energy crops, woody forestry residues and lignocellulosic fraction of industrial and municipal solid wastes (MSW) as feedstocks [23]. 3G biorefineries will rely on different freshwater and marine algal biomass as the feedstocks for biofuel and biomaterial production. It is distinctively ascertained that the feedstocks used in the 1G biorefineries are having food/feed value and are fit for human consumption, whereas all feedstocks of the

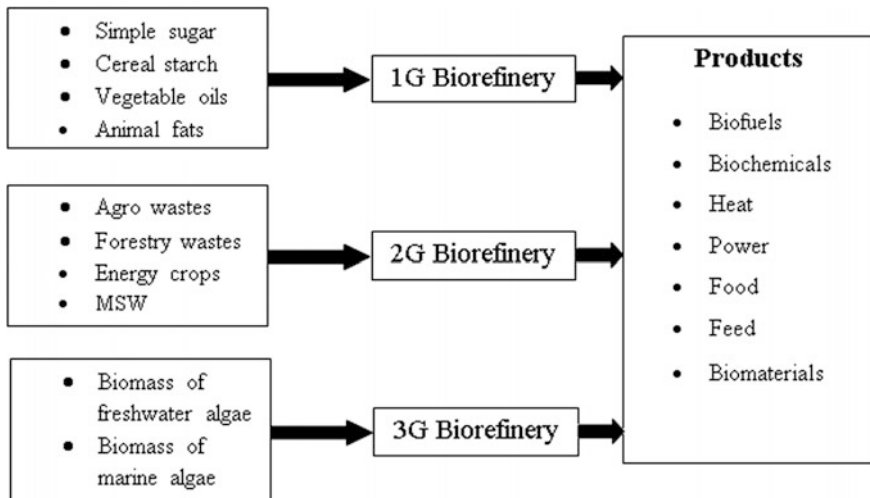


Fig. 1 Three classes of biorefineries based on feedstock sourcing

2G biorefineries are completely non-food in nature [28, 29]. This distinction in feedstock resourcing renders superiority of the 2G biorefineries over the 1G ones from the perspective of ‘food versus fuel’ issues, which makes the 1G technology highly unsustainable [28, 29]. In our discussion, we will specifically focus on the 2G biorefineries meant for the conversion of various Indian lignocellulosic agro-wastes to biofuels and multiple added-value products. The usage of dedicated energy crops has been intentionally excluded due to another controversial issue of ‘land versus fuel’ [28], which should be avoided in an exclusively agriculture-oriented country like India. Most compatible combinations of ‘feed-stocks and conversion routes’ will be assessed and recommended for future implementation based on the maximized level of attainable sustainability standard in the Indian context.

3 Categorization of Indian Agro-wastes

Before planning the utilization of different Indian agro-wastes as feedstock for biofuel production either through individual conversion routes or in a 2G biorefinery facility, proper categorization is a requisite. This will greatly help in assessing the probable economic value of the particular feedstocks and eventual valorization through policy making from the perspective of their usage in biofuel and biochemical production. This is rather a difficult job because of the existence of extremely diverse types of Indian agro-biomass [18–20]. To categorize the Indian agro-wastes, primarily they have been divided into two distinct classes, depending

on their appearance on the supply chain (from the cultivation field to the agro-processing sectors). First class is the agro-wastes directly produced during or after the harvesting of the crop/agricultural plants, termed as ‘post-harvesting residues’. Post-harvesting leftovers may also be regarded as the ‘field residues’ as most of the times these are left in the field at/or close to the site of cultivation. Second class of agro-biomass is represented by the remainings generated as by-products of different processing units handling the crops to harness the edible parts, termed as ‘post-processing residues’. Varieties of different major Indian agricultural crops and the residual agro-wastes derived from them [18, 19, 30], both post-harvesting and post-processing, have been tabulated in Table 1.

Depending on the variation in climatic conditions and soil properties, different types of agricultural crops are cultivated in different parts of India. Rice, being the staple food of majority of Indians, is the most prominently cultivated crop in India. Rice is cultivated in mass scale in 21 states among the total 28 major states of the country [30]. Naturally, quantity-wise a huge fraction of the Indian agro-wastes is dominated by the residues produced from rice. Besides rice, the other crop varieties cultivated in large scale are reported in Table 1 along with the agro-wastes subsequently produced from them. The lignocellulosic agro-wastes generated from all these crops can serve as potential feedstocks for generation of bioenergy through different conversion routes.

Table 1 Major types of Indian crops and the post-harvesting and post-processing residues derived from them

Indian crops	Post-harvesting residue	Post-processing residue
Rice	Straw/stalk, leaves, stubble,	Husk/hull
Wheat	Straw/stalk, leaves, stubble	Pod/panicle
Sugarcane	Top, leaves	Bagasse
Maize	Stalks	Cobs
Banana	Leaves, pseudo-stem, fruit branch	Pith, fruit peels
Mustard	Stalks	Husk, press cakes
Sesame	Stalks	Press cakes
Castor	Stalks	Husk, press cakes
Soybean	Stalks	N.A.
Coconut	Fruit brunch, fronds	Husk/coir, pith, shell
Areca nut	Fruit brunch, fronds	Husk
Groundnut	Stalks	Shell
Bajra	Stalks	Husk, cobs
Jowar	Stalks	Husk, cobs
Ragi	Stalks	N.A.
Pulses*	Stalks	Husk

Sourced from [18, 19, 30], *Arhar, gram, masoor, moong, urad

4 Availability and Conventional Use of Indian Agro-wastes

Table 1 provides an overview of the extremely diversified agro-waste varieties produced in India. Most of the tabulated agro-wastes are available round the year due to the continuous production of the crops in rotational manner for the production of food and feed to satiate the hunger of the huge population of India. As a natural consequence, the non-edible lignocellulosic agro-residues originating from the cultivation and processing of the Indian food crops are absolutely huge for the prime crop varieties [18, 19, 30]. Regarding the quantity, agro-wastes produced from rice, wheat, sugarcane, maize, banana, oilseed crops (mustard, sesame, castor), nuts (coconut, areca nut, ground nut), millets (jowar, bajra, ragi) and pulses are substantially huge in India [19]. Annually available amount of these agro-wastes have been tabulated and presented in Table 2.

From the data presented in Table 2, it is evident that among the Indian agro-wastes generated through the cultivation and processing of crops, residues of rice hold the majorly significant fraction of produced agro-wastes. Other than rice, wheat, sugarcane, banana, maize, coconut, groundnut, jowar, bajra are the other Indian crop varieties, which produce significantly high amount of lignocellulosic wastes. Agro-wastes produced from the oilseeds are also considerably high, particularly for mustard (Table 2). However, the availability of data on the quantity of the 'press cakes' produced as post-processing residues from the oilseeds is scarce, which can be significantly added to the agro-wastes of Indian oilseeds. Also, quantitative data on the amount of stubble of rice and wheat are not available, which are important lignocellulosic agro-wastes of these two cereal crops.

Clearly, there is an absolute abundance of agro-wastes in India, which also poses difficulties in proper management and handling of the massive volume of solid biomass continuously being produced. In India, there are mainly two conventional ways/methods, through which the agro-wastes are managed. The first method has a long history of traditional usage in India, which is the use of dry agro-residues as solid fuel in earthen/clay ovens or house stoves in the rural areas for cooking and producing heat [31]. Huge amount of GHGs (particularly CO_2 , NO_x , SO_x) and respirable particulates are produced during the burning of the lignocellulosic agro-residues in this method of usage [31]. This is neither an eco-friendly nor a healthy way of utilization of the agro-wastes. It notably adds up to the atmospheric GHG load in one hand, and on the other, it adversely affects the respiratory system of the persons directly exposed to the smoke caused during the burning [31]. The straws or stalks, residual leaves, nut shells and fronds of the crop plants are primarily used through this method. The second way of agro-waste management practiced in India is leaving the wet parts of the agro-wastes openly in the site of cultivation for the amendment of soil by the fertilizer produced through the microbial decay of the biomass. This process, although apparently looks harmless, causes emission of another potent GHG, viz. CH_4 to the environment in mass scales. The CH_4 is produced during the microbial degradation of the agro-biomass

Table 2 Annual availability of agro-wastes of major agricultural crop varieties of India

Indian crops (corresponding agro-wastes)	Annual availability (Kt/year)	Reference
Rice waste	161893.00	[20]
Rice straw	141120.00	
Rice husk	20773.00	
Wheat (straw)	122991.00	[20]
Sugarcane wastes	114761.00	[20]
Sugarcane bagasse	73775.00	
Sugarcane tops and leaves	40986.00	
Maize waste	33720.00	[20]
Maize straw	28396.00	
Maize cobs	5324.00	
Banana waste	67776.00	[20]
Banana fruit peels	393.00	
Banana pseudo-stem	67383.00	
Mustard waste	16877.00	[20]
Mustard press cake	2681.00	
Mustard seedpod	1355.00	
Mustard stalks	12841.00	
Sesame (stalks)	1207.70	[19]
Soybean husk	671.00	[20]
Coconut waste	9060.00	[20]
Coconut fronds	7769.00	
Coconut shell	726.00	
Coconut coir pith	565.00	
Areca nut (fronds, husk)	1000.80	[19]
Groundnut (shells)	1385.00	[20]
Bajra(stalks, cobs, husk)	15831.80	[19]
Jowar (cobs, stalks, husk)	24207.80	[19]
Ragi (straw)	2630.20	[19]
Cotton waste	38281.00	[20]
Cotton stalks	35397.00	
Cotton hull	2884.00	
Pulses* (stalks, husk)	13462.90	[19]

*Arhar, gram, masoor, moong, urad

by the native decaying microorganisms present in the soil. So, from an environmental perspective, this method is also not eco-friendly. This method is particularly used for the agro-biomass of the pulses for recycling back the nitrogen into the soil in a traditional belief. Another commonly practiced method for managing the enormous volume of straw and stubble is the open-field burning for mass destruction of the dry agro-wastes [32, 33]. It is easily understandable that this is an environmentally detrimental process due to the massive GHG (CO₂, CO, NO_x, SO_x etc.) emission, during the open-air combustion of the carbonaceous straws/stubbles [33]. Lack of awareness and infrastructural inabilities are the two major reasons for the persistence of these malpractices in India. True valorization of the

Indian agro-wastes through proper identification of their prospects for the production of biofuels and additional value-added products is urgent to stop the mis-handling of the immensely valuable agro-wastes.

5 Characterization of Indian Agro-wastes

It is of crucial importance to clearly understand the physico-chemical characteristics of the lignocellulosic agro-wastes to facilitate optimal processing and efficient conversion into biofuels and other value-added products in a 2G biorefinery. Principal components of all of the tabulated agro-wastes, both post-harvesting and post-processing, are the three complex biopolymers, namely lignin, cellulose and hemicellulose [34]. Lignin is the rigid aromatic hetero-biopolymer which forms the outermost protective layer of all lignocellulosic biomass [35]. The polysaccharide duo, cellulose and hemicellulose form the core carbohydrate moiety of lignocelluloses and are the target components for biofuel production [35]. Contents of lignin, cellulose and hemicellulose substantially vary among various lignocellulosic biomass depending on species, season, region and climatic conditions [19, 30, 34, 35]. Owing to the natural recalcitrance and compositional complexity, lignin content plays the pivotal role regarding the choice of the conversion route, namely biochemical or thermochemical or their hybrid, for the generation of biofuels from the agro-residues. Hence, it seems beneficial to primarily select the route of conversion for the Indian agro-wastes to biofuels based on the lignin content; this strategy is discussed in detail in a later section. Lignin, cellulose and hemicellulose contents of some major agricultural wastes have been presented in Table 3.

5.1 Lignin-Based Classification of Indian Agro-wastes

Based on the lignin contents of the Indian agro-wastes, as reported in Table 3, a three-class categorization has been done. The three classes of agro-wastes are namely low lignin (LL), medium lignin (ML) and high lignin (HL). The characteristic range of lignin contents (%) of the three classes are 1–10 (LL), 10–20 (ML) and HL (above 20), respectively. According to this lignin-based classification, the distribution of different agro-wastes (Table 3) is as follows:

1. HL: rice husk, sugarcane tops, sugarcane leaves, coconut shell, groundnut shell, barley straw.
2. ML: rice straw, wheat straw, sugarcane bagasse, maize stems, coconut coir.
3. LL: mustard stalks, soybean husk, sesame press cake, banana pseudo-stem.

Table 3 Lignocellulose contents of different Indian agro-wastes

Agro-waste	Lignin (%)	Hemicellulose (%)	Cellulose (%)	Reference
Rice straw	17.00	22.00	42.00	[20]
Rice husk	24.60	31.60	43.80	[34]
Wheat straw	13.00	30.00	42.00	[20]
Mustard press cake	–	3.00	4–5	[46]
Mustard stalks	2.20	18.70	39.50	[47]
Soybean husk	9.88	17.15	33.49	[48]
Sesame press cake	1.00	–	–	[49]
Sugarcane bagasse	13.40	9.20	58.20	[20]
Sugarcane tops	21.70	32.00	39.70	[50]
Sugarcane leaves	22.70	28.70	40.80	[50]
Maize stems	19.90	21.10	–	[51]
Coconut shell	28.70	25.10	36.30	[52]
Coconut coir	17.80	25.90	47.70	[52]
Banana pseudo-stem	8.07	18.40	44.00	[53]
Groundnut shell	30.20	18.70	35.70	[52]
Barley straw	20.78	–	–	[54]

5.2 Elemental Analysis

The elemental composition of different Indian agro-wastes has been presented in Table 4.

5.3 Energy Potential of Indian Agro-wastes

Estimation of total energy potential of candidate agro-wastes in a year-wise basis is an important consideration to select the most promising feedstocks for 2G biorefinery. This will help in the primary decision-making process considering the abundance and higher heating value (HHV) of a particular agro-waste ensuring its uninterrupted availability. The elemental composition, particularly C–H–O analysis of any lignocellulosic biomass, affects the energy content of the feedstock. The higher heating values (HHV) of the Indian agro-wastes have been calculated using the Dulong's equation as follows [36]:

$$\text{HHV(kJ/kg)} = [(337.7 \times \text{C}) + \{1437.9 \times (\text{H} - (\text{O}/8))\}] \quad (1)$$

The values of C, H and O have been obtained from Table 4.

Table 5 represents the quantitative data on the HHV and total energy potential of some major Indian agro-wastes, calculated based on the annual availability of the wastes, as provided in Table 2.

Table 4 Elemental composition of different agro-wastes and their higher heating values

Agro-waste	C (%)	H (%)	O (%)	N (%)	S (%)	Reference
Rice straw	38.80	6.70	38.80	0.20	0.20	[55]
Rice husk	39.80	5.70	39.80	0.50	0.20	[55]
Wheat straw	41.70	5.00	41.70	0.40	0.30	[55]
Mustard press cake	40.26	6.03	46.14	6.46	1.11	[46]
Mustard seedpod	44.30	8.80	43.00	0.38	0.19	[20]
Mustard stalks	43.80	5.90	43.80	0.30	0.30	[55]
Castor shell	49.80	5.30	43.90	0.90	0.10	[56]
Soybean husk	43.10	6.40	44.50	0.80	0.09	[20]
Sesame press cake	45.19	7.55	39.27	7.26	0.72	[57]
Sesame stalks	49.16	6.59	34.06	0.85	0.31	[58]
Sugarcane bagasse	48.60	5.90	42.80	0.16	0.04	[20]
Sugarcane tops and leaves	39.80	5.60	46.80	1.70	–	[20]
Maize straw	47.09	5.54	39.79	0.81	0.12	[20]
Maize cobs	41.40	6.00	51.30	0.14	0.01	[20]
Coconut fronds	48.60	5.80	42.40	–	–	[20]
Coconut shell	52.30	6.60	39.50	0.30	0.80	[20]
Coconut coir pith	50.30	5.10	39.60	0.45	0.16	[20]
Banana pseudo-stem	43.28	6.23	49.02	0.98	0.49	[59]
Banana fruit peels	35.58	4.62	57.16	2.19	0.45	[59]
Areca nut husk	44.70	3.80	51.20	0.40	–	[60]
Groundnut shell	33.90	2.00	59.90	1.10	0.12	[20]
Cotton stalks	41.50	6.20	47.50	1.81	0.02	[20]
Cotton hull	50.40	8.40	39.80	1.40	0.10	[20]
Barley straw	45.67	6.15	38.26	0.43	0.11	[61]
Barley chaff	46.77	5.94	39.98	1.45	0.15	[61]

From the data presented in Table 5, it is evidently seen that agro-wastes derived from rice possess the highest annual energy potential and are much greater than any other agro-wastes. This is followed by wastes of wheat, banana, sugarcane, cotton and maize; the annual energy potentials of which are also significantly high for India. Other noteworthy agro-wastes with substantially high energy potential ranging between 100 and 200 PJ/year are namely mustard and coconut. Hence, it is assessed that agro-wastes of these crops can serve as abundant source of feedstocks for an Indian agro-waste-based 2G biorefinery. Total annual energy potential of the agro-wastes of 8591.67PJ is comparable to the total coal-based thermal power of 194553 MW in India [37]. The actual potential is, however, dependent on the efficiency of the conversion process to be selected for the generation of energy from the wastes.

Table 5 Total annual energy potential of selected Indian agro-wastes

Agro-waste	HHV (MJ/kg)	Energy potential in PJ/year (= Annual availability * HHV)	Reference
Rice straw	15.76	2224.05	[55]
Rice husk	14.48	300.79	[55]
Wheat straw	13.77	1693.58	[55]
Mustard press cake	13.97	37.45	[46]
Mustard seedpod	19.88	1.37	[20]
Mustard stalks	15.40	197.75	[55]
Soybean husk	15.76	10.57	[20]
Sesame stalks	19.95	24.09	[58]
Sugarcane bagasse	17.20	1268.93	[20]
Sugarcane tops and leaves	13.52	554.13	[20]
Maize straw	16.72	474.78	[61]
Maize cobs	13.39	71.29	[20]
Coconut fronds	17.06	132.54	[20]
Coconut shell	20.05	14.55	[20]
Coconut coir pith	17.20	9.72	[20]
Banana pseudo-stem	14.77	995.25	[59]
Banana fruit peels	8.38	3.29	[59]
Groundnut shell	3.55	4.91	[20]
Cotton stalks	14.39	509.36	[20]
Cotton hull	21.94	63.27	[20]
Total		8591.67	

6 Biomass Conversion Processes of 2G Biorefinery Platform

Lignocellulosic biomass can be converted to an array of various biofuels and chemicals/biochemicals via selection of different route of conversion. Both thermochemical and biochemical conversion processes are in common practice worldwide [9, 38]. As individual processes, all of the biomass conversion routes produce some energy products (heat and fuels) and some material products (chemicals, biochemicals, biomaterials). In a 2G biorefinery platform, more than one of these processes are advantageously used together to increase the extent of biomass conversion, number of marketable products and reduction of waste generation. However, selection of particular conversion processes in 2G biorefinery platforms in different countries is highly dependent on several factors. Type and availability of biomass, awareness and willingness of the biomass producers to supply biomass residues to conversion plants, progress in biomass conversion technologies and proper planning of utilization by the bioenergy leaders are some

prime driving factors. As a primary focus of this chapter, suitability of different conversion routes for the conversion of Indian agro-wastes, categorized on the basis of lignin content, has been assessed. Table 6 provides the thermochemical, biochemical conversion routes and their hybrids under consideration.

7 Strategies for the Utilization of Indian Agro-wastes in 2G Refinery

Lignin is the most recalcitrant substance present in all lignocellulosic materials, including the agro-wastes; it highly influences the rate of conversion of biomass through any route, particularly the biochemical ones [35]. Hence, it seems beneficial to primarily select the specific route, either thermochemical or biochemical, to ensure maximum biomass conversion with enhanced efficiency. It is understandable that biomass with very high percentage of lignin is not suitable as feedstocks for biochemical routes due to the requirement of extensive pre-treatments. Although it is not very easy to assess the difficulties or advantages of using any agro-waste as feedstock for any conversion route, an assessment considering major influencing factors is necessary. To facilitate the clear understanding on proper and specific selection of biomass and its most compatible conversion route, a strategic decision-making approach has been adopted here. In the approach, lignin content of the agro-wastes has been considered as the first basis of categorization to be used for the selection of the best conversion route among available options. Afterwards, a well-known strategic decision-making tool has been used to assess the feasibility of agro-waste conversion in a 2G biorefinery framework shown in Fig. 2.

Figure 2 depicts the overall scheme of the proposed 2G biorefinery framework comprising all options of biomass classes, pre-treatment units, conversion routes and product series. In Fig. 2, the three-class categorization of lignin-based biomass has been shown along with their probable point of entry in different option of conversion routes. For the three biomass classes, a total of five conversion routes (Table 6) have been proposed as options as following:

- A. Thermochemical routes (no biomass pre-treatment is considered)
 1. Gasification (GA)
 2. Gasification followed by Fischer–Tropsch synthesis (GA-FT)
 3. Pyrolysis (PY)
- B. Biochemical routes (acid hydrolysis (AH) of biomass is considered as an initial step)
 1. Anaerobic digestion (AH-AD)
 2. Alcohol fermentation (AH-AF)
- C. Hybrid process (thermochemical + biochemical)
 1. Gasification followed by alcohol fermentation (GA-ALF)

Table 6 The biomass conversion processes of the 2G biorefinery platform

Conversion process	Technology used	Reactions	Product uses
Thermochemical processes	Gasification	$C + O_2 \rightarrow CO_2$ $CO_2 + C \rightarrow 2CO$ $C + H_2O \rightarrow CO + H_2$ $CO + H_2O \leftrightarrow CO_2 + H_2$ $C + 2H_2 \rightarrow CH_4$	Fuel
	Gasification followed by: Fischer-Tropsch	$nCO + (2n + 1)H_2 \xrightarrow{\text{Catalyst}} C_nH_{2n} + 2 + nH_2O$ $nCO + 2nH_2 \xrightarrow{\text{Catalyst}} C_nH_{2n} + nH_2O$	Fuel
	Pyrolysis	<pre> graph TD Biomass --> Pyro-char Biomass --> Pyro-gas Biomass --> Pyro-oil </pre>	Char: adsorption and soil amendment; Oil: fuel and biochemical Gas: fuel
Biochemical processes	Alcohol fermentation	$C_6H_{12}O_6 \xrightarrow{\text{Microorganisms}} 2C_2H_5OH + 2CO_2$	Alcohol: Fuel Lignin residues: Chemical
	Biogas production	<pre> graph TD Biomass -- 1 --> Simple_sugars[Simple sugars] Simple_sugars -- 2 --> Volatile_fatty_acids[Volatile fatty acids] Volatile_fatty_acids -- 3 --> Acetic_acids[Acetic acids] Acetic_acids -- 4 --> CH4_CO2[CH4 + CO2] </pre>	Biogas: Fuel; Solid waste: Fertilizer
Hybrid process	Syngas fermentation	$6CO + 3H_2O \rightarrow CH_3CH_2OH + 4CO_2$ $2CO_2 + 6H_2 \rightarrow CH_3CH_2OH + 3H_2O$	Lower alcohols: Drop-in fuel; Higher alcohols: Drop-in fuel

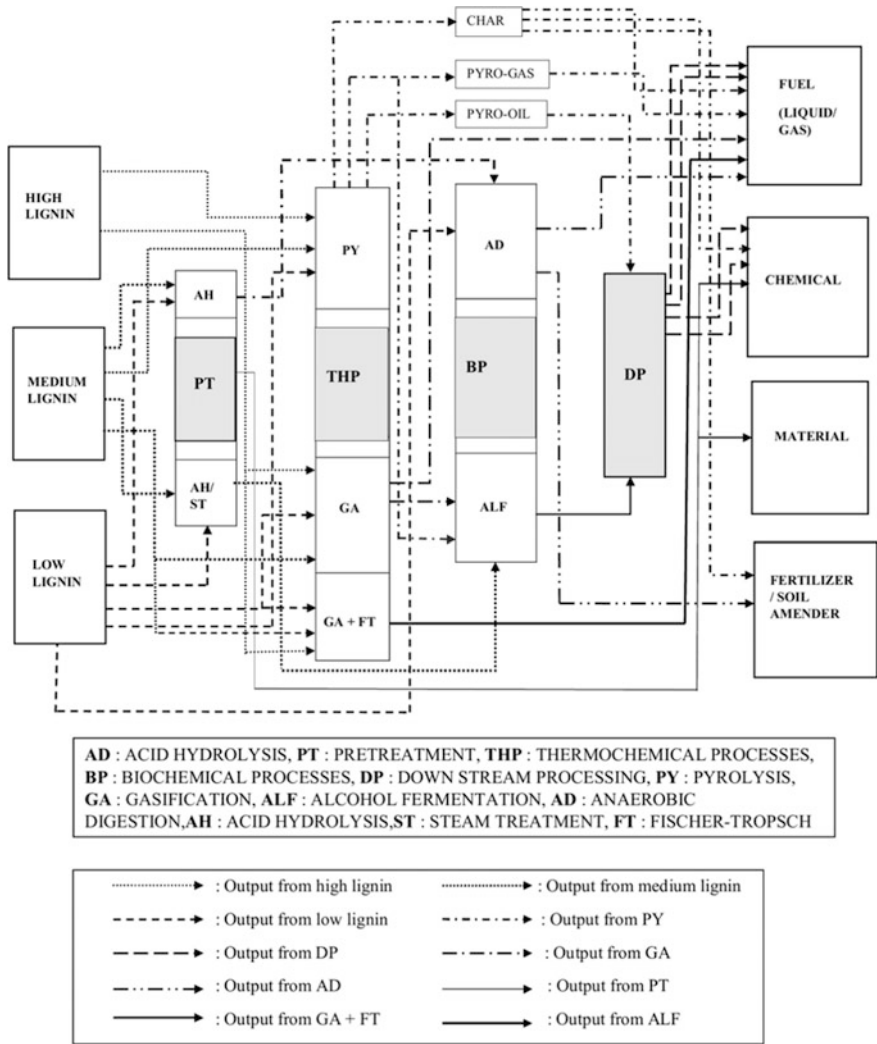


Fig. 2 Schematic of the Indian agro-waste-based 2G biorefinery framework

After defining all the available options for biomass and conversion routes, feasibility analysis has been conducted to clearly assess the suitability of conversion of particular agro-wastes from Indian context.

7.1 Analytical Hierarchical Process (AHP) Model

The analytical hierarchical process (AHP) in this study has been carried out using the super decision software following the basic steps proposed by Saaty [39–43]. The AHP used in this study is a four-tier structure consisting of one goal, one criteria cluster, one sub-criteria cluster and one alternatives cluster illustrated in Fig. 3.

The goal of this study is to find out the best compatible route for conversion of biomass of varying lignin content in the Indian context. The criteria set for the analysis is environmental aspects, economical aspects and the maturity of the technologies considered for conversion of biomass. The sub-criteria have been set to be different lignin content of biomass, i.e. high lignin content, medium lignin content and low lignin content. The alternatives chosen are pyrolysis (PY), gasification followed by alcohol fermentation (GA-ALF), gasification followed by Fischer–Tropsch process (GA-FT), anaerobic digestion with acid hydrolysis as pre-treatment (AH-AD) and alcohol fermentation with acid hydrolysis as

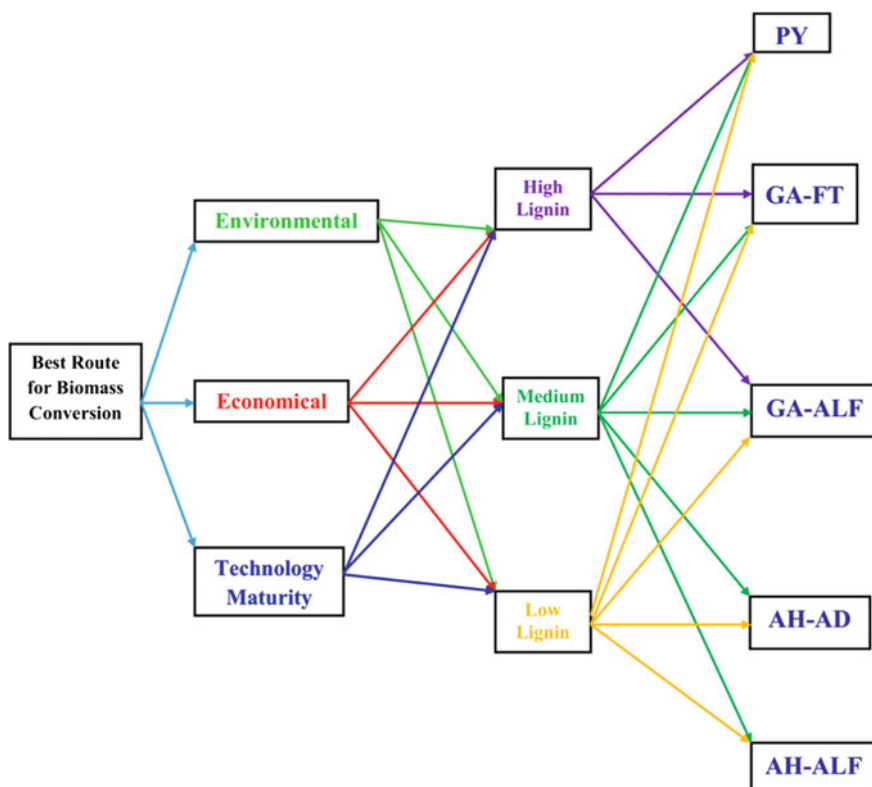
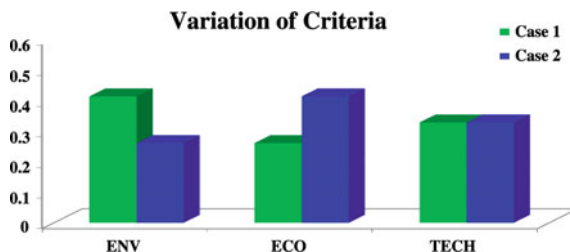


Fig. 3 Four-tier AHP model of the Indian agro-waste-based 2G biorefinery

Fig. 4 Variation of criteria in case 1 and 2



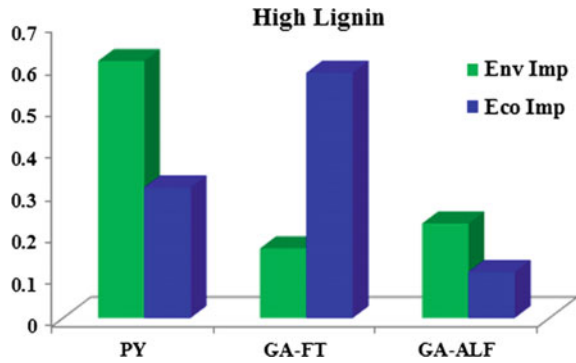
pre-treatment (AH-ALF). Since direct conversion through biochemical route is impracticable for high lignin biomass, the alternatives are set to PY, GA-ALF and GA-FT. For both medium and low lignin biomass, all the five alternatives are applicable. The ratings have been provided by means of detailed literature review, subsequent analysis and brain-storming sessions. The Saaty scale has been strictly followed for this purpose [44, 45]. In order to avoid any ambiguity and biasness towards the ratings, the AHP has been carried out twice by assigning different weightage to the environmental and economic criteria, defined as case 1 and case 2, respectively (Fig. 4). The technological maturity has been left unperturbed as that dictates a fact or current status about that technology, and introducing perturbation in that is meaningless. On a scale of 100, for case 1, weightages on economics, environmental impact and technological maturity are set in the ratio of 26:41.2:32.8. In case 2, the weightages on environment and economics have been interchanged. Thus, the eco: env: tech is set as 41.2:26:32.8.

7.2 AHP Results for Three Classes of Biomass

7.2.1 High Lignin Biomass

For high lignin content biomass, for case 1, the pyrolysis is the most preferable route followed by GA-ALF and GA-FT. This is justifiable as pyrolysis has lesser environmental footprint than gasification process. In addition to that, the pyro-char obtained as a product of pyrolysis is used in soil fixation which has positive environmental footprint. With respect to the economical preference (case 2) for high lignin biomass, GA-FT is the best suitable route followed by GA-ALF. In this case, GA-FT is the best solution because the economics of this process is well established and the demands of the final products are also high. Also, gasification is a self-sustained process compared to pyrolysis, and no additional cost is required to maintain an inert atmosphere inside the reactor. Pyrolysis comes as second option as the process is economically feasible more than the GA-ALF process as the yield is less in case of GA-ALF. The results are depicted in Fig. 5.

Fig. 5 AHP rating for suitable conversion processes for HL



7.2.2 Medium and Low Lignin

For medium and low lignin biomass, pyrolysis followed by AH-AD and AH-ALF is the most suitable options, and GA-ALF and GA-FT are the least suitable options when the analysis is biased on environmental impact. Due to the positive environmental footprints, as discussed before, pyrolysis comes up as the best preference compared to AH-AD and AH-ALF, as both the latter processes have energy requirement and water footprint. In addition to that, AH-AD have higher footprint if methane leakage occurs. GA-ALF and GA-FT are least preferable options as the overall environmental footprint is much higher. For case 2 with higher biasness to economics, AH-AD, pyrolysis and GA-FT are the best suitable routes, whereas AH-ALF and GA-ALF are the least suitable routes. AH-ALF and GA-ALF lag behind mainly due to low conversion. AH-AD dominates the top position as installation cost, operating cost and maintenance cost are less compared to pyrolysis and GA-FT. The results are depicted in Fig. 6.

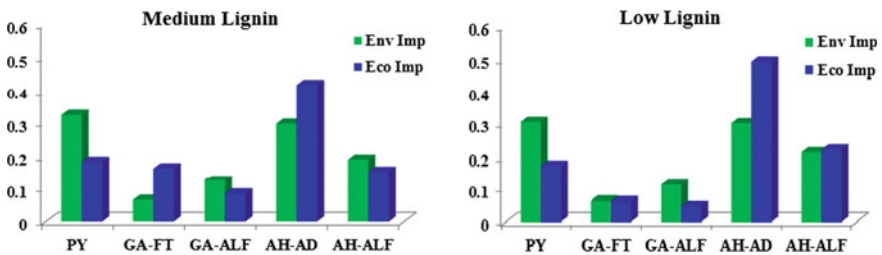


Fig. 6 AHP rating for suitable conversion processes for ML and LL

8 Recommendation on Strategic Decision on Feasible Conversion Processes

From the AHP analysis, it is clear that the choice of the conversion processes to be used in the 2G biorefineries depends on the type of agro-waste and the environmental and economic impacts of the process. Different sets of conversion processes are suitable if the biasness on environment and economics is interchanged. Therefore, for the setting up of a 2G refinery in any agricultural hub, the policy makers have to decide on the priority consideration, i.e. whether environmental impact or economic returns is to be given more stress. For the same level of environmental impact, better economy is expected if the technological maturity increases. Hence, more thrust should be given on research and development to unwind the mechanisms to address the challenges of the conversion processes. The analysis also indicates that parallel processing of high, low and medium lignin feedstocks should be done using different conversion processes in the same 2G biorefinery to exploit the maximum benefit from all agro-residues.

9 Conclusions

From the available database, an assessment on the abundance of Indian agro-residues and their overall energy potential has been made. Based on the lignin content, the residues have been classified as high lignin, medium lignin and low lignin ones. Considering an array of thermochemical, biochemical and hybrid processes, an AHP model has been developed to draw a guideline for the strategic decision on the utilization of the conversion path for different types of biomass in a single 2G refinery. The analysis clearly indicates that the suitability of routes changes with the interchange of priority on environmental impact and economic return. It is expected that the findings presented in the article will be useful for the scientists to focus on the research and development on suitable conversion processes for different types of agro-residues and for the policy makers to decide on setting up of 2G biorefineries near agricultural hubs in rural sectors.

Acknowledgements The corresponding author acknowledges INNO-INDIGO for the selection of collaborative CONVER-B project on Biobased Energy. All authors acknowledge the valuable comments made by the learned reviewers for the upgradation of the quality of the manuscript.

References

1. Viaggi D, Mantino F, Mazzocchi M, Moro D, Stefani G (2012) From agricultural to bio-based economics? Context, state of the art and challenges. *Bio-based Appl Econ* 1(1):3–11
2. Priefer C, Jörissen J, Frör O (2017) Pathways to Shape the Bioeconomy. *Resources* 6(1):10

3. Philp JC, Pavanan KC (2013) Bio-based production in a bioeconomy. *Asian Biotechnol Develop Rev* 15(2):81–88
4. De Jong E, Higson A, Walsh P, Wellisch M (2012). Bio-based chemicals value added products from biorefineries. IEA Bioenergy Task42 Biorefinery
5. Sun R (2010) Cereal straw as a resource for sustainable biomaterials and biofuels: chemistry, extractives, lignins, hemicelluloses and cellulose. Elsevier
6. Mtui GY (2009) Recent advances in pretreatment of lignocellulosic wastes and production of value added products. *African J Biotechnol* 8(8)
7. Rooni V, Raud M, Kikas T (2017) Technical solutions used in different pretreatments of lignocellulosic biomass: a review. *Agron Res* 15(3):848–858
8. Wi SG, Cho EJ, Lee DS, Lee SJ, Lee YJ, Bae HJ (2015) Lignocellulose conversion for biofuel: a new pretreatment greatly improves downstream biocatalytic hydrolysis of various lignocellulosic materials. *Biotechnol Biofuels* 8(1):228
9. Brethauer S, Studer MH (2015) Biochemical conversion processes of lignocellulosic biomass to fuels and chemicals—a review. *CHIMIA Int J Chem* 69(10):572–581
10. Nanda S, Mohammad J, Reddy SN, Kozinski JA, Dalai AK (2014) Pathways of lignocellulosic biomass conversion to renewable fuels. *Biomass Convers Biorefinery* 4(2):157–191
11. Limayem A, Ricke SC (2012) Lignocellulosic biomass for bioethanol production: current perspectives, potential issues and future prospects. *Prog Energy Combust Sci* 38(4):449–467
12. Sarkar A, Chowdhury R (2016) Co-pyrolysis of paper waste and mustard press cake in a semi-batch pyrolyzer—optimization and bio-oil characterization. *Int J Green Energy* 13(4):373–382
13. Arvidsson M, Morandin M, Harvey S (2015) Biomass gasification-based syngas production for a conventional oxo synthesis plant—greenhouse gas emission balances and economic evaluation. *J Clean Prod* 99:192–205
14. Hill J, Nelson E, Tilman D, Polasky S, Tiffany D (2006) Environmental, economic, and energetic costs and benefits of biodiesel and ethanol biofuels. *Proc Natl Acad Sci* 103(30):11206–11210
15. Gowen MM (1989) Biofuel v fossil fuel economics in developing countries: How green is the pasture? *Energy Policy* 17(5):455–470
16. Sasana H, Ghazali I (2017) The impact of fossil and renewable energy consumption on the economic growth in Brazil, Russia, India, China and South Africa. *Int J Energy Econ Policy* 7(3):194–200
17. Ahmed K (2017) Revisiting the role of financial development for energy-growth-trade nexus in BRICS economies. *Energy* 128:487–495
18. Singh J, Gu S (2010) Biomass conversion to energy in India—a critique. *Renew Sustain Energy Rev* 14(5):1367–1378
19. Kumar A, Kumar N, Baredar P, Shukla A (2015) A review on biomass energy resources, potential, conversion and policy in India. *Renew Sustain Energy Rev* 45:530–539
20. Cardoen D, Joshi P, Diels L, Sarma PM, Pant D (2015) Agriculture biomass in India: Part 1. estimation and characterization. *Resour Conserv Recycl* 102:39–48
21. Gabhane J, Tripathi A, Athar S, William SP, Vaidya AN, Wate SR (2016) Assessment of bioenergy potential of agricultural wastes: a case study cum template. *J Biofuels Bioenergy* 2(2):122–131
22. Abraham A, Mathew AK, Sindhu R, Pandey A, Binod P (2016) Potential of rice straw for bio-refining: an overview. *Biores Technol* 215:29–36
23. Demirbas A (2010) Biorefineries for biomass upgrading facilities. *Green Energy Technol*
24. De Jong E, Jungmeier G (2015) Biorefinery concepts in comparison to petrochemical refineries. *Ind Biorefineries White Biotechnol* 3–33
25. Cherubini F, Jungmeier G, Wellisch M, Wilke T, Skiadas I, Van Ree R, De Jong E (2009) Toward a common classification approach for biorefinery systems. *Biofuels, Bioprod Biorefin* 3(5):534–546

26. Naik SN, Goud VV, Rout PK, Dalai AK (2010) Production of first and second generation biofuels: a comprehensive review. *Renew Sustain Energy Rev* 14(2):578–597
27. Alaswad A, Dassisti M, Prescott T, Olabi AG (2015) Technologies and developments of third generation biofuel production. *Renew Sustain Energy Rev* 51:1446–1460
28. Valentine J, Clifton-Brown J, Hastings A, Robson P, Allison G, Smith P (2012) Food vs. fuel: the use of land for lignocellulosic ‘next generation’ energy crops that minimize competition with primary food production. *GCB Bioenergy* 4(1):1–19
29. Thompson PB (2012) The agricultural ethics of biofuels: the food vs. fuel debate. *Agriculture* 2(4):339–358
30. Mohanty P, Pant KK, Naik SN, Das LM, Vasudevan P (2011) Fuel production from biomass: Indian perspective for pyrolysis oil
31. Ingale LT, Dube KJ, Sarode DB, Attarde SB, Ingle ST (2013) Monitoring and respiratory health assessment of the population exposed to cooking fuel emissions in a rural area of Jalgaon District, India. *Asia Pacific J Public Health* 25(6):463–475
32. Paliwal U, Sharma M, Burkhart JF (2016) Monthly and spatially resolved black carbon emission inventory of India: uncertainty analysis. *Atmos Chem Phys* 6(19):12457–12476
33. Trivedi A, Verma AR, Kaur S, Jha B, Vijay V, Chandra R, Prasad R (2017) Sustainable bio-energy production models for eradicating open field burning of paddy straw in Punjab, India. *Energy* 127:310–317
34. Katakari R, Chutia RS, Mishra M, Bordoloi N, Saikia R, Bhaskar T (2015) Feedstock suitability for thermochemical processes
35. Ghosh S, Chowdhury R, Bhattacharya P (2017) Sustainability of cereal straws for the fermentative production of second generation biofuels: a review of the efficiency and economics of biochemical pretreatment processes. *Appl Energy* 198:284–298
36. Sarkar S (1974) Fuels and combustion. Universities Press
37. <http://powermin.nic.in/en/content/power-sector-glance-all-india>
38. Tanager P, Field JL, Jahn CE, DeFoort MW, Leach JE (2013) Biomass for thermochemical conversion: targets and challenges. *Frontiers Plant Sci* 4
39. Debnath B, Biswas NT, Baidya R, Ghosh SK (2014) Nanotechnology in waste water treatment: a review. *Ecol Urban Areas* 2014:563
40. Saaty TL (2002) Decision making with the analytic hierarchy process. *Scientia Iranica* 9(3):215–229
41. Saaty TL (2008) Decision making with the analytic hierarchy process. *Int J Serv Sci* 1(1):83–98
42. Saaty TL, Kearns KP (2014) Analytical planning: the organization of system, vol 7. Elsevier
43. Baidya R, Ghosh SK, Debnath B (2015) Analysis of parameters for green computing approach using the analytical hierarchy process. In: 2015 International conference on energy economics and environment (ICEEE), pp. 1–4. IEEE
44. Saaty TL (1980) The analytic hierarchy process. McGraw—Hill, New York
45. Saaty TL (1985) Decision making for leaders. *IEEE Trans Sys Man Cybern* 3:450–452
46. Sehwal S, Das M (2015) A brief overview: present status on utilization of mustard oil and cake
47. Raj T, Kapoor M, Gaur R, Christopher J, Lamba B, Tuli DK, Kumar R (2015) Physical and chemical characterization of various Indian agriculture residues for biofuels production. *Energy Fuels* 29(5):3111–3118
48. Brijwani K, Vadlani PV (2011) Solid state fermentation of soybean hulls for cellulolytic enzymes production. *Soybean-Appl Technol*
49. Balan V, Rogers CA, Chundawat SP, da Costa Sousa L, Slininger PJ, Gupta R, Dale BE (2009) Conversion of extracted oil cake fibers into bioethanol including DDGS, canola, sunflower, sesame, soy, and peanut for integrated biodiesel processing. *J American Oil Chemists’ Soc* 86(2):157–165
50. Franco H CJ, Pimenta MTB, Carvalho JLN, Magalhães PS, Rossell CEV, Braunbeck OA, Rossi Neto J (2013) Assessment of sugarcane trash for agronomic and energy purposes in Brazil. *Scientia Agricola* 70(5):305–312

51. Xiao B, Sun X, Sun R (2001) Chemical, structural, and thermal characterizations of alkali-soluble lignins and hemicelluloses, and cellulose from maize stems, rye straw, and rice straw. *Polym Degrad Stab* 74(2):307–319
52. http://shodhganga.inflibnet.ac.in/bitstream/10603/17540/7/07_chapter%202.pdf
53. Fernandes ERK, Marangoni C, Medeiros SHW, Souza O, Sellin N (2012) Slow pyrolysis of banana culture waste: leaves and pseudostem. In: 3rd International conference on industrial and hazardous waste management
54. Ross K, Mazza G (2011) Comparative analysis of pyrolysis products from a variety of herbaceous Canadian crop residues. *World J Agric Sci* 7(6):763–776
55. Raj T, Kapoor M, Gaur R, Christopher J, Lamba B, Tuli DK, Kumar R (2015) Physical and chemical characterization of various Indian agriculture residues for biofuels production. *Energy Fuels* 29(5):3111–3118
56. Mohammed TH, Lakhmiri R, Azmani A, Hassan II (2014) Bio-oil from pyrolysis of castor shell. *Int J Basic Appl Sci* 1–5
57. Sarkar A, Mondal B, Chowdhury R (2014) Mathematical modeling of a semibatch pyrolyser for sesame oil cake. *Ind Eng Chem Res* 53(51):19671–19680
58. Li J, Chen Y, Yang H, Zhu D, Chen X, Wang X, Chen H (2017) The correlation of feedstock and bio-oil compounds distribution. *Energy Fuels*
59. Abdullah N, Sulaiman F, Miskam MA, Taib RM (2014) Characterization of banana (*Musa spp.*) pseudo-stem and fruit-bunch-stem as a potential renewable energy resource. *Int J Biol Vet Agric Food Eng* 8(8):712
60. Pilon G (2007) Utilization of arecanut (*Areca catechu*) husk for gasification
61. Ramachandra TV, Kamakshi G (2005) Bioresource potential of Karnataka (No. 109). Technical report

Energy Conservation and Sustainability Due to Passive Daylight System of Light Pipe in Indian Buildings

Abdus Salam Azad and Dibakar Rakshit

Abstract With continuous increase in energy usage in Indian building sector, share of electricity has risen to 35% of total electricity consumption. Therefore, achieving energy efficiency in buildings by adopting solar passive design strategies is lucrative. It is important to mention that in India, electricity consumption in lighting a commercial building is high and about 25% of the total electricity consumption. It is therefore imperious to evolve techniques that cut down the energy consumption for lighting load and thus develop energy efficient buildings. Tubular light guide is modern and innovative system which can be used to improve illumination for buildings that require more electrical light during daytime. This is done by utilizing the natural light to illuminate the interior space and save a significant amount of lighting energy. The study involves analytical and experimental investigation of a tubular light pipe for prediction of illuminance distribution inside a room of $3 \times 3 \times 2.7 \text{ m}^3$. For this purpose, predictive performance of existing empirical models has been compared with two commercially available software EnergyPlus and Holigilm. The daylight penetration factor (DPF) has been evaluated on the horizontal working plane through available empirical models. The DPF obtained by these empirical models and software is compared with experimental values and is found to have a good agreement. Besides this, annual energy saving potential having windows and light pipe in a room for different Indian climatic conditions has been evaluated.

Keywords Daylighting · DPF · Light pipe · Lighting energy

A. S. Azad · D. Rakshit (✉)
Centre for Energy Studies, Indian Institute
of Technology Delhi, New Delhi 110016, India
e-mail: dibakar@iitd.ac.in

A. S. Azad
e-mail: esz148318@iitd.ac.in

1 Introduction

In Indian building sector, residential and commercial buildings share 23 and 12% of the total electricity demand, respectively [1]. Lighting systems consume 25 and 28%, respectively, of the total electricity in commercial and residential buildings, respectively [2]. The electrical energy demand in the buildings will continue to rise, as it is estimated that the construction industry in the country is growing at a rapid growth rate of over 9% per year [3]. Therefore, energy conservation in buildings is a major challenge nowadays.

In energy efficient buildings, reduction in energy consumption can be achieved by adopting low energy/solar passive design strategies, such as proper orientation, shading, natural ventilation and daylighting. Sharma et al. [4] have analysed the performance of a building with respect to orientation, and thus, it has been appraised that longer facade to be in north–south direction for Indian conditions. Daylighting [5] is an important passive method of building design in achieving energy conservation. Effective utilization of daylight can be achieved by the effective positioning of windows and skylights, along with the lighting controls that respond according to the daylight available.

It is also important to develop new techniques that utilize the renewable energy (most importantly solar energy) in yielding sustainable buildings. Use of natural light from the sun can reduce significant amount of lighting energy consumption. Therefore, modern and passive technique of tubular light pipes [6, 7] has been invented which provides natural light to interior windowless parts of the buildings. In daytime, light pipe can effectively utilize the sunlight to illuminate the interior space, and hence, a significant amount of lighting energy can be conserved.

2 Scope of Energy Conservation in Lighting

Artificial lights consume major portion of energy usage in buildings. The use of artificial lighting also adds to the cooling load of the building by dissipating waste heat. In order to improve the situation, new lighting fixtures with increased efficiency are being developed. Due to the result of research and testing conducted by researchers, nowadays LEDs having luminous efficacy of 100 lm/W are available in the market. Along with this, it is always recommended that daylight should be integrated in building design to conserve lighting energy. However, familiarizing daylight into buildings is not as simple as having glazed areas or windows on the building facade. Architect or building designers should understand the mechanism of how daylight works and how to incorporate daylight in intelligent way to ensure the visual and thermal comfort inside the building.

2.1 *Passive Methods of Daylighting*

There are several passive methods of daylighting being in practice. Most useful and popular methods have been summarized and discussed below:

2.1.1 Windows

Windows considered as potential passive technique in contributing to lighting energy in any type of building since past. Daylight received through windows can significantly contribute in reducing lighting energy consumption and improving the visual comfort. Installing window also has impact on the cooling load of the building as solar gain through exterior envelop is a major contributor to the thermal load. In buildings, the net energy gain through windows depends on the thermal properties of the glazing material. Therefore, many researches have been carried out by different researchers [8, 9, 6], and it has been found that different commercially available glazed windows are suitable in different conditions.

Singh and Garg [10] explored the capability of daylighting in reducing electrical lighting load for various Indian climatic conditions. In the study, analysis was carried out of an office building for four different types of windows (all double glazed) equipped in all four directions. Lighting energy saving was calculated by using both daylighting software ADELIN 3.0 and Perez model and was compared. Ihm et al. [11] developed and validated a simplified method for estimation of annual energy savings associated with electrical lighting. The simplified method includes the building geometry, the window size and the type of glazing. They investigated the potential of daylighting to save energy utilizing the dimming and stepped daylighting control strategies for an office building.

Fasi and Budaiwi [12] conducted a study with the purpose to investigate the impact of different glazed windows type on energy and visual comfort inside the building in the hot climate of Saudi Arabia. The influence of daylight integration with electrical lighting to increase the energy savings while maintaining the visual comfort was assessed. The results showed that reduction of 16% in total annual energy consumption can be achieved for double-glazed low-E windows with daylight integration.

2.1.2 Skylight

A skylight is an opening surface having a slope of less than 60° from the horizontal plane (Plate 1). It is installed with the roof system providing daylighting and ventilation to the building. As the skylights are located on the roof, they may have adverse effects in terms of unwanted solar heat gain during period of summers and heat leakage during winters. Skylight glazing is usually glass or acrylic material, although advanced glazing technologies have been developed and can be used for

Plate 1 Skylight

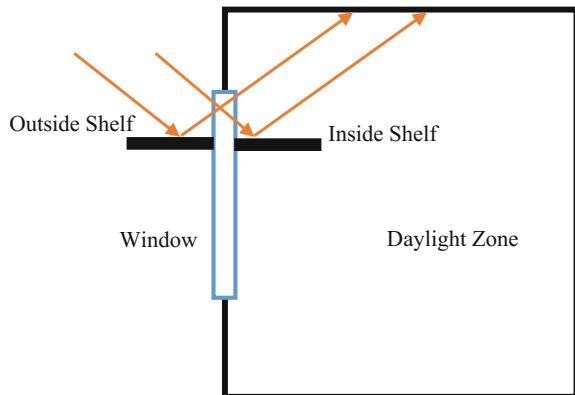


solar heat control. The size of skylight significantly affects the illumination level and heat leakage to the space below. The position of skylight plays an important role to maximize daylighting and/or passive solar heating potential. Al-Obaidi et al. [13] reviewed several skylight systems for Malaysian climatic conditions, but they found it inappropriate for the practical application because of the energy imbalance between thermal and lighting loads. Therefore, they suggested that these systems should be integrated with shading, glare control, advanced glazing systems and taking advantage of different geometries.

2.1.3 Light Shelves

Light shelves are passive technique to enhance daylighting from windows, and this can be obtained by placing a horizontal reflective surface outside the window. It has three main components: a window, an inside shelf and outside shelf (Fig. 1). The inside shelf reflects the all transmitted light from the upper window onto the room ceiling. The outside shelf reflects the incident light upward to illuminate the room

Fig. 1 Light shelves (Source Ref. [14])



ceiling. This reflected light to the ceiling reduces the need of artificial illumination. The window is divided into two window surfaces. Only the upper interacts with the daylighting and provides way to reflected rays.

It has also been found that by integrating shelves on south-facing facades of the buildings, the daylighting quality increases significantly and improves the inner space illumination through the enhancement of light distribution. This leads to the reduction in glare and increases the degree of human health and comfort [15].

2.1.4 Light Pipe

Tubular light pipes are modern, but passive technique which utilizes the daylight to illuminate the interior space of the buildings. The use of light pipe can provide illuminance without the use of artificial light and hence can significantly reduce the lighting energy consumption in a building. It works on the principle of propagation of light from ambient to indoor due to multi-reflections on high reflective internal surfaces. Light pipes mainly have three components (Fig. 2): receiving part (hemispherical dome) in which sunlight gets collected, the received light goes to multi-reflections through the reflecting tube, and the lower part (diffuser) is responsible for uniform distribution of light throughout the space.

Shin et al. [16] conducted experimental studies for Korean climatic conditions. For the prediction of internal illuminance, they developed a prediction model for straight light pipe with two aspect ratios and found good agreement with experimental values. Energy conservation and CO₂ mitigation potential of light pipe at test room were also evaluated for the considered location. Patil [17] fabricated a windowless test room on the roof fitted with light pipe in composite climatic zone of



(a) Test room with light pipe set-up (b) Light pipe with dome (c) Diffuser

Plate 2 a Test room with light pipe set-up, Plate b light pipe with dome and Plate c diffuser

New Delhi, India. External illuminance and internal illuminance under clear, intermediate and overcast sky were measured. Effects of sky clearance index on internal illuminance and on daylight penetration factor (DPF) were analysed.

2.2 Advantage of Light Pipe Over Other Daylight Methods

Light pipe utilizes about two-third of the available global illuminance in a clear sky day. It receives both direct and diffuse components of sunlight, which transmitted and diffused into the interior space of the building. Because of having long and sealed reflecting part, it has additional advantage of reducing unnecessary solar heat gain [18].

To increase daylight inside the building, larger window exposure is not recommended because it will add more cooling load on the air-conditioning system. In place, utilizing light pipe with window gives us an opportunity to reduce glare and further improve the balance of daylight within the interior space. We receive redirected and diffused daylight from light pipe; it can reduce the problem of glare and would give daylight of better uniformity. Skylight introduces diffuse light inside the building; increasing the facade area to admit more diffuse light can be responsible for adding undesirable sunlight. In place, light pipe transmits both direct and diffuse light by multi-reflection mechanism. Therefore, we can receive more uniform and diffused daylight than that by a skylight.

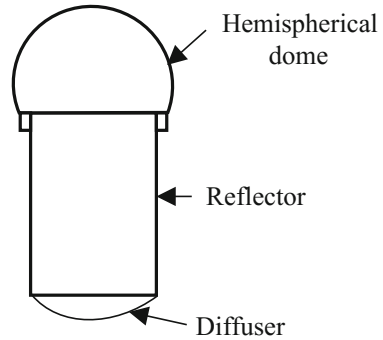
In this study, it is aimed to model tubular light pipe for the prediction of illuminance distribution inside a small room. For this purpose, tubular device is modelled using two existing prediction models as well as two simulation softwares (EnergyPlus™ Version 8.3 and Holigilm™). The DPF has been computed using both predictions models and simulation software and has been compared and validated. Secondly, the energy saving opportunities utilizing different glazing with varied glazed areas and light pipe have been assessed for different Indian climatic conditions. Both the analyses have been carried out in separate sections.

3 Evaluation and Analysis of DPF for Light Pipe System

3.1 Methodology

In present study, experimental observations have been carried out in the composite climatic zone of New Delhi, India. The monitoring period was during the month of March–May of a year. The experimental observations have been conducted for a windowless test room made up of wooden ply boards sized 3 m × 3 m × 2.7 m (Plate 2a). During the experimental observations, the door was remain closed to keep the room interior free from ambient conditions. To avoid the effect of light

Fig. 2 Tubular light pipe



reflectance from the inner walls and ceilings, they were painted black. The light pipe installed on roof along with diffuser is shown in Plate (2b, c). The light pipe has a diameter of 23 cm, with a pipe length of 1 m getting aspect ratio of 4.3.

The horizontal working plane (floor) has been divided into grid of 5×5 (Fig. 3). The hourly illuminance distribution at different points of the working plane has been measured using photosensors and luxmeter. The observations have been conducted for worst case scenario.

In next sections, the expression of DPF is described. The prediction models used in the study is explored. Simulation parameters used by the EnergyPlus and Holigilm for the study are also presented.

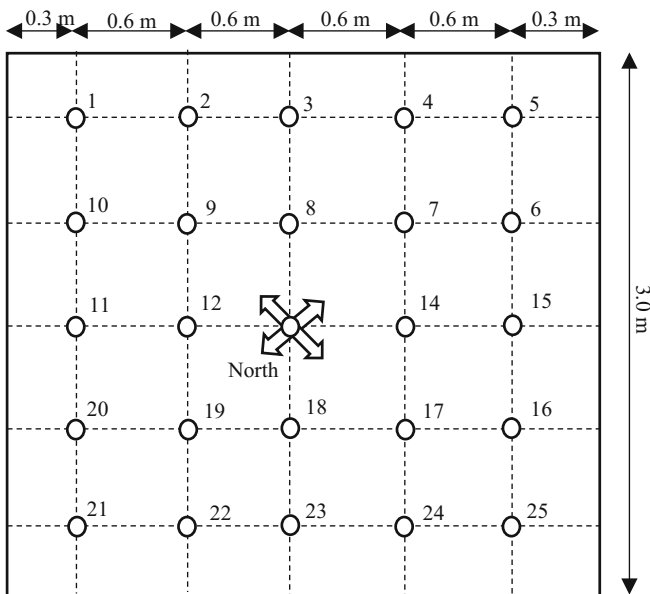


Fig. 3 Grid points of horizontal working plane (floor)

3.2 Daylight Penetration Factor (DPF)

It is defined as the ratio of internal illuminance at a given point inside any building to the external global illuminance (E_{ext}) on the horizontal plane. It is a dimensionless factor similar to daylight factor (DF). Advantage of DPF over DF is that it also includes the effect of both internal and external environmental factors and light pipe configuration. It can be noticed that the ratio is dependent on the points of interest. Mathematically,

$$\text{DPF}_{(x,y,z)} = \frac{E_{\text{int}(x,y,z)}}{E_{\text{ext}}} \times 100 \quad (1)$$

where $E_{\text{int}(x,y,z)}$ is the internal illuminance at the given point $P_{(x,y,z)}$, and $\text{DPF}_{(x,y,z)}$ is daylight penetration factor for the given point.

Using DPF, the internal illuminance at a given point with coordinates (x, y, z) due to a given light pipe can be calculated from the Eq. (2),

$$E_{\text{int}(x,y,z)} = \text{DPF}_{(x,y,z)} \times E_{\text{ext}} \quad (2)$$

3.3 Light Pipe Prediction Models

To predict the daylight performance of light pipes, several prediction models have been developed by researchers. The semi-empirical models considered in the study require light pipe's configuration and the local climatic condition as input parameters.

3.3.1 Zhang–Muneer Model

Based on the experiments conducted by the authors [19], a mathematical model was developed. The model includes the input parameters of light pipe's length and diameter as well as solar altitude (α_s) and sky clearness index (k_t), which is given by:

$$\begin{aligned} \text{DPF}_{(x,y,z)} = & (62.5 - 17.2k_t + 2.6\alpha_s) \\ & \times \rho^{(136 + 4.3A_p + 1.1 \cot \alpha_s - 0.4A_p \cot \alpha_s)} R^2 \left(\frac{V_l}{D}\right)^{1.3} / D^2 \end{aligned} \quad (3)$$

where

- k_t sky clearance index,
- α_s solar altitude,
- ρ light pipe reflectance,
- L length of the light pipe
- R diameter of the light pipe
- r radius of light pipe
- A_p aspect ratio of the light pipe (L/R)
- V_1 vertical distance from the diffuser to the point of interest
- D direct distance from the diffuser to the point of interest

Internal illuminance (E_{int}) is given by:

$$E_{int} = E_{ext} \times DPF \tag{4}$$

3.3.2 Jenkins–Muneer Model

This semi-empirical model has been developed by Jenkins et al. [20], for prediction of the output from the light pipe. The model can be used for straight light as well as bent type. The model estimates illuminance distribution at any point below the diffuser. The outline of model is based on the cosine rule of light propagation. The required input parameters are external illuminance along with light pipe configuration as shown in the Fig. 4.

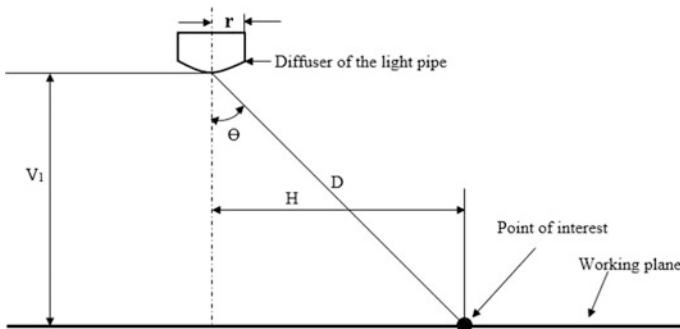


Fig. 4 Input parameters of Jenkins–Muneer model

Indoor illuminance (E_{int}) on the working plane due to straight light pipe is given as:

$$E_{\text{int}} = 0.494 \times \frac{\varphi \cos^4 \theta}{V_l^2} \quad (5)$$

$$\varphi = 0.82 \times E_{\text{ext}} e^{-0.11A_p} \times \Pi r^2 \quad (6)$$

$$E_{\text{int}} = E_{\text{ext}} \times 0.402 \times e^{-0.11A_p} \times \Pi r^2 \frac{\cos^4 \theta}{V_l^2} \quad (7)$$

3.4 Overview of Simulation Tools and Parameter

Among many available lighting simulation tools, only three are used to model the tubular device. For our comparative study, we have considered EnergyPlus and Holigilm. EnergyPlus is an internationally accepted tool, and Holigilm is dedicated to modelling of light pipe. Apart from these two, DIALux also simulates the tubular device.

3.4.1 EnergyPlus

EnergyPlus is new generation simulation engine, which integrates the best features of two energy simulation engines DOE-2 and BLAST. EnergyPlus is developed by the help of Lawrence Berkeley National Laboratory (LBNL) and U.S. Department of Energy (DOE). To predict more accurate results, EnergyPlus has been validated with building energy simulation tests (BESTests)—developed by the International Agency of Energy (IAE).

In addition to its versatile application, the EnergyPlus also predicts daylighting through windows, skylight, tubular light guide, etc., inside the building. For daylighting prediction, EnergyPlus uses DELight [21]. The calculation method is based on daylight factor (DF) interpolation for the direct daylight coming from sun.

To model a light pipe in EnergyPlus, it is considered as a separate zone on the top of the daylight zone as depicted in the Fig. 5. The daylight zone considers no window opening. The tubular light pipe model includes simultaneously three distinct and related phenomena: daylighting, solar gains and conductive/convective gains.

Simulation of solar and conductive/convective gains is based on zone heat balance, though daylighting is simulated separately. To include the advantage of many of the standard daylighting and heat transfer sequences, the dome and diffuser are treated as special window surface (Fig. 6) for both daylighting and heat balance simulations. Dome and diffuser are together considered as “receiver” and “transmitter”, respectively, i.e., radiation entering the dome ends up the diffuser.

Fig. 5 Light pipe modelled in EnergyPlus

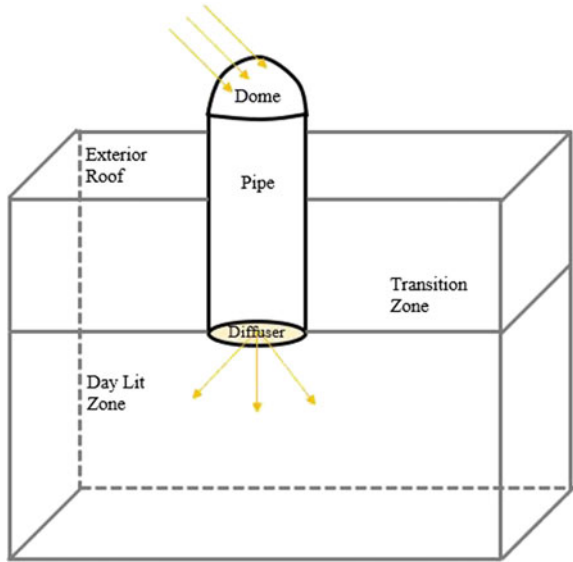
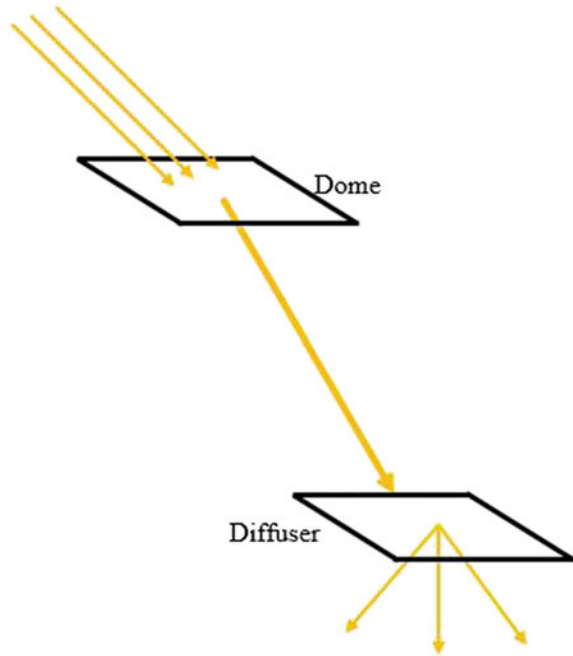


Fig. 6 Dome and diffuser surfaces



The reflecting tube (pipe) is simulated by an independent code module. Though several different empirical models for characterizing tubular light pipe performance are present [22, 7], using the transmittance of the light pipe is most compatible with the existing EnergyPlus daylighting and heat balance code.

3.4.2 Holigilm

Holigilm is a calculation tool developed to predict indoor illuminance from the straight and tubular hollow light guides. The name HOLIGILM is an abbreviation of hollow light guide interior illumination method.

The modelling using Holigilm is based on classical and analytical approach of integrating sky and sun illuminances developed by Kocifaj et al. [23]. The program does not use a weather file, and it is only based on the theoretical calculations of the solar position. One more limitation of the programme is it only simulates straight and tubular pipe equipped with a Lambertian or transparent diffuser.

The simulation parameters assumed to model tubular light pipe in EnergyPlus and Holigilm have been summarized in Table 1.

3.5 Results and Discussion

From the observations, it has been found that the illuminance distribution through the diffuser is uniform. The illuminance received in afternoon is sufficient to illuminate a small room, though in morning and evening time it will be required to use

Table 1 Simulation parameters in EnergyPlus and Holigilm

	Energy Plus	Holigilm
Building	Length: 3.0 m	Length: 3.0 m
	Width: 3.0 m	Width: 3.0 m
	Height: 2.7 m	Height: 2.7 m
	Orientation: 45°	Orientation: 45° (Azimuth)
Working Plane	Horizontal floor	Horizontal floor
Weather file	IND_New.Delhi.421820_ISHRAE	13 CIE Clear polluted, urban
Dome and diffuser	Rectangular (0.21 m × 0.21 m) Transmittance of the dome: 0.92 Transmittance of the diffuser: 0.9 (Lambertian)	Transmittance of the dome: 0.92 Transmittance of the diffuser: 0.75 (Lambertian) Grid density on the optical interface: Medium
Reflecting pipe	Reflectance: 0.95 Length: 1 m Diameter: 0.23 m Position: centre of the room	Reflectance: 0.934 Length: 1 m Diameter: 0.23 m Position: centre of the room

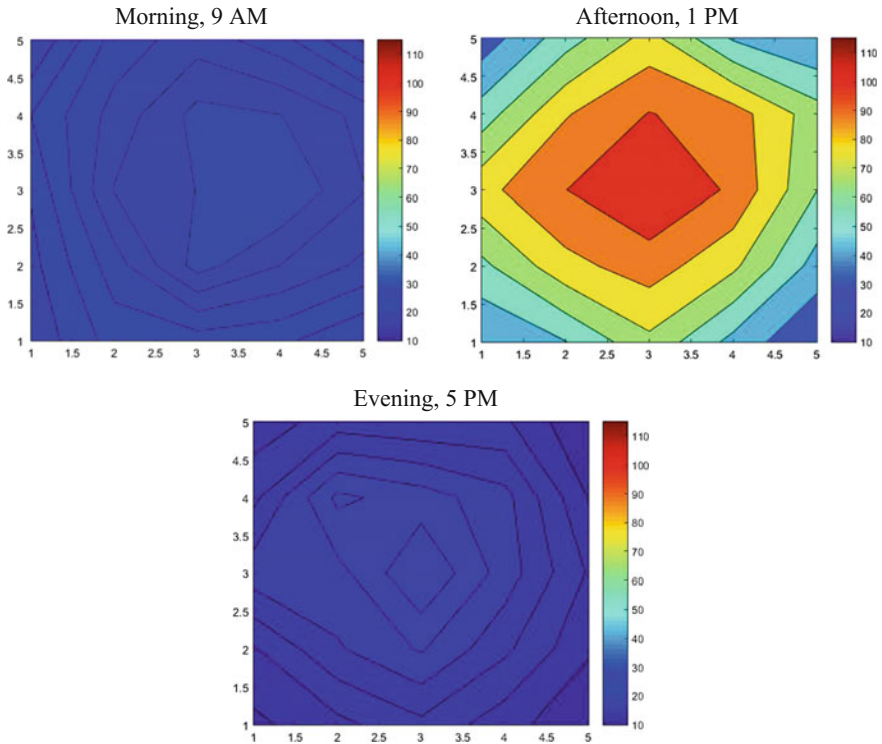


Fig. 7 Illuminance distribution through the light pipe in morning, afternoon and evening time

artificial light along with light pipe. The illuminance is measured on the floor (worst case scenario); therefore, it is possible to achieve adequate amount of light on the working level. Utilization of two light pipes in the same room can provide more light in achieving the adequate lighting level [24]. The illuminance distribution in morning, afternoon and evening has been depicted in the Fig. 7.

3.5.1 Analysis of Daylight Penetration Factor (DPF)

As mentioned before, the DPF being a dimensionless ratio, we can get more inference in the results which relate us with external weather conditions. This parameter is very useful in showing the deviation in the results obtained from the prediction models and selected software. A series of DPF has been computed for different set of points on the working plane. Variation of DPF for three points has been shown in the Figs. 8, 9 and 10.

Figure 8 shows that most of the DPF values lie between 0.05 and 0.15% for the point below the diffuser. Exceptions are the values computed from Jenkins–Muneer model and EnergyPlus software. The computed DPFs from Jenkins–Muneer model

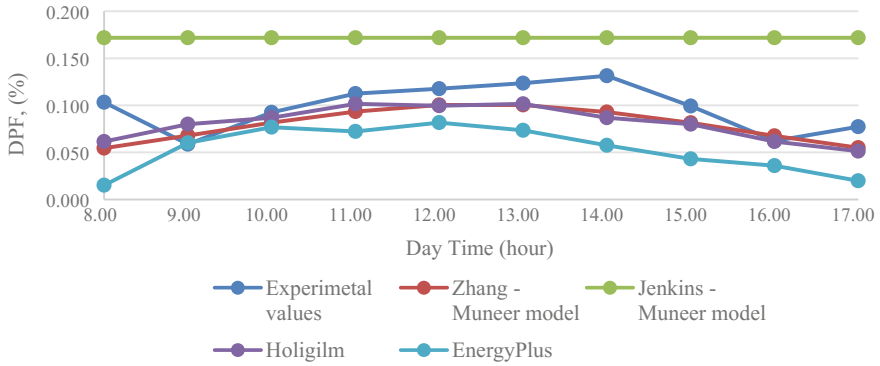


Fig. 8 DPF under the diffuser (point 13) on March 19, 2016

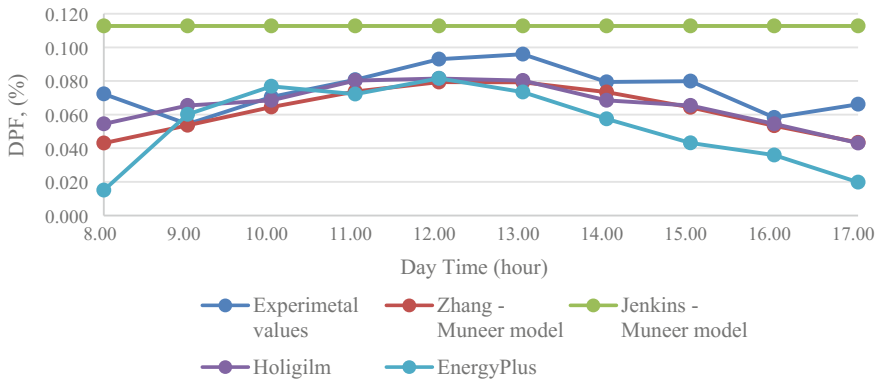


Fig. 9 Average DPF of points 7, 9, 17 and 19 during March 19, 2016

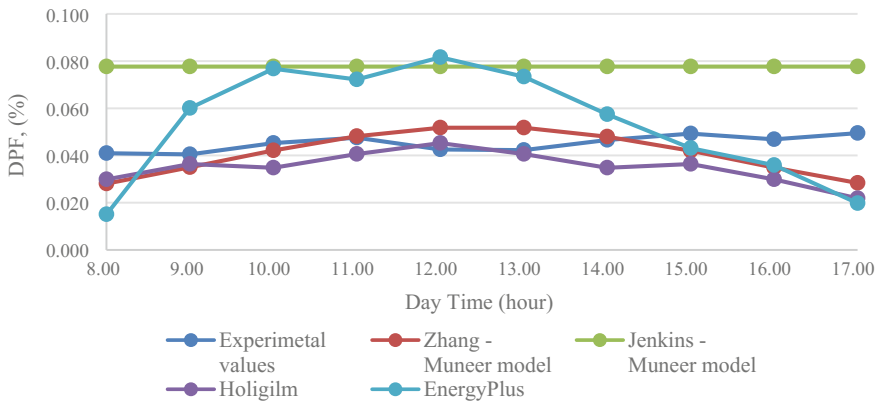


Fig. 10 Average DPF of points 1, 5, 21 and 25 during March 19, 2016

are little higher compared to experimental values and are constant throughout the day. On the other hand, the computed DPFs using EnergyPlus are little lower. It can be observed that the DPFs are minimum in morning time, reach the maximum in afternoon and then decrease.

As the points (7, 9, 17 and 19) are symmetrically placed with respect to central point, the computed average DPFs of the points have been shown in the Fig. 9. Most of DPF values lie between 0.04 and 0.1%. The values are again little higher for Jenkins–Muneer model as compared to experimental values. The trend for increase and decrease is same as that of the previous case.

For the farthest points (1, 5, 21 and 25) on the working plane, the computed DPFs values lie between 0.02 and 0.08% as shown in Fig. 10, almost following the similar pattern as witnessed in the previous plots.

Considering the three Figures (Figs. 8, 9 and 10) together, it can be concluded that for the point below the diffuser (centre), DPF value is higher. As we move away from this point, the DPF decreases and is lowest for the farthest points. It can also be observed that DPFs are lower in morning and evening time because of low external illuminance. As the high external illuminance, DPFs reach the maximum in afternoon. In all the cases as per Jenkins–Muneer model, the DPF is constant for particular point irrespective of the daytime. Reason for this is model is dependent on constant input parameters of light pipe configuration only. While in case of Zhang–Muneer model, the model is dependent on the variable input parameters of sky clearness index and solar altitude angle. Also, it has been inferred that Zhang–Muneer model and Holigilm software show good agreement with experimental values, while Jenkins–Muneer model and EnergyPlus software show a little deviation in the results compared to others.

4 Input Data for Energy Savings in Lighting

In the section, the energy saving opportunities utilizing different glazing with varied glazed areas and light pipe have been assessed for different Indian climatic conditions. The building has been modelled using DesignBuilder and simulated using EnergyPlus. Simulations were performed for a standard conference/meeting room sized 5.5 m × 5.5 m × 3.5 m. Diametrical representation of the building sample is shown in Fig. 11. Construction details of external wall and roof have been depicted in Fig. 12a, b, and layer-by-layer material details are given in the Table 2. Four different types of glazing (Table 3) have been taken into consideration with glazed area (window to wall ratio) varied from 10 to 40%. The visible light transmittance (VLT) for the glazed materials varied from 0.07 to 0.88. Considering window installed on the specified orientation, simulation has been carried out in all four directions. The occupancy schedule is taken as from 8:00 AM to 6:00 PM. During the period, the room temperature is maintained at 25 °C. The illuminance level of 400 lx is maintained at the working height of 0.8 m as recommended by BEE [2]. Continuous dimming is used to control the illuminance level inside the room. It is

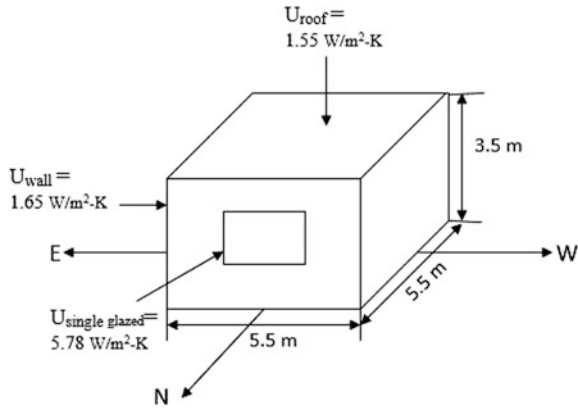


Fig. 11 Model of building for simulation

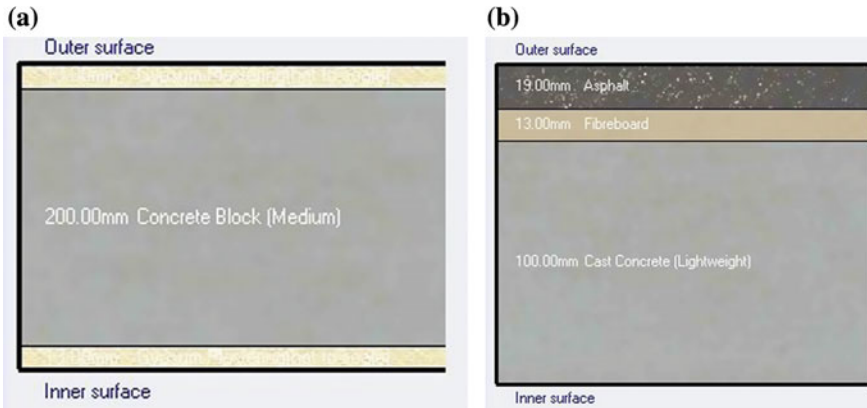


Fig. 12 a and b Construction details of external wall and Roof

Table 2 Layer-by-layer material details of external wall and Roof

	Layer-by-layer materials (outer surface to inner)	Thickness (mm)	U-value (W/m ² K)
External wall	Gypsum plaster	13	1.65
	Concrete block (medium)	200	
	Gypsum plaster	13	
Roof	Asphalt	19	1.55
	Fibreboard	13	
	Cast concrete (lightweight)	100	

Table 3 Properties of different glazing

Glazing type	Glass thickness and air gap (mm)	U-value (W/m ² K)	SHGC	VLT
Single glazed, clear	6	5.78	0.82	0.88
Double glazed, clear	6, 12	3.16	0.76	0.81
Double glazed, tinted, low e-coated	6, 6	2.43	0.40	0.44
Double glazed, clear, reflective	6, 13	2.22	0.14	0.07

assumed that there is a sensor which senses the total lux at the interior space and adjusts the electric light accordingly in a continuous mode. Lighting power density (LPD) is assumed 14 W/m² as per Indian building standard [25]. No other internal load (equipment and occupancy load) is being considered in the study as they will be remain constant and do not have any effect on analysis.

The light pipe also has been modelled in DesignBuilder and simulated using EnergyPlus for the same above input parameters. The modelled light pipe is having diameter of 0.23 m and length 1.0 m.

4.1 Energy Saving Assessment

The energy saving assessment has been carried out for four different Indian climatic conditions. One location from each climatic zone [26] is being considered (Table 4). The location from the cold climatic zone is being ignored as the analysis is based on the cooling load calculations. Simulated results obtained from EnergyPlus present the annual energy usage in terms of kWh/m²-yr. In the study, effect of varied area for different glazing on lighting and cooling load has been analysed. Due to varied glazed area, the lighting and cooling load will be different for different glazed windows. Also, the total annual energy saving per unit area has been computed for evaluating the overall effect.

In Table 5, the lighting, cooling and total energy saved for different types of window glazing, different glazed areas and for different orientations have been summarized for New Delhi. As the LPD is 14 W/m² and required illuminance level

Table 4 Details of different locations in Indian climatic zone

Climatic zones	Location	Latitude (°) (°N)	Longitude (°) (°E)	Elevation (m)	Standard Pressure (Pa)
Composite	New Delhi	28.58	77.20	216	98,757
Hot and dry	Bikaner	28.0	73.30	224	98,663
Moderate	Pune	18.53	73.85	559	94,787
Warm and humid	Chennai	13.0	80.18	16.0	101,133

Table 5 Delhi: Annual lighting, cooling and total energy saved for different types of window, different glazed area and for different orientation

Window type	% Glazing area	Lighting energy saved (kWh/m ² -yr)						Cooling energy saved (kWh/m ² -yr)						Total Energy Saved(kWh/m ² -yr)					
		North	South	East	West	North	South	East	West	North	South	East	West	North	South	East	West		
Single glazing	10	21	22.2	28	17.6	11.9	11	14	9.7	33	33.1	42	27.3						
	20	30.4	30.5	30.9		14.8	15.9	15.5	14.8	45.2	46.4	46.4	43.7						
	30	31.2	31.2	31.3	30.7	15.1	17.2	15.9	15.5	46.3	48.4	47.3	46.2						
	40	31.5	31.4	31.5	31.3	15.2	18.7	16.2	15.9	46.7	50.1	47.7	47.2						
Double glazed, clear	10	19.4	20.5	27.1	16.2	13.6	11.4	10	9	30.8	30.5	40.8	25.2						
	20	30	30.1	30.7	28.3	14.8	15.7	15.4	14.5	44.8	45.8	46.1	42.9						
	30	31.1	31.0	31.2	30.3	16.5	17.1	16	15.5	47.5	48.1	47.2	45.8						
	40	31.4	31.3	31.4	31.1	15.3	18.6	16.3	15.9	46.7	49.9	47.7	47						
Double glazed, e-coated	10	5.9	8.4	19.8	7.0	4.6	3.2	10.2	4.7	10.5	11.6	30	11.7						
	20	25.1	26.1	27.6	23.1	13.4	12.9	13.9	12	38.5	39	41.5	35						
	30	28.4	29	29.8	26.5	14.4	14.9	15	13.7	42.9	43.9	44.8	40.2						
	40	29.6	30.1	30.4	28.3	14.8	16	15.4	14.6	44.4	46.1	45.9	42.9						
Double glazed, reflective	10	2.5	2.8	4.6	3.5	1.4	1.2	2.5	2	3.9	4.1	7.2	5.5						
	20	4.9	5.8	8.8	6.4	2.7	2.5	4.5	3.5	7.6	8.3	13.3	9.8						
	30	6.8	8.4	11.6	9.1	3.8	3.8	5.9	4.9	10.6	12.2	17.6	14.1						
	40	8.3	10.8	13.5	11.3	4.6	4.9	6.9	6	13	15.7	20.3	17.3						
Light pipe, dia 0.23 m		0.8			19.8									20.6					

is 400 lx, the maximum total energy saving of 50.1 kWh/m²-yr has been achieved. The maximum energy saved utilizing daylight is achieved for the single-glazed south-oriented window with 40% glazed area. It has been observed that when VLT is high (e.g. 0.88 for single-glazed clear glass and 0.81 for double-glazed clear glass), the total energy saved is maximum which is about 46.7–50.1 kWh/m²-yr. The energy saved is low for small glazed area, increases with increase in glazed area and remains almost constant for 30–40% glazed area. For high-VLT glasses, total energy saved is almost same for all orientations. Only exception is for low glazed area; total energy saved is highest for east orientation.

The lighting energy savings have direct impact on cooling energy saved, as the waste heat is generated by the artificial lights. It can be concluded that utilizing daylight through window has greater impact on lighting load than on cooling load, which is opposite in case of light pipe. Savings in both lighting and cooling energy increase with increase in glazed area. As the VLT decreases, the amount of energy saved reduces and is lowest for the double-glazed reflective window (VLT of 0.04 only). Reason for this is: less amount of visible light is transmitted inside the room.

The energy saving is also computed for a light pipe with diameter of 0.23 m. For this case, no glazed area is being considered on the building walls. The daylight enters through the light pipe installed on the roof. The total energy saved due to light pipe is comparable to the high-VLT glasses and low glazed areas & with low-VLT glasses and high glazed areas.

In Fig. 13, the effect of window orientation on energy savings has been depicted for New Delhi. The results are shown for 30% glazed area only (for other glazed area, refer to Table 4). It can be inferred from the plot that when the transmittance of glass is high (VLT > 0.80), energy savings are nearly same in all directions.

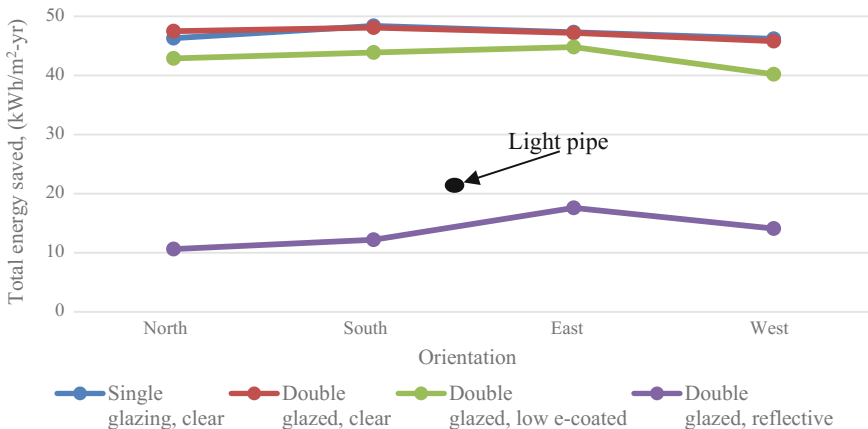


Fig. 13 Effect of orientation on total energy saved for glazed area of 30%

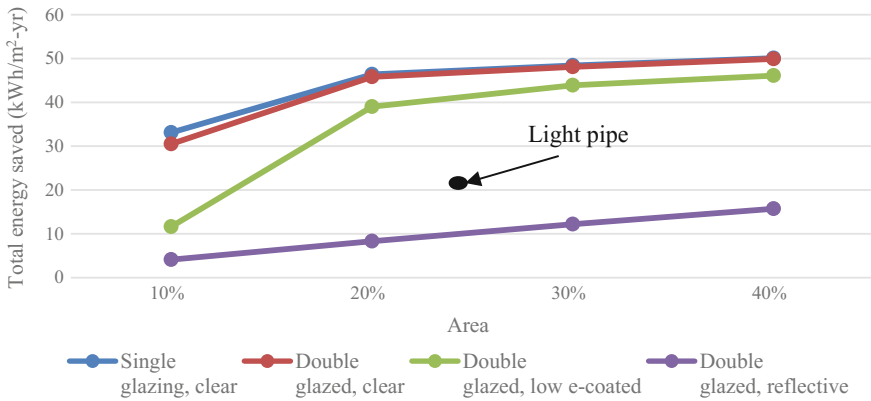


Fig. 14 Effect of glazed area on total energy saved for glazed area in south direction

Reason of this is: more visible radiation is entering through these windows, and this is ample to maintain illuminance level of 400 lx. It is also prevailing that when transmittance is low ($VLT < 0.07$), the energy saving is minimum for north orientation. As the light pipe is independent of any orientation, the energy saving has been shown as separate point. The energy saving from the light pipe is very significant and in fact higher than low-VLT glasses.

The effect of variation of glazed area on total energy savings for south direction is shown in the Fig. 14. It can be seen that energy saving increases with increase in glazed area. When the glazed area increases to more than 20%, energy saving becomes significant. When VLT is high, total annual energy saving of 50 kWh/m^2 can be achieved for 40% glazed area. But when VLT is low, the maximum of only 15.7 kWh/m^2 of total annual energy saving can be achieved which is lower than the energy saved from the considered light pipe.

Simulated results for other locations from different climatic zones are presented in the Tables 6, 7 and 8. It can be concluded that for varied glazed area and that of different orientation, the energy saving trends of these locations are similar to that of New Delhi. However, the total annual energy saved that was achieved for Chennai and Pune is slightly higher.

The annual energy saving for varied glazed areas and for double glazing, clear type installed in south direction along with light pipe for four locations from different climatic zones has been presented in the Fig. 15. It can be observed that as glazed area increases, energy saving for all the locations increases. But, when the glazed area is 30–40%, the difference in energy saving is not very significant. The energy saved from the light pipe is lower compared to any glazed areas.

Table 6 Bikaner: Annual lighting, cooling and total energy saved for different types of window, different glazed area and for different orientation

Window type	% Glazing area	Lighting Energy saved (kWh/m ² -yr)						Cooling Energy saved (kWh/m ² -yr)						Total Energy Saved(kWh/m ² -yr)					
		North	South	East	West	North	South	East	West	North	South	East	West	North	South	East	West		
Single glazing, clear	10	19.4	21.8	28.3	16.3	12.0	12.1	15.1	9.8	31.4	33.9	43.4	26.1						
	20	29.7	30.7	31.3	28.1	16.0	18.1	17.2	15.8	45.7	48.8	48.5	43.9						
	30	30.9	31.5	31.7	30.2	16.5	19.5	17.6	17	47.4	51	49.3	47.1						
	40	31.5	31.7	31.8	31.0	16.6	20.1	18.1	17.6	48.1	51.8	49.9	48.7						
Double glazed, clear	10	17.6	20.0	27.3	15.0	11.2	10.5	15	9.1	28.9	30.5	42.2	24.1						
	20	29.2	30.3	31.2	27.4	16.0	17.7	17.7	15.5	45.2	48	48.3	42.9						
	30	30.6	31.3	31.6	29.7	16.5	19.4	17.6	16.9	47.2	50.7	49.3	46.6						
	40	31.3	31.6	31.8	30.7	16.8	20.1	18.1	17.6	48	51.7	49.9	48.3						
Double glazed, e-coated	10	4.3	7.7	19.3	6.4	3.8	3.1	10.8	4.5	8.1	10.9	30.1	11						
	20	23.9	25.7	27.8	22.2	13.9	13.9	15.3	12.6	37.9	39.6	43.1	34.7						
	30	27.5	29.0	30.3	25.5	15.4	16.6	16.6	14.5	42.8	45.6	46.9	40						
	40	28.8	30.3	30.9	27.4	15.9	18.2	17.2	15.7	44.8	48.6	48.1	43.1						
Double glazed, reflective	10	2.3	2.8	4.6	3.2	1.4	1.3	2.7	1.9	3.7	4.1	7.4	5.1						
	20	4.5	5.6	8.8	6.4	2.7	2.7	5	3.7	7.3	8.4	13.8	10.1						
	30	6.4	8.2	11.7	9.3	3.8	4.1	6.5	5.4	10.2	12.3	18.2	14.7						
	40	7.8	10.6	13.4	11.2	4.7	5.3	7.5	6.5	12.5	15.9	20.9	17.7						
Light pipe, dia 0.23 m									23.9				24.9						

Table 7 Chennai: Annual lighting, cooling and total energy saved for different types of window, different glazed area and for different orientation

Window type	% Glazing area	Lighting energy saved (kWh/m ² -yr)				Cooling energy saved (kWh/m ² -yr)				Total Energy Saved(kWh/m ² -yr)			
		North	South	East	West	North	South	East	West	North	South	East	West
Single glazing	10	26.0	20.5	28.2	20.2	17.7	14.1	19.3	13.7	43.7	34.3	47.5	33.9
	20	31.2	30.2	30.6	30.6	21.0	20.6	20.9	20.7	52.3	50.5	51.5	51.3
	30	31.5	30.9	31.2	31.4	21.2	21.0	21.2	21.3	52.7	52.0	52.4	52.7
	40	31.6	31.2	31.4	31.6	21.2	21.2	21.3	21.3	52.9	52.4	52.7	53.0
Double glazed, clear	10	24.9	18.5	27.6	18.7	17.1	12.7	19.0	12.7	42.0	31.2	46.6	31.3
	20	31.1	29.9	30.4	30.2	21.1	20.5	20.8	20.5	52.1	50.4	51.2	50.7
	30	31.4	30.8	31.0	31.3	21.3	21.1	21.3	21.3	52.7	51.9	52.3	52.6
	40	31.6	31.1	31.3	31.5	21.4	21.3	21.4	21.5	53.0	52.4	52.7	53.0
Double glazed, e-coated	10	12.1	5.7	21.4	8.0	8.4	3.9	14.7	5.4	20.6	9.6	36.1	13.4
	20	28.8	24.9	28.0	25.1	19.5	17.0	19.2	16.9	48.3	41.9	47.1	42.0
	30	30.4	28.7	29.5	28.6	20.6	19.6	20.2	19.4	51.0	48.3	49.8	48.0
	40	30.9	29.8	30.1	30.1	20.9	20.4	20.7	20.4	51.8	50.2	50.8	50.6
Double glazed, reflective	10	3.3	2.5	5.1	3.0	2.2	1.7	3.5	2.0	5.5	4.1	8.6	5.0
	20	6.4	5.0	9.5	6.2	4.4	3.4	6.6	4.1	10.8	8.4	16.1	10.3
	30	8.9	7.3	12.5	9.0	6.1	4.9	8.6	6.0	15.0	12.2	21.1	15.0
	40	10.8	9.2	14.5	11.0	7.4	6.3	10.0	7.3	18.2	15.5	24.5	18.3
Light pipe, dia 0.23 m		0.5			23.3				23.8				

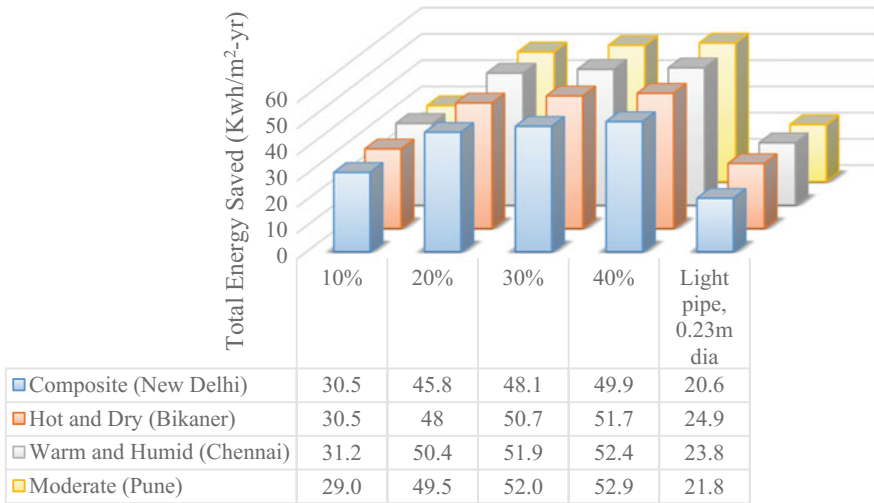


Fig. 15 Effect of climatic zones on annual energy saved. Window is double glazing, clear type and south-oriented

5 Conclusions

The DPF of light pipe system has been computed using semi-empirical models and two commercially available softwares (EnergyPlus & Holigilm). A graphical comparison of all the computed DPF values has been shown, and a good agreement has been found for Zhang–Muneer model and Holigilm software. Although, a little deviation has been observed for Jenkins–Muneer model and EnergyPlus. The DPF achieved from the light pipe is found low in morning and evening time, but by changing the light pipe configuration (length and diameter), we can enhance its performance.

The energy saving opportunity utilizing daylight from passive techniques of window and light pipe has been assessed. It has been found that when VLT is low, the energy saving increases with increase in glazed area and maximum for east-oriented window. When VLT is high, energy saving first increases and then becomes constant for 30–40% glazed area irrespective of window orientation. From the previous studies, it has been found that the longer facade of a building should be in north–south direction for Indian conditions. But, no orientation has been clearly found suitable for the present case studied. For the present analysis within the range of parameters studied, it has can be seen that weather conditions of a particular station have little impact on energy savings.

The energy saving achieved from the considered configuration of light pipe is quite significant and comparable with energy saved from low-VLT glasses and high-VLT glasses with less glazed area. Therefore, it is always appreciable to look for utilization of passive methods inside any building which in turn has positive environmental impact and leads towards sustainability.

References

1. A report on energy efficiency and energy mix in the Indian energy system (2030), Using India energy security scenarios, 2047. Niti aayog, April 2015
2. Bureau of Energy Efficiency (BEE) (2006) BEE Code, Lighting. Under Ministry of Power, Government of India, New Delhi
3. USAID ECO-III Project. Energy Assessment guide for commercial building. A report, 2009
4. Sharma P, Azad AS, Rakshit D (2015) Quantitative evaluation of directional influence on building performance in India. In: International conference on advances in power generation from renewable energy sources (APGRES 2015), Kota, India, June 15–16
5. Kamaruzzaman SN, Edwards R, Zawawi EMA, Che-Ani AI (2015) Achieving energy and cost savings through simple daylighting control in tropical historic buildings. *Energy Build* 90:85–93
6. Mohelnikova J (2008) Daylighting and energy savings with tubular light guides. *WSEAS Trans Environ Dev* 4(3):200–209
7. Zhang X, Muneer T, Kubie J (2002) A design guide for performance assessment of solar light pipes. *Lighting Res Technol* 34(2):149–169
8. Aguilar JO, Xamán J, Olazo-Gómez Y, Hernández-López I, Becerra G, Jaramillo OA (2017) Thermal performance of a room with a double glazing window using glazing available in Mexican market. *Appl Therm Eng* 119:505–515
9. Lu L, Law KM (2013) Overall energy performance of semi-transparent single-glazed photovoltaic (PV) window for a typical office in Hong Kong. *Renew Energy* 49:4–250
10. Singh MC, Garg SN (2010) Illuminance estimation and daylighting energy savings for Indian regions. *Renew Energy* 35:703–711
11. Ihm P, Nemri A, Krarti M (2009) Estimation of lighting energy savings from daylighting. *Build Environ* 44:509–514
12. Fasi MA, Budaiwi IM (2015) Energy performance of windows in office buildings considering daylight integration and visual comfort in hot climates. *Energy Build* 108:307–316
13. Al-Obaidi KM, Ismail M, Rahman AMA (2014) A study of the impact of environmental loads that penetrate a passive skylight roofing system in Malaysian buildings. *Frontiers Architectural Res* 3:178–191
14. Engineering Reference. EnergyPlus™ version 8.3 Documentation. LBNL laboratory, California, US
15. Malin N (2007) Light louver offers low-profile alternative to light shelves. Retrieved from <https://www.buildinggreen.com/product-review/lightlouver-offers-low-profile-alternative-light-shelves>
16. Shin JY, Yun GY, Kim JT (2011) Evaluation of daylighting effectiveness and energy saving potentials of light-pipe systems in buildings. *Indoor Built Environ* 000(000):1–8
17. Patil KN (2014 May) Energy conservation studies in buildings through daylighting and natural ventilation for space conditioning. PhD thesis, IIT-Delhi, New Delhi
18. Zhang X Daylighting performance of tubular solar light pipes: measurement, modelling and validation. PhD. Thesis, 2002
19. Zhang X, Muneer T (2000) A mathematical model for the performance of light-pipes. *Lighting Res Technol* 32(3):141–146
20. Jenkins D, Muneer T, Kubie J (2005) A design tool for predicting the performances of light pipes. *Energy Build* 37:485–492
21. Malet-Damour B, Boyer H, Fakra AH, Bojic M (2014) 2013 ISES Solar World Congress: light Pipes Performance Prediction: inter model and experimental confrontation on vertical circular light-guides. *Energy Procedia* 57:1977–1986

22. Harrison SJ, McCurdy GG, Cooke R (1998) Preliminary evaluation of the daylighting and thermal performance of cylindrical skylights. In: Proceedings of international daylight conference, Ottawa, Canada, pp 205–212
23. Kocifaj M, Darula S, Kittler R (2008) HOLIGILM: hollow light guide interior illumination method—An analytic calculation approach for cylindrical light-tubes. *Sol Energy* 82 (3):247–259
24. Azad AS, Rakshit D (2017) Experimental study of tubular light pipe system: influence of light reflector on its performance. World Renewable Energy Congress XVI, Murdoch University, Western Australia, Australia
25. ECBC (2007) *Energy Conservation Building Code*. Ministry of Power, Govt. of India, India
26. MNRE. Chapter 2: Climate and buildings. <http://www.mnre.gov.in/solar-energy/ch2.pdf>

Thermal Performance Evaluation of Building Roofs Embedded PCM for Multi-climatic Zones

Pranaynil Saikia, Abdus Salam Azad and Dibakar Rakshit

Abstract Phase change material (PCM) is used as a thermal energy storage medium in building roofs and walls, which reduces heat gain and temperature fluctuation inside buildings by virtue of latent heat property. Different geographical regions experience different values of climatic parameters such as ambient temperature, sky clearness, intensity of solar radiation, precipitable water quantity. All these parameters affect the thermal performance of the PCM used in a particular geographical region. As the performance of PCM is sensitive to a large number of climatic parameters, estimation of the performance of a PCM in a particular region requires the knowledge of the variation of the thermal performance of PCM with respect to each of the climatic parameters and then computing the performance of the PCM for specific values of the parameters for that region. The estimation of the performance of PCM will be less tedious if the thermal performance can be assessed as a function of a single parameter rather than a set of parameters. This study aims at finding such a composite parameter which alone can determine the thermal performance of PCM in a particular climate. In this study, a mathematical model is developed for the purpose of computing and comparing the thermal performances of three different PCMs in three different climatic conditions. The study specifically focuses on variation of climatic parameters in hot atmosphere where PCM is used to reduce interior heat gain and temperature fluctuation.

Keywords Phase change material · Heat gain · Roof · Climate
Latent heat

P. Saikia · A. S. Azad · D. Rakshit (✉)
Centre for Energy Studies, Indian Institute of Technology Delhi,
New Delhi 110016, India
e-mail: dibakar@iitd.ac.in

P. Saikia
e-mail: pranayxs4@gmail.com

A. S. Azad
e-mail: esz148318@iitd.ac.in

Nomenclature

t	Time (s)
T	Temperature of the heat-conducting material (K)
T_i	Inside temperature of the room (K)
T_o	Outside temperature (K)
h_i	Heat transfer coefficient (HTC) from PCM to inside air ($\text{W/m}^2\text{K}$)
h_o	Heat transfer coefficient (HTC) from PCM to outside air ($\text{W/m}^2\text{K}$)
I_g	Global solar radiation (W/m^2)
abs	Absorptivity
ϵ	Emissivity
α	Thermal diffusivity (m^2/s)
k	Thermal conductivity (W/m K)
ρ	Density (kg/m^3)
T_{sol}	Sol-air temperature (K)
m	Total mass of PCM (kg)
L_f	Latent heat of fusion (J/kg)
C	Specific heat capacity of any material in general (J/kg K)
C_s	Specific heat of solid phase (J/kg K)
C_l	Specific heat of liquid phase (J/kg K)
Q_{in}	Heat input to PCM (W)
Q_{out}	Heat going out of PCM (W)
B_i	Biot number
F_o	Fourier number
ΔR	Long-wavelength radiation exchange (W/m^2)

1 Introduction

Buildings consume about one-third of the total energy usage and emit around 24% in terms of CO_2 . In Indian building sector, residential and commercial buildings share 23 and 12% of the total electricity demand, respectively [1]. The electrical energy demand in the buildings will continue to rise, as it is estimated that the construction industry in the country is growing at a rapid growth rate of over 9% per year [2]. Therefore, energy conservation in buildings is a major challenge nowadays. To reduce heat ingress inside the building through building envelop, one of the important methods is incorporating thermal insulation [3, 4]. In similar manner, another method is utilization of latent heat thermal energy storage (LHTES) materials. LHTES using phase change materials (PCMs) can improve the energy performance and indoor thermal comfort of building.

PCMs provide a large heat capacity over a limited temperature range, and they can act like an almost isothermal reservoir of heat. Due to its ability to exhibit high

enthalpy of fusion in a relatively small volume, PCMs store or release large amounts of energy as latent heat during melting and solidification. The ability of a material to store a large quantity of heat as latent heat without undergoing change in temperature promises wide use of PCM in construction industries. PCM included inside concrete walls and roofs of buildings can reduce fluctuation of room air temperature which brings thermal comfort inside the building.

Soares et al. [5] explored the evaluation of how and where PCMs are used in passive latent heat thermal energy storage (LHTES) systems and how these construction solutions contribute to building's energy efficiency. It was concluded that improvement can be made in indoor thermal comfort using PCM in LHTES systems. Pomianowski et al. [6] studied the various PCM technologies integrated in building applications. The methods to determine the correct thermal properties of PCM materials were identified and discussed. Also, the procedures to determine the energy storage and saving potential were explored. Many authors have studied the different methods of incorporating PCM in building walls [7–12], and a detailed review of the applications of PCM in buildings can be found in the literature [13–16].

Kylili and Fokaides [17] investigated the effect of natural convection in the liquid phase of PCM as it melts under incident solar radiation. They also highlighted the importance of natural convection within the liquid PCM using numerical simulation. They identified several factors which can directly improve the thermal performance of the PCM. Waqas and Kumar [18] studied the use of PCM in hot and dry climate of South Asia region. It was reported that PCM can be used as better heat source for ambient air during hot daytime. The stored heat can be easily discharged due to cooler night temperatures.

Researchers have also conducted studies incorporating PCMs in the building roofs, which is major source of heat ingress inside the building. Alqallaf and Alawadhi [19] carried out study on the thermal performance of building roofs with cylindrical holes containing PCM. The objective of incorporating PCM in roof was to reduce heat gain inside a room during peak hours of electricity demand by utilizing its latent heat of fusion. A similar study was conducted by both of them [20] where building roof was constructed with vertical conical holes containing PCM. The PCM n-eicosane filled inside conical frustum showed improved performance with a heat flux inside the room reduced up to 39%.

Vakialtojar and Saman [21] developed a latent heat storage system encompassing two different PCMs which can be utilized for producing thermal comfort during both summer and winter months. Ravikumar and Sirinivasan [22] reported that heat ingress inside the room can be attenuated by about 50% when the PCM is integrated in the roof of a building. Hamza et al. [23] studied the consequences of integrating two different PCM layers in the roof of a building. They also evaluated the optimum thickness and location of the PCMs to minimize energy usage while maintaining thermal comfort inside the building.

Recently, melting and solidification phenomenon of the PCMs has been investigated experimentally [24–26] by some authors. Pasupathy et al. [27] conducted experimental investigation to analyze thermal performance of the roof

utilizing PCM for Chennai City, India. They also carried detailed study on the effects of variation in the ambient condition through the year, variation in heat transfer coefficient on the outer surface of the roof, and the PCM panel thickness.

Several practical experiments have been carried out to determine thermal performances of different PCMs under different climatic conditions. But for estimating the performances of a large number of PCMs in different climatic conditions, a mathematical model will be very useful for quick assessment and comparison purposes. This study involves the development of such a mathematical model along with its application for computing and comparing the thermal performances of three different PCMs in three different climatic zones. Also the effects of different climatic parameters are combined into a single parameter which can determine the relative thermal performance and suitability of PCM in different climates.

2 Problem Statement and Modeling Method

The mathematical model and the numerical solution methodologies for a PCM-embedded concrete roof system are presented in this section.

2.1 Problem Statement

When solar radiation is incident on the PCM-embedded roof, it absorbs heat. At the same time, the PCM roof exchanges heat with the ambient and room interior by convection. If heat input to the PCM is more than heat lost by the PCM, then there is accumulation of heat in the PCM. This accumulated heat serves to change the phase of the PCM from solid to liquid while at constant temperature. If heat accumulation proceeds further, the whole PCM melts and after that sensible heating (superheating) of the liquid occurs.

If the heat input to the PCM is less than the heat loss by the PCM, then there will be reduction in the net heat stored in the PCM. This will facilitate phase change from liquid to solid. If the whole PCM solidifies and still the input radiation is less than the heat lost by PCM, there will be sensible cooling (subcooling) of the solid PCM.

It is desirable to minimize sensible heating and cooling of the PCM as the aim of incorporating PCM in concrete roofs is to keep inside temperature constant. Once sensible heating or cooling of PCM begins, its thermal behavior becomes similar to that of concrete material and it ceases to serve its purpose of latent heat storage.

A change in the geographical region results in variation of climatic parameters which alters the performance of PCM. The variation of performance of PCM with respect to variation of climate is discussed in the present study.

2.2 Model Geometry

The schematic of the geometry is presented in Fig. 1. The concrete properties are typically those of a reinforced concrete [28].

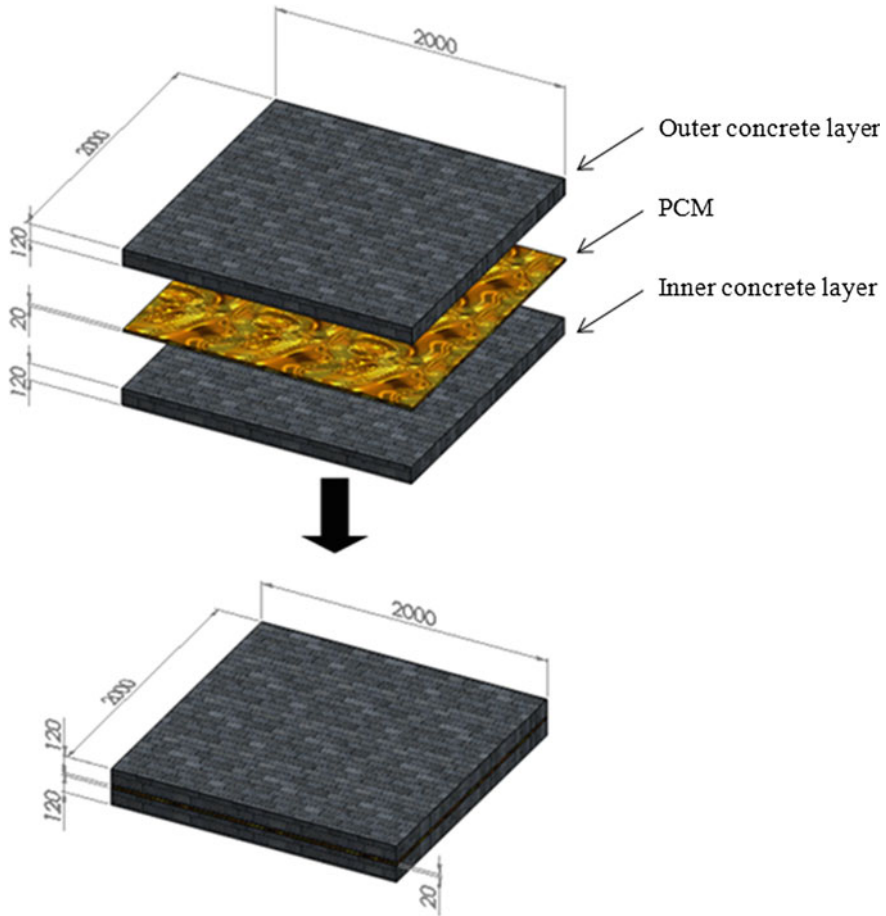
Following are dimensions of the roof containing PCM:

Thickness of outer concrete = 12 cm

Thickness of PCM = 2 cm

Thickness of inner concrete = 12 cm

Area = 2 m × 2 m



All dimensions are in mm

Fig. 1 Dimensions of the PCM-embedded roof

2.3 Mathematical Model

For the mathematical model of the above-stated problem, following assumptions are made:

- i. One-dimensional heat transfer (x-direction only).
- ii. Temperature is uniform over the PCM surface.
- iii. 15% void is maintained initially in the space inside the concrete roof where the PCM is incorporated (to accommodate the volumetric changes in phase transition and possible superheating/subcooling of PCM).
- iv. Temperature inside the room is kept constant at 300 K by some air-conditioning unit. The purpose of incorporating PCM in the concrete roof is to minimize temperature fluctuation on the inner surface of the concrete roof so that variation in convective heat transfer between the inner surface of the concrete roof and room air is reduced.

The governing equation and the boundary condition are developed as below. Governing equation for heat transfer by conduction with no internal heat generation is given by

$$\frac{\partial^2 T}{\partial x^2} + \frac{\partial^2 T}{\partial y^2} + \frac{\partial^2 T}{\partial z^2} = \rho C dT / k dt \quad (1)$$

where x , y , and z are three mutually perpendicular directions. ' T ' is the temperature of the heat-conducting material having density ' ρ ,' specific heat capacity ' C ,' and thermal conductivity ' k .' ' dT ' is the change in temperature in time ' dt .'

Governing equations for latent and sensible heating of PCM can be expressed as

$$(Q_{in} - Q_{out})dt = mL_f \quad (\text{Phase transformation}) \quad (2)$$

$$(Q_{in} - Q_{out})dt = mC_l dT \quad (\text{Superheating of liquid}) \quad (3)$$

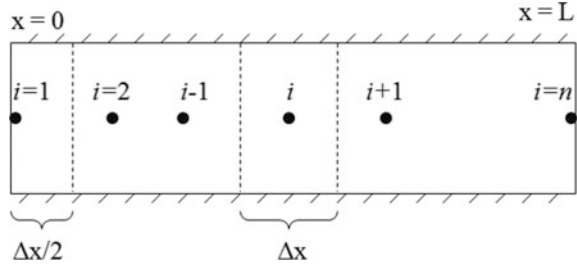
$$(Q_{out} - Q_{in})dt = mC_s dT \quad (\text{Sub cooling of solid}) \quad (4)$$

where Q_{in} is the heat input to the PCM and Q_{out} is the heat going out of the PCM. The inner and outer concrete layers are subdivided into smaller nodes of size equal to that of the PCM. Basic energy conservation equation is applied to all the nodes considering all the thermal properties of the concrete and PCM.

The current heat transfer problem includes two independent variables x (along the direction of roof thickness) and t (time) and a dependent variable T (temperature).

$$T = f(x, t) \quad (5)$$

Fig. 2 Transient heat transfer along the thickness of the PCM-embedded roof



For transient one-directional heat transfer, the time derivative of temperature is written in the following explicit form [29] as shown in Fig. 2.

$$\frac{dT}{dt} = \frac{T(x, t + \Delta t) - T(x, t)}{\Delta t} \tag{6}$$

The nodal form of Eq. (6) is given as

$$\frac{dT}{dt} = \frac{T_{i,j+1} - T_{i,j}}{\Delta t} \tag{7}$$

where the nodal variable ‘j’ is defined by $t = (j - 1) \times \Delta t$ and $j = 1$ corresponds to $t = 0$.

The x (thickness) derivative of temperature is expressed by the following explicit equation.

$$\frac{\partial^2 T}{\partial x^2} = \frac{T(x - \Delta x, t) - 2T(x, t) + T(x + \Delta x, t)}{\Delta x^2} \tag{8}$$

The nodal form of Eq. (8) is as follows:

$$\frac{\partial^2 T}{\partial x^2} = \frac{T_{i-1,j} - 2T_{i,j} + T_{i+1,j}}{\Delta x^2} \tag{9}$$

Combining Eqs. (6) and (8), we get the explicit Eq. (10) which facilitates temperature calculation at any node at any time step.

$$T(x, t + \Delta t) = \frac{\alpha \Delta t}{\Delta x^2} [T(x - \Delta x, t) + T(x + \Delta x, t)] + \left[1 - 2 \frac{\alpha \Delta t}{\Delta x^2} \right] T(x, t) \tag{10}$$

The nodal form of Eq. (10) can be expressed as follows:

$$T_{i,j+1} = \frac{\alpha \Delta t}{\Delta x^2} [T_{i-1,j} + T_{i+1,j}] + \left[1 - 2 \frac{\alpha \Delta t}{\Delta x^2} \right] T_{i,j} \tag{11}$$

For the first element ($i = 1$) which is exposed to ambient, following equation is used to compute the temperature at any time step t .

$$T_{1,j+1} = T_{1,j}[1 - 2F_o(1 + B_i)] + 2F_o B_i T_o + 2F_o T_{2,j} \quad (12)$$

where F_o is the Fourier number defined by $F_o = \frac{\alpha \Delta t}{\Delta x^2}$ and B_i is Biot number defined by $B_i = \frac{h \Delta x}{k}$.

The case discussed in the study involves heat input to outer concrete by radiation, conduction of heat through PCM and concrete. Then, there is convective heat transfer between ambient and outer concrete surface and again between inner surface of concrete and room. Such boundary condition is known as Robin-type boundary condition. Since rate of heat transfer varies with time, the analysis is transient. For the inner concrete surface, the heat transfer coefficient for horizontal surface is taken as $h_i = 7.7 \text{ W/m}^2\text{-K}$ from [28]. Considering the effect of wind velocity, average outer surface heat transfer coefficient is taken as $h_o = 22.7 \text{ W/m}^2 \text{ K}$. Also from [30], monthly average solar insolation (global radiation, I_g and water precipitable, w) and ambient temperatures, T_a , of different cities of Bikaner (hot-dry), Chennai (warm-humid), and Hyderabad (composite) in India have been taken. Summer and monsoon months of May, June, and July are chosen for the assessment of thermal performance of the PCM.

Sol-air temperature for roof has been calculated from the collected solar insolation data for the different cities from the below expression [31]:

$$T_{\text{sol}} = T_a + \frac{\text{abs } I_g}{h_o} - \frac{\epsilon \Delta R}{h_o} \quad (13)$$

where T_{sol} is sol-air temperature, abs is absorptivity of the surface (taken as 0.8 for the concrete roof), ϵ is emissivity of the surface (taken as 0.8 for concrete roof), and ΔR is long-wavelength radiation exchange (taken as 63 W/m^2 for the horizontal surface) [28].

3 Methodology

The general procedure for the numerical simulation can be summarized in the following steps:

1. Data collection and material selection.
2. Validation of the numerical model.
3. Initial simulation and check for the cycle independence.
4. Final simulation run, save, and stop.

3.1 Data Collection and Material Selection

The numerical simulation requires solar irradiance on horizontal surface, ambient temperature, and precipitable water which has been presented in the Tables 1, 2, and 3. The data has been collected from the weather files available on the EnergyPlus Web site [30]. The weather data contains database of average of 25 years measured values for different cities.

Sol-air temperature for roof has been computed using the Eq. 13. Hourly variations of sol-air temperatures for roof along with ambient temperature for three consecutive days are depicted in Fig. 3.

PCMs considered in the study have melting temperatures in the range of 302–309 K. Reason for selecting the PCMs in this temperature range is that their melting temperatures are closer to the ambient temperature in the daytime. Therefore, the

Table 1 Monthly mean hourly global solar irradiance, ambient temperature, and precipitable water for Bikaner location

Time (h)	Global radiation (W/m ²)			Ambient Temp. (°C)			Precipitable water (mm)		
	May	June	July	May	June	July	May	June	July
1	0	0	0	31.1	32.5	31.1	23	36	48
2	0	0	0	30.2	31.8	30.5	23	36	47
3	0	0	0	29.4	31.0	30.0	23	36	47
4	0	0	0	28.5	30.3	29.4	23	36	47
5	0	0	0	27.6	29.6	28.8	24	37	48
6	0	0	0	26.8	28.8	28.2	24	37	49
7	69	75	49	28.3	30.4	29.2	25	38	50
8	246	228	189	30.3	32.0	30.6	25	38	51
9	438	399	351	32.5	33.7	32.1	25	38	51
10	614	548	467	34.5	35.3	33.5	24	38	51
11	722	682	570	36.3	36.9	34.7	24	37	51
12	829	774	633	37.8	38.2	35.7	23	37	50
13	882	830	681	39.1	39.3	36.5	23	36	50
14	859	766	674	40.0	40.0	37.1	22	36	49
15	764	706	638	40.4	40.3	37.5	22	36	49
16	635	611	533	40.4	40.4	37.5	23	36	50
17	465	446	373	39.9	39.9	37.1	23	37	50
18	278	262	238	38.8	39.0	36.5	24	37	51
19	86	109	101	37.3	37.8	35.6	24	38	52
20	0	0	0	36.2	36.7	34.6	24	38	52
21	0	0	0	35.2	35.8	33.9	24	38	52
22	0	0	0	34.2	34.9	33.2	24	38	51
23	0	0	0	33.1	34.0	32.5	24	37	50
24	0	0	0	32.1	33.2	31.7	23	37	49

Table 2 Monthly mean hourly global solar irradiance, ambient temperature, and precipitable water for Chennai location

Time (h)	Global radiation (W/m ²)			Ambient Temp. (°C)			Precipitable water (mm)		
	May	June	July	May	June	July	May	June	July
1	0	0	0	30.3	29.4	25.8	56	48	51
2	0	0	0	29.7	28.8	25.3	55	48	51
3	0	0	0	29.1	28.2	24.9	55	47	50
4	0	0	0	28.5	27.7	24.5	54	47	50
5	0	0	0	27.8	27.1	24	54	47	50
6	0	0	0	27.3	26.5	23.6	54	47	50
7	82	72	57	28.7	27.8	24.7	57	49	52
8	269	237	213	30.3	29.4	26.6	59	51	54
9	479	415	376	32.1	31.0	28.5	61	52	55
10	661	572	513	33.8	32.6	30.5	62	52	55
11	768	692	627	35.2	34.0	32.2	62	53	55
12	852	730	717	36.3	35.0	33.8	62	52	55
13	855	749	723	37.2	35.8	35	62	52	55
14	810	717	686	37.7	36.3	35.8	62	52	54
15	688	630	564	37.8	36.5	36.1	62	52	54
16	522	489	478	37.5	36.3	36	62	52	55
17	320	307	300	36.7	35.6	35.2	62	52	55
18	119	118	128	35.5	34.5	33.9	62	53	55
19	0	5	10	34.7	33.4	32.5	62	53	55
20	0	0	0	34.0	32.7	31.6	62	53	55
21	0	0	0	33.2	32.0	30.8	61	52	55
22	0	0	0	32.4	31.3	29.9	60	51	54
23	0	0	0	31.7	30.7	29.1	59	50	53
24	0	0	0	30.9	30.0	28.3	57	49	52

PCMs can be easily get melted by absorbing heat during daytime and getting have enough time to release the heat during nighttime. If we choose PCMs having lower range of melting temperature, most of the PCMs will easily get melted to liquid state in short time and no more heat will be added. Also, because of high ambient temperature during nighttime, they will not be able release heat and will remain in liquid state. Other important properties which influenced the results are latent heat of fusion (L_f), thermal conductivity (k), and specific heat (C). The properties of PCM considered in the study are listed in Table 4 [26, 16].

Table 3 Monthly mean hourly global solar irradiance, ambient temperature, and precipitable water for Hyderabad location

Time (h)	Global radiation (W/m ²)			Ambient Temp. (°C)			Precipitable water (mm)		
	May	June	July	May	June	July	May	June	July
1	0	0	0	30.0	26.7	25.4	31	37	40
2	0	0	0	29.2	26.1	25.0	31	37	40
3	0	0	0	28.5	25.5	24.5	31	37	40
4	0	0	0	27.8	24.9	24.1	31	37	40
5	0	0	0	27.1	24.3	23.6	32	37	40
6	0	0	0	26.3	23.7	23.1	32	37	40
7	78	68	55	28.0	25.1	24.1	33	39	41
8	261	215	213	29.9	26.7	25.5	33	40	42
9	474	368	340	32.0	28.3	26.7	33	40	43
10	659	506	454	34.0	29.8	27.8	33	41	43
11	782	591	557	35.7	31.1	28.8	33	41	43
12	852	642	624	37.1	32.1	29.7	32	40	43
13	860	641	635	38.1	32.8	30.3	32	40	42
14	848	620	619	38.8	33.3	30.7	31	40	42
15	712	567	531	39.0	33.5	30.8	31	40	42
16	537	447	408	38.7	33.4	30.6	32	40	42
17	357	307	275	37.9	32.8	30.2	32	41	43
18	154	167	143	36.6	31.9	29.5	33	41	43
19	16	28	27	35.1	30.7	28.5	33	41	43
20	0	0	0	34.2	30.0	28.0	33	41	43
21	0	0	0	33.3	29.3	27.5	33	41	43
22	0	0	0	32.5	28.6	26.9	33	40	43
23	0	0	0	31.6	27.8	26.4	32	39	42
24	0	0	0	30.8	27.1	25.8	32	39	41

3.2 Numerical Model Validation

The results of the numerical model are validated by comparing with the results of the experimental work carried out by Pasupathy et al. With similar input data such as PCM properties, incident solar radiation, ambient temperature variation, the numerical model can successfully replicate the temperature variation profile of PCM for a diurnal cycle as obtained by Pasupathy et al. (Fig. 4). Slight discontinuities occur because the incident solar radiation values obtained from EnergyPlus may deviate to some extent from the actual values of incident solar radiation during the experiment of Pasupathy et al.

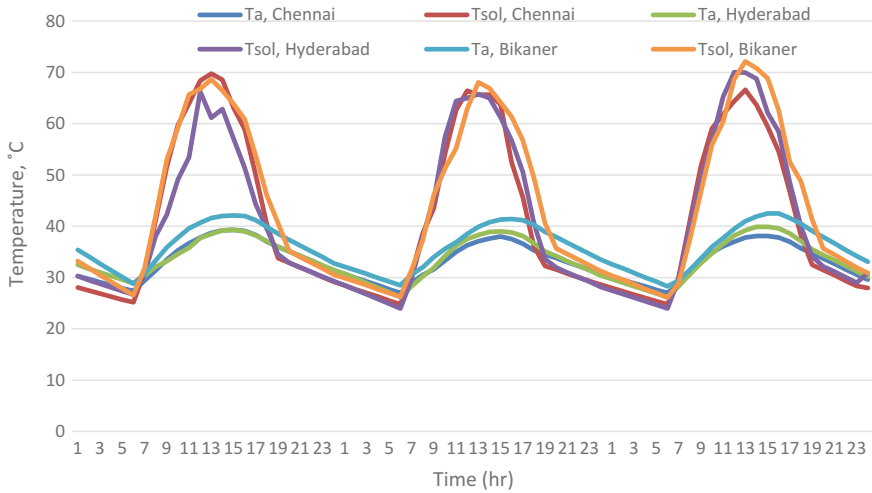


Fig. 3 Variation of ambient temperature and sol-air temperature for the selected locations (Bikaner, Chennai, and Hyderabad) w.r.t. time

4 Results and Discussion

The numerical simulation yields the values of net heat gain into the room through the roof for the months of May, June, and July in the cities Bikaner, Chennai, and Hyderabad. A few sample plots of net heat gain versus time have been depicted in Figs. 5, 6, and 7. From net heat gain data, average daily heat gain through the roof is calculated for the three cities and for the three months (Tables 5, 6, 7, 8, 9, and 10). Two different cases are studied for the three cities. First is without considering the effect of wind (still air), and the second includes the effect of wind on heat gain and PCM performance.

4.1 Thermal Performance of PCM Roof in the Absence of Wind

The heat transfer coefficient for a horizontal surface in contact with still air can be conveniently taken as $7.7 \text{ W/m}^2\text{K}$. Under such condition, the performances of the three PCMs (BioPCM, OM32, and OM35) are evaluated in three different places which belong to three different climatic zones of India. All the three PCMs give maximum average daily heat gain for the month of May (Tables 5, 6, 7, 8, 9, and 10). It is observed that the amount of precipitable water quantity is minimum in May (Tables 1, 2, and 3) which is an indicator of clear sky with more incident solar radiation on the roof. Ambient temperature is also high in May. All these factors lead to increased heat gain into the room. In May, BioPCM gives minimum average

Table 4 Properties of PCMs

PCM	Melting point (T_m) (K)	Latent heat of fusion (L_f) (kJ/kg)	Density of solid phase (ρ_s) (kg/m ³)	Density of liquid phase (ρ_l) (kg/m ³)	Thermal conductivity of solid phase (k_s) (W/m-K)	Thermal conductivity of liquid phase (k_l) (W/m K)	Specific heat of solid phase (C_s) (J/kg-K)	Specific heat of liquid phase (C_l) (J/kg-K)
BioPCM	302	219	860	860	0.2	0.2	1970	1970
OM32	305	200	928	870	0.219	0.145	1950	2300
OM35	309	197	900	870	0.20	0.16	1650	2300

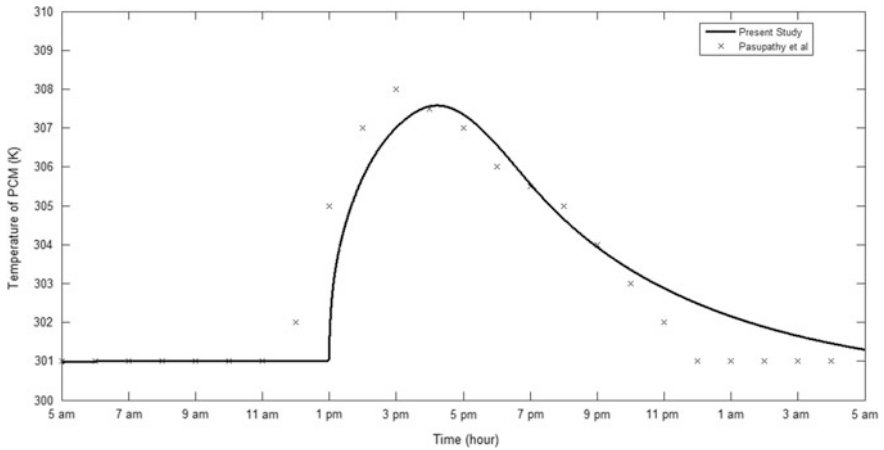


Fig. 4 Validation of the numerical model

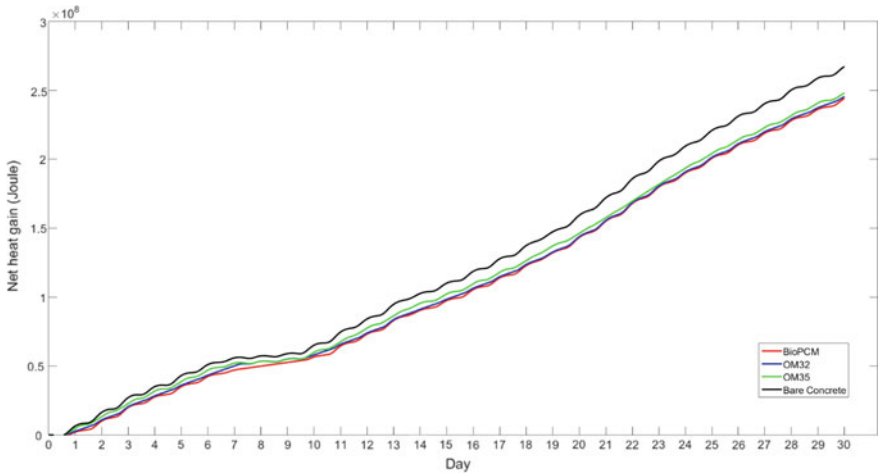


Fig. 5 Net heat gain through the roof in the presence of wind (Bikaner, June)

daily heat gain into the room and OM32 gives maximum heat gain into the room out of the three PCMs studied. In June and July, the precipitable water quantity is greater than in the month of May. This indicates a relatively overcast weather in June and July resulting in less amount of solar radiation incident on the roof. As a result, heat gain into the room reduces. A change in the trend of relative performances of PCM is observed in June and July. Now, BioPCM gives minimum heat gain into the room and OM35 gives maximum heat gain. Heat gain for OM32 lies in between that for BioPCM and OM35. The heat gain values through all PCMs are less than the corresponding values for a bare concrete roof.

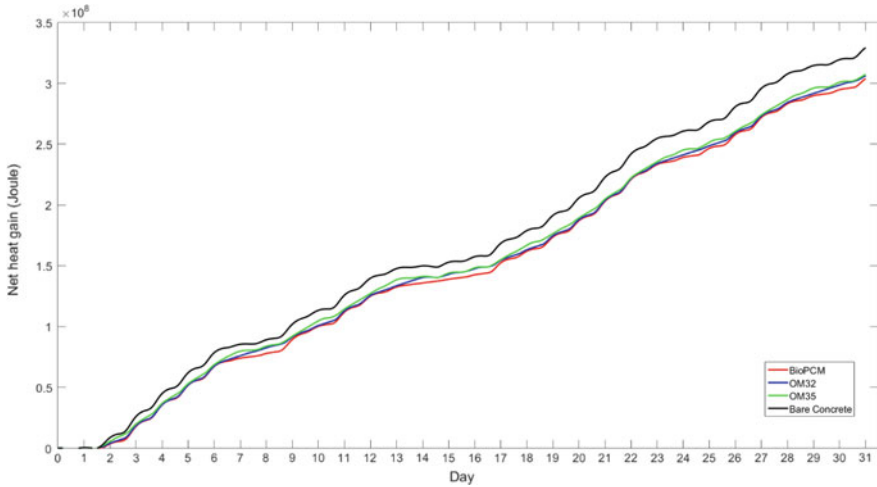


Fig. 6 Net heat gain through the roof in the absence of wind (Hyderabad, July)

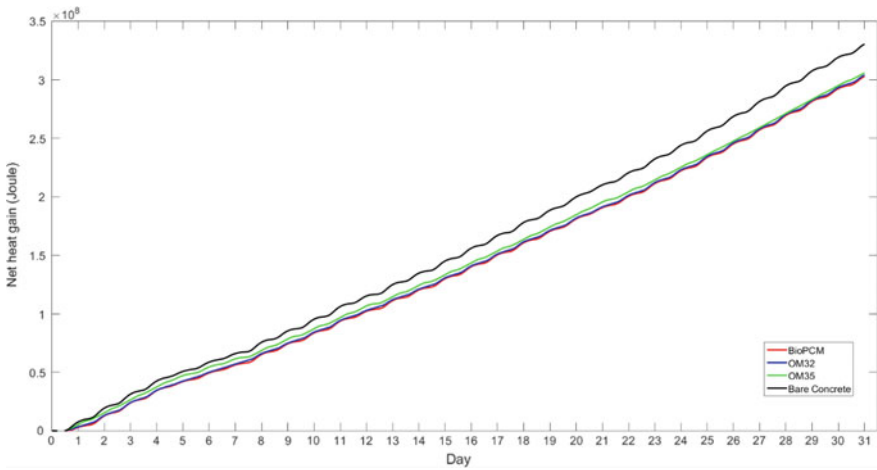


Fig. 7 Net heat gain through the roof in the presence of wind (Chennai, May)

4.2 Thermal Performance of PCM Roof in the Presence of Wind

The effect of wind is primarily to increase heat transfer rate from the roof to the air resulting in a decrease in the average daily heat gain to the room. It is observed that the relative performances of all the three PCMs follow the same trend in the presence of wind. Here, BioPCM gives the minimum average daily heat gain and OM35 gives the maximum average daily heat gain (Tables 8, 9, and 10).

Table 5 Average daily heat gain in the absence of wind (Bikaner)

	Average daily heat gain (kJ/day)			3 months average
	May	June	July	
BioPCM	19385	15548	12869	15934
OM32	19430	15590	12902	15974
OM35	19410	15598	12911	15973
Bare Concrete	20818	16748	13896	17154

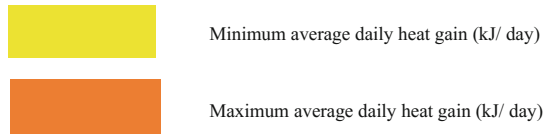
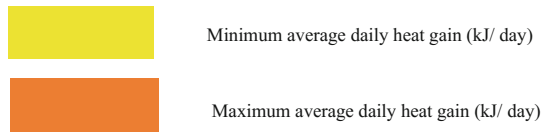


Table 6 Average daily heat gain in the absence of wind (Chennai)

	Average daily heat gain (kJ/day)			3 months average
	May	June	July	
BioPCM	16960	13502	11639	14033.7
OM32	17001	13539	11671	14070.3
OM35	16990	13554	11689	14077.7
Bare Concrete	18240	14575	12588	15134.3



The performance of OM32 falls between BioPCM and OM35. The heat gain values through all PCMs are less than the corresponding values for a bare concrete roof.

Referring to Tables 5, 6, and 7, it is observed that the relative performances of the three PCMs change above and below a critical value of average daily heat gain through the bare concrete roof. If we look specifically in Table 5, we can observe the shift in the trend of relative performances of PCM. In third column (June month), the average daily heat gain through bare concrete is 16,748 kJ/day and OM35 gives maximum heat gain through the roof out of the three PCMs. But if we

Table 7 Average daily heat gain in the absence of wind (Hyderabad)

	Average daily heat gain (kJ/day)			3 months average
	May	June	July	
BioPCM	18510	9763	9802	12691.7
OM32	18553	9833	9879	12755
OM35	18539	9871	9915	12775
Bare Concrete	19888	10541	10625	13684.7



Minimum average daily heat gain (kJ/ day)



Maximum average daily heat gain (kJ/ day)

Table 8 Average daily heat gain in the presence of wind (Bikaner)

	Average daily heat gain (kJ/day)			3 months average
	May	June	July	
BioPCM	11708	8141	6957	8935.3
OM32	11742	8185	6987	8971.3
OM35	11751	8275	7067	9031
Bare Concrete	12740	8915	7642	9765.7



Minimum average daily heat gain (kJ/ day)



Maximum average daily heat gain (kJ/ day)

Table 9 Average daily heat gain in the presence of wind (Chennai)

	Average daily heat gain (kJ/day)			3 months average
	May	June	July	
BioPCM	9775	7221	5751	7582.3
OM32	9808	7265	5797	7623.3
OM35	9870	7345	5883	7699.3
Bare Concrete	10664	7926	6342	8310.7



Minimum average daily heat gain (kJ/ day)



Maximum average daily heat gain (kJ/ day)

Table 10 Average daily heat gain in the presence of wind (Hyderabad)

	Average daily heat gain (kJ/day)			3 months average
	May	June	July	
BioPCM	11265	4106	4627	6666
OM32	11301	4165	4735	6733.7
OM35	11324	4170	4769	6754.3
Bare Concrete	12264	4471	5119	7284.7



Minimum average daily heat gain (kJ/ day)



Maximum average daily heat gain (kJ/ day)

look at the 3 months' average column where the average daily heat gain through bare concrete is 17,154 kJ/day, then OM32 gives the maximum heat gain. Therefore, the critical value lies between 16,748 and 17,154 kJ/day. And similar trend can be observed in all other tables. Whenever the value of average daily heat gain through bare concrete is above 17,000 kJ/day, the trend of relative performances of PCMs is different than the cases with average daily heat gain through bare concrete being lower than 17,000 kJ/day. It is difficult to pinpoint the exact value in the interval between 16,748 and 17,154 kJ/day in Table 5 where the shift in the trend occurs primarily because average daily heat gain cannot be varied as an independent variable in the mathematical model as it is the combined effect of all the climatic and roof configuration parameters. Therefore, a ballpark number of 17,000 kJ/day can be considered for the shift in relative performances of the PCMs.

Thus, the combined effect of variation in incident solar radiation, ambient temperature, precipitable water quantity, and wind speed for different climatic zones on the relative performances of PCMs can be summarized into a single factor which takes into account all these climatic factors. This single factor is average daily heat gain into the room. Firstly, average daily heat gain into the room through bare concrete roof is computed. If average heat gain through the concrete roof is below 17,000 kJ/day, then BioPCM is the most suitable PCM out of the three for all the climatic zones studied, while OM35 is the least suitable one. If the value exceeds 17,000 kJ/day, then BioPCM is the most suitable PCM and OM32 is the least suitable PCM. This conclusion is supported by the fact that the three PCMs' relative performance depended on this threshold value of average daily heat gain in all the three different climatic zones. In order to account for roofs of different dimensions, heat gain per unit area of the roof can be considered. For a horizontal plane roof of any surface area, if the average daily heat gain through unit surface area of the bare concrete roof is more than 4250 kJ, then OM32 is the least suitable PCM and if the average daily heat gain per unit area of the bare concrete roof is less than 4250 kJ, OM35 is the least suitable PCM (BioPCM being the best PCM in both the cases).

Another round of computation is performed by taking PCM thickness of 4 cm (in place of 2 cm PCM thickness in the previous cases thereby increasing the total thickness of the PCM roof by 2 cm) and in the absence of wind. The results obtained from the numerical model are presented in Tables 11, 12, and 13. As can be seen from the new results, the critical value of average daily heat gain through bare concrete still lies within the interval of 16,748–17,154 kJ/day as determined from Table 5. Table 11 further shows that the trend shift occurs somewhere near 16,835 kJ/day which is close to 17,000 kJ/day as determined before. Changing PCM and roof thickness may affect the value of average daily heat gain for a particular place in a particular month, but the critical value where the shift in the trend of relative performances of the PCMs occurs remains unaltered.

Table 11 Average daily heat gain in the absence of wind (Bikaner) with 4 cm PCM thickness

	Average daily heat gain (kJ/day)			3 months average
	May	June	July	
BioPCM	18183	14648	12063	14964.667
OM32	18243	14700	12104	15015.667
OM35	18216	14703	12113	15010.667
Bare Concrete	20351	16498	13656	16835



Minimum average daily heat gain (kJ/ day)



Maximum average daily heat gain (kJ/ day)

Table 12 Average daily heat gain in the absence of wind (Chennai) with 4 cm PCM thickness

	Average daily heat gain (kJ/day)			3 months average
	May	June	July	
BioPCM	15926	12667	10936	13176.333
OM32	15980	12712	10975	13222.333
OM35	15963	12725	10989	13225.667
Bare Concrete	17879	14333	12423	14878.333



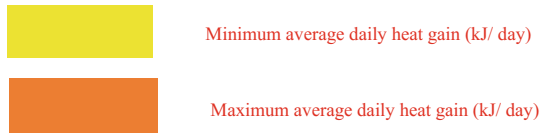
Minimum average daily heat gain (kJ/ day)



Maximum average daily heat gain (kJ/ day)

Table 13 Average daily heat gain in the absence of wind (Hyderabad) with 4 cm PCM thickness

	Average daily heat gain (kJ/day)			3 months average
	May	June	July	
BioPCM	17342	9219	9206	11922.333
OM32	17400	9489	9295	12061.333
OM35	17380	9562	9541	12161
Bare Concrete	19431	10506	10519	13485.333



5 Conclusion

The comparative study demonstrates that heat gain through the roof can be considered as a deciding factor which takes into account several climatic factors affecting the performance of PCM in building roofs. Suitability of PCM can be determined by computing the heat gain through the bare concrete roof. The temperature of the inner surface of the roof can be measured by simple temperature measuring instruments, and applying convective heat transfer equation between inner surface of roof and room interior (kept at constant temperature by air conditioner), one can compute the heat gain. After this, a suitable PCM can be selected based on the computed value. This method is an easy alternative to determine relative performances of PCMs in different geographical regions rather than considering the effect of each climatic factor (such as ambient temperature, wind, precipitable water quantity) individually on the performance of PCM and then drawing an overall conclusion.

References

1. A Report on Energy Efficiency and Energy Mix in the Indian Energy System (2030), Using India energy security scenarios, 2047. NITI Aayog, April 2015
2. USAID ECO-III Project (2009) Energy Assessment guide for commercial building. A report
3. Azad AS (2013) Energy saving analysis of high performance commercial buildings in India. M.Tech. Thesis, Jamia Millia Islamia University, New Delhi, 100 pp
4. Sullivan GP (1995) Energy conservation and thermal comfort in buildings in northern Pakistan. MS Thesis, Massachusetts Institute of Technology (MIT)

5. Soares N, Costa JJ, Gaspar AR, Santos P (2013) Review of passive PCM latent heat thermal energy storage systems towards buildings' energy efficiency. *Energy Build* 59:82–103
6. Pomianowski M, Heiselberg P, Zhang Y (2013) Review of thermal energy storage technologies based on PCM application in buildings. *Energy Build* 67:56–69
7. Feustel HE, Stetiu C (1997) Thermal performance of phase change wallboard for residential cooling application. Lawrence Berkeley National Laboratory, Report LBL-38320
8. Bouguerra EH, Hamid A, Retiel N (2011) Reduction of HVAC Energy in Buildings by Incorporating Phase Change Materials. In: *Proceedings of the Global Conference on Global Warming 2011*, Lisbon, Portugal
9. Kissock JK, Hannig JM, Whitney TI, Drake ML (1998) Testing and simulation of phase change wallboard for thermal storage in buildings. In: *Proceedings of the international solar energy conference*, New York, USA, pp 45–52
10. Huang MJ, Eames PC, Hewitt NJ (2006) The application of a validated numerical model to predict the energy conservation potential of using phase change materials in the fabric of a building. *Sol Energy Mater Sol Cells* 90:1951–1960
11. Peippo K, Kauranen P, Lund PD (1991) A multicomponent PCM wall optimized for passive solar heating. *Energy Build* 17:259–270
12. Shapiro M (1989) Development of the enthalpy storage materials. Mixture Florida Solar Energy Center
13. Cabeza LF, Castell A, Barreneche C, de Gracia A, Fernández AI (2011) Materials used as PCM in thermal energy storage in buildings: a review. *Renew Sustain Energy Rev* 15:1675–1695
14. Khudhair A, Farid M (2004) A review on energy conservation in building applications with thermal storage by latent heat using phase change materials. *Energy Convers Manage* 45:263–275
15. Saikia P, Yagnamurthy SS, Rakshit D (2016) Fabric heat gain assessment of phase change materials as passive space heating medium. In: *International Conference on Materials Science & Technology (ICMTECH 2016)*. VBRI Press, Linköping. <https://doi.org/10.5185/icmtech.2016>
16. Zhang Y, Zhou G, Lin K, Zhang Q, Di H (2007) Application of latent heat thermal energy storage in buildings. *Build Environ* 42:2197–2209
17. Kylili A, Fokaides PA (2015) Numerical simulation of phase change materials for building applications: a review. *Adv Build Energy Res* 11:1–25. <https://doi.org/10.1080/17512549.2015.1116465>
18. Waqas A, Kumar S (2011) Utilization of latent heat storage unit for comfort ventilation of buildings in hot and dry climates. *Int J Green Energy* 8(1):1–24. <https://doi.org/10.1080/15435075.2010.529406>
19. Alqallaf HJ, Alawadhi EM (2013) Concrete roof with cylindrical holes containing PCM to reduce the heat gain. *Energy Build* 61:73–80
20. Alawadhi EM, Alqallaf HJ (2011) Building roof with conical holes containing PCM to reduce the cooling load: numerical study. *Energy Convers Manage* 52:2958–2964
21. Vakialtojjär S, Saman W (2000) Domestic heating and cooling with thermal storage. In: *Proceedings of the 8th international conference on thermal energy storage*, 28 Aug–1 Sept 2000, Stuttgart, Germany, pp 381–386
22. Ravikumar M, Sirinivasan PSS (2011) Year round performance of PCM filled RCC roof for thermal management. *Eur J Sci Res* 3:424–433
23. Hamza H, Hanchi N, Abouelkhyrat B, Lahjomri J, Oubarra A (2016) Location and thickness effect of two phase change materials between layers of roof on energy consumption for air-conditioned room. *J Therm Sci Eng Appl* 8:021009, 1–7
24. Li W, Wang YH, Kong CC (2015) Experimental study on melting/solidification and thermal conductivity enhancement of phase change material inside a sphere. *Int Commun Heat Mass* 68:276–282
25. Motahar S, Khodabandeh R (2016) Experimental study on the melting and solidification of a phase change material enhanced by heat pipe. *Int Commun Heat Mass* 73:1–6

26. Yang XH, Lu TJ, Kim T (2011) Temperature effects on the effective thermal conductivity of phase change materials with two distinctive phases. *Int Commun Heat Mass* 38 (10):1344–1348
27. Pasupathy A, Athanasius L, Velraj R, Seeniraj RV (2008) Experimental investigation and numerical simulation analysis on the thermal performance of a building roof incorporating phase change material (PCM) for thermal management. *Appl Therm Eng* 28:556–565
28. Ministry of New and Renewable Energy (MNRE). *Solar energy*, Chap. 4 (Thermal Performance of Buildings)
29. Venkateshan SP (2009) *Heat transfer*, 2nd edn. Ane Books Pvt. Ltd., New Delhi
30. EnergyPlus (2017) “Weather Data by Region,” National Renewable Energy Laboratory, Golden, CO. https://energyplus.net/weather-region/asia_wmo_region_2/IND%20%20. Accessed 5 January 2017
31. Sharma P, Rakshit D (2016) Quantitative assessment of orientation impact on heat gain profile of naturally cooled buildings in India. *Adv Build Energy Res*. <https://doi.org/10.1080/17512549.2016.1215261>

Enhancement of Energy Efficiency at an Indian Milk Processing Plant Using Exergy Analysis

Babji Srinivasan, Jaideep Pal and Rajagopalan Srinivasan

Abstract The dairy sector in India is the largest milk producer in the world. Substantial amounts of freshwater and energy are consumed during milk processing with concomitant impacts on sustainability. In this chapter, we study the energy efficiency at India's largest milk processing plant and propose retrofits for improving the plant's sustainability. Specifically, we report on exergy analysis of a milk powder manufacturing unit. Exergy of a system at a certain thermodynamic state is the maximum amount of work that can be obtained when the system moves from that state to one of equilibrium with its surroundings. In contrast to a conventional energy analysis, which maps the energy flows of the system and suggests opportunities for process integration, an exergy analysis pinpoints the locations, causes, and magnitudes of thermodynamic losses. The milk powder plant that is the focus of the current study consists of two sections—an evaporation section and a drying section. Our results reveal that exergy efficiency of certain units is very low (<20%). Significant improvements in energy efficiencies can be achieved through simple, low-cost retrofits to these units.

Keywords Energy efficiency · Dairy industry · Process integration
Exergy · Retrofit

B. Srinivasan · J. Pal · R. Srinivasan (✉)
Indian Institute of Technology Gandhinagar, Gandhinagar, India
e-mail: raj@iitm.ac.in

R. Srinivasan
Department of Chemical Engineering,
Indian Institute of Technology Madras, Chennai 600036, India

© Springer Nature Singapore Pte Ltd. 2018
S. De et al. (eds.), *Sustainable Energy Technology and Policies*, Green Energy
and Technology, https://doi.org/10.1007/978-981-10-7188-1_19

Nomenclature

Letter Symbols

C_p	Specific heat capacity at constant pressure (in kJ/kg K)
e_x	Specific exergy (in kJ/kg)
h	Specific enthalpy (in kJ/kg)
\dot{m}	Mass flow rate (in kg/s)
p	Pressure of a system (in bar)
\dot{Q}	Heat flow (in kJ/s or kW)
R	Mass-based (substance dependent) gas constant (in kJ/kg K)
s	Specific entropy (in kJ/kg K)
t	Time (in s)
T	Temperature of a system (in °C or K)
\dot{W}	Power (or work per time) (in kW)

Greek Symbols

Δ	Change in property
η	Exergy efficiency

Superscript

P	Pressure
T	Temperature

Subscripts

0	Thermodynamic state with ambient conditions
1	Thermodynamic state
2	Thermodynamic state
a	Fluid a
b	Fluid b
cv	Control volume
ex	Exergy
i	Initial
in	Inlet stream
f	Final
out	Outlet stream
p	Constant pressure
vap	Vaporization

1 Introduction

Increasing the energy efficiency of the industrial sector has the potential to significantly reduce the greenhouse gas emissions associated with the consumption of fossil fuels and the operating costs associated with energy use [1]. In the dairy processing industry, a very small amount of processing energy is actually stored in the final products and hence the vast majority of processing heat is eventually wasted. Since recovery of the waste heat and its subsequent utilization imply reduction in the net purchased energy, recovery of this waste heat is highly necessary [2].

India is now the largest producer of milk [3] owing to “Operation Flood” [4], a project launched by National Dairy Development Board (NDDB) in 1970 and led by late Dr. Verghese Kurien. India, with its enormous vegetarian population, is the largest consumer of its own dairy products such as butter, cheese, ghee, milk powder as these are the only acceptable sources of animal protein for the vegetarians [5]. Thus, dairying is a persistent source of income for the rural India. As per NDDB, the Indian dairy industry is all set to experience high growth rates in the next few years with demand likely to reach 200 million tonnes by 2022 [6].

The subject of this case study, Kaira District Co-operative Milk Producers’ Union Limited, widely known as Amul Dairy, is located in Anand, Gujarat. Amul is the largest food brand in India majoring in production of milk and milk products. Back to 1946, this dairy was the significant center of “white revolution.” It is run by collection of milk from around 700 thousand villagers [5]. With a daily milk handling capacity of 4.5 million liters, it manufactures ghee, butter, processed milk, milk powder, and flavored milk. Every unit has its own production capacity. This dairy processes 1800 m³ of raw milk per day. It produces 75 metric tonnes of milk powder, 75.5 metric tonnes of butter, 25 metric tonnes of flavored milk, 14 metric tonnes of ghee, and 55 metric tonnes of skim milk powder every day. The milk packaging section packs 90 m³ of processed milk every day.

The rest of the chapter is organized as follows: Sect. 2 gives a brief overview of exergy analysis. The milk powder production process is described in Sect. 3. Section 4 describes its exergy analysis. Two strategies are devised to make the overall plant more energy efficient. These are also discussed in this section.

2 Exergy Analysis

The term *Exergy* was first used by Rant [7] in 1956, and it refers to the Greek words *ex* meaning external and *ergos* meaning work. Szargut [8] defined exergy as: “Exergy is the amount of work obtainable when some matter is brought to a state of thermodynamic equilibrium with the common components of its surrounding nature by means of *reversible* processes, involving interaction only with the above-mentioned components of nature” [8]. Since the term reversible processes is

involved, in other words, the exergy of a system at a certain thermodynamic state is the *maximum* amount of work that can be obtained when the system moves from particular state to a state of equilibrium with the surroundings. Thus, the basic difference between the first and second laws of thermodynamics is that the former states that energy is conserved but makes no distinction between energy forms, while the latter states that the energy transformation processes in a system can only proceed from a higher-quality form to a lower-quality form unless there is some net input of energy quality (such as work) from the surroundings, thereby inferring that different energy forms have different energy qualities.

Energy can be broadly classified into: (1) high-grade energy and (2) low-grade energy. High-grade form of energy is highly organized in nature, and conversion of such energy to some other high-grade form ($W \rightarrow W$, such as electrical energy \rightarrow thermal energy in electrical heater) is not dictated by the second law of thermodynamics. Conversion of high-grade energy to low-grade energy, although not desirable, takes place in our environment. This is because of dissipation of heat due to friction (e.g., mechanical work \rightarrow electricity; some losses are there due to the friction in bearing of machineries). Thus, both the first and second laws of thermodynamics are to be considered for the analysis. Low-grade energy such as heat due to combustion, fission, fusion reactions and internal energies are highly random in nature, and their conversion to high-grade form ($Q \rightarrow W$) has been of interest. But the second law of thermodynamics dictates that complete conversion of low-grade energy (Q) to high-grade energy (W) is never possible. That part of low-grade energy which is available for conversion is termed as available energy, availability, or exergy, and the part which gets rejected is known as unavailable energy or irreversibility [9]. Thus, the exergy analysis provides comprehensive and deeper insight into the process and new unforeseen ideas for improvements and hence is applicable for process evaluation and optimization purposes [10]. Not only does it help to determine the type, location, and magnitude of energy losses in a system, but by enabling the engineers to recognize the individual components efficiency it also helps to find means to reduce these losses to make the system more energy efficient [10, 11].

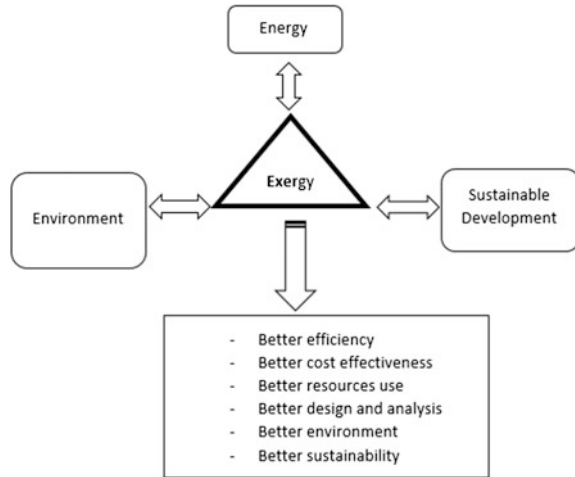
For the determination, quantification, and prioritization of possible energy savings in complex and large-scale industrial processes, including dairy production process, several scientific and engineering methods exist and are in continuous development [1]. One such method is the basic energy analysis which is a traditional approach to estimate various energy consumption processes [12]. The energy analysis is based on the first law of thermodynamics, which expressed the principle of conservation of energy. However, it provides no information about the irreversibility aspects of thermodynamic processes. The energy analysis is unable to distinguish the different qualities of energy such as heat quality which is dependent on the heat source temperature [13]. Due to these deficiencies and shortcomings of energy analysis, the exergy analysis which provides a more realistic view of the systems and processes has proved to be a more powerful tool for engineering evaluations. This is because exergy analysis considers the maximum amount of work obtainable from a stream of matter, heat, or work when some matter is

brought to a state of thermodynamic equilibrium with the common components of natural surroundings by means of reversible processes, and is a measure of the potential of a stream to cause change, as a consequence of not being completely stable relative to the reference environment [14–17].

In a real processing operation, there are many product and waste streams—some requiring heating and others requiring cooling—and each stream may have different start and end temperatures, different flows and heat capacities. If a process stream needs to be cooled over a particular temperature range, it can take place against another process stream that needs to be heated over a similar temperature interval using a heat exchanger between the streams—and this is more attractive than using steam to heat one stream, and chilled water to cool the other. This situation presents a range of options for arranging heat transfer between these streams. This technique has been developed to formalize this design process: A process integration analysis of a processing operation will consider all the process streams that require heating collectively, and develop a representation of their total heat requirement in each temperature interval; the analysis will then do the same for all the process streams that require cooling [2].

Exergy analysis gained importance in chemical engineering after the year 1990. The current applications of exergy analysis in distillation operation, membrane technology, and CO₂ capture are reviewed by Luis [18]. Review of exergy analysis of energy-intensive processes like cement, paper, iron, and steel is carried out by Luis and Bruggen [19]. Exergy analysis of methanol production shows that convective reforming process is 40% more exergy-efficient process than the steam reforming process [20]. The refrigeration cycle in the petrochemical plant that uses ethylene and propylene as refrigerant shows more losses in compressor and evaporator [21]. Energy efficiency, waste minimization, and effective raw material use can be measured and optimized by using utilizable exergy coefficient in chemical process design. Exergy load distribution analysis carried out for final optimal flow sheet topology shows an increase in exergy efficiency by 10% [22]. Second law concept is used to reduce energy consumption in the chemical industry by following some consequences suggested by Leites et al. [23]. Exergy analysis by Gao et al. shows that polygeneration systems for the production of energy and a chemical are promising in the future [24]. Thus, it can be seen that many design-related applications of exergy analysis are helpful to evaluate, compare, and improve the process. Bühler et al. [25] analyzed the energy and exergy efficiencies, as well as the destroyed and lost exergy, of 22 industrial sectors in Denmark for the years 2006 and 2012 [25]. The paper showed that the thermal process efficiencies range from 12 to 56% while industries with high-temperature processes such as cement and metal production achieve the highest efficiencies. The paper also gave a basis for future analyses toward undertaking energy efficiency measures in the industry by targeting the high-temperature processes, where large quantities of energy was found to be recoverable. Ertesvåg [26] compared the exergy scenario of different societies with the motivation that such studies may be able to create an awareness of the notion of

Fig. 1 Interdisciplinary triangle of exergy [54, 55]



energy quality and degradation of energy. His findings explain that societies with a large contribution from thermal power plants had relatively low total efficiencies while the industries generally had a higher efficiency [26].

The exergy-based performance evaluation and subsequent optimization of drying facilities have been a growing interest among the researchers in recent years. The main objective of exergy analysis of drying systems is to provide a clear picture of the process, to quantify the sources of inefficiency, to distinguish the quality of energy consumption, to select optimal drying conditions, and to reduce the environmental impact of drying systems [13]. Energy, exergy, and their impact on the environment are closely related as shown in Fig. 1. For instance, we all know that the environmental impact of emissions can be reduced by increasing the efficiency of resource utilization. However, increasing efficiency has sustainability implications as it lengthens the lives of existing resource reserves, but generally entails greater use of materials, labor, and more complex devices. Depending on the situation and the players involved, the additional cost may be justified by the added security associated with a decreased dependence on energy resources, by the reduced environmental impact, and by the social peace obtained through increased productive employment. Thus, it is suggested that the impact of energy resource utilization on the environment and the achievement of increased resource-utilization efficiency are best addressed by considering exergy. On the other hand, since these topics are critical elements in achieving sustainable development, exergy also appears to provide the basis for developing comprehensive methodologies for sustainability (shown in Fig. 2). Since the exergy of an energy form or a substance is a measure of its usefulness or quality to cause a change, it should be able to provide the basis for an effective measure of the potential of a substance or energy form to impact the environment [27].

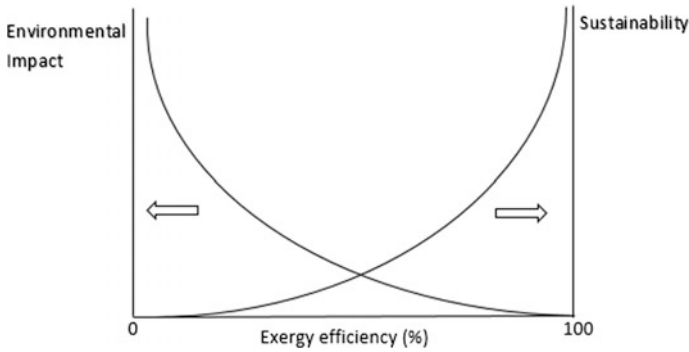
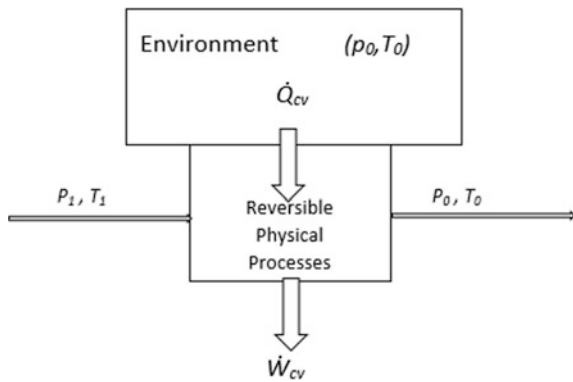


Fig. 2 Qualitative illustration of the relation between the environmental impact and sustainability of a process, and its exergy efficiency [15, 16]

Fig. 3 A reversible device (module) for determining thermomechanical energy [28]



2.1 Methodology

A process stream with temperature T_1 and pressure P_1 with negligible kinetic and potential energies, undergoing reversible physical processes as shown in Fig. 3, is considered. The heat transfer to/from the ideal reversible module shown in Fig. 3 takes place at ambient temperature T_0 , and the work produced is the maximum possible (the processes being reversible in nature) when the process stream at a state P_1, T_1 is brought to equilibrium with its natural surroundings (referred to as the environment), which is at the thermodynamic state of P_0, T_0 . An energy balance for this system yields the following[28]:

$$\frac{dE_{cv}}{dt} = 0 = \dot{Q}_{cv} - \dot{W}_{cv} + \dot{m}(h_1 - h_2) \tag{1}$$

Similarly, the entropy balance assuming no irreversibility yields the following [28]:

$$\frac{dS_{cv}}{dt} = 0 = \frac{\dot{Q}_{cv}}{T_0} + \dot{m}(s_1 - s_2) \quad (2)$$

Equation (2) can then be solved to establish an expression for specific heat transfer [28]:

$$\frac{\dot{Q}}{\dot{m}} = T_0(s_1 - s_2) \quad (3)$$

Equation (1) can then be solved with respect to specific work and rearranged to give the following [28]:

$$\frac{\dot{W}_{cv}}{\dot{m}} = T_0(s_1 - s_2) - (h_0 - h_1) \quad (4)$$

The specific exergy of the process stream entering the ideal device can be derived from Eq. (4) as follows [28]:

$$e_{x,1} = T_0(s_0 - s_1) - (h_0 - h_1) = (h_1 - h_0) - T_0(s_1 - s_0) \quad (5)$$

The change in specific exergy when a system undergoes a process from thermodynamic state 1 to state 2 is then given by the following expression (the enthalpy and entropy functions at the surrounding conditions (h_0 , s_0) cancel due to subtraction) [28]:

$$\Delta e_x = (e_{x,2} - e_{x,1}) = (h_2 - h_1) - T_0(s_2 - s_1) = \Delta h - T_0\Delta s \quad (6)$$

This change in specific exergy, if negative, accounts for irreversibility, I.

A fundamental difference between energy and exergy is that while the former is conserved, the latter is destroyed in all real processes due to irreversibility. This exergy is lost in two different ways: internal losses caused by irreversibility in the process like chemical reaction, mixing, unrestricted expansion and external losses due to effluent streams like exhaust gases, purge, and bleed streams that are not utilized. Thus, it is common to define exergy efficiency as a ratio of useful exergy from the process to total exergy to the process and given by:

$$\eta_{e_x} = \left(\sum e_x \right)_{out} / \left(\sum e_x \right)_{in} \quad (7)$$

where the subscripts out and in denote the outgoing and incoming streams, respectively. The reversible device can be replaced with real industrial equipment like evaporator, dryer, heat exchanger.

For instance, in case of heaters and heat exchangers, the working fluid is to a higher temperature and hence the entropy change is given as follows:

$$S_f - S_i = mC_p \ln(T_f/T_i) \tag{8}$$

Then, the irreversibility and efficiency are calculated with the help of the following equations:

$$I = T_0[(S_{2a} - S_{1a}) + (S_{2b} - S_{1b})] \tag{9}$$

$$\eta = \frac{[(m_b h_{x2b} - m_b h_{x1b}) - (T_0 S_{x2b} - T_0 S_{x1b})]}{[(m_a h_{x1a} - m_a h_{x2a}) - (T_0 S_{x2a} - T_0 S_{x1a})]} \tag{10}$$

where

- T_0 Ambient temperature (298 K)
- $C_{p, \text{milk}}$ 3.93 kJ/kg K
- $C_{p, \text{water}}$ 4.18 kJ/kg K.

In pumps, compressors, and the thermal vapor recompression (TVR) unit, the work input which is the work done by electricity is to be considered in the calculation of irreversibility, I . The total exergy is calculated by taking into account the change in exergy caused by change in temperature as well as change in pressure in these devices. Thus, the exergy expression is given by the following equations:

$$e_x(T) = C_p [T - T_0(1 + \ln(T/T_0))] \tag{11}$$

$$e_x(P) = T_0 R \ln(T/T_0) \tag{12}$$

$$e_x = e_x(T) + e_x(P) \tag{13}$$

From here on, irreversibility and efficiency are calculated with the help of Eqs. 14 and 15:

$$m e_{x1} + W_{\text{elec}} = m e_{x2} + I \tag{14}$$

$$\eta = \frac{W_{\text{elec}}}{[m(e_{x1} - e_{x2})]} * 100\% \tag{15}$$

In evaporators, due to the heating potential of the generated vapors, the exergy of the vapors needs to be considered as a part of useful exergy obtained from the process and is given as follows:

$$\eta = 100 * ((e_{x,a1} - e_{x,a2}) + e_{x,\text{vap}} / (e_{x,b2} - e_{x,b1}))\% \tag{16}$$

$$I = (e_{x,a1} - e_{x,a2}) + (e_{x,b2} - e_{x,b1}) \quad (17)$$

where

- a1 Heating medium (steam/vapor)
- a2 Condensate
- b1 Incoming working liquid
- b2 Outgoing working liquid.

However, in dryers no such added exergy term is used in efficiency calculation due to the absence of any vapor. This is the basic difference between an evaporator and a dryer in terms of calculating exergy efficiency even though both the equipments are used to increase the concentration of the working fluid. The exergy efficiency of the dryer is given as follows:

$$\eta = 100 * ((e_{x,a1} - e_{x,a2}) / (e_{x,b2} - e_{x,b1})) \% \quad (18)$$

$$I = (e_{x,a1} - e_{x,a2}) + (e_{x,b2} - e_{x,b1}) \quad (19)$$

Applying the above equations, irreversibility and exergy efficiencies can be obtained for various equipments in the process.

3 Milk Powder Production

Milk drying is an energy-intensive process as it usually requires hot air as heating medium to allow simultaneous heat and mass transfer between the drying air and the milk. For dairy products, the most widely used technique for dehydration is spray drying after evaporation. These processes preserve food properties as they do not involve severe heat treatments and allow storage of powders at an ambient temperature [29]. The drying operation generally takes place in three sequential stages: (i) spray chamber, in which drying occurs within a few seconds; (ii) internal stationary fluid bed, added at the conical base of the spray chamber to better control particle agglomeration and drying [30]; and (iii) external fluid bed to fine-tune the powder moisture and to cool the out-feed product stream.

When the milk receives enough energy in the form of heat, its water molecules escape as vapor. The rate at which the water molecules escape depends on various factors, viz. temperature of milk, temperature of surroundings, the pressure above the milk surface, and the rate of heat transfer. Milk powder possesses various physio-chemical and functional properties which are important to both industrial and consumer uses.

3.1 Process Description

Milk powder manufacturing involves the gentle removal of water at the lowest possible cost under stringent hygiene conditions while retaining all the desirable natural properties of the milk—color, flavor, solubility, nutritional value [31]. During the process, the water present in the milk is removed by boiling the milk under reduced pressure at low temperature in a process known as evaporation. The resulting concentrated milk is then sprayed in a fine mist into hot air to remove further moisture, thereby producing the powder. Approximately 13 kg of whole milk powder (WMP) or 9 kg of skim milk powder (SMP) can be made from 100 L of whole milk [31]. The conventional process for the production of milk powder starts with taking the raw milk received at the dairy factory and pasteurizing and separating it into skim milk and cream using a centrifugal cream separator. If whole milk powder is to be manufactured, a portion of the cream is added back to the skim milk to produce milk with a standardized fat content.

There are two sections in milk powder production: the evaporation section and the spray drying section. The pasteurized milk at 6–10 °C with around 13–14% solids is pumped into the five-effect evaporators, each accompanied with a pre-heater, where the water present in the milk gets vaporized with the help of vapor fed in the reverse direction. In Fig. 4, the hyphenated lines represent the flow direction of the pasteurized milk from left to right in the evaporation section, while the dotted lines represent the flow direction of the steam or vapor from right to left. Preheating causes a controlled denaturation of the whey proteins in the milk along with

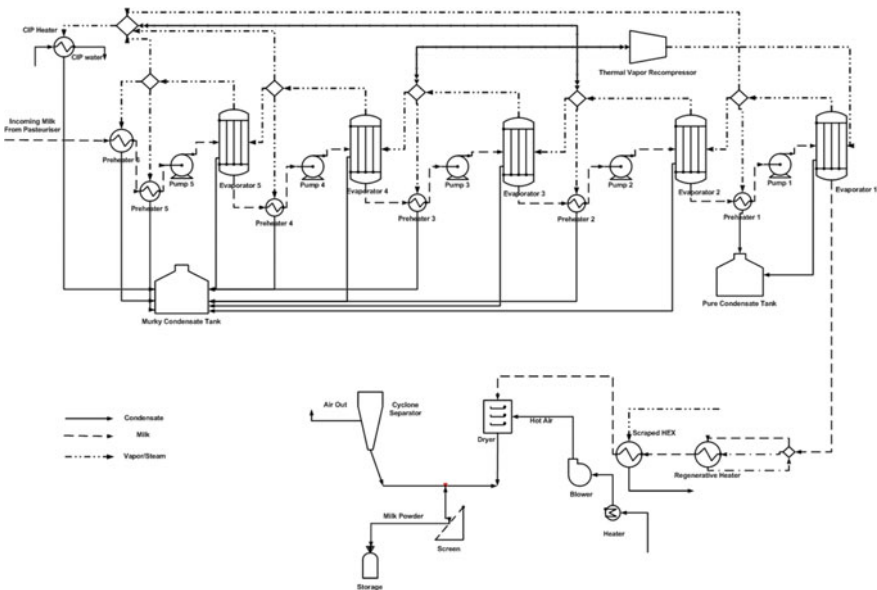


Fig. 4 PFD of base scenario

destroying bacteria, inactivating enzymes and generating natural antioxidants thereby imparting heat stability [31]. The steam which is fed in the first effect is generated by thermally compressing a part of the vapor generated in the third effect. The pressure in the five effects ranges from around 650 mmHg in first effect to around 500 mmHg in the last effect with a difference of about 30–50 mmHg between any two adjacent effects. The vapor generated in the evaporator-preheater assembly is split into three parts where first part is sent to the next effect, the second part to its accompanying preheater for heat exchange, and the third part for CIP water heating, thereby ensuring that no external source of heating is required (can be observed from Fig. 4). Condensate from the first effect, because of being in large amount as compared to other effects, gets collected in the pure condensate tank, while for all the other effects, the condensates get collected in the murky condensate tank as these condensates carry traces of solids present in the milk. The concentrated milk leaving the evaporation section has a temperature of around 92–93 °C and a solid content of around 30% [32].

A part of the milk leaving the five effects is flash cooled to around 58 °C and fed to the scraped surface heat exchanger where it is heated to 75 °C before being fed to the spray dryer (refer Fig. 4). Spray drying involves atomizing the milk concentrate from the evaporator into fine droplets. This is done inside a large drying chamber in a flow of hot air at a temperature of 180–200°C using either a spinning disk atomizer or a series of high-pressure nozzles. The milk droplets are cooled by evaporation, and they never reach the temperature of the air. The concentrate may be heated prior to atomization to reduce its viscosity and to increase the energy available for drying. The atomized particles come in contact with hot air, and water in it gets evaporated leaving a fine powder of around 4% moisture content with a mean particle size typically of <0.1 mm diameter which is collected in the silos [31]. Sometimes a secondary drying takes place in a fluidized bed through which hot air is blown to remove some more water to give a product with a moisture content of 2–4% [31]. Some amount of dried product may also get entrained with the exhaust air which is then separated in a high-efficiency cyclone separator and recycled back to the chamber. As shown in Fig. 4, the milk powder formed is then collected at the bottom of the dryer in bags or silos and sent for storage. More details about the process conditions with respect to the process flow diagram have been provided in Sect. 4.1 of the chapter.

3.2 Energy Efficiency Studies

There are a number of heat-recovery issues specific to the manufacturing dairy industry. For semi-batch operations, the availability or duty cycle of the source and target streams must be checked carefully. Heat exchangers can develop leaks, and heat recovery creates the possibility of contamination between streams. This is unacceptable in milk processing, and isolation by pressure differential double-plate heat exchangers or intermediate circuits is essential in such cases. Also many gas

and liquid waste streams carry contaminants which may affect the surfaces of heat-recovery equipment. Good engineering solutions are available for most of these problems, but surface cleaning must be designed into the heat-recovery equipment. In the recovery of gas from waste gas streams, there is also the possibility of contaminants presenting a fire hazard. Many waste gas streams contain significant moisture that will condense if the temperature is lowered significantly. It is quite possible to design heat exchangers for operation with a gas stream below the dew point, and indeed such streams often represent large heat sources. There are significant problems of physically installing major heat-recovery equipment as dairy processing buildings are frequently crowded. Large heat exchangers impose back pressure on boilers and spray dryers. The ability of original equipment to tolerate this back pressure must be checked. In this context, the optimized use of the condensate should also be considered for the recovery of the condensate imparts some added benefits to the milk drying process such as savings of (i) water and water treatment costs, for replacing the lost condensate, (ii) heat, for prewarming new boiler feed water, and (iii) wastewater, because less condensate gets into the wastewater [2].

Reducing energy use associated with milk powder production has been the subject of numerous studies. Previous studies have mainly focused on three areas: (i) heat recovery from the spray dryer exhaust air, including source/sink integration options [33], industrial case studies [34, 35], and heat exchanger modeling [36], (ii) zonal and total site heat integration of dairy factories, including integration of the milk treatment process that occurs preceding the drying operations [37] and the application [38, 39] and design [40] of heat-recovery loops to semi-continuous processes, and (iii) an overview of good energy-efficient practices in spray drying [41]. More recent studies have looked heat-recovery targeting methods and heat exchange synthesis between the evaporator and spray dryer operations of a powder process.

Some energy analyses of the dairy industry in terms of exergy have been conducted in the last few decades. However, these have primarily analyzed the milk processing [42, 43] or the drying process [44]. Quijera et al. [42, 45] use the pinch and exergy methods to evaluate and optimize the integration of solar thermal technologies for the production of cheese and yoghurt. An exergy analysis of milk pasteurization was performed by Fang et al. [43], where the process was also optimized. The usefulness of exergy as a tool for the dairy industry was discussed by Vidal et al. [46]. A milk powder production facility in New Zealand was analyzed in this study, and product input/output states were studied on a component-wise basis. The exergy losses of flavored yoghurt production were determined by Sorgüvan and Özilgen [47]. The production of other ingredients than milk was also included from a cumulative exergy perspective. A study by Trägårdh [48] used exergy as a quality factor. Dincer and Sahin [49] proposed a new thermodynamic model for drying processes, based on exergy analysis. Evaporation in food processes was discussed in [50, 51], and different evaporator configurations for citrus processing were analyzed. Winchester [52] analyzed the modeling and operation of falling film evaporators at the example of a dairy plant. Choi in [53]

focused on exergy analysis of thermal vapor recompression evaporators, suggesting new designs and operating parameters. From the above examples, it can be concluded that exergy analysis is a promising approach to study the energy efficiency for Amul's milk powder production process.

4 Improving Energy Efficiency by Process Integration

In this section, the simulation of the normal operation of the milk powder plant which is the base scenario will be presented followed by its exergy analysis. With the exergy analysis, first the regions where the heat loss is comparatively more will be located which will be followed by developing strategies through process integration to make the entire plant much more energy efficient.

4.1 Simulation Results: Base Scenario

The process conditions of milk powder production are presented in Table 1. The model presented in Fig. 4 was simulated in CHEMCAD, and the simulation results are summarized in Table 2. These were validated with plant measurements. The drying of moisture from the milk takes place in two parts as discussed earlier—first in the evaporator and then in the dryer. Apart from these two sections, there is one more section where the regenerative heating and cooling of the milk takes place. The following gives a detailed picture of the simulation results in these three regions of the milk powder plant.

Table 1 Process conditions for milk powder production

Sl. No.	Condition	Value
01.	Incoming milk temperature	6–10 °C
02.	Incoming milk solid concentration	13–4%
03.	Milk flow rate	25–30 m ³ /h
04.	Pressure in the evaporators	650 mmHg in E1 to 500 mmHg in E5
05.	Pressure drop between consecutive effects	30–40 mmHg
06.	Net rise in milk temperature in the five effects	2 °C
07.	Rise in CIP water temperature	10 °C
08.	Temperature of milk entering scraped HEX after it is flash cooled in the regenerative heater	55–58 °C
09.	Temperature of milk entering spray dryer	70–75 °C
10.	Incoming hot air temperature	180–200 °C
11.	Dryer temperature	80–90 °C

Table 2 Simulation results of base scenario

No.	Simulation condition	Value
1	Temperature of milk leaving the evaporators	93.75 °C
2	Solid concentration of milk leaving the evaporators	30.03%
3	Pure condensate collected	400.9 kmol/h
4	Murky condensate collected	819.9 kmol/h
5	Solid concentration of milk leaving the dryer	95.79%
6	Moisture content of milk powder	4.21%

Evaporation: As shown in Fig. 4, the evaporator used in the plant is of backward feed type which means that the milk and vapor flow in opposite directions. The reason behind using backward effect evaporator in food processing industries like milk powder production is that here the milk of highest concentration will remain in the first, that is, the hottest effect. Therefore, the viscosity of the milk will remain low, leading to a high heat transfer coefficient which, in turn, will enhance the capacity of the system. So the pasteurized milk enters the evaporator at 6 °C where it gets concentrated from 14.9% solids to 30.03% solids. The pressure in the five effects ranges from 630 mmHg in first effect to 500 mmHg in fifth effect with a difference of about 30 mmHg between two adjacent effects. The partially concentrated milk leaving the evaporator section is at a temperature of 93.75 °C with an overall rise of 1.5–2 °C in the five effects. The extent of evaporation in the second and the third effects (21.44% in second and 25.61% in third) was found to be significantly more than the rest of the effects (<7%). This is due to the splitting of the vapor stream in the split fractions. To utilize the full potential of these two effects, the vapor splitters just preceding these two effects, that is, splitter first and second were given a fraction of 0.75 in favor of the vapors entering the second and third effects, respectively, while the remaining 0.25 was split between the vapors fed to the preheaters and that sent for CIP heating for each of these two effects. The water used for CIP cleaning is heated from 25 to 34.33 °C with a part of vapor generated in the evaporators. The amount of pure condensate and the amount of murky condensate collected are 400.9 kmol/h and 819.9 kmol/h, respectively. The pure condensate collected from first effect is sometimes used as CIP water or pumped back to boiler house depending on requirement.

Regenerative heating and cooling: The milk leaving the evaporator section (at 93.75 °C) is then sent to the regenerative heater where a part of the milk is cooled to 58.75 °C by flash cooling and the other part is heated to 94.21 °C (shown in Fig. 4). The latter is fed back for regenerative purpose. The part of the milk which is leaving at 58.75 °C is then fed to the scraped surface heat exchanger, where it is heated to 75.75 °C by steam at 3000 mmHg and fed to the spray dryer for removing the remaining moisture and concentrating it to the required solid concentration.

Spray drying: The milk leaving the scraped heat exchanger at 75.75 °C enters the spray dryer from the top where it gets atomized by a series of high-pressure nozzles. The dryer temperature is maintained at around 85 °C. The vaporization of

Table 3 Exergy result for base scenario

No.	Equipment	Irreversibility (KJ/h)	Efficiency (%)
1	Preheater 1	5.35×10^4	22.02
2	Preheater 2	6.615×10^4	12.58
3	Preheater 3	9.784×10^3	50.61
4	Preheater 4	1.2799×10^4	16.79
5	Preheater 5	1.11×10^4	43.76
6	Preheater 6	1.287×10^5	41.81
7	CIP heater	1.397×10^6	65.64
8	Regenerative heater	1.532×10^6	69.94
9	Scraped HEX	7.64×10^5	56.24
10	Thermal vapor recompressor	1.0053×10^6	32.36
11	Pump 1	6.133×10^4	61.60
12	Pump 2	1.88×10^5	63.38
13	Pump 3	2.24×10^5	61.23
14	Pump 4	2.59×10^5	56.63
15	Pump 5	5.23×10^6	31.62
16	Evaporator 1	2.662×10^7	22.03
17	Evaporator 2	4.475×10^7	25.87
18	Evaporator 3	1.17×10^8	17.17
19	Evaporator 4	2.399×10^7	48.8
20	Evaporator 5	1.945×10^7	21.59
21	Dryer	2.09×10^7	68.28

moisture from the milk takes place due to the transfer of heat from the hot air to the milk. As a result, the atomized milk gets dried from 30.03% solids to 95.79% solids when it comes in contact with hot air blown from the bottom at a temperature of 185 °C and a pressure of 2000 mmHg (refer Fig. 4). The milk powder formed at a temperature of 40 °C and a moisture content of 4.21% is then collected at the bottom of the dryer and sent for storage. In this context, it can be mentioned that the final moisture content of the milk powder that is obtained is in sync with that of the actual process, which is around 4%.

4.2 Exergy Analysis of Base Scenario

To find the extent of heat loss in each section of the plant, exergy analysis of the base scenario was performed with the help of the equations discussed in Sect. 2 and the results are shown in (Table 3). From the results obtained, it could be concluded that some of the major equipments of the plant were running on significantly low energy efficiencies due to major heat losses which in turn bring down the energy efficiency of the entire plant. On close investigation, it was observed that major

Table 4 Simulation results of Scenarios 1 and 2 with respect to base scenario

No	Condition	Value with respect to base scenario	
		Scenario 1	Scenario 2
1	Temperature of milk leaving the evaporators	+0.12 °C	+0.21 °C
2	Solid concentration of milk leaving the evaporators	+1.37%	2.27%
3	Pure condensate collected	+37.7 kmol/h	+52.6 kmol/h
4	Murky condensate collected	-16.49 kmol/h	+49.22 kmol/h
5	Solid concentration of milk leaving the dryer	+0.12%	+0.197%
6	Moisture content of milk powder	-0.12%	-0.197%

exergy destruction occurs in equipment which is a part of the evaporation section while the equipment present in the drying section shows relatively compatible efficiencies.

Preheaters, CIP heater, Regenerative heater, and Scraped heat exchanger:

For equipment like preheaters, CIP heater, regenerative heater, and scraped surface heat exchanger, the method employed for calculating the exergy efficiency is same for all these four types of equipment, the working fluids (water for CIP heater and milk for the rest) do not exhibit any change of state. First, the change in entropy is calculated for both the two fluids between which the heat exchange is taking place. The net entropy change in both the fluids is then multiplied by the ambient temperature to obtain the irreversibility or net loss in heat in these equipments, which is nothing but the difference in exergy change of the cold stream and that of the hot stream. The exergy efficiency was then calculated by taking the ratio of the exergy gained by the cold stream (output exergy) to the exergy lost by the hot stream (input exergy). Compiling the results, it was observed that among the preheaters, only the ones belonging to the third (50.61%) and fifth (43.76%) effects showed decent efficiencies while the CIP heater, regenerative heater, and the scraped surface heat exchanger exhibited above par exergy efficiency values (55–70%); hence, they do not require any improvement as such.

TVR and pumps: For equipment like the pumps and the thermal vapor recompression unit, the work done by electricity also comes into the picture while doing the exergy analysis. An energy balance between the work done by electricity and the exergy content of the incoming and outgoing fluids gives us the value of the net irreversibility developed. One more key feature of this exergy analysis is the fact that here the exergy is contributed both by temperature and pressure because in these equipments the working fluid undergo change in temperature as well as change in pressure. The exergy efficiency was then calculated by dividing the work done by electricity by the net change in exergy of the working fluid.

The vapor from the third effect enters the TVR at 90.6 °C with a flow rate of 1754 kg/h, and the steam leaves at 271.66 °C. The enthalpy values corresponding to the inlet and outlet temperatures are -2.27×10^7 kJ/h and -1.89×10^7 kJ/h, respectively. The work done by electricity is 4.81×10^5 kJ/h. By using

$C_p = 4.18$ kJ/kg K, $T_o = 298$ K, and $R = 0.462$ kJ/kg in Eqs. (11), (12), and (13) (along with the process conditions), e_{x1} and e_{x2} were found to be -20.68 kJ/kg and 279.83 kJ/kg, respectively. These details are used in Eqs. (14) and (15) to get the lost heat or irreversibility as 1.0053×10^6 kJ/h and efficiency as 32.36%.

Thus, the results obtained showed that the efficiency of TVR is below par considering the significance of the equipment in the entire process. Most of the pumps, on the other hand, exhibited above par efficiencies (>55–60%). Observing the result, the fact that the thermal vapor recompression unit, one of the most integral parts of the process, showed considerably low efficiency became prominent. Thus, it was determined that the primary approach toward devising a strategy to improve on the current scenario should first focus on reducing the exergy loss in this unit.

Evaporator and dryer: For the evaporator and the dryer, the methodology followed for doing the exergy analysis is more or less similar. The hot utility which is steam or vapor for the evaporators, is hot air for the dryer and the corresponding counterparts at the exit are condensates and exhaust for the evaporator and dryer, respectively. The only difference between these two equipments is that while calculating the exergy efficiency, the exergy content of the generated vapor must be included for the evaporators while no such exergy addition is needed for the dryer as no vapor is generated in this case. The reason being, the exergy of the vapor is considered as a part of exergy improvement as the energy content of this vapor is later utilized to vaporize the moisture content of the milk in the next effect or even CIP heating for that matter. It was observed that among the evaporators, the third effect, the one from which a part of the vapor is sent for thermal compression into steam, showed the least efficiency (17.17%). The dryer, on the other hand, turned out to be exhibiting one of the highest efficiency values (68.28%) in the whole analysis.

Thus, it is concluded that the exergy efficiency varies from a large extent in different sections of the milk powder plant and there is a wide scope in devising strategies to improve the situation. After verification of the above-mentioned exergy results, a couple of such strategies are discussed in the next chapter of the work where some of the flaws of the base scenario have been duly addressed.

4.3 Strategies to Improve Energy Efficiency

To reduce the amount of heat loss in the equipment and thereby improve the energy efficiency of the plant, different strategies that have the potential to improve the present situation were analyzed. As discussed earlier, it was identified that not only was the third effect showing the least efficiency among the evaporators, but also the thermal vapor recompression unit, where a part of the vapor generated in the third effect is thermally compressed into steam, also showed below par efficiency. This analysis presented us with a scope to devise a strategy to improve the exergy situation by keeping these two equipments at the focal point. Thus, there can be two

options that can be pursued in this regard, which are to send either the vapor generated from second effect or that from fourth effect for thermal compression in place of that from the third effect.

First, the fourth effect was tried in the analysis. A part of the vapor generated in the fourth effect which was earlier being sent for CIP heating is now sent for thermal compression to steam which would then be fed to the first effect as the primary source of evaporation, while the part of vapor which was earlier sent for thermal compression is now sent to the CIP heater. Subsequent simulation of this new strategy followed by its exergy analysis yielded results which turned out to be below par even when compared to that of the base scenario. Earlier, the exergy efficiencies of TVR and third effect were 32.36 and 17.17%, respectively. After this new development, these values have further decreased to 28.96 and 15.72%, respectively. One reason of such an occurrence can be attributed to the fact that vapor sent to CIP heater from fourth effect is lesser than the vapor from third effect which is sent for thermal compression. Since these two have been interchanged in the new strategy, both TVR and third effect have suffered more losses. Hence, this strategy was dismissed.

Next, the second effect vapor is partly sent to TVR instead of the fourth effect and the portion which was earlier being sent to TVR is now sent to the CIP heater as before. Simulating this second model followed by its exergy analysis gave a glimpse of a better result with respect to the TVR and the third effect as compared to the base scenario. A detailed exergy analysis showed significant improvement in a few other major equipments, and this in turn formed the first strategy which could be proposed to Amul. The second strategy was developed by using the murky condensate as a hot utility to heat up the CIP water instead of the vapors, thereby utilizing the full potential of the vapors to evaporate the water present in the milk in all the five effects. These proposed strategies, believed to bring better results when implemented in the dairy, are discussed in the following.

4.3.1 Scenario 1

It is observed that in the base scenario, the part of the vapor leaving the third effect that is sent for CIP heating is more than the part sent for thermal compression into steam. Since, for the purpose of drying, the CIP heating is not of major priority, it can be concluded that there are scopes for the improvement in this section of the plant. Also, the amount of vapor sent for CIP heating from the second effect is much more than that from third effect (because of the split ratio at the splitters). Hence, the vapor from second effect which was earlier sent for CIP heating is now sent for thermal compression to steam and the vapor from third effect that was earlier sent for thermal compression is now sent for CIP heating in the new strategy (shown in Fig. 5). The following describes the simulation results obtained after implementing this new strategy:

Evaporation: With this new strategy now implemented in the existing plant operations, the milk leaving the evaporators now has a solid concentration of

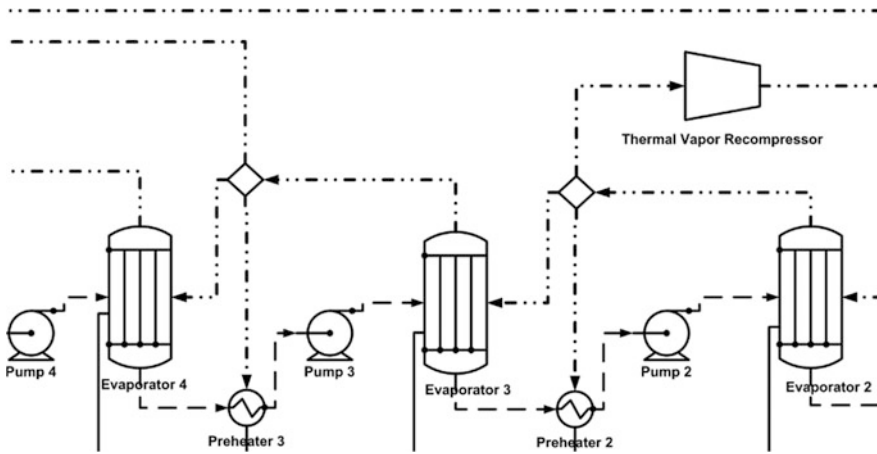


Fig. 5 PFD of Scenario 1 (modification only)

31.4%, which earlier used to be 30.03%. The milk temperature has also risen a little to 93.87 °C. The pure condensate generated from first effect has increased from 400.9 to 438.6 kmol/h due to the fact that the amount of steam fed to first effect is more now, due to which the pure condensate obtained is also more. But the amount of murky condensate is reduced from 819.9 to 803.41 kmol/h due to the fact that now the vapor used for CIP heating is comparatively lesser which in turn results in lesser condensate generation (as shown in Table 4). At the exergy front, the efficiency of TVR in this scenario has showed a jump from 32.36% to 46.47% which is more than 10% while the efficiency of the third effect is at par with that of base scenario (shown in Table 5). Along with this, the first- and second-effect evaporators including their corresponding preheaters have showed a significant jump in efficiency (around 20%). The rest of the equipment has shown only minor variations.

Regenerative heating and cooling: The partially concentrated milk from the evaporators entered this section at 93.87 °C, and a part of it is again flash cooled to its design value of 58.75 °C. It is then heated to 75.75 °C in the scraped heat exchanger and fed to the spray dryer. This shows that there are not many changes in the process conditions involved at this section, and hence, the exergy values are more or less at par with that of base scenario. The regenerative heater now has an exergy efficiency of 69.7%, a minute drop from 69.94%, value in case of base scenario while the scraped surface heat exchanger shows a slight upward growth from 56.24% at base scenario to 56.98% in this new strategy.

Spray Drying: The fact that in the evaporators, milk already got concentrated to 31.4% (1.37% more than the base scenario) had a direct effect in the extent of drying as well. The final dried powder in this new strategy had an overall moisture content of 4.09%, which is 0.12% lesser than the base scenario (shown in Table 4).

Table 5 Exergy results of Scenarios 1 and 2 with respect to base scenario

No	Equipment	Irreversibility (KJ/h)		Efficiency (% change with respect to base scenario)	
		Scenario 1	Scenario 2	Scenario 1	Scenario 2
1	Preheater 1	3.13×10^4	2.981×10^4	+16.74	+19.11
2	Preheater 2	3.97×10^4	3.24×10^4	+19.81	+24.76
3	Preheater 3	1.01×10^4	9.82×10^3	-3.24	-0.59
4	Preheater 4	1.52×10^4	9.88×10^3	-0.34	+6.92
5	Preheater 5	1.48×10^4	1.003×10^4	-0.84	+0.43
6	Preheater 6	1.462×10^5	9.76×10^4	-0.61	+3.59
7	CIP heater	1.52×10^6	1.453×10^6	-3.86	-2.29
8	Regenerative heater	1.58×10^6	1.61×10^6	-0.24	-0.73
9	Scraped HEX	7.42×10^5	7.428×10^5	+0.74	+0.66
10	Thermal vapor recompressor	1.001×10^6	1.0007×10^6	+14.11	+14.86
11	Pump 1	5.84×10^4	5.37×10^4	+0.70	+0.95
12	Pump 2	1.823×10^5	1.83×10^5	+2.13	+2.09
13	Pump 3	2.49×10^5	2.52×10^5	-0.34	-0.47
14	Pump 4	2.81×10^5	2.823×10^5	-0.22	-0.74
15	Pump 5	5.47×10^6	5.561×10^6	-0.29	-1.22
16	Evaporator 1	2.083×10^7	2.004×10^7	+21.75	+24.75
17	Evaporator 2	3.477×10^7	3.238×10^7	+22.31	+25.29
18	Evaporator 3	1.1743×10^8	1.159×10^8	-0.58	+4.58
19	Evaporator 4	2.469×10^7	2.35×10^7	-0.66	+0.64
20	Evaporator 5	1.98×10^7	1.47×10^7	-0.48	+5.34
21	Dryer	2.04×10^7	2.01×10^7	+0.82	+1.50

The final solid temperature was also maintained at around 40 °C in the presence of hot air blown from the bottom of the dryer at 185 °C and 2000 mmHg. As a result, the dryer efficiency rose a little from 68.28% in the base scenario to 69.1% in Scenario 1.

Thus, it is clear from Table 4 that in Scenario 1, due to improved efficiency of evaporation in first and second effects, the overall drying has improved. Thus, this strategy more or less addressed those equipments which were earlier exhibiting low exergy efficiency under base scenario and improved them to decent values. In the second scenario, another strategy is devised which when implemented with this Scenario 1 will show further improvement in the exergy results.

4.3.2 Scenario 2

In the previous model, vapor generated in the evaporators was used to heat the CIP water (for its 10 °C rise). But it was observed that instead of using the vapor if the condensate was used for CIP heating (since it is not a major priority in milk drying), then the energy efficiencies could be further improved. On implementing this change in Scenario 1, it showed significant rise in the efficiency values and reduction in the heat losses due to the fact that now more amount of vapor, which was earlier sent for CIP heating, was now used for the evaporation of the water present in the milk in the five effects. The modification made in Scenario 2 with respect to Scenario 1 is shown in Fig. 6. A detailed picture of the simulation results is presented in the following:

Evaporation: Adding this new strategy along with Scenario 1 has resulted in an increase in solid concentration in the milk leaving the evaporation effects from 31.4% solids in Scenario 1 to 32.3% solids under this combined strategy. The total water removal in all the five effects has also jumped further, from 51.77% in Scenario 1 to 52.54% under the present scenario. Since now more amount of vapor is being sent for evaporation, the condensates collected in both the pure and murky condensate tanks have increased (pure condensate: 453.5 kmol/h from 400.9 kmol/h in base scenario and murky condensate: 869.12 kmol/h from 819.9 kmol/h in base scenario). The final temperature of the CIP water, which is now 34.72 °C, is also found to have increased a little in this scenario (34.33 °C in base scenario and 34.41 °C in Scenario 1). From the exergy perspective, significant growth has been noticed in the third effect, both in the evaporator and in its corresponding preheater. Compared to Scenario 1, where the efficiency values of third evaporator and preheater were 16.59 and 47.37%, respectively, these values have now jumped to 21.75 and 50.02%, respectively. The detailed results are shown in Table 5. All the preheaters under this new strategy have shown decent improvement, while rest of the equipment exhibited minor variations.

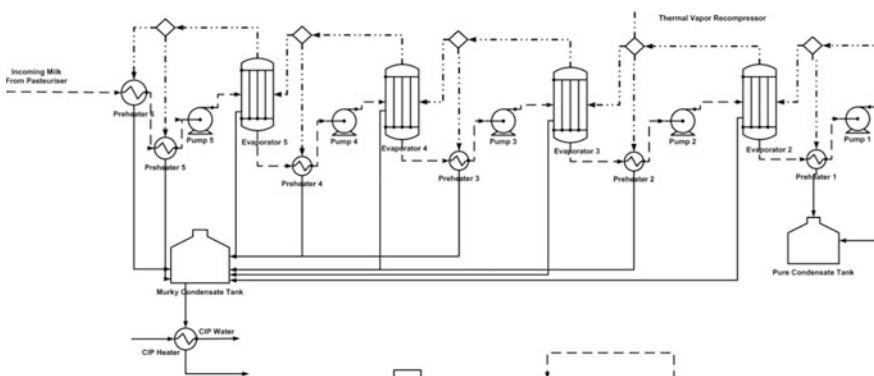


Fig. 6 PFD of Scenario 2 (modification only)

Regenerative heating and cooling: The milk now leaves the evaporator at a temperature of 93.96 °C, which is a slight rise from Scenario 1 where the milk leaving the five effects and entering this section had a temperature of 93.87 °C. A part of the milk is cooled to its designed value of 58.75 °C and fed to the scraped surface heat exchanger where it is heated to 75.75 °C before being fed to the spray dryer. The exergy efficiency of both the regenerative heater and the scraped surface heat exchanger showed a slight drop, negligible enough to affect the overall exergy scenario of the whole plant.

Spray drying: The improvement in solid concentration in the evaporation section had a direct effect in the final moisture content of the milk powder as well. There had been a rise of 2.27% in the overall solid concentration in Scenario 2 from the base scenario, as a result of which the milk powder moisture content has reduced from 4.21% in base scenario to 4.013% in Scenario 2. These details are shown in Table 5. The final solid temperature remained within its designed limit of around 40 °C. All these have resulted in an improvement in the dryer efficiency, from 68.28% in base scenario and 69.1% in Scenario 1 to 69.78% in this combined strategy.

These two scenarios discussed above clearly depict how process integration helps to improve the overall efficiency of any process. A graphical representation depicting the comparative analysis of all the three scenarios for those equipments which show significant improvements has been presented in Fig. 7.

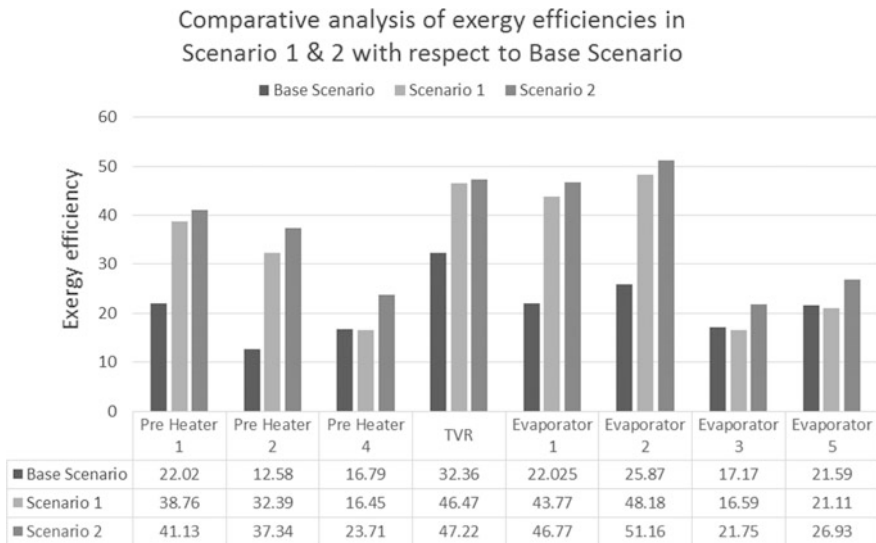


Fig. 7 Graphical representation of the exergy results for the major equipment

5 Summary

This work addresses opportunities to improve energy efficiency of a large-scale milk powder production unit through process integration based on exergy studies. A model of the milk powder plant of Amul Dairy was built and simulated in CHEMCAD to get an idea of all the equipment efficiencies under the normal operation of the plant. On the basis of exergy analysis, two strategies were proposed which if implemented can lead to significant improvement (more than 20% in some major equipment) in the exergy efficiencies.

The proposed approach for improving the energy efficiency can be extended to develop a holistic framework that can foster water and energy sustainability. This framework can be realized by an optimization approach that minimizes the energy and water usage using the proposed techniques while accounting for cost constraints and plant dynamics through appropriate models. The strategies suggested here are best applicable to milk powder plants worldwide and can be further generalized for various other industries to promote water and energy sustainability, respectively.

Acknowledgements The authors gratefully acknowledge Mr. S.S. Sundaran (OSD, Public Relations) and Mr. Deepak R. Sharma (Deputy Manager, Production) of Amul Dairy, Anand, for their constant support in this project.

References

1. Bühler F, Nguyen T, Jensen JK, Elmegaard B (2016) Energy, exergy and advanced exergy analysis of a milk processing factory. In: Proceedings of ECOS 2016: 29th International conference on efficiency, cost, optimization, simulation and environmental impact of energy systems.
2. Bulletin of the International Dairy Federation 401/2005, 2005 Energy use in dairy processing
3. Department of Dairying Fisheries and Animal husbandary (2013) Annual Report—2012–13. Ministry of Agriculture, Government of India 15(1):1. <https://doi.org/10.1016/j.parkreldis.2008.12.001>
4. Banerjee A (2001) Dairying Systems in India. FAO Corporate Document Repository
5. Tiwari S, Srinivasan B (2017) Water conservation, reuse and challenges: a case study performed at Amul dairy. The water-food-energy nexus: processes, technologies and challenges, CRC Press ISBN: 9781498760836
6. National Dairy Development Board (2014) Annual Report, 2013–14
7. Rant Z (1956) Exergy, a new word for “technical available work”. *Forschung auf dem Gebiete des Ingenieurwesens* (in German) 22:36–37
8. Szargut J (1980) International progress in second law analysis. *Energy* 5(8–9):709–718
9. Chapter 3: Exergy analysis Available at: http://www.iitg.ernet.in/scifac/qip/public_html/cdcell/chapters/p_mahanta_adv_engg_thermo/Chapter-3.pdf
10. Kaushik SC, Siva RV, Tyagi SK (2011) Energy and exergy analyses of thermal power plants: a review. *Renew Sustain Energy Rev* 15:1857–1872
11. Siva RV, Kaushik SC, Tyagi SK (2012) Exergetic analysis of solar concentrator aided natural gas fired combined cycle power plant. *Renew Energy* 39:114–125

12. Nazghelichi T, Aghbashlo M, Kianmehr MH (2011) Optimization of an artificial neural network topology using coupled response surface methodology and genetic algorithm for fluidized bed drying. *Comput Electron Agric* 75(1):84–91
13. Aghbashlo M, Mobli H, Rafiee S, Madadlou A (2013) A review on exergy analysis of drying processes and systems. *Renew Sustain Energy Rev* 22:1–22
14. Dincer I (2002) On energetic, exergetic and environmental aspects of drying systems. *Int J Energy Res* 26:717–727
15. Dincer I, Rosen MA (2007) *Exergy: energy, environment, and sustainable development*. Elsevier, Amsterdam
16. Dincer I (2011) Exergy as a potential tool for sustainable drying systems. *Sustain Cities Soc* 1:91–96
17. Pandey AK, Tyagi VV, Park SR, Tyagi SK (2012) Comparative experimental study of solar cookers using exergy analysis. *J Therm Anal Calorim* 109:425–431
18. Luis P (2013) Exergy as a tool for measuring process intensification in chemical engineering. *J Chem Technol Biotechnol* 88(11):1951–1958
19. Luis P, Van der Bruggen B (2014) Exergy analysis of energy-intensive production processes: advancing towards a sustainable chemical industry. *J Chem Technol Biotechnol* 89:1288–1303
20. Rosen MA, Scott DS (1988) Energy and exergy analyses of a production process for methanol from natural gas. *Int J Hydrogen Energy* 13:617–623
21. Fábrega FM, Rossi JS, d'Angelo JVH (2010) Exergetic analysis of the refrigeration system in ethylene and propylene production process. *Energy* 35:1224–1231
22. Sorin M, Hammache A, Diallo O (2000) Exergy load distribution approach for multi-step process design. *Appl Therm Eng* 20:1365–1380
23. Leites IL, Sama DA, Lior N (2003) The theory and practice of energy saving in the chemical industry: some methods for reducing thermodynamic irreversibility in chemical technology processes. *Energy* 28:55–97
24. Gao L, Jin H, Liu Z, Zheng D (2004) Exergy analysis of coal-based polygeneration system for power and chemical production. *Energy* 29:2359–2371
25. Bühler F, Nguyen T, Elmegaard B (2015) Energy and exergy analysis of the danish industry sector. In: *Proceedings of the 10th conference on sustainable development of energy, water and environment systems*
26. Ertesvåg IS (2001) Society exergy analysis: a comparison of different societies. *Energy* 26:253–270
27. Rosen MA, Dincer I (2001) Exergy as the confluence of energy, environment and sustainable development. *Exergy Int J* 1(1):3–13
28. Gundersen T (2011) An introduction to the concept of exergy and energy quality. *Energy Process Eng version 4*
29. Schuck P, Dolivet A, Méjean S, Jeantet R (2008) Relative humidity of outlet air: the key parameter to optimize moisture content and water activity of dairy powders. *Dairy Sci Technol* 88:45–52
30. Birchal VS, Passos ML (2005) Modeling and simulation of milk emulsion drying in spray dryers. *Braz J Chem Eng* 22(2):293–302
31. Milk Powder—New Zealand Institute of Chemistry Available at: <https://nzic.org.nz/ChemProcesses/dairy/3C.pdf>
32. Training Manual—Amul 3 Powder Plant, Amul Dairy, Anand
33. Holland CR, McCann JB (1980) Heat recovery in spray drying systems. *Int J Food Sci Technol* 15:9–23
34. Mercer AC (1986) Improving the energy efficiency of industrial spray dryers. *J Heat Recovery Syst* 6:3–10
35. Miller J (1987) The use of recovered heat for preheating air to spray driers. *New Zealand Energy Research and Development Committee Report*. Palmerston North, New Zealand
36. Atkins MJ, Walmsley MRW, Neale JR (2011) Integrating heat recovery from milk powder spray dryer exhausts in the dairy industry. *Appl Therm Eng* 31:2101–2106

37. Robert C (2005) Bulletin of the IDF No. 401/2005- Energy use in dairy processing
38. Atkins MJ, Walmsley MRW, Neale JR (2010) The challenge of integrating non-continuous processes—milk powder plant case study. *J Clean Prod* 18:927–934
39. Atkins MJ, Walmsley MRW, Neale JR (2012) Process integration between individual plants at a large dairy factory by the application of heat recovery loops and transient stream analysis. *J Clean Prod* 34:21–28
40. Walmsley MRW, Walmsley TG, Atkins MJ, Neale JR (2012) Area targeting and storage temperature selection for heat recovery loops. *Chem Eng Trans* 29:1219–1224
41. Baker CGJ, McKenzie KA (2005) Energy consumption of industrial spray dryers. *Drying Technol Int J* 23:365–386
42. Quijera JA, Labidi J (2013) Pinch and exergy based thermosolar integration in a dairy process. *Appl Therm Eng* 50:464–474. <https://doi.org/10.1016/j.applthermaleng.2012.06.044>
43. Fang Z, Larson DL, Fleischmen G (1995) Exergy analysis of a pilot milk processing system. *Trans ASAE* 38:1825–1832
44. Erbay Z, Koca N (2012) Energetic, exergetic, and exergoeconomic analyses of spray-drying process during white cheese powder production. *Dry Technol* 30:435–444. <https://doi.org/10.1080/07373937.2011.647183>
45. Quijera JA, Alriols MG, Labidi J (2011) Integration of a solar thermal system in a dairy process. *Renew Energy* 36:1843–1853. <https://doi.org/10.1016/j.renene.2010.11.029>
46. Vidal M, Martin L, Martin M (2014) Can exergy be a useful tool for the dairy industry? In: 24th European Symposium Computer Aided Process Engineering—ESCAPE 24, vol 33, Elsevier, Amsterdam, pp 1603–1608. <https://doi.org/10.1016/B978-0-444-63455-9.50102-1>
47. Sorgüven E, Özilgen M (2012) Energy utilization, carbon dioxide emission, and exergy loss in flavored yoghurt production process. *Energy* 40:214–225. <https://doi.org/10.1016/j.energy.2012.02.003>
48. Traegardh C (1981) Energy and exergy analysis in some food processing industries. *Leb Und—Technologie* 14:213–217
49. Dincer I, Sahin AZ (2004) A new model of thermodynamic analysis of a drying process. *Int J Heat Mass Transf* 47:645–652. <https://doi.org/10.1016/j.ijheatmasstransfer.2003.08.013>
50. Leo MA (1982) Energy conservation in citrus processing. *Food Technol* 36:231–233
51. Balkan F, Colak N, Hepbasli A (2005) Performance evaluation of a triple-effect evaporator with forward feed using exergy analysis. *Int J Energy Res* 29:455–470. <https://doi.org/10.1002/er.1074>
52. Winchester J (2000) Model based analysis of the operation and control of falling film evaporators. Massey University
53. Choi HS, Lee TJ, Kim YG, Song SL (2005) Performance improvement of multiple-effect distiller with thermal vapor compression system by exergy analysis. *Desalination* 182:239–249. <https://doi.org/10.1016/j.desal.2005.03.018>
54. Bejan A, Dincer I, Lorente S, Reis AH, Miguel AF (2004) Porous media in modern technologies: energy, electronics. Biomedical and environmental engineering. Springer, New York p 396
55. Dincer I, Rosen MA (2005) Thermodynamic aspects of renewables and sustainable development. *Renew Sustain Energy Rev* 9:169–189

Erratum to: Sustainable Energy Technology and Policies

Sudipta De, Santanu Bandyopadhyay, Mohsen Assadi
and Deb A Mukherjee

Erratum to:

S. De et al. (eds.), *Sustainable Energy Technology
and Policies*, Green Energy and Technology,
<https://doi.org/10.1007/978-981-10-7188-1>

The original version of the book was inadvertently published with incorrect Foreword version which has been now updated with correct version in Frontmatter. The erratum book has been updated with the change.

The updated online version of this book can be found at
<https://doi.org/10.1007/978-981-10-7188-1>

© Springer Nature Singapore Pte Ltd. 2018
S. De et al. (eds.), *Sustainable Energy Technology and Policies*, Green Energy
and Technology, https://doi.org/10.1007/978-981-10-7188-1_20